Geotechnics for Catastrophic Flooding Events

Editor: Susumu Iai

CRC Press
Taylor & Francis Group
A BALKEMA BOOK

GEOTECHNICS FOR CATASTROPHIC FLOODING EVENTS

This page intentionally left blank

PROCEEDINGS OF THE FOURTH INTERNATIONAL CONFERENCE ON GEOTECHNICAL ENGINEERING FOR DISASTER MITIGATION AND REHABILITATION (4th GEDMAR), 16–18 SEPTEMBER 2014, KYOTO, JAPAN

Geotechnics for Catastrophic Flooding Events

Editor

Susumu Iai
Disaster Prevention Research Institute, Kyoto University, Japan

CRC Press
Taylor & Francis Group
Boca Raton London New York Leiden

CRC Press is an imprint of the
Taylor & Francis Group, an **informa** business
A BALKEMA BOOK

CRC Press/Balkema is an imprint of the Taylor & Francis Group, an informa business

Typeset by MPS Limited, Chennai, India
Printed and bound in Great Britain by CPI Group (UK) Ltd, Croydon, CR0 4YY.

Published by: CRC Press/Balkema
P.O. Box 11320, 2301 EH Leiden, The Netherlands
e-mail: Pub.NL@taylorandfrancis.com
www.crcpress.com – www.taylorandfrancis.com

ISBN: 978-1-138-02709-1 (Hardback + CD-ROM)
ISBN: 978-1-315-73698-5 (eBook)

Geotechnics for Catastrophic Flooding Events – Iai (Ed)
© 2015 Taylor & Francis Group, London, ISBN 978-1-138-02709-1

Table of contents

Workshop on guidelines and recommendations for local governments to mitigate flooding disasters

Panel Discussions "How to meet catastrophic flooding events?"

Geotechnics for Catastrophic Flooding Events – Iai (Ed)

Preface

This book is prepared for sharing knowledge and improving understanding of the geotechnical engineering issues associated with catastrophic flooding events. The book will discuss hurricane, rainstorm and storm surge induced riverine and coastal flooding events, such as the 2004 Sumatra earthquake in Indonesia, the 2005 Hurricane Katrina disaster in New Orleans, USA, Typhoon Morakot, which devastated parts of Taiwan in 2009 and the 2011 earthquake and tsunami disaster in Eastern Japan.

Combined failure mechanism, multiple hazards, and rare event with significant consequence exemplified by Fukushima accident and lessons learned are just a few examples characterizing this book. The book also includes contributions to a workshop on liquefaction experiment and analysis projects (LEAP) and a workshop for developing guidelines and recommendations for local governments to mitigate the risk of coastal and river flooding disasters.

The book is compiled at the Fourth International Conference on Geotechnical Engineering for Disaster Mitigation and Rehabilitation (4th GEDMAR), held on 16–18 September, 2014, Kyoto, Japan. The 4th GEDMAR provided a forum for members of ISSMGE and built on the tradition of previous successful GEDMAR conferences held in Singapore, Nanjin/China, and Semarang/Indonesia since 2005.

The editor hopes that the book will further advance the geotechnics for catastrophic flooding events. In compiling the manuscripts, the assistance by Ms. Chihiro Tsurui, Kyoto University and Ms. Waka Yuyama, FLIP Consortium, are gratefully acknowledged.

Susumu Iai
Editor

This page intentionally left blank

Keynote Lectures

This page intentionally left blank

Geotechnics for Catastrophic Flooding Events – Iai (Ed)
© 2015 Taylor & Francis Group, London, ISBN 978-1-138-02709-1

Combined failure mechanism of breakwaters and buildings subject to Tsunami during 2011 East Japan earthquake

S. Iai
Disaster Prevention Research Institute, Kyoto University, Japan

ABSTRACT: In this study, a centrifuge model tests and effective stress analyses are performed on a breakwater and a steel frame building with pile-foundation subject to Tsunami such as those seriously damaged during 2011 East Japan Earthquake (Magnitude 9.0). The centrifuge model tests at a scale of 1/200 are performed to simulate the failure of a breakwater subject to Tsunami. The centrifuge model tests are also performed to simulate the overturning of a building subject to combined effects of soil liquefaction and Tsunami. With the effective stress analyses, this study demonstrates the importance of the mechanism of failure in the rubble mound due to seepage flow of pore water and the combined effects of soil liquefaction at pile foundation in addition to the external force of Tsunami.

1 INTRODUCTION

An earthquake with a Japan Meteorological Agency (JMA) magnitude 9.0 hit north east Japan at 14:46, March 11, 2011. JMA named this earthquake '2011 Tohoku-Pacific Ocean earthquake'. This earthquake is the greatest in its magnitude since the modern earthquake monitoring system was established in Japan.

Recorded heights of the Tsunamis were higher than 7.3 m at Soma, higher than 4.2 m at Oarai, and higher than 4.1 m at Kamaishi. The impact of the Tsunamis is also the greatest since the existing design methodology was adopted for designing breakwaters. The existing design methodology of a breakwater is based on limit equilibrium by considering wave force acting from the lateral side and additional pressure acting underneath the caisson as shown in Figure 1.

1.1 *Damage to breakwaters*

The most typical example of the damage to breakwater was the one at the Kamaishi Harbor. In this example,

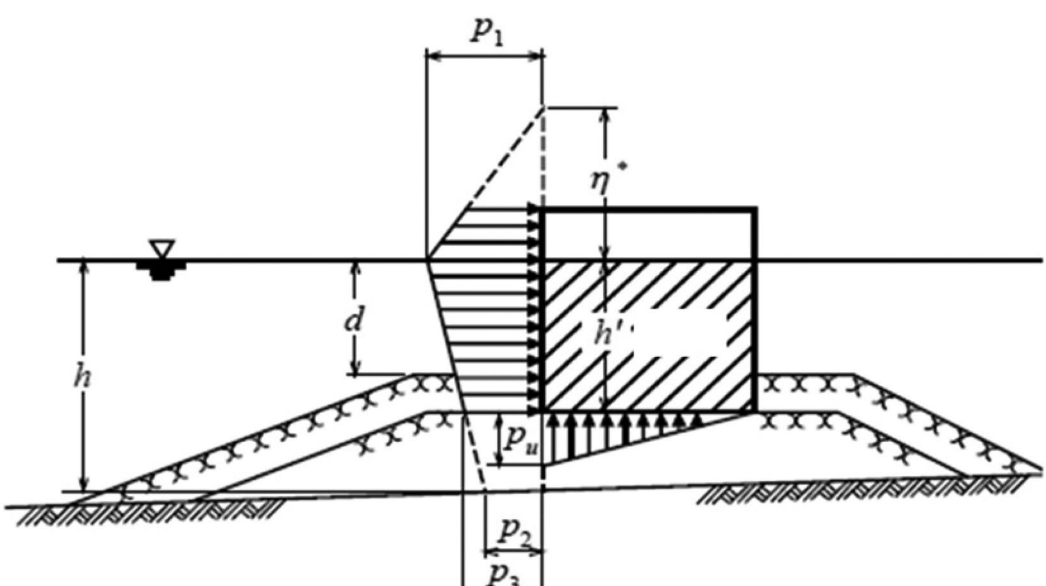

Figure 1. Existing design procedure of a breakwater.

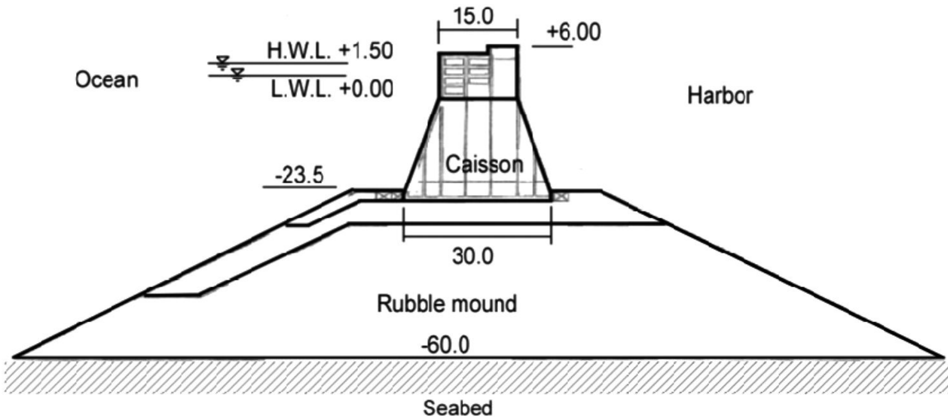

Figure 2. Cross section of a composite breakwater at Kamaishi Harbour (unit in m).

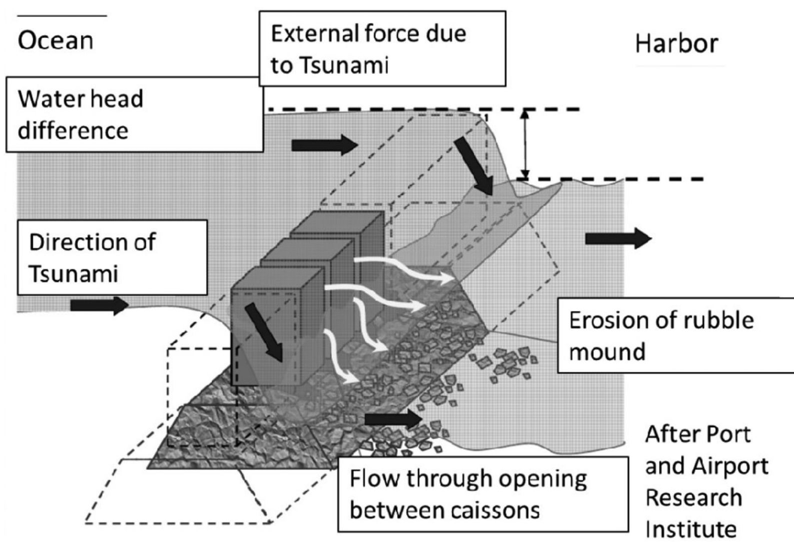

Figure 3. Primary mechanism of failure hypothesized by a hydrodynamics expert group.

the breakwater was specifically designed for protection against the impact of Tsunami and constructed at the mouth of the Kamaishi harbor at a depth of 63 m or less over the length of 990 m in the northern part and 670 m in the southern part with an opening of 300 m in between. However, the breakwater was devastated by the Tsunami. This may be partly due to the failure of design procedure then adopted but also a symbolic event for indicating the serious impact by the Tsunami.

Figure 2 shows a typical cross section of the break water. The breakwater is a composite of caisson and rubble mound. Based on the visual data (video) monitored from the coastal line, the first arrival of the Tsunami was at about 15:24 (about 40 minutes after the earthquake). The break water was not damaged by this first arrival of the Tsunami.

However, there was a continual overtopping of water at the top of the breakwater. At about 15:32, when the height of the Tsunami was reduced, serious devastation of the breakwater was visually confirmed by the monitored visual data. At 15:59, the devastation was progressed further and many of the caissons fell into the harbor side from the rubble mound. The rubble mound was also seriously devastated even to the extent that about half of its original body of the rubble mound was lost.

In order to investigate the primary mechanism of failure of this type of a breakwater due to Tsunami, a series of centrifuge model tests and effective analyses are performed in this study. As a straight forward extension of the existing design procedure shown in Figure 1, the primary mechanism of failure was considered by a hydrodynamics expert group due to erosion of rubble mound by the water flow through opening between caissons as shown in Figure 3. As parallel efforts to that group, this study was performed

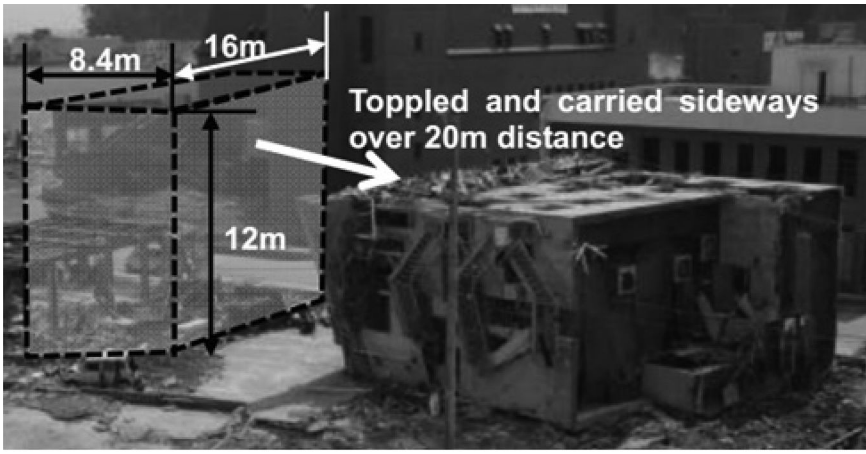

(a)

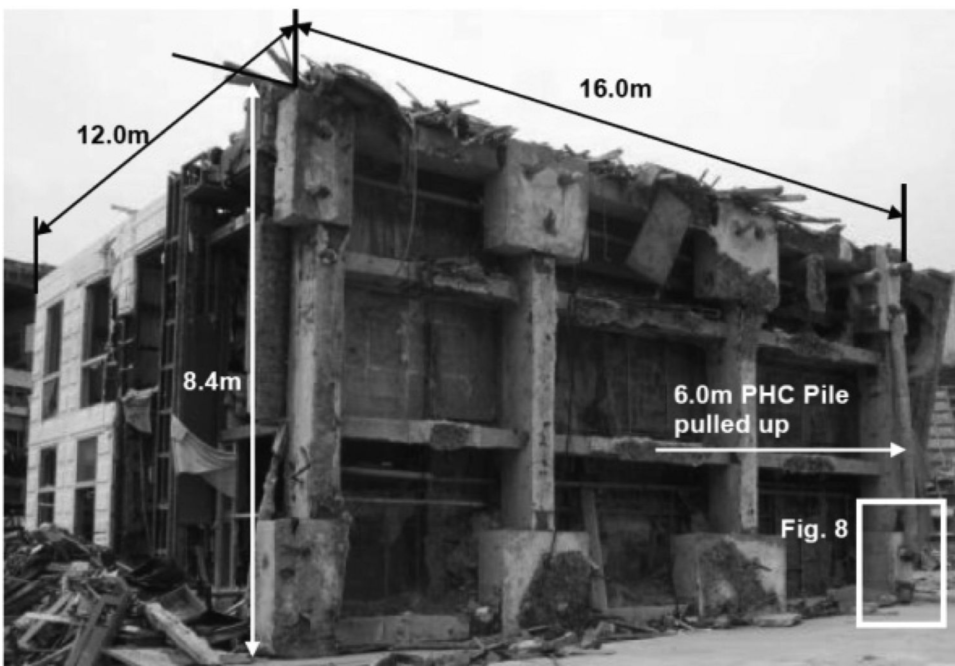

(b)

Figure 4. Toppling of a four story steel frame building with pile-foundation at Onagawa city during 2011 East Japan earthquake (after JSCE, 2011).

with the objective of evaluating the effect of seepage flow through the rubble mound due to water head difference due to Tsunami in combination with the wave force action.

1.2 *Damage to RC and steel frame buildings with pile-foundations*

The most typical example of the damage to buildings was the one at Onagawa city. In this example, the RC or steel frame buildings supported by pile foundations were washed away and toppled down due to Tsunami. These types of buildings were supposed to resist the external force due to Tsunami and expected to function as evacuation facilities. Consequently, the damage to these types of buildings, including the pull-out of pile foundation, was unexpected, posing a new engineering problem related to the effects of Tsunami.

Figure 4 shows a typical damage to the steel frame buildings at Onagawa city. The four story building had dimension of 8.4 wide, 12 m high, and 16 m in depth, receiving Tsunami force toward the shortest dimension. This building was overturned together with the footing, and pile was damaged at the pile top near the

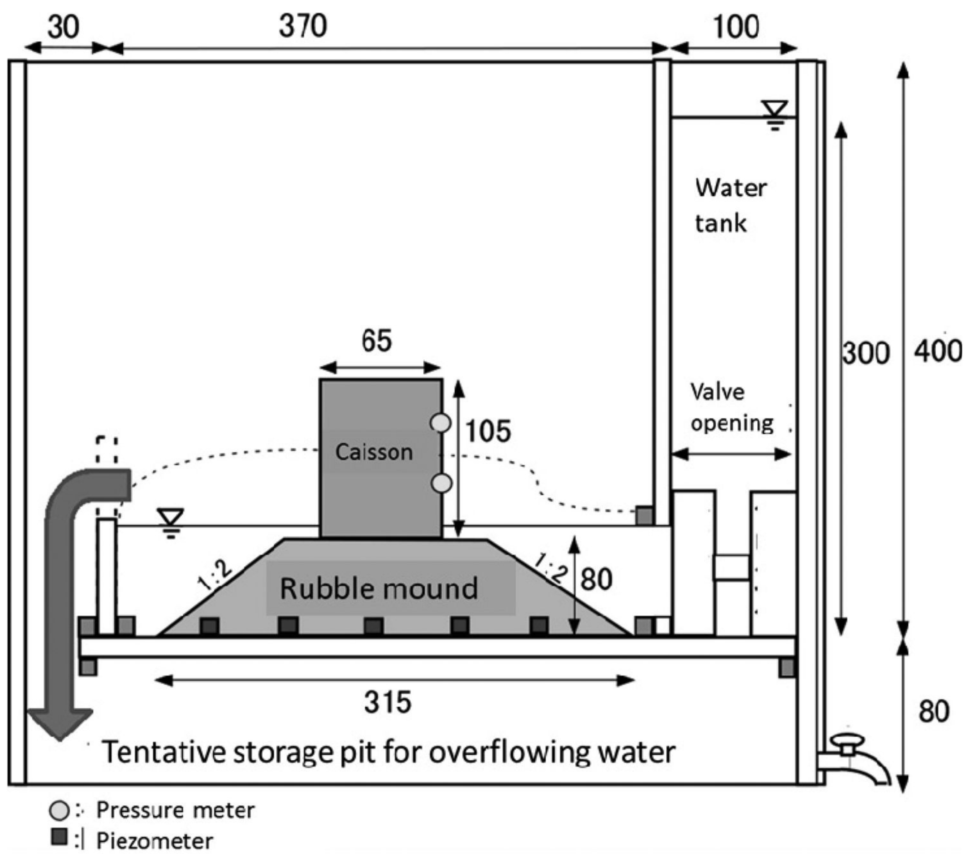

Figure 5. Equipment for simulating Tsunami in centrifuge model tests and model of a breakwater (unit in mm in model scale).

footing. At the right side of the photo, a pulled out pile is dragged down from the footing. After Tsunami, this building was found washed away 20 m over a parking area in the vicinity of the original location of the building.

The mechanism of failure of this type of damage to buildings was speculated due not only to Tsunami force, but also combined effects due to liquefaction of foundation ground. In order to investigate the primary mechanism of failure of this type, another series of the centrifuge model tests and effective analyses are performed in this study.

2 CENTRIFUGE MODEL TESTS

2.1 *Tsunami generator in centrifuge and model test conditions*

The centrifuge at Disaster Prevention Research Institute, Kyoto University, (effective radius 2.5 m) was used for the centrifuge model tests in this study. The equipment for simulating Tsunami in the centrifuge is shown in Figure 5. In this equipment, the remote-control valve at the bottom of the water tank is opened for generating Tsunami-like water flow toward a structure such as a breakwater or a building and overflowing water at the other end of the model (left in this figure) is absorbed in a tentative storage pit for reducing the effect of reflecting wave from the (left side) wall of the container.

The centrifuge model tests of a breakwater were performed for a caisson 21 m high in prototype with a scaling factor of 1/200 by adopting the generalized scaling relation (Iai et al. 2005) in a 25 g centrifugal acceleration field. Four cases were performed by varying initial sea water level and water level difference due to Tsunami as shown in Table 1. The material of rubble mound was also varied by using Silica No.1 sand that

Table 1. Model test cases of a breakwater.

Case	Mound	Relative density	Sea water level	Water level difference
Case 1	Silica #1 sand	55.5%	6.23 m	14.4 m
Case 2	Silica #1 sand	60.3%	12.6 m	10.3 m
Case 3	Silica #4 sand	58.0%	8.15 m	15.2 m
Case 4	Silica #4 sand	65.8%	13.0 m	10.9 m

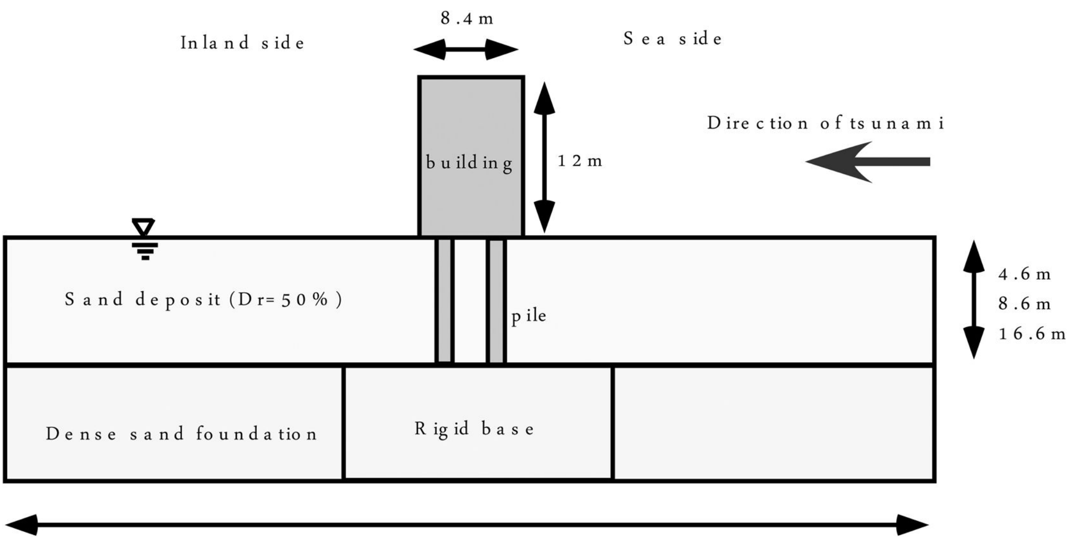

Figure 6. Centrifuge model of a building with pile foundation at liquefiable sand deposit (unit in m in prototype scale).

consists of particles scaled in 1/200 of the prototype rubble and Silica No. 4 sand that artificially reduces the effect of seepage flow in the rubble mound. Pure water was used for centrifuge tests. The rubble mound model was made by water pluviation.

The centrifuge model tests of a building with pile foundation were performed for a building 12 m high, 8.4 m by 16 m wide, in prototype with a scaling factor 1/200 by adopting the generalized scaling relation in a 20 g centrifugal acceleration field. The cross section of the model is shown in Figure 6. In this model, piles were made of solid stainless steel rods, 1.2 m in diameter with a density of 7.93 t/m^3. Pile tops were fixed to the base of the rigid model building but pile ends were placed on a rigid base made of a metal block, allowing separation from the rigid base when piles are pulled out.

Silica No.7 sand with a relative density of 50% was used for liquefiable sand deposit. Figure 7 shows liquefaction resistance curve of this sand obtained from a series of cyclic triaxial tests. Thickness of this sand deposit was varied from 4.6 m to 16.6 m. Pile length was adjusted to the same as the thickness of the sand deposit. Viscous fluid was used following the generalized scaling relationship. Pure water was used for Tsunami wave because the effect of seepage flow from the ground surface is considered negligibly small.

Building was made of a mortar block with a unit weight adjusted to the bulk density of RC building. In case of the model tests of a building, whole equipment for simulating Tsunami was mounted on a shaking table in the centrifugal force and shaken by a sinusoidal motion of 0.54 Hz, with a maximum acceleration of 0.25 g before the arrival of Tsunami. Three cases of model tests were performed by varying the thickness of sand deposit and pile lengths as shown in Table 2. Each case consists of model tests with and without the effects of excess pore water pressure in the sand deposit when Tsunami reaches the building.

Table 2. Model test cases of a building with pile foundation.

Case	Pile length m	Excess pore pressure (at the time of Tsunami)
Case 1-1	4.6	remaining
Case 1-2	4.6	fully dissipated
Case 2-1	8.6	remaining
Case 2-2	8.6	fully dissipated
Case 3-1	16.6	remaining
Case 3-2	16.6	fully dissipated

2.2 *Centrifuge test results of a breakwater*

Figure 8 shows the results of the centrifuge tests of a breakwater for Cases-2 and 4 with respect to the deformation. As described earlier, Case-2 was performed for simulating the prototype condition. As shown in (a-1) in this figure, when the Tsunami at the water level difference of 10.3 m acts on the caisson, the caisson remains standing without deformation. At the same time, bubbles appear on the bay side (left side), indicating that a seepage flow of water through the rubble mound begins at this instance. After a certain period of time ((a-2) in the same figure), rubble mound gradually deforms in a bearing capacity failure mode with inclined load together with the caisson toward the direction of Tsunami wave force. The caisson eventually falls down from the rubble mound and the rubble mound exhibits a residual failure mode that resembles the classic circular failure mode.

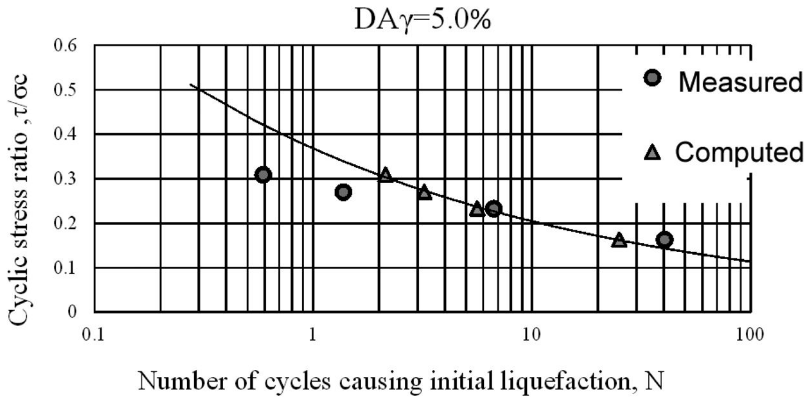

Figure 7. Liquefaction resistance curve of Silica No.7 sand.

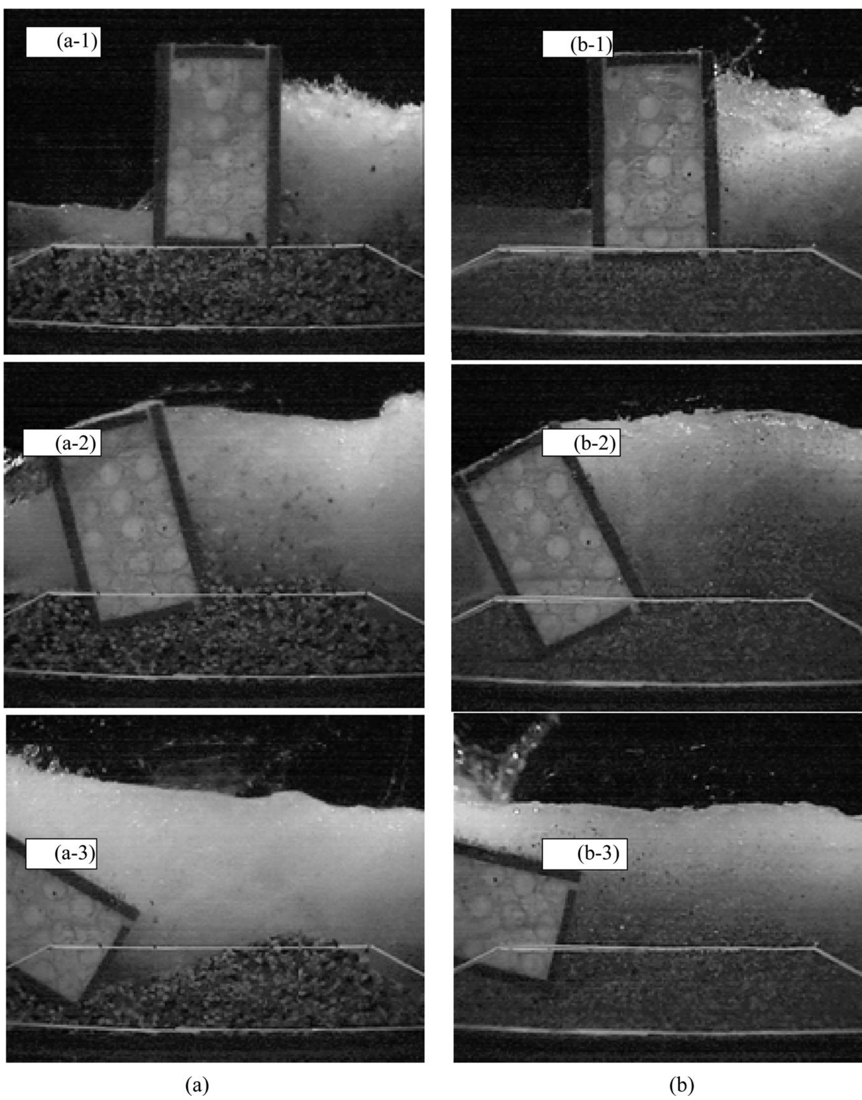

Figure 8. Deformation of caisson and rubble mound of a breakwater model.

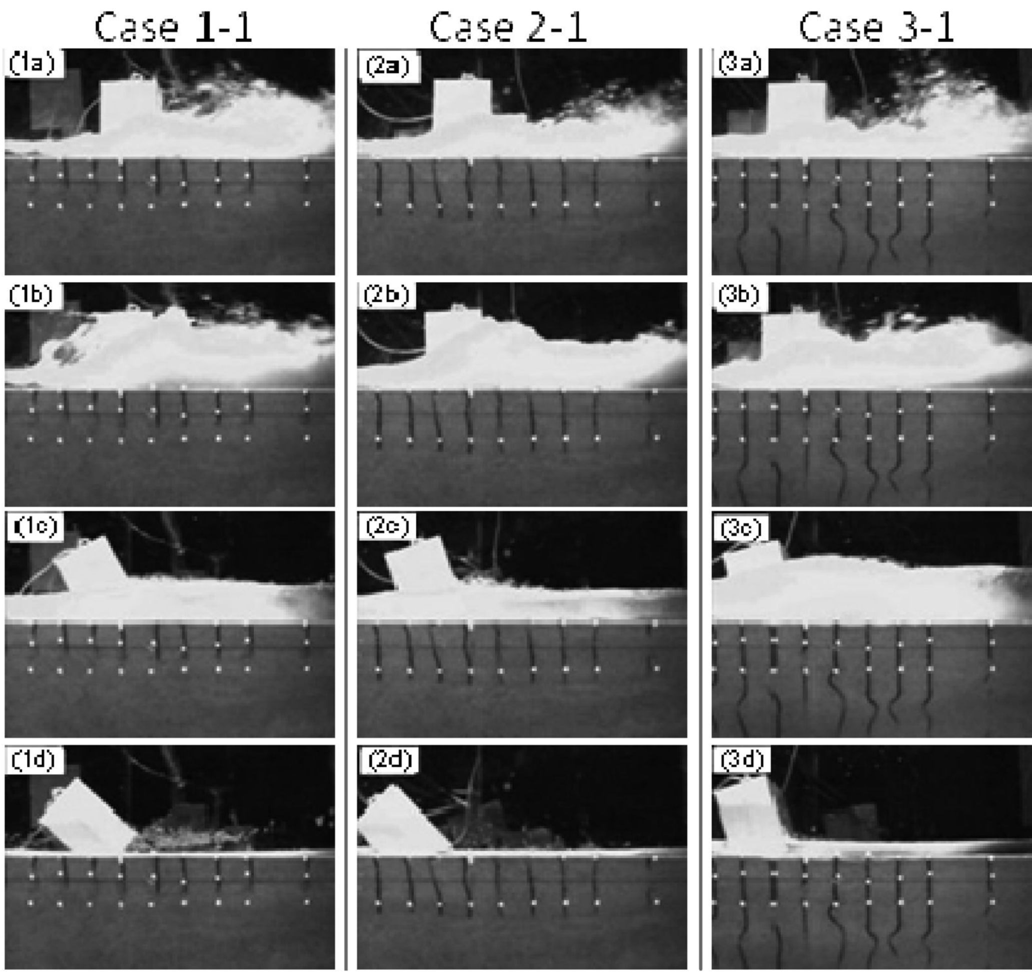

Figure 9. Deformation of a building with pile foundation when Tsunami arrives immediately after shaking (with remaining excess pore water pressures in the liquefiable sand deposit): Cases 1-1, 2-1, and 3-1.

These failure modes of the caisson and the rubble mound are consistent with those investigated and identified at Kamaishi Harbour after 2011 East Japan earthquake. This fact is indicative of the fact that the mechanism of failure due to Tsunami is considered due to the combined effect of seepage flow and wave action. However, the mechanism of erosion progressing from the harbor side also produces the similar failure mode. Thus, the mechanism of failure has to be studies further by performing effective stress analysis as described later.

Case-4 was performed as comparison to Case-2 by artificially reducing the effect of seepage flow in the rubble mound. Even if artificially reduced, the effect of seepage flow still exists so that a combined failure mode is also observed as shown in (b-1) through (b-3) in Figure 8. However, the failure mode in Case-4 is more or less dominated by sliding of caisson rather than deep failure mode of rabble mound. This fact indicate that if there is no seepage flow, then sliding failure mode will be dominant as often considered in the existing design procedure described earlier.

2.3 *Centrifuge test results of a building with pile foundation*

Figure 9 shows the results of the centrifuge tests of a building with pile foundation when Tsunami arrives immediately after shaking (Case 1-1, 2-1, and 3-1). Figure 10 shows the results of the centrifuge tests of a building when Tsunami arrives long after shaking with excess pore water pressure in the sand deposit fully dissipated (Case 1-2, 2-2, and 3-2).

As shown in Figures 9 (1b), (2b), and (3b), when the Tsunami arrives and Tsunami force is applied to the building, the building begins to tilt about 5 degrees

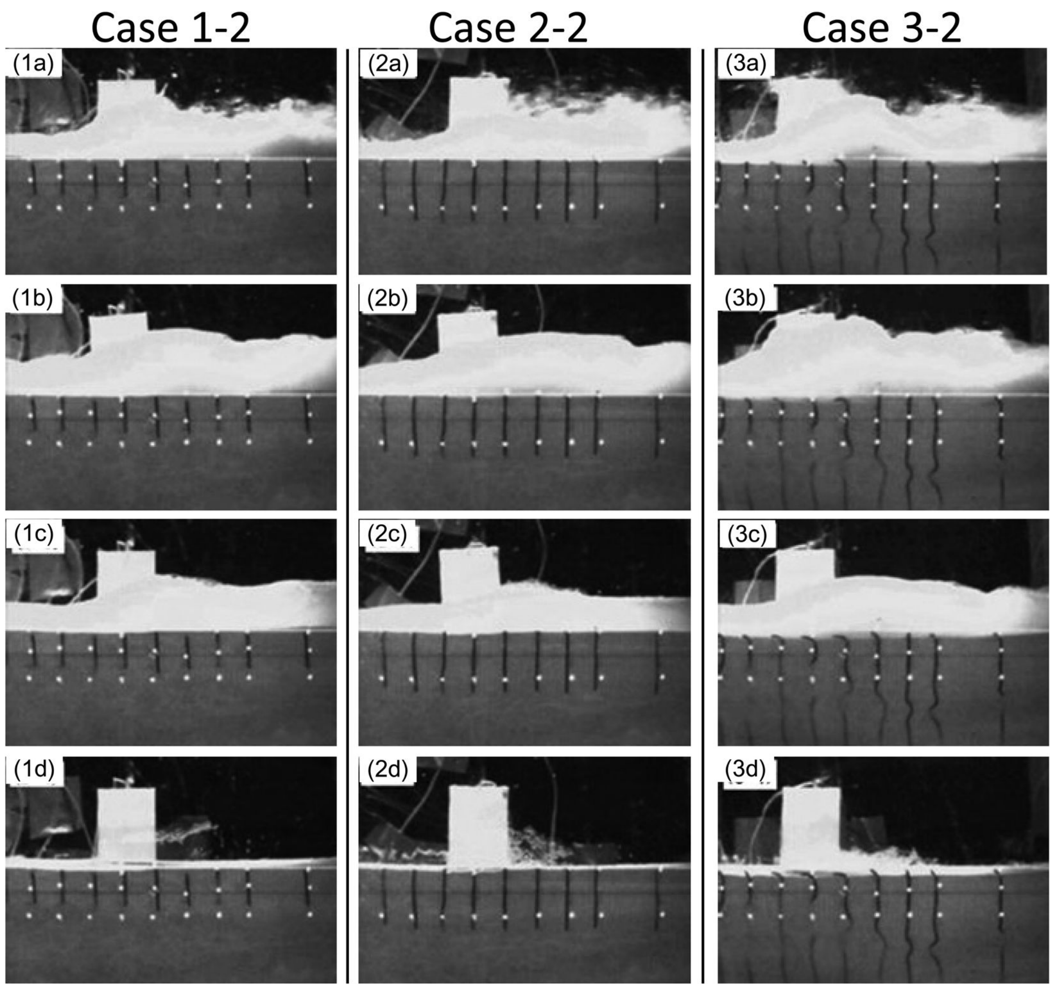

Figure 10. Deformation of a building with pile foundation when Tsunami arrives long after shaking (with fully dissipated excess pore water pressures in the liquefiable sand deposit): Cases 1-2, 2-2, and 3-2.

toward the downstream side of Tsunami. This degree of deformation is commonly observed in Figure 10 (1b), (2b), and (3b). However, difference between the results shown figures 9 and 10 becomes distinct in (1c), (2c), and (3c) or (1d), (2d), and (3d). The tilting of the building continue to progress when Tsunami arrives immediately after shaking whereas the building gets back to the original straight position when Tsunami arrives long after shaking.

Thus, the centrifuge model tests of a building successfully demonstrated that combined effects of liquefaction of ground with Tsunami force can be the major mechanism of failure of the building with pile foundation.

The model test also demonstrated that the degree of tiling is larger for a building supported by shorter piles. This trend should be considered as one of the important factor when studying mitigation measures against the possible failure of a building with pile foundation in liquefiable ground.

3 EFFECTIVE STRESS ANALYSIS

3.1 *Effective stress model*

For the effective stress analysis of a breakwater subject to seepage flow and wave action and also of a building subject to combined effects of soil liquefaction and wave action, the strain space multiple mechanism model with a cocktail glass model is used (Iai et al. 2011). In the strain space multiple mechanism model, the effective stress, defined as extension positive, is given based on a dyad defined by the unit vector **n** along the direction of the branch between the particles in contact with each other and the unit vector **t** normal to **n** as follows:

$$\boldsymbol{\sigma}' = -p\mathbf{I} + \frac{1}{4\pi}\iint q\left\langle \mathbf{t}\otimes\mathbf{n}\right\rangle \mathrm{d}\omega\mathrm{d}\Omega \qquad (1)$$

$$\left\langle \mathbf{t}\otimes\mathbf{n}\right\rangle = \mathbf{t}\otimes\mathbf{n} + \mathbf{n}\otimes\mathbf{t} \qquad (2)$$

where p denotes effective confining pressure (compression positive), $\mathbf{I}$ denotes second order identity tensor, q denotes micromechanical stress contributions to macroscopic deviator stress due to virtual simple shear mechanism (called virtual simple shear stress), and $\langle \mathbf{t} \otimes \mathbf{n} \rangle$ denotes second order tensor representing the virtual simple shear mechanism. Out of the double integration, the integration with respect to ω (=0 through π) is taken over a virtual plane spanned by the direction vectors $\mathbf{n}$ and $\mathbf{t}$ with $\omega/2$ being the angle of $\mathbf{n}$ relative to the reference local coordinate defined in the virtual plane, while the integration with respect to the solid angle Ω is taken over a surface of a unit sphere to give a three dimensional average of two dimensional mechanisms.

The integrated form of the constitutive equation, i.e. direct stress strain relationship, is derived by relating the macroscopic strain tensor $\boldsymbol{\varepsilon}$ to the macroscopic effective stress $\boldsymbol{\sigma}'$ through the structure defined by Equation (1). The first step to derive this relationship is to define the volumetric strain ε (extension positive) and the virtual simple shear strains γ as the projections of the macroscopic strain field to the second order tensors representing volumetric and virtual simple shear mechanisms as follows:

$$\varepsilon = \mathbf{I} : \boldsymbol{\varepsilon} \tag{3}$$

$$\gamma = \langle \mathbf{t} \otimes \mathbf{n} \rangle : \boldsymbol{\varepsilon} \tag{4}$$

where the double dot symbol denotes double contraction. In order to take into account the effect of volumetric strain due to dilatancy ε_{d}, effective volumetric strain ε' is introduced by

$$\varepsilon' = \varepsilon - \varepsilon_{\mathrm{d}} \tag{5}$$

where the rate of volumetric strain due to dilatancy is given by the projection of strain rate field to a second order tensor $\mathbf{I}_{\mathrm{d}}$ as

$$\dot{\varepsilon}_{\mathrm{d}} = \mathbf{I}_{\mathrm{d}} : \dot{\boldsymbol{\varepsilon}} \tag{6}$$

The scalar variables defined in Equations (4) and (5) as the projection of macroscopic strain field are used to define the isotropic stress p and virtual simple shear stress q in Equation (1) through path dependent functions as

$$p = p(\varepsilon') \tag{7}$$

$$q = q(\gamma) \tag{8}$$

In the strain space multiple mechanism model, the virtual simple shear mechanism is formulated as a nonlinear hysteretic function, where a back-bone curve is given by the following hyperbolic function;

$$q(\gamma) = \frac{\gamma / \gamma_{\mathrm{v}}}{1 + |\gamma / \gamma_{\mathrm{v}}|} q_{\mathrm{v}} \tag{9}$$

The parameters q_{v} and γ_{v} defining the hyperbolic function are the shear strength and the reference strain of the virtual simple shear mechanism, respectively.

The isotropic component in Equation (7) is defined by a hysteretic tangential bulk modulus depending on the loading/unloading (L/U) condition as

$$K_{\mathrm{L/U}} = -\frac{\mathrm{d}p}{\mathrm{d}\varepsilon'} = r_K K_{\mathrm{U0}} \left(\frac{p}{p_0} \right)^{l_K} \tag{10}$$

where p_0: initial confining pressure, K_{U0}: tangential bulk modulus at initial confining pressure.

Dilatancy in Equation (5) in the Cocktail glass model is decomposed into contractive component ε_d^c and dilative component ε_d^d as

$$\varepsilon_{\mathrm{d}} = \varepsilon_{\mathrm{d}}^{\mathrm{c}} + \varepsilon_{\mathrm{d}}^{\mathrm{d}} \tag{11}$$

In this study, dilatancy of the liquefiable sand deposit was idealized based on the liquefaction resistance shown in Figure 7. Using the model parameters of dilatancy calibrated to the liquefaction resistance, computed results are also shown in Figure 7. Effect of dilatancy in the dense foundation ground below the liquefiable sand deposit and the rubble mound for a breakwater model was assumed negligibly small and dilatancy was ignored.

3.2 *Load conditions for simulating Tsunami and seepage flow acting on a breakwater subject to Tsunami*

The effective stress analysis of a breakwater was performed for a prototype scaled from the centrifuge model, including the caisson 21 m high. As shown in Figure 11, joint element is specified at the bottom of the caisson to allow sliding and separation between the caisson and the rubble mound. After static gravity analysis to set the initial conditions for dynamic Tsunami analysis, Tsunami wave force was applied on the caisson as equivalent static distributed force as shown in Figure 12. In order to analyze the effect of seepage flow due to sea level difference, excess pore water pressure was applied at the rubble mound. External force due to sea level difference is also simulated by equivalent lateral static force on the caisson.

Distribution and magnitude of the wave force due to Tsunami adopted for the analysis (Figure 12) was determined based on the proposal by Tanimoto et al. (1984). This proposal has been also adopted in the existing design procedure of a breakwater (Figure 1).

The effective stress analyses were performed for Cases-1 through 4 with the material parameters used for the rubble mound shown in Table 3. These parameters were determined by undrained cyclic shear tests using hollow cylinder specimen and by permeability test with constant water level difference. The initial sea levels for Cases-1 through 4 were simplified for

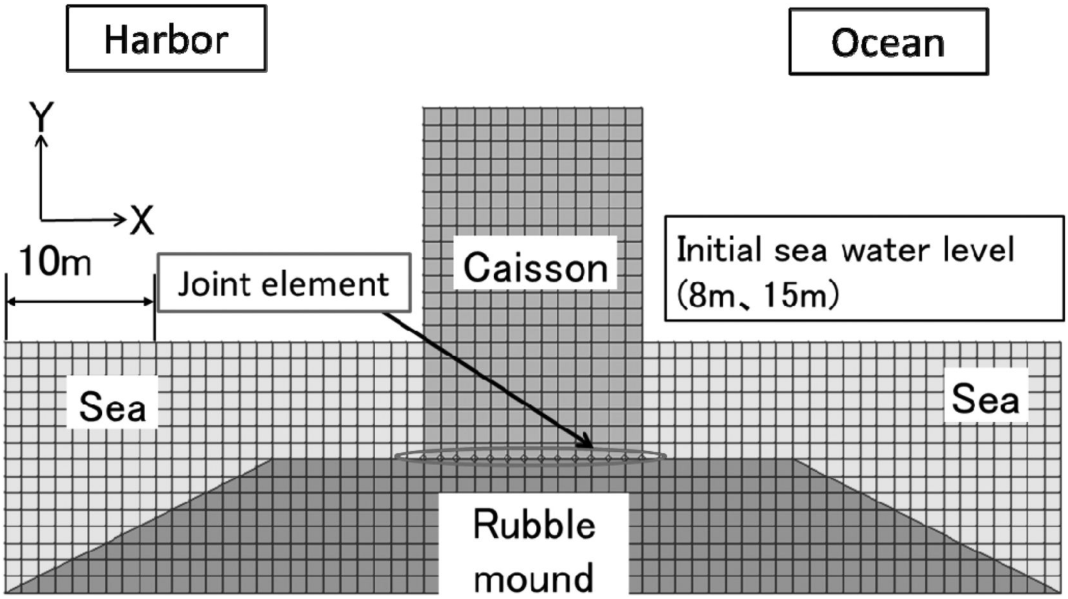

Figure 11. Finite element mesh of a breakwater for analysis (prototype scale).

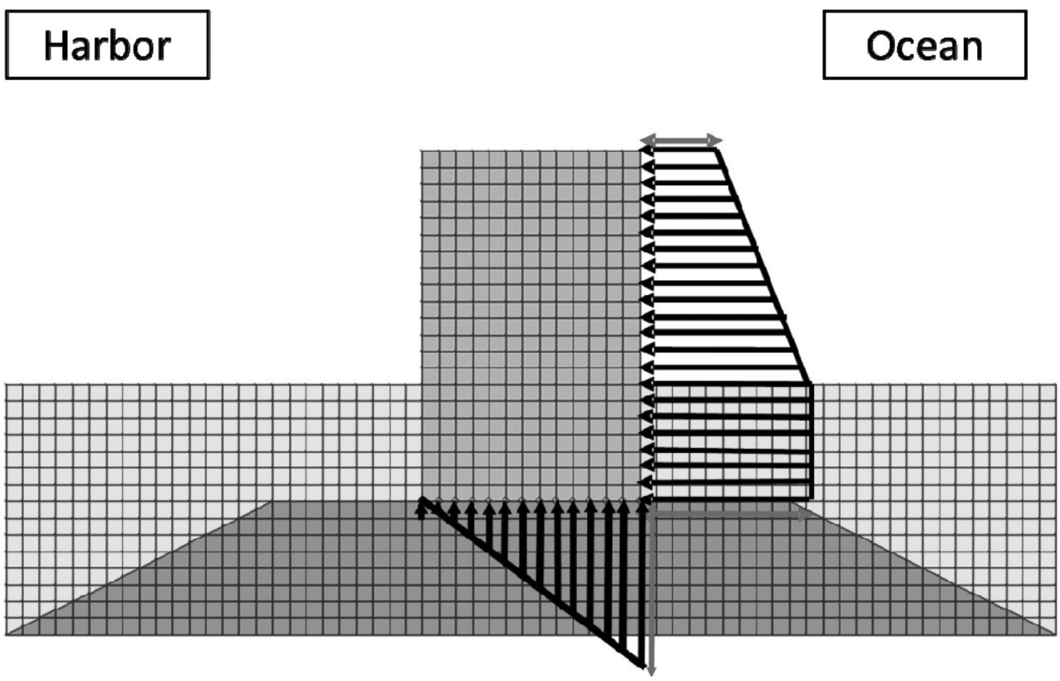

Figure 12. Load conditions for simulating wave force due to Tsunami.

Table 3. Material parameters of rubble mound.

Mound	Density	Permeability	Shear modulus	ϕf	Cohesion
Silica #1	1.91 (t/m3)	7.06×10^{-2} (m/s)	6.15×10^{4} (kPa)	40.8°	0 (kPa)
Silica #4	1.90 (t/m3)	1.56×10^{-3} (m/s)	7.67×10^{4} (kPa)	38.7°	0 (kPa)

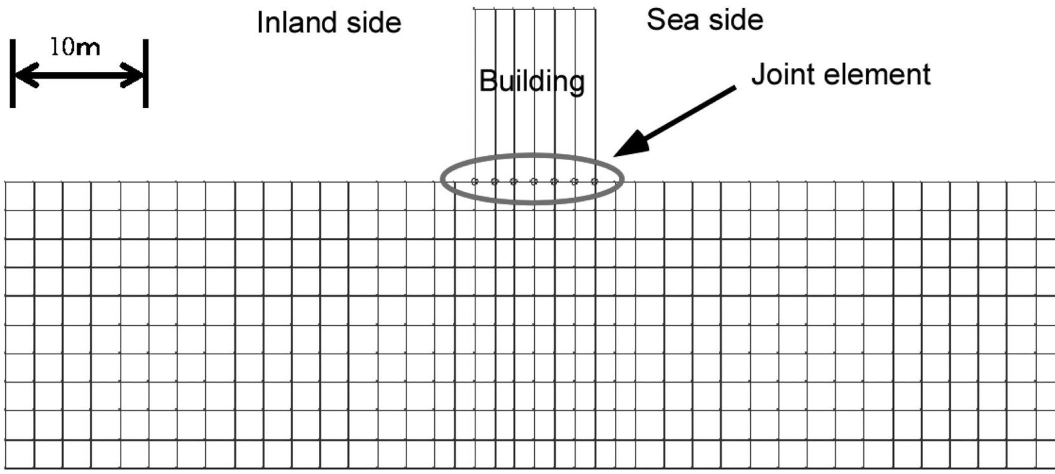

Figure 13. Finite element mesh of a building for analysis (prototype scale) and load conditions for simulating Tsunami wave force.

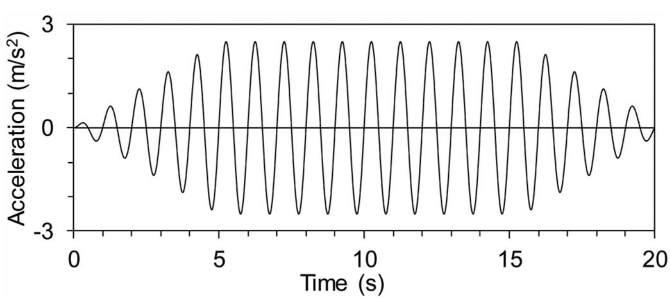

Figure 14. Input motion for a building with pile foundation.

the analysis as shown in Figure 11. The sea level differences were also simplified as 15m for Cases-1 and 3, and 11m for Cases-2 and 4.

3.3 *Load conditions for simulating Tsunami and effect of liquefaction acting on a building with pile foundation*

The effective stress analysis of a building with pile foundation was performed for a prototype scaled from the centrifuge model, including the building 12 m high. As shown in Figure 13, joint element is specified at the bottom of the building to allow sliding and separation between the building footing and foundation ground. After static gravity analysis to set the initial conditions of building-foundation system, a sinusoidal input motion for a duration of 20 seconds, shown in Figure 14, was applied at the base of the foundation soil, and then after certain period for allowing dissipation of excess pore water pressure from the foundation ground, a Tsunami wave force was applied on the building as equivalent static distributed force as shown in Figure 15.

For simplicity, the analysis was performed with (Case 1) and without (Case 2) shaking before arrival of Tsunami. In Case 1, ten seconds were allowed between the end of shaking and arrival of Tsunami. Increasing rate of Tsunami height was simulated for allowing 40 seconds from the arrival of Tsunami to the maximum Tsunami height of 6.0 m.

3.4 *Results of the effective stress analysis of a breakwater*

The results of analysis of Case-2 of a breakwater are presented below. Figure 16 (a) shows residual deformation of a breakwater with both Tsunami wave force on the caisson and seepage flow in the rubble mound. The tilting of the caisson is associated with a significant deformation of rubble mound. This mode of failure is consistent with that observed at the centrifuge model test. In comparison to this result, deformation of a breakwater due to Tsunami wave force only is negligibly small as shown in Figure 16 (b). These results of the analyses indicate that primary mechanism of failure of a breakwater due to Tsunami is combined failure

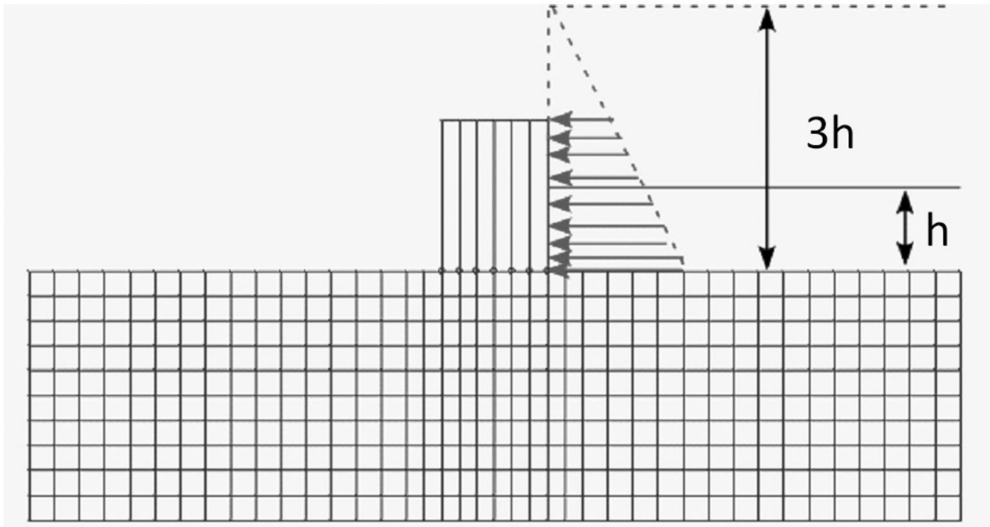

Figure 15. Load conditions for simulating wave force due to Tsunami.

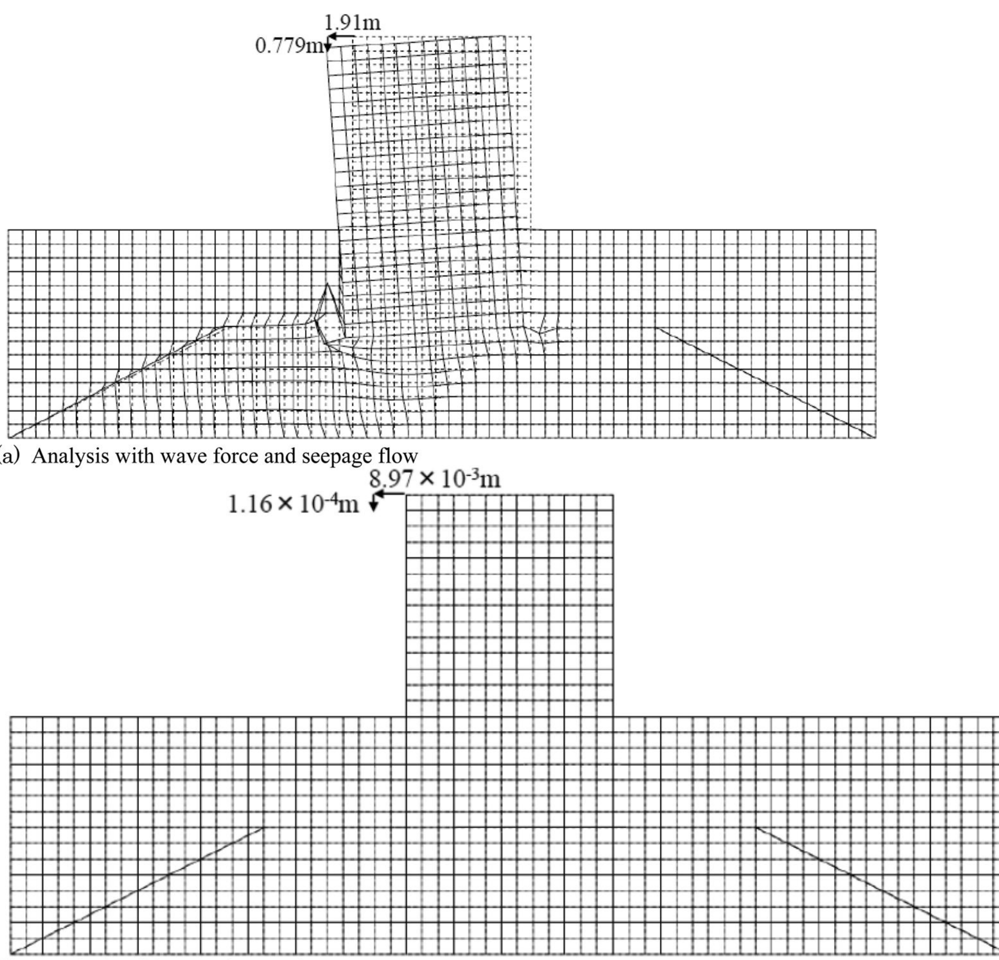

(a) Analysis with wave force and seepage flow

(b) Analysis with wave force only

Figure 16. Residual deformation of a breakwater.

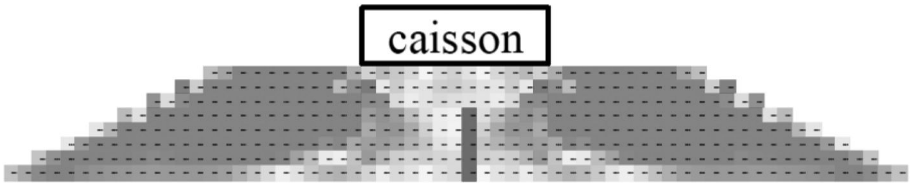

(a) Initial condition for dynamic analysis

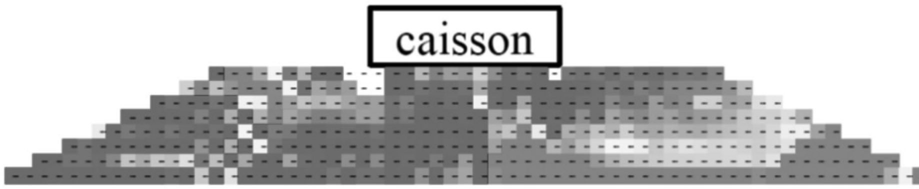

(b) Residual status due to Tsunami wave force and seepage flow

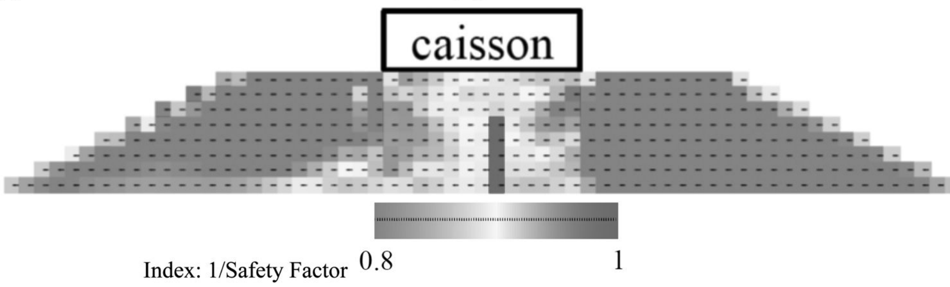

(c) Residual status due to Tsunami wave force only

Figure 17. Distribution of 1/Safety Factor in the rubble mound.

mechanism due to Tsunami wave force and seepage flow in the rubble mound due to water level difference associated with Tsunami.

In addition, distribution of an inverse of safety factor with respect to Mohr-Coulomb failure criterion in the rubble mound is shown in Figure 17. As shown in Figure 17(a), the rubble mound beneath the caisson undergoes a compression shear due to the overburden from the caisson before Tsunami. When the Tsunami wave force and seepage flow act on the rubble mound, significant area of cross section of rubble mound are brought close to a shear failure condition as shown in Figure 17(b). However, if only the Tsunami wave for acts, there is not a significant change in the rubble mound with respect to its stress status. These results also supports the previous notion that the primary mechanism of failure of a breakwater due to Tsunami is combined failure mechanism involving seepage flow in the rubble mound.

3.5 *Results of the effective stress analysis of a building with pile foundation*

The results of analysis of Case-2-1 & 2-2 of a building with pile foundation are presented below. Figure 18 (a) shows residual deformation of a breakwater with both Tsunami wave force on the building with foundation ground at the state of liquefaction. The tilting of the building is associated with a significant deformation of pile foundation and foundation ground. This mode of failure is consistent with that observed at the centrifuge model test. In comparison to this result, deformation of a building due to Tsunami wave force only is small as shown in Figure 18 (b). These results of the analyses indicate that prima-ry mechanism of failure of a building with pile foundation due to Tsunami is combined failure mechanism due to Tsunami wave force and liquefaction of foundation ground.

4 CONCLUSIONS

In this study, a centrifuge model tests and effective stress analyses are performed on a breakwater and a building with pile foundation subject to Tsunami such as those serious damaged during 2011 East Japan Earthquake (Magnitude 9.0). For a breakwater, both the centrifuge model tests at a scale of 1/200 and the effective stress analyses demonstrate the importance of the mechanism of failure in the rubble mound due to seepage flow of pore water in addition to the wave force of Tsunami action. For a building with pile foundation, both the centrifuge model tests at a scale of 1/200 and the effective stress analyses demonstrate the importance of the combined mechanism of failure with the effect of liquefaction of foundation ground in addition to the wave force of Tsunami action.

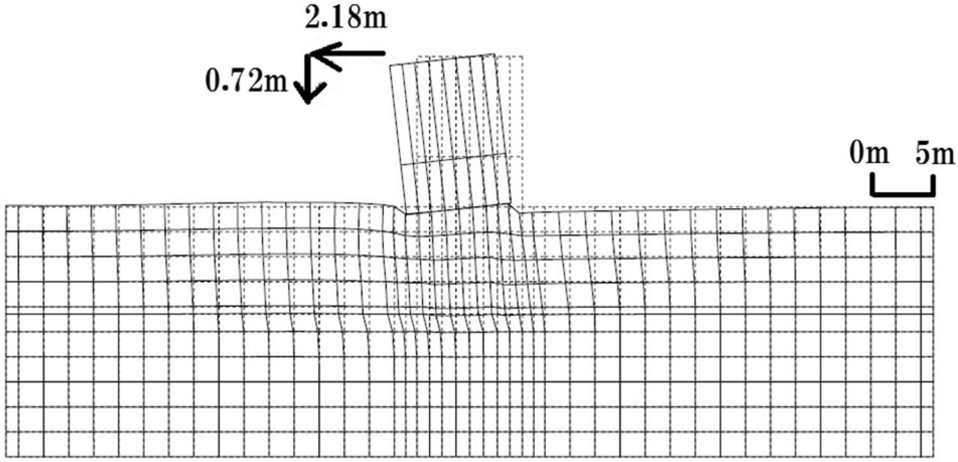

(a) Analysis with liquefaction and wave force

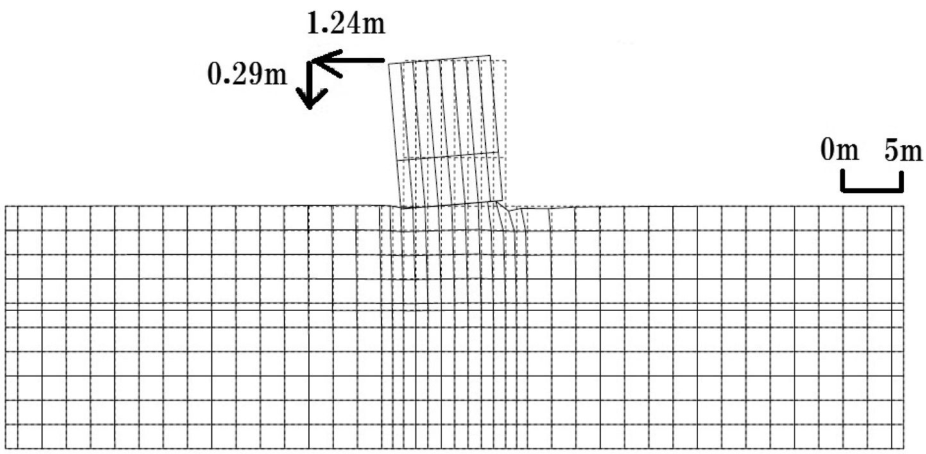

(b) Analysis with wave force only

Figure 18. Residual deformation of a building with pile foundation.

As a whole, this study demonstrates the importance of combined failure mechanism associated with action of water on soil-structure systems.

PREFERENCES

Iai, S., Tobita, T. & Nakahara, T. 2005. Generalized scaling relations for dynamic centrifuge tests, *Geotechnique*, 55(5): 355–362.

Iai, S., Tobita, T., Ozutsumi, O. & Ueda, K. 2011. Dilatancy of granular materials in a strain space multiple mechanism model, *International Journal for Numerical and Analytical Methods in Geomechanics*, 35(3): 360–392.

JSCE (Earthquake Engineering Committee) 2011. 2011 East Japan earthquake reconnaissance report, JSCE, No.20 (in Japanese)

Tanimoto, K., Tsuruya, K., & Nakano, S. 1984. Tsunami wave force and failure mechanism of bulkhead due to Tsunami during 1983 Nihonkai-chubu earthquake, *Proc. 31th Research Conference on Coastal Engineering*, 257–261 (in Japanese)

Geotechnics for Catastrophic Flooding Events – Iai (Ed)
 ISBN 978-1-138-02709-1

Performance-based assessment of liquefaction hazards

Steven L. Kramer
University of Washington, Seattle, Washington, USA

Yi-Min Huang
Feng Chia University, Taichung City, Taiwan

Michael W. Greenfield
University of Washington, Seattle, Washington, USA

ABSTRACT: Advances in the development of performance-based earthquake engineering, which seeks to predict the seismic performance of structures and facilities in ways that are useful to a wide variety of stakeholders, offer important opportunities for more rational, objective, and consistent evaluation of liquefaction hazards. Performance-based procedures for evaluation of liquefaction potential have been shown to provide more consistent and accurate indications of the actual likelihood of liquefaction in areas of different seismicity than conventional procedures. These procedures can be extended to include effects of liquefaction such as lateral spreading and post-liquefaction settlement. This paper reviews the evolution of performance-based earthquake engineering, discusses the notion of performance and its description, and describes a recently developed framework for performance-based liquefaction hazard evaluation. The integration of procedures for estimation of liquefaction susceptibility, potential, and effects are described. The procedures are illustrated with examples of the evaluation of liquefaction potential and liquefaction-induced settlement hazards.

1 INTRODUCTION

Liquefaction hazards are generally assessed by evaluating (a) the susceptibility of a soil deposit to liquefaction, (b) the potential for initiation of liquefaction under some anticipated level of loading, and (c) the physical effects, or consequences, of liquefaction. The level of loading considered in the assessment is conventionally expressed in terms of a ground motion intensity measure at a single return period. In practice, liquefaction susceptibility, potential, and effects are usually evaluated deterministically.

The development of performance-based earthquake engineering concepts allow probabilistic evaluations of susceptibility, initiation, and effects to be combined with a probabilistic evaluation of ground motion hazards to produce more rational and consistent estimates of liquefaction hazards. The purpose of this paper is to show how performance-based concepts can allow uncertainties in susceptibility, initiation, and effects to be incorporated into liquefaction hazard assessments, and how performance-based predictions of such hazards compare with conventional predictions.

2 CONVENTIONAL PROCEDURES FOR ASSESSMENT OF LIQUEFACTION HAZARDS

The assessment of liquefaction hazards can be broken down into three primary components (Kramer, 1995) – evaluation of liquefaction susceptibility, evaluation of the potential for initiation of liquefaction, and evaluation of the effects of liquefaction. If the susceptibility evaluation indicates that liquefiable soils are not present, liquefaction hazards do not exist and there is no need to evaluate initiation and effects. If the soil is susceptible to liquefaction, but the anticipated level of shaking is not strong enough to initiate liquefaction, liquefaction hazards do not exist and there is no need to evaluate the potential effects of liquefaction. If the soil is susceptible and the shaking strong enough to trigger liquefaction, however, then the performance of structures, lifelines, and other facilities will be strongly influenced by the effects of liquefaction, which must be explicitly evaluated. These effects can be compared with some allowable, or limit state, value in order to determine whether or not performance is expected to be satisfactory.

2.1 *Liquefaction susceptibility*

The primary difficulty in evaluating liquefaction susceptibility at this time lies in the susceptibility of fine-grained soils of marginal plasticity and coarse-grained soils with high fines contents. For many years, such soils were considered to be non-susceptible to liquefaction. Then, after silty soils had been observed to liquefy in a number of earthquakes, the modified Chinese criteria were recommended (Seed and Idriss, 1982; Seed et al., 1985) for evaluation of liquefaction susceptibility of fine-grained soils. Following more recent observations of liquefaction in fine-grained soils for which the Chinese criteria indicated non-susceptibility, extensive research on the liquefaction susceptibility of fine-grained soils was undertaken. At this stage, two major studies by Boulanger and Idriss (2005) and Bray and Sancio (2006) have proposed criteria for evaluating the liquefaction susceptibility of fine-grained soils. These criteria are consistent for many conditions but differ for others; however, both indicate the unreliability of the Chinese criteria. Both were developed using the results of field observations and laboratory tests by well-respected leaders of the geotechnical engineering profession. For the majority of conditions where the two approaches do not agree, the proposers of both recognize that high-quality sampling is feasible and recommend that behavior be evaluated by laboratory testing. At the present time, data sufficient to prove one or the other to be more appropriate do not exist. As a result, both must be considered plausible, and both should be considered in a liquefaction susceptibility evaluation.

2.1.1 *Boulanger and Idriss*

Boulanger and idriss (2005) reviewed case histories and laboratory tests involving cyclic loading of different fine-grained soils. Boulanger and idriss identified two types of behavior that they described as "sand-like" and "clay-like" on the basis of stress normalization and stress-strain behavior. Soils exhibiting sand-like behavior were considered susceptible to liquefaction and soils exhibiting clay-like behavior were not, although Boulanger and idriss pointed out that some (e.g., sensitive clays) may be susceptible to behavior that can lead to earthquake damage.

Boulanger and Idriss found that soil plasticity characteristics determined whether an individual soil was likely to exhibit sand-like or clay-like behavior, and proposed that the distinction could be made based on plasticity index, PI. Figure 1 shows the transition between sand-like and clay-like behavior observed by Boulanger and Idriss – the soil is clearly sand-like at PI < 3 and clay-like at PI > 8.5. While the transitional nature of the soil behavior was emphasized, a simple (and conservative) guideline of PI = 7 was recommended when a distinct indication of susceptibility is required and detailed laboratory testing results are not available.

To quantify the transitional nature of observed sand-like to clay-like behavior, a numerical relationship

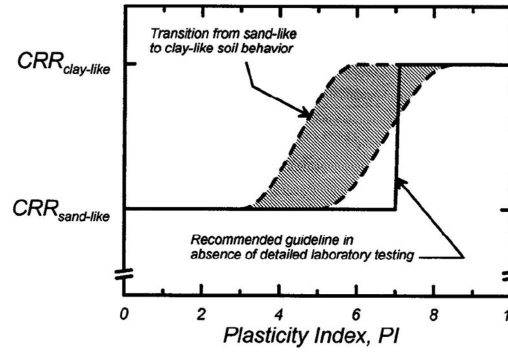

Figure 1. Transition from sand-like to clay-like behavior with plasticity index for fine-grained soils (Boulanger and Idriss, 2005).

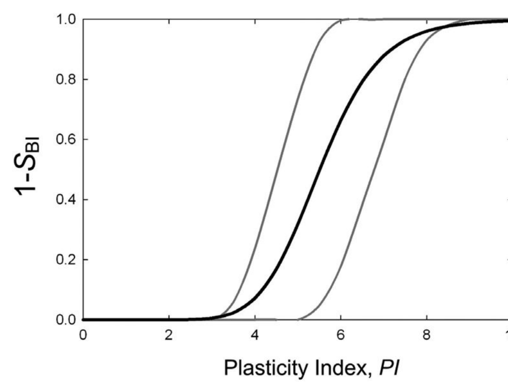

Figure 2. Relationship between S_{BI} and Boulanger and Idriss (2005) transition zone boundaries.

can be established. The *PI* transition from clay-like to sand-like behavior from Boulanger and Idriss (2005) can be described using a susceptibility index, defined as

$$S_{BI} = \left[1 + \left(\frac{\ln(PI + 0.0001)}{1.843}\right)^{11.483}\right]^{-2.0} \tag{1}$$

which has a value of 0.0 for clay-like (non-susceptible) behavior and 1.0 for sand-like (susceptible) behavior. The relationship between S_{BI} and the graphical relationship presented by Boulanger and Idriss is shown in Figure 2.

2.1.2 *Bray and Sancio (2006)*

Bray and Sancio (2006) investigated fine-grained soils that liquefied during 1994 Northridge, 1999 Kocaeli, and 1999 Chi-Chi earthquakes and proposed new compositional criteria for liquefaction susceptibility evaluation. In addition to plasticity index, Bray and Sancio found the ratio of water content to liquid limit (w_c/LL) to also influence liquefaction susceptibility. Bray and Sancio found soils with $PI < 12$ and $w_c/LL > 0.85$ to be consistently susceptible, and soils with PI > 18

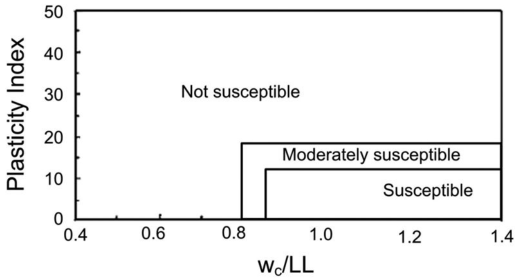

Figure 3. Ranges of *wc/LL* and plasticity index for various susceptibility categories according to Bray and Sancio (2006).

or $w_c/LL < 0.80$ to be consistently non-susceptible to liquefaction. Other soils were considered to be moderately susceptible with testing recommended to further establish their liquefaction susceptibility. Figure 3 shows the boundaries of susceptible, moderately susceptible, and non-susceptible zones of liquefaction susceptibility recommended by Bray and Sancio (2006).

A function similar to that used to approximate the Boulanger and Idriss criterion can be developed to quantify Bray and Sancio's susceptibility criteria. The equation is simply the product of two terms which have a form similar to that of Equation 1, i.e.,

$$S_{BS} = \left[1+\left(\frac{\ln(PI+0.0001)}{2.778}\right)^{33.077}\right]^{-2.0} \times \left[1+\left(\frac{4.401}{\ln(w_c/LL)}\right)^{360.471}\right]^{-2.0} \quad (2)$$

These equations were determined by assuming the boundary between susceptibility and non-susceptibility to be uniformly distributed within the 'moderately susceptible' zone of Bray and Sancio, and fitting a function that would have the same mean and variance with respect to both PI and w_c/LL. As in Equation 1, a value of 0.0 corresponds to non-susceptibility and 1.0 to susceptibility. A three-dimensional view of S_{BS} is shown in Figure 4.

2.1.3 *Clay-like or non-susceptible soils*

It should be acknowledge that soils that are deemed clay-like or non-susceptible to liquefaction using the Boulanger and Idriss or Bray and Sancio screening criteria may still experience strength loss as a result of seismic shaking. Sensitive or highly overconsolidated clays may reach their peak strength at relatively small strains, resulting in remolded shear strengths following seismic shaking (Anderson et al., 2007). The strength loss of soils that are deemed non-susceptible to liquefaction is generally minor compared to the strength loss observed in liquefiable soils, but the concepts of initiation and effect of liquefaction may still apply.

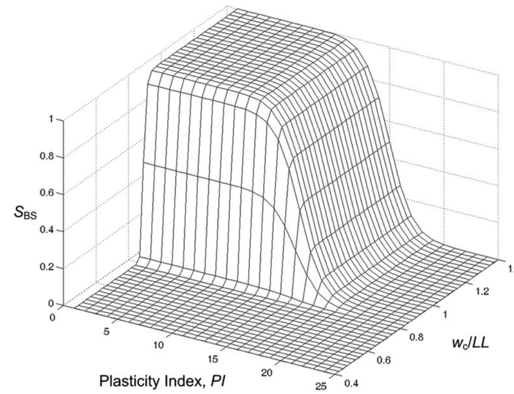

Figure 4. Illustration of variation of S_{BS} with plasticity index and *wc/LL* ratio.

2.2 *Initiation of liquefaction*

Liquefaction potential is generally evaluated by comparing consistent measures of earthquake loading and liquefaction resistance. It has become common to base the comparison on cyclic shear stress amplitude, usually normalized by initial vertical effective stress and expressed in the form of a cyclic stress ratio, *CSR*, for loading and a cyclic resistance ratio, *CRR*, for resistance. The potential for liquefaction is then described in terms of a factor of safety against liquefaction,

$$FS_L = CRR/CSR \quad (3)$$

2.2.1 *Characterization of earthquake loading*

The cyclic stress ratio is most commonly evaluated using the "simplified method" first described by Seed and Idriss (1971), which can be expressed as

$$CSR = 0.65\frac{a_{\max}}{g}\cdot\frac{\sigma_{vo}}{\sigma'_{vo}}\cdot\frac{r_d}{MSF} \quad (4)$$

where $a_{\max}$ = peak ground surface acceleration, g = acceleration of gravity (in same units as $a_{\max}$), σ_{vo} = initial vertical total stress, σ'_{vo} = initial vertical effective stress, r_d = depth reduction factor, and MSF = magnitude scaling factor, which is a function of earthquake magnitude. The depth reduction factor accounts for compliance of the soil profile and the magnitude scaling factor acts as a proxy for number of cycles, or ground motion duration. It should be noted that two pieces of ground motion information, $a_{\max}$ and magnitude, are required for estimation of the cyclic stress ratio.

2.2.2 *Characterization of liquefaction resistance*

The cyclic resistance ratio is generally obtained by correlation to insitu test results, principally from standard penetration (SPT), cone penetration (CPT), or shear wave velocity (V_s) tests. Of these, the SPT has been most commonly used and will be used in the remainder of this paper. A number of SPT-based procedures

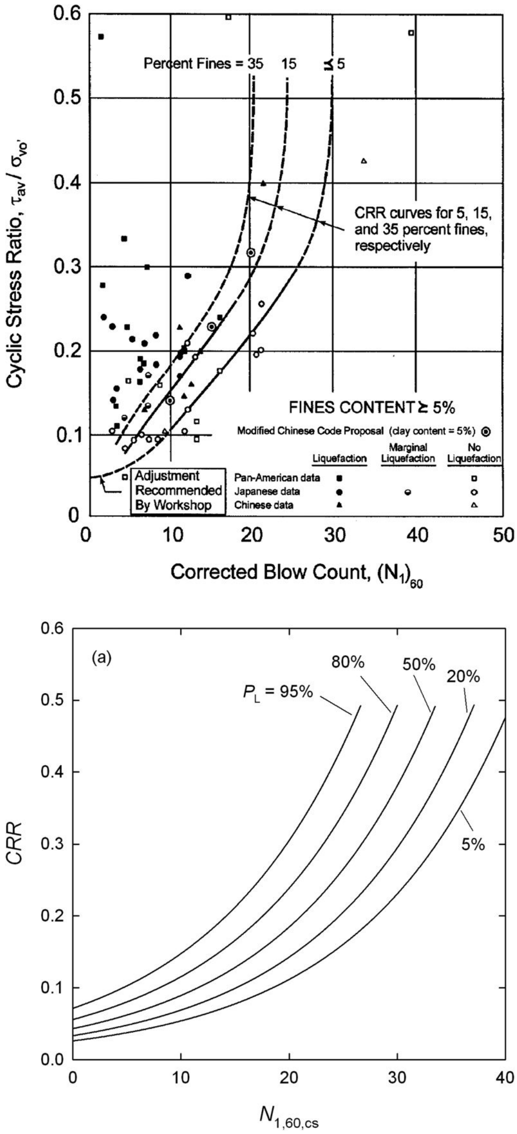

Figure 5. (a) Deterministic cyclic resistance curves proposed by Youd et al., (2001), and (b) cyclic resistance curves of constant probability of liquefaction with measurement/estimation errors by Cetin et al., (2004).

for deterministic (Seed and Idriss, 1971; Seed et al., 1985; Youd et al., 2001, Idriss and Boulanger, 2010) and probabilistic (Liao et al., 1988; Toprak et al., 1999; Youd and Noble, 1997; Juang and Jiang, 2000; Cetin et al., 2004; Boulanger and Idriss, 2014) estimation of liquefaction resistance have been proposed.

2.2.3 *Effects of liquefaction*

The initiation of liquefaction can have several effects that can be damaging to buildings, bridges, dams, embankments, lifelines and other facilities. The most significant of these are usually associated with permanent deformations that develop as a result of the softening and/or weakening of soils associated with excess porewater pressure development. In cases where very loose soils exist under relatively large initial shear stresses (e.g., under moderate to steep slopes) catastrophic flow slides producing large horizontal deformations can result from liquefaction. Lateral deformations ranging from small to large can also be caused by lateral spreading; these deformations are generally smaller than those associated with flow slides, but they occur much more frequently. Permanent vertical deformations in the form of post-earthquake settlement can also be caused by liquefaction – this effect will be used to illustrate performance-based liquefaction hazard evaluation in the remainder of this paper.

The most common form of liquefaction-induced settlement is that which results from the volumetric compression that occurs when excess porewater pressures dissipate under level-ground conditions (i.e., when shearing deformations are insignificant). The contractive nature of sands subjected to vibratory loading has been recognized for many years. Silver and Seed (1971) showed experimentally that the densification of dry sands subjected to cyclic loading depended on the density of the sand, the number of cycles of loading applied to the sand, and the amplitude of the cyclic shear strain induced in the sand. Over the years, several procedures for estimating the post-liquefaction settlement of sands have been proposed.

Tokimatsu and Seed (1987) reviewed previous laboratory test data, which showed post-liquefaction volumetric strain to be related to relative density and peak shear strain. They then related relative density to SPT resistance and peak shear strain to cyclic stress ratio to develop curves relating volumetric strain to $(N_1)_{60}$ and *CSR* (Figure 6a). The curves in Figure 6(a) show that post-liquefaction volumetric strain increases with increasing loading and decreasing SPT resistance and suggest that volumetric strains can be as large as 10 percent in extremely loose sands. They also show that, for strong levels of shaking, the soil reaches a limiting volumetric strain. The Tokimatsu and Seed procedure computes ground surface settlement by integrating volumetric strain over the depth of the liquefiable layer, i.e., as

$$\Delta H = \int \varepsilon_v dz \qquad (5)$$

This integral is usually evaluated numerically by dividing the soil profile into a series of sublayers of constant SPT resistance, and then summing the computed settlements of the individual sublayers. Other investigators (Ishihara and Yoshimine, 1992; Shamoto et al., 1998; Wu and Seed, 2004) have proposed similar relationships; that of Wu and Seed (2004) is shown in Figure 6(b). This relationship, like several others, does not suggest the existence of a limiting volumetric strain for moderately dense soils (corrected SPT resistances above about 10). Recently, Cetin et al., (2009)

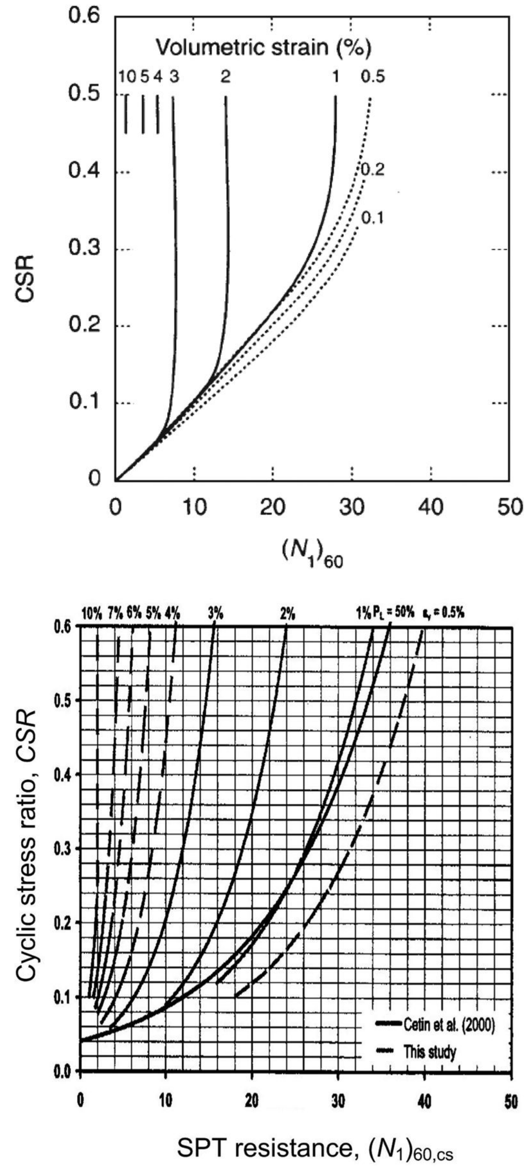

Figure 6. Variation of volumetric strain with corrected SPT resistance and cyclic stress ratio (a) Tokimatsu and Seed (1987), and (b) Wu and Seed (2004).

proposed a probabilistic procedure for estimation of volumetric strain following liquefaction that indicates lower uncertainty than the preceding procedures.

3 PERFORMANCE-BASED LIQUEFACTION HAZARD ASSESSMENT

In practice, liquefaction hazards are usually evaluated for a single hazard level, for example, for ground motions with a 10% probability of exceedance in a 50-yr period (475-yr return period). In some cases, two hazard levels may be considered, but different performance objectives (e.g. minimum factors of safety or levels of settlement) would typically be required for the different hazard levels. For a given performance objective, only one hazard level is usually considered. In reality, liquefaction hazards can be caused by a wide range of ground shaking levels ranging from weaker motions that occur relatively frequently to stronger motions that occur only rarely.

Performance-Based Earthquake Engineering (PBEE) is generally formulated in a probabilistic framework to evaluate the risk associated with earthquake shaking at a particular site. The risk can be expressed in terms of economic loss, fatalities, or other measures. The Pacific Earthquake Engineering Research (PEER) Center has developed a probabilistic framework for PBEE (Cornell and Krawinkler, 2000; Krawinkler, 2002; Deierlein et al., 2003; Krawinkler and Miranda, 2004).

The PEER PBEE framework computes risk as a function of ground shaking through the use of several intermediate variables. The ground motion is characterized by an *Intensity Measure*, *IM*, which could be any of a number of ground motion parameters. The effects of the *IM* on the response of a system of interest are expressed in terms used primarily by engineers in the form of *Engineering Demand Parameters*, or *EDP*s. For a liquefiable site, the geotechnical engineer's initial contribution to this process for evaluating liquefaction hazards comes primarily in the evaluation of the conditional probability distribution of *EDP* given *IM*. In the PEER framework, the mean annual rate of exceeding some value of $EDP = edp$ is given by

$$\lambda_{EDP}(edp) = \sum_{i=1}^{N_{IM}} P[EDP > edp \mid IM = im_i]\Delta\lambda_{IM}(im_i) \quad (6)$$

Within the context of the previously described susceptibility/initiation/effects evaluations for liquefaction hazard assessment, the effects of liquefaction (e.g., settlement) would be taken as the *EDP*, and the susceptibility and initiation considerations would need to be addressed as intermediate steps in the evaluation of liquefaction effects. The evaluation of the conditional probability of *EDP* given *IM* would then take the following form

$$P[EDP > edp \mid IM] = P[EDP > edp \mid IM, initiation] \times P[initiation \mid IM, susceptibility] P[susceptbility] \quad (7)$$

The evaluation of this conditional distribution therefore requires evaluation of the probability that a given element of soil is susceptible to liquefaction, the probability that liquefaction will be triggered by ground motions of various intensities, and the probability that some level of effects will be reached given the intensity level and the fact that liquefaction has been initiated.

3.1 *Susceptibility*

The susceptibility indices given by Equations 1 and 2 can be interpreted in different ways. Neither were developed in a sufficiently formal manner as to represent probabilities of liquefaction susceptibility in the frequentist sense. However, they could be interpreted as degrees of belief, or subjective probabilities, that a soil would be susceptible to liquefaction in that they have values of zero for conditions in which Boulanger and Idriss (2005) and Bray and Sancio (2006) indicate clear non-susceptibility and value of 1.0 where they indicate clear susceptibility. Differences between the two approaches could be treated as epistemic uncertainty using a two-branched logic tree.

3.2 *Initiation*

As indicated previously, a number of probabilistic liquefaction initiation models have been proposed over the past 20 years. The model of Cetin et al., (2004) provides a convenient example of such methods. For a soil of a given density, the Cetin et al., (2004) model allows computation of a probability of liquefaction initiation for a liquefaction-susceptible soil, which can be expressed as

$$P[initiation|\, IM, susceptbilty] = \Phi\left[-\left(\frac{1}{\sigma_\varepsilon}\right)\left((N_1)_{60}(1+\theta_1 FC) - \theta_2 \ln CSR_{eq} - \theta_3 \ln M_w - \theta_4 \ln\left(\sigma'_{vo}/p_a\right) + \theta_5 FC + \theta_6\right)\right] \tag{8}$$

where Φ is the standard normal cumulative distribution function, $(N_1)_{60} =$ corrected SPT resistance, $FC =$ fines content (in percent), $CSR_{eq} =$ cyclic stress ratio (Equation 4 without MSF, which serves as the IM in this case), $M_w =$ moment magnitude, $\sigma'_{vo} =$ initial vertical effective stress, p_a is atmospheric pressure (in same units as σ'_{vo}), σ_ε is a measure of the estimated model and parameter uncertainty, and θ_1–θ_6 are model coefficients obtained by regression. In this form, CSR and M_w form a vector IM.

3.2.1 *Example*

To explore the level of inconsistency in conventional liquefaction potential evaluations, a series of conventional and performance-based analyses were made at several locations within the state of California. California's seismicity is dominated by the San Andreas fault, which runs in a generally north-south direction along the Pacific coast. The seismic hazard is generally highest near the coast and diminishes eastward towards the central valley. Near the eastern boarder of California, several local crustal fault zones, such as the Cedar Mountain, Surprise Valley, and Hilton Creek faults, present significant seismic hazard, although these hazards are generally lower than the seismic hazards of the coast. A generic soil profile was assumed at nine major cities and three east-west profiles in the north, central, and south portions of the state. The profile consisted of a 9 m-thick deposit of clean sand with a groundwater level 2 m below the ground surface. The corrected SPT resistances at each site location were adjusted to provide a factor of safety of 1.5 against triggering of liquefaction for 975-yr ground motions using the Cetin et al., (2004) deterministic triggering relationship. The conventional procedure indicated the liquefaction potential of each of these site was equal, even though the seismic hazard varied significantly between the sites. A performance-based liquefaction potential evaluation was then performed on each adjusted profile, and the results expressed in terms of a return period of liquefaction. If the conventional procedures produced consistent indications of actual liquefaction potential, the computed return periods would be equal. The results show, however, that the actual return periods of liquefaction varied greatly, even over relatively short distances. Sites in San Francisco, Oakland, and San Jose, which would all fall within a 67-km-diameter circle, had return periods ranging from 2,680 yrs to 5,430 yrs. Los Angeles and Long Beach, 17 km apart and both home to large sea ports of tremendous economic value to their regions, have return periods of 2,720 and 4,640 yrs, respectively. Return periods of liquefaction across the state range from about 450 year to over 7,000 years.

The return period of liquefaction also depends on the selection of magnitude used in the conventional liquefaction triggering evaluation. Deaggregation of the PSHA provides estimates of mean and modal earthquake magnitudes, neither of which fully represent the liquefaction hazard at a site. The modal magnitude represents the source contributing the greatest hazard to the site, while the mean magnitude represents a weighted average of the magnitude contributions to PGA hazard at the site. Modal magnitudes usually exceed mean magnitudes, so the differences between the mean return periods considering mean or modal magnitudes is not unexpected. The computed return periods at the sites selected for this example using conventional analysis procedures with a magnitude scaling factor based on mean and modal magnitudes are shown in Figure 7. The average (mean) return periods at the sites considered in this example are 2,250 and 3,560 yrs using the mean and modal earthquake magnitudes, respectively. In general, the mean magnitude tends to provide a more consistent return period of liquefaction across the different locations – the coefficients of variation of the return periods are 0.38 and 0.46 for the mean and modal magnitudes, respectively. These coefficients of variation are both very large, indicating the geographic variation of the hazards using performance-based analysis are very different, even though the conventional procedures indicate the seismic hazards are identical.

3.3 *Effects of liquefaction – settlement*

Huang (2008) developed a probabilistic post-liquefaction settlement model based on interpretation of previous laboratory test results presented by Tokimatsu and Seed (1987), Ishihara and Yoshimine (1992), Shamoto et al., (1998), and Wu and Seed (2004). The relationship between SPT resistance, cyclic stress ratio, and median vertical strain, $\hat{\varepsilon}_v$,

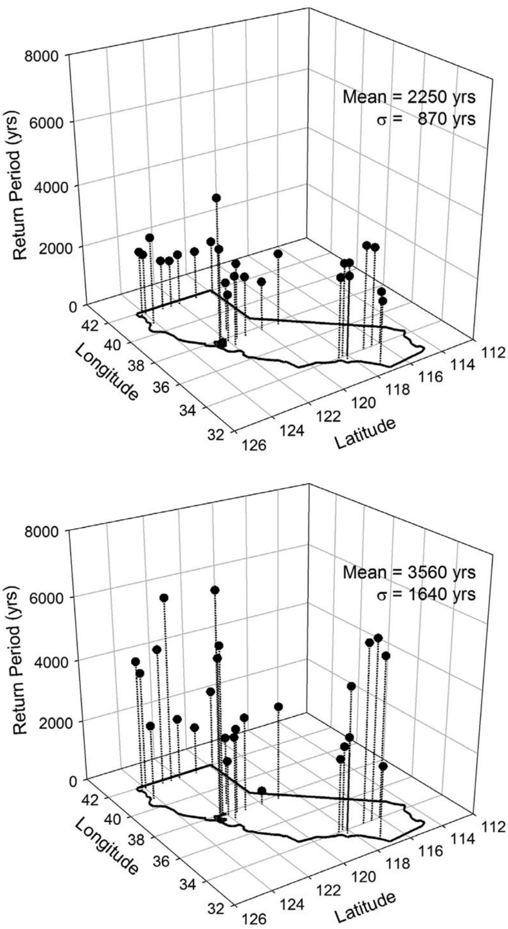

Figure 7. Return periods of liquefaction at sites for which $FS = 1.5$ using 975-yr peak ground acceleration and magnitude scaling factor based on (a) mean magnitude, and (b) modal magnitude.

based on Wu and Seed's graphical model was expressed as

$$
\begin{aligned}
&(N_1)_{60,cs} = \frac{CSR + D}{A + B(CSR + D)}, \text{ where} \\
&A = 0.002152\hat{\varepsilon}_v + 0.003322 \\
&B = b_1\hat{\varepsilon}_v{}^2 + b_2\hat{\varepsilon}_v + b_3, \\
&b_1 = -0.00003725\,\hat{\varepsilon}_v^2 - 0.0001581\hat{\varepsilon}_v + 0.004152, \\
&b_2 = 0.0007936\,\hat{\varepsilon}_v^2 - 0.002052\hat{\varepsilon}_v + 0.002547, \\
&b_3 = -0.001089\,\hat{\varepsilon}_v^2 - 0.0006875\hat{\varepsilon}_v + 0.01696, \\
&D = -0.0123652\hat{\varepsilon}_v + 0.02709.
\end{aligned} \tag{9}
$$

The quality of the fit given by this expression is illustrated in Figure 8(b). Equation 9 requires an iterative solution for $\hat{\varepsilon}_v$ as a function of SPT resistance

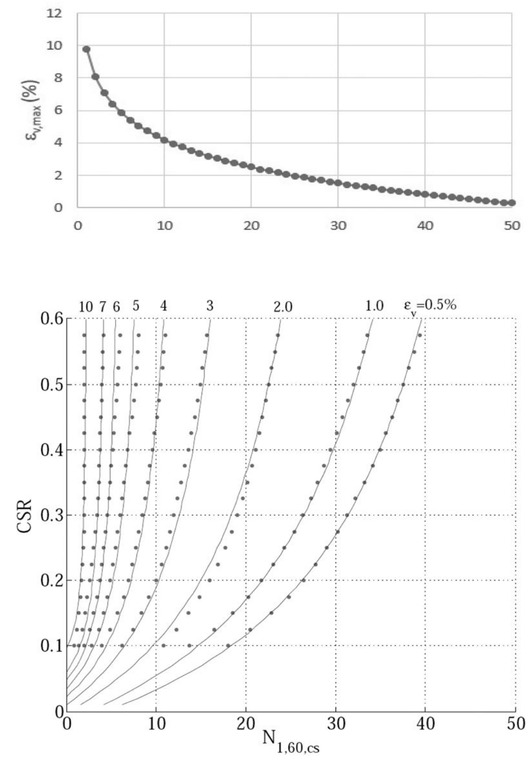

Figure 8. Representation of Wu and Seed graphical curves (data points) by Equation 8 (solid curves). Upper plot shows variation of $\bar{\varepsilon}_{v,\max}$ with $(N_1)_{60,cs}$.

and cyclic stress ratio. The mean value of ln ε_v can then be computed as

$$\mu_{\ln \varepsilon v} = \ln(\hat{\varepsilon}_v) \tag{10}$$

which allows the vertical strain fragility relationship for a given CSR and $(N_1)_{60}$ to be described by

$$P[\varepsilon_v > \varepsilon_v^* \mid CSR\ , N] = \Phi\left[\frac{\mu_{\ln \varepsilon v} - \ln \varepsilon_v^*}{\sigma_{\ln \varepsilon_v}}\right] \tag{11}$$

where $\Phi(\cdot)$ is the standard normal cumulative distribution function.

The fact that the Wu and Seed (2004) curves do not become vertical at high CSR levels implies that volumetric strain continues to increase without bound with increasing CSR. However, considerable experimental evidence suggests that the continued vibration of soil leads to densification only to some limiting void ratio or density. Therefore, there must exist some limiting volumetric strain for a soil of a given initial density. Because the performance-based approach integrates response over all levels of ground motion hazard (Equation 6), extrapolating the Wu and Seed

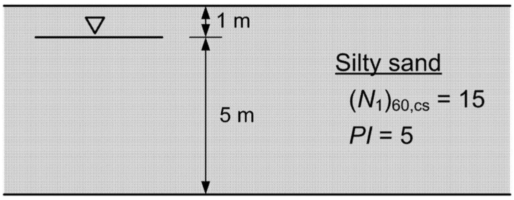

Figure 9. Hypothetical soil profile in Seattle, Washington.

(2004) curves to the very high *CSR* values that can exist in areas of high seismicity can lead to unrealistically high volumetric strain levels. Huang (2008) reviewed data from compaction, minimum void ratio, drained cyclic tests, and consolidation tests following cyclic loading to establish a relationship between maximum volumetric strain and SPT resistance. The relationship can be approximated by

$$\bar{\varepsilon}_{v,\max}(\%) = 9.765 - 2.427\ln[(N_1)_{60,cs}] \qquad (12)$$

Recognizing the approximate nature of this relationship, Huang (2008) assumed that $\varepsilon_{v,\max}$ was uniformly distributed over a range of 0.5 $\bar{\varepsilon}_{v,\max}$ to 1.5 $\bar{\varepsilon}_{v,\max}$.

3.3.1 *Example*

Performance-based evaluation of liquefaction hazards offers significant advantages over conventional procedures. It considers the complete range of expected ground motions – from weak motions that occur relatively frequently to strong motions that occur only rarely, and thereby gives a more complete representation of the seismic environment. It also accounts for uncertainties in liquefaction susceptibility, initiation, and effects, and thereby treats those phenomena more objectively and consistently than conventional procedures, which generally apply some form of conservatism that varies inconsistently from engineer to engineer and site to site.

To illustrate the performance-based settlement evaluation procedure, a simple, hypothetical site in Seattle, Washington (Figure 9) is assumed. The site consists of 6 m of loose, silty sand with a groundwater level 1 m below the surface. The sand has a corrected clean sand SPT resistance, $(N_1)_{60,cs} = 15$ and PI = 5. The variation of $\bar{\varepsilon}_{v,\max}$ with $(N_1)_{60,cs}$ is illustrated in Figure 7(a).

To illustrate the roles of susceptibility, initiation, and maximum volumetric strain, the post-liquefaction settlement hazard for the site is computed for four different cases. Case 1 makes the conservative assumption that P[*susceptibility*] = 1.0, P[*initiation*] = 1.0, and that no maximum volumetric strain exists. For this case, the curves of Wu and Seed (2004) shown in Figure 8 are extrapolated to large *CSR* values. Case 2 is identical to Case 1, except that the existence (and distribution) of maximum volumetric strain is taken into account. Case 3 is the same as Case 2, except that the probability of initiation of liquefaction is also computed and accounted for. Finally, Case 4 accounts for

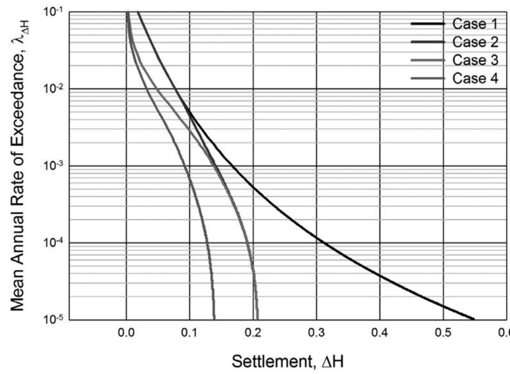

Figure 10. Post-liquefaction settlement (m) hazard curves.

the probability of liquefaction susceptibility, the probability of initiation, and the existence of a maximum volumetric strain.

The computed settlement hazard curves for all four cases are shown in Figure 10. For Case 1, the settlement hazard curve shows steadily increasing settlement with increasing return period (decreasing mean annual rate of exceedance). At long return periods, the unbounded settlement relationship implies settlement of over 0.5 m, which would correspond to average volumetric strains (over the 5 m saturated thickness) in excess of 10%. Referring back to Figure 7, a volumetric strain of 10% for a soil with $(N_1)_{60,cs} = 15$ would require extremely high *CSR* values that would be associated with extremely long return period ground motion levels; this volumetric strain would exceed that which has been observed in laboratory tests. The mean value of $\varepsilon_{v,\max}$ predicted by Equation 12 for such a soil would be approximately 3.2%, so the upper limit according to Huang (2008) would be less than 5%. While these extraordinary levels of volumetric strain are reached at extremely long return periods, they are nevertheless unrealistic and, therefore, inappropriate.

For Case 2, in which the existence of a maximum volumetric strain was considered, the settlement hazard curve matches the Case 1 curve at short return periods where volumetric strains do not approach the maximum value. At return periods beyond about 250 yrs, however, the shaking becomes strong enough that the maximum volumetric strain begins to affect the settlement hazard. At longer return periods, the Case 2 settlement hazard curve drops below the Case 1 curve and eventually becomes asymptotic to a maximum settlement slightly greater than 0.2 m. This settlement would correspond to an average maximum volumetric strain of about 4% under the strongest possible shaking, a value that is consistent with the results of laboratory tests and therefore more realistic than that of Case 1.

The Case 2 curve assumes that liquefaction is initiated at all return periods. For the relatively weak shaking expected at short return periods, however, the probability of liquefaction may be less than 1.0. The

Case 3 curve accounts for the probability of liquefaction initiation, and therefore drops below the Case 2 curve at short return periods. For return periods longer than about 1,000 years, the probability of initiation is virtually 1.0 so the Case 3 curve converges to the Case 2 curve, as expected.

Finally, the settlement hazard curves for the first three cases all assume that the $PI = 5$ soil is susceptible to liquefaction. This PI level, however, would be in the transitional zone identified by Boulanger and Idriss (2005) and shown in Figure 1 and would be assigned a value of $S_{BI} = 0.68$ according toEquation 1. Taking S_{BI} as a subjective probability of susceptibility, the expected value of settlement drops to the Case 4 curve shown in Figure 9. Consideration of the probabilities of susceptibility and initiation, and the existence of a maximum volumetric strain, reduce the 475-yr settlement value from approximately 17 cm to approximately 9 cm.

4 SUMMARY AND CONCLUSIONS

Performance-based concepts can allow objective and consistent evaluation of liquefaction hazards. By properly combining uncertainties in ground motions with uncertainties in liquefaction susceptibility, initiation, and effects, the actual return period for a given level of effects can be computed. The application of these concepts to the problems of liquefaction triggering and post-liquefaction settlement prediction is illustrated in the paper.

Performance-based triggering analyses include contributions from all peak ground accelerations and all earthquake magnitudes, and also consider uncertainties in liquefaction potential given peak acceleration and magnitude. The result is a more complete and accurate indication of liquefaction potential than is achieved with conventional procedures which consider only one level of ground shaking and treat liquefaction potential deterministically. Analyses of sites distributed across California with equal liquefaction potential as indicated by conventional procedures were shown to have very different actual liquefaction hazards – return periods of liquefaction varied by factors of two over even short distances and factors up to about 15 for different locations within the state.

The fact that performance-based settlement estimates are based on all levels of ground motion, including very strong levels that may only occur very rarely, requires the consideration of bounding values on volumetric strain. An approximate model for maximum volumetric strain was developed and implemented, and found to have a significant effect on post-liquefaction settlement at long return periods.

The implementation of this probabilistic settlement model into a performance-based framework that allows probabilistic characterization of liquefaction susceptibility and the potential for initiation of liquefaction allows the most consistent and objective estimates of post-liquefaction settlement hazards to be evaluated.

REFERENCES

Anderson, D. L., Byrne, P. M., DeVall, R. H., Naesgaard, E., Wijewickreme, D. (2007). *Geotechnical Design Guidelines for Buildings on Liquefiable Sites in Accordance with NBC 2005 for Greater Vancouver Region*. Greater Vancouver Task Force Report, Vancouver, BC.

Boulanger, R. W., and Idriss, I. M. (2005). Evaluating cyclic failure in silts and clays. *Proceedings, Geotechnical Earthquake Engineering Satellite Conference on Performance Based Design in Earthquake Geotechnical Engineering: Concepts and Research*. Prepared by TC4 Committee of ICSMGE, Japanese Geotechnical Society, Tokyo, 78–86.

Boulanger, R.W. and Idriss, I.M. (2014). CPT and SPT based liquefaction triggering procedures, *Report No. UCD/CGM-14/01*, Center for Geotechnical Modeling, University of California, Davis, 134 pp.

Bray, J.D. and Sancio, R.B. (2006). Assessment of the Liquefaction Susceptibility of Fine-Grained Soils. *Journal of Geotechnical and Geoenvironmental Engineering,* Vol. 132, No. 9, pp. 1165–1177.

Cetin, K.O., Seed, R.B., Der Kiureghian, A., Tokimatsu, K., Harder, L.F., Kayen, R.E., and Moss, R.E.S. (2004). Standard penetration test-based probabilistic and deterministic assessment of seismic soil liquefaction potential, *Journal of Geotechnical and Geoenvironmental Engineering, ASCE*, 130(12), 1314–1340.

Cetin, K.O., Bilge, H.T., Wu, J., Kammerer, A.M., and Seed, R.B. (2004). "Probabilistic model for the assessment of cyclically induced reconsolidation (volumetric) settlements," *Journal of Geotechnical and Geoenvironmental Engineering*, ASCE, 132(3), 387–398.

Cornell, C.A. and Krawinkler, H. (2000). Progress and challenges in seismic performance assessment, *PEER News*, April, 1–3.

Deierlein, G.G., Krawinkler, H., and Cornell, C.A. (2003). A framework for performance-based earthquake engineering, *Proceedings, 2003 Pacific Conference on Earthquake Engineering.*

Huang, Y. (2008). Performance-Based Design and Evaluation for Liquefaction-Related Seismic Hazard, *PhD Thesis*, University of Washington, Seattle, WA.

Idriss, I. M., and Boulanger, R. W. (2010). "SPT-based liquefaction triggering procedures." Report UCD/CGM-10/02, Department of Civil and Environmental Engineering, University of California, Davis, CA, 259 pp.

Ishihara, K. and Yoshimine, M. (1992). Evaluation of settlements in sand deposits following liquefaction during earthquakes, *Soils and Foundations*, Vol. 32, No. 1, pp. 173–188.

Juang, C.H. and Jiang, T. (2000). Assessing probabilistic methods for liquefaction potential evaluation, *Soil Dynamics and Liquefaction 2000*, R.Y.S. Pak and J. Yamamuro, eds., Geotechnical Special Publication 107, ASCE, New York, 148–162.

Kramer, S.L. (1995). *Geotechnical Earthquake Engineering*, Prentice-Hall, Englewood Cliffs, New Jersey, 653 pp.

Krawinkler, H. (2002). A general approach to seismic performance assessment, *Proceedings, International Conference on Advances and New Challenges in Earthquake Engineering Research*, ICANCEER, 2002, Hong Kong.

Liao, S.S.C., Veneziano, D., and Whitman, R.V. (1988). Regression models for evaluating liquefaction probability, *Journal of Geotechnical Engineering, ASCE*, 114(4), 389–409.

Seed, H.B. and Idriss, I.M. (1971). Simplified procedure for evaluating soil liquefaction potential, *Journal of the Soil Mechanics and Foundations Division, ASCE*, 107(SM9), 1249–1274.

Seed, H.B. and Idriss, I.M. (1982). *Ground motions and soil liquefaction during earthquakes*, Earthquake Engineering Research Institute, Berkeley, California, 134 pp.

Seed, H.B., Tokimatsu, K., Harder, L.F., and Chung, R.M. (1985). Influence of SPT procedures in soil liquefaction resistance evaluations, *Journal of Geotechnical Engineering*, Vol. 111, No. 12, pp.1425–1445.

Shamoto, Y., Zhang, J.-M., and Tokimatsu, K. (1998). Methods for evaluating residual post-liquefaction ground settlement and horizontal displacement, *Soils and Foundations*, Special Issue No. 2, 69–83.

Silver, N.L. and Seed, H.B. (1971). Volume changes in sands during cyclic loading, *Journal of the Soil Mechanics and Foundations Division, ASCE*, Vol 97, No. SM9, pp. 1171–1180.

Tokimatsu, K. and Seed, H.B. (1987). Evaluation of settlements in sand due to earthquake shaking, *Journal of Geotechnical Engineering, ASCE*, Vol. 113, No. 8, pp. 861–878.

Toprak, S., Holzer, T.L., Bennett, M.J., and Tinsley, J.C. III. (1999). CPT- and SPT-based probabilistic assessment of liquefaction, *Proc., 7th U.S.-Japan Workshop on Earthquake Resistant Design of Lifeline Facilities and Countermeasures Against Liquefaction*, Seattle, Multidisciplinary Center for Earthquake Engineering Research, Buffalo, NY, 69–86.

Wu, J. and Seed, R.B. (2004). Estimation of liquefaction-induced ground settlement (case studies), *Proceedings, Fifth International Conference on Case Histories in Geotechnical Engineering*, New York, pp. 1–8.

Youd, T.L. and Noble, S.K. (1997). Liquefaction criteria based on statistical and probabilistic analyses, *Proceedings of the NCEER Workshop on Evaluation of Liquefaction Resistance of Soils*, National Center for Earthquake Engineering Research, Buffalo, NY, 201–205.

Youd, T.L. et al., (2001). Liquefaction resistance of soils: Summary report from the 1996 NCEER and 1998 NCEER/NSF workshops on evaluation of liquefaction resistance of soils, *Journal of Geotechnical and Geoenvironmental Engineering, ASCE*, 127(10), 817–833.

Geotechnics for Catastrophic Flooding Events – Iai (Ed)

Progresses on disaster mitigation and rehabilitation technologies for embankment dam in China

H.L. Liu
Institute of Geotechnical Engineering, Chongqing University, Chongqing, China
Key Laboratory of Ministry of Education for Geomechanics and Embankment Engineering, Hohai University, Nanjing, China

ABSTRACT: The progresses on danger-control and reinforcement techniques for embankment dams in China are reviewed in this paper. Based on observed static and dynamic embankment dam behaviours, three main types of damage mechanism for embankment dams are summarized, namely the seepage deformation, dam instability and insufficient earthquake-resistant capability. Aiming at remediating three types of dam damage, commonly employed reinforcement measures for embankment dams are introduced, followed by a discussion of their future developments.

1 INTRODUCTION

Since 1949, a large number of dams and reservoirs have been constructed in China. Through 65-year development, complete and multi-functional flood control engineering systems have been established on most large rivers, which are capable of blocking, discharging, detaining and diverting flood through the constructed reservoirs, embankments, detention basins and division channels, where remarkable and effective effect has been achieved on flood control and disaster reduction. According to the "National special planning of danger-control and reinforcement project for dangerous reservoirs" (The Ministry of Water Resources, 2007), there are 90,020 reservoirs in China, including 508 large-scale ones, 3,209 medium-scale ones and 69,059 small-scale ones, where 38,019 reservoirs are assessed in dangerous status. Furthermore, the constructed river embankments in China are approximately 250,000 km long, including 65,700 km long main embankments. Taking the two longest Chinese rivers, Yangtze River and Yellow River, for example, the total length of embankments on Yangtze River is 30,000 km, including 3,600 km long main embankments, and the length of embankments on Yellow River is 1,400 km (downstream after Mengjin City) (Bao and Wu, 1990). However, during the construction of these hydraulic projects, due to insufficient geological investigation, lacking of laboratory test data and poor quality of construction materials, the qualities of these embankment dams were not reasonably controlled. After several-decade operation, these factors have essentially resulted in various risks for the safety of reservoirs and embankment dams, influencing functional operation of these hydraulic projects, limiting economic development and even threatening the safety of millions of people living in the downstream areas. It is observed that these risky reservoirs have increasingly weakened the whole flood control system, and therefore it is necessary and urgent to conduct danger-control and reinforcement measures on dangerous reservoirs and embankment dams in China.

2 DAMAGE TYPES FOR EMBANKMENT DAMS

Based on the statistical data, 95% of dams in China are earth and rockfill dams which was reported by Zhang (2001), mostly constructed in 1950s–1970s. However, due to the restricted construction techniques in that period, limitations existed in densification of dam materials and foundation seepage prevention measures. These limitations have caused various types of seepage deformation on embankment dams under operation, such as piping, soil flow and contact erosion, which can further lead to dam cracking and slope slide. Concerning other hydraulic structures, i.e. masonry dams, concrete dams, spillways and conveyance tunnels, due to the poor construction quality or incomplete foundation treatment, as time passing, various damages would appear, such as the carbonisation, cracking, steal exposure, stripping, erosion, lioxiviation and leakage, which significantly affect the structural and seepage safety of these structures. Overall, the damage mechanisms of embankment dams in China can be categorized into three types, illustrated as follows:

2.1 *Seepage deformation*

Seepage deformation on embankment dams behaves as water leakage on dam bodies or dam foundations, which can result in piping, soil flow and contact

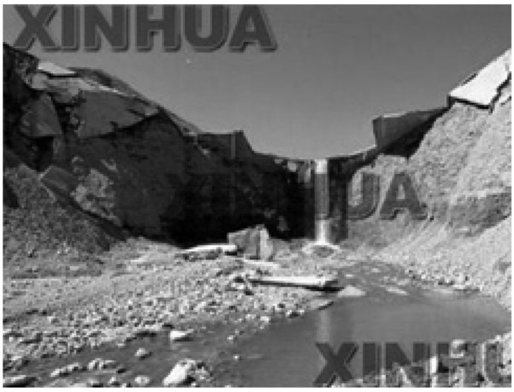

Figure 1. Failure of Gouhou reservoir dam.

Figure 2. Cracks on Wanquanhe dam (Qionghai, Hainan Province).

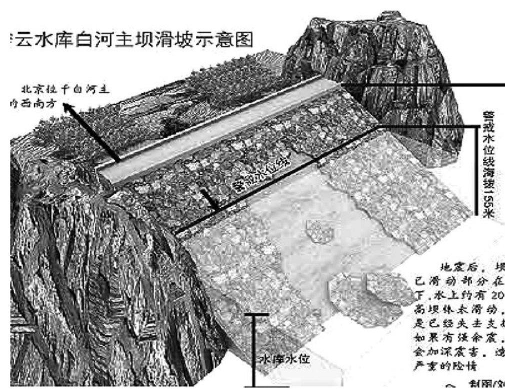

Figure 3. Slope slide on Baihe dam of Miyun reservoir.

erosion for earth and rockfill dams, and lioxiviation problems for masonry dams. According to different leakage locations, seepage deformation can be categorized into three types, which are dam body leakage, foundation leakage and bypassing leakage. Seepage deformation is mainly induced by poor construction quality, incomplete drainage facilities, ineffective or broken seepage prevention facilities, weak foundation rock or even freezing environment. Under the condition of reservoir impounding, these negative factors could lead to different leaking locations on the downstream dam side, resulting in concentrated leakage or large-area infiltration, which can further induce piping, soil flow, and slope slide, significantly threatening dam safety. Figure 1 shows the failure of Gouhou reservoir dam on 27th August, 1997, in Gonghe County of Qinghai Province, China, which was a reinforced concrete face gravel-fill dam. Investigation observes that after reservoir impounding, leakage existed in the joints between the concrete face and the toe slab of the parapet wall, where however, effective filtering layers were not constructed in the dam. Furthermore, the coefficients of uniformity of the dam materials were found to be considerably high. These two factors essentially induced seepage channels inside the dam body, where contact erosion existed between the concrete face and gravel-fill materials, and piping occurred in the dam. Long-term seepage led to saturated dam materials and high saturation line, which finally resulted in local static failures on the dam crest.

2.2 *Dam instability*

Dam instability can lead to significant deformation on dam bodies and foundations, i.e. dam cracking, slope slide and plastic failure on dam bases (see Figure 2), which are mainly due to the fact that the structural strength and anti-sliding stability of dams cannot satisfy design standards. In particular, investigation shows that steep dam slopes can reduce anti-sliding capability of dams, broken protection slopes can threaten dam safety, and poor construction quality and incomplete dam foundation treatment can weaken structural strength and anti-sliding stability of dams.

2.3 *Insufficient earthquake-resistant capability*

This type of dam damage mechanism is induced when earthquake-resistant capability cannot satisfy the corresponding seismic design standards. According to the statistical data presented by Zu (2004), the earthquake-resistant capabilities of 13 large-scale and numerous medium and small-scale reservoir dams in China were not sufficiently designed. It is observed that either the originally adopted designing earthquake intensity is smaller than the modified one from the latest Earthquake Intensity Zoning Map, or the original design did not consider earthquake loading conditions, where through later-on seismic evaluations, the earthquake-resistant capability could not satisfy designing standards. At 03:42 CST, on 27th August, 1997, the Tangshan earthquake (ML = 7.8) occurred in China, which resulted in devastating destruction to this city. The Baihe dam of Miyun reservoir in Beijing experienced severe damages, where local failures were found on different locations of the dam, as shown in Figure 3. Furthermore, after the 8.0 MS Wenchuan

Figure 4. Cracks on Shidaojiao reservoir dam in Guanyuan City after Wenchuan earthquake.

earthquake (2008, China), a large number of dams were found to have been damaged in different degrees (see Figure 4).

3 DANGER-CONTROL AND REINFORCEMENT TECHNIQUES FOR EMBANKMENT DAMS

Danger-control and reinforcement projects for embankment dams are considerably critical for millions of people and economic development in the downstream areas. Since 1949, Chinese government has significantly increased the investment on construction of embankment dams. Particularly after the 1998 great flood, the danger-control and reinforcement work for embankment dams has reached a peaking level, and the corresponding techniques have obtained significant development, where a variety of new technologies, equipments and materials have been proposed and employed. Progresses on danger-control and reinforcement techniques for embankment dams are introduced in the following part, aiming at remediating different types of dam damage.

3.1 *Seepage prevention techniques for embankment dams*

Seepage deformation is the most common potential danger for reservoirs dams and river embankments, and therefore seepage prevention work is considered to be one of the most urgent reinforcement projects. The basic principles of seepage prevention work for embankment dams include blocking and drainage. More specifically, at the upstream dam side, the blocking work aims to block seepage inlets and maximally extent seepage path, including horizontal and vertical seepage prevention measures. At the downstream dam side, the drainage work adopts diverting and filtering facilities, in order to quickly and safely discharge leaking water while without bring soil particles. Before 1970s, only simple and less advanced seepage prevention techniques were employed in China (Yang 2011), where typical measures included increasing dam dimensions, such as heightening and thickening dam bodies, riprap and seepage diversion channels. However, since 1970s, seepage prevention techniques have been quickly developed, providing sufficient new equipments and technologies for reinforcement measures of embankment dams.

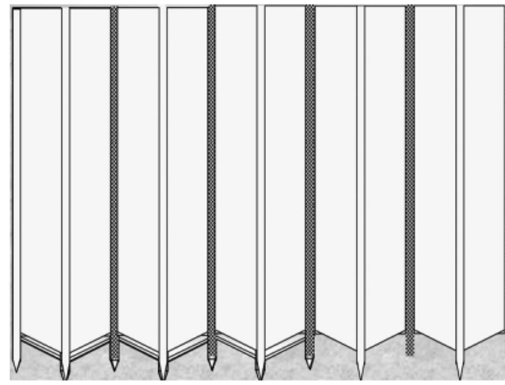

Figure 5. Schematic construction graph for polymer grouting cut-off wall.

3.1.1 *Polymer grouting cut-off wall technique*

Polymer materials occupy impermeable and highly elastic characteristics. When grouted in soil structures, polymer materials can penetrate between soil particles and produce cementing effect on soil materials. Concerning the application of polymer grouting cut-off wall, precast moulds of different shapes are penetrated inside embankment dams at different distances by static pressure equipments (see Figure 5), forming a continuous mould wall. After grouted into the precast moulds, polymer materials expand along the direction induced by moulds and consist a polymer grouting cut-off wall (Xu et al. 2012). Polymer grouting cut-off wall technique has been successfully employed to solve the leakage problems on Tiandu masonry dam (Hainan Province, China) and Shixianhang reservoir dam (Henan Province, China), in terms of foundation seepage and dam body seepage problems respectively. It was observed that after employing the polymer grouting cut-off walls, saturation lines were effectively lowered and seepage amount and water head were significantly reduced, achieving obvious seepage prevention effects (Guo 2012). It should be noted that polymer grouting cut-off wall technique predominates over typical seepage prevention measures, in terms of fast installation, light self weight, low permeability, small dimension, safe and eco-friendly materials and favourable durability.

3.1.2 *Vibration sinking mould cut-off wall*

The vibration-sinking-mould is a new technique for constructing the seepage cut-off wall. As compared to the conventional construction means, this technique has various advantages such as ease to achieve the desired wall continuity, verticality and integrity, and

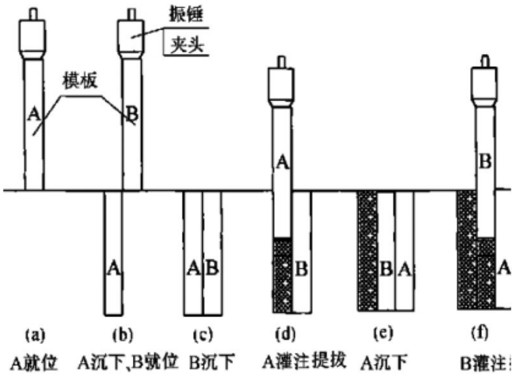

Figure 6. The construction procedure for vibration sinking mould cut-off wall.

Figure 7. Multi-head, small diameter, deep mixing for constructing the thin cut-off wall.

the favourable evenness and uniformity of the wall thickness. Its other desirable features include the rapid installation, satisfactory imperviousness and low cost (Pan et al. 2002; Qian and Yin 2008)[8–9]. As such, it has been widely applied to stabilizing and reinforcing embankments. As Figure 6 illustrates, its construction procedure starts with penetrating (or more specially 'sinking') the hollow steel mould made up of two metal templates (template A and B in Figure 6), with the aid of vibration generated by a powerful vibrator with high-frequency. As soon as the mould penetrates to the designed depth, imperious material is first filled into the space inside the template A, which is then immediately withdrawn and re-penetrated at the other side of template B. The exactly same procedure will be repeated on the template B. Repeatedly penetrating template, filling impervious material, and retracting template eventually forms a continuous seepage cut-off wall. Such a construction technique has now been practiced on various occasions, e.g. seepage cut-off walls built in the project of waterway from Huai River to the sea and cut-off walls constructed inside the right earth embankment of Yuhang River levee of Hangzhou.

3.1.3 *Thin cut-off wall constructed by multi-head, small diameter, deep mixing*

The multi-head, small diameter deep mixing, utilizing cement as the curing agent, can be used to construct the continuous seepage cut-off wall. It has a specially-designed multi-head, small diameter mixer, which can forcedly inject the binder slurry (cement) into soil and simultaneously mix soil with cementitious binder slurry to construct cement-treated soil columns. When these columns are densely located and overlapped, it can form a continuous cut-off wall. A series of mechanical and chemical actions are involved in the multi-head, small diameter deep mixing process which can produce continuous cement-treated soil walls (or curtains) having desirable strength and integrity as well as low permeability. This approach was found to be helpful to control the seepage and improve slope stability of the gravity dam foundation (Zhang and Gao 2007). The construction sequence of multi-head, small diameter deep mixing includes: first positioning the mixer to the targeted locations, then levelling the equipment and activating an array of drilling heads. A powerful drill advances drilling heads to penetrate to designed depths. They are subsequently retracted and in the meantime the binder slurry is injected into soil with the aid of high pressure. Additional soil mixing is achieved in their retraction process. This process can construct rows of overlapping columns which as a whole serve as the seepage cut-off wal (Wang 2000). This approach is applicable to a wide range of soils including clay, silty clay, silt, sand and gravel with a diameter less than 0.05 m, boulder with a diameter less than 200.0 mm. Moreover, its construction process does not interfere with the normal functioning of reservoirs when used for seepage control underneath the embankment foundation. Figure 7 shows the construction of thin cut-off walls by employing the multi-head, small diameter and deep mixing technique.

3.1.4 *Vertical placement of plastic membrane for seepage prevention*

Vertical placement of plastic membrane is a new water-blocking technique, which vertically places the plastic membrane into a trench created inside embankment or below the embankment base (i.e. the embankment foundation). This has proven to be an effective means to mitigate the potential seepage problems such as embankment or dam leakage or soil piping (Ren et al. 2006; Chen and Zhu 2000). Its construction sequence is: trench extraction – vertical placement of plastic membrane – trench backfilling. Its trench excavator can be broadly classified into three categories namely: scraper type machine, reciprocating machine and rotatory type machine. Vertical placement of plastic membrane is applicable to the seepage control of the embankment as well as dam foundation. It can also be utilized for the seepage prevention inside the embankment and dam body which is made of soils ranging from sandy soil, clay loam, sand to gravel. The scraper type machine is workable for sand and gravel with diameters up to 18.0 cm; the reciprocating machine is mainly applicable for silty soil, clay loam, sand and gravel with diameters up to 8.0 cm; the rotatory type machine is suitable for sandy soils.

3.2 *Stabilization and reinforcement techniques for embankment dams*

There are sorts of structural safety issues associated with embankment which encompass the deformation of embankment body and foundation, cracking and slope failure of embankment body, plastic failure of soil at the heel of embankment. Various measures exist to enhance the structural safety of embankment such as remedying embankment sections, which previously experienced collapse or slope failure, and fortifying the embankment base as well as its slope. The general principle for stabilizing and reinforcing the embankment is minimizing the sliding force, maximizing sliding resistance and increasing the relatively density of soil. In line with the preceding principle, there exist a number of feasible solutions such as flattening the unstable slope, reducing the slope gradient, excavating and backfilling, opening channel to guide the seepage flow, etc. In cases where there is sludge or weak soil layers below the embankment base, it is advisable to conduct dredging, crushing sludge, imposing high pressures on the embankment heel and so on. Aside from the above, in the recent years new means have been devised.

3.2.1 *Riprap for protecting embankment heel*

Riprap (also known as rock armour) is the most commonly adopted techniques for protecting the embankment heel with proven efficacy. For example, underwater riprap was used to protect the heel of Xiaonan embankment in Xiaonan City County of Hubei Province (Figure 8). One apparent shortcoming of riprap, however, is its high construction cost. Besides, due the absence of reversed filter, soil below ripraps remains susceptible to erosion caused by water torrents. The erosion of soil leads to further settlement of ripraps, which thus requires frequent maintenance. To remedy this deficiency necessitate the placement of reversed filter, which usually consists of sand and gravels at certain combination ratios. Nevertheless, this remedial measure is expensive and not resilient to water torrent. One plausible solution is to use the reverse filter made up of geomembrane and geotextile. This is in principle a feasible and may improve the effectiveness of riprap greatly. As the equipment and skill for underwater installation of geotextile and geomembrane is still immature, more research work is necessary to exploit this approach.

Figure 8. Underwater riprap at Xiaonan embankment.

3.2.2 *Geo-bags for embankment stabilization*

Geo-bag is produced by sewing up two identical pieces of geotextile, which, then filled with cement mortar, can serve as optimal material for embankment stabilization after cement setting. If classified in different ways, geo-bag can be grouped into different categories. For instance, according to whether it has been equipped with filtration opening, the geo-bag can be classified into two main categories: geo-bag with filtration opening and that without filtration opening. According to its connection mode, geo-bag can be grouped into the chain-type geo-bag and the grid-type geo-bag. Moreover, according to whether it is woven, the geo-bag fall into two distinct categories: the woven geo-bag and non-woven geo-bag. Virtues of the geo-bag include good adaptability to a diverse range of terrains, desirable integrity, strong resilience to scouring and erosion, ease to install, good durability, cost-efficiency and readiness for underwater manipulation. However, on occasions with severe water torrents and great water depths, its construction machinery as well as construction skills have to be further improved to guarantee the satisfactory construction quality. Such improvement works is currently being undertaken in relevant institutes.

3.2.3 *Geomembrane mattress for embankment stabilization*

Soft geomembrane mattress is made up of large pieces of inter-connected geomembrane, which as a hole form a huge mattress. The existing geomembrane mattress can be broadly classified into two categories namely geomembrane mattress with ballasts and mattress with sand-filled bags. As an innovative, economical embankment stabilization solution, the soft geomembrane mattress has performed remarkably well in projects involved.

Soft geomembrane mattress with ballasts: geomembranes are first sewed up to form a huge mattress and the latter is then ballasted to stabilize the embankment. The ballast materials can be big heavy stones, soil pillows, soil bags, rock-filled wire gabion, chained

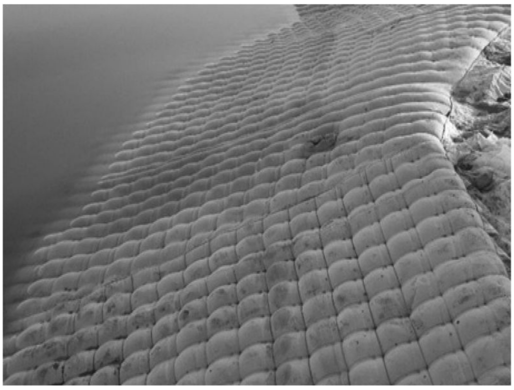

Figure 9. Soft geomembrane mattress.

Figure 10. Installation of composite soft geomembrane mattress at Xinjiawan of Anhui Province.

concrete slabs, etc. The soft geomembrane mattress with ballasts has been extensively practiced in embankment stabilization projects all over the world. It is particularly suited to be practiced on the ice or under shallow water. In situation with great water thickness and harsh water torrents, its application may be constrained.

Soft geomembrane mattress with sand-filled bags: the sand-filled bag is fist prepared by sewing the geotextile up, into which sand is then fed. There two types of sand bags which are currently used in China. One type is obtained by sewing up two layers of geotextile into arrays of discrete bags, each of which has its own opening for sand filling. The other is made by sewing the geotextile into long tubes with closed ends, which is then attached to geomembrane mattress. Sand is subsequently filled into bags to ballast. The geomembrane mattress with sand-filled bags is readily fabricated and its sand filling process can also be mechanized. During its installation, the mattress can fall under its own self-weight, with no requirement of further loading. The filling material can be reviver sand. Nevertheless, to prevent the leakage of filled sand, it is more advisable to add the cementitious material or binder as a part of its filling material. As Figure 10 shows, the composite geomembrane mattress was adopted to stabilize and reinforce the embankment section of Huai River near the Xinjiawan in Huaibei City of Anhui Province (Figure 9).

3.2.4 *Soil slope curing technology*

As a new technology for slope protection, soil slope curing technology makes use of soil stabilizer to cure topsoil of embankment to achieve anti-erosion, anti-freeze, anti-wave, and anti-seepage purposes. Soil stabilizer was previously used for road construction. The first trial of soil stabilizer for slope protection was on Yiyang River estuary of Zijiang levee in Hunan Province in 1999, from which the obtained experimental data and construction process can be used as references for similar projects (Ding et al. 2000).

3.3 *Seismic reinforcement techniques for embankment dams*

Loose sand may be subjected to liquefaction induced by earthquakes. The basic anti-liquefaction measures include replacement method, encryption method and increasing weights method (Cao 2003; Fu 2000_). Replacement method involves dredging the sand in liquefaction zone and refilling gravel and other materials with better anti-liquefaction properties. The objective of encryption method is to improve the density of sand through vibro-compaction, making it more resistible to seismic loadings. Increasing weights method works through imposing pressure on the surface of the liquefaction zone to improve the effective stress of sand layer. The commonly adopted techniques include: riprap weights technology, continuous concrete wall sealing technology and vibro flotation technology.

3.3.1 *Riprap weights technology*

Riprap is adopted to impose pressure on foot of the upstream dam. After placement of the riprap, the liquefied area can be constrained to 10.0 m outside of the dam foot, indicating that the effect is significant. In addition, riprap weights can effectively increase the stabilizing force, thus increasing the safety factor against sliding of the upstream dam. Furthermore, this technique is cost-effective and the construction process is simple, making it easy to meet the technical requirements. Figures 11 and 12 illustrated the riprap weight reinforcements of Bashan reservoir dam in Shandong Province and Qingan reservoir dam in Jiangsu Province, respectively.

3.3.2 *Continuous concrete wall sealing technology*

To solve the problem of embankment liquefaction, continuous concrete walls at both the upstream and downstream toes along the axis of embankment are built to enclose the liquefied foundation. As trenching is followed by concreting, the construction quality can be assured. The continuous concrete wall is of good continuity and integrity, and adaptable to the lateral deformations. The construction of continuous concrete wall causes minimal impact on nearby ground transportations, even under narrow ground conditions.

Figure 11. Reinforcement of Bashan reservoir dam.

Figure 12. Reinforcement of Qingan reservoir dam.

3.3.3 *Vibro flotation technology*

Vibro flotation was proposed by Steuerman in 1936, involving charging water into the hole, a method of vibro reinforcement (Wen 2002). Based on the reinforcement mechanism, vibro flotation can be divided into two types: vibro replacement and vibro compaction. Considering the large permeability of gravels, the reinforcement effect of vibro replacement gravel pile is significant, since the pore water pressure generated by the earthquake can be quickly dissipated. Vibro compaction method is mainly adopted in reinforcing loose sand, making the saturated sand layer liquefied through strong vibros first. Then the sand particles rearrange, and thus porosity is reduced. In the construction process, the exciting force within the 1.0 m range from vibroflot can produce 1.0 g of acceleration; the acceleration is less than 0.5 g from 2.0 m outside the vibroflot, implying that its vibration effect is far more significant than 0.15 g that generated by a

Figure 13. Reinforcement of Xiakou dam using vibro replacement stone column method.

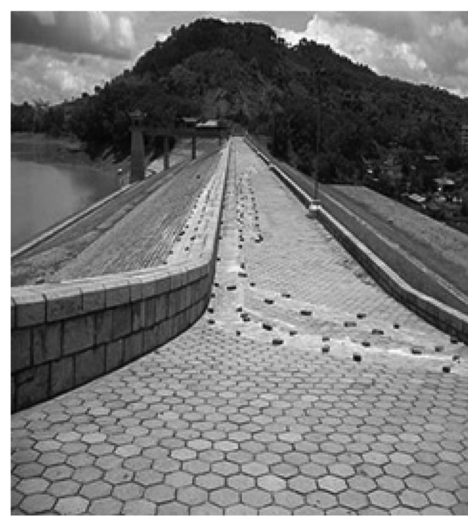

Figure 14. Reinforcement of Donger reservoir using vibro replacement stone column method.

8 magnitude earthquake. It is anticipated that the preliquefaction effects generated by vibro compaction will considerably improve the liquefaction resistance of dam foundation. No accident has been reported in Japan about liquefaction of sand foundation treated by vibro replacement stone column method. Figures 13 and 14 showed the applications of vibro replacement stone column method in Xiakou dam in Yunan Province and Donger River levee, respectively.

4 CONCLUSIONS AND FUTURE WORKS

China is the country owning the largest number of reservoirs and rivers. Reinforcement and protection measures to ensure stability and functional operation of reservoirs and embankment dams are essential. Type, location and severity of embankment quality problems may differ. To achieve effective reinforcement purposes, the principle of technical reliability and economic rationality should be adhered to. The reinforcement measures should be reasonably determined according to the geological conditions, data specificity and complexity of problems. This paper briefly discusses the main technical methods with regard to the reservoir and dam reinforcements in China. Research on danger-control and reinforcement for engineering structures should be extended in the fields of: (1) new technologies with more significant effect and more practical use; (2) novel construction techniques with systematic development, easy operation, and low cost; (3) new materials with good properties of seepage prevention, anti-erosion and carbonation resistance; (4) environmentally friendly, danger-control and reinforcement technology development should take into account the protection of the environment.

ACKNOWLEDGEMENTS

The financial support of Program for Changjiang Scholars and Innovative Research Team in University (Grant No. IRT1125) is acknowledged.

REFERENCES

Bao CG, and Wu CY. (1990). Dike construction technology and development in China. *Yangtze River* 30 (10): 15–16.

Chen HF, Zhu FC. (2000). Vertical Plastic processing and its application in the levee seepage. *Water Resources Development & Management* 20(2): 52–53.

Cao XC. (2003). Dam safety accident prevention and reinforcement technique. *Beijing Soft Electronic Press*

Ding LQ, Guo J, Yuan XY. (2000). Progress dike reinforcement. *China Water Resources* 3: 27–28.

Fu L. (2000). Seismic rehabilitation design of an earth dam. *Journal of hydraulic engineering* 8: 16–20.

Guo CC. (2012). Study on Non-water Reacted Polymer Curtain Grouting for Seepage Control of Dykes and Dams. PhD thesis. *Dalian University of Science and Technology*, China.

Pan WZ, Bai YN, Zhang CF, Wang WX. (2002). Wall seepage test vibro-sinking new technologies. *Advances In Science and Technology of Water Resources* 22(4): 38–40.

Qian YL, Yin ZZ. (2008). Mechanism of Wall Formation for the Impervious Wall with Vibration Sinking Mould and Its Application., *Geotechnical Investigation & Surveying*, 11:33–36.

Ren YP, Xie XY, Li B. (2006). Applications vertical plastic technology., *Water Conservancy Science and Technology and Economy* 12(10): 710–711.

The Ministry of Water Resources. (2007). The Special Program of Countrywide Ill- Conditioned And Dangerous Reservoirs. *Ministry of Water Resources*. Beijing, China.

Wang JS. (2000). The Application of Vertical Anti-seepage Wall Technology in the Yangtze River Important embankment Hidden Project., *China Water Resources* 7: 16–17.

Wen YH. (2002). Vibrating and Impact reinforcement technology. *Proc. of Progress of Rock Mechanics and Western Development geotechnical problems cum Chinese Society of Rock Mechanics and Engineering Seventh Conference*, Xian, China.

Xu JG, Wang FM, Zhong YH, Wang B, Li, XL, and Sun, N. (2012). Stress analysis of polymer diaphragm wall for earth-rock dams under static and dynamic loads. *Chinese Journal of Geotechnical Engineering* 34(9): 1699–1704.

Yang BS. (2011). Elaborate on dam seepage reinforcement and application of innovative technologies. *China Water Transport* 7: 2.

Zhang YB, Gao ZC. (2007). Long small diameter cement mixing pile in the reservoir reinforcement. *China Rural Water and Hydropower* 5: 91–92.

Zhang YM. (2001). Technical papers of national ill- conditioned and dangerous reservoirs sluices. *China Water Power Press*.

Zu L. (2004). Safety management of dangerous reservoirs in China. *Changjiang Publishing*, Wuhan, China.

Geotechnics for Catastrophic Flooding Events – Iai (Ed)
© 2015 Taylor & Francis Group, London, ISBN 978-1-138-02709-1

Development of seismic risk microzonation maps of Jakarta city

Masyhur Irsyam, Daniel Hutabarat, M. Asrurifak, Iswandi Imran, Sri Widiyantoro, Hendriyawan, Imam Sadisun & Bigman Hutapea
Research Center for Disaster Mitigation, Institut Teknologi Bandung, Indonesia

Taufik Afriansyah & Haris Pindratno
Jakarta Industry and Energy Department, The Government of Jakarta, Indonesia

Anita Firmanti & M. Ridwan
Research Institute for Human Settlement, Ministry of Public Works, Indonesia

Sri Woro Haridjono & Rakhindo Pandhu
Agency of Meteorology, Climatology, and Geophysics, Indonesia

ABSTRACT: Development of seismic risk microzonation study is required for disaster preparedness, risk and hazard mitigation decisions for the Government of Jakarta. The study includes estimation of seismic hazard, site characterization, site specific response analysis and risk assessment. Seismic hazard is performed based on deterministic and probabilistic approachs considering seismic sources influencing Jakarta. Geotechnical parameters are intrepreted from previous and recent measurements and depth of engineering bedrock is estimated based on microtremor array measurement. Identification of local site effects is conducted by carrying out one-dimensional ground response analysis considering the behavior of soil non-linearity. The result of the hazard microzonation study includes the distribution of site response such as spectral acceleration and amplification ratio. The results are then combined with building fragility that is determined based on the FEMA 154. Two building fragility curves are formulated corresponding to existing building type in Jakarta which are the confined masonry and in-filled frame structures.

1 INTRODUCTION

Several damaging earthquakes in the last decades in Indonesia have alerted the Government of Republic of Indonesia to mitigate future damages due to earthquake. Figure 1 show several massive earthquakes in the last decade, for example, Aceh 2004, within 150 kilometers of Aceh Province that followed by a massive tsunami, 2005 Nias Earthquake (Mw 8.7), the 2009 Tasik Earthquake (Mw 7.3), and the latest 2009 Padang Earthquake (Mw 7.6). These earthquakes have caused thousands of casualties, destruction and damage to thousands of infrastructure and buildings, as well as billion of dollars for rehabilitation and reconstruction.

In 2011, the Coordinating Ministry for People's Welfare appointed a national team to develop seismic risk microzonation maps for Jakarta city in order to enhance disaster preparedness, risk reduction and hazard mitigation. The team members consist of experts from national agencies and university research center including: Research Center for Disaster Mitigation of ITB, Government of Jakarta; Ministry of Public Works; Bureau of Meteorology, Climatology and Geophysics; National Disaster Management Agency; Ministry of Energy and Mineral Resources; Ministry of Research and Technology; Agency for Assessment and Application of Technology; and National Agency for Surveying & Mapping. The team members also collaborate with experts from Australian National University through AIFDR.

Jakarta is located in the North of Java Island with total land area approximately 664 km^2 with total population, from national census in 2010, approximately 10 million people with density about 15 thousand people for every km^2 area. It makes that seismic microzonation study is crucial to be completed immediately. The Indonesia seismic hazard maps published by the Ministry of Public Works in 2010 show that Jakarta is subjected to about 0.3–0.4 g ground acceleration at bedrock for the hazard level 2% probability of exceedance in 50 years. Seismic microzonation study is generally recognized as one of effective method to perform seismic hazard assessment and risk evaluation which is defined as the zonation with respect to ground motion characteristics taking into account source and site conditions (ISSMGE/TC4, 1999). This paper present several aspects in seismic microzonation in Jakarta city including the seismotectonic condition, geological condition, site amplification and risk

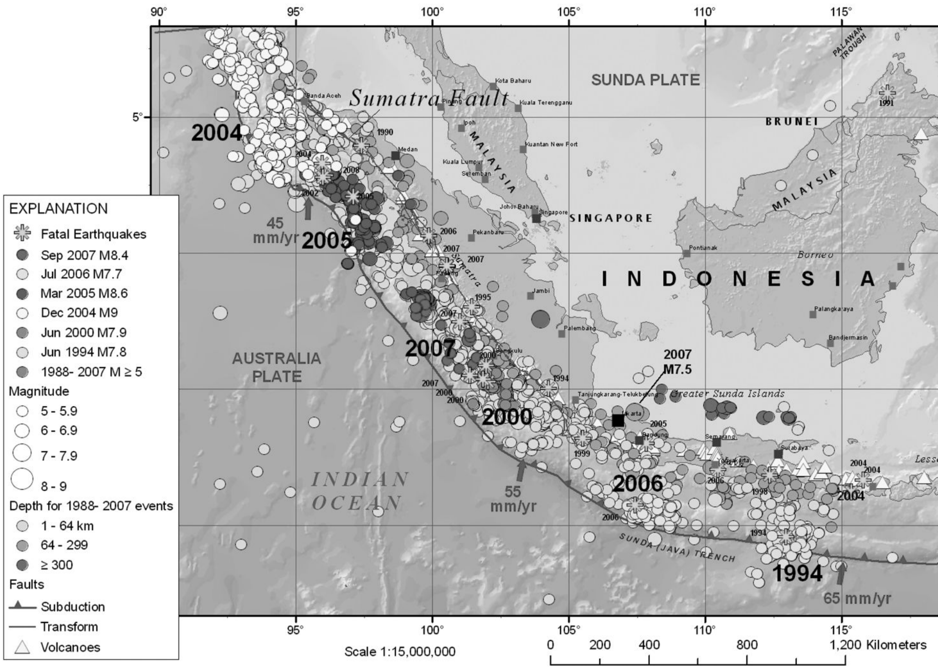

Figure 1. Seismic activity and seismotectonic condition in Sumatra and Java Island, Indonesia for the last few decades. (Modified from USGS).

evaluation by taking into account the building fragility. The microzonation level is graded based on the scale of investigation and method of ground motion assessment. Based on the technical committee on earthquake geotechnical engineering, TC4 of the International Society of Soil Mechanics and Geotechnical Engineering (1999), the seismic microzonation process methodology and level of study of Jakarta city is performed according to ISSMGE/TC4, 1999.

Seismic microzonation study in Jakarta requires rigorous input parameters regarding the seismic hazard in Jakarta, depth of engineering bed-rock, geotechnical condition and parameters, ground water level, ground response analysis and quantification of building vulnerability. It means that the seismic microzonation process are divided into 4 steps:

a. Evaluation of the input motion at bedrock or outcrop.
b. Site Specific Response Analysis
c. Seismic hazard microzonation
d. Seismic risk microzonation by taking into account the building fragility.

2 SEISMIC SOURCES INFLUENCING JAKARTA CITY

As mentioned previously by Irsyam et al., (1999 and 2011), Indonesia is located in a tectonically very active area at the point of convergence of three major plates and nine smaller plates as developed by Bird (2003). The Eurasian, Pacific and Australian-Indian plates, along with some smaller plates (i.e. Philippine Sea plate), are all actively moving toward each other in the Southeast Asia region creating a complex network of plate boundaries.

The earthquake data recorded by numerous national and international institutions show that the total number of earthquake occurring in Indonesia region between 1900–2000 with a magnitude $Ms > 5.0$ is approximately more than 8000 occurrences, where 5 percent of occurrences occurred in or near Java Island. Western Indonesia, where Jakarta is located, tectonically consists of the Sunda Shelf which includes the islands of Sumatra, Java, Bali, Borneo, and the southwestern part of Sulawesi (Hamilton, 1979).

The active tectonics of western Indonesia is dominated by convergence of the Australia plate with Sumatra and Java. Along Sumatra the direction of convergence is highly oblique to the trench strike, and is partitioned into nearly arc-perpendicular thrusting at the trench and arc-parallel, right lateral slip at the Sumatran fault (Bock et al., 2003).

Seismotectonic map showing the faults locations, geological setting and historical earthquakes influencing Jakarta is shown in Figure 2. Seismotectonic study has been collected in a circular area for detail with having radius of about 250 km around Jakarta. The seismotectonic map for Jakarta city contains several major fault lines in western Java with historical maximum magnitudes (Moment Magnitude, M_W) ranging from 6.5–7.6, and subduction zone either megathrust or deep intraslab subduction (Benioff) sources in sea with historical maximum M_W ranging from 7.8 to 9.0.

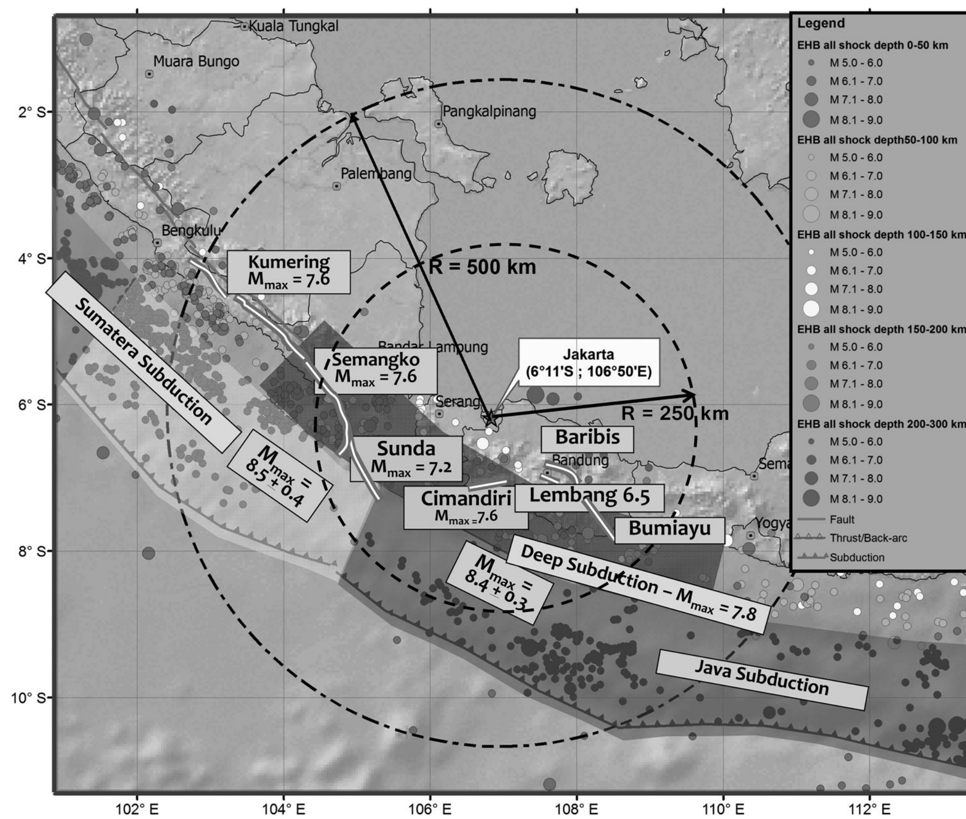

Figure 2. Seismotectonic map of Sumatra and Java Island which show the seismic sources influencing Jakarta city.

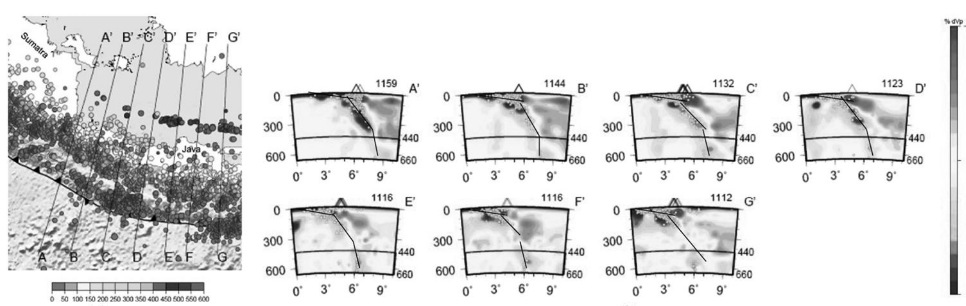

(a) (b)

Figure 3. Distribution of earthquake epicenters based on relocated events. (Enghdal et al., 2007); (a) Hypocentre depths (colouring) distribution from 1964 and 2007; (b) Vertical sections across the convergent margin in Java through the P-Wave model (Kennet et al., 1995).

The source models were derived based upon seismogenic conditions, focal mechanisms and earthquake catalogs. This seismogenic conditions include geometry and geomorphological of tectonic plate such as faults and subduction zones.

The Sunda Strait segment is located in the transitional zone between the Sumatera and Java segments of the Sunda Arc subduction zone. The angle of the subducted plate is depicted by vertical section shown in Figure 3. The dip angle of the megathrust represents important input for PSHA. Therefore, dip angles were investigated further by using carefully relocated events of Engdahl et al., (2007) using a 3D velocity and a double-difference (DD) technique (Pesicek et al., 2010). Figure 4 shows the dip angles of megathrust zone and can be depicted well.

In this study, several fault lines sources in Sumatra and Java Island are included. The 1900-km long Sumatran fault zone (SFZ) traverses the back-bone of Sumatra, within or near the active volcanic arc (Katili and Hehuwat, 1967; Sieh and Natawidjaja, 2000). Other fault sources that are also considered include

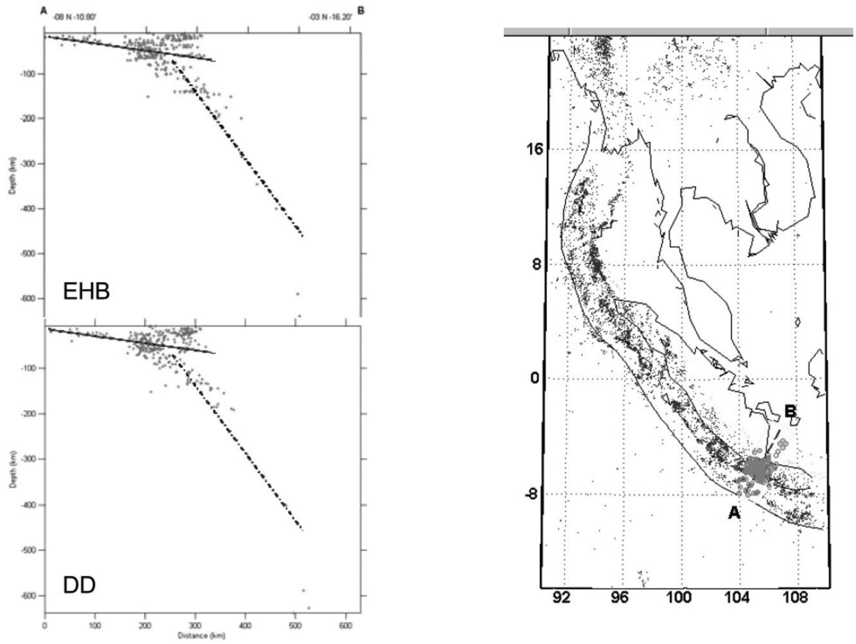

Figure 4. Vertical sections across the Sunda strait through the global data set by Enghdahl et al., 2007 (EHB) and relocated events using a double-difference (DD) method and 3D velocity model. (Pesicek et al., 2010, Widiyantoro et al., 2011).

Table 1. Identified active seismic sources within 250 km radius from Jakarta city.

Sources	Name	Mechanism	M_{max}	Length (km)	Activity Slip rate (mm/yr)	GR Parameter a	GR Parameter b
Fault	Cimandiri	Strike-slip	7.2	62.2	4	–	–
	Lembang	Strike-slip	6.6	34.4	1.5	–	–
	Semangko	Strike-slip	7.2	65	5	–	–
	Sunda	Strike-slip	7.6	150	5	–	–
	Kumering	Strike-slip	7.6	150	11.0		
Subduction	South Sumatra Megathrust	Reverse	9.0	–	–	5.76	1.05
	Java Megathrust	Reverse	9.0	–	–	6.14	1.1

the East Lampung fault (Semangko) and the Sunda Strait fault line.

In Java Island, the nearest fault sources which have been proven as active shallow crustal faults are the Cimandiri and Lembang faults. The Cimandiri fault is considered as an active fault based on micro earthquake monitoring and geomorphic expression instead of the slip rate calculation (Kertapati, 1984). Table 1 sumarizes the activity both for the fault and subduction zone influencing Jakarta city.

3 SEISMIC HAZARD ANALYSIS OF JAKARTA

Seismic hazard analysis is performed based on both probabilistic and deterministic approaches. The analysis is conducted using similar procedures used by the Team for Revision of Seismic Hazard Maps of Indonesia 2010 (Irsyam et al., 2010a, Irsyam et al., 2010b, Irsyam et al., 2011, Irsyam et al., 2013a, and Irsyam et al., 2013b). Seismic sources are devided into subduction, fault, and background zones by considering recurrence relationship that includes truncated exponential model, pure characteristic model, and combined models. Earthquake source parameters are derived based upon earthquake catalog, geological, and seismological information of active faults.

3.1 *Probabilistic seismic hazard analysis (PSHA)*

Three seismic source models are utilized in this analysis; fault zone, subduction zone, and gridded seismicity for shallow background and deep intraslab.

The source models were selected using seismogenic conditions, focal mechanisms and earthquake catalogs. This seismogenic conditions include geometry and geomorphological of tectonic plate such as faults and subduction zones.

The modeling of the subduction sources is conducted based on well-identified seismotectonic data such as location of subduction in latitude and longitude coordinates, slope of subduction plane (dip), rate, and b-value from historical earthquake catalogues, and limit depth of subduction zones. The subduction zone that is shallower than 50 km is considered as the Megathrust or interface zone, whereas, the earthquake occurence deeper than the Megathrust zones is classified as the Benioff zone and considered as deep background sources (Irsyam et al., 2013b).

Fault source is treated as a plane in 3-D space for calculation of distance from a site to a certain point at the plane. Parameters of fault required for input of PSHA include fault traces, focal mechanism, sliprate, dip, length and width of the fault. Location of each fault was determined based on information obtained from previous publications and relocated epicenters. The information was then used to trace each fault on the Shuttle Radar Topographic Mission (SRTM) that indicates geomorphology. Using this procedure, coordinate and length of each fault can be obtained. Other input data required for analysis was obtained from publications and technical discussions (Irsyam et al., 2010a and Irsyam et al., 2013b).

Gridded (smoothed) seismicity model are utilized to determine the rate of occurrence of small earthquakes on mapped faults and random earthquakes on unmapped faults (Petersen et al., 2008). This model is used to predict the likelihood of bigger earthquake for region in which lack of seismogenic data but has seismic activities report from small to moderate earthquakes.

A truncated-exponential or Gutenberg-Richter (Gutenberg and Richter, 1954) magnitude-frequency distribution between M5.0 and M6.5 is used to model rates for different sizes of earthquakes in every grid. The composite catalog was used as input for background seismicity and it was divided into five depth intervals, i.e. shallow earthquakes (0–50 km), intermediate earthquakes (50–100 km and 100–150 km), and deep earthquakes (150–200 km and 200–300 km) (Irsyam et al., 2010a, Irsyam et al., 2010b, Irsyam et al., 2011, and Irsyam et al., 2013b).

3.2 *Attenuation functions*

Based on the previous researches in the development of Indonesia seismic hazard maps (Irsyam et al., 2010a, Irsyam et al., 2011, and Irsyam et al., 2013) a number of attenuation functions from worldwide historical earthquake data record is adopted to estimate the ground shaking in Jakarta city.

Attenuation from Atkinson-Boore intraslab seismicity world data BC-rock condition (Atkinson and Boore, 1995), Geomatrix slab seismicity rock (Youngs et al., 1997), and Atkinson-Boore intraslab (Atkinson and Boore, 2003) were used for Benioff (deep background sources). Attenuation from Chiou-Young NGA (Chiou and Youngs, 2008), Boore-Atkinson NGA (Boore and Atkinson, 2008), and Campbell-Bozorgnia NGA (Campbell and Bozorgnia, 2008) were chosen for faults and background sources. Attenuation from Geomatrix subduction (Youngs et al., 1997), Atkinson-Boore BC rock and global Source (Atkinson and Boore, 2003) and Zhao et al., with variable Vs-30 (Zhao et al., 2006) were chosen for Megathrust zone (subduction interface).

3.3 *Seismic hazard level of Jakarta City*

Based on the earthquake sources listed on Table 1 and the attenuation function determined before, the PSHA is carried out to obtain the hazard level for Jakarta. The analysis considers two hazard levels; 10% and 2% probability of exceedance in 50 years. Figure 5 shows the distribution of peak ground acceleration (PGA) for Jakarta city. The value of PGA at bedrock ranges from 0.18–0.22 g and from 0.33–0.39 g for 10% and 2% probability of exceedance in 50 years.

3.4 *De-aggregation & time histories development*

The probabilistic seismic hazard analysis that was mentioned previously allows computation of the mean annual rate of exceedance at particular site location based on the cumulative risk from potential earthquake sources having different magnitude occurring at different source-site distance. The computed rate of exceedance is not associated with any particular earthquake magnitude or source-site distance. In order to estimate the most likely earthquake magnitude and the most likely source-site distance, de-agregation process is conducted. The process requires that the mean annual rate be expressed as a function of magnitude and distance (the representing/controlling earthquakes). The results of de-agregation is then used to select existing ground motion records, which recorded in earthquake of similar magnitude and at similar source-site distance. The de-aggregation results are summarized in Table 2.

The seismic hazard curves for PGA, 0.2 and 1.0 second spectral period are developed and de-aggregated to obtain representing magnitudes and distances for return periods of 500 and 2500 years for Jakarta city. Selection of input motions is conducted based on the magnitude and distance in Table 2. Modified time histories are then generated based on recorded ground motion from previous historic earthquake event and estimated target spectrum at bedrock using the spectral matching method proposed by Abrahamson (1998).

3.5 *Deterministic seismic hazard analysis*

In addition to probabilistic approach, deterministic seismic hazard analysis (DSHA) is also performed

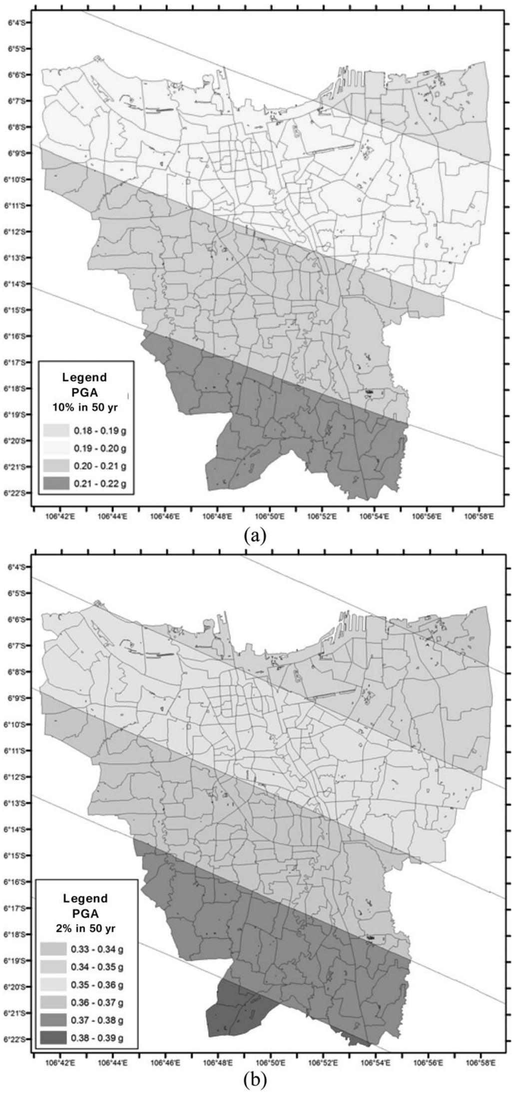

Figure 5. Contour of PGA value at bedrock in Jakarta city with (a) 500 yr return period and (b) 2500 yr return period.

in the development of seismic micro-zonation maps of Jakarta. DSHA for Jakarta is carried out first by selecting the matrix combination of magnitude and distance to represent earthquake scenarios due to earthquake sources surrounding Jakarta. The matrix is used as a basis to choose appropriate ground motion from worldwide historical earthquake records.

Each of scenarios for a specific earthquake source with certain magnitude and distance is represented by appropriate time-histories of ground motion records for input motions in shear wave propagation analysis. Historical earthquake records with magnitude ranging from 5.0 to 7.0 and distance from 20 km to 60 km are collected for crustal fault. The scenarios for subduction sources including deep intraslab utilize various historical earthquake with magnitude ranging from 7.0–9.0 and distance ranging from 150–450 km. Site response analysis using 1-D shear wave propagation procedure is then conducted once the input motions corresponding to a specific earthquake scenario are selected.

4 GEOLOGICAL & GEOTECHNICAL CONDITION OF JAKARTA CITY

Based on the geological map of Jakarta and Seribu Islands Quadrangle, Java (Turkandi et al., 1992), the Great Jakarta city area are founded on Quaternary sediments which are consists of river to coastal alluvium deposits, beach ridge sediments, alluvium fan deposits and volcanic tuff. These sediments occupy the whole of thick sedimentary basin knowing as the Ciputat Sub-Basin (Fachri et al., 2002), which bordered by Tinggian Tangerang to the west, Tinggian Rengasdengklok to the east and the Bogor Antiklinorium zone to the south.

The sediment thickness in this area may locally reach more than 500 m and unconformably overlying the older Tertiary sediment formation, such as Serpong Formation, Genteng Formation, Kaliwangu Formation, Subang Formation, Parigi Formation, Bojongmanik Formation and Jatiluhur Formation as shown in Figure 6.

Table 2. De-aggregation results of Jakarta city for various return period.

		Megathrust		Shallow crustal		Benioff	
Return Period	Period	Magnitude	Distance	Magnitude	Distance	Magnitude	Distance
years	sec	(M_w)	(km)	(M_w)	(km)	(M_w)	(km)
500	PGA	8.07	113.04	5.90	55.23	6.78	120.88
	0.2 s	8.05	191.44	5.94	58.07	6.71	122.79
	1.0 s	8.05	202.32	6.47	70.62	6.96	134.01
2500	PGA	8.03	165.78	5.96	45.19	7.03	112.87
	0.2 s	8.09	189.51	5.97	47.38	6.91	111.07
	1.0 s	8.11	199.80	6.41	49.56	7.16	117.38

4.1 *Identification of engineering bedrock of Jakarta*

The depth of engineering bedrock is one of required parameters used to perform the site response analysis. Because of the location of bedrock of Jakarta is not well identified until now, therefore, investigation of bedrock depth is urgently required. Microtremors array survey has becomed an effective method to estimate engineering bedrock based on S-wave velocity structures because it is very simple in the field operation and without active sources. Analysis of dispersion curve of microtremors can be performed by Spatial Auto-Correlation (SPAC) method which was developed by Aki (1957) and expanded by Okada (1998) on the circular array with distance r between two stations. The microtremor study is expected to provide the estimation of depth at which the material is measured its shear wave velocity.

Ridwan et al., (2013) applied microtremors array to obtain the 1D and 2D S-wave velocity profiles in some locations in Jakarta. Estimation of the bedrock depth in Jakarta is based on S-wave velocity parameters. The spatial autocorrelation method was used to estimate dispersion curves, while S-wave velocity structure is derived by genetic algorithm. The result of 2D construction of S-wave velocity structure shows stratigraphy cross section that consists of four layers, where the bedrock depths in northern Jakarta can be depicted in the range from 518 m to 542 m and in the southern part is in the range from 359 m to 398 m (Ridwan et al., 2014). Figure 7 show the location of instrumentation in Jakarta city and the contour map showing the depth of recorded shear wave velocity greater than 750 m/s.

Reffering to the Geological condition in Jakarta where layers thickness increases to the North, hence, microtremors survey was designed in one line from the South to the North across Jakarta. The triangular arrays configuration was used for each sites by using 4 instrument and the time duration for microtremors data record was 1–2 hours for each array. 1D S-wave velocity profile resulted by individual inversion was used to construct 2D profile after conducted second inversion. The results of microtremors array analysis shows that the subsurface models for Jakarta consist of four layers where engineering bedrock can be estimated at the forth layers (359–608 m depth) as shown in Figure 8.

4.2 *Soil condition of Jakarta city*

Site characterization is carried out by interpreting the results of field measurements including in-situ testing such as standard penetration test (SPT), Dutch cone penetration test (DCPT), shear wave velocity measurement using seismic downhole test and laboratory tests. Field and laboratory data are obtained by collection

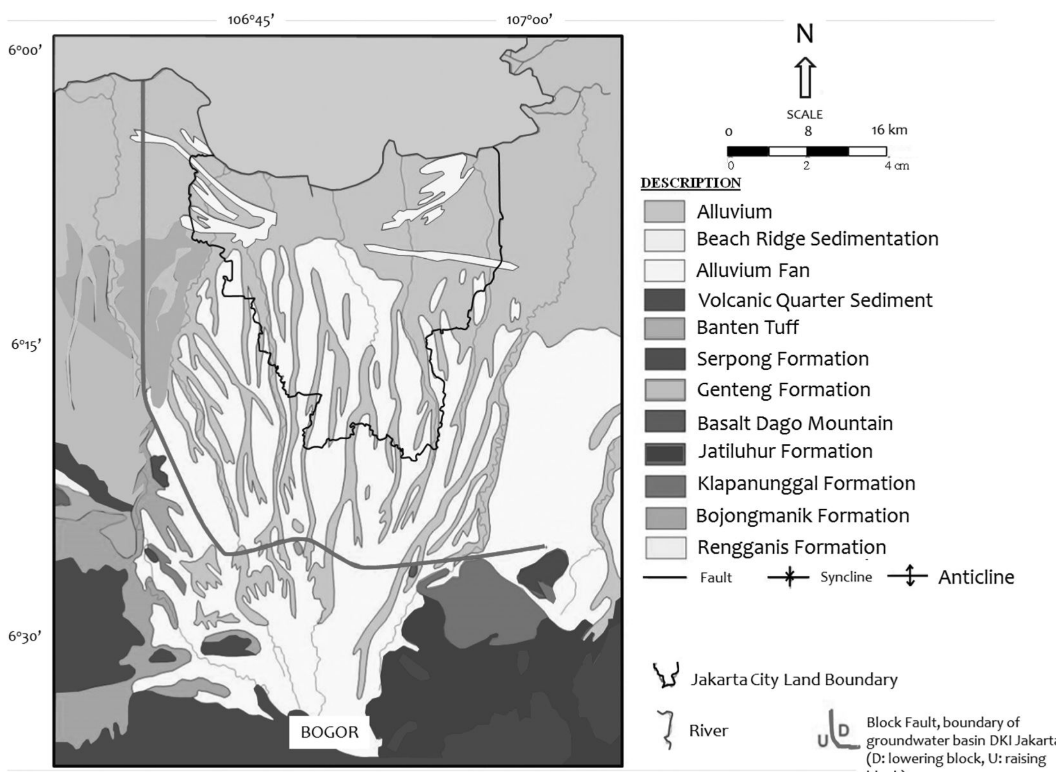

Figure 6. Geological map of the Greater Jakarta Area and surrounding Area (After Fachri et al., 2002).

of previous soil investigation results conducted previously by various consultants and by performing new additional soil investigation conducted by the Government of Jakarta. Figure 9 shows the distribution of borehole points in all part of Jakarta city used for the development of seismic microzonation maps.

Further study to identify the dynamic soil properties is also conducted to encounter limited data of shear wave velocity profiles in Jakarta. An empirical correlation between N-SPT with shear wave velocity has been developed based on 42 borehole points from 22 different location in Jakarta. The borehole data is

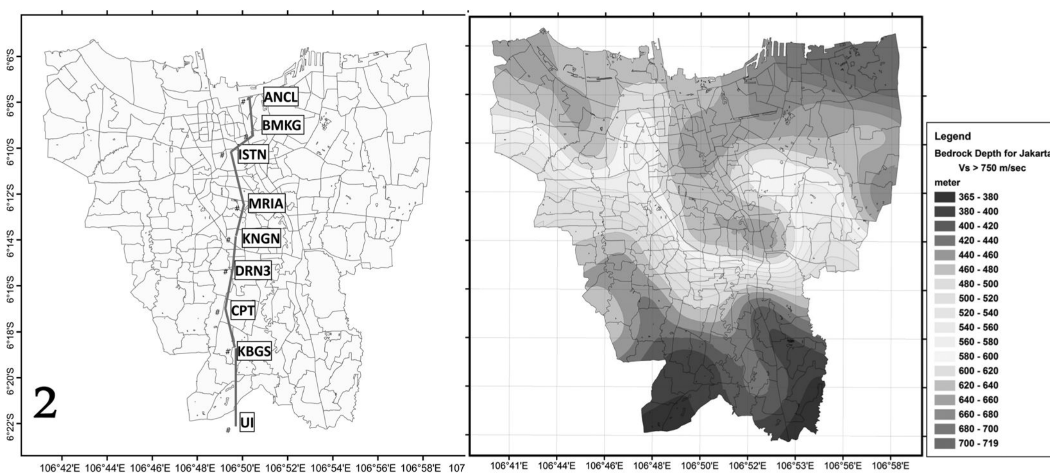

(a) (b)

Figure 7. Microtremor measurement to identify engineering bedrock in Jakarta (Ridwan et al., 2013); (a) Location of Instrumentation.; (b) Contour map of depth of engineering bedrock (Vs > 750 m/s) identified by microtremor array.

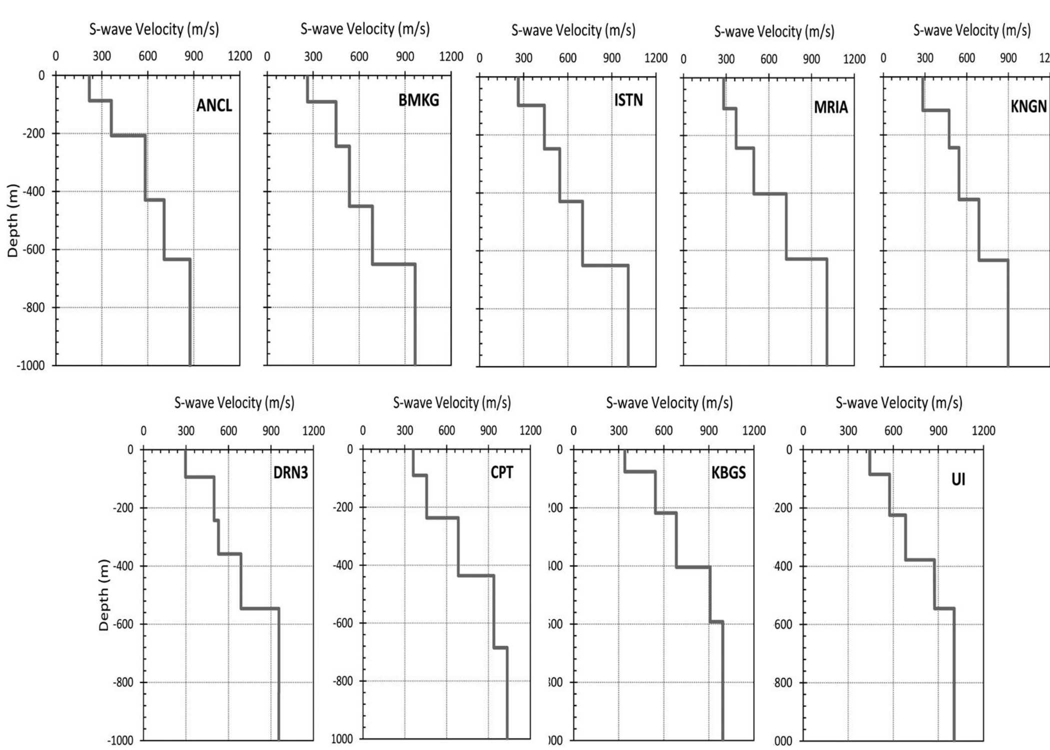

Figure 8. Shear wave velocity profile across Jakarta from the North to the South that shows the estimated engineering bedrock. (Ridwan et al., 2013).

collected from high rise building projects spread across the city and the data is plotted in Figure 10.

Figure 10 indicates that the correlation between N-SPT with shear wave velocity is quite scatter. It shows

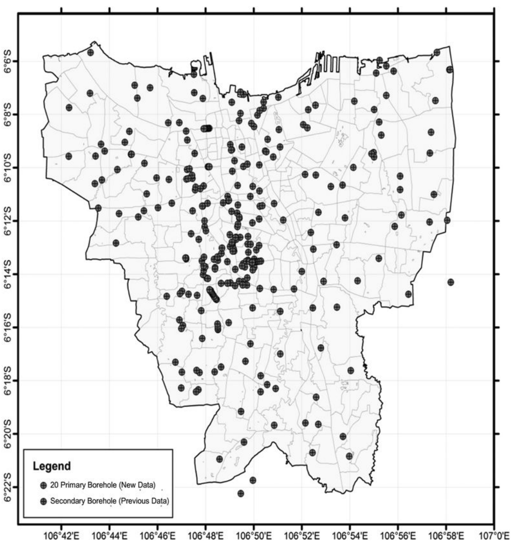

Figure 9. Distribution of borehole points in Jakarta city for site response analysis.

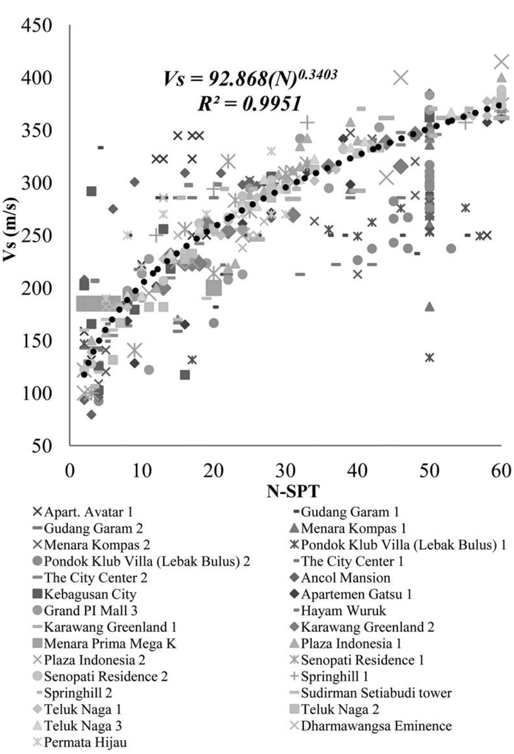

Figure 10. Variation of V_s (m/s) and N-SPT value in several locations in Jakarta (after Yunita, 2013).

that the tendency of plotted data is eligible as a basis to develop the empirical equation to estimate shear wave velocity value. The shear wave velocity profile in other borehole is etimated based on this empirical equation shown in Figure 10. Based on the result developed by Yunita (2013), the result show that the equation proposed by Imai and Tonouchi (1982) is the closest relationship for shear wave velocity estimation based on N-SPT value for Jakarta city.

Site classification study for Jakarta is performed based on the N-SPT_{30} according to the NEHRP site classification standard as shown in Figure 11. The study show that most of location in Jakarta city is classified as the soft soil site (SE) and medium soil (SD) with N-SPT value less than 15 and ranging from15 to 30 respectively.

4.3 *Fragility curves*

In this study, the seismic risk is considered only for building, neglecting the impact on people. With this definition, the seismic risk is obtained by the convolution of seismic hazard and building vulnerability only. Building vulnerability is considered for different building typologies and is represented using fragility curves.

Fragility curves have been derived for two types of low rise buildings that dominate the residential building population in Jakarta, i.e. confined masonry and in-filled frame structures in this study. The fragility curves are derived based on FEMA 154 procedures for different levels of damage (i.e. Slight, Moderate, Extensive and Complete Damages) and the ground motion severity in these curves are expressed in terms of Peak Surface Acceleration (PSA) shown in Figure 12. The fragility curves allow the estimation of the probability of reaching or exceeding certain levels of damage ($P(x \geq X)$ for a given PSA. These fragility curves are later applied to each area in Jakarta to determine the vulnerable area at which the building type distribution is known. Building types distribution in the area considered is obtained through building survey.

5 RESULTS & DISCUSSION

The results of the seismic microzonation study of Jakarta city include: probabilistic and deterministic peak acceleration, amplification factors, spectral acceleration, and hazard level at ground surface; and risk maps for Jakarta city. The work is still on going and is expected to be completed next year. Tentative results are presented in the following paragraphs.

5.1 *Seismic hazard microzonation*

Site response analysis is conducted to obtain peak acceleration, amplification factors, spectral acceleration, and hazard level at ground surface due to

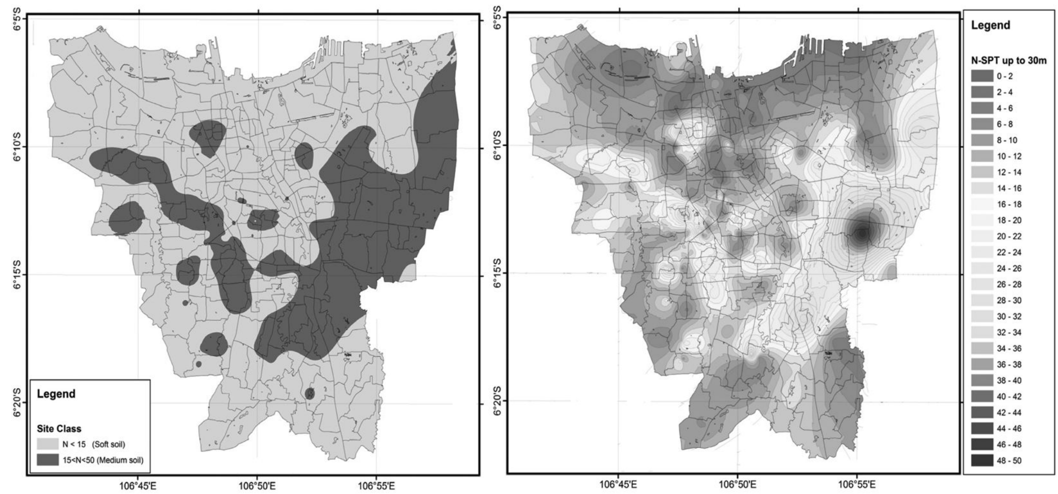

(a) (b)

Figure 11. Site classification study in Jakarta city based on N-SPT value; (a) Site classification based on NEHRP classification. (b) Contour map of N-SPT_{30} value in Jakarta city.

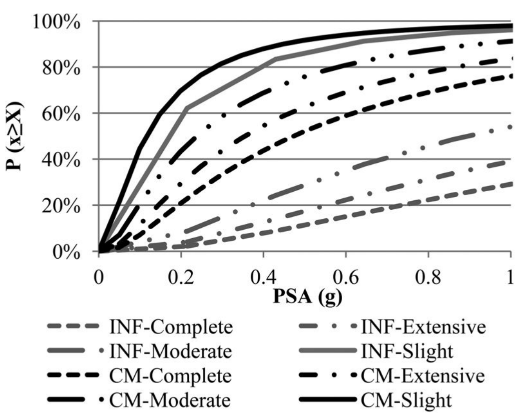

Figure 12. Fragility curves for In-Filled Frame (INF) and Confined Masonry (CM).

ground motions at bedrock obtained from probabilistic and deterministic seismic hazard analysis. The site response analysis is performed based on the 1-D non linear wave propagation procedure using the constitutive model proposed by Iwan and Mroz (1967) and by utilizing the free software NERA (Bardet & Tobita, 2001). Figure 13.a and b present the site amplification factor due to ground motions from fault source with magnitude M = 6.5 and distance R = 20 km and megathrust source with magnitude M = 9.0 and distance R = 200 km. The maps indicate that the amplification factor ranges from 0.8 to 2.2 and at the center of Jakarta where most of major high rise buildings are located the value varies from 1.2 to 1.6.

Figure 14.a shows peak surface acceleration due to ground motions from fault source with magnitude M = 6.5 and distance R = 20 km. The peak acceleration at ground surface varies from 0.14 to 0.24 g for fault sources. Figure 14.b present probabilistic peak surface acceleration for 2500 years earthquake occurence period where the peak acceleration at ground surface ranges from 0.2 to 0.4 g.

5.2 *Seismic risk microzonation*

The seismic risk microzonation maps is developed by combining the seismic hazard with the building fragility. Figures 15–16 show the examples of the maps of seismic risk microzonation, for example, in East Jakarta (Cipayung and Duren Sawit Districts). The seismic scenario used is the deterministic shallow crustal earthquake, with magnitude M = 6.5 and distance R = 20 km. Due to this earthquake, the PSA in East and North Jakarta is in between 0.12–0.26 g. The color scale in Figures 15–16 is different for each risk level it is divided into 5 risk level start from the Very High (Brown), High (Red), Medium (Orange), Low (Yellow) and Very Low (Green).

It can be seen from those figures the different seismic risk levels in Jakarta due to the seismic scenario applied. These seismic risk maps can be useful instrument for risk reduction or disaster mitigation program in Jakarta. These maps can be used for establishing intervention priorities for population of buildings in certain area in the city, in order to reduce the risk.

6 CONCLUSION

The development of seismic microzonation hazard and risk map have been carried out for Jakarta city as the

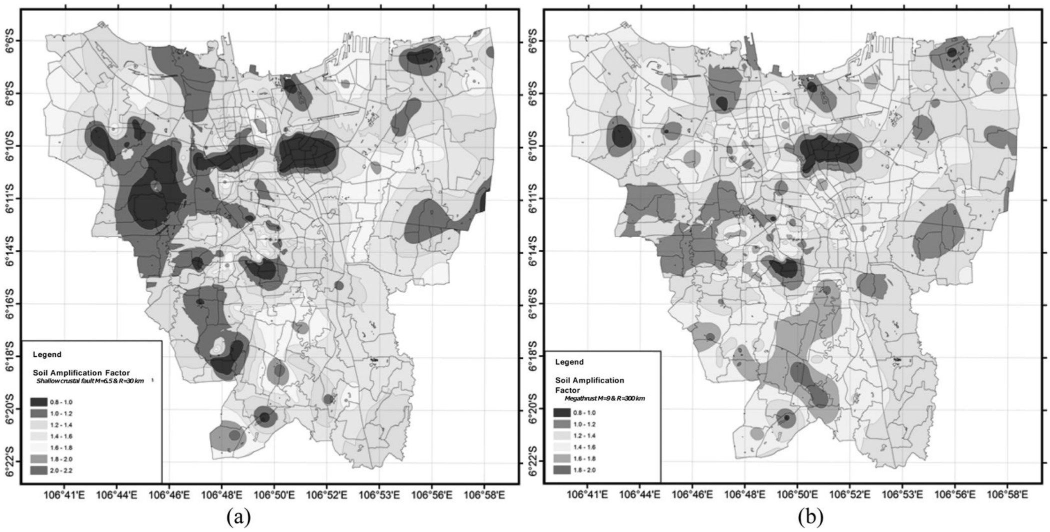

Figure 13. Contour map of deterministic amplification factor for: (a) Scenario-30, fault sources with $M_w = 6.5$ and $R = 20$ km; (b) Scenario-36, megathrust sources with $M_w = 9.0$ and $R = 200$ km.

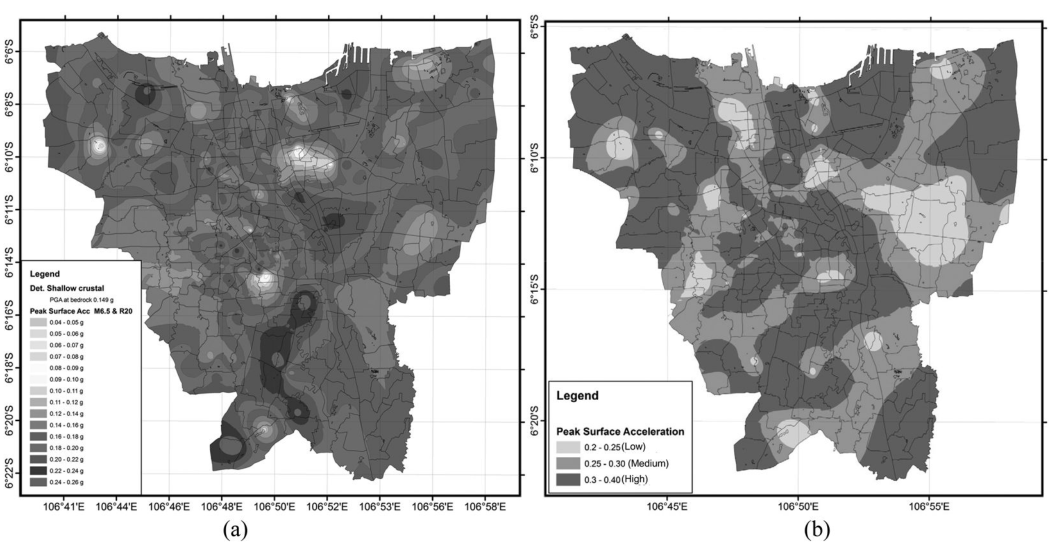

Figure 14. Contour map of; (a) Peak Surface Acceleration (PSA), Scenario-30, fault sources with $M_w = 6.5$ and $R = 20$ km; (b) Probabilistic Peak Surface Acceleration with 2% probability of exceedance in 50 years.

capital city of Republic Indonesia. The study includes the identification of major seismic sources influencing Jakarta city, probabilistic and deterministic seismic hazard analysis (using worst case earthquake scenario), de-aggregation & probabilistic time histories development, the identification of engineering bedrock by using microtremor array, site characterization and interpolation of soil dynamic properties, ground response analysis and estimation of the soil amplification factor and peak surface acceleration. Moreover, the seismic risk mapping in micro-scale of every part in the Jakarta city (district scale) is developed by identification of building typologies, formulating fragility curves for different building typologies, determination of the vulnerable area for each building type distribution in every district, and calculating the seismic risk. This study then is expected as a basic consideration for disaster preparedness to the government in planning further land planning and development of Jakarta city.

Figure 15. Seismic Risk Map in Cipayung District, East Jakarta.

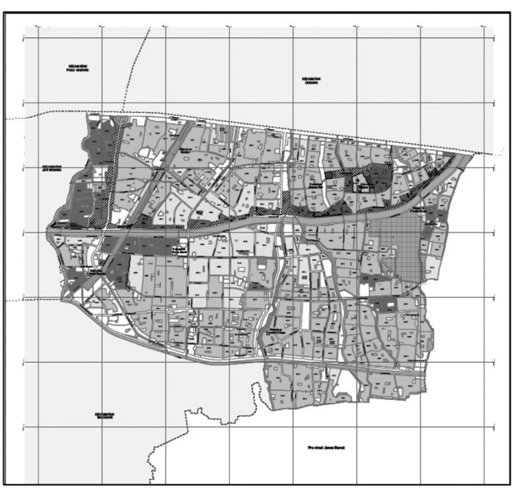

Figure 16. Seismic Risk Map in Duren Sawit District, East Jakarta.

ACKNOWLEDGEMENT

The authors want to express grateful thanks to Dedy-Dharmawansyah and Partogi Simatupang for their supports in this research and also to Department of Industry and Energy – Government of Jakarta; Institut Teknologi Bandung, the Ministry of Public Works; Bureau of Meteorology, Climatology and Geophysics; National Disaster Management Agency; Ministry of Energy and Mineral Resources; Ministry of Research & Technology; and Australian National University through Australia-Indonesia Facility for Disaster Reduction for their supports and assistances during this study.

REFERENCES

Abrahamson, N.A. (1998). Non-Stationary Spectral Matching Program RSPMATCH. PG&E Internal Report, February.

Aki, K. (1957). Space and Time Spectra of Stationary Stochastic Waves, with Special Reference to Microtremors. *Bulletin of the Earthquake Research Institute*, University of Tokyo, 35, 415–456.

Atkinson, G.M., dan Boore, D.M, (2003), Empirical Ground-Motion Relations forSubduction-Zone Earthquakes and Their Application to Cascadia and OtherRegions, *Bulletin of the Seismological Society of America, Vol. 93, No. 4*, pp 1703–1729.

Bardet, J.P. and Tobita, T. (2001) : NERA A Computer Program for Nonlinear Earthquake site Response Analyses of Layered Soil Deposits, Departement of Civil Engineering University of Southern California.

Bird, P., (2003), An updated digital model of plate boundaries: *Geochemistry, Geophysics, Geosystems*, v. 4, no. 3, 1027, doi:10.1029/2001GC000252,

Bock, Y., et al., (2003), Crustal motion in Indonesia from Global Positioning System measurements, *Journal of Geophysical Research*-Solid Earth, 108, 2367.

Boore, D.M., and Atkinson, G.M., (2008), Ground-motion prediction equations for the average horizontal component of PGA, PGV, and 5%-damped PSA at spectral periods between 0.01 s and 10.0 s: *Earthquake Spectra, v. 24*, no. 1.

Campbell, K.W., and Bozorgnia, Y., (2008), Ground motion model for the geometric mean horizontal component of PGA, PGV, PGD and 5% damped linear elastic response spectra for periods ranging from 0.01 to 10.0 s: Earthquake Spectra, v. 24, no. 1.

Chiou, B., and Youngs, R., (2008), A NGA model for the average horizontal component of peak ground motion and response spectra: *Earthquake Spectra, v. 24*, no. 1.

Engdahl, E. R., Villasenor, A., DeShon, H. R., dan Thurber, C. H., (2007): Teleseismic Relocation and Assessment of Seismicity (1918–2005) in The Region of The 2004 Mw 9.0 Sumatra–Andaman and 2005 Mw 8.6 Nias Island Great Earthquakes, *Bull. Seismol. Soc. Am., 97*, S43–S61.

Fachri, M., Djuhaeni., Hutasoit, M. L. and Ramdhan, M. A., (2002). Stratigraphy and hydrostratigraphy of Jakarta Groundwater Basin. *Buletin Geologi, Vol. 34*, No. 3, pp. 169–189.

FEMA 154. (2002). Rapid Visual Screening of Buildings for Potential Seismic Hazard, 2nd Edition. NEHRP. Washington,DC, USA.

Hamilton, W., (1979). Tectonics of the Indonesian region, U.S. *Geol. Survey Prof. Paper*, 1078, 345 pp.

Imai, T., Tonouchi, K. (1982): Correlation of N-value with S-wave Velocity and Shear Modulus, *Proceeding of The 2nd European Symposium of Penetration Testing, Amsterdam*, 57–72.

Iwan, W.D. (1967): On A Class of Models for The Yielding Behavior of Continuous and Composite Systems, *Journal of Applied Mechanics*, ASME, Vol. 34:612–617.

Irsyam, M., Subki B., Himawan A., Suntoko H., (1999), Analisis Seismisitas untuk Semenanjung Muria, Prosiding Konferensi Nasional Rekayasa Gempa, Pemanfaatan Perkembangan Rekayasa Kegempaan dalam Rangka Penyempurnaan Peraturan dan Peningkatan Kepedulian Masyarakat Terhadap Bencana Gempa di Indonesia, hal VI-9–VI-20.

Irsyam, M., Dangkua, D.T., Hendriyawan, Hoedayanto, D., Hutapea, B.M., Kertapati, E., Boen, T., Petersen, M.D.

(2008), Proposed Hazard Seismic Maps of Sumatera and Java Islands and Microzonation Study of Jakarta city, Indonesia,*Journal of Earth Science System, 117,* S2, November.

Irsyam, M., Asrurifak, M., Hendriyawan, Budiono, B., Triyoso, W., Merati, M., Sengara, I.W., and Firmanti, A., (2009), Development of Spectral Hazard Map for Indonesia Using Probabilistic Method by Considering Difference Values of Mmax for Shallow Background Sources, *The 1st International Seminar on Sustainable Infrastructure and Built Environment in Developing Countries*, Bandung, November.

Irsyam, M., Sengara, I.W., Asrurifak, M., Ridwan, M., Aldiamar, F., Widiyantoro, S., Triyoso, W., Natawijaya, D.H., Kertapati, E., Meilano, I., and Suhardjono (2010a), Summary: Development of Seismic Hazard Maps of Indonesia for Revision of Seismic Hazard Map in SNI 03-1726-2002, *reseach report submited to the Ministry of Public Works by Team for Revision of Seismic Hazard Maps of Indonesia*, July.

Irsyam, M., Asrurifak, M., Hendriyawan, Budiono, B., Triyoso, W., and Firmanti, A., (2010b), Development of Spectral Hazard Maps for Proposed Revision of Indonesia Seismic Building Code, *Geomechanics and Geoengineering an International Journal*, Vol. 5. No. 1.

Irsyam, M., Hendriyawan, Asrurifak, M., Razali, R., Fermanti, A. (2011), Combined Hazards: Seismic Hazard maps of Indonesia and Geotechnical and Tsunami Hazard Assessment for Banda Aceh, Chapter 8 of '*Geotechnical and Earthquake Geotechnics towards Global Sustainability*' edited by Susumu Iai, ISBN 978-94-007-0469-5, Springer.

Irsyam, M., Hendriyawan, Asrurifak, M., Ridwan, M., Aldiamar, F., Sengara, I.W., Widiyantoro, S., Triyoso, W., Natawijaya, D.H., Kertapati, E., Meilano, I., Suhardjono, and Firmanti, A. (2013), Past Earthquakes in Indonesia and New Seismic Hazard Maps for Earthquake Design of Buildings and Infrastructures, Chapter 3 of part 1 of '*Geotechnical Predictions and Practice in Dealing with Geohazards*' edited by Chu, Jian, Wardani, S.P.R., and Lizuka, A., due April 2013, ISBN 978-94-007-5674-8, Springer.

Katili, J., and F. Hehuwat (1967). On the occurrences of large transcurrent faults in Sumatra, Indonesia. J. Geosci., Osaka City Univ., 10, 5–17.

Kennett, B. L. N., Engdahl, E. R. & Buland, R., (1995). Constraints on seismic velocities in the Earth from travel times, *Geophys. J. Int., 122*, 108–124.

Kertapati, E.K. (1984), Studi Seismotektonik Selat Sunda, Prosiding Pertemuan Ilmiah tahunan IAGI, Bandung.

Mroz, Z. (1967): On The Description of Anisotropic Workhardening, *Journal of Mechanics and Physics of Solids*, Vol.15: 163–175.

Okada, H. (1998), Microtremors as an Exploration Method. Geo¬exploration Handbook, Vol. 2, *Society of the Exploration Geophysicists of Japan*.

Pesicek, J. D., Thurber, C. H., Zhang, H., DeShon, H. R., Engdahl, E. R. & Widiyantoro, S., (2010). Teleseismic Relocation of Earthquakes along the Sumatra-Andaman Subduction Zone, *J. geophys. Res.*

Petersen, Mark D., Mueller, Charles S., Frankel, Arthur D., Zeng, Yuehua, (2008), Spatial Seismicity Rates and Maximum Magnitudes for Background Earthquakes, USGS Open-File Report.

Ridwan, M., Widiyantoro,S., Afnimar, Irsyam, M., (2013) Identification of Engineering Bedrock in Jakarta by Using Array Observations of Microtremors. *3rd International Symposium on Earthquake and Disaster Mitigation*, Procedia Earth and Planetery Scienc Elsevier.

Ridwan, M (2013) Personal Communication

Sieh, K., and Natawidjaja, D. (2000). Neotectonics of the Sumatran fault, Indonesia. *Journal of Geophysical Research*, 105, 28, 295–28, 326.

Turkandi, T., Sidarto, Agustyanto, D.A. and Hadiwidjoyo, M.M.P., (1992). Geological Map of Jakarta and Seribu Islands Quadrangle, Java. *Geological Research and Development Center*, Bandung.

TC-4 Committee of the Internation Society of Soil Mechanics and Geotechnical Engineering (ISSMGE). (1999). "Manual for Zonation on Seismic Geotechnical Hazards", The Japanese Geotechnical Society, Tokyo, Japan.

Widiyantoro, S., Pesicek, J.D., Thurber, C.H., (2011). Subducting slab structure below the eastern Sunda arc inferred from non-linear seismic tomographic imaging. *Geological Society, London, Special Publications*; v. 355; p.139–155 doi: 10.1144/SP355.7

Youngs, R.R., Chiou, S.J., Silva, W.J., dan Humphrey, J.R., (1997), Strong ground motion attenuation relationships for subduction zone earthquakes. *Seismol. Res. Lett.* 68, 58–73.

Yunita, H (2013), Studi efek Kondisi Tanah Lokal dan Sumber Gempa Dalam Analisis Respons Dinamik Tanah dan Implementasinya Dalam Pembuatan Peta Mikrozonasi Kota Jakarta. *Doctoral Thesis*. Institut Teknologi Bandung, Bandung, Indonesia.

Zhao John X., Zhang, J., Asano, A., Ohno, Y., Oouchi, T., Takahashi, T., Ogawa, H., Irikura, K., Thio, H., dan Somerville, P., (2006), Attenuation Relations of Strong Motion in Japan using site classification based on predominant period, *Bull. Seismol. Soc. Am.,* 96, 898.

This page intentionally left blank

Geotechnics for Catastrophic Flooding Events – Iai (Ed)
© 2015 Taylor & Francis Group, London, ISBN 978-1-138-02709-1

Use of biogeotechnologies for disaster mitigation

J. Chu & V. Ivanov
Iowa State University, USA

J. He & M. Naeimi
Nanyang Technological University, Singapore

ABSTRACT: In this paper, the principles of microbial geotechnologies are discussed. Studies for the establishment of three different applications of the microbial methods to disaster mitigation or rehabilitation are presented. These include biogas desaturation method for mitigation of soil liquefaction which may become the most cost-effective method for the reduction of liquefaction risks; bioshotcrete method for levees to prevent erosion and seepage failure; and biogrouting method for road construction and repair using biogrout made of waste materials. Although biogeotechnological based methods have not been commonly adopted for real disaster mitigation projects yet, it offers many advantages over the existing methods in terms of both costs and simplicity in construction and thus have the potential to become a major geotechnological approach for both soil improvement and hazard mitigation in the future.

1 INTRODUCTION

We have entered into an era where dealing with disasters becomes a routine task rather than a special requirement. There is an urgent need to enhance our disaster mitigation and rehabilitation capabilities so our infrastructures and constructed facilities can be better protected. We also need more cost-effective solutions to allow disaster mitigation measures to be applied to a larger area within a limited budget. For example, liquefaction has long been identified as one of the major hazards as seen in the recent earthquake disasters in New Zealand and Japan. However, ground treatment for mitigation of liquefaction hazard is normally only carried out for sites where important infrastructures such as sea ports and airports are constructed. This is because the cost involved in ground treatment for liquefaction is high. If a much cheaper liquefaction mitigation method can be developed, ground treatment for liquefaction can thus be applied over a wider range of projects to reduce the impacts of the damages associated with liquefaction.

New methods or new technologies come from new research and new developments. Thus the role of research and innovation for the improvement of the disaster mitigation capability cannot be over emphasized. Geotechnical constructions involve in the use of materials for construction and the construction process itself. Therefore, the areas where innovation will play an important role are likely to be the use of new materials and the use of alternative construction processes. For disaster mitigation or rehabilitation projects, costs of the materials and speed of construction become important considerations. We need to use inexpensive materials as much as possible to bring down the cost and at the same time to complete the project as quick as possible to save life or reduce the suffer or inconvenience experienced by the people affected by disasters. Another consideration is to use as less heavy equipment as possible as mobilization of heavy machines may be difficult in disaster affected areas. To be innovative in materials and construction processes, one needs to draw ideas from other disciplines. It will be shown by examples how microbial technologies can be adopted in geotechnologies and how new technologies and methods can be developed through interdisciplinary studies and benefit geotechnical engineering as a whole.

In this paper, a new biogeotechnological based liquefaction mitigation method is presented. This new method is only part of a new development in the new interdisciplinary area of biotechnologies, in particular, the microbial technologies. In addition to this liquefaction mitigation method, a few other biotechnological based methods that could be applied for disaster mitigation and rehabilitation will also be presented. These include the use of biogrouting for prevention of levee failure due to overtopping and erosion; construction of temporary water storage pond in sandy soil; and road repair using biogrout made of waste. Some of the methods presented here are still new and needed to be developed further before they can be used in practice. Nevertheless, any great technology starts from a less than perfect method and then gets improved with time. One of the main objectives of this paper is to share some of the ideas and new attempts so more people may start to be interested in these methods and adopt them in the projects in the future. In this way, we will have a better chance to turn some of the ideas into sound technologies and make some positive social and economic impacts.

2 PRINCIPLES OF MICROBIAL GEOTECHNOLOGY

One of the common approaches to improve the engineering properties of soft or weak soil is to use cement or chemicals to increase the shear strength of soil. The same approach can be used to reduce the water conductivity of soil or the rate of water flow in soil. However, the use of cement or chemicals for construction or soil improvement is not sustainable in the long run as cement or chemicals require a considerable amount of natural resource (for example limestone) and energy to produce. The production process also generates carbon dioxide, dust and possibly other toxic substances and thus is not environmentally friendly. The use of cement or chemicals for soil improvement is also expensive and time consuming. Using the latest microbial biotechnology, a new type of construction material, biocement, has been developed as an alternative to cement or chemicals (Whiffin, 2004; Ivanov and Chu, 2008). Biocement is made of naturally occurring microorganisms at ambient temperature and thus requires much less energy to produce. It is sustainable as microorganisms are abundant in nature and can be reproduced easily at low cost. The microorganisms that are suitable for making biocement are non-pathogenic and environmentally friendly. The application of microbial biotechnology to construction may also simplify some of the existing construction processes. For example, the biocement can be in either solid or liquid form. In liquid form, the biogrout has much lower viscosity and can flow like water. Thus, the delivery of biocement into soil is much easier compared with that of cement or chemicals. Furthermore, when cement is used, one has to wait for 28 days for the full strength to be developed, whereas when biocement is used, the reaction time can be much reduced if required.

The principle of microbial treatment is to use the microbially-induced calcium carbonate precipitation or other approaches to produce bonding and cementation in soil so as to increase the strength and reduce the water conductivity of soil. A number of studies have been carried out in recent years (Mitchell and Santamarina, 2005; Ivanov and Chu, 2008; Van der Ruyt and van der Zon, 2009; Van Paassen et al., 2010). Much of the work still stays at the experimental stage. However, the scale of treatment has increased rapidly with time and has reached 100 m^3 in the recent years (Van Passen et al., 2010).

The microbiological processes induce calcium carbonate crystals, other minerals or slimes as illustrated by examples shown by Van der Ruyt and van der Zon (2009), Van Paassen et al., (2010) and Chu (2012). Those minerals or slimes act as cementing agencies between sand grains to increase the shear strength of soil and/or to fill in the pores in soil to reduce the water conductivity as illustrated schematically in Figure 1. The two processes to increase strength and reduce conductivity have been called biocementation and bioclogging respectively (Ivanov and Chu, 2008). The process to deliver the biocement in-situ to achieve biocementation or bioclogging is called biogrouting. The materials used to produce biocementation or bioclogging effect are called biocement. The existing study so far shows that the biocement method is effective in both increasing the shear strength and reducing the water conductivity of soil. Normally bonding materials to produce biocementation will also reduce the permeability of soil at the same time due to the reduction in the pore space. However, there are biocements that will only produce biocement or bioclogging only. The viscosity of biogrout is generally as low as water. So it is possible to pump the biogrout into ground without mixing for sandy soil. This will enable the construction process to be simplified.

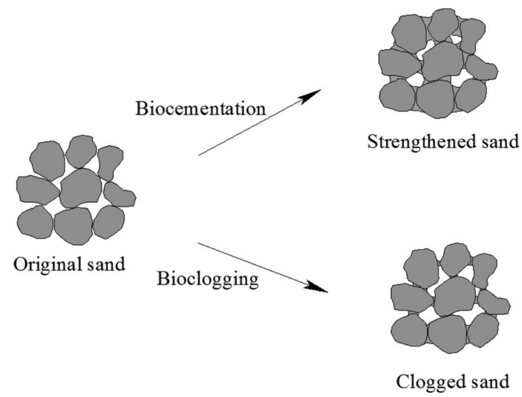

Figure 1. Schematic Illustration of (a) biocementation and (b) bioclogging process.

There are also other processes for microbial treatment such as the generation of slime for biopolymer for bioclogging. Another microbial process is the generation of biogas which can also be used beneficially for geotechnical problems as illustrated in the next section.

The biogrouting methods have the following advantages:

1) Biocement is produced at ambient temperature and thus requires much less energy to produce;
2) Biogrout has much lower viscosity and can flow like water;
3) It is sustainable as bacteria can be reproduced easily at low cost;
4) The bacteria that are used for biocement are non-pathogenic and environmentally friendly.

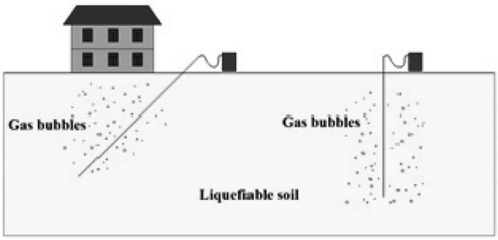

Figure 2. Mitigation of soil liquefaction by air injection.

3 BIOGAS DESATURATION FOR MITIGATION OF LIQUEFACTION

Soil liquefaction often occurs in sandy soil during earthquake. It is one of the major causes for earthquake related disasters. More recently liquefaction was largely responsible for extensive damage to residential properties in the eastern suburbs and satellite townships of Christchurch, New Zealand during the 2010 Canterbury earthquake and more extensively again following the Christchurch earthquakes that followed in early and middle 2011. The common methods that can be adopted for mitigation of liquefaction include the following four broad categories: (1) Replacement or physical modification; (2) Densification; (3) Pore water pressure relief; and (4) Foundation reinforcement, as summarized by Chu et al., (2009). However, it is difficult to treat ground for the purpose of mitigation of liquefaction because the scale of the ground to be treated is normally huge and thus too expensive to be implemented. Therefore, there is a need for more cost-effective solutions for liquefaction treatment.

A new approach for the mitigation of liquefaction potential of sand is to introduce gas bubbles into potentially liquefiable, saturated sand. The main cause of liquefaction is the generation of pore water pressure. Several studies (e.g., Okamura et al., 2006; Yegian et al., 2007) have shown that when saturated sand is made slightly unsaturated (with a degree of saturation between 85 to 95%) by inclusion of gas bubbles, the excess pore water pressure generated in soil under a dynamic load will be greatly reduced.

However, it is difficult to introduce gas into ground to maintain the sand desaturated for a long time. This is because the gas bubbles tend to dissolve in water or escape from the ground over time. Pumping can be used as illustrated conceptually in Fig. 2. However, the distribution of gas bubbles introduced by pumping will not be even. Furthermore, the gas pumped into ground tends to present in the form of aggregated gas pockets rather than individual bubbles. As a result, the sizes of the gas bubbles or aggregates are not small enough to be kept in the ground for a long period of time.

One innovative way to overcome the above problems is to generate tiny gas bubbles in-situ using microorganisms. This method is promising as it has the following three advantages: (1) It consumes the least energy as the low viscosity bacteria and nutrient fluid can be delivered easily into sand; (2) The gas generated by bacteria can be distributed more evenly than other means; (3) The gas bubbles generated by bacteria are tiny so the gas bubbles are less prone to escape from the ground. This so-called biogas desaturation method for mitigation of liquefaction has been developed by our research group (He et al., 2013; He and Chu, 2014).

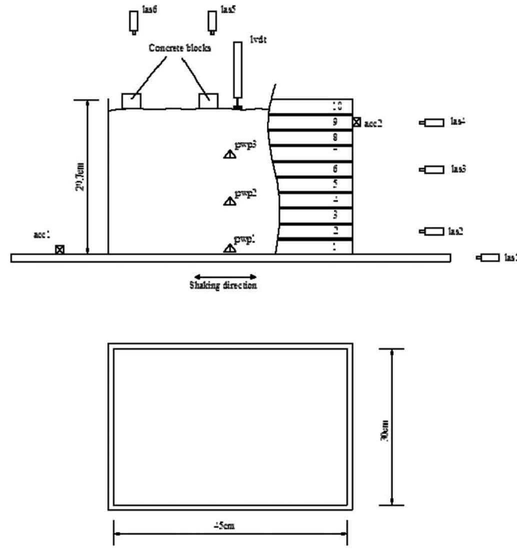

Figure 3. Laminar box and instrumentations used for shaking table tests (acc: accelerometer; pwp: pore water pressure transducer; and las: laser displacement transducer).

To verify the effectiveness of the biogas method, shaking table tests using a laminate box as shown in Fig. 3 were carried out on saturated sand and sand desaturated to a degree of saturation S_r of 95, 90 and 80% using biogas. Some of the results are presented in Fig. 4, where the pore water pressures generated during ground shaking under an acceleration of 1.5 m/s^2 are plotted. Fig. 4a shows the pore water pressure for a saturated sample and Fig. 4b the pore water pressure for a sample with a degree of saturation of 80%. The pore pressures were measured at 3 different locations as shown in Fig. 3. It can be seen from Fig. 4 that by merely reducing the degree of saturation using biogas, the amount of pore water pressure generation can be much reduced.

Fig. 5 shows the pore water pressure ratio obtained from each shaking table test plotted against the relative density of the sand for samples with different degree of saturation S_r. The pore water pressure ratio is defined as the ratio of maximum excess pore water pressure to the initial effective overburden stress. When the pore water pressure ratio is close to 1, liquefaction becomes possible. The normal design requirement is to control the pore pressure ratio to be less than 0.5. The samples with the degree of saturation less than 100% in these tests were created using nitrogen gas produced by denitrifying bacteria. The ground acceleration applied was 1.5 m/s^2. It can be seen from Fig. 4 that the pore

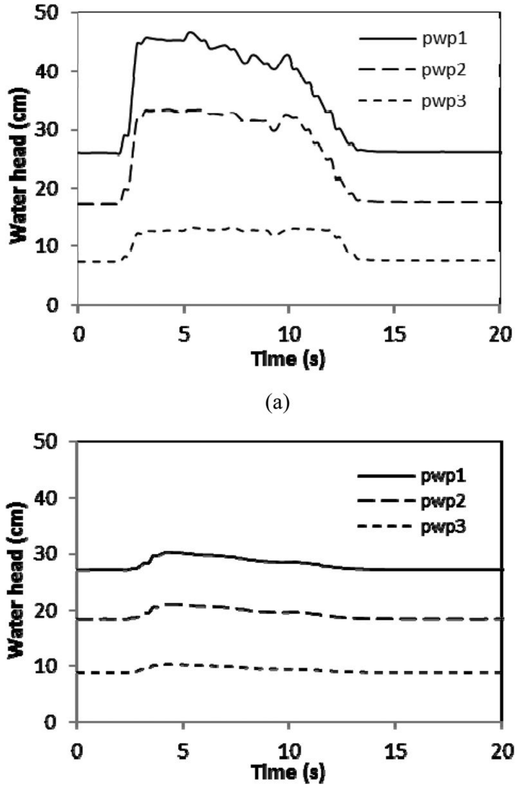

Figure 4. Pore water pressures generated during shaking at an acceleration of 1.5 m/s^2: (a) for sample with $D_r = 0.52$ and $S_r = 100\%$; and (b) for sample with $D_r = 0.43$ and $S_r = 80\%$.

water pressure ratio for the saturated sand with a relatively density of 50% is as high as 1 and thus the sand liquefied under the applied ground acceleration.

One of the conventional ways to prevent liquefaction from happening is to increase the relative density of sand. This requires energy intensive soil improvement methods such as dynamic compaction to be used. However, if the degree of saturation of the sand is lowered down to 95%, the pore pressure ratio would reduce to 0.4 for sand with the same density (Fig. 5). The cost and energy required to low down the degree of saturation from 100% to 95% is much less. If we lower down the degree of saturation to be 90%, the pore water pressure ratio can be controlled to be even less than 0.2. Therefore, the biogas method can be very effective for liquefaction mitigation. It is also less expensive compared with any conventional methods.

A comparison of ground settlement for a fully saturated sand layer and a sand layer treated with biogas with a degree of 95% is made in Figure 6. The settlement is expressed as a settlement ratio with the maximum settlement for fully saturated sand as 100%. It can be seen from Figure 6 that with only 5% of gas replacement, the ground settlement generated under ground shaking with an acceleration of 1.5 m/s^2 can be

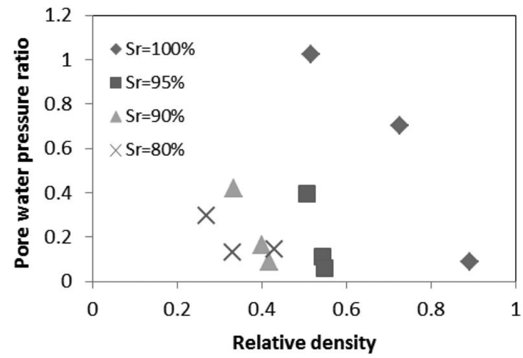

Figure 5. Plot of pore water pressure ratios against relative densities under a_{max} 1.5 m/s^2 for samples with different degree of saturation (with the pore water pressure measured by transducer pwp2, as shown in Fig. 3).

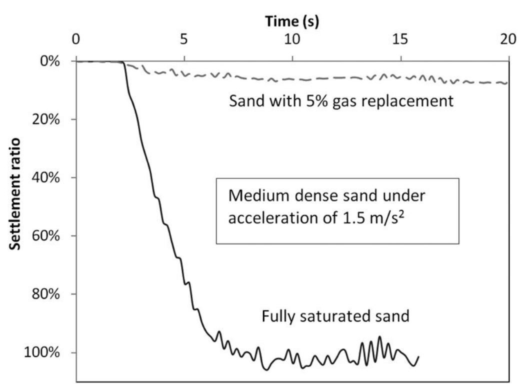

Figure 6. Comparison of ground settlement induced by ground shaking under an acceleration of 1.5 m/s^2 for a saturated sand layer and a sand layer with 5% gas replacement.

reduced by more than 90%. Thus, the biogas method is effective in preventing the occurrence of soil liquefaction as well as reducing the damage caused by liquefaction.

4 BIOGROUT FOR PROTECTION OF LEVEES

By using the microbially-induced calcium carbonate precipitation method, the shear strength of soil can be increased. When cement or chemicals are used to treat soil, the amount of improvement in the shear strength of soil is dependent on the amount of cement or chemical used. Similarly, when biocement is used, the shear strength of soil is affected by the amount of metal precipitated. In one study by Van der Ruyt and van der Zon (2009), the uniaxial compressive strength (UCS) of biocement treated sand was measured for specimens having different calcium carbonate contents. The results are shown in Figure 7. It can be seen that the UCS strength increases with increasing calcium carbonate content. The highest UCS obtained is 27 MPa.

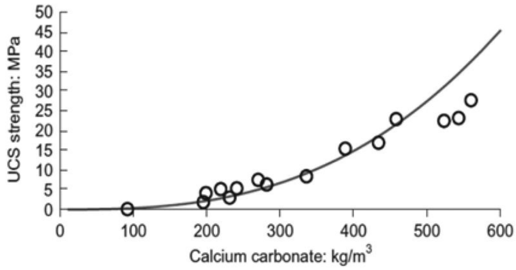

Figure 7. The unconfined compression strength (UCS) versus calcium carbonate content relationship for biocement treated sand (after Van der Ruyt and van der Zon, 2009).

For normal applications, the UCS strength required is less than 3 MPa. This will only require a calcium content of 100 to 200 kg/m^3. To achieve the same UCS strength for sand using cement grouting, the amount of cement used would be between 250 to 300 kg/m^3. As the production of biocement can be cheaper as discussed by Ivanov and Chu (2008), the overall cost for biogrouting can be potentially lower.

Biocement can also be used to reduce the water conductivity of sand through bioclogging as illustrated in Fig. 1. One of the methods that has been developed by our research group is to use urea reducing bacteria to precipitate a layer of calcium carbonate on top of sand as shown in Figure 8. This hard layer of crust has a water conductivity of less than 10^{-7} m/s (Chu et al., 202) and thus can be used as an impervious layer for water storage or for erosion control of beach or riverbank. As the layer of treatment is rather thin, the amount of biogrout used is small. Thus the method can be more economical than conventional methods. The detail of this method is described in Chu et al., (2012).

The method shown in Fig. 8 has provided a method for making temporary water storage for special need or during disaster mitigation or rehabilitation process. The method does not require special construction equipment, but a spreader to spread the biocement solution onto the soil surface.

A method for rehabilitation of levees using biogrout to enhance its ability against erosion under overtopping and seepage through the levee and the base of the levee has been proposed. This so-called bioshotcrete method is illustrated in Fig. 9.

In this method, bacteria solution and biogrout consisting of fiber, calcium source, and urea are sprayed on top of the levee surface to form a biocoating. Biogrouting columns can also be installed to below the levee to form a cutoff wall as shown in Fig. 9.

To evaluate the effectiveness of this method, model tests using a hydraulic flume were carried out. In conducting this test, a levee model made of standard Ottawa sand and then treated using biogrout. The dimension of the levee model is shown in Fig. 10. The biogrouting solution was applied by spraying the surface of the levee model with this solution for 6 times.

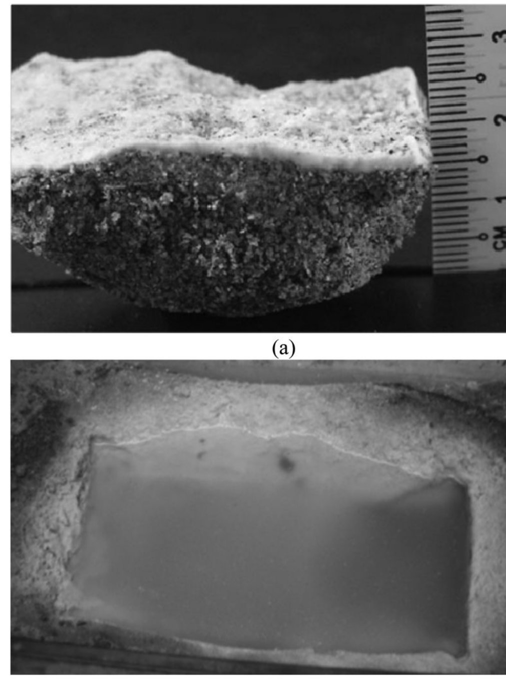

(a)

(b)

Figure 8. Formation of (a) a thin impervious layer on top of sand using a biogrouting method and (b) a water pond model in sand using this method.

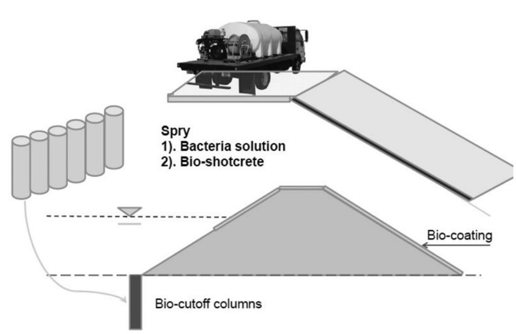

Figure 9. Methods for using biogrout for levee treatment.

The biogrout included urease-producing bacteria suspension solution, calcium chloride, and urea. A levee model after treatment is shown in Fig. 11. The model was then placed inside a hydraulic flume as shown in Fig. 12 for testing. More detail on the model tests is given in Naeimi (2014).

After model tests in the hydraulic flume, samples were taken from the model to determine the unconfined compressive strength (UCS). The UCS determined for samples taken from different depths are shown in Fig. 13. It can be seen that UCS within the top 30 mm is much higher indicating the formation of a crust on top of the levee. It is this strong crust that protects the levee from erosion and seepage flow

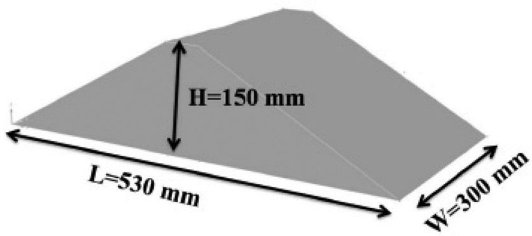

Figure 10. Dimension of the levee model used for the model tests in a hydraulic flume.

Figure 11. A levee model after treatment using biogrout.

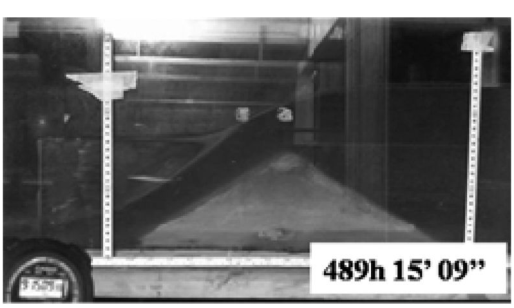

Figure 12. A levee model undergoing overtopping flow in a hydraulic flume.

through the levee. The calcium carbonate content distribution with depth in the model levee is also shown in Fig. 13. A good correlation with the UCS strength is seen. It can also be seen that there are also some precipitation of calcium carbonate in the soil below the 30 mm crust which also contributes to the overall stability of the levee. The permeability of the soil also reduced with the calcium carbonate content as shown

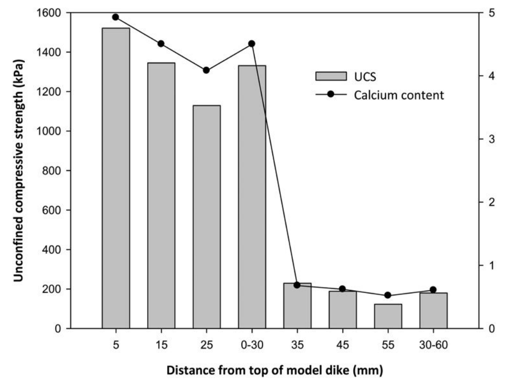

Figure 13. Unconfined compressive strength and precipitated calcium carbonate content distribution along the depth of the levee model.

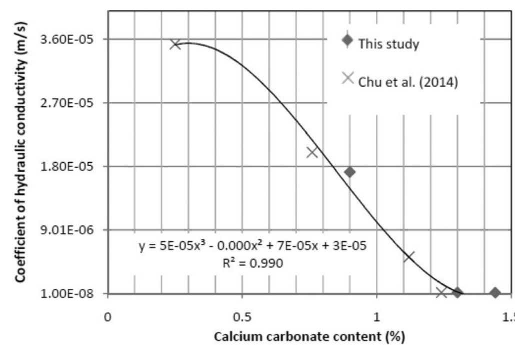

Figure 14. Change in permeability of sand with the calcium carbonate content to sand ratio (% w/w).

in Fig. 14 and the permeability value can be reduced to be below 10^{-7} m/s as shown in Fig. 14. Thus, this strong crust layer also forms an impervious layer for the levee surface to cutoff seepage. Similar methods can be used to install cutoff wall for the base of the levee.

The model tests presented above have shown that the biogrouting method is effective in protecting the levee from erosion. However, it should be pointed out that the strong crust formed on top of the levee is relatively thin. The thickness of this crust can be increased if required as shown in Naeimi (2014). Alternatively, geosynthetic fiber should be used together with the biogrout to increase the ductility of the crust. The use of fiber will also increase the strength of the crust and preventing it from cracking under allowable deformation. Thus, the bioshotcrete method will be a viable method to be used for levees.

5 BIOGROUT FOR ROAD CONSTRUCTION OR REPAIR

Biogrout can also be used for road construction or repair in a way similar to the use of cement grout. To

Figure 15. Production of biogrout using solutions made of limestone fines and corn cobs with the addition of biomass and urea.

Figure 16. Applying the biogrout directly on top of base and subbase of the road.

reduce further the cost of biogrout, a method to produce biogrout using mining and agricultural byproduct has been developed. In this method, limestone fines – a byproduct of limestone mine and corn cobs or any other agricultural byproduct can be used to produce soluble calcium salt using an acidogenic fermentation process. The soluble calcium salt can be used together with biomass to form biogrout for road construction and repair.

Some laboratory tests have been carried out to establish the procedure for this method. A fermenter was used to produce soluble calcium solution with limestone residuals in it as shown in Fig. 15 as the white solution in the container. Bacteria solution and urea were then added to the soluble calcium solution to form a biogrout solution. This solution can be applied directly on top of soil or a crushed stone layer as shown in Fig. 16. Once this layer is dried up, a biogrouted slab is formed as shown in Fig. 17.

In general, the cost of biotreatment is lower than the conventional methods such as the use of cement or chemicals. However, a direct cost comparison may not be made at this stage. This is because the biocement production may have to be made in a factor setting. For

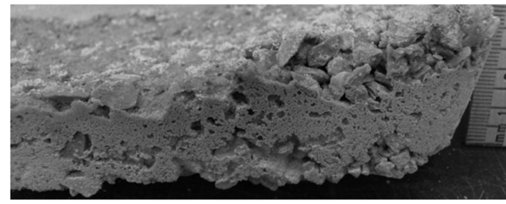

Figure 17. Formation of biogrouted slab.

example, the fermentation process adopted to produce biogrout introduced above is very complicated and its operation may not be well controlled. This has to be done in a factor when a large quantity of biocement is required for construction. Until the production lines are in place, the cost of biocement will not be able to be evaluated realistically.

6 CONCLUSIONS

In this paper, the principles of microbial geotechnologies are discussed. Studies for the establishment of three different applications of the microbial method are presented. These include biogas desaturation method for mitigation of soil liquefaction; bioshotcrete method for levees for erosion and seepage control; and biogrouting for road construction and repair. The main conclusions are summarized as follows:

1. The biogrouting method has four major advantages: it is produced at ambient temperature and thus requires much less energy to produce; it has much lower viscosity and can flow like water; it is sustainable as bacteria can be reproduced easily at low cost; and the bacteria that are used for biocement are non-pathogenic and environmentally friendly.
2. Denitrifying bacteria can be used to produce nitrogen gas ins-situ and enhance the liquefaction resistance of soil through desaturation. This method has the potential to be the most cost-effective method for mitigation of liquefaction hazard;
3. A bioshotcrete method is proposed for the rehabilitation of levees. In this method, fiber mixed biogrouting is used to treat the surface of a levee to form a strong crust to protect the levees from erosion and seepage failure.
4. Biogrouting materials can be produced using mining and agricultural byproducts and used for road construction and repair.

REFERENCES

Chu, J. 2012. General report on biogrout & other grouting methods, General Report, *Proc. ISSMGE – TC 211 International Symposium on Ground Improvement*, Brussels, 31 May & 1 June, 1: 177–187.

Chu, J., Stabnikov, V. and Ivanov, V. 2012. Microbially induced calcium carbonate precipitation on surface or in the bulk of soil, *Geomicrobiology Journal*, 29: 544–549.

He, J. and Chu, J. 2014. Undrained responses of microbially desaturated sand under static monotonic loading, *Journal of Geotechnical and Geoenvironmental Engineering*, ASCE, 140(5): 04014003-1 to 8.

He, J., Chu, J., and Ivanov, V. (2013). "Mitigation of liquefaction of saturated sand using biogas." *Geotechnique*, 63(4): 267–275.

Ivanov, V. and Chu, J. 2008. Applications of microorganisms to geotechnical engineering for bioclogging and biocementation of soil in situ. *Reviews in Environmental Science and Biotechnology* 7(2): 139–153.

Mitchell, J.K. and Santamarina, J.C. 2005. Biological Considerations in Geotechnical Engineering. *Journal of Geotechnical and Geoenvironmental Engineering*, *ASCE,* 131(19): 1222–1233.

Naeimi, M. 2014. Biocementation of sand in geotechnical engineering, *PhD thesis*, Nanyang Technological University, Singapore.

Okamura, M., & Soga, Y. 2006. Effects of pore fluid compressibility on liquefaction resistance of partially saturated sand. *Soils and Foundations*. 46(5): 695–700.

Yegian, M.K., Eseller-Bayat, E., Alshawabkeh, A. and Ali, S. 2007. Induced-partial saturation for liquefaction mitigation: experimental investigation. *J. Geotech. Geoenviron. Eng.*, ASCE, 133(4): 372–380

van Paassen, L.A., Ghose, R., van der Linden, T.J.M. van der Star, W.R.L. and van Loosdrecht, M.C.M. 2010. Quantifying biomediated ground improvement by ureolysis: Large-scale biogrout experiment, *Journal of Geotechnical & Geoenvironmental Engineering*, *ASCE* 136(12): 1721–1728.

van der Ruyt, M., & Van der Zon, W. 2009. Biological in situ reinforcement of sand in near-shore areas *Geotechnical Engineering*, 162(1): 81–83.

Whiffin V.S., 2004. Microbial $CaCO_3$ precipitation for the production of biocement, *Ph.D. Thesis*, Murdoch University.

Geotechnics for Catastrophic Flooding Events – Iai (Ed)

Damage to river levees by the 2011 Off the Pacific Coast Tohoku earthquake and prediction of liquefaction in levees

M. Okamura
Ehime University, Matsuyama, Japan

S. Hayashi
Kobe Electric Railway Co. Ltd.,Kobe, Japan

ABSTRACT: More than 2000 river levees were damaged by the 2011 Off the Pacific Coast of Tohoku Earthquake and liquefaction of soils in levees is considered to be the fundamental mechanism of about 80% of the damaged levees. Vulnerability assessment of existing levees and execution of remedial countermeasure for this newly realized mechanism will be the next challenge. In this study the validity of the liquefaction evaluation method used in the current practice was examined. It was revealed that the current method provides the factor of safety against liquefaction, F_L, for relatively thin saturated layers in levees excessively on the safe side. A possible reason for this is considered to be drainage of generated excess pore pressure during the earthquake shaking. An attempt was made to improve the liquefaction evaluation method by taking the drainage effects into account.

1 INTRODUCTION

In order to fight against riverine flooding that has continued to produce devastating consequences, in both life and economic losses, several tens of thousands of kilometers of river levees have been constructed over centuries since the Edo era in Japan. Even though the construction efforts have been continuously devoted, approximately 40% of levees in Japan does not have enough height and width. Raising and widening the levees still have a highest priority in the current engineering practice of river levee management.

On the other hand, although river levees have repeatedly been damaged by earthquakes, it was rarely the case that the damage to levees resulted in devastating consequences of flooding, and thus seismic effects on levees had not been considered in the engineering practice. In 1995, Hogoken-nambu earthquake caused severe damaged to the levees of the Yodo river and Osaka city, the second largest city of Japan, was in real danger of flooding. Thick loose alluvium sand deposits liquefied and the 5 m high levees subsided as much as 3 m. Since the dominant mechanism of the seismic damage to levees in past large earthquakes was believed to be the liquefaction of foundation soils, execution of liquefaction countermeasure for foundation soils of vulnerable levees has started after the Hyogoken-nambu earthquake.

Regarding the seismic damage, occurrence of crest settlement larger than half of the embankment height is not unusual when foundation soils liquefy (Matsuo, 1999). Levees resting on non-liquefiable soil, however, were considered to have rarely experienced severe damage. Recorded crest settlement due to the deformation of soft foundation clay was, at the largest, 15% of the levee height (River Front Center, 1999). In 1993, the Kushiro-oki earthquake hit the northern part of Japan and the Kushiro river levees were severely damaged. The incident attracted attention of engineers since damaged levees were underlain by a non-liquefiable peat deposit. It was presumed that the surface of the highly compressible and less permeable peat deposits below the levees had subsided in a concave shape, creating saturated zone in the levees, as shown in Figure 1 (Sasaki et al., 1995). More recently, more than 2000 river levees were damaged by the 2011 off the Pacific Coast of Tohoku Earthquake (River Bureau, Ministry of Land, Infrastructure and Transport, 2011) and a considerable number of levees failed in this mechanism. Assessment of vulnerable existing levees and execution of countermeasure for this newly realized mechanism will be a next challenge.

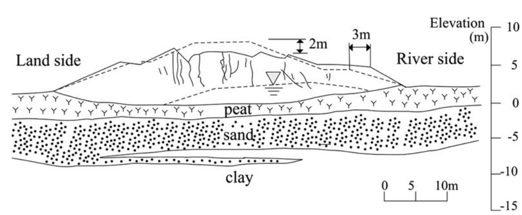

Figure 1. Damaged levee of the Kushiro river (Sasaki et al., 1995).

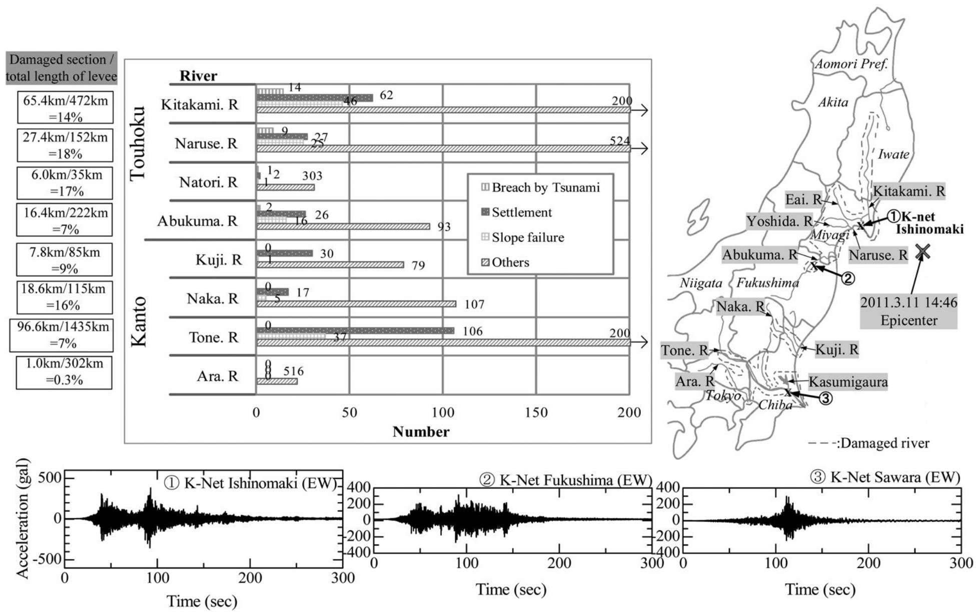

Figure 2. Locations and number of damaged levees caused by the 2011 Off the Pacific coast Tohoku Earthquake (after River Bureau of MLIT, 2011).

2 LIQUEFACTION IN LEVEES BY 2011 OFF THE PACIFIC COAST TOHOKU EARTHQUAKE

The Off the Pacific Coast Tohoku Earthquake of moment magnitude 9.0 occurred on March 11, 2011, with its hypocenter located at 130 km from the coast and a depth of 24 km. Figure 2 shows locations and the number of damaged levees as well as typical acceleration time histories observed with K-Net. Maximum accelerations of the main shock observed in coastal areas of soft soil profiles ranged from about 0.3 g to 0.6 g in the Tohoku district and from about 0.2 g to 0.4 g in the Kanto district. The main shock lasted more than 2 minutes, followed by a large number of aftershocks. 416 aftershocks of moment magnitude higher than 5.0 were recorded by the end of March 2011, in 20 days after the main shock. A total of some 2000 damaged river levees extended widely from northern part of Iwate Prefecture to Tokyo as indicated with the broken lines in the figure and a total length of damaged levee sections added up to 241 km. On heavily damaged levees which no longer had a function to resist high-water, such as levees with crest height lower than high-water level or those with significant cracks and deformation, detailed in-situ investigation was conducted including SPT, CPT, Swedish weight sounding, ground water level monitoring, sampling and laboratory tests and even direct observation by completely dissecting levees. It was confirmed that soil liquefaction was the dominant mechanism to cause the heavy damage. From a viewpoint of locations of liquefied soil layers, damaged levees are broadly classified into three types as illustrated in Figure 3. The first one is such that a liquefied soil layer existed in the levee on a thick clay deposit; the second one is such that the liquefied sand layer existed only in the foundation soil and the levee was consisted of non-liquefiable soil; and the third type is the combination of the first and the second. For type 1 levees, the surface of the compressible and less permeable clay deposit below the levee had subsided in a concave shape, creating a saturated zone in the leveeas shown in Figure 1. For such levees, expected deformation mechanisms is lateral spreading of levees with limited deformation of foundation soil. Figure 4 depicts the toe of such levee where the levee spread laterally on the surface of foundation soil towards hinterland side without any noticeable deformation detected on the ground surface outside the levee toe.

The number of levee failed in the first and third mechanisms was some 80% of the damaged levees. Liquefaction of soils in levees was certainly the dominant mechanism.

Figure 5 illustrates a cross section of such a damaged levee, the left bank levee of the Naruse river at 30.3 km from the mouth, which was originally approximately 9 m high and rested on a thick alluvium clay deposit (Tohoku Regional Development Bureau, MLIT, 2011). The water table in the levee observed 7 weeks after the earthquake with excavated boreholes was more than 2 m above the foundation clay layer (Ac1), indicating that the lower part of the levee (Bs) was saturated. The soils of the levee (Bs) was mostly silty sands with the SPT N-values lower than 5. The levee spread laterally on the rice pad which remained

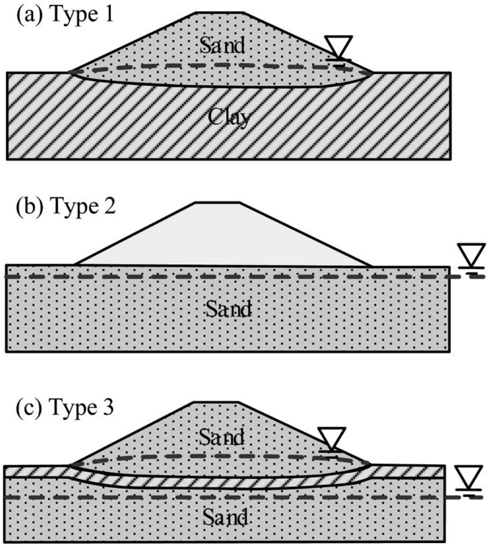

Figure 3. Three types of levee and foundation soil classified based on location of liquefied soil layers (TRDB, 2011).

Figure 4. Naruse River, R12.0k (River division, NILM). The levee spread laterally on the surface of foundation soil toward hinterland side. There was not any detected deformation outside the levee toe.

intact and many cracks and fissures appeared on the slope were partly filled with boiled sand. All these facts suggest that the levee liquefied. It is interesting to note that neighboring undamaged levees and their foundation soil conditions were quite similar to those of the damaged levees in all aspects with an exceptionof the water table in the levee being slightly lower (Tohoku Regional Development Bureau, MLIT, 2011). The loose saturated soil layer at the base of the levee with a thickness of about 2 m in the damaged section liquefied and caused serious damage to the levee, and the undamaged levees had the saturated soil with a smaller thickness which presumably did not liquefy. This alludes effects of drainage of pore water from saturated soil layers on occurrence of liquefaction and severity of damage.

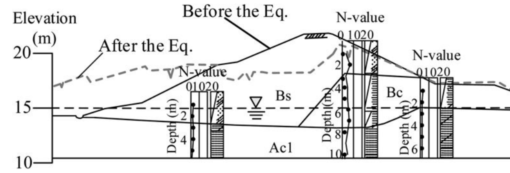

Figure 5. Damaged levee of the Naruse river (TRDB, Ministry of Land, Infrastructure and Transport, 2011.

3 LIQUEFACTION ASSESSMENT OF DAMAGED AND UNDAMAGED LEVEES

In order to assess vulnerability to liquefaction of levees, the validity of the evaluation method of in-situ liquefaction susceptibility is important. In this chapter, the liquefaction evaluation method used in the current practice is examined.

The author picked out 18 severely damaged levees where liquefaction of soils inside the levees are considered as a main cause of damage (the first type in Figure 3). Another 12 undamaged levees in the neighborhood of those damaged levees were also selected and their properties are summarized in Table 1. Figure 6 depicts variation in crest settlement and soil profile in the longitudinal direction of a typical section containing damaged and undamaged levees. Subsided and cracked significantly in the section between 30.9 k and 31.6 k, the levee in the section between 30.6 k and 30.9 k practically suffered from no damage despite conditions were similar in all aspects including levee height, foundation clay thickness, SPT-N values and soil type with an exception of the thickness of saturated zone in the levees. The saturated levee soil had evidently larger thickness in the heavily damaged section than the slightly damaged and non-damaged section.

The safety factors against liquefaction, F_L $(= R_L/L)$, of all the 30 levees were calculated with the method of the Japan Road Association (JRA, 2012). SPT-N values and fines content obtained at the sites after the earthquake were used to estimate the liquefaction resistance of the soils, R_L. These levees have been built up and extended over decades without following modern standards and construction technique, the levee soils were generally loose. The normalized SPT-N values, N_1 $(=(170N/(70+\sigma_v'))^{0.5})$, of the saturated soil layers were in a range between 0 and 10, as indicated in Figure 7. Distribution of N_1 values of damaged and undamaged levees are quite similar to each other and N_a values, the normalized N value with the effects of fines content taken into account, are also the case.

Cyclic stress ratio developed at the sites, L, were estimated from following equation,

$$L = c_w \frac{a_{\max}}{g} \frac{\sigma_v}{\sigma_v'} r_d \tag{1}$$

where σ_v and σ_v' denote the total and effective vertical overburden stress calculated simply using overlying soil thickness, respectively, and $a_{\max}$ is the maximum ground acceleration. Because of the large moment

Table 1. Summary of damaged and undamaged levees used for validation of F_L methods.

No.	River	Location*	Levee height m	Crest settlement m	Thickness of saturated layer m	D_{10} mm	Permeability k (Hazen) m/s	N	N_1	N_a	FC %	Estimated max acc. gal
(a) Damaged levee												
1	Abukuma	R22.5k + 70 (H)	5.8	2.2	2.2	0.0090	1.1×10^{-4}	3	4	6.5	29	341
2		L28.8 + 85k (H)	4.6	0.2	2.3	0.0020	3.0×10^{-6}	2	3	3.3	15	341
3		R31.0k + 50 (H)	5.7	2.0	2.4	0.0100	1.3×10^{-4}	3	4	8.2	39	341
4		R32.9k + 70 (H)	6.6	1.1	2.5	0.0130	2.3×10^{-4}	3	4	6.4	32	341
5	Naruse	L11.5k (H)	5.6	2.4	1.7	0.1020	1.4×10^{-2}	3	6	11.2	31	657
6		R12.0k (C)	5.4	0.9	3.8	0.0070	6.5×10^{-5}	1	1	4	48	657
7		R12.0k (H)	5.4	0.9	3.3	0.0070	6.5×10^{-5}	3	4	7.7	40	657
8		R12.0k (R)	5.4	0.9	2.6	0.0070	6.5×10^{-5}	2	3	4.1	20	657
9		L29.1k (R)	6.2	2.6	0.9	0.0100	1.3×10^{-4}	3	6	7.5	21	568
10		L30.3k (H)	7.5	5.5	2.9	0.0015	3.0×10^{-6}	2	4	14.3	75	568
11	Yoshida	L14.8k (C)	7.8	1.5	2.8	0.0100	1.3×10^{-4}	6	5	7.9	31	657
12		L14.8k (R)	7.8	1.5	1.2	0.0100	1.3 × 10v-4	3	4	8.9	47	657
13	Eai	R14.15k (C)	4.1	1.5	3.0	0.0015	3.0×10^{-6}	1	1	4.6	56	463
14		R14.35k (C)	4.3	1.3	1.7	0.0020	5.3×10^{-6}	0	0	2.5	55	463
15		L14.4k (C)	3.0	1.4	1.1	0.0045	2.7×10^{-5}	1	1	3.2	36	463
16		L14.61k (C)	4.0	1.2	3.6	0.0050	3.3×10^{-5}	1	1	3.9	45	463
17		L27.7k (C)	3.4	2.5	2.2	0.0150	3.0×10^{-4}	3	4	2.4	0	326
18	Shin eai	R2.8k + 40 (C)	6.7	1.4	1.9	0.0020	5.3 × 10-6	4	4	11.7	64	568
(b) Undamaged levee												
1	Abukuma	L29.123k (C)	4.6	0	0.6	0.0130	2.3×10^{-4}	10	10	13.7	26	341
2		L28.75k (C)	4.6	0	1.2	0.0130	2.3×10^{-4}	12	11	15	29	341
3	Naruse	L11.7k (H)	5.6	0	0.4	0.0100	1.3×10^{-4}	4	6	11	37	341
4		R11.9k (C)	5.4	0	2.9	0.0100	1.3×10^{-4}	4	6	11.2	37	657
5		R29.0k (R)	6.8	0	0.5	0.0020	3.0×10^{-5}	3	5	19	81	657
6		L30.7k (H)	7.0	0	0.5	0.0020	5.3×10^{-6}	2	3	12	75	568
7	Yoshida	L14.9k (C)	7.8	0	1.8	0.0100	1.3×10^{-4}	2	2	5.1	47	568
8		L15.3k (H)	8.4	0	1.7	0.0060	4.8×10^{-5}	2	3	12	75	657
9	Eai	L14.7k (H)	4.0	0	0.5	0.102	1.4×10^{-2}	3	4	4.2	15	463
10		R26.69k (C)	3.8	0	0.6	0.010	1.3×10^{-4}	3	3	10.8	65	326
11		L27.9k (H)	3.4	0	0.6	0.008	8.5×10^{-5}	8	10	14	29	326
12	Kitakami	L5.2k + 2 (C)	4.7	0	2.2	0.052	3.6×10^{-3}	6	6	6.3	11	398

Location* C: crest, H: hinterland side slope R: riverside slope

magnitude and the large number of significant acceleration cycles contained in the main shock of the earthquake, the correction factor C_w was assumed to be unity for the first approximation (Tokimatsu and Yoshimi, 1983; Idriss & Boulanger, 2006). The stress reduction factor r_d was also assumed to be unity since the elevation of the soil layer to be assessed was similar to that of level ground surface.

Maximum ground accelerations at each levee were invoked based on those estimated by the National Institute for Land and Infrastructure Management (EDPD, 2012). EDPV has analyzed acceleration data recorded at strong motion seismograph observatories of K-NET, Kik-NET (National Research Institute for Earth Science and Disaster Prevention) as well as MLIT, and provided the interpolated maximum ground accelerations at a small interval. The factor of safety against liquefaction, F_L, is indicated in Figure 8. Being lower than unity for both damaged and undamaged levees, the factors of safety are not a good index to distinguish damaged levees from non-damaged levees.

It is of interest to note that the factors F_L lower than unity are inevitable for cases of such a sever event with peak accelerations higher than 300 gals, those 12 levees survived without any noticeable damage. A possible explanation to the fact may be that the soils in the saturated zones of those levees did not liquefy probably because generated excess pore pressures dissipated swiftly during earthquake owing to shorter drainage distances and higher permeability of soils. Okamura & Tamamura (2010) and Okamura et al. (2012)conducted a series of dynamic centrifuge tests on embankments with thin saturated liquefiable zones at the base, with the thickness ranging between 0.8m and 1.2m and with the different drainage boundary conditions. They demonstrated that crest settlement of the embankment due to the shaking increased with an increase in the thickness of the saturated zone, with

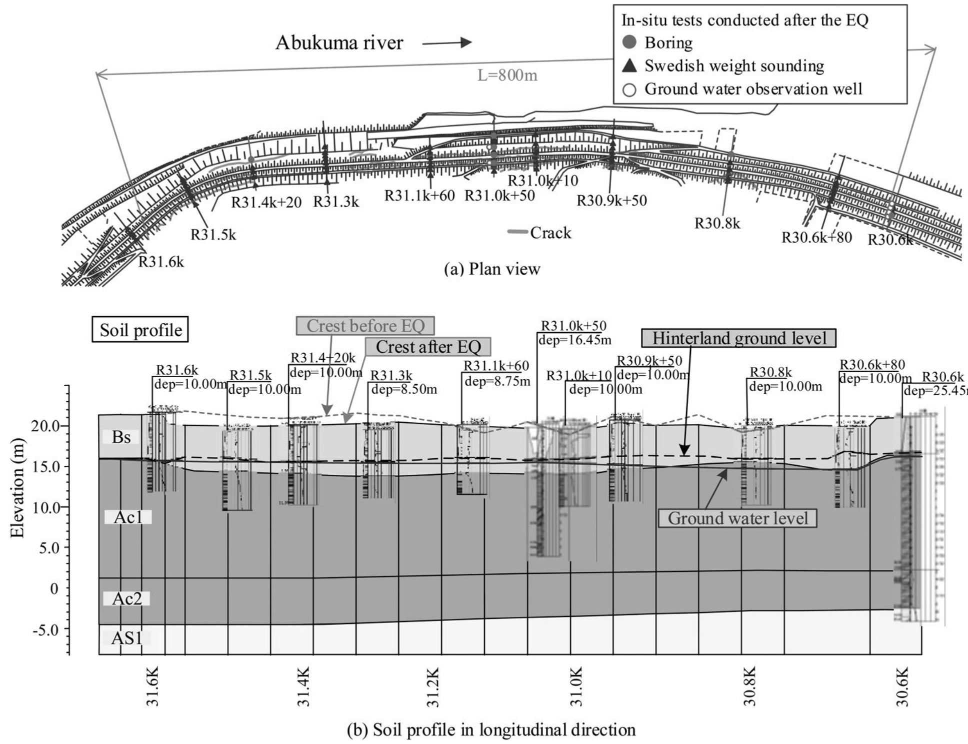

Figure 6. Variations of ground water level and soil profile in longitudinal direction of damaged levee.

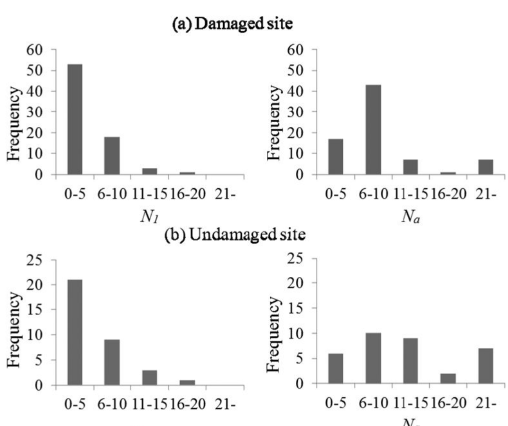

$$N_1 = 170N/(\sigma_v'+70) \qquad N_a = c_1 N_1 + c_2$$

$$c_1 = \begin{cases} 1 & (0 \le Fc \le 10\%) \\ (Fc+40)/50 & (10 \le Fc \le 60\%) \\ Fc/20-1 & (60 \le Fc) \end{cases}$$

$$c_2 = \begin{cases} 0 & (0 \le Fc \le 10\%) \\ (Fc-10)/18 & (10 \le Fc) \end{cases}$$

Figure 7. Frequency distribution of N_1 and N_a values.

the settlement being larger for the zone with undrained boundaries. In the following sections, in order to verily the hypothesis that undamaged levees were survived due largely to the drainage effects, the drainage effects on the liquefaction potential of thin sand layers is studied in the following sections.

4 CENTRIFUGE TEST

In this section, a series of centrifuge tests performed in this study is described which aimed to investigate how the drainage during shaking affects pore pressure responses and accelerations needed to liquefy relatively thin sand layers.

4.1 *Model preparation and test condition*

Two types of models shown in Figure 9 were tested in a centrifuge at 25 g. The model 1 consisted of a 1m deep uniform sand deposit with the ground water table coincided to the ground surface, while the model 2 was the uniform sand deposit with the same density as model 1 and with the thickness two times larger than that of model 1. The ground water table was at 1m deep from the ground surface.

The soil used to build the models was Toyoura sand of which index physical properties are $\rho s = 2.64$, $e_{max} = 0.973$ and $e_{min} = 0.609$. Dry Toyoura sand was rained through air to a relative density of 45% or 70% in a rigid container with internal dimensions of 420 mm in width and 120 mm in length. During the sample preparation, accelerometers and pore pressure cells were installed at the locations indicated in the

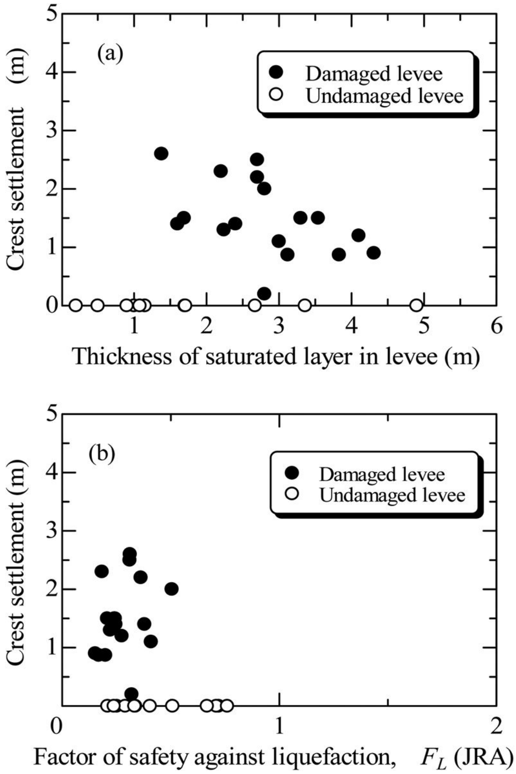

Figure 8. Variations in factor of safety assessed with JRA method and thickness of saturated layer in levees.

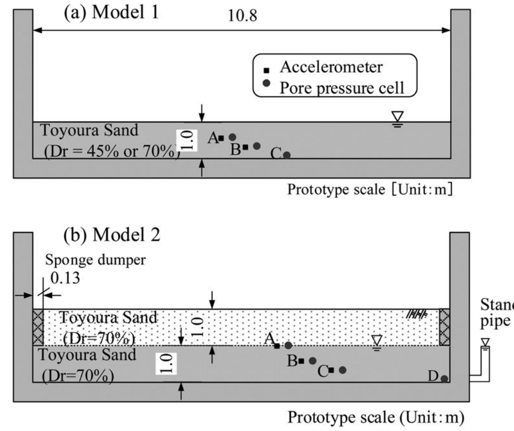

Figure 9. Centrifuge model configurations.

figure. For model 2, 5 mm thick sponges were glued on the side walls to allow the upper unsaturated sand layer to displace horizontally during shaking.

The models were fully saturated with water or viscous fluid in a vacuum chamber at a vacuum pressure of −95 kPa with the aid of CO_2 replacement technique to a degree of saturation higher than 99.5%, which was measured with the method developed by Okamura & Kitayama (2008) and Okamura & Inoue (2010). The viscous fluid was a mixture of water and hydroxypropyl methylcellulose (Type 65SH-50), termed Metolose by the Shin-etsu Chemical Company. In this study viscosity of Metolose solution was varied from 5cSt to 1000cSt by changing the concentration of the solution. The consequence of using the pore fluid with a viscosity ν times higher than that of water in the centrifuge tests at 25 g to model the liquefaction of the water-saturated prototype soil in the field is that the actual prototype permeability being simulated was $k_{\text{prototype}} = k_{\text{model}}/\nu * 25$ (Tan & Scott, 1985). The coefficients of permeability of Toyoura sand k_{model} are 2.5×10^{-4} m/s at $Dr = 45\%$ and 1.8×10^{-4} m/s at $Dr = 70\%$.

The model was set on the geotechnical centrifuge at Ehime University and the centrifugal acceleration was gradually increased to 25 g. For model 2, the pore fluid was drained through a stand pipe until the ground water table stabilized at the proper height. Horizontal base shaking was imparted to the models with a mechanical shaker, with the basic shape of acceleration time histories shown in Figure 12. The shaking intensity was varied by changing the rotation rate of a cam shaft in the shaker. The predominant frequencies of input motions were, for instance, 0.64 Hz for $a_{\max} = 0.8\,\text{m/s}^2$ and 1.0 Hz for $a_{\max} = 1.7\,\text{m/s}^2$. Test conditions are summarized in Table 2.

4.2 *Result and discussion*

Figure 10 shows typical time histories of acceleration and excess pore pressure responses during shaking observed in tests of model 1 with $Dr = 70\%$. The excess pore pressures depend apparently on the permeability, $k_{\text{prototype}}$; the model with $k_{\text{prototype}} = 6.4 \times 10^{-5}$ m/s liquefied in a few cycles of shaking with an acceleration amplitude 140 gal, while the model with the higher permeability $k_{\text{prototype}} = 5.0 \times 10^{-4}$ m/s needed a higher acceleration of 205 gal to liquefy. This clearly suggest that permeability of the soil and thus drainage has significant effects of liquefaction behavior of the soil layers. The maximum acceleration amplitudes of the input motions until the soil liquefied are plotted against the prototype permeability for all tests of models 1 and 2 in Figure 11. For cases of model 1, the acceleration amplitudes seems to be constant for $k_{\text{prototype}}$ lower than 10^{-5} m/s and increases with increasing $k_{\text{prototype}}$ for the higher permeability, with the acceleration amplitude being higher for higher relative density.

It should be mentioned in Figure 10 that the more permeable sand layer needed the higher acceleration to liquefy and the liquefaction lasted shorter duration. The excess pore pressure of the model with $k_{\text{prototype}} = 5.0 \times 10^{-4}$ m/s started to decrease about 5 seconds after the sand liquefied even though the shaking continued, while for the model with $k_{\text{prototype}} = 6.4 \times 10^{-5}$ m/s the liquefaction lasted more than 15 seconds. Liquefied soil is capable of continuously developing large cyclic shear strains even under

Table 2. Centrifuge test conditions represented in prototype scale.

Model	Dr %	Viscosity of pore fluid, ν cSt	$k_{\text{prototype}}$ m/s	Input acc. amplitude, $a_{\max}$ gal	Frequency Hz	Number of cycles to liquefy
Model 1	45	1	6.3×10^{-3}	255	1.2	3
		5	1.3×10^{-3}	169	1.0	2
		10	6.3×10^{-4}	152	1.0	3
		24	2.6×10^{-4}	112	0.84	2
		120	5.2×10^{-5}	104	0.74	4
		120	5.2×10^{-5}	73	0.64	7
		500	1.3×10^{-5}	81	0.68	7
		1000	6.3×10^{-6}	82	0.64	8
	70	9	5.0×10^{-4}	205	1.1	3
		18	2.5×10^{-4}	198	1.1	5
		27.5	1.6×10^{-4}	198	1.1	11
		50	9.0×10^{-5}	190	1.0	5
		70	6.4×10^{-5}	140	0.92	4
		220	2.0×10^{-5}	104	0.72	15
		1000	4.5×10^{-6}	105	0.72	2
Model 2	70	9	5.0×10^{-4}	455	2.0	2
		29	1.6×10^{-4}	324	1.2	3

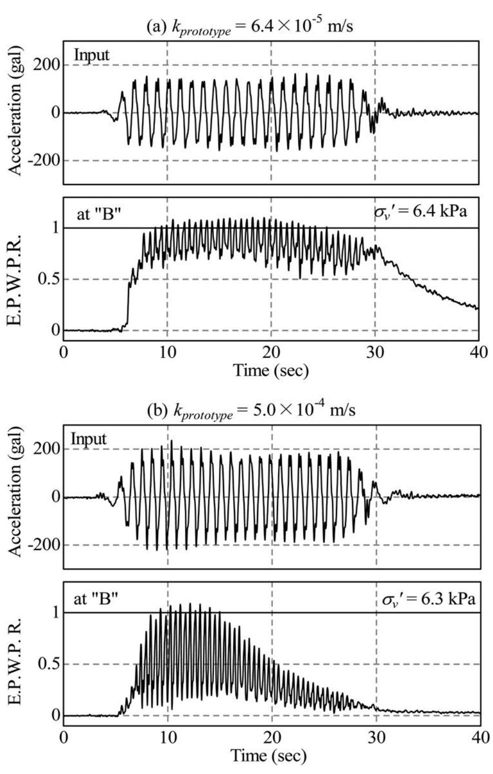

Figure 10. Typical acceleration and excess pore pressure time histories of Model 1 ($Dr = 70\%$).

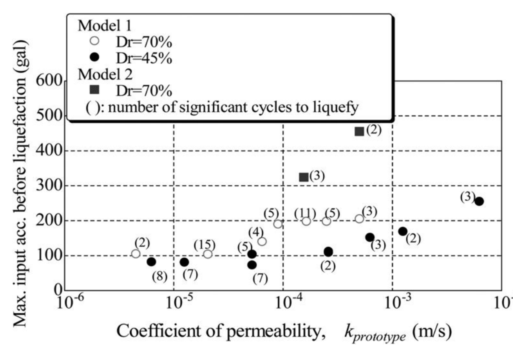

Figure 11. Variation in input acceleration to liquefy the sand layer with coefficient of permeability.

small accelerations. Okamura et al. (2001) has suggested that weak vibration or aftershocks acting on the already liquefied and continuously liquefied soil may contribute significantly to the continued deformation accumulation. For the cases of an earthquake with a long duration such as that shown in Figure 2, the permeability of sand must be a dominant factor on both the occurrence of liquefaction and the accumulated deformation.

The accelerations for model 2, in which liquefiable sand layers were overlain by unsaturated layers, are higher than those for model 1 as shown in Figure 11. Existence of the overlying unsaturated soil layer which decreased the cyclic stress ratio is responsible for this. Factors of safety against liquefaction F_L for each tests were estimated as follows. Because of the different number of cycles to liquefy in each test as indicated in Figure 11, cyclic stress ratios corresponding to the number of cycles were employed as liquefaction resistance R_L,

$$R_L = CSR_{(N)} \frac{1 + 2K_0}{3} \tag{2}$$

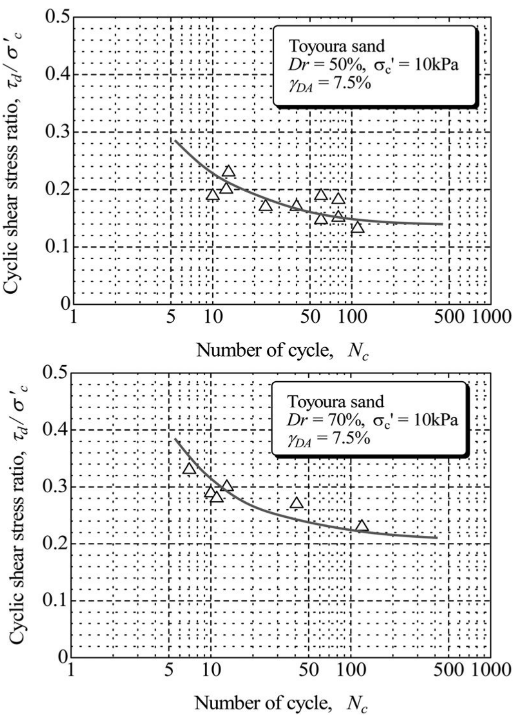

Figure 12. Liquefaction strengths obtained from torsional cyclic shear tests at low confining stress (Tanaka et al., 2009).

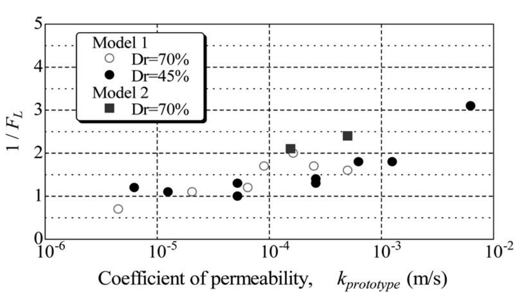

Figure 13. Variation in $1/F_L$ with permeability of sand.

where $CSR_{(N)}$ and K_0 denote the cyclic stress ratio at number of cycles N and the coefficient of earth pressure at rest (=0.5), respectively. Undrained cyclic torsional shear test results on Toyoura sand indicated in Figure 12 (Tanaka et al., 2009) were used for this purpose, of which test conditions were similar to those of the centrifuge including the initial effective confining pressure (10 kPa) and relative densities (50% and 70%). Maximum accelerations $a_{\max}$ used to estimate the cyclic stress ratio were the maximum input acceleration before the soils liquefied. The test results were approximated with liner relationships between cyclic stress ratio and number of cycles in log-log space (Liu et al., 2001) and indicated in the figure. The inverse of the factor of safety, $1/F_L$,is shown in Figure 13. $1/F_L$ is approximately unity in the range of $k_{\text{prototype}}$ lower than 10^{-5} m/s and increases with increasing $k_{\text{prototype}}$ regardless of the relative densities and the overburden pressure.

In model 2, the liquefied sand layers were overlain by unsaturated sand layers with a lower permeability, drainage at the surface of the liquefied layers might be impeded. It is well documented in the literature that overlying impermeable soil layers imposed the undrained condition to underlying soil layers (e.g. Kokusho & Kojima, 2002). In Figure 13, however, there are no distinct differences in F_L value between model 1 and 2. In a saturated sand layer with overburden pressure, the hydraulic gradient will be significantly high at the surface of the layer, which might accelerate drainage at shallower depth. In fact, the excess pore pressure ratios at shallower location (labeled "A" in Figure 9(b)) of model 2 tend to be lower than locations B and C at the beginning of shaking, which was unlike model 1. The drainage boundary condition at the surface of liquefied soil layer of model 2 had little effects on drainage during the shaking.

5 VOLUMETRIC STRAIN DUE TO DRAINAGE

It is common practice to assume the undrained condition to access a potential for liquefaction, however, the centrifuge test results described above indicates that the undrained condition does not hold true depending on permeability. An apparent liquefaction resistance increased with increasing permeability and thus with amount of drained water from the layer during shaking. An increase in the apparent liquefaction resistance have also been observed in studies related to the membrane penetration and imperfect saturation of specimen (e.g. Chaney, 1978; Tokimatsu,1990; Yoshimi et al., 1988).

It is well recognized that unsaturated soils exhibit higher liquefaction resistance than fully saturated soils. The underlying mechanisms that enhance liquefaction resistances of the unsaturated sand is such that air in a partially saturated sand mass plays a role of absorbing generated excess pore pressures by reducing its volume (Okamura and Soga, 2006; Kazama et al., 2006; Unno et al., 2008).Okamura & Soga (2006) derived influential factors of the liquefaction resistance of a partially saturated sand from theoretical consideration and examined effects of the factors through a series of triaxial tests on a clean sand. They assumed that air in the soil contracted according to excess pore pressure and defined the potential volumetric strain, ε_v^*, as,

$$\varepsilon_v^* = \frac{\sigma_c'}{p_0 + \sigma_c'}\left(1 - S_r\right)\frac{e}{1+e} \tag{3}$$

where S_r is degree of saturation, σ_c' is initial effective confining pressure and p_0 is initial pore pressure (in absolute pressure). The potential volumetricstrain is a volumetric strain that will be attained when the excess pore pressure reaches its maximum value, the initial effective stress. They found the unique relationship between liquefaction resistance ratios, LRR, that is the ratio of cyclic shear stress ratio for a sand to that of fully a saturated sand, and the potential volumetric strain as shown in Figure 14. They approximatedthe relation with the following equation.

$$LRR = \log\left(6500\, \varepsilon_v^{*} + 10\right) \tag{4}$$

Since the drainage during shaking and reducing pore volume of unsaturated soils, both result in the contraction in soil volume,may have similar effects on liquefaction resistance, an attempt is made in this study to estimate the amount of water expelled from the saturated sand layers during shaking and resulting volumetric strains. Being a direct and promising method, measurement of surface settlement in a good accuracy was difficult especially for the thin sand layers in the centrifuge. Amount of water to be drained during a time duration t_d from a sand layer with a thickness H with an impermeable boundary at the base is estimated as follows.

$$V_d = k \cdot i \cdot t_d \tag{5}$$

When the excess pore water pressure ratio of the sand layer reaches unity, hydraulic gradient attains its maximum value as,

$$i_{max} = \sigma_v'/\gamma_w \quad H \tag{6}$$

The volumetric strain due to the drainage can be expressed as,

$$\varepsilon_{v\,\max} = \frac{k\sigma_v'}{\gamma_w H^2} t_d \tag{7}$$

where σ_v' and γ_w denotes the effective overburden pressure and the unit weight of water, respectively. In this calculation, t_d is assumed as the time duration from the beginning of the significant acceleration cycle till the sand liquefied. Corresponding excess pore pressure ratios during the time duration were approximately from 30% and 100%.

The factors $1/F_L$ of the centrifuge models are plotted against the volumetric strain in Figure 15 together with LRR, the empirical relationship obtained from the cyclic triaxial tests on unsaturated sands. The centrifuge test results from different models at the different relative densities lay almost on a unique curve. Although the factors $1/F_L$ or the apparent liquefaction resistance begin to increase at lower volumetric strain than LRR, both $1/F_L$ and LRR increase in a quite similar tends. This strongly suggests that the drainage during shaking and the compression of air in soils, both allow volumetric contraction of soils, have similar effects on the liquefaction resistance. Possible causes for the difference between $1/F_L$ and LRR may be time duration t_d and permeability coefficient em ployed in the calculation of volumetric strain.

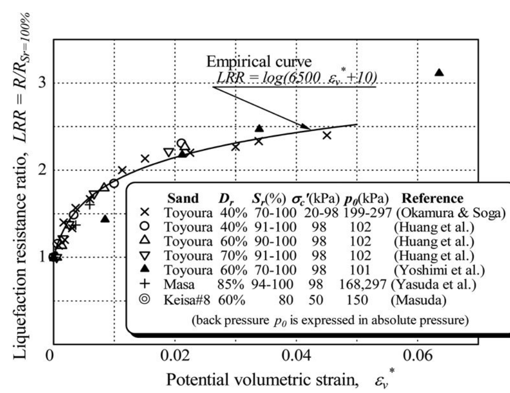

Figure 14. Relationship between hypothetical volumetric strain and liquefaction resistance of partially saturated sand (after Okamura & Soga, 2006).

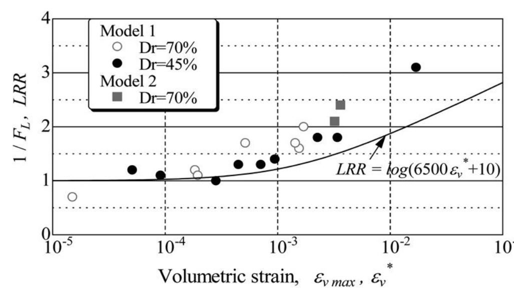

Figure 15. Relationship between rates of increase in apparent liquefaction resistance and volumetric strain due to drainage.

It should be mentioned here that there is a distinct difference in the flow of pore water depending on depth. The drainage effect arises as the result of upward flow of pore water towards the drainage boundary. A soil at the bottom of liquefied layer dissipates generated excess pore pressures by expelling the amount of water which is equivalent to the volume of contraction of soil skeleton, while for a soil at shallower depth amount of outflow water to dissipate excess pore pressure is amount of inflow water from underlying soil in addition to that equivalent to contraction of soil skeleton. For a uniform sand layer the amount of outflow water increases with decreasing the depth, while the flow rate is restricted by the permeability of soil. The resulting consequence is that liquefaction condition begins at the surface and propagates downward as observed in many 1g and centrifuge tests on saturated uniform sand deposits without overburden pressure (e.g. Dobry, 1995). Heterogeneous excess pore pressure ratio will be the typical case for thick deposits and excess pore pressures ratio distributes more or less uniformly in such thin sand layers as models tested in this study.

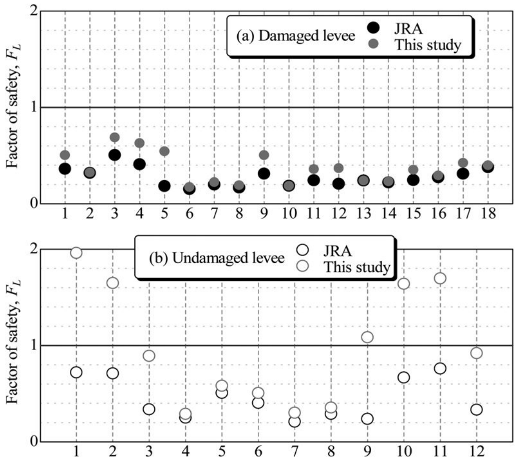

Figure 16. Factor of safety against liquefaction with and without taking drainage effect into account.

6 QUEFACTION ASSESSMENT CONSIDERING DRAINAGE EFFECT AND ITS VILIFICATION

Factor of safety F_L of all the damaged and undamaged levees are evaluated again with taking the effect of drainage into account. Volumetric strain of liquefiable soils in each levees are calculated with equation (5) and the liquefaction resistance ratio, *LRR* derived from equation (4), was multiplied to F_L value from JRA method already derived in the chapter 3. Coefficient of permeability was determined from grain-size data with the Hazen formula as,

$$k\,(\text{m/s}) = 1.3{D_{10}}^2 \tag{9}$$

where D_{10} is diameter of grains in the 10th percentile expressed in millimeters. The obtained factors of safety for all the 30 levees are shown in Figure 16.F_L for undamaged levees significantly increased by taking the drainage effect into account; F_L of seven levees out of 12 undamaged levees became higher than or almost equals to unity. While for the damaged levees, F_L of all the levees stays below unity. The results of liquefaction susceptibility assessment was improved considerably by taking the damage effect into account especially for levees with relatively thin saturated layers.

7 CONCLUDING REMARKS

More than 2000 river levees were damaged by the 2011 Off the Pacific Coast of Tohoku Earthquake and liquefaction of soils in levees is considered to be the fundamental mechanism of about 80% of the damaged levees. Vulnerability assessment of existing levees and execution of remedial countermeasure for this newly realized mechanism will be the next challenge.

In assessing susceptibility to liquefaction of levees, the validity of the evaluation method of in-situ liquefaction susceptibility is important. In this study the validity of the liquefaction evaluation method used in the current practice was examined. Liquefaction assessment on eighteen damaged and twelve undamaged levees conducted in this study revealed that the current method provides the factor of safety against liquefaction, F_L, for relatively thin saturated layers in levees excessively on the safe side. Estimated factors F_L for not only the damaged levees but also all the undamaged levees were lower than unity. A possible reason for this was considered to be drainage of generated excess pore pressure during the earthquake shaking. An attempt was made to improve the liquefaction evaluation method by taking the drainage effects into account.

A series of centrifuge tests was conducted on thin sand layers to investigate effects on shaking acceleration necessary to liquefy the layers of factors including relative density and permeability of sand and overburden pressures. The input acceleration necessary to cause liquefaction and thus an apparent liquefaction resistance increased with increasing permeability of the sand. Since the drainage of pore fluid is suggested to be responsible for the increase in the apparent liquefaction resistance, volume of drained fluid and the resultant volumetric strain before the sand liquefied was estimated. It was found that the apparent liquefaction resistance ratio increased uniquely with the volumetric strain due to the drainage.

It has been known that the liquefaction resistance of sands increases with degreasing degree of saturation. Existence of air allows nearly saturated sand to contract even in the undrained condition and this volumetric strain is believed to enhance the liquefaction resistance. It was found that the relationship between the apparent liquefaction resistance ratio and volumetric strain obtained from the centrifuge tests was in close similarity with that from undrained cyclic triaxial tests on unsaturated sands.

Liquefaction assessment with the effects of drainage taken into account was conducted for the damaged and undamaged levees by the 2011 earthquake. Results of assessment was much improved by considering the drainage effect. Factors of safety stayed lower than unity for all the damaged levees while factors were higher than unity for more than half of the undamaged levees.

REFERENCES

Chaney, R.C. 1978. Saturation effects on the cyclic strength of sands, *Earthquake engineering and oil dynamics, GED, ASCE* 1: 342–358.

Dobry, R., Taboada, V. & Liu, L. 1995. Centrifuge modeling of liquefaction effects during earthquakes, *Proc. 1st Int. Conf. on Earthquake Geotechnical Engineering* 3: 1291–1324.

Ishihara, K., Iwamoto, S., Yasuda, S. & Takatsu, H. 1977. Liquefaction of anisotropically consolidated sand. *Proc. the*

Ninth International Conference on Soil Mechanics and Foundation Engineering, Tokyo 2: 261–264.
Japan Road Association, 2001. *Specifications for Highway Bridges, Part V, Earthquake Resistant Design*. Maruzen (in Japanese).
Kokusho, T. & Kojima, T. 2002. Mechanism for post-liquefaction water film generation in layered sand, *J. Geotechnical and Geoenvironmental Engineering* 128(2): 129–137.
Earthquake Disaster Prevention Division, National Institute for Land and Infrastructure Management. 2012. http://www.nilim.go.jp/lab/rdg/earthquake/milim-distri bution 2.zip.
Idriss, I. M. & Boulanger, R. W.2006. Semi-empirical procedures for evaluating liquefaction potential during earthquakes, *Soil Dynamics and Earthquake Engineering* 26(2–4): 115–130.
Kazama, M., Takamura, H., Unno, T., Sento, N. & Uzuoka, R. 2006. Liquefaction mechanism of unsaturated volcanic sandy soils, *J. Geotechnical Engineering, JSCE* 62(2): 546–561.
Liu, A. H., Stewart, J. P., Abrahamson, N. A. and Moriwaki, Y. 2001. Equivalent number of uniform stress cycles for soil liquefaction analysis, *J Geotechnical and Geoenvironmental Engineering* 127(12): 1017–1026.
Matsuo, O., 1999. Seismic design of river embankments. *Tsuchi-to-kiso, JGS* 47(6), 9–12 (in Japanese).
Maeda, T. & Okamura, M. 2012. Effect of thickness of saturated zone in an embankment on liquefaction induced embankment, *Prod. 47th Japan National Conference on Geotechnical Engineering, JGS* (in Japanese).
Okamura, M., Abdoun, T., Dobry, R., Sharp, M.& Taboada, V. 2001. Effects of sand permeability and weak aftershocks on earthquake-induced lateral spreading, *Soils and Foundations* 41(6): 63–78.
Okamura, M. & Inoue, T. 2010. Preparation of fully saturated model ground. *Proc. the Seventh International Conference on Physical Modelling in Geotechnics, Zurich 2010,* 1.: 147–152.
Okamura, M. & Kitayama, H. 2008. Preparation of fully saturated model ground in centrifuge and high accuracy measurement of degree of saturation. *Proc. Japanese Society of Civil Engineers* 64 (3): 662–671 (in Japanese).
Okamura, M. & Tamamura, S. 2011. Seismic stability of embankment on soft soil deposit, *Int. J. Physical Modelling in Geotechnics* 11(2): 1–8.
Okamura, M., Tamamura, S. & Yamamoto, R. 2013. Seismic stability of embankments subjected to pre-deformation due to foundation consolidation, *Soils and Foundations* 53(1), 11–22.
River Front Center, 1999. Personal Communication.
Sasaki, Y., Tamura, K., Yamamoto, M. & Ohbayashi, J. 1995. Soil improvement work for river embankment damage by 1993 Kushirooki earthquake. *Proc. the First International Conference on Earthquake Geotechnical Engineering, Tokyo* 1: 43–48.
River Bureau, Ministry of Land, Infrastructure and Transport. 2011./http://www6.river.go.jp/riverhp_viewer/entry/y2011eb4071ffc52db6d40a124e92f499b12b83125342f.htmlS.
Tanaka, T., Yasuda, S. & Naoi, K. 2009. Liquefaction and post-liquefaction deformation characteristics of some silica sands under low confining pressure, *Proc. the 30th JSCE Earthquake Engineering Symposium*.
Tohoku Regional Development Bureau, Ministry of Land, Infrastructure and Transport, 2011. /http://www.thr.mlit.go.jp/Bumon/B00097/K00360/Taiheiyouokijishinn/kenntoukai/110530/houkokusho.pdfS.
Tokimatsu, K. & Yoshimi, Y. 1983. Empirical correlation of soil liquefaction based on SPT N-value and fines content, *Soils and Foundations* 23(4): 56–74.
Tokimatsu, K. 1990. System compliance correlation from pore pressure response in undrained cyclic triaxial tests, *Soils and Foundations* 26(1): 14–22.
Tan, T.S. & Scott, R.F. 1985. Centrifuge scaling considerations for fluid particle systems. *Geotechnique* 35 (4), 461–470.
Unno, T., Kazama, M., Uzuoka, R. & Sento, N. 2008. Liquefaction of unsaturated sand considering the pore air pressure and volume compressibility of the soil particle skelton, *Soils and Foundations* 48(1): 87–100.
Yoshimi, Y., Tanaka, K. & Tokimatsu, K. 1988. Liquefaction resistance of a partially saturated sand, *Soils and Foundations* 17(1): 23–38.

This page intentionally left blank

Geotechnics for Catastrophic Flooding Events – Iai (Ed)

Geoenvironmental issues for the recovery from the 2011 East Japan earthquake and tsunami

T. Katsumi, T. Inui, & A. Takai
GSGES, Kyoto University, Japan

K. Endo & H. Sakanakura
National Institute for Environmental Studies, Tsukuba, Japan

H. Imanishi
Tohoku Institute of Technology, Sendai, Japan

M. Kazama
Tohoku University, Sendai, Japan

M. Nakashima
Kokusai Environmental Solutions, Co., Ltd., Tokyo, Japan

M. Okawara
Iwate University, Morioka, Japan

Y. Otsuka
Okumura Corporation, Morioka, Japan

H. Sakamoto
Fujita Corporation, Tokyo, Japan

H. Suzuki
Nippon Koei, Co., Ltd., Tsukuba, Japan

T. Yasutaka
National Institute of Advanced Industrial Science and Technology, Tsukuba, Japan

ABSTRACT: Several geoenvironmental issues have been caused by the 2011 earthquake off the Pacific coast of Tohoku. This paper presents two issues, namely (1) treatment of disaster debris and utilization in geotechnical applications and (2) countermeasures against nuclide contamination. Use of the treated disaster debris for the recovery of infrastructures have been conducted at the disaster affected areas, in particular at the areas subsided by this disaster. Characterization, standardization, and strategic utilization of the recovered soils obtained from the disaster debris are presented. Countermeasures against soils and wastes contaminated with nuclides require the approach from several geoenvironmental viewpoints, such as the design and performance evaluation of containment system for contaminated materials.

1 INTRODUCTION

An earthquake of magnitude 9.03 (Mw), referred to as the 2011 earthquake off the Pacific coast of Tohoku, occurred at 14:46 on March 11, 2011, and was one of the five most powerful earthquakes in the world since modern record-keeping started. The earthquake triggered a tsunami that reached heights of up to 40.5 m at maximum in Miyako city, Iwate Prefecture, and travelled up to 10 km inland in the Sendai plane in Miyagi Prefecture. "Totally" and "half" collapsed buildings counted more than 129,000 and 254,000 respectively. The recovery from this catastrophic disaster has been a crucial issue in Japan.

This earthquake and subsequent tsunami caused several serious geoenvironmental problems mainly in the coastal area of the Tohoku and North-Kanto Regions in Japan. These geoenvironmental problems include (1) generation of disaster debris and tsunami deposits, (2) contamination with salt, (3) land subsidence, and (4) geoenvironmental contamination with nuclides caused by the Fukushima Daiichi Nuclear Power Plant. Among these geoenvironmental issues, this paper focuses on the management of disaster debris and tsunami deposits, as well as the countermeasures against nuclide contamination.

Treatment of the disaster debris in the affected areas was conducted and completed in most places by March 2014. Since the disaster debris and tsunami deposits include a significant amount of soil fractions, proper treatment to recover these soils and utilization of such recovered soils in geotechnical applications in reconstruction works of disaster recovery have strongly been encouraged. In the second section characterization and potential utilization of such soils recovered from the disaster debris are presented.

As for the nuclide contamination related to geoenvironmental engineering, radioactive Cesium exists in (1) wastes and incinerator ashes, (2) sewage sludges, (3) soils and wastes generated from nuclide decontamination works, (4) excavated soils and wastes from construction works, etc. Countermeasures against such soils and wastes contaminated with nuclides require the approach from several geoenvironmental viewpoints, including the design and performance evaluation of containment system for contaminated materials. These issues are summarized in the third section.

2 DISASTER DEBRIS AND RECOVERED MATERIALS

2.1 *Generation and treatment*

Immediately after the 2011 earthquake off the Pacific coast of Tohoku and subsequent tsunami, the government estimated that approximately 20,000 Gg (20,000,000 ton) of disaster debris and 10,000 Gg of tsunami deposit had been generated through this disaster mostly in Iwate, Miyagi, and Fukushima Prefectures (see Figure 1 for the locations of these prefectures). Tsunami deposits are the soils transported by the tsunami and also require proper treatment as well as the disaster debris. These numbers are comparable to those generated at the previous catastrophic disasters such as 2010 Haiti earthquake, 2008 Sichuan earthquake in China, etc (Brown et al. 2011). It was geographically and economically unrealistic to construct new waste disposal facilities with sufficient capacities to accept these wastes, which amount to several times the annual generation of municipal solid waste in each local municipality. Reutilization of these materials was therefore required. Since the national government decided that treatment of debris and tsunami deposits should be completed by 2014 March, proper treatment and utilization of the materials treated from these disaster wastes have strongly been expected.

Treatment of the disaster wastes generated by this earthquake has been a big challenge, since such a large amount of such mixed wastes had never been generated in Japan before. A significant fraction of these wastes corresponds to tsunami deposit soils. Figure 2 shows the fractions of generated waste materials in Iwate and Miyagi prefectures (MOE 2014).

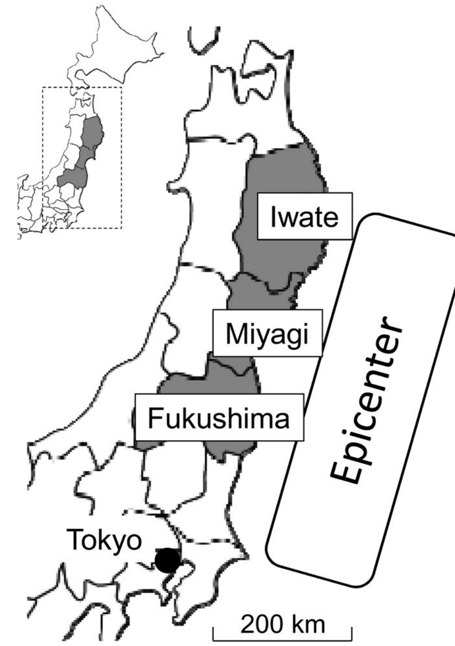

Figure 1. Location of Iwate, Miyagi, and Fukushima Prefectures.

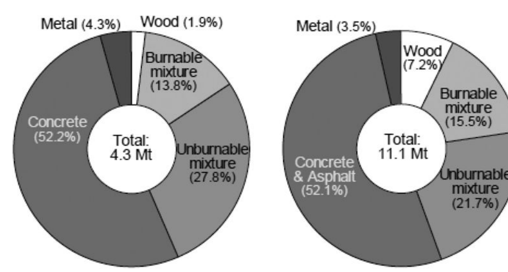

Figure 2. Composition of disaster debris in Iwate (left) and Miyagi (right) Prefectures (MOE 2014).

Primarily in Japan, local municipal governments are responsible for disaster debris treatment. As for the 2011 East Japan earthquake and tsunami, the national government decided to complete disaster waste treatment within 3 years by way of a national subsidy. While the detailed processes of disaster debris treatment vary by municipality, a common system can be illustrated in Figure 3. First, the debris was cleared at the affected sites, collected, and transported to the primary storage sites, which counted more than 300 sites at maximum. At the primary storage sites, wastes were stockpiled depending on the separation upon collection, such as waste mixtures dominant with burnable materials such as collapsed wooden houses,

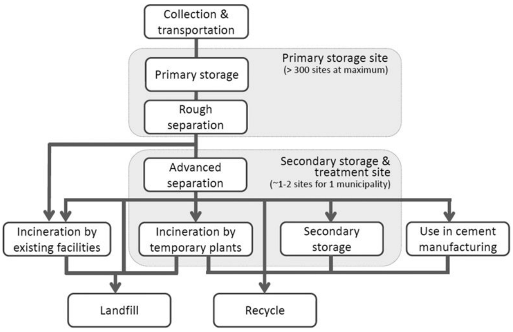

Figure 3. Basic flow of disaster waste management.

concrete-dominant stockpiles, tatami mat dominant stockpiles, soil-dominant stockpiles, etc. Only rough separation, such as separation using operation vehicles and manual separation, was conducted. After the rough separation, "advanced treatment" was conducted at the secondary storage and treatment sites, which were set 1 or 2 sites per one municipality (approximately 30 sites in Miyagi and Iwate prefectures). This "advanced treatment" can also be called "mechanical treatment" because various mechanical equipments and/or machineries were installed, and also be called "advanced separation" because most of the systems installed in each municipality result in the separation. "Separation" systems mostly consist of several processes of "crushing" and "separating". The basic idea of the separation system is to separate mixed wastes into fractions based on the substances, such as burnable materials, unburnable materials, metals, etc, as shown in Figure 4(a) illustrating the general flow of disaster waste treatment. As a result, a significant amount of soils and other fine fractions can be obtained. As for the soil-dominant stockpiles which are mainly the collections of tsunami deposits, only sieving (separation using sieve) was mostly conducted to separate soils from the wastes as shown in Figure 4(b).

The materials obtained from the advanced separation were subjected to incineration treatment in existing incineration plants, incineration using temporary plants, secondary storage, utilization, landfill, and use for cement manufacturing, as shown in Figure 3. Since the capacity of the existing incineration plants in the local areas was limited, the treatment site of each municipality installed temporal incineration plants. Discussion has been made on the utilization, in geotechnical application, of incinerator ashes discharged from these temporary plants. In Iwate prefecture, disaster wastes after advanced separation were used as raw or energy materials for cement manufacturing, because one cement factory exists in the coastal area. This cement factory was damaged by tsunami, recovered in several months, and started to produce cement using disaster debris treated materials in 2011 November after some trials. As for the separated soils, or recovered soils, some of them have been utilized in reconstruction works, while some have been stored in secondary storage sites to wait

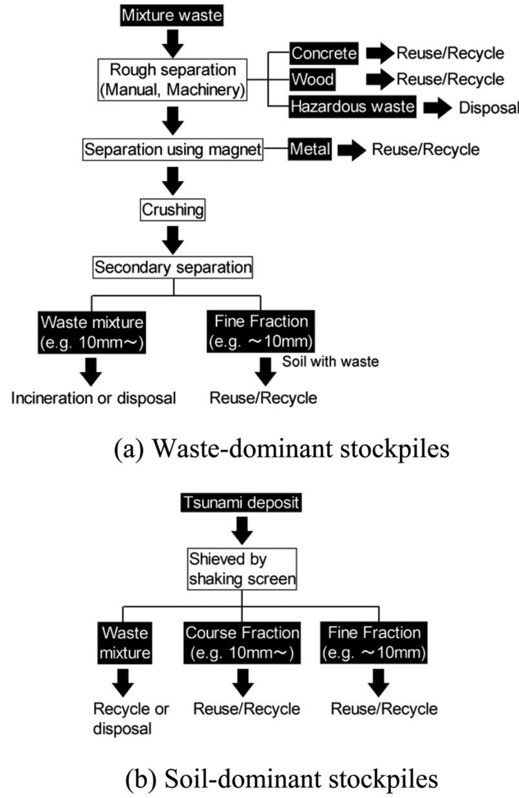

Figure 4. Typical flow chart for the treatment of waste-dominant disaster debris and tsunami deposits or soil-dominant disaster debris (Inui et al. 2012).

for their utilization. As mentioned the following subsections, utilization of such separated soils has been an important geoenvironmental challenge.

The system of "advanced treatment" varied from sites to sites, depending on the different given conditions of materials to be treated (amount of disaster debris generation, primary separation and storage, type of original soil, etc.), site environments (area limitation, air pollution risks, number of primary storage sites, etc.), and local resources (waste incinerators, cement plants, etc.). At most municipalities, construction companies were engaged in the advanced treatment business of such mixed wastes based on their own proposals. One example of these systems is illustrated in Figure 5, in which three "separation" processes using sieving machines (vibrating screen, 35-mm-opening rotating screen, 15-mm-opening rotating screen), one "crushing" process, and three "separation" processes using manual separation, and two "separation" processes using special machines to separate burnable fractions from waste mixtures. Evaluation of these treatment systems from the viewpoint of treatment efficiency and recycle is a next inevitable consideration.

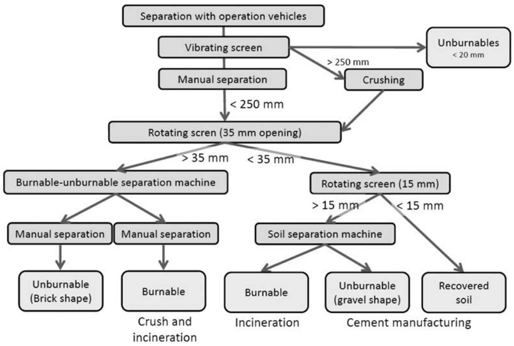

Figure 5. Example of disaster waste treatment system.

2.2 *Policies and limitations for utilization*

At the affected areas, ground subsidence occurred due to the earthquake. For example, maximum lateral and vertical movements were recorded as 5.3 m and −1.2 m respectively at Oshika Peninsula in Miyagi Prefecture. Many other places along the Pacific coast at Iwate, Miyagi, and Fukushima Prefectures suffered more than 0.5 m ground subsidence (Geospatial Information Authority of Japan 2011). These ground subsidence cases are considered mostly permanent, and caused secondary problems such as difficulty in recovery and resettlement, and sanitary problems due to insufficient drainage. Embankment is therefore necessary for the recovery both for residential, commercial, and green areas. Utilization of the materials treated from the disaster wastes and tsunami deposits have been strongly expected. In particular, the geotechnical utilization of the soil fraction in disaster debris and tsunami deposits has become a big challenge for geotechnical engineers since temporal and spatial variations in the geotechnical properties of waste-mixed soils or recovered soils should be considered if a large amount of these soils are used for constructing embankments and levees against tsunami in reconstruction projects.

To promote the utilization of disaster debris in recovery works, the Japanese Ministry of Land, Infrastructure, Transports and Tourism (MLIT) established two technical guidelines to construct (1) parks and green spaces as a redundancy zone against tsunamis in which embankments be constructed using disaster wastes as shown in Figure 6 and (2) fill embankments at the areas where ground subsidence occurred significantly due to the earthquake (MLIT 2012a and 2012b). It was proved that green areas had a positive effect on reducing the energy of tsunami and trapping the flowing obstacles such as cars, while some trees did not have sufficient root depth, which resulted in insufficient resistance against tsunami. Therefore, embankment construction for green areas has been considered advantageous to provide a sufficient distance from groundwater table to the ground surface.

The material criteria proposed by the above guideline are shown in Table 1. There have been several

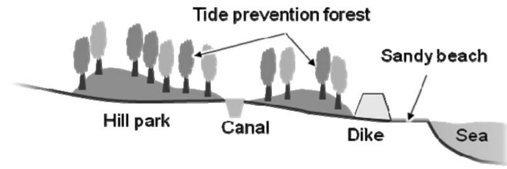

Figure 6. Green park construction for disaster recovery using waste materials (MLIT 2012a).

Table 1. Criteria for the materials treated from disaster wastes used for embankment (MLIT 2012b).

Item	Criteria
Maximum grain size	<300 mm
Cone index	>400 kN/m^2
Salt content (in principle)	<1 mg/g
Electrical conductivity	<200 mS/m
pH	6.0–9.0
Swelling (at CBR soaking)	>3%

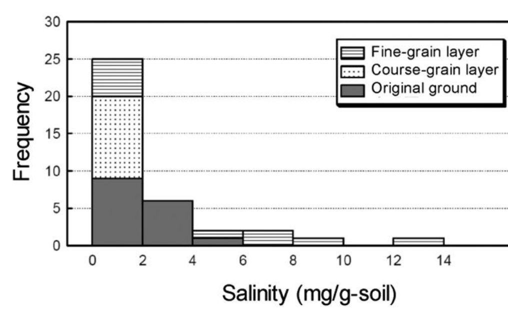

Figure 7. Salinity of the tsunami deposits collected at farmlands in Fukushima Prefecture (Takai et al. 2013).

discussions about these criteria. As for the salt content, to prevent the corrosion of underground steel materials, such as steel piles, and adverse impacts on vegetation, a salt content lower than 1 mg/g is generally required. However, this technical guideline might consider the situation to construct embankments at the tsunami affected areas, in which the salt concentration is already high because they are located close to the ocean, although significant portion of the materials such as tsunami deposits may exceed this criteria of salt content as shown in Figure 7 indicating the results of salt content of tsunami deposits (Katsumi et al. 2013a). It was anticipated that the strict application of this criteria might limit the utilization of materials. Therefore, this technical guideline also covers the utilization of the materials having a salt content higher than 1 mg/g.

Another concern of such materials is the potential of degradability which may cause the generation of gas and leachate and ground settlement. In the field of waste management engineering, ignition loss has been normally used to evaluate the degradability. However, the ignition loss is not only reflected by degradable materials, but also by other components

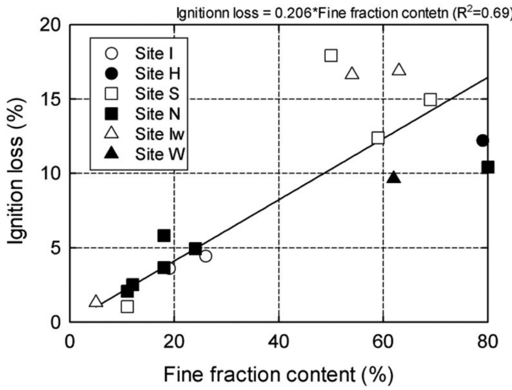

Figure 8. Relationship between the fine fraction content and ignition loss of tsunami deposits (Inui et al. 2012).

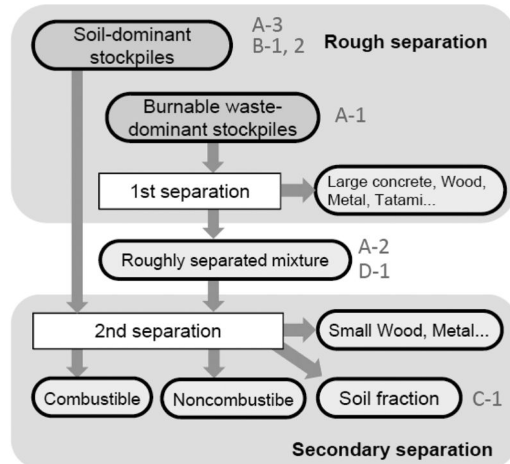

Figure 9. Typical treatment procedure of waste mixed soil (Morita et al. 2012, Katsumi et al. 2013a).

such as hydration products and organic components naturally contained in the original soil. Also, while the standardized test for ignition loss uses samples smaller 2 mm in particle size, if the materials (soils) are rich in fine fraction, they will exhibit higher ignition loss as shown in Figure 8. It is therefore required to establish comprehensive criteria to evaluate the intactness of materials.

2.3 *Characterization of recovered soils*

Evaluating the engineering properties of tsunami deposits and soils separated and/or obtained from disaster waste mixture has been an important issue to ensure their performance, such as stability of the earthen structures if they are used in geotechnical applications in recovery works. However, no experience or knowledge on the treatment and geotechnical properties of such waste mixed soils were accumulated before. Evaluation of the engineering properties of such soils obtained from the disaster debris have therefore been carried out by researchers and engineers, including the JGS (Japanese Geotechnical Society) Geoenvironmnetal Technical Committee on the 2011 East Japan Earthquake and Tsunami chaired by the first author (Okawara et al. 2013).

As mentioned in the previous sub-section, large size wastes were removed from the mixture at a primary temporary storage site (rough separation), and further separation was conducted using trommels, vibrating screens, or other machineries/equipments, at a secondary storage site (secondary separation). Morita et al. (2012) sampled soil-waste mixtures and separated soils from several temporary storage sites, and conducted experiments to evaluate their basic properties such as particle density, particle size distribution, ignition loss, waste composition, compaction, and cone index. Non-separated soil (samples A-1, A-3) and roughly separated soil (A-2) were taken at a first temporary storage site in Town A, and non-separated soil (B-1, B-2) were collected at a storage site in Town B. Secondary separated soil (C-1) was taken at a secondary storage site in Town C. Roughly separated soil (D-1), which passed through a 20-mm opening screen, was taken at a temporally storage site in Town D. The samples used in Morita et al. (2012) are indicated in Figure 9.

One of the most important considerations is the effect of combustible substances on the engineering properties, since these combustibles may be deteriorated, resulting in the emission of gas and leachate, and ground settlement. Ignition loss test conducted on the sample sieved by a 2 mm opening screen according to JIS A 1226 does not consider all the organic matters in the soil-waste mixture mainly consisting of combustible wastes such as wood chips, paper scraps or plastic, etc., because most of these combustible materials exhibit particle size larger than 2 mm. Manual separation in which the fractions over 2 mm were separated into combustible, noncombustible, and soil particles was conducted.

Compaction characteristics of each sample are shown in Figure 10 (Morita et al. 2012). The numbers listed to left side of each compaction curve represent the combustible content larger than 2 mm of each sample, obtained according to the aforementioned method. From this result, the samples of high combustible content such as A-1 and D-1 exhibited a high optimum water content for obtaining the maximum dry density. Besides, the maximum dry density values of such samples are low (1.1 to 1.4 g/cm^3) compared to other samples (1.7 to 2.0 g/cm^3). This is because the samples that contain large amounts of combustible substances cannot be properly compacted, and the densities of combustible substances are low. The samples that contain smaller volumes of combustible substances exhibited lower optimum water contents and higher maximum dry densities, and have clear peaks of compaction curves. Therefore, it is expected that such samples can be used

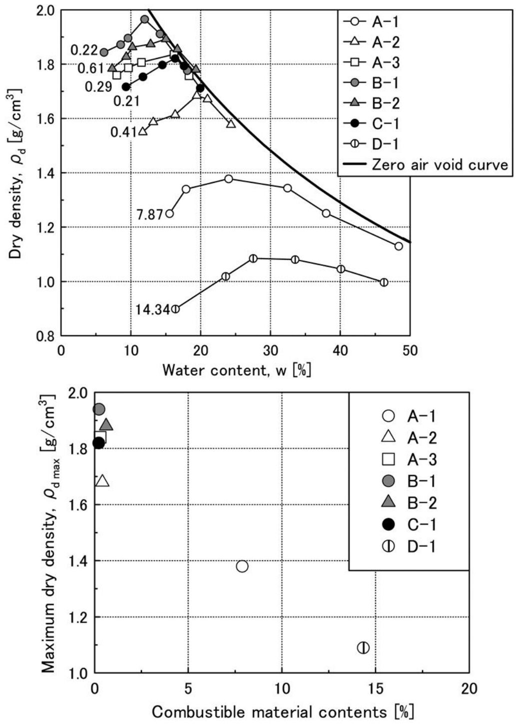

Figure 10. Compaction curves of the soils recovered from disaster debris (upper, Numbers are the content of combustible substances in percentage) and maximum dry density versus combustible contents (lower) (Morita et al. 2012).

Table 2. Classification of recovered soils designated by Iwate prefecture (2012).

Classes	Contents
Recovered Soil Class A	Soils separated from soil-dominant stockpiles
Recovered Soil Class B	Soils separated from waste-mixed stockpiles, and satisfying the criteria for utilization
Separated fine fractions (Recovered Soil Class C)	Fine fractions obtained through the treatment process of disaster waste

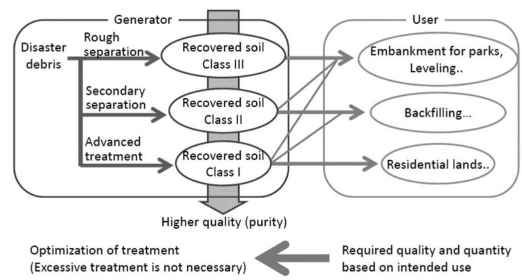

Figure 11. Ideal basic concept of optimization of disaster debris treatment based on the utilization of recovered soils in geotechnical applications (Katsumi et al. 2013a).

as geo-materials with sufficient compaction. Further investigation should evaluate how the waste and combustible matters will affect the engineering properties for a long term by their decomposition if the waste mixed soils or separated soils be used in geotechnical applications.

2.4 *Recovered soils in civil engineering applications*

There are several types of soils recovered from the disaster debris, depending on the original soil, the collection manner and stockpiles, the treatment system, etc. as shown in the previous sub-chapter. Based on the presented results, as well as on the results obtained by the JGS Geoenvironmental Technical Committee on the 2011 East Japan Earthquake and Tsunami (Okawara et al. 2013, Yamane et al. 2013), a "Guideline for Utilization of Treated Wastes for the Recovery Works" has been published by Iwate Prefecture (2013), in which "recovered soils" are categorized into three classes, namely, "Recovered Soil Class A," "Recovered Soil Class B," and "Separated Fine Fractions (Recovered Soil Class C)," depending on their origin and nature. "Recovered Soil Class A" is the soils separated from the soil-dominant stockpiles, mostly tsunami deposits, while "Class B" and "Class C" are the finer fractions (mostly soils) obtained from waste-dominant stockpiles, after rough and secondary separations respectively. This categorization intended the strategic utilization of the recovered soil materials. Class A recovered soils started to be used in the applications for recovery of seaside forests in Iwate Prefecture in 2012 fall.

There was hesitation to promote the utilization of the soils recovered from the disaster debris, in particular from the waste-dominant stockpiles. Construction sectors of the local governments were rather conservative against the utilization of the soils obtained from the disaster wastes, because long-term properties are not well known, as mentioned in the previous chapter. Since the governmental sectors assigned to manage the construction works are different from the sectors responsible of the disaster waste management, utilization would not occur voluntarily, even if a manual or guidelines were established. The creation of incentives to use these soils is also important.

Higher quality recovered soils may be obtained depending on the treatment. In general, the more expensive treatment system might result in the higher quality of the recovered soils. Such high quality soils may not, however, be required for some applications, while for other applications they may be. Therefore, if we have the information about what types of applications are expected, what qualities and quantities of soils are required for these applications, and when these soils are needed, constructing the optimum system of

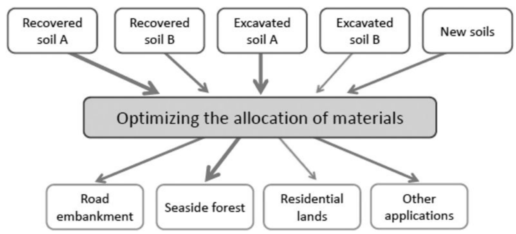

Figure 12. Concept of integrated management of the soils for the disaster recovery discussed by JGS Technical Committee on Recovered Geo-Materials (2014).

disaster waste treatment might have been possible, as shown in Figure 11 for the future disaster.

The recovery and reconstruction works have been done by the environmental, construction, and forestry sections of national, prefectural, and municipal governments, as well as by the private sectors, including railway companies. There are not only recovered soils but also excavated soils, generated in large quantities to cut mountains to create new residential space. In some places, the new soil materials are used due to the scarcity of natural materials. Awareness of the necessity of integrated management of the soil materials beyond these sections started in the related institutions.

The Japanese Geotechnical Society established a Technical Committee on Recovered Geo-Materials in 2013 with the supports from the National Institute for Environmental Studies and the Mud Recycling Association, to present a proposal to tie the different institutions and sections to promote the effective use of soils, either recovered, excavated, or new (Figure 12). In this proposal, three important concepts are presented, namely (1) construction of resilient infrastructures, (2) promotion of use of the recovered materials, and (3) optimization of combined projects, but not single projects, in the area.

3 NUCLIDE CONTAMINATION

Management of the radioactive contamination of surface soils caused by the accident at Fukushima Daiichi Nuclear Power Plant, which includes fall-out radioactive materials such as ^{134}Cs and ^{137}Cs, has been a serious geoenvironmental issue. The tsunami generated by the earthquake caused great damage to widespread coastal areas in the Tohoku Region including Fukushima prefecture where the Fukushima Daiichi Nuclear Power Plant is located. On March 14, 2011, hydrogen explosions occurred in both the No.3 and No.1 reactors. As a result of the explosions, large amounts of radioactive materials including ^{131}I, ^{134}Cs, and ^{137}Cs were released into the atmosphere. Radioactive Cesium exists in (1) wastes and incinerator ashes, (2) sewage sludges, (3) soils and wastes generated from nuclide decontamination works, and (4) excavated soils and wastes from construction works, etc. Countermeasures against such soils and wastes contaminated with nuclides require the approach from several geoenvironmental viewpoints.

The issues may be categorized into three levels, namely (1) the site of the nuclear power plants, (2) area with restricted access due to nuclide concentration, and (3) non-restricted area with low level presence of nuclides. At the site of the plants, issues are the control of contaminated water mainly contaminated with Sr and ^{3}H and safety management of damaged plants and nuclear decommissioning requiring the consideration against several types of nuclides. The detail of these issues is presented by Muto (2014) in this conference.

In the area with restricted access, and also other areas as well, decontamination works have been conducted to reduce the radiation. Large amount of soils and wastes are generated through the decontamination works. Storage and containment of such soils and wastes are an important geoenvironmental consideration, which is presented in the next subsection. The management against ^{134}Cs and ^{137}Cs is required at present.

Even in the non-restricted areas, nuclides are widely present with low concentrations. Through the waste management, such nuclides are concentrated in MSW (municipal solid waste) incinerator ashes. The issue is how to landfill such MSW incinerator ashes because of the presence of nuclides and increase in concentration due to incineration. For this subject, ^{134}Cs and ^{137}Cs are the target nuclides at this moment.

3.1 *Soils and wastes generated through decontamination works*

"Decontamination" work is to remove the soils, plants, trees, and any other materials contaminated with nuclides from our environment to reduce the radiation and decrease the risk of exposure. Currently, the Japanese government has designated three areas, including (1) area where the residence will be difficult, (2) area where the current residence is restricted, and (3) area where over-night stay is restricted. In such areas, decontamination projects are conducted by the national budgets.

Since nuclides fell out all over the ground, all the grasses and soils should be removed to reduce the radiation. From the purpose of decontamination, "shaving" of only 1-cm thick soil is considered sufficient. It is however difficult to shave such thin soil layer, and thicker layer of soils, e.g., 5 cm, are therefore removed, which results in a larger quantity of contaminated soils to be stored and contained. These soils might contain grasses and other organic materials which will be subjected to degradation causing gas, heat, and leachate generations and reduction in volume. Containment of such materials requires consideration against such phenomena. Gas permeable geomembranes developed are applied at such temporary storage sites (Ishida et al. 2014).

Through this decontamination works, large amounts of soils and wastes have been generated. For the

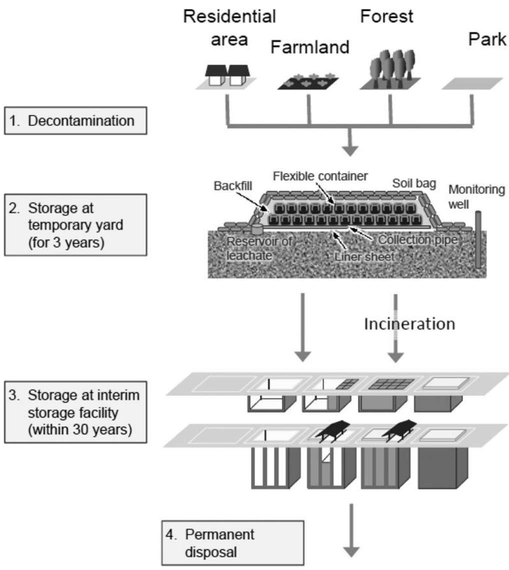

Figure 13. Disposal scenario of radioactive contaminated soils and wastes (MOE 2011).

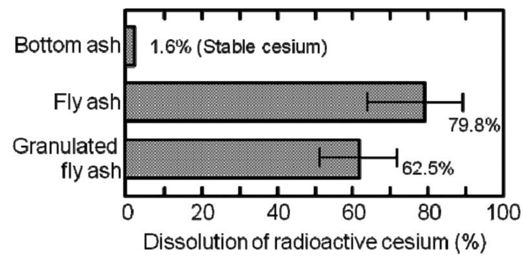

Figure 14. Leaching ratio of radioactive cesium from MSW in-cinerator ashes (NIES 2012).

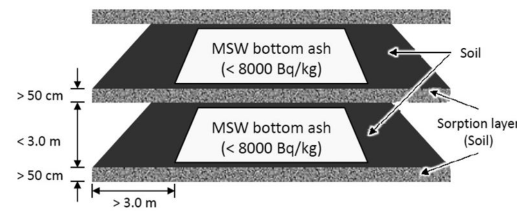

Figure 15. Landfill of MSW bottom ash lower than 8000 Bq/kg with lower dissolution (edited from NIES (2012)).

waste soils and plants discharged through decontamination works, the scenario consisting of storage at a temporary storage yard (for ~3 years), then at an interim storage facility (for ~30 years), and finally at a permanent disposal site, has been decided by the national government (Figure 13). The MSW higher than 100,000 Bq/kg are also considered under this scenario. Currently, only temporary storage sites have been facilitated, because of the difficulty in receiving the agreements for the construction of interim storage facilities. At the interim storage facilities, as well as at the permanent disposal sites, establishment of design method including the use of geosynthetics for reinforcement, hydraulic, and chemical barrier, filtration, and other functions, is strongly anticipated. Soils and wastes that require management are estimated to be more than 20,000,000 m^3. Management of such materials in terms of logistics is another important consideration.

3.2 *MSW incinerator ashes with nuclides*

Sewage and waste materials may contain radioactive substances concentrated through natural and artificial processes in some areas in the Tohoku and Kanto regions in Japan. The wastes that contain radioactive materials lower than 8,000 Bq/kg are allowed to be disposed of at existing MSW (municipal solid waste) landfill sites, according to regulations. However, these regulations only consider the exposure of radioactive substances to workers, but not the fate and transport of these substances in the subsurface, including landfill sites. Leachate with nuclide contamination exceeding regulatory satisfactory level should not be generated, because existing leachate treatment facilities installed at landfill sites do not have a capability to treat nuclide contamination. Leaching from the landfilled materials is an important consideration. For example, the leaching ratios are very different between MSW bottom ash and fly ash, as shown in Figure 14, even though they may contain the same level of concentration of radioactive cesium. While radioactive cesium in MSW bottom ash may be stable in terms of the leaching (only 1.6% leaching ratio), 79.8% cesium from fly ash, and 62.5% from granulated fly ash, will leach out (NIES 2012).

It should also be noted that the basic concept of Japanese MSW landfills is to allow the infiltration of rainfall into the waste layer, and to accelerate the biodegradation under semi-aerobic condition, as well as to wash out the contaminants that may be dissolved. At the landfill sites designed following such basic concept, if the leaching ratio of radioactive cesium in the disposed wastes is high, it will be important to evaluate its fate and transport, because the existing landfill leachate treatment facilities will not be able to treat the radioactive cesium. Installing soil layers to act as a sorption layer against radioactive cesium is required for MSW bottom ash as shown in Figure 15, while soil layers both for hydraulic barrier and for sorption are required for MSW fly ash which exhibits higher leaching potential as shown in Figure 16.

Since these soil layers may be constructed over the existing waste layer, differential settlement and chemical compatibility should be taken into account. Geosynthetic reinforcement such as geogrids and/or geosynthetic barriers such as GCLs may be considered for the safe disposal of such waste materials. Researches on the applications of such geosynthetics against differential settlement and chemical compatibility are expected (Katsumi et al. 2012, Kimura et al.

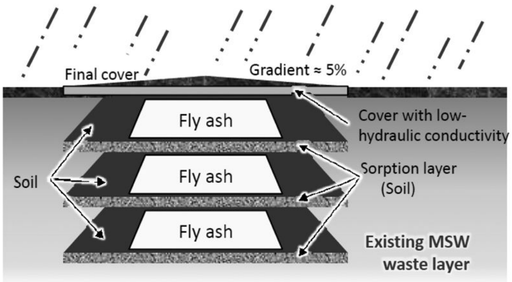

Figure 16. Landfill of MSW fly ash lower than 8000 Bq/kg with higher dissolution (edited from NIES (2012)).

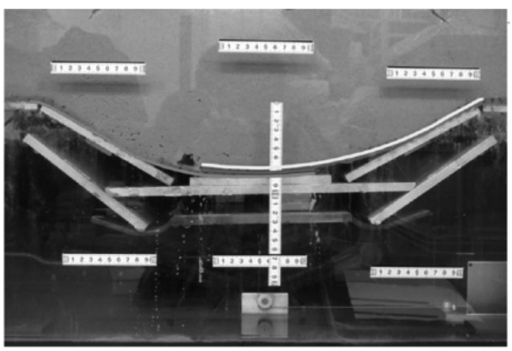

Figure 17. Trapdoor experiment to evaluate the effect of differential settlement on overlapped GCLs: Upper GCL in yellow, lower GCL in blue, and overlapped section in red for image analysis. (Ogawa et al. 2013).

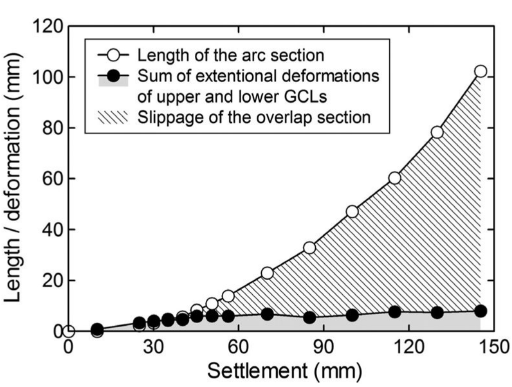

Figure 18. Profiles of extensional deformations of GCLs and slippage of the overlap section (Ogawa et al. 2013).

2013, Ogawa et al. 2013). Figure 17 shows an experimental apparatus to evaluate effects of the differential settlement on hydraulic barrier performance of overlapped needle-punched GCLs presented in Ogawa et al. (2013). The overlapped GCLs deformed with the shape of an arc as the differential settlement progressed. The overlapped section was subjected to slippage, and the overlap length decreased from 151 mm to 56 mm after the test. Extensional deformations were also observed in both upper and lower GCLs. These results present that both slippage and extensional deformation contributed to the change in length of the arc section due to differential settlement. Change in the contributions of extensional deformation and overlap slippage with the settlement of the trapdoor plate is presented in Figure 18. When the settlement was less than 45 mm, no slippage occurred at the GCLs overlap section, due to the sufficient frictional forces acting on the interfaces between upper/lower GCLs and GCL/soil. As further settlement progressed and the tensile force became larger, the overlap section started to slip. Once the slippage occurred, extensional deformation of GCLs did not developed anymore. Such mechanisms of deformation of soil layers should be discussed under different conditions, such as types of GCLs, soils, wetting conditions, overburden pressures, etc. to provide the proper design and construction of these soil layers.

4 CONCLUDING REMARKS

Among the geoenvironmental issues caused by the 2011 East Japan earthquake and tsunami, the generation of disaster debris and tsunami deposits and the geotechnical investigations on the soils recovered from the disaster debris, as well as the countermeasures against nuclide contamination of soils and wastes, are presented in this paper. Utilization of disaster debris for the recovery works after proper treatment has been proposed at the disaster affected areas, in particular at the areas where significant subsidence occurred due to earthquake. Characterization of waste mixed soils obtained from the disaster debris that was conducted to evaluate the applicability to construction materials for disaster recovery requires further research in understanding the physical, chemical, and biochemical effects. As for the nuclide contamination due to nuclear power plant accident, concerns should be addressed to the storage and containment of the soils and wastes generated from nuclide decontamination works, as well as the MSWs and incinerator ashes generated even in the area without restricted access but with low level presence of nuclides. Fate and transport of radioactive cesium including leaching from MSW bottom and fly ashes is an important consideration. Performance of sorption and barrier layers applied in the existing MSW landfill sites should be discussed from the viewpoints not only of chemical phenomenon but also physical and mechanical phenomenon.

ACKNOWLEDGEMENTS

Contributions and discussions provided by the members of JGS (Japanese Geotechnical Society) Geoenvironmental Technical Committee on the 2011 East Japan Earthquake and Tsunami chaired by the first author are greatly appreciated. Many individuals from

Iwate, Miyagi, and Fukushima Prefectural Governments, Japan Ministry of Land, Infrastructure, and Transport, Ministry of Environment, Forestry Agency, Reconstruction Agency, National Institute for Environmental Studies, Mud Recycling Association, and other institutions provided valuable information and discussion.

REFERENCES

Brown, C., Milke, M., and Seville, E. (2011): Disaster waste management: A review article, *Waste Management,* Vol.31, pp. 1085–1098.

Geospatial Information Authority of Japan (2011): Land subsidence caused by 2011 Tōhoku earthquake and tsunami, http://www.gsi.go.jp/sokuchikijun/sokuchikijun40003.html (accessed on 2013 August 10, in Japanese).

Inui, T., Yasutaka, T., Endo, K., and Katsumi, T. (2012): Geo-environmental issues induced by the 2011 off the Pacific Coast of Tohoku Earthquake and tsunami, *Soils and Foundations,* Vol.52, Issue 5, pp. 856–871.

Iwate Prefecture (2013): Guideline for Utilization of Treated Wastes for the Recovery Works (Revised version), http://ftp.www.pref.iwate.jp/download.rbz?cmd=50&cd=43951&tg=3 (accessed on 2013 August 10, in Japanese)

JGS Technical Committee on Recovered Geo-Materials (2014): Use of Recovered Geo-Materials for the Disaster Recovery, https://www.jiban.or.jp/index.php?option=com_content&view=article&id=1540&Itemid=148 (in Japanese).

Ishida, M., Yamamoto, K., Toyooka, S., Akai, T., Nishimura, M., and Kamon, M. (2014): Comparative experiments on covers for temporary storage sites of contaminated waste with radioactive materials, *Geosynthetics Technical Information,* IGS Japan Chapter, Vol.30, No.1, pp. 22–27 (in Japanese).

Katsumi, T., Kotake, N., and Viswanadham, B.V.S. (2012): Geosynthetics for environmental protection – Compatibility and integrity, *Geosynthetics Asia 2012 – 5th Asian Regional Conference on Geosynthetics,* D.T. Bergado (ed.), pp. 47–68.

Katsumi, T., Inui, T., Takai, A., Endo, K., Sakanakura, H., Yasutaka, T., Otsuka, Y., Suzuki, H., Sakamoto, H., Okawara, M., and Imanishi, H. (2013a): 2011 East Japan earthquake and tsunami – Geoenvironmental challenges, *Coupled Phenomena in Environmental Geotechnics – From Theoretical and Experimental Research to Practical Applications,* M. Manassero, A. Dominijanni, S. Foti, and G. Musso (eds.), CRC Press, pp. 335–340.

Katsumi, T., Endo, K., Imanishi, H., Inui, T., Okawara, M., Otsuka, Y., Sakamoto, H., Sakanakura, H., Suzuki, H., Takai, A., and Yasutaka, T. (2013b): Geoenvironmental challenges –Beyond the 2011 East Japan earthquake and tsunami, *IGS 2013 Indian Geotechnical Conference – Geotechnical Advances and Novel Geomechanical Applications,* Indian Geotechnical Society Roorkee Chapter, (on CD).

Kimura, F., Naka, A., Inui, T., Takai, A., and Katsumi, T. (2013): Cesium sorption characteristics of sodium bentonite affected by coexisting cations in leachate, *Geo-Environmental Engineering 2013 – 12th Global Joint Seminar on Geo-Environmental Engineering,* Seoul National University, pp. 40–43.

Ministry of Environment (MOE) (2011): Guidelines on the Treatment of Waste Contaminated by Accidental Nuclides (in Japanese).

Ministry of Environment (MOE) (2014): Treatment of disaster debris from 2011 East Japan earthquake, http://kouikishori.env.go.jp/table/pdf/shori140425.pdf (in Japanese).

Ministry of Land, Infrastructure, and Transport (2012a): Technical Guideline on the Development of Parks and Green Spaces in the Reconstruction from the off the Pacific coast of Tohoku Earthquake Disaster, http://www.mlit.go.jp/common/ 000205823.pdf (access on 2013 August 10, in Japanese).

Ministry of Land, Infrastructure, and Transport (2012b): Basic Concepts on the Utilization of Recycled Materials in Constructing Fill Embankment to Accelerate the Revitalization from the Earthquake Disaster, http://www.mlit.go.jp/common/000208618.pdf (access on 2013 August 10, in Japanese).

Morita, K., Katsumi, T., Takai, A., and Inui, T. (2012): Characterization of waste mixed tsunami sediments generated by the 2011 East Japan earthquake and tsunami, *Geo-Environmental Engineering 2012 – Proceedings of the 11th Japan-Korea-France-Canada Joint Seminar on Geoenvironmental Engineering,* Caen University, pp. 33–42.

Muto, S. (2014): Fukushima Accident: What happened and lessons learned, *Fourth International Conference on Geotechnical Engineering for Disaster Mitigation and Rehabilitation* (in press).

National Institute for Environmental Studies (2012): Proper waste treatment and disposal considering the fate and transport of radionuclide – Ver.2 (in Japanese).

Ogawa, S., Sumoto, S., Inui, T., Takai, A., and Katsumi, T. (2013): Hydraulic barrier performance of overlapped geosynthetic clay liners subjected to differential settlements, *Geosynthetics Engineering Journal,* Vol.28, pp. 103–108 (in Japanese with English abstract).

Okawara, M., Otsuka, Y., Sakamoto, H., Takai, A., Imanishi, H., Endo, K., Omine, K., Kazama, M., Katoh, M., Kotake, N., Shuku, T., Suzuki, H., Nakagawa, M., Nakano, M., Nishimura, S., Fujikawa, T., Matsuyama, Y., Yamanaka, M., and Katsumi, T. (2013b): Properties of separated soil generated through disaster waste treatment, *Proceedings of 10th JGS Symposium on Environmental Geotechnics,* JGS, pp. 355–360 (in Japanese).

Takai, A., Endo, K., Yasutaka, T., Inui, T., and Katsumi, T. (2013): Characterization of tsunami deposits toward utilization followed by the 2011 East Japan Earthquake and tsunami, *Proceedings of Congrès GESeD (Gestion Environnementale des Sédiments de Dragage),* O21 (on CD).

Yamane, K., Morita, K., Takai, A., Inui, T., Katsumi, T., and Otsuka, Y. (2013): Physical properties of the soils separated from disaster wastes, *Geo-Environmental Engineering 2013 – 12th Global Joint Seminar on Geo-Environmental Engineering,* Seoul National University, pp. 130–136.

Geotechnics for Catastrophic Flooding Events – Iai (Ed)
© 2015 Taylor & Francis Group, London, ISBN 978-1-138-02709-1

Fukushima Accident: What happened and lessons learned

Sakae Muto
Former Chief Nuclear Officer and Executive Vice-president of TEPCO, Tokyo, Japan

ABSTRACT: On 11th March, 2011, a massive earthquake of magnitude 9.0, the fourth largest ever recorded worldwide, caused huge tsunami along the Pacific coast of Japan. The quake was caused by simultaneous move of several regions with area of 500 km × 200 km slipped off the coast along the trench. The tsunami significantly exceeded stations design bases to cause station blackout including emergency power supply. It caused core meltdown to release large amount of radio activities. Now reactor cores are all cooled by circulating water. Road map for decommissioning work has been set, and work is now in progress. Many lessons have been learned through the accident. Measures have been taken in other nuclear power stations to enhance safety. To be prepared for the unpredicted in more flexible way is the key point to increase resilience against large natural disaster including huge tsunamis.

1 THE EARTHQUAKE AND TSUNAMI

1.1 *Great East Japan Earthquake*

Great East Japan Earthquake of M9.0 broke out at off the coast of the Pacific Ocean on 11th of March 2011 at around 14:46 in Friday afternoon. The hypocenter was off the Sanriku coast (38° 6.2′N, 142′51.6′E) with focal depth of 24 km. The Japan Meteorological Agency Seismic Intensity Scale, which has seven Ranges with ten Grades (Range: 0–7, 10 grades with 5-Upper/Lower, 6-Upper/Lower) was 7 in Kurihara City, Miyagi Prefecture, 6-Upper in Naraha, Tomioka, Okuma, and Futaba Towns in Fukushima Prefecture where Fukushima Daiichi and Fukushima Daini Nuclear Power Station are sited.(*1) (Fig.1) The acceleration at the station was at around the level of design basis of those stations. No damage by quake in safety related equipments is reported. (Table 1)

1.2 *Tsunami*

The tsunami height at those power stations, however, significantly exceeded the design bases. All of Japanese nuclear power plants including Fukushima have been designed against tsunami by Japan Society of Civil Engineers (JSCE) Tsunami Evaluation Methodology published in 2002. That methodology has set a standard for tsunami evaluation for nuclear power station design. The methodology was made through discussions by academic expert as well as industry specialist in JSCE Nuclear Power Committee. The method is based on many historical data in various regions with the state-of-the-art simulation technology. It defines eight regions for tsunami evaluation along the Pacific coast from Hokkaido to Boso. (1 through 8 in Fig. 2) (*2) The methodology has been referred in IAEA Safety Standards "Meteorological and Hydrological Hazards in Site Evaluation for Nuclear Installations" (SSG-18)(*3)

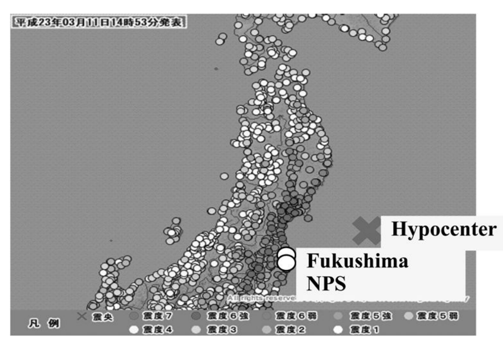

Figure 1. Great East Japan Earthquake and its Japan Meteorological Agency seismic intensity scale.

The methodology shows wave sources for each region which is needed for tsunami height evaluation.

The wave source of 3–11 earthquake, however, was much larger and slipped area included multiple areas in the methodology. Simultaneous move of multiple regions caused much higher tsunami than the value given by JSCE methodology. (Fig.3) (*4) No organization including JSCE and The Headquarters for Earthquake Research Promotion (HERP), one of Governmental organizations, indicated possibility of simultaneous move of multiple regions before 3–11.

Originally Fukushima Nuclear Power Station was designed with historical maximum tsunami height along Fukushima coast of 3 meters which was recorded by Chilean earthquake. The design was done in 1960's, and the license was still legally valid on 3–11 with the

Table 1. Observed Acceleration vs. Design.

Observation point (R/B basemat)	Observed Acceleration (Gal			Design Base Acceleration (Gal)		
	NS direction	EW direction	UD direction	NS direction	EW direction	UD direction
Unit 1	460	447	258	487	489	412
Unit 2	348	550	302	441	438	420
Unit 3	322	507	231	449	441	429
Unit 4	281	319	200	447	445	422
Unit 5	311	548	256	452	452	427
Unit 6	298	444	244	445	448	415

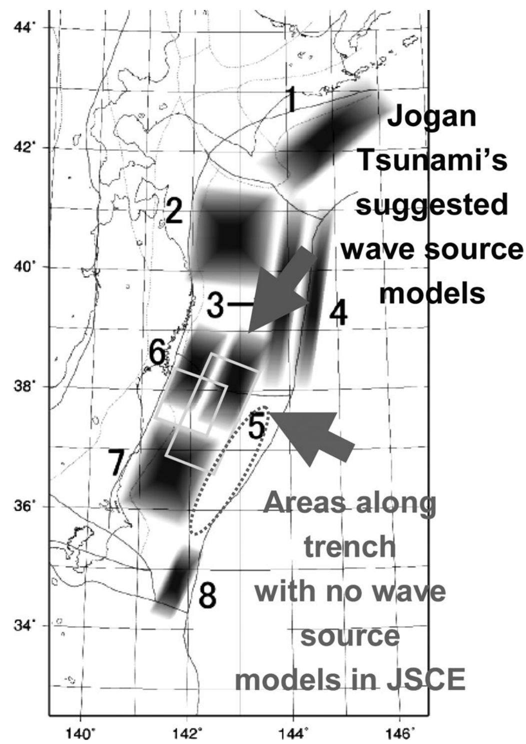

Figure 2. JSCE wave sources.

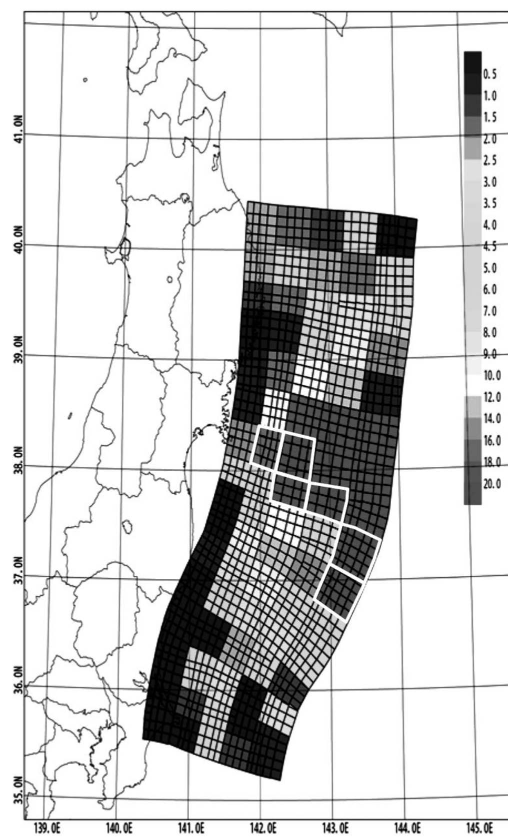

Figure 3. Actual sources.

height. After the plate tectonics theory evolved, the JSCE's methodology with numerical simulations was developed based on the theory. It had given 6 meters design basis for Fukushima. It has been reported to the regulatory body. The original design height was doubled and measures to raise height of sea water pump motors at pump yard have been implemented. Other nuclear power stations in Japan also applied the methodology and increased the design bases as well.

Even though JSCE methodology had been believed to give comfortable margin because of its extensive approach with conservative simulations, TEPCO started to discuss if any other wave sources should be added to the methodology for higher safety.

One was as to areas along Japan Sea Trench off the Fukushima coast where no record existed in history that caused tsunami in past. The other is how to handle Jogan tsunami in 9th century (AD869), where some researchers had suggested possible wave sources. (Fig. 2)

JSCE methodology divided Japan Sea Trench into several areas and defined wave sources for each. HERP, on the other hand, issued a report, "Long term evaluation of earthquake activities in Sanriku coast to Boso coast" also in 2002.(*5) The report treats the areas as one long block without excluding off the coast of Fukushima where there was no earthquake recorded in history. The reason to handle the area as such was not clearly stated by HERP. It did not give any wave source data required for tsunami simulation.

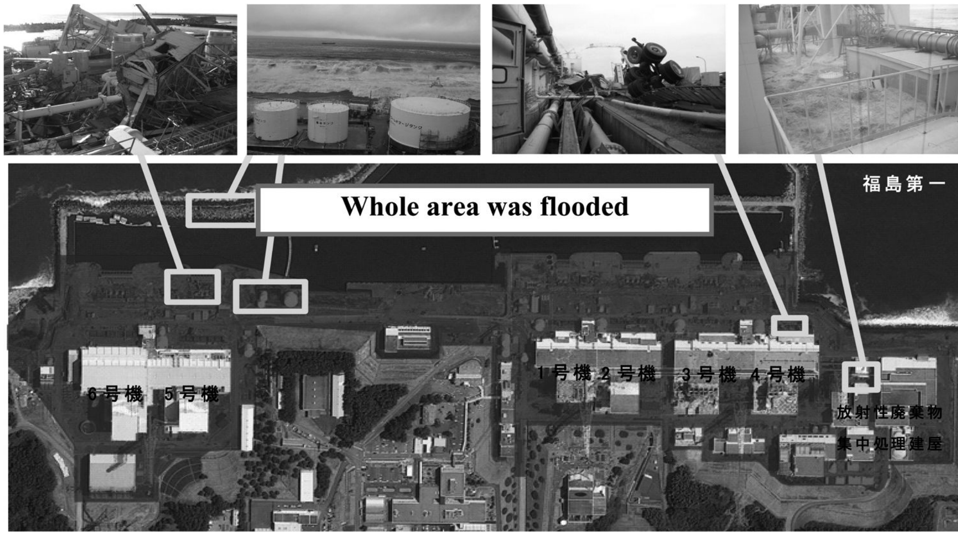

Figure 4. Flooded Area of Daiichi (Blue Part).(*4)

Since back-check of seismic safety was required in 2008, where deterministic evaluation was needed, TEPCO started to do some trial calculations for higher safety with very hypothetical assumptions for those areas where JSCE methodology did not define wave source. It resulted in higher tsunami height than JSCE methodology. JSCE had tried to study those beyond design tsunami with probabilistic approach in past but the method was not yet ready for practical application.(*6)

It resulted in asking JSCE to deliberate whether or not it would be appropriate to consider those in the methodology. JSCE was in final stage to conclude the results, when the huge tsunami came on 3-11. The Central Disaster Management Council in Cabinet did not include these tsunamis in the disaster management planning either.(*7)

As to Jogan, since the suggested wave sources were based on survey in Miyagi far north from Fukushima down to northern Fukushima, TEPCO had surveyed tsunami deposit along the Fukushima coast down south to confirm if it had any traces around. It resulted in no significant record around nuclear power stations.

The wave source of 3-11, which is some 200 km in width and 500 km in length, is significantly different and larger than suggested Jogan or hypothetical calculations. The source of 3-11 shows that seven or eight wave sources in the JSCE methodology had moved simultaneously. Thus, it caused far beyond the design basis tsunami, which was not predicted beforehand.

1.3 *Impact of earthquake and tsunami*

The reactor or turbine buildings are located at 10 to 13 meters above sea level in Fukushima Daiichi. Sea water pumps for both normal and emergency cooling are located in pump yard at 4 meters above sea level.

The tsunami inundation height was about 15 meters above sea level, and all of six units in Fukushima Daiichi were flooded severely.

Also the tsunami brought many debris scattered around, which along with many aftershocks made the access to the field after the accident very difficult.

The direct cause of the accident is that tsunami had crippled ability to cool. Even though all of reactors in operation were safely shut down automatically ("SCRAM"ed), decay heat has to be removed by cooling system. Losing cooling capability would lead to damages and melting of cores.

In-coming nine off-site power transmission lines in Fukushima Daiichi had been lost by the earthquake, but emergency diesel generators had supplied power until tsunami hit the power station. There were 13 emergency diesel generators in Fukushima Daiichi Nuclear Power Station. Tsunami caused those all except for one in Unit 6 inoperable by flooding diesel generator itself or flooding sea water cooling pumps for diesels. One in Unit 6 which was air-cooled, continued to supply power to Unit 5 and 6 after the tsunami. That differentiated the result of Unit 5 and 6 which was safely cooled down.

Most of switch gears which distribute power to equipments were also flooded, which made the recovery work difficult.

Identified inundation routes are such as building entrance, equipment hatches, emergency diesel generator air intake louvers, and so forth. All of those route lead to flooding emergency diesel generators as well as switch gears and even DC batteries to supply power to control systems.

Loss of seawater system had made generators which were not flooded inoperable except for one in Unit 6.

Since incoming AC power had been lost by the quake, losing those means losing all of the AC and DC power sources to cause complete station blackout.

Table 2. Status of Emergency Diesel Generators.(*4)

Locations of EDGs and damage by the tsunami

		Fukushima Daiichi NPS						Fukushima Daini NPS			
		Unit 1	Unit 2	Unit 3	Unit 4	Unit 5	Unit 6	Unit 1	Unit 2	Unit 3	Unit 4
Tsunami height *1		Approximately +13 m						Approximately +9 m			
Site height		O.P.+10m				O.P.+13m		O.P.+12m			
Flood depth around major buildings [Flood height]		Approx. 1.5 ~ approximately 5.5m [O.P. approximately+11.5 ~ approximately +15.5m]*2				Approx. 1.5m or less [O.P. approximately+13 ~ approximately 14.5m]		Approximately 2.5m or less (almost zero apart from around Unit 1) [O.P. approximately +12 ~ approximately 14.5			
D/G installation building [installed floor]	subsystem-A	turbine building [1st basement floor]	turbine building [1st basement floor]	turbine building [1st basement floor]	turbine building [1st basement floor]	turbine building [1st basement floor]	reactor building annex [1st basement floor]	reactor building annex [2nd basement floor]	reactor building annex [2nd basement floor]	reactor building annex [2nd basement floor]	reactor building annex [2nd basement floor]
	subsystem-B	turbine building [1st basement floor]	shared pool building [1st floor]	turbine building [1st basement floor]	shared pool building [1st floor]	turbine building [1st basement floor]	D/G building [1st floor]	reactor building annex [2nd basement floor]	reactor building annex [2nd basement floor]	reactor building annex [2nd basement floor]	reactor building annex [2nd basement floor]
	HPCS system						reactor building annex [1st basement floor]	reactor building annex [2nd basement floor]	reactor building annex [2nd basement floor]	reactor building annex [2nd basement floor]	reactor building annex [2nd basement floor]

The main D/G unit was flooded

The main D/G unit was not flooded

*1: Tsunami height at the tidal stations. Due to instrument damage, the actual height of the tsunamis at the tidal stations are not known.
*2: Local area where O.P. approximately +16 ~ approximately +17 m [flooding depth approximately 6~7 m] in the southwest part of said area
*3: Local area where O.P. approximately +15 ~ approximately +16 m [flooding depth approximately 3 ~ 4 m] from the south side of

-EDG for Fukushima Daiichi Unit 5 is installed in the turbine building
-This main EDG unit was not flooded

-EDG for Fukushima Daini Unit 1 is installed in the reactor building annex
-This main EDG unit was flooded

Practice in licensing then was to assume half an hour loss of power in design, and the battery capacity lasts for eight hours, but the blackout state lasted for days to cause melting down of three cores.

Tremendous water force of tsunami was observed in the station. Very large heavy machineries were adrift and very thick door for physical protection were breached easily by massive tsunami. Breakwater was collapsed in water intake. Along with aftershocks, those also made the recovery work onsite difficult.

1.4 *Sequence of accident*

There are six nuclear power units in Fukushima Daiichi and four in Fukushima Daini totaling ten units.

Two stations are separated by 12 km with Daiichi in north. Out of ten, seven were in operation on 3-11.

<Fukushima Daini and Fukushima Daiichi Unit 5/6>

All of Fukushima Daini units were at the rated power. All of Fukushima Daiichi and Daini Units except for Unit 3 of Daini lost their heat sink because they lost pumps at 4m above sea level. In Daini, however, there remained power. In-coming off-site power was available in Daini. It made possible for Daini to monitor reactor status and to succeed to depressurize reactors and used make-up water pumps (MUWP) to inject water to cores as defined in accident management procedures.

Total of 9 km length of temporary cables were installed to activate the newly brought-in temporary sea water pumps which were either air- or land-carried to the station and cold shut down was achieved in all of Daini Units by 15th of March.

Installing cables required two hundred electric technicians who were also brought in from Transmission and Distribution Division of TEPCO.

In Fukushima Daiichi Unit 5 and 6, the situation is similar to Fukushima Daini, though these two were in outages. There was power supplied by diesel generator, which made it possible to monitor the status by instruments. Temporary sea water pumps were installed to recover the ultimate heat sink.

<Fukushima Daiichi Unit 1, 2, 3, and 4>

The situation was very different in Unit 1 through 4 of Daiichi. All the power was lost both in-coming power and emergency diesels as well as most of DC batteries. It deprived of all instruments and lightings in buildings except for Unit 3 where DC batteries survived and supplied power to instruments for a while.

Monitoring of critical plant parameters such as reactor water level or containment pressure was done with brought-in temporary batteries and portable generators. Those were connected to instruments, which were read by flash lights.

Equipments and procedures arranged for beyond the design base accident, which is referred as accident management, could not be applied because of flooding and/or complete station blackout. Those procedures were applied to Fukushima Daini units and it worked to cool down reactors, but in Daiichi, cooling had to be done with equipments or procedures which had not been prepared beforehand.

Fire engines were used to inject fresh- and then sea-water to cores for cooling. The core, however, was overheated and melted to generate hydrogen by metal-water reaction. Hydrogen that was leaked out to reactor building (R/B) exploded in Units 1, 3, and 4. Explosion of Unit 4 was believed to be caused by hydrogen from Unit 3, as Unit 4 was in refueling outage and no fuel was loaded in core. In Unit 2, blowout panel was incidentally opened up by explosion on Unit 1, so that no hydrogen was accumulated.

The core temperature was lowered to below 100 degrees C by 16th of December, 2011 by sea water and then fresh water injection for those units.

Figure 5. The assistant shift supervisor working at his desk with temporary lighting.

1.5 *Difficulty on site*

Because tsunami devastated the whole site along with no power available, the operation in Fukushima Daiichi damaged units after tsunami was extremely difficult.

Lighting was lost inside and outside of buildings. No instruments except for Unit 3 were available, and debris were scattered in field to make it difficult to access.

Communication tools were limited. Personal handy phone which was used in daily onsite operation was not operable because of power failure or loss of its repeater station itself by tsunami. Public cell phone was available at the beginning but was difficult to connect, and then it also went out because probably the base station lost power as well. It made communication between main control room, emergency response center, and/or field very difficult.

Transportation was also difficult because many roads were broken and fell. Aftershocks made workers stay at high locations for long as a precaution for another tsunami, and they had to be called back many times as they felt aftershocks even if they were allowed to go outside for work.

In the evening of the first day, the core of Unit 1 was damaged, and radiation level inside and outside of building increased that made another major obstacle for work. Full face mask were required for preventing inhalation, which impaired operability significantly.

Symptom based operation guide was prepared, which was believed to be useful in case of severe accidents, but the situation overwhelmed those predetermined emergency procedures.

TEPCO report[*4] states some employee's testimony, which well indicates those difficulties. These are part of those testimonies.

"At the time when the tsunami arrived I saw the lamps on the Unit 1 and 2 power panels flicker and then all go out at once. The D/G (Diesel Generator) stopped and lamps started to go out one by one, I had no idea what was happening."

"When we were about halfway down the corridor (turbine building basement corridor) the fire alarm went off and we turned back sensing danger. Then suddenly the lights went out and we could hear that the D/G had stopped. We just started running, passed the M/C room and up the stairs when suddenly a large amount of water started pouring through the airtight door to the D/G room."

"With the power out I felt more of a sense of helplessness than fear. Young operators looked uneasy. Some started yelling, "We can't do anything, there is no reason for us to be here, why do we have to stay!?" (In response to being asked about how the situation resolved itself) I bowed my head and said, "Please stay" at which point another shift supervisor also bowed his head in silence. We told two young trainees to evacuate to the seismic isolated building and asked for a nod of approval from everyone else."

"We had undergone extensive training but none of that was applicable. It was as if we had had our legs and arms cut off and were just sitting there looking at the data that was available. Then when the first hydrogen explosion occurred some people start to lose it."

"The power station I had been so accustomed to seeing underwent a complete change. Not just the reactor buildings that exploded, but everywhere I could see had suffered damage and a copious amount of debris had been scattered about. Also, heavy fuel oil tanks had been washed up to the site which is 10 m above sea level and were blocking roads, and tons of cars and been turned over. The night was dark and eerily silent."

"When I went to the suppression chamber (S/C) after being told to check if S/C vent valves were open, my shoes melted. I could not see the valve because it was at the very top. When I put my foot on the torus to check the temperature my sole melted instantly. I decided I shouldn't proceed."

Figure 6. Temporary batteries were connected to instruments to power them.

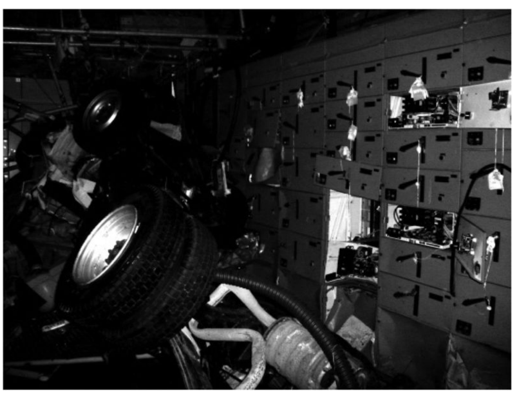

Figure 7. Truck that had been stuffed into the back of the Unit 4 truck bay (photographed in the days after the disaster).

"Aftershocks caused the most trouble. We'd leave and have to come back, leave and come back. And, it took time to confirm safety in each instance. When there was a large aftershock we would rush back as if our life was in danger. So, we weren't ready to merely head back out after the quake ended and usually needed two hours or so to recover after which we headed back out."

"There was water in the electrical equipment room. I had to work in rubber boots. I assumed that no current was flowing, but it was scary because there was a possibility of lethal electrocution."

2 RELEASED ACTIVITIES AND OFF-SITE EVACUATION

The government had ordered evacuation and sheltering from right after the accident. The source term (amount of activities released at origin) could not be measured in case of Fukushima.

In design bases, the plant is designed so as to measure those amounts by radiation monitors installed at stack. The radiation levels surrounding station are also

Figure 8. Heavy fuel oil tank swept up by the tsunami and blocking the road (Diameter: 11.7 m Height: 9.2 m).

monitored by monitoring posts which covers all directions continuously. Those data are transferred on-line to government, which will make appropriate orders including evacuation possible.

In case of Fukushima, because there was no power, the stack monitors or the on-line system did not work. The plant status could be barely monitored by hooking up temporary batteries, and available mobile monitoring cars monitored radiation doses at some points, they were not enough to estimate source term in real time.

Still the government ordered evacuation or sheltering at early stage of the accident. At 21:23 on 3-11, evacuation in 3 km radius and taking shelter in 10 km radius of Fukushima Daiichi was ordered. The area was expanded gradually including Fukushima Daini.

On April 21, 20 km radius of Fukushima Daiichi is designated as "Restricted Area", and on 22, "Deliberate Evacuation Area" was set for the areas in northwest beyond 20 km radius where doses were regarded high and cumulative dose might reach 20 mSv in a year.

It is believed that high level of radiation in those northwest areas was results of releases from Unit 2 in the morning of March 15.

Total amount of released activities was estimated by several organizations after the accident. TEPCO also evaluated it inversely from the environmental monitoring data obtained by some monitoring cars. Since there were no stack monitors and monitoring posts available, there are many assumptions. It was evaluated that the release was 500 peta Bq (5×10^{17}) Bq as iodine 131.

If we compare Fukushima with Chernobyl, and TMI, in Fukushima the released activity is about one order of magnitude larger than TMI and about 20 percent of Chernobyl. More than 100 thousands people were evacuated and still they are. No acute fatality by radiation is reported in Fukushima. (Fig. 9)

It should be noted that the consequences of meltdown of three cores are not acceptable in any sense and rigorous corrective actions should, and actually are to be taken. On the other hand it is noteworthy as well that no acute fatalities were recorded for even on-site workers. Delayed health effects are not expected either for public. In General Assembly of United Nations, it is stated that the assessment of the United Nations Scientific Committee on Human Exposure to Radiation shows that there was "no significant adverse health

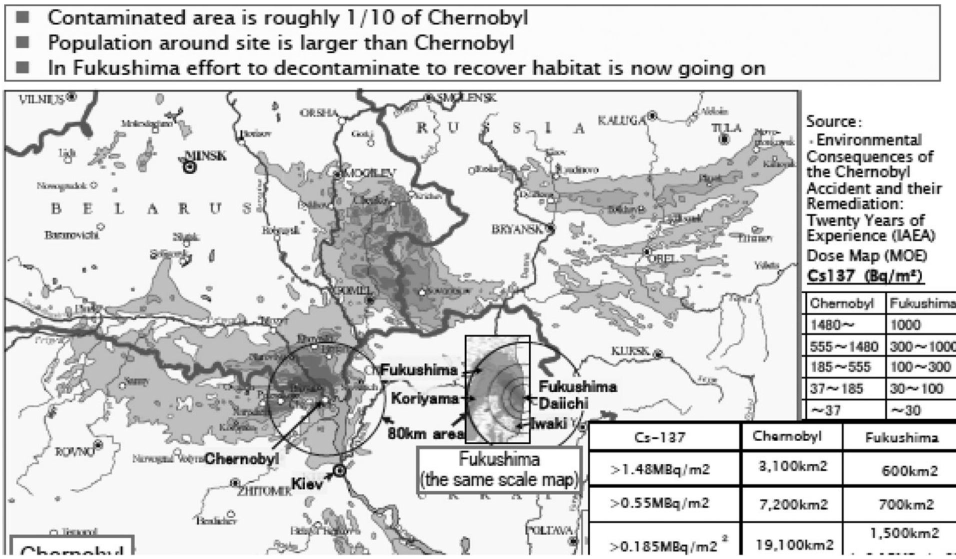

Figure 9. Contaminated Area in Chernobyl and Fukushima in the same scale.

effect" observable in the exposed population so far in connection with the 2011 Fukushima accident.(*8)

Chernobyl was an accident that failed to shut down the reactor with core-wide reactivity excursions. Fukushima succeeded to shut reactors down, but it failed to cool. Also the containment is in the part of design in Fukushima. The differences of fatalities can be largely traced back to aspect of accident and the engineered safeguard prepared beforehand in design. The shortcomings in Fukushima are correctible, and now various measures are implemented over the world.

The primary objective of safety design is of course to protect public. As ASME points out after the Fukushima accident, however, the consequences of past severe accidents seem to bear more broad socio-political and economic aspects along with the safety of radioactivity itself.(*9) Understanding and consensus of low level radiation dose effects on human body should be more thoroughly elaborated. The confusion as to the target level of decontamination could be largely attributed to the mix-up of LNT (Linear Non Threshold) model for radiation protection and actual specific estimation of damages.

3 CURRENT STATUS OF SITE

Now the cores are cooled by circulating water injected by pumps. Spent fuel pools are cooled by heat exchangers. Temperatures have been stable.

In unit 1 a cover surrounding reactor building was made in 2011. In unit 2 there was no explosion because the blowout panel of the reactor building was opened up by explosion on other unit so that hydrogen did not accumulate. In unit 3 works to remove rubbles on the top floor have been done. In unit 4, structures for fuel removal has been built and fuel bundles in spent fuel pool are now transferred to the common pool.

Identifying core status and where about of debris are still in process. The exact status and location of the cores are not known yet. Efforts have been paid to identify the location of fuel by doses, temperatures, and visual inspections. Very high dose rate inside the reactor building and water accumulated on underground floor make it difficult to perform surveillance. Many robotics are in use. Inserting instruments through existing penetrations or bored holes have been tried.

In unit 1, 3, and 4, because of hydrogen explosion, structures like roof or wall, and refueling machines fell in pools. Also sea water was injected to pools at the early stage of the accident to add the water inventory in units 2, 3, and 4. The precise condition is still up to further inspections in units 1, 2 and 3. In unit 4, fresh fuel bundles taken out of spent fuel pool have been inspected. No damage has been observed on those fuel bundles.

As to the radiation dose in site field, there are some high spots but in general the doses around the reactor buildings are of the order of one tenth to one mSv per hour level.

Fukushima Daiichi is a fairly large site with the area of 3 and a half million square meters or 860 acres, and the dose rate at the boundary is of the order of a few micro-Sv per hour.(*10)

The radiation level in sea around the station is low. Also the dust inside the station is low except for the near field of reactors. Alpha emitting nuclides such as plutonium has been monitored, and they are low and of the order of past fall out level by atmospheric weapon tests.

Radio activity release from buildings has been decreased as time goes by. As of now, it is conservatively estimated to be about 10 million Bq / hour by dust concentration at the building. Its contribution to the dose rate at the site boundary is 0.03 mSv/h

Figure 10. Cover of Unit 1.

so that the already existent contamination has much larger contribution to the total dose.

4 ROADMAP FOR DECOMISSIONING

Since the decommissioning of Fukushima Daiichi will be decades long project, roadmap has been drawn to carry out the project safely and progressively. The roadmap consists of three phases. The first phase is time frame up to removal of fuels from pool which looks at next two years. Second phase is time frame up to starting debris removal which corresponds to next ten years. Third phase includes debris removal and rest of decommissioning work including waste disposal which is expected to last for 30-40 years from now.[(*11)]

Key issue is how to remove debris, and since the optimal method may depends on doses, location of debris, availability of exiting equipments, and many other factors such as seismic evaluation of existing buildings which are to be investigated, revised roadmap has several options to be determined. That gives some flexibility as to the future plan of how to remove fuel and debris.

For instance, in Unit 1, already a cover around the reactor building was built in the fall of 2011. In order to remove spent fuel or debris, first the removal of that cover is needed. Then there are three options:

Plan 1 is to retrofit the existing cover for defueling and then to make separate container that covers the whole reactor building to house equipments for debris removal.

Plan 2 is an option to add upper structures on the existing reactor building and then to retrofit the cover to container for debris removal.

Plan 3 is first to build cover for defueling the spent fuel and then to build separate container for debris removal.

Evaluation will be made based on the feasibility of retrofitting cover, and also feasibility to maintain seismic safety of the building with structures on it.

Similar flexible plans have been made for each unit.

5 CONTAMINATED WATER

5.1 *Contaminated water and purification system*

The other issue is contaminated water. 300 tons of water is injected for cooing into three cores per day. The water injected to core is leaked out to buildings, though exact pass has not been identified yet. The water is pumped up and fed back again to the cores.

Also the underground water level around buildings is high, and it is estimated that 400 tons of water is getting into the buildings per day.

That incoming water is mixed with the contaminated water in the buildings resulting steady increase of the contaminated water inventory.

In order to lower the activities in stored water, three water treatment systems have been installed to purify activities. Purified water is stored in tanks as well.

There are three issues to handle this contaminate water. One is to prevent underground water from coming into buildings, that is, to lower underground water level. Two is to enhance water treatment systems to increase capacity. Three is to increase storage capacity as well as their reliability.

In order to decrease the incoming water to buildings, lowering the underground water level is needed. In the station the underground water flows from mountain side to the ocean through permeable layers.

Several wells were made at upper stream side to pump up underground water which is expected to reduce the underground water level around the buildings. Waterproof walls at sea side is now under construction to prevent from contaminating ocean.

Evaluation of building frozen underground wall around the buildings is now made. Wells would be drilled to the depth on low permeability layers and cooling medium would be circulated to freeze soils to construct frozen wall. There are several issues to be evaluated such as dealing with underground structures like ducts. Also it has to be taken note that lowering the level too low would contaminate underground water by leak-out of contaminated water inside the buildings.

5.2 *Storage tanks and its reliability*

Storage tanks are needed for both purified water and water before treatment. From right after the accident, to prevent contaminated water from leaking to ocean, tanks have been continuously built. It is planned to increase the capacity to 800 thousands tons.

In early stages, tanks were needed urgently so that bolted tanks were used which could be built much faster than the welded type. It, however, caused leakage.

In August 2013, 300 tons of contaminated water leaked to ground from tank. Cesium and salt was removed by treatment systems but it contained strontium and other nuclides to be removed by water treatment system. Water was soaked in soil but monitoring was enhanced without excluding possibility

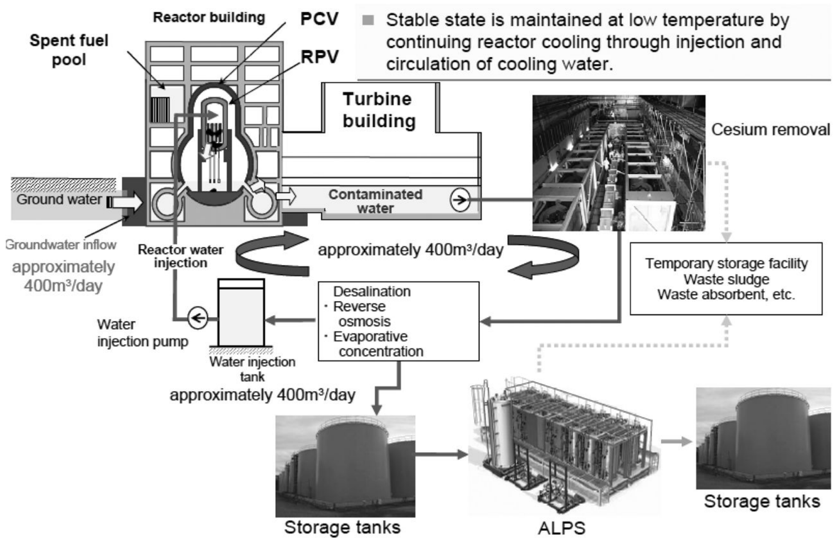

Figure 11. Water treatment system.

that it might reach ocean. Water in leaked tank has been transferred: and removal of contaminated soil was done.

Now tanks quickly built right after the accident for preventing high level water leak-out are being replaced with more robust welded tanks. The work has been accelerated and flange-type tanks are scheduled to be replaced by the end of FY2015. Storage capacity will be increased as well.

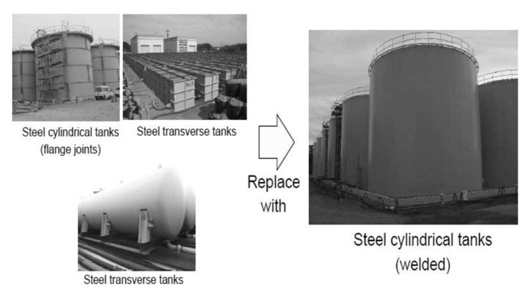

Figure 12. Tank replacement for higher reliability.

6 PROGRESS ON SITE AND FURTHER ACTIVITIES

6.1 *Fuel removal in Unit 4*

Even though hydrogen exploded in Unit 4, the radiation level in the building is low, as there was no fuel damage in the unit. Dose rate is low enough to make it possible to work inside the building in Unit 4.

Since the roof and wall of top floor of reactor building has been destroyed, new structure to house cranes for defueling was newly constructed. The structure has been already made and defueling started in November last year.

On site dry storage casks and common pool which was not damaged by the earthquake will receive fuel from pool.

6.2 *Debris removal process*

For decommissioning work, after the removal of fuel from the pools, removal of debris from cores will be critical process.

In other units than Unit 4, to defuel from spent fuel pool: 1) rubbles in the upper level of reactor building has to be removed, 2) a cover or a container for entire reactor building has to be constructed, and fuel handling equipment be installed, and also 3) design and manufacturing of containment casks have to be made.

At the same time, 4) the fuel stored in common pool be moved to casks to make vacancy in common pool for the fuel removed from the spent fuel pool to be transported there.

Even though status of debris is not known yet, current roadmap is based on the concept of underwater fuel debris removal. After finishing removal of fuel from pool, it is planed to remove fuel debris with filling up primary containment vessel with water.

It is believed that basic structure of primary containment vessel is intact, but there are leaks because water injected to cool the cores is coming out to reactor buildings. So it is needed to inspect leaks of primary containment vessel as well as buildings and to seal those leaks before the removal of debris.

Already some water pass have been identified, still extensive decontamination of buildings is needed for those works.

7 LESSONS LEARNED

The accident was caused by tsunami which led to loss of cooling. It caused fuel damage and melting of cores. Metal-water reaction produced large amount of hydrogen which then exploded inside the reactor buildings.

Specific lessons learned are now implemented in nuclear power station in the world. They should well prevent the same type of accident from happening again. Also those can be amalgamated into more generic sublimated lessons. Those are my personal views and may not represent the parties concerned.

7.1 *Enhancing safety by both soft- and hard-ware*

Measures have been taken so that Fukushima will never ever happen. They are multiple and diversified and it follows the concept of defense in depth.

Prevention

<Tsunami height evaluation and measures>

The tsunami significantly exceeded the design bases. To be prepared for newly defined design base tsunami height, new breakwater is constructed. Reactor building doors are reinforced for waterproof. Camera to monitor tsunami is installed. In rooms that houses important equipments, water sealing of penetration is reinforced.

Mitigation

<Power>

To mitigate the events and to prevent core damage, power supplies are enhanced. It includes air-cooled gas turbine generators, diesel power generators on truck, emergency switch gear panel, pre-installed cables from the panel, batteries and cables in store, and enhancement of incoming power transmission lines.

<Water>

Water supply was critical for cooling. Water storage ponds are built. Tanks are seismically strengthened. Procedure to utilize sea water is prepared.

<Injection and depressurization>

There should be pumps to inject water both at high pressure before depressurizing reactors and at low pressure after then. Fire engines are stored at high locations. For depressurization, batteries and gas cylinders are in store for activation of electrically or pneumatically operated valves.

<Ultimate heat sink>

To cool down reactors, ultimate heat sink should be provided. Drop-in sea water pumps and heat exchangers are also in store.

<Spent fuel pool cooling>

Cooling pool required mobile concrete pumps which can reach top floor of the building. Those are in store.

<Containment and hydrogen control>

There are many other measures including filtered venting of primary containment vessel and hydrogen detector and recombiners.

<Habitability and monitoring>

Habitability of main control room is improved. Power source of monitoring post is enhanced. Communication measures such as satellite phone are installed.

<Rabble removal>

To remove rabbles, heavy machineries are in storage.

Operational aspects

<Drills>

There are many lessons in operations. Many activities have to depend on knowledge based judgment rather than predetermined rules, and importance of realistic drills should be addressed. That should include blind drills which will envisage real difficulties in emergency.

<Command and control>

Basic principle of command and control should be reconfirmed. The accident will not happen in a way as we imagine beforehand, and well-established command and control is more strongly needed in extreme case. Blind drills will reveal those problems.

<Credence among parties>

All of emergency activities were based on the idea that plant status were designed to be shared by emergency response support system, or computerized system. But in Fukushima it did not work because power was completely lost. Lack of communication had led anxiety and disbelief. Sharing information as well as well established mutual credence among parties is a must for difficult operations such as Fukushima.

<Resources and logistics>

Accidents at multiple units have caused much difficulty as well. The accident was in weekday afternoon, but that may not be always the case. Enough resources should be allocated in short period of time, which requires well prepared logistic measures. Also it should be noted that the time length of operation may extend far longer than drills. Human resources are difficult to be renewed after the accident. That may degrade the quality of operations in a long run.

Experiences in Fukushima tell that the plant has to be kept safe for a few days without relying on newly brought in resources. Transportation of last ten miles to site may be very critical.

<Simulator training>

Operators are well trained in simulators. The past simulator, however, did not include core degradation process. With experiences in Fukushima, it seems that simulator training that includes post core degradation in its simulators should be deliberated. Also the simulator did not include fields such as manually operated valves in containment. It is not practical to include the whole system in simulation, but still it should be noted that cooperation with people in field and operators in main control room was one of the critical elements in Fukushima. Procedures are now established to activate high pressure injection system manually even in case of power failure.

<Industry-wide depots>

There are many materials which will be needed in case of extreme accidents. Protective materials such as masks, or people doing monitoring tasks, fuel, food and other very essential materials and resources can be in short in any case. Equipments and parts are to be needed for activities to mitigate the accident and to monitor radio activities in flexibly depending on situations. A shared industry-wide system that such resources are prepared beforehand and to be delivered

Figure 13. Flooded switch gear in unit 6.

and dispatched to the site automatically with or without request would help the work much.

From right after the accident, the Japanese utilities dispatched hundreds of people from their power stations to Fukushima with monitoring equipments and monitoring cars voluntarily.

7.2 *Resilience*

<Uncertainty in evaluation>

Tsunami has shown that evaluation of natural phenomena even with the state-of-the-art technology may include large uncertainty. It is important to narrow the gap by continuous efforts. The engineering design, however, should cope with that uncertainty to well protect the public. The consequences of such accidents are not in any way acceptable. For that, the plant design and operation has to be more resilient in an extreme case such as Fukushima. All of those countermeasures in previous chapter can be attributed to increase resilience as a whole. It should be noted that it has a different aspect from just expanding its design boundary outward to include more severe cases in design. Resilience is needed where the case exceeds the design boundary.

<Resilience after human factors and safety cultures>

Three Mile Island accident in 1979 focused on the importance of "human factors". Chernobyl accident in 1986 addressed dissemination of "safety culture" in the organization. In Fukushima, far beyond the design base tsunami had crippled the cooling capability. We should note the importance of resilience in the whole system.

In nuclear power station design, safety will be assured by assuming design bases. Within the boundary of design bases, designers will handle expected abnormal transients and accidents well within the predetermined criteria. After TMI and Chernobyl, accident management procedures have been established. But in Fukushima, unfortunately the tsunami exceeded those assumptions. Even though those certainly helped mitigating the consequence of the accident, it was not sufficient to save the critical situation.

Expanding the boundary of design based on the specific experience is a must. It, however, may not be sufficient enough in other extreme cases. The system has to be more resilient in those cases.

<Rules, Skills, and Knowledge>

To systematize operation, rules and skills are important. They will give bases for safety and quality of daily operations. In past, the nuclear industry has worked hard to implement best practices in the industry. Also operational experiences and outcome of corrective action programs are applied not only to their own station but also they are shared and applied in other places over the world. Those are reflected on new rules and skills are refined through rigorous trainings based on those experiences. Those remain important even after Fukushima.

Being resilient means "to be prepared for the unpredicted" in more flexible way. That in some sense contradictory statement requires more flexible knowledge-based application of resources in hands on site which may not be covered by predetermined rules or skills.

Safety culture is defined as:[(*12)]

"Safety culture is that assembly of characteristics and attitudes in organizations and individuals which establishes that, as an overriding priority, nuclear plant safety issues receive the attention warranted by their significance."

It can be said that "to give attention by their significance" requires sound base of knowledge. In order to be resilient, the whole organization has to maintain its knowledge bases that would save the case where skills and rules could not cover the overall situation. Again it addresses the importance of safety culture as well.

The risk will be dominant in the area that is beyond the design boundaries. (Beyond Design Base Accident: BDBA) Within the boundary, the consequences of design base accidents (DBA) should be also within the predetermined limits, which are regarded allowable in design. The capability of plants is improved by implementing various lessons by extending design boundaries, and in order to exploit those, "hockey stick" like capability curve should be as flat even beyond the design boundaries. Smaller "head" with broader angle in the beyond the design region in the hockey stick curve will give higher resilience. (Fig. 14) Those may be embedded in its design at the beginning with defense in depth as its basic concept. DC batteries in Unit 3 survived the tsunami because of its high location. It is an example of more resilient design, which cannot be differentiated by its design base boundary. Also the importance of keeping sound knowledge in operation base can be addressed as well. Cooling cores by fire engines or hooking batteries to instruments in Fukushima were not based on rules.

7.3 *International collaboration*

Fukushima has given tremendous impact on nuclear industry in the world. Though the policy around the nuclear power may differ from country to country, the nuclear safety is a common interest.

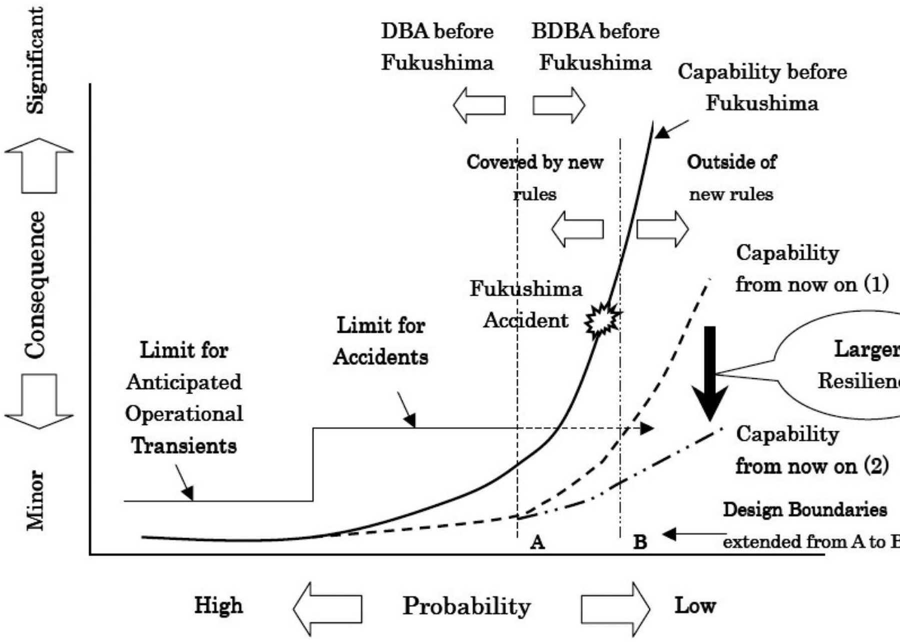

Figure 14. Resilience beyond design boundaries.

The lessons learned should be shared and measures should be implemented. Also decommissioning work in Fukushima is, and continued to be, unprecedented challenge.

In that context, the importance of international collaboration, collecting versatile knowledge and experience cannot be overstressed.

Already Cooperation with IAEA, OECD/NEA is carried out, and International Advisory Team has been set up.

International Research Institute for Nuclear Decommissioning (IRID) which is composed of 17 corporations in Japan to utilize expertise in the world has been founded in August 2013.

With sharing experiences and information, the project is open to any expertise and nuclear communities around world. IRID management states that it will best utilize the abilities of companies, research institutes, and experts from around the world in addressing and resolving the difficult issues. (*13)

8 SUMMARY

The most important lessons learned through Fukushima accident is the importance of "being prepared for the unpredicted". Even though the ordinary daily operation largely depends on skills and rules, it should be addressed that the knowledge based operation is required and plays important roles in case of extreme emergency. Preparation of hardware equipments is a must. Also the design should be resilient even beyond the design base. It should be addressed that keeping abundant and sound knowledge bases in the organization is important. That is the key factor to make the operation robust and making the whole system resilient in case of emergency.

There are many technical challenges in decommissioning of Fukushima. High dose rate has to be overcome for identifying location of debris and its removal. Also contaminated water issue has to be solved. Water treatment and its storage should be handled safely. Waste and dose of working forces have to be managed with long term view.

Process choices, and its R&D, definition of end status, as well as safety / quality of field work have challenging aspects as well. Risk management in whole project has to be handled. Socially, credibility to safe operation and convincing transparency are important. Collecting international experiences, expertise and knowledge are all important.

The project requires decades long dedication of parties concerned. Expertise has to be well kept and maintained in the industry, which will dictate the outcome of unprecedented challenge of Fukushima.

REFERENCES

(*1) The 2011 Great East Japan Earthquake Portal (Japan Meteorological Agency) – http://www.jma.go.jp/jma/en/2011_Earthquake/2011_Earthquake.html
(*2) Tsunami Assessment Method for Nuclear Power Plants in Japan (February 2002 Japan Society of Civil Engineers) http://committees.jsce.or.jp/ceofnp/system/files/JSCE_Tsunami_060519.pdf
(*3) IAEA Safety Standards Meteorological and Hydrological Hazards in Site Evaluation for Nuclear Installations

(2011 IAEA) http://www-pub.iaea.org/MTCD/ publications/PDF/Pub1506_web.pdf
(*4) The Fukushima Nuclear Accidents Investigation Report (June 2012 TEPCO) http://www.tepco.co.jp/en/press/corp-com/release/2012/1205638_1870.html
(*5) Long term evaluation of earthquake activities in Sanriku coast to Boso coast (in Japanese, July 2002 HERP) http://www.jishin.go.jp/main/chousa/02jul_sanriku/tenpu.pdf
(*6) Analytical Methodology of Probabilistic Tsunami Hazard (in Japanese, JSCE) http://committees.jsce.or.jp/ceofnp/system/files/PTHA20111209_0.pdf
(*7) Task Force Report on Trench-type Earthquakes in the Vicinity of the Japan and Chishima Trenches (in Japanese, Jan. 2006 Central Disaster Management Council, Cabinet Office) http://www.bousai.go.jp/kaigirep/chuobou/senmon/nihonkaiko_chisimajishin/pdf/houkokusiryou2.pdf http://www.bousai.go.jp/kaigirep/chuobou/senmon/nihonkaiko_chisimajishin/pdf/kanmatsu1.pdf
(*8) Sixty-eighth General Assembly Fourth Committee 14th Meeting (Oct. 2013 United Nations) http://www.un.org/News/Press/docs/2013/gaspd539.doc.htm
(*9) Forging a New Nuclear Safety Construct (Jun. 2012 ASME) https://www.asme.org/getmedia/193b225c-6019-4c76-bdb4-d3d193400b32/Lessons-Learned-Full-Report.aspx
(*10) Fukushima Daiichi NPS Survey Map and other data (in Japanese TEPCO) http://www.tepco.co.jp/nu/fukushima-np/f1/surveymap/index-j.html http://www.tepco.co.jp/nu/fukushima-np/f1/smp/index-j.html
(*11) Progress Status and Future Challenges of the Mid-and-Long-Term Roadmap towards the Decommissioning of TEPCO's Fukushima Daiichi Nuclear Power Station Units 1-4 (February 2014 METI) http://www.meti.go.jp/english/earthquake/nuclear/decommissioning/pdf/20140227-e.pdf
(*12) SAFETY SERIES No.75-INSAG-4 (1991 IAEA) http://www.pub.iaea.org/MTCD/publications/PDF/Pub882_web.pdf
(*13) International Research Institute for Nuclear Decommissioning http://www.irid.or.jp/en/index.html
(*14) Photos were provided by TEPCO or quoted from TEPCO Accident Report and its WEB. http://www.tepco.co.jp/en/press/corp-com/release/2012/1205638_1870.html

This page intentionally left blank

Workshop on liquefaction experiment and analysis project (LEAP)

This page intentionally left blank

Geotechnics for Catastrophic Flooding Events – Iai (Ed)
© 2015 Taylor & Francis Group, London, ISBN 978-1-138-02709-1

Liquefaction Experiment and Analysis Projects (LEAP) through a generalized scaling relationship

S. Iai
Disaster Prevention Research Institute, Kyoto University, Japan

ABSTRACT: Liquefaction Experiment and Analysis Projects (LEAP) aims at achieving high accuracy in evaluation of geohazards, such as liquefaction induced damage during large earthquakes, through scaled model tests in centrifugal field. In particular, generalized scaling relationship is expected to allow the use of larger scaling factors, ranging from 1/100 to 1/1000, than those of 1/50 applicable to conventional centrifuge tests. In the approach of LEAP, more than three groups of numerical modelers and more than three groups of physical modelers through centrifuge participate to perform predictions of geohazards with respect to the same prototype. Through this new approach, LEAP is expected to achieve higher accuracy in evaluation of geohazards than that achieved by the conventional approach.

1 INTRODUCTION

Studies on evaluation of geohazards, such as liquefaction induced damage during large earthquakes, have been advanced through model tests and effective stress analyses since 1970s. In particular, since 1990s, application of effective stress analysis in practice for evaluating failure mode and degree of damage to soil-structure systems has been actively pursued by geotechnical engineering community. However, complexity and dimension of urban infrastructures have been increasingly expanded and, thereby, limitation of conventional model tests, including conventional centrifuge tests, have been widely recognized. The

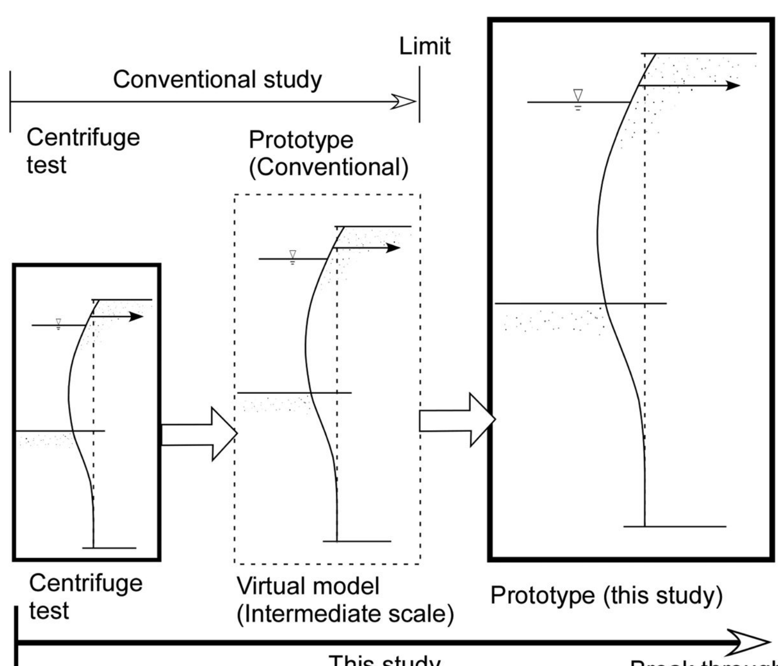

Figure 1. Concept of generalized scaling relationship (taking an example of a sheet pile retaining wall model).

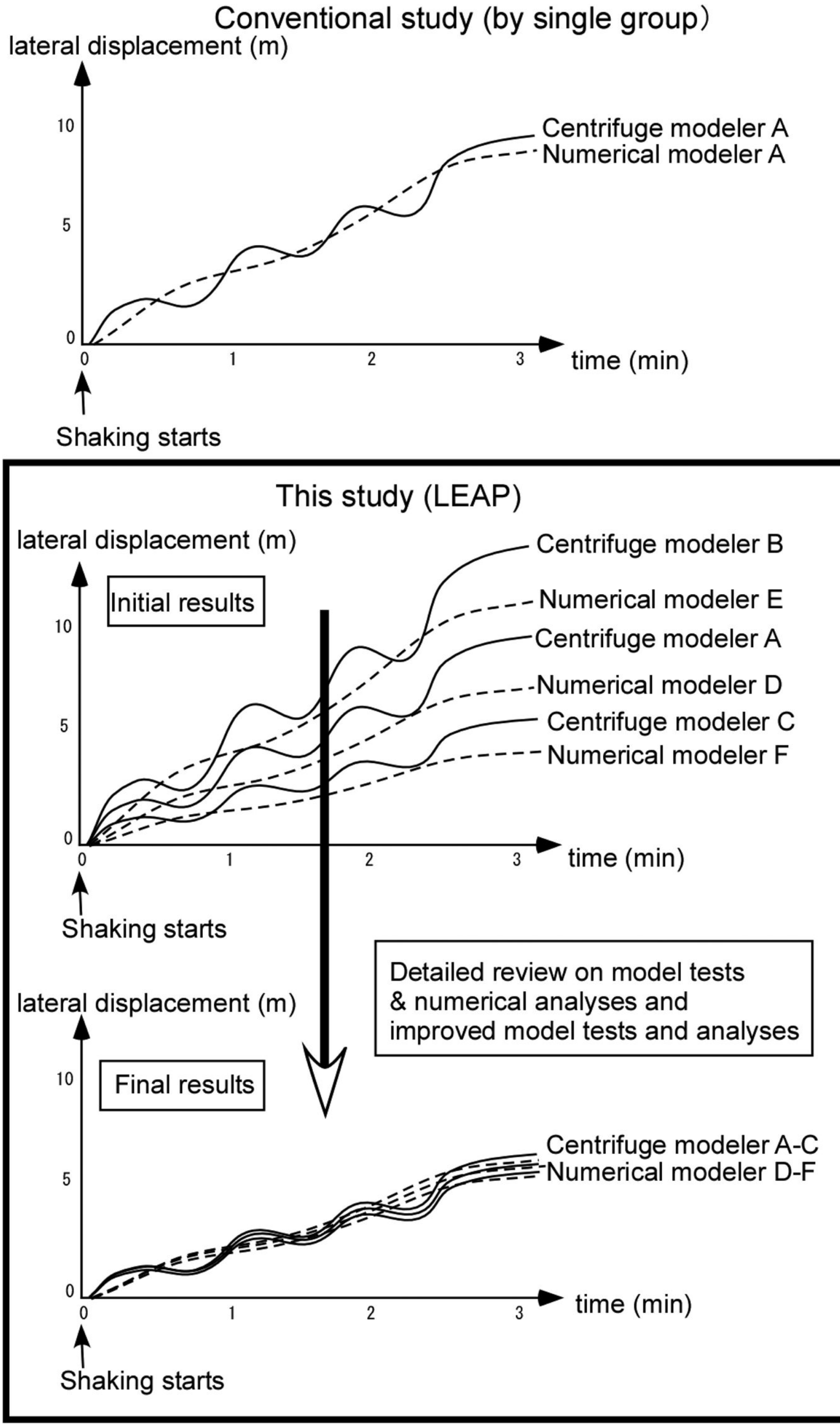

Figure 2. Group approach in LEAP (taking an example of lateral displacement of inclined ground).

limitation in scaling factor, e.g. 1/50 for typical centrifuge facilities for dynamic model tests, has come to be the primary problem to meet these situations in evaluation of geohazards to urban infrastructures.

In this paper, a new approach that is expected to solve this problem in a framework of a cooperative project is described.

2 LEAP

2.1 *Generalized scaling relationship*

Trend toward physical modelling of larger prototypes triggers the move for expanding the current capability of dynamic centrifuge tests. Generalized scaling relationship (Iai et al 2005) is based on the concept of two stage scaling that allows expanded use of the currently available facilities. Through the two stage scaling, a prototype is scaled down, in the first stage, into an intermediate virtual model based on the scaling relations in 1g field with a scaling factor of μ (=prototype/virtual model). In the second stage, the intermediate virtual model is scaled down into a physical model using the conventional scaling relations in centrifugal field with a scaling factor of η (=virtual model/physical model). In this manner, a large scaling factor $\lambda = \mu\eta$ (=prototype/physical model) can be broken down into the smaller scaling factors μ and η and thus the centrifuge model tests can be performed with the smaller scaling factor η. In effect, the limits in the scaling factor for the currently available centrifuge facilities can be expanded by a factor of μ (Figure 1).

Applicability of generalized scaling relationship has been studied for level ground subject to seismic motion (Tobita et al 2011). However, more general type of geohazards, such as lateral displacement of ground in wide area, has not been studied for applicability of generalized scaling relationship. Consequently, there is a strong need for initiating a new study in this regard.

2.2 *Group study approach in LEAP*

Lateral displacement of ground in wide area associated with soil liquefaction is one of the difficult subjects to predict while the lateral displacement can directly bring damage to urban areas. In the conventional approach, study is performed by a single research group as schematically shown in top graph in Figure 2. In this approach, it is possible to confirm the consistency between physical model tests and numerical analyses. However, accuracy and generality in the results of the study are not fully understood by this approach. It is necessary to wait for other research groups to perform similar studies until the results of the study are fully established.

In the group approach in LEAP, more than three groups of numerical modelers and more than three groups of physical modelers through centrifuge test participate to perform predictions of geohazards with respect to the same prototype.

In the initial round of the study through the LEAP group study approach, discrepancy among the results obtained by different research groups can be large, depending on the complexity of the soil-structure systems or the geotechnical and structural conditions as shown in middle graph in Figure 2. In the Leap group study approach, the research groups participating the project get together at the point and exchange information and discussions to identify the source of the discrepancy among the results. The research groups, then, improve or modify the procedure for physical model testing and numerical analysis and move on to the next round of the study.

In the final round of the study, most of the factors to cause the discrepancy will be identified, and all the results will converge to a consistent result as shown in the bottom graph in Figure 2. At this point, the study through the LEAP group study is expected to achieve higher accuracy in evaluation of geohazards than that achieved by the conventional approach.

3 CONCLUSIONS

Outline of LEAP through a generalized scaling relationship is described in this paper. The limits in the scaling factor for the currently available centrifuge facilities can be expanded by a factor of μ through the generalized scaling relationship. In the approach of LEAP, more than three groups of numerical modelers and more than three groups of physical modelers through centrifuge participate to perform predictions of geohazards with respect to the same prototype. Through this new approach, LEAP is expected to achieve higher accuracy in evaluation of geohazards than that achieved by the conventional approach.

REFERENCES

Iai, S., Tobita, T. & Nakahara, T. 2005. Generalized scaling relations for dynamic centrifuge tests, *Geotechnique* 55(5), 355–362.

Tobita, T., Iai, S., von der Tann, L. & Yaoi, Y. 2011. Application of the generalised scaling law to saturated ground." *International Journal of Physical Modelling in Geotechnics*, 11(4), 138–155.

Geotechnics for Catastrophic Flooding Events – Iai (Ed)
© 2015 Taylor & Francis Group, London, ISBN 978-1-138-02709-1

Proposed outline for LEAP verification and validation processes

B.L. Kutter
University of California, Davis, California, USA

M.T. Manzari
The George Washington University, Washington DC, USA

M. Zeghal
Rensselaer Polytechnic Institute, Troy, New York, USA

Y.G. Zhou
Zhejiang University, Hangzhou, Zhejiang, China

R.J. Armstrong
Division of Safety of Dams, Sacramento, California, USA

ABSTRACT: The Liquefaction Experiments and Analysis Project (LEAP) is an international collaboration between universities in the US, Japan, UK, Taiwan and China to evaluate the capabilities of constitutive models for liquefaction problems. In developing this international collaboration, a key step is to develop and define the verification and validation procedure that will be used in this study. This paper will outline the current state of thinking of the validation and verification procedure to be used in LEAP and will include description of the procedure for the constitutive model and numerical model verification process as well as validation process using element and centrifuge test data. Specific details, requirements, and purposes of each of the exercises within the verification and validation procedure is described.

1 INTRODUCTION

This paper describes a proposed procedure for comparing the quality of numerical simulation tools used for the prediction of effects of soil liquefaction. The development of this procedure is part of a collaboration of several universities and industry partners in the US, Japan, UK, and China. This project is called LEAP (Liquefaction Experiments and Analysis Projects). It is envisioned that there will be a series of asynchronous validation exercises (e.g. LEAP 1, LEAP 2, …, LEAP n) hosted by different universities in the collaboratory. Each "LEAP" may focus on a certain issue related to liquefaction or a class of liquefaction problems (e.g., earth dams, lateral spreading, retaining structures, or waterfront structures). Ideally, the validation process will be similar from LEAP to LEAP, but evolution of this process is anticipated.

The LEAP workshop in Kyoto in September 2014 is one of the first LEAP exercises in this collaborative effort. This paper is presented at this workshop as a proposal for consideration for implementation in future LEAP exercises. An updated version of the proposed LEAP verification and validation process, along with a working draft of the evolving document is to be posted in a public folder on NEEShub, the data archiving website for the Network for Earthquake Engineering Simulation (NEES). This paper describes the current state of thinking about this verification and validation (V&V) procedure. Because the success of this project requires community consensus, it is important to present and discuss the V&V procedure prior to adoption in future LEAP projects.

2 CONCEPT OUTLINE FOR LEAP V&V PROCESS

The LEAP project documentation will include templates that the participants in numerical simulation exercise use to describe their constitutive and numerical models as well as laboratory and model test data used in the validation process. LEAP documentation will also describe the formats for submission of shared results that allow for meaningful and fair evaluation and side-by-side comparison of the capabilities and limitations of the models. The documentation will eventually attempt to establish metrics to score the quality of predictions on a variety of objective scales.

As described by Jeremic et al (2009) and others, the verification and validation process is differentiated as follows. *Verification* is the process of determining that a model implementation accurately represents the developer's conceptual description and specification; verification provides evidence that the model is solved correctly. *Validation* is the process of determining the degree to which a model accurately models the intended real world behavior.

The evolving concept for LEAP verification and validation includes the above philosophy, but also requires the verification and validation results be clearly understood and fairly compared so that users of these models can accurately and practically assess their capabilities and limitations. This is important for decision makers, such as leaders of regulatory agencies that determine the safety of infrastructure and allocate resources accordingly. It is envisioned that the verification and validation process not only verifies and validates – it also must illustrate the quality of the verification and validation to users and to decision makers that are not necessarily numerical modeling experts.

Thus, the suggested LEAP V&V process may be outlined as follows.

- Constitutive model *verification*: description of physics intended to be modeled with graphical presentations to illustrate predicted constitutive behavior for specific standard test paths.
- Numerical model *verification*: description of discretization and solution schemes with graphical comparisons to illustrate their stability and accuracy in selected numerical tests.
- Element test *validation*: predictions of constitutive model are compared to data from laboratory test data (e.g., triaxial, simple shear, and one-dimensional consolidation tests).
- Class C *validation* by comparing predictions of numerical models to data from:
  - Benchmark centrifuge model tests (relatively simple geometry such as 1-D saturated sloping ground)
  - System physical model tests (e.g., more complex problems such as dams, cases involving soil-structure interaction, etc.)
  - Benchmark simulations of liquefaction in the field (e.g., validation against observed liquefaction in the Christchurch earthquakes of 2010–2011)
- Class A *validation*:
  - New benchmark centrifuge model tests (relatively simple geometry such as 1-D saturated sloping ground)
  - New system centrifuge tests (e.g. dams, soil-structure interaction, etc.)

Similar to Lambe's (1973) explanation, we differentiate the classes of validation as follows. *Class A* is a true prediction of an event made prior to the event. A *Class B* prediction is after the event, but with results unknown to the predictor. A *Class C* validation is after the event, with results known to the predictor. For class C validation, the individual(s) conducting the modeling (herein called "predictor(s)") may or may not iteratively adjust the model parameters to improve the quality of the agreement between calculations and observations.

The verification steps (first two bullets in the above list) will identify which models have which capabilities, often with a yes/no or black/white binary classification. The verification steps do not require comparison to experimental data; but they do require demonstrating the model's ability to provide consistent results. However the validation against experimental data (the last three bullets in the above list) requires metrics for assessing the quality of validation. Because validation involves comparison to experimental data, there will be inevitable questions about data consistency and accuracy. The LEAP process will endeavor to establish relaiable calibration data and to develop reasonably robust validation metrics.

At the time of this paper submission, the verification steps (first two bullets in the above outline) have been developed to a greater extent than the validation steps (last three bullets). Hence this paper focuses more attention to verification than to validation.

3 CONSTITUTIVE MODEL VERIFICATION

Constitutive model verification is intended to develop a clear understanding of the range of behaviors that are intended to be simulated by the code and an illustration of the ability of the code to predict this behavior. Data will be collected in a standard format to allow systematic comparisons of the predictions from multiple constitutive models. Blank tables will be provided to encourage predictors to provide results in a format for easy cross-comparison of their constitutive model results with those of other researchers.

Verification of the constitutive models will involve the developers answering several key questions about their constitutive models (3.1) and conducting a series of specific verification tests (3.2) using a generic set of soil data like that found in Table 1.

3.1 *Constitutive model questionnaire*

The numerical modelers will be asked to provide detailed papers and reports explaining their constitutive models. In addition, the following questions will be asked to enable tabulated comparisons of the capabilities of different models.

1. What are the mathematical equations for stress and strain parameters used in the constitutive model (e.g., p, q, Lode angle, $b = (\sigma_2 - \sigma_3)/(\sigma_1 - \sigma_3)$, volumetric strain, shear strain)?
2. Is the model formulated in the general stress-strain pace or is it designed for a special case such as plane strain condition?
3. Does the model account for rotation of the direction of the principle stresses? How?

Table 1. Default hypothetical soil descriptions for verification of constitutive model.

Soil Type	Dense (D)	Medium Dense (M)	Loose (L)
Relative Density	80	50	20
Init. void ratio	0.55	0.7	0.85
Permeability	0.015 mm/s	0.03 mm/s	0.05 mm/s
Method of Placement	Dry pluviation	Dry pluviation	Dry pluviation
Crit. State Friction Angle	32°	32°	32°
Crit. Void Ratio at p' = 100 kPa	0.8	0.8	0.8
Gradation, D_{60}/D_{10}	2	2	2
Gradation, D_{50}	0.2 mm	0.2 mm	0.2 mm

4. Critical state:
   a. Does the model prescribe a critical state for which the void ratio or relative density at critical state is a function of the confining pressure?
   b. Does the model prescribe a critical state friction angle?
5. What are the dependent (embedded in code) and independent (user specified) parameters of the constitutive model and what behaviors they control?
6. What is the flow rule in the deviatoric plane and in various planes that contain the hydrostatic axis?
7. Does the model account for effects of grain crushing on the location of the critical state and normal compression lines in the e-p space?
8. Does the model include an ingredient to capture size effects and post-localization response?
9. Are strain-rate or aging effects included? If yes, describe the rate and aging effects.
10. Hysteretic damping.
    a. Does the constitutive model include damping or hysteretic energy dissipation at very small strains?
    b. Is it expected or typical to use numerical damping at the system equation level (e.g. Rayleigh damping) to account for energy dissipation at the constitutive level?
11. What are other important limitations and capabilities of the constitutive model?

3.2 *Constitutive model verification test results*

At least five classes of verification tests were identified and are described next with blank tables when appropriate to provide an example of how data may be input. As mentioned earlier, blank tables like the ones shown in this paper will be provided to predictors to encourage them to provide results in a format for easy cross-comparison of their constitutive model results with those of other researchers.

Table 2. Example of results template for isotropic and 1-D consolidation verifications.

Isotropic Consolidation		1-D Consolidation		
p' (kPa)	Void Ratio, e	σ'_v (kPa)	Void Ratio, e	σ'_h (kPa)
10	0.7	10	0.7	10
1		1		
10		10		
100		100		
10		10		
1		1		
0.1		0.1		
0		0		
1		1		
10		10		
100		100		
1000		1000		
10000		10000		
1000		1000		
100		100		
10		10		
1		1		

3.2.1 *Isotropic consolidation*

Consider a medium density fine sand (see Table of default soil properties) that is pluviated in air and is normally consolidated to the initial state indicated in Table 2. The verification test is to subject the soil to isotropic consolidation for a sequence of mean effective stresses indicated in the Table 2. The blank columns in the table would be filled out by the predictors.

This sequence of stresses is designed to identify typical volumetric strain behavior; how the model behavior changes as it transitions from overconsolidated to normally consolidated states, to visually show how the model handles volumetric strains at very low effective stresses (some models introduce a minimum pressure parameter below which the constitutive behavior is simplified), and finally to show if the model is able to account for crushing.

3.2.2 *One-dimensional consolidation*

Consider a medium density fine sand (see Table 1) that is pluviated in air and normally consolidated to the initial state indicated in Table 2, with the initial coefficient of lateral earth pressure, $K_o = 1$. The verification test is to show the evolution of K_o and void ratio under the sequence of vertical stresses indicated in Table 2.

3.2.3 *Monotonic drained test paths*

This specific verification test is to calculate the monotonic drained test paths for conventional drained triaxial conditions with constant horizontal stress, σ_r, beginning with the initial void ratio described in Table 1, initially isotropically normally consolidated to

Table 3. Typical calculated test paths for default soils in triaxial tests.

	Soil and test path							
	Loose ICDC		Medium Dense ICDC		Dense ICDC		Medium Dense ICDE	
$\lvert\varepsilon_a\rvert_{(\%)}$	q	e	q	e	q	e	q	e
0	0	0.85	0	0.7	0	0.55	0	0.7
0.001								
0.01								
0.1								
0.2								
0.4								
1								
2								
3								
5								
7								
10								
20								
30								

$p' = 100$ kPa, will be calculated. Table 3 shows the format for submission of predicted test paths. For the strains specified, the void ratio and deviatoric stress $q = (\sigma_a - \sigma_r)$ will be reported. Compression test paths will be applied to loose, medium and dense samples, and an extension path will be applied to medium dense sand. Note that ICDC stands for Isotropically Consolidated Drained Compression and ICDE stands for Isotropically Consolidated Drained Extension.

In addition to the cases listed in Table 3, the predicted paths for direct simple shear tests should also be predicted in a similar format. Instead of reporting values of q and axial strain, shear stress, and shear strains as well as the evolution of the horizontal effective stress will be calculated while the effective vertical stress is held constant. If a numerical procedure is not able to simulate one of these prescribed load paths, the table will be left blank.

The data collected in this way will allow assessment of the effective shear modulus as a function of shear strain as well as the ability of the constitutive model to predict dilatancy, peak and critical state friction angles and void ratios at critical state.

3.2.4 *Monotonic constant volume shearing*

This specific verification test is to calculate the monotonic undrained test paths for conventional consolidated undrained triaxial conditions beginning with the initial void ratio described in Table 1, initially isotropically normally consolidated to p' = 100 kPa. A data template similar to that for drained tests will be provided, except that instead of reporting q and e as a function of strain, data regarding q, and p' will be reported for triaxial compression (ICUC) tests and extension (ICUE) tests. Compression test paths will be applied to loose, medium and dense samples, and an extension path will be applied to a medium dense sand sample.

In addition to the cases listed in Table 3, the predicted path for simple shear tests should also be predicted in a similar format. Instead of reporting values of q and p', shear stress, shear strain and the evolution of the horizontal effective stress will be reported while the effective vertical stress is held constant.

The data collected in this way will allow assessment of undrained behavior for dilatant and contractive soil, and to demonstration of the influence of the test path (triaxial compression, triaxial extension, and simple shear) on the undrained test path.

Table 4. CRR curves to for verification.

CRR curve	Soil Density	$(\tau_{static})/(\tau_{cyclic})$	Consol. stress (kPa)	OCR	Test path	Threshold strain
1 a,b,c	D	0	100	1	DSS	1,3,10
2 a,b,c	M	0	100	1	DSS	1,3,10
3 a,b,c	L	0	100	1	DSS	1,3,10
4 a,b,c	D	1.5	100	1	DSS	1,3,10
5 a,b,c	M	1.5	100	1	DSS	1,3,10
6 a,b,c	L	1.5	100	1	DSS	1,3,10
7	M	0	100	10	DSS	3
8	D	0	1000	1	DSS	3
9	M	0	1000	1	DSS	3
10	L	0	1000	1	DSS	3
11	M	0	100	1	Triax	3
12	M	0.5	100	1	Triax	3
13	M	1.5	100	1	Triax	3

3.2.5 *Cyclic undrained shearing*

For cyclic undrained shear the verification test will be to determine the relationship between the CRR (cyclic resistance ratio) and number of cycles of loading for uniform loading. The CRR is defined as the cyclic stress ratio to cause development of a selected threshold strain. For simple shear conditions the cyclic stress ratio is defined as the ratio of cyclic shear stress to the initial consolidation stress prior to the undrained cyclic loading.

Figure 1 shows a hypothetical effect of the soil density on the cyclic stress to cause 3% strain. In addition to the effects of density on the CRR curves, the effects of other factors listed in Table 4 on CRR curves will be demonstrated.

The static shear stress is also known to have an important effect on cyclic loading. One of the factors affecting the importance of static shear stress is the reversal of shear stress direction after passing through zero shear stress. If the shear stress never actually reaches zero, then the soil particles must maintain effective stress contact. This factor is controlled by the ratio $(\tau_{\mathrm{static}})/(\tau_{\mathrm{cyclic}})$; when this ratio is greater than 1, the shear stress does not pass through zero as illustrated by the dashed path in Figure 2. For the solid line, the cyclic shear stress is greater than the static shear stress.

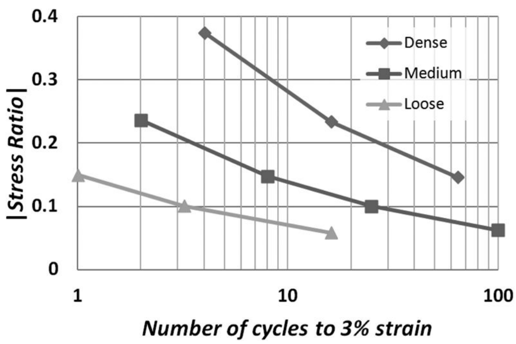

Figure 1. Hypothetical cyclic resistance ratio (CRR) curves predicted by numerical model.

As reconsolidation following cyclic loading causes volumetric strains and settlement, as a general practice, for every undrained cyclic loading test simulated, the cyclic loading should be terminated when the threshold strain is achieved, and then the soil should be reconsolidated back to the initial consolidation stress and static shear stress. The strains during reconsolidation will be reported as a function of the reconsolidation pressure.

3.2.6 *Other features affecting liquefaction*

Various constitutive models have unique features that will not be demonstrated in the above verifications. For example, some recent models (e.g., Manzari & Dafalias 1997, Dafalias & Manzari, 2004) account for the evolution of fabric that develops during cyclic loading.

Models that are true 3-D models will also have some capability to model the effects of multidirectional shaking. The predictors will be encouraged to provide specific simulation data to demonstrate the model's other capabilities.

4 NUMERICAL MODEL VERIFICATION

Similar to the constitutive model verification, the numerical model verification will consist of first asking developers several key questions about their numerical model (4.1) and conducting a series of specific verification tests (4.2).

4.1 *Numerical model questionnaire*

The numerical modelers will be asked to provide detailed papers and reports explaining the detailed theory and implementation of numerical solutions. In addition, the following questions are asked to enable tabulated comparisons of capabilities of different models.

1. What is the discretization approach (Finite Element, Finite Difference, a meshless method, or otherwise)?

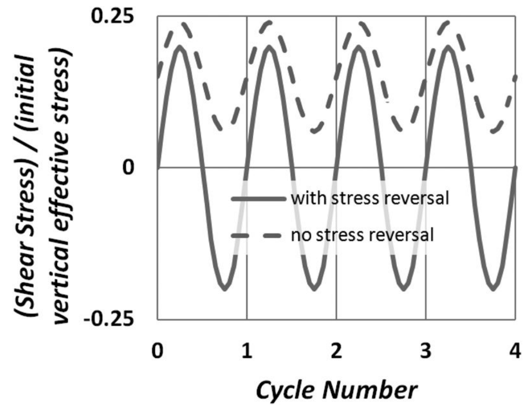

Figure 2. Illustration of cyclic stress as a function of cycle number for cyclic loading with and without reversal of the direction of the shear stress.

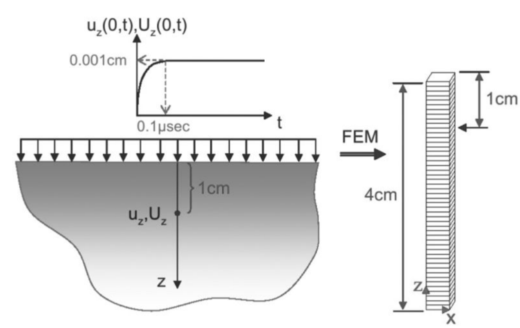

Figure 3. Physical problem analyzed by Jeremic et al (2001).

2. What types of elements (number of nodes and integration points are used in the simulation, u-p, u-p-U, etc)?
3. Is the approach capable of accounting for large deformations and large rotations? How?
4. What integration procedure is used for stress-strain relationship?
5. Is Rayleigh damping used? If so, is the damping matrix determined by the tangent stiffness, the initial stiffness, or both?

4.2 *Numerical verification results*

4.2.1 *Time-rate of one-dimensional consolidation*

Using a specified set of material properties (permeability, porosity, and elastic moduli the numerical solution to Terzaghi's theory of consolidation should be presented.

4.2.2 *Free vibration of an elastic column*

A 1-dimensional column of soil 10 m thick will be subject to a shear stress step function applied at the ground surface. The shear wave will propagate to the base of the specimen and the time of arrival of the stress wave will be compared to that of the theoretical travel time

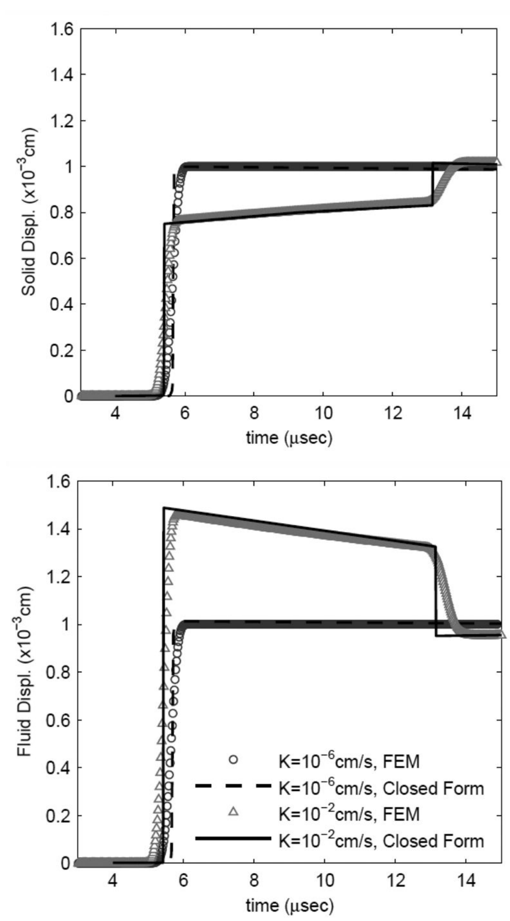

Figure 4. Comparison between closed form solution and predicted displacement under a p-wave generated by a sudden surface load. (a) Solid displacement and (b) fluid displacement. (From Jeremic et al., 2001).

$t = H/V_s$ where H = 10 m and $Vs = (G/\rho)^{0.5}$. In addition the free vibration of the column will be displayed and the numerical damping during free vibration will be assessed.

4.2.3 *Verification of Biot formulation and integration procedure*

Following Jeremic et al. (2001), the implementation of the Biot formulation and accuracy of numerical integration will be illustrated by comparing the numerical model predictions to closed form solutions of shock wave propagation in poro-elastic material by Gajo (1995). Figure 3 illustrates the configuration of the validation scenario. A unit step function of displacement is applied to the surface, with amplitude 0.01 mm while the pressures and displacements of the fluid and solid phases are compared. Computed results by Jeremic et al. (2001) for this problem are compared to the closed form solution by Gajo (1995). Figure 4 shows the comparison between the numerical solution and the closed form solution.

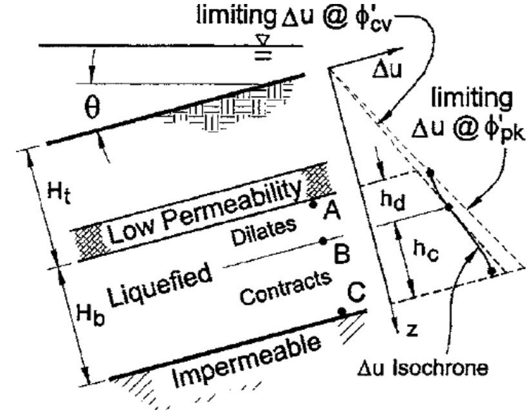

Figure 5. Slope involving liquefying sand covered by a lower permeability soil (After Malvick et al. 2006).

4.2.4 *Void migration beneath impermeable layer.*

Malvick et al. (2006) presented centrifuge model tests of sloping liquefiable ground capped with an impermeable layer that traps the upward flowing water in the liquefying ground near the interface. They show that the soil loosens under the cap as illustrated in Figure 5. Researchers have attempted to capture this phenomenon numerically with some difficulty. The accumulation of water at this interface facilitates dilation (loosening of the soil near the interface); but the softening at the interface can lead to localization of strains and numerical instability. This appears to be a challenging issue that is not yet resolved; a generic submerged slope composed of medium dense sand, similar to that depicted in Figure 5 should be analyzed with the proposed numerical modeling frameworks.

4.2.5 *Illustration of how shear strain localization is modeled*

The sensitivity the relation between nominal stress-nominal strain to the mesh size shall be compared for a medium dense sand in plane strain biaxial compression loading. Results may be compared to predictions from a single element, a 10×10 mesh of elements, 100×100 mesh of elements.

4.2.6 *Illustration of large strains are modeling.*

For a model of a DSS specimen consisting of a 10×10 mesh of elements, show the predicted path for monotonic shearing to global apparent strain of 1000% strain. If a large strain formulation is used, show a comparison of a large strain simulation to a simulation with the large strain provision is turned off.

5 VALIDATION AGAINST ELEMENT TEST DATA

Up to this point all of the requested verification exercises may be completed without comparison to any experimental data. This section focuses on the validation of the constitutive models by comparing predictions of the constitutive model to the response measured in element tests such as triaxial, rotational shear, and DSS (direct simple shear) monotonic and cyclic loading tests. For each LEAP exercise, a different soil may be used. For the centrifuge or field experiments descried in the next section of this paper, element test data will be provided to help the predictors simulate the results of the centrifuge or field experiments.

This outline below describes the element test data that will ideally be made available to predictors and attempts to describe the metrics that will be used to evaluate the quality of the comparison between experiments and predictions:

1) Isotropic and 1-D consolidation comparison between experiment and calculation.
   a) Metrics for evaluation of comparison.
      i) Average difference between e measured and e predicted (over the important range of pressures)
      ii) Area of the hysteresis loop?
   2) ICD monotonic
   3) ICU monotonic
   4) ICU cyclic
      i) p-q, q-ε_q, p-ε_q,
   b) CSR vs Number of cycles to 3.5% strain
      i) Dr = 30, 50, 90?
      ii) Confining stress/$P_{atmospheric}$ = 0.2, 1, 5
   c) ACU cyclic
      i) Initial Static shear stress ratio = 0, 0.1
   d) Elastic behavior (V_s or G_{max}) as a function of confining pressure
   e) Reconsolidation volumetric strains following liquefaction
5) Experimentally developed shear modulus reduction curves.

6 CLASS C VALIDATION

Class C validation is considered to be comparison of numerically calculated response with known experimental data. Class C validation against one particular response to one particular loading case is not particularly illuminating because it is always possible for a predictor to adjust parameters to obtain a decent fit to a limited data set. On the other hand, validation against a series of cases can be very illuminating; for example, prediction of the response of a centrifuge model to a sequence of shaking events (small, intermediate and intense shaking, or shaking with different ground motions), while attempting to predict deformed shape, pore pressure contours, and spectral accelerations at multiple points. Even if the input properties and liquefying model responses are known, it may not be possible for any model to accurately predict all aspects

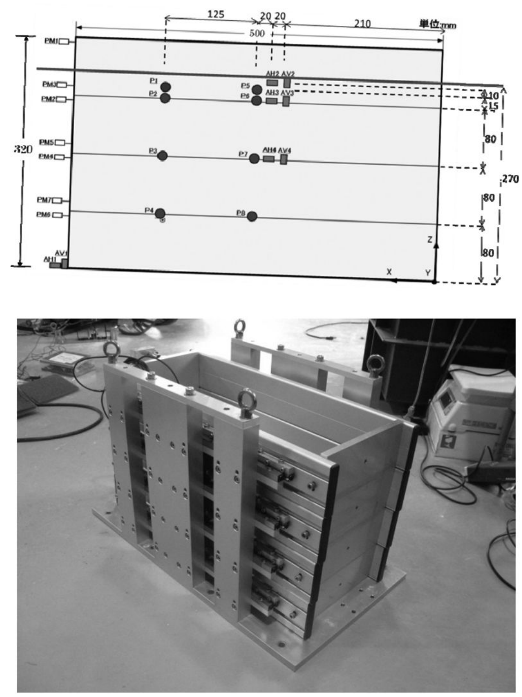

Figure 6. Example of a LEAP benchmark tests performed for a workshop in Kyoto in 2013. (a) Top figure shows the model dimensions and instrument locations. (b) Bottom is a photograph of the actual container used for experiments at Kyoto University.

of the response without changing the model parameters. If the results are known a priori, the ability of a model to duplicate a sequence of Class C validation events, without changing parameters from event to event will be much more meaningful than a simulation that predicts a single event.

It is envisioned that LEAP will archive (and make available to everyone) standard sequences of experiments archived especially for the purpose of validation of numerical models. Some of these experiments (Benchmark Model Tests) will be quite simple geometry, and others (System Model Tests) may attempt to model more realistic prototype situations with realistic geometries and heterogeneities.

6.1 *Class C validation of benchmark tests*

Benchmark tests will include, for example:

- uniform level ground sites with different densities modeled in laminar containers,
- uniform soil layers with sloping ground as in an infinite slope configuration,
- uniform submerged embankment on a rigid foundation

The details of the model and apparatus configuration along with all the input data will be archived and shared for free access for interested parties.

This data includes a description of the experiment, model container, experimental apparatus, achieved input motions, soil properties measured in flight before shaking, dimensions, location and sensitivity of all sensors, and all other necessary information in more detail than can be explained in this paper.

Finally, each benchmark will have its own description and its own set of validation metrics.

6.1.1 *Description of model container*

Scrutiny of Figure 6 may beg the question: 'What is the influence of the container on the results?' Several researchers have considered model container effects on test results. Kutter (1995) discusses the importance of developing complementary shear stresses in laminar containers and on the damping that may be introduced by the shaker and container. Taboada and Dobry (1998) explain how the weight of the rings of a laminar container changes the effective ground slope – the model slope represents a prototype slope perhaps two or three times steeper. Others have investigated other aspects of container effects. The properties of the model container (e.g., mass, stiffness, and friction) should be carefully documented for the finalized Class C validation benchmark tests. While there is some benefit to using complex containers designed to minimize boundary effects (such as that shown in Figure 6(b), complex containers have the disadvantage of being more difficult to model numerically. On the other simple containers (e.g., rigid box) are easy to model in an analysis, but they might be significantly constraining the model behavior. As each type of container has its advantages, validation benchmark tests will include tests in simple rigid containers as well as sophisticated, laminar containers. Detailed properties of each container along with their measured performance in satisfying their intended utilities will be documented and made available to predictors.

6.2 *Example benchmark: Sloping ground in 1-D laminar container*

6.2.1 *Description of the benchmark*

The benchmark will be described briefly with overview sketches similar to those in Figure 6, but the major source of information for predictors will be a complete data report archived in the project repository. This data report includes a complete description of the input data materials used, construction procedure, basic properties of materials and apparatus, sensor locations, calibrations, data processing techniques, and input ground motions. The report also summarizes some key results of the experiment and provides detailed instructions that allow predictors to find all of the output data, photographs, and video documentation of the experiments. Such documentation is already available for several experiments in NEEShub, the data archive for the Network for Earthquake Engineering Simulation. An example of such an archive is Allmond and Kutter (2014). The textual description of the experiment (Allmond and Kutter 2013), is also available on NEES

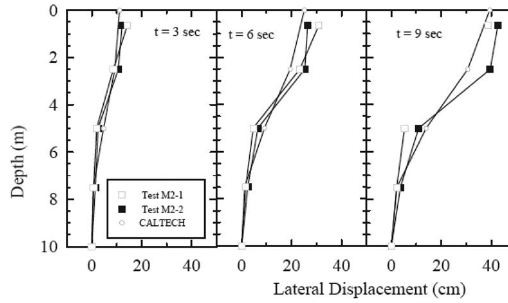

Figure 7. Lateral displacement profiles for centrifuge tests of the same physical model (of a sloping deposit) conducted at RPI and Caltech (Dobry and Taboada 1994).

hub or from the Center for Geotechnical Modeling at UC Davis.

6.2.2 *Input motions*

The benchmark will require predictions to be made on a sequence of ground motions. This will test the ability of the models (using one set of input parameters) to

- account for seismic history,
- account for motions of varying shaking intensity, and,
- account for motions with different frequency content.

6.2.3 *Validation metrics*

The appropriate degree of complexity of validation metrics is difficult to describe. Instead of validating against the amplitude of response, the quality of capturing the important mechanisms of response is perhaps as important as matching the amplitude of response.

Figure 7 is an example from VELACS (Dobry & Taboada 1994) of an excellent way to demonstrate the quality of agreement between different simulations, in this case experimental simulations. As can be seen, for these particular experiments the deformed shape is reasonably similar, and this should receive a high validation grade.

To reduce the apparent agreement displayed in Figure 7 to a numerical score or grade may require subjective grading by a team of experts.

Possible comparisons to be made to perform the validation might include, for example:

1) Deformed shape contours at different stages of the test.
2) Surface settlement profile and lateral inclinometer profiles at the middle and at the end walls – before shaking, after 1 pulse of shaking, at the end of shaking, after consolidation.
3) Time history of settlement, including magnitude and frequency content at centerline and near end walls of laminar box type container.
4) Time history of lateral displacement at centerline and end walls.

5) Time history of acceleration at base, mid-depth, and surface.
6) Time history of pore pressure at base, mid-depth, and surface.
7) Response spectrum of base motion, mid depth and surface.
8) Evaluation of how well the boundary conditions at the soil-container interface are modeled.

What has not yet been determined is to provide an objective score for each of the comparisons. While it may be difficult to provide an objective score, it might be necessary to resort to expert opinion and judgment. As class C simulations are done after the event, and after other simulations have been "scored", the scoring criteria for class C simulations may be known prior to the simulation efforts. This knowledge will bias reported predictions.

6.3 *List of potential benchmark experiments archived for class C simulations*

- Sloping uniform ground with unidirectional shaking
    - $D_r = 40, 60, 80\%$
    - Slope angle = 0, 0.03, 0.1 radians
- Level uniform ground, with bi-directional horizontal shaking
- Homogeneous trapezoidal embankment

6.4 *List of potential system experiments for class C simulations*

- Sloping ground with an impermeable layer, similar to Figure 5
- Embankment dam with zones of different soils
- Ground improvement options
- Waterfront earth retaining structures
- Soil-structure interaction in liquefiable soils

7 CLASS A AND B VALIDATIONS

We anticipate that most LEAP events will include at least one more formal class A or class B prediction contest. Class A predictions are based upon the planned experiment, not the actual experiment. Thus errors in comparisons between Class A predictions and the experiments may arise due to errors in the performance of the experiment in addition to errors in the simulation.

Class B predictions, conducted after the experiment is completed but without knowledge of the results, may be based upon as-built properties and measured input data. In cases where there are significant differences between the planned and performed experiments, much may be learned from Class B validations.

7.1 *Complexity*

Class A simulation exercises could attempt to match experiments of widely varying complexity. The complexity might vary from predicting the results of element tests to large scale centrifuge models of soil-structure interaction involving heterogeneous soil layers with multidirectional earthquake shaking.

7.2 *Similarity to previous calibration exercises*

Some Class A validation exercises might be quite similar to the previously reported Class C benchmarks. Class C benchmarks could include soils with relative density of 40% with a slope of 3% shaken by a sinusoidal motion while a later class A experiment involves layer of soil with relative density 60% and a slope of 3% shaken by a series of realistic earthquake motions.

7.3 *Duplication of experiments*

Although it may not be feasible for all prediction exercises, the experiments should be repeated at least once, and ideally the experiment should be repeated at a different facility or through modeling of models.

8 DISCUSSION AND CONCLUSIONS

Presently, there are many numerical techniques and constitutive models being used in research and practice, and validation standards are arbitrary and different for every numerical procedure. It is very difficult for owners and decision makers to have confidence in the results of numerical simulations if there is no standard for validation. The goal of LEAP is to attempt to establish a standard process for validation of numerical models associated with liquefaction. This will be hopefully be accomplished over a number of LEAP exercises occurring over the next several years.

This paper has outlined a concept for systematic comparison and validation of numerical simulation tools. This plan is in a state of evolution and we expect to modify the plan after each LEAP. The LEAP session at this GEDMAR 2014 conference is one of the first LEAPs.

One of the goals of this paper is to stimulate the discussion of how validation should be done. Following the GEDMAR 2014 conference, we expect to hold an additional workshop(s) to expand upon and add detail to the plans for systematic and accurate verification and validation.

ACKNOWLEDGEMENT

The planning phase of the LEAP project has been funded by the US National Science Foundation NEES research program directed by Dr. Richard Fragaszy, through the grants CMMI-1344705, CMMI-1344630, and CMMI-1344619 to the George Washington University, the University of California Davis, and Rensselaer Polytechnic Institute, respectively. This support is gratefully acknowledged.

REFERENCES

Allmond, J.D., Kutter, B.L. (2014). "JDA02: Centrifuge Testing of Rocking Foundations on Saturated and Submerged Sand", Network for Earthquake Engineering Simulation (distributor), Dataset, DOI:10.4231/D37D2Q74Z.

Allmond, J.D., and Kutter, B.L. (2013). "Centrifuge testing of rocking foundations on saturated and submerged sand: Centrifuge Data report for JDA02. Report No. UCD/CGMDR-13/01, Center for Geotechnical Modeling, University of California, Davis, February.

Dafalias, Y. F. and Manzari, M. T. (2004). "Simple Plasticity Sand Model Accounting for Fabric Change Effects." *ASCE Journal of Engineering Mechanics*, 130(6), 622–634.

Dobry, R. and Taboada, V. (1994). "Possible Lessons from VELACS model No. 2 Results," Verification of Numerical Procedures for the Analysis of Liquefaction Problems, Arulanandan and Scott (eds.), Proceedings of Intl. Conf., Davis, CA, October 17–20, 1993, Vol. 2, A.A. Balkema, Rotterdam, The Netherlands, pp. 1341–1352.

Gajo, A. (1995). Influence of viscous coupling in propagation of elastic waves in saturated soil. ASCE Journal of Geotechnical Engineering, 121(9):636–644, September.

Gajo, A. and L. Mongiovi. (1995) An analytical solution for the transient response of saturated linear elastic porous media. International Journal for Numerical and Analytical Methods in Geomechanics, 19(6):399–413.

Jeremic, B., Taiebat, M., Tafazzoli, N., Tasiopoulou, P. (2009) Verification and Validation in Computational Geomechanics. GheoMat Conference, Masseria Salamina, Italy, June.

Jeremic, B. Cheng, Z., Taiebat, M., and Dafalias, Y. (2001) Numerical Simulation of Fully Saturated Porous Materials, Int. J. Numer. Anal. Meth. Geomech. 01:1–6.

Kutter, B. L. (1995). Recent advances in centrifuge modeling of seismic shaking. In *Proc., 3rd Int. Conf. on Recent Advances in Geotechnical Earthquake Engineering and Soil Dynamics* (Vol. 2, pp. 927–942). Rolla, MO: Univ. of Missouri.

Lambe, T. W. (1973). Predictions in Soil Engineering, Geotechnique, 23(2), 151–201.

Malvick EJ, Kutter BL, Boulanger RW, Kulasingam R (2006). Shear localization due to liquefaction-induced void redistribution in a layered infinite slope. J Geotech Geoenviron Eng ASCE 132(10):1293–1303.

Manzari, M. T. and Dafalias, Y. F. (1997). "A Critical State Two-Surface Plasticity Model for Sands." Geotechnique, Vol. 49, No. 2, pp. 252–272.

Taboada, V. and Dobry, R. (1998). "Centrifuge modeling of earthquake-induced lateral spreading in sand" J Geotech Geoenviron Eng ASCE 124 (12), pp. 1195–1206.

Geotechnics for Catastrophic Flooding Events – Iai (Ed)
© 2015 Taylor & Francis Group, London, ISBN 978-1-138-02709-1

LEAP projects: Concept and challenges

M.T. Manzari
The George Washington University, Washington DC, USA

B.L. Kutter
University of California, Davis, California, USA

M. Zeghal
Rensselaer Polytechnic Institute, Troy, New York, USA

S. Iai & T. Tobita
Disaster Prevention Research Institute, Kyoto University, Kyoto, Japan

S.P.G. Madabhushi & S.K. Haigh
Cambridge University, Cambridge, UK

L. Mejia
URS Corp., Oakland, CA, USA

D.A. Gutierrez & R.J. Armstrong
Division of Safety of Dams, Sacramento, CA, USA

M.K. Sharp
US Army Corps of Engineers, Mississippi, USA

Y.M. Chen & Y.G. Zhou
Zhejiang University, Hangzhou, Zhejiang, China

ABSTRACT: The Liquefaction Experiment and Analysis Project (LEAP), an international research collaboration among researchers from the US, UK, Japan, China and Taiwan, is a validation campaign to assess the capabilities of existing numerical/constitutive models for liquefaction analysis by using laboratory experiments and centrifuge tests. The nature, goals, and scope of the project are presented in this paper. The goals of the planning phase of the project that is currently ongoing in the US are briefly discussed. The main components of the validation campaign and their corresponding challenges are outlined.

1 BACKGROUND

1.1 *The need for a new validation campaign*

Liquefaction-induced permanent deformations and failure in geo-structures such as retaining structures, soil slopes, and earth embankments remain a major concern to the geotechnical engineering community. Following large earthquakes, recorded data, field investigations, and various case studies have often been used to understand the mechanisms of failure and to establish a link to key features of soil stress-strain-strength behavior. Furthermore, intensive efforts have been undertaken by researchers towards the development of constitutive and numerical modeling tools capable of predicting cyclic and permanent deformations of liquefaction prone soils (e.g., Zienkiewicz et al., 1998; Elgamal et al., 2003; Manzari and Dafalias, 1997; Dafalias and Manzari, 2004; Jeremic, et al., 2008). Except for occasional efforts such as that by EPRI (1993), thorough assessment and validation of these computational tools has been limited.

In a recent paper, Perlea and Beaty (2010) explain how advanced numerical methods are now being used by the US Army Corps of Engineers to evaluate the effects of seismic loading and liquefaction on dams. They describe the use of three different codes including FLAC (with a hypoplasticity model, Wang et al., 2006; with UBCSand model, Byrne et al., 2003; and with an empirical pore pressure generation model, Dawson et al., 2001), DYNAFLOW (Prevost, 1983), and TARA (Finn et al., 1986) in the assessment of the seismic response of a number of earth dams. The extensive computational work reported in Perlea and Beatty (2010) clearly demonstrates the continuing need of practicing engineers for validation and assessment of modern numerical tools that are now available for geotechnical analysis.

In the early 1990's, over 20 teams of numerical modelers participated in an elaborate prediction exercise that was meant to VErify Liquefaction Analyses by Centrifuge Studies (VELACS) (Arulanandan and Scott 1993-1994). Centrifuge tests were conducted and duplicated at different centrifuge facilities in the US (UCD, RPI, University of Colorado at Boulder, and Princeton University) and Cambridge University in the UK. A large number of "Class A" (i.e., true prediction of an event made prior to the event) numerical simulations of these centrifuge tests were submitted and compared at a symposium. The two key lessons learned from this exercise were that: (1) none of the numerical techniques available at that time were reliable for producing high quality predictions of liquefaction problems, and (2) there was significant variability in many of the centrifuge test results.

Over the past few decades, the geotechnical engineering community has seen remarkable advances in experimental and computational simulation capabilities. Experimental research using increasingly reliable element scale laboratory tests, in-situ tests, and centrifuge experiments have provided the community with significantly improved understanding of the response of geosystems to earthquake loading.

In the same vein as the VELACS project, a recent exercise was conducted in Italy, on predicting the tunnel-soil interaction using numerical procedures that are matched to centrifuge test data. This project titled Round Robin Tunnel Tests (RRTT) has involved seven different numerical modeling teams that were involved in predicting the centrifuge test results in terms of tunnel lining forces and bending moments amongst other parameters, Bilotta et al., (2014).

The tremendous advances in computational power and computational methods have provided an unprecedented opportunity for the analysis of very large geostructural systems using sophisticated constitutive and numerical modeling techniques. Compared to 25 years ago, there are far better computational and numerical modeling techniques available for the analysis of soil liquefaction and its consequences. In the realm of constitutive modeling, there are several well-established constitutive models for saturated granular soils (Elgamal, et al., 2003; Ling and Yang, 2006; Manzari and Dafalias, 1997; Cubrinovski and Ishihara, 1998; Dafalias and Manzari, 2004; Taiebat, 2009). Moreover, several commercial finite element/finite difference codes (e.g., FLAC) provide nonlinear fully-coupled effective stress capabilities for analysis of geostructures involving liquefiable soils. New advances in meshfree (Manzari and Regueiro, 2005), finite element analysis (Regueiro and Borja, 2001; Manzari, 2004; Manzari and Yonten, 2010, 2011-a, 2011-b) and discrete element techniques (Zeghal and El Shamy, 2004) have provided the community with powerful tools to model liquefaction as well as post-failure response of geostructures.

All these advanced computational tools still need to be assessed and validated against high-fidelity experiments. Without validation, the profession will remain rightfully skeptical and reluctant to adopt such tools. Given the significant advances in numerical modeling over the past twenty five years, it is time for a reassessment of the reliability of modern numerical modeling techniques in analysis of geotechnical engineering problems involving liquefaction.

1.2 *Development of LEAP*

The Liquefaction Experiments and Analysis Project (LEAP) is an international effort to produce a set of high quality centrifuge test data that can be used for validation of existing numerical simulation procedures for liquefaction analysis in a class-A prediction exercise. Evaluation of a wide range of analysis procedures requires a wide range of experiments and analysts. International collaboration widens the scope, gravitas, and impact of the findings. LEAP is an ongoing collaboration that encompasses the writers and their research groups and a team of researchers from the UK led by Cambridge University, the geotechnical earthquake engineering research group at Kyoto University, the geotechnical engineering group at National Taiwan University, and researchers from Zhejiang University in China.

The birth of the LEAP collaboration may have been in November 2011 when the writers submitted a NEESR proposal that included significant international collaboration. The writers had shared their proposal with a team of Japanese and a team of UK researchers, and in return they committed to submit parallel proposals to their respective national funding agencies.

Fortunately, the Japanese proposal, led by Susumu Iai from Kyoto University, was successfully funded and they began performing experiments and analyses at multiple institutions in Japan in 2012. Manzari, Kutter, and Madabhushi were invited to attend a meeting in Kyoto on January 30-31 2013 that included a first phase prediction exercise.

On the first day of the meeting simulations of experiments from three different centrifuge facilities were compared. The experiments modeled liquefying level and sloping ground. Simulations included use of numerical simulation codes such as FLIP ROSE, FLIP TULIP, LIQCA (Iai et al., 1992, 2011), and the FE simulation software developed by Manzari. These comparisons reminded us how important it is to carefully model boundary conditions in both the centrifuge and the analyses, and proved once again that nonlinear finite element simulations of liquefaction can be prone to error, and experiments of liquefaction can produce variable results when using different equipment.

On the second day of the Kyoto meeting a smaller group of international collaborators (from Taiwan, Japan, UK and the US) met to discuss how international efforts could be synergistically coordinated. The group came up with the name *LEAP* (Liquefaction Experiments and Analysis Project), and an overall objective/goal: To evaluate the capability of a wide range of analysis procedures to accurately predict the response (especially deformations) of geotechnical structures including effects of liquefaction.

Details of the project are further discussed in the next sections.

2 NATURE AND GOALS OF THE PROJECT

2.1 *Kyoto document*

A document describing the nature and goals of the collaboration was produced following the Kyoto meeting. The Kyoto document states that at least 3 LEAP "projects", each involving a focused set of experiments and simulations are presently envisioned. For example: (1) Level ground and sloping ground, (2) retaining structure (sheet pile or seawall), (3) embankment and/or embankment dams, and (4) additional focused sets of experiments depending on the sub disciplines of the funding agencies (tunnels, ports, transportation infrastructure, levees, etc.).

It is envisioned that each project under LEAP could proceed in parallel but out of phase with the other projects. Each LEAP project would be led and hosted by one national LEAP team, but international participants will be invited and expected to participate. The leader of each LEAP project will become a member of the international steering committee, which provides a mechanism for coordination.

Protocols for specifying experiments, simulations, material properties and constitutive model calibrations, as well as results of experiments and simulations would be shared amongst all the LEAP projects. A core group for each project will make the specifications for the experiment and simulations for each blind prediction exercise. Broader participation by other physical and/or numerical simulation teams will then be invited. Each LEAP project would culminate in an international prediction symposium. The plan has the following benefits and advantages:

- LEAP will involve different problem-focused projects that will each attract different agencies and sub disciplines.
- Lessons learnt in the earlier projects can benefit planners of the later LEAP projects.
- Class A prediction data developed in one LEAP project can be used as Class C (i.e., predictor validates a model by comparing results to known data) prediction data in later LEAP projects
- Material properties and constitutive law calibrations developed in one LEAP project can be used in later LEAP projects
- Making LEAP projects asynchronous allows different international teams to have different levels of activity at different times depending on the ebb and flow of their team's funding.
- Feedback from physical modelers to numerical analysts and vice versa in successive LEAP projects will lead to a gradual improvement in the process of experimental validation of numerical procedures and best practices for experiments and analysis.

2.2 *Planning phase of LEAP in the US*

The writers are currently involved in a research project that lays the ground for a LEAP in the US. The current activities consist of six complementary components that are discussed in the following sections.

- Organization of Existing Experimental Data for Class-C Predictions and Calibrations,
- New Complementary Laboratory Element Tests,
- System Identification Analysis of a Select Set of Existing Centrifuge Experiments,
- Class-C Predictions and Numerical Simulation of Existing Centrifuge Tests,
- Preparation for a Numerical Prediction (Validation) Exercise in a follow-on research project,
- An international workshop for planning the next phase of the project.

3 SCHEDULE

The US project has started in early fall 2013 and is currently in a planning phase to lay the ground for future centrifuge experimental campaign to investigate liquefaction and its consequences. It is expected that the planning phase will conclude in late 2015 and the experimental phase of the project will begin in 2016.

4 CURRENT STATUS OF THE PLANNING PROJECT

The planning phase of the project that is carried out by the US team is currently focused on the following efforts:

1. Prepare a preliminary set of guidelines and protocols that can be used for future comparisons of the centrifuge experiments with numerical simulations. This effort will also encompass the development of the minimum information required to present a numerical and/or constitutive model and the key stress/strain paths that should be simulated to assess the performance of a model (Kutter et al., 2014).
2. A thorough review of the centrifuge experiments documented in NEEShub and identification of a small number of high quality experiments that can be used for class-C simulations by LEAP researchers and by future modelers who intend to assess or calibrate their numerical/constitutive modeling tools (Zeghal, et al., 2014).
3. A critical review of the numerical simulation techniques, currently available and commonly used for analysis of soil liquefaction and its consequences,

in order to identify the key properties required for their proper calibration.

5 VALIDATION CAMPAIGN: CHALLENGES AND OPPORTUNITIES

The LEAP project is an ambitious attempt to validate existing numerical and constitutive modeling approaches available for liquefaction analysis through the use of high quality experimental data that are mainly based on element tests and centrifuge modeling. The key elements of this campaign are reliable experimental data and a thorough procedure to assess the capabilities of the numerical/constitutive modeling techniques. These components are further discussed in the following sections.

5.1 *Availability and reliability of the experimental data*

Many existing constitutive/numerical procedures for soil liquefaction have been built based on the observed response of soil. Moreover, to use these procedures one needs to calibrate them against the results of laboratory tests. For example, to obtain the essential constants/parameters of an advanced elastoplastic model the following information may be needed:

a) Shear modulus degradation and damping characteristics of the soil at very small to small strain levels.
b) Stress-strain-strength properties of the soil at small to relatively large strain levels which are normally obtained through monotonic triaxial compression tests. To be useful for critical state based models, these experiments must be done up to a stage where the critical state can be identified.
c) Cyclic stress-strain response of the soil in drained and undrained conditions via cyclic triaxial, direct simple shear, or torsional shear tests.

All the above mentioned tests must be done on representative samples of the soil that reproduce the fabric of the soil in the centrifuge experiments which will eventually be used to assess the predictive capabilities of the model in a boundary value problem. Moreover, these tests must be repeated to establish their reliability for the use in model calibration.

The next and even more challenging step is the undertaking of centrifuge experiments that can serve as a basis for all future validation exercises. The soil specimens must be prepared with extra care to reproduce the intended boundary value problem. Here in addition to the usual precautions regarding scaling laws, use of appropriate pore fluid, and proper representation of far-field boundary conditions, one must carefully consider the proper placement of sensors, sensitivity of the sensors to the wide range of responses that soil exhibits during earthquake loading, interaction of sensors with the soil in the near liquefaction stage, difficulties in controlling the base excitation, and the consequences of the unintended movements of the soil container due to the base excitation. Centrifuge experiments must be repeated and potential sources of data scatter should be established.

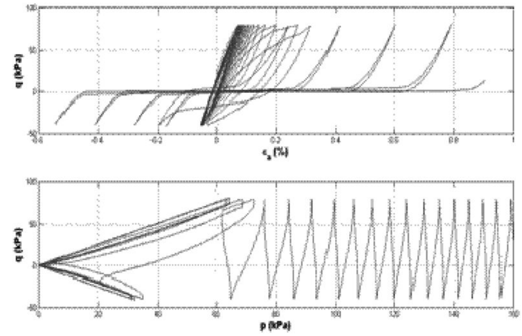

Figure 1. Performance of a soil plasticity model in simulation of an undrained cyclic triaxial shear test when a fully-implicit integration technique is used.

5.2 *Assessment of constitutive models*

It is expected that a number of existing and future soil constitutive models will be used to simulate the experimental database produced by LEAP projects. A majority of existing models use plasticity (including elastoplasticty, hypoplasticity, hyperplasticity, etc.) as the main framework. However they may differ significantly in their ingredients, e.g. elastic response, yield surface, flow rule, and hardening laws. Some of these models are based on critical state soil mechanics and may require substantial experimental data (laboratory based element tests or in-situ tests) for determination and calibration of model parameters. Moreover, constitutive models that are developed for liquefiable soils may be designed to capture shear-induced volume change but may lack proper ingredients to model the volume change caused under loading with constant shear stress ratio. In some occasions, a model appears to perform well in pore pressure generation stage but is unable to reproduce the deformations caused by soil-reconsolidation. Most models are unable to properly simulate void ratio redistribution resulting from water flow induced by excess pore pressure gradients.

Implementation of the constitutive model is also an important aspect of the entire simulation tool. Time integration of the rate equations is performed by using a variety of explicit, explicit-implicit, and fully implicit techniques. The accuracy of these techniques will have significant impact on the overall simulation results. Figure 1 shows the stress path and the stress-strain response of a soil plasticity model in an undrained cyclic triaxial test when a fully implicit integration technique is used.

Figure 2 shows the performance of the same constitutive model in the simulation of the same test when an explicit technique without strict error control is used.

Instead of a smooth stress path, this time the stress path shows locally erratic patterns due to spurious unloading during plastic loading. The spurious

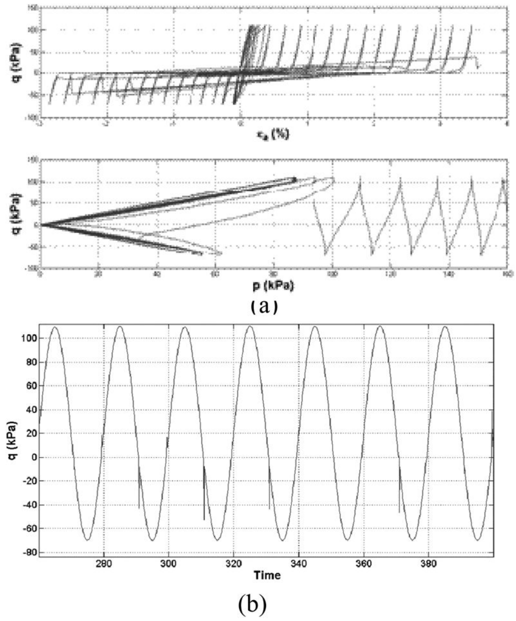

Figure 2. Performance of a soil plasticity model in simulation of an undrained cyclic triaxial shear test when a simplified explicit integration technique is used.

unloading is more visible in the q-time graph shown Figure 2(b).

Hence, it is important that this aspect of the model implementation be well documented in the course of the validation exercise envisioned in the LEAP projects. To allow for a more thorough assessment of the constitutive models used in the simulation phase of LEAP projects, it is planned to document the performance of these models in a variety of stress/strain paths, so that potential versatility as well as shortcomings of these models in the simulation of more complex boundary value problems can be correlated with their performance in the simulation of element tests.

To this end, Kutter et al., (2104) propose a set of basic experiments that a soil constitutive model needs to simulate before it is used in the simulation of boundary value problems.

5.3 *Assessment of numerical modeling tools*

A plethora of numerical simulation platforms are now available for geotechnical engineering simulations involving liquefaction. While a majority of commonly used techniques are mesh-based (e.g., finite difference and finite element methods), there have been significant new developments on particle-based techniques such as meshfree and material point methods (MPM). In addition to these continuum-based methods, new developments in the realm of discrete element methods are also quite promising and are being used to study dynamic response of liquefiable granular soils.

Continuum-based methods are expected to be the dominant choice for the simulation phase of LEAP projects. Most available simulations tools (such as OpenSEES, FLAC, PLAXIS, etc) treat the saturated soil as two-phase media in which the differential equations governing the motion of soil and flow of pore water are formulated by using Biot's theory or mixture theory. Implementation and application of these formulations involve several key components that need to be clearly described to achieve a thorough assessment of their performance in a boundary value problem. The following issues are of particular interest to LEAP projects:

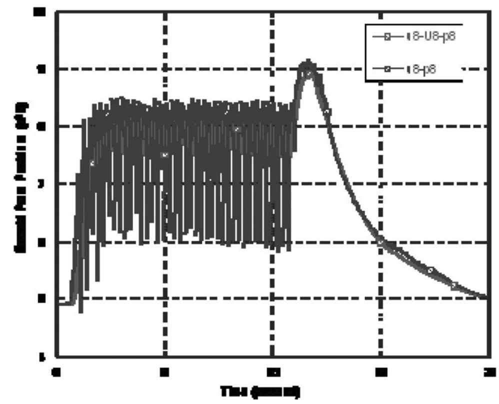

Figure 3. Comparison of two different formulations in seismic analysis of a saturated sand deposit.

a) The main formulation used in the numerical simulation.
b) The element type used in finite element simulations using a particular formulation
c) The method of time integration.

For example, Zienkiewicz and Shiomi (1984) have described three different formulations for dynamic analysis of saturated porous media, i.e. **u**-p, **u**-**U**, and **u**-**U**-p, where **u**, **U**, and p represent the displacements of the soil skeleton, displacements of pore water, and pore pressure, respectively. The **u**-**U**-p formulation provides the most complete formulation, but it requires a significantly larger number of unknowns per node.

Through an analysis of an elastoplastic column of soil subjected to a dynamically varying surface pressure, Zienkiewicz and Shiomi (1984) showed that for some earthquake problems the **u**-p formulation may be able to provide solutions with sufficient accuracy. A recent work by Manzari (2014) has shown that while the results of the two methods may be close in many earthquake engineering problems, there may be significant numerical oscillations when a finite element-based **u**-p formulation is used in liquefaction analysis. Figure 3 shows the excess pore pressure time histories computed near the ground surface in a uniform sand deposit that is subjected to 20 cycles of a sinusoidal motion with maximum amplitude of 0.25 g.

Eight-noded brick elements using **u**-**U**-p and **u**-p formulations were used in the simulations. The 3D elements were constrained in the direction perpendicular to the direction of ground motion. Large oscillations

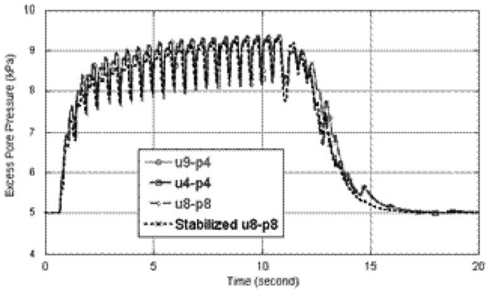

Figure 4. Comparison of pore pressure time histories near ground surface in a sloping ground; performance of different finite elements using **u**-p formulation.

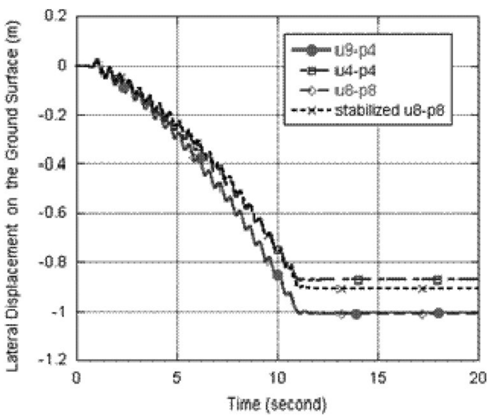

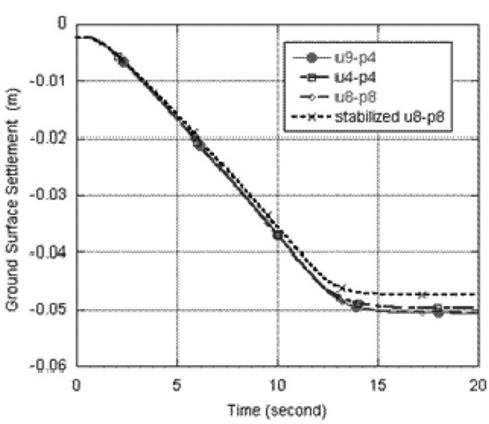

Figure 5. Comparison of the performance of different finite elements using **u**-p formulation.

are observed in the results obtained by the **u**-p formulation. The oscillations seem to be an artifact of the numerical scheme rather than the true response of the soil.

A similar analysis for a fully submerged mildly sloping ground shows that with the **u**-p formulation, the choice of the finite element has an impact on the simulation results. Figures 4 and 5 compare the results of seismic analyses using the **u**-p formulation with different finite elements. In these Figures, **u**4-p4 and **u**9-p4 are plane strain finite elements with 4 and 9 degrees of freedom for displacement of the soil skeleton and 4 degrees of freedom for pore pressure. The **u**8-p8 element is an 8-noded brick element with displacement and pore pressure degree of freedoms for all nodes. Finally the stabilized **u**8-p8 is a stabilized version of the traditional **u**8-p8 element when only one integration point is used in the analysis.

The observed differences in the computed lateral displacements are larger while the impact on computed pore water pressure is not as significant.

Given the above mentioned observations, it is important to document details of the numerical procedures used in the simulation phase of the LEAP project.

Examples of the details that need to be specified when a numerical simulation is submitted are:

- Type of the simulation platform (mesh-based, particle-based, etc.),
- General formulation used to formulate the governing equations,
- Nature of interpolation functions used in mesh-based or particle-based methods,
- Numerical scheme used in numerical integration of integrals leading to the final matrix equations,
- Numerical scheme used in time integration of the governing equations along with the parameters used,
- Return algorithms used for integration of the constitutive rate equations,
- Solution scheme used in the solution of nonlinear matrix equations.

A detailed set of information needed for submission of the numerical simulations is being developed and a preliminary set is reported by Kutter et al., (2014).

6 CONCLUSION

This paper presented an overview of the concept behind the *Liquefaction Analysis and Experiment Project* (LEAP), an ongoing international collaboration among researchers from the US, the UK, Japan, China, and Taiwan. The nature and goals of the project as well as the current state of the planning phase of the project in the US were discussed. Some key challenges and opportunities that face LEAP as a validation campaign for assessment of numerical/constitutive models for liquefaction analysis were presented.

ACKNOWLEDGEMENT

The planning phase of the LEAP project has been funded by the US National Science Foundation NEES research program directed by Dr. Richard Fragaszy, through the grants CMMI-1344705, CMMI-1344630, and CMMI-1344619 to the George Washington University, the University of California Davis, and Rensselaer Polytechnic Institute, respectively. This support is gratefully acknowledged.

REFERENCES

Arulanandan, K., and R. F. Scott (1993–1994). "Verification of Numerical Procedures for the Analysis of Soil Liquefaction Problems," Proceedings of the International Conference on the Verification of Numerical Procedures for the Analysis of Soil Liquefaction Problems, Vols. 1 and 2, A. A. Balkema, Rotterdam, the Netherlands.

Bilotta, E., Lanzano, G., Madabhushi, S.P.G. and Silvestri, F., (2014), A round robin on tunnels under seismic actions, *accepted by* ACTA Geotechnica, Italy.

Byrne, P.M. (1991). "A Cyclic Shear-Volume Coupling and Pore-Pressure Model for Sand", Proceedings: Second Int. Conf. on Recent Advances in Geotechnical Earthquake Engineering and Soil Dynamics, St. Louis, Paper No. 1.24, 47–55.

Byrne, P.M., Park, S.S., and Beaty, M. (2003). "Seismic liquefaction: centrifuge and numerical modeling"' *Proc., 3rd International FLAC Symposium,* Sudbury, Canada.

Byrne, P.M., Park, S.S., Beaty, M.L., Sharp, M.K., Gonzalez, L., and Abdoun, T. (2004). "Numerical modeling of liquefaction and comparison with centrifuge tests". Canadian Geotechnical Journal, Vol. 41(2), 193–211.

Cubrinovski, M. and Ishihara, K. (1998). "State concept and modified elastoplasticity for sand modeling." *Soils and Foundations* 38(4): 213–225.

Dawson, E.M., Roth W.H., Nesarajah, S., Bureau, G., and Davis, C.A. (2001). "A Practice-Oriented Pore Pressure Generation Model," Proceedings 2nd International FLAC.

Dafalias, Y. F. and Manzari, M.T. (2004). "Simple Plasticity Sand Model Accounting for Fabric Change Effects." ASCE Journal of Engineering Mechanics, 130(6), 622–634.

Elgamal, A.-W., Adalier, K. Zeghal, M. (1994). "Overview and relevance of experimental data from VELACS project, models 4a,4b, and 6" *Verification of Numerical Procedures for the Analysis of Liquefaction Problems*, Arulanandan and Scott (eds.), Proceedings of Intl. Conf., Davis, CA, October 17–20, 1993, Vol. 2, A.A. Balkema, Rotterdam, The Netherlands, pp. 1681–1702.

Elgamal, A.-W., Zeghal, M., Parra, E., and Gunturi, R. (1996). "Identification and Modeling of Earthquake Ground Response, I: Site Amplification," *Soil Dynamics and Earthquake Engineering*, Vol. 15, No. 8, pp. 499–522.

Elgamal, A., Yang, Z., Parra, E., and Ragheb, A., (2003). "Modeling of Cyclic Mobility in Saturated Cohesionless Soils," *International Journal of Plasticity*, Pergamon, Elsevier Science Ltd., Vol. 19, Issue 6, pp. 883–905.

El Shamy, U., Zeghal, M., Dobry, R., Thevanayagam, S., Elgamal, A, Abdoun, T., Medina, C., Bethapudi, R., and Bennett, V. (2010). "Micromechanical Aspects of Earthquake-induced Lateral Spreading," *ASCE International Journal of Geomechanics*, v.10, p. 190.

EPRI (1993). Electric Power Research Institute. Guidelines for determining design basis ground motions. Palo Alto, California: Electric Power Research Institute, vol. 1–5, EPRI TR-102293.

Finn, W.D. Liam, Yogendrakumar, M., Yoshida, N. and Yoshida, H. (1986). *"TARA-3: A Program to Compute the Response of 2-D Embankments and Soil-Structure Interaction Systems to Seismic Loadings,"* University of British Columbia, Department of Civil Engineering, Vancouver, Canada.

Finn, W.D. Liam and Yogendrakumar, M. (1989). *"TARA-3FL: Program for Analysis of Liquefaction Induced Flow Deformations"*, University of British Columbia, Department of Civil Engineering, Vancouver, Canada.

Iai, S., Matsunaga, Y., and Kameoka, T. (1992). "Strain space plasticity model for cyclic mobility," Soils Foundations, 32(2), pp. 1–15.

Iai, S., Tobita, T. and Ozutsumi, O. (2011). "Induced Fabric Under Cyclic And Rotational Loads In A Strain Space Multiple Mechanism Model For Granular Materials." International Journal for Numerical and Analytical Methods in Geomechanics. 37: 1326–1336. doi: 10.1002/nag.2087

Jeremic, B., Cheng, Z., Taiebat, M., and Dafalias, Y. F. (2008). "Numerical Simulation Of Fully Saturated Porous Materials." International Journal for Numerical and Analytical Methods in Geomechanics, 32(13), 1635–1660.

Kutter, B. L. et al., (2014). "Proposed Outline for LEAP Verification and Validation Processes." Proceedings of the Fourth International Conference on Geotechnical Engineering for Disaster Mitigation and Rehabilitation, Kyoto, Japan.

Ling, H.I. and Yang, S. (2006). "A Unified Sand Model based on Critical State and Generalized Plasticity." Journal of Engineering Mechanics, ASCE, 132, 1380-1391.

Manzari, M. T. and Dafalias, Y. F. (1997). "A Critical State Two-Surface Plasticity Model for Sands." *Geotechnique,* Vol. 49, No. 2, pp. 252–272.

Manzari, M.T. (2004). "Application of Micropolar Plasticity to Post-failure Analysis in Geomechanics Problems." International Journal of Numerical and Analytical Methods in Geomechanics, 28(10), 1011–1032.

Manzari, M.T. and Regueiro, R.A. (2005). "Gradient Plasticity Modeling of Geomaterials in a Meshfree Environment, Part I: Theory and Variational Formulation." International Journal of Mechanics Research Communications, 32, 36–546.

Manzari, M. T. (2009-a). "On Material versus Structural Response of Saturated Granular Soils." DiMaggio Symposium, in Proceedings of the Fourth Biot Conference on Poromechanics including the second Frank L. Dimaggio Symposium, Columbia University, June 8–10, 2009, H. I. Ling, A. Smyth, and R. Betti (eds.), DESTech Pub., pp. 1033–1039.

Manzari, M. T. (2009-b). "An Evaluation of Liquefaction Potential of Sands at Low Confining Pressure." Proceedings of the International Conference on Performance-Based Design in Earthquake Geotechnical Engineering, from case history to practice, (IS-Tokyo 2009), 15–18 June 2009, pp. 1257–1260.

Manzari, M. T. and Yonten, K. Y. (2010). "Analysis of Geostructures using a Two-Scale Constitutive Model." Proceedings of the first International Conference on Advances in Interaction and Multiscale mechanics, May 30–June 3, 2010, South Korea.

Manzari, M. T. and Yonten K. (2011-a). Comparison of Two Integration Schemes for a Micropolar Plasticity Model, Comp. Meth. Civil Eng., 2 (2011) 21–42.

Manzari, M. T. and Yonten K. (2011-b), "Analysis of Post-Failure Response of Sands using a Critical State Micropolar Plasticity Model." Interaction and Multiscale Mechanics, Vol. 4, No. 3, 187–206.

Manzari, M. T., Yonten, K. Y., El Ghoraiby, M. A., and Beyzaei, C.Z. (2011). "On Analysis of Liquefaction-Induced Displacement in a Caisson Quay Wall." III ECCOMAS Thematic Conference on Computational Methods in Structural Dynamics and Earthquake Engineering, M. Papadrakakis, M. Fragiadakis, V. Plevris (eds.), Corfu, Greece, 26–28 May 2011.

Manzari, M. T. and Yonten, K. Y. (2013). "C1-Finite Element Analysis of Gradient Enhanced Continua."

Journal of Mathematical and Computer Modeling, 10.1016/j.mcm.2013.01.003.

Manzari, M. T. (2014). “On Finite Element Analysis of Liquefaction using Elastoplasticity.” Proceedings of 17th US Congress on Theoretical and Computational Mechanics, June 15–20, 2014.

Perlea, V.G., and Beaty, M.H. (2010). “Corps of Engineers’ Practice in the Evaluation of Seismic Deformation of Embankment Dams.” Proc., Fifth International Conference on Recent Advances in Geotechnical Earthquake Engineering and Soil Dynamics, May 24–29, San Diego. Special Lecture SPL-6, (pp. 1–30).

Prevost, J.H. (1998). *“DYNAFLOW, Version 98, Release 02.A”*, Princeton University, Department of Civil Engineering & Op. Res., Princeton, New Jersey.

Regueiro, R.A. and Borja, R.I. (2001). “Plane Strain Finite Element Analysis of Pressure Sensitive Plasticity with Strong Discontinuity.” Int. J. Solids Struct., 38(21): 3647–3672.

Taiebat, M. (2009). Advanced Elastic-Plastic Constitutive and Numerical Modeling in Geomechanics. LAP Lambert Academic Publishing. ISBN 978-3-8383-1123-4, 264 pages.

Wang, Z.L. and Makdisi, F.I. (1999). “Implementing a bounding surface hypoplasticity model for sand into the FLAC program.” FLAC and Numerical Modeling in Geomechanics, A.A. Balkema, Netherlands, 483–490.

Zeghal at al. (2014). “LEAP: selected data for class C calibrations and class A validations.” the Fourth International Conference on Geotechnical Engineering for Disaster mitigation and Rehabilitation (4th GEDMAR), 16–18 September, 2014, Kyoto, Japan.

Zienkiewicz, O. C., Chan, A. H. C., Pastor, M., Schrefler, B. A., and Shiomi, T. (1998). *Computational Geomechanics with Special Reference to Earthquake Engineering*. John Wiley and Sons, England.

Geotechnics for Catastrophic Flooding Events – Iai (Ed)
© 2015 Taylor & Francis Group, London, ISBN 978-1-138-02709-1

LEAP: Selected data for class C calibrations and class A validations

M. Zeghal
Rensselaer Polytechnic Institute, Troy, New York, USA

M.T. Manzari
George Washington University, Washington, DC, USA

B.L. Kutter
University of California, Davis, CA, USA

T. Abdoun
Rensselaer Polytechnic Institute, Troy, New York, USA

ABSTRACT: The Liquefaction Experiments and Analysis Projects (LEAP) is an international effort to produce a set of high quality test data which will then be used for validation of existing computational models and simulation procedures for liquefaction analysis. This paper presents an overview and discusses the limitations of some of existing data that may be used in class-C predictions (or calibration). The paper also discusses some of the requirements for validation data and presents some thoughts for a future series of high quality centrifuge tests aimed at soil model validations using class A (blind) predictions within LEAP.

1 INTRODUCTION

Soil liquefaction during earthquake excitations is a pervasive problem often associated with large permanent ground deformations leading to failure of geosystems of different types such as retaining structures, soil slopes, and earth embankments. Laboratory tests of soil samples and system (physical) models have been intensively used to understand the soil stress-strain-strength behavior and associated mechanisms of failure. Data recorded during earthquakes, field investigations and various case studies were also employed to complement the information provided by these tests. On the other hand, intensive efforts have been undertaken by researchers towards the development of constitutive and numerical modeling tools capable of predicting cyclic and permanent deformations of liquefaction prone soils (e.g., Zienkiewicz et al., 1998; Elgamal et al., 2003; Jeremic, et al., 2008). Given the significant advances in numerical modeling over the past twenty years, there is currently an urgent need for validation and assessment of the reliability of modern numerical modeling techniques in predicting the response of geotechnical systems in the event of liquefaction. The Liquefaction Experiments and Analysis Projects (LEAP) is an international effort to produce high quality experimental data sets and to use this data in a systematic effort to validate existing computational models of the dynamic response and liquefaction of saturated granular soils (Manzari et al., 2014 and Kutter et al., 2014).

The geotechnical community has been addressing the validation and calibration of computational tools for a long time through, the so-called, class A, B and C predictions. Professor Lambe (1973) explained these predictions in his Rankine Lecture as follows:

> "A type A prediction of settlement, for example, would be made before construction and based entirely on data available at that time. A type B prediction of settlement would be made during the construction and would have available data obtained during the initial parts of the construction, such as measurements made during excavation, foundation construction etc. The outcome of the event being predicted may be unknown (type B) or known (type Bl). A type C prediction is one made after the event being predicted has occurred. The Profession is in great need of simple techniques to make type A predictions. Even though type B predictions may be helpful, they are normally not nearly as useful as type A predictions. Type C predictions are autopsies. Our professional literature contains the results of more type Cl predictions than of any other type. Autopsies can of course be very helpful in contributing to our knowledge. However, one must be suspicious when an author uses type Cl predictions to 'prove' that any prediction technique is correct."

With few exceptions (e.g., Arulanandan and Scott, 1993, 1994), the geotechnical engineering community has been relying mostly on C1 predictions to assess the capability of our computational tools using problems for which the results are known before the assessment is made. Such predictions are valuable, but are often more calibration than validation efforts. In contrast, class A (blind) predictions ensure an independence between computational and experimental results and are, thus, actual validations (Oberkampf et al., 2010). The community can become more confident of the geotechnical computational tools if class A predictions are systematically used with standardized validation methodology and metrics.

Historically, the early validation efforts in soil liquefaction (Arulanandan and Scott, 1993, 1994) were hindered by the quality and resolution of the experimental data. In contrast, the last two decades were marked by a significant development in testing and data acquisition capabilities. Current tests of soil samples and small-scale centrifuge models produce superior experimental data in terms of both quality and quantity. These conditions are more favorable and conducive for systematic validation efforts such as LEAP (see Manzari et al., 2014 for an overview of this project). This paper: (1) gives an overview of a number of important liquefaction problems that require attention and should be included in such efforts, (2) presents some of the experimental data available for class C predictions, and (3) discusses a number of benchmark and system centrifuge tests for future class A predictions to consistently validate computational models of soil liquefaction.

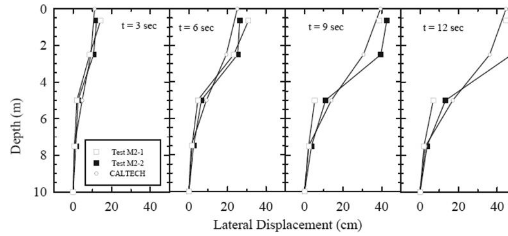

Figure 1. Lateral displacement profiles for centrifuge tests of the same VELACS physical model (of a sloping deposit) conducted at Rensselear and Caltech (Dobry and Taboada 1994).

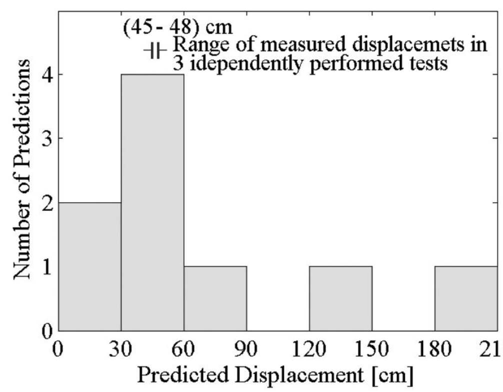

Figure 2. Histogram of predicted lateral displacements compared to 3 centrifuge results from Figure 1 (Dobry and Taboada 1994).

2 SOIL LIQUEFACTION ANALYSES AND VALIDATION NEEDS

The dynamic response of saturated granular soils under extreme loading conditions is complex and exhibits patterns associated with the particulate discrete nature of granular soils and the effects of pore pressure buildup. These soils may deform as a solid, liquefy or, eventually, flow as a fluid depending on the level of confining stresses and pore water pressures. The response may also exhibit patterns that are distinct of that of soil and fluid such as dilation and void redistribution. As mentioned above, numerous computational tools were developed over the last decades, and are now able to handle the multitude of response characteristics associated with excess pore pressure buildup and liquefaction with different levels of realism. The developed tools are often calibrated through personal efforts using class C predictions, and, frequently, theses efforts are limited and in some instance lack consistency due mostly to a lack of coordination. In other words, there was no thorough assessment and validation of the computational tools used to analyze soil liquefaction, except for few occasional efforts such as that by EPRI (1993) and the VELACS project (Arulanandan and Scott, 1993 and 1994).

2.1 *VELACS and lesson learned*

An extensive suite of centrifuge tests and duplicates were conducted in the in the early 1990's at different facilities in the US and UK (UCD, RPI, University of Colorado at Boulder, Princeton University, and Cambridge University) to generate data for Verification of Liquefaction Analyses by Centrifuge Studies (VELACS). A total of 12 models were tested and represented various soil systems, including level sites, sloping ground, embankments and shallow foundations. There was significant variability in the centrifuge test results. Some experiments showed a large degree of consistency in results, while others had low level of repeatability.

Over 20 teams of numerical modelers participated in an elaborate prediction exercise of the conducted tests. Numerous class A (blind) numerical simulations of these centrifuge tests were submitted and compared at a symposium. Figures 1 and 2 illustrate the limitations of some of the employed state-of-the art numerical modeling techniques (at the time of VELACS) for one of the tested models that showed a large degree of consistency in experimental results. The experimental measurements of surface lateral displacement of a sloping deposit model varied from 45 to 48 cm, but numerical simulations spanned the range

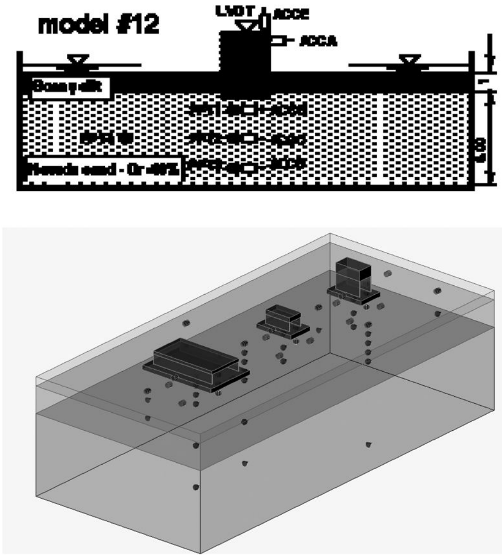

Figure 3. Advances in testing technologies: (a) VELACS Model 12 with 10 sensors (Prevost and Popescu 1994) compared to (b) a recent centrifuge experiment archived in NEEShub by Dashti et al., (2008) with three model structures supported on a layered soil deposit and more than 100 sensors.

from 0 to 210 cm. Other centrifuge models tested in VELACS showed a significant scatter in experimental results and numerical predictions. This was especially the case for relatively complex systems. For instance, the settlement of the shallow foundation in VELACS Model 12 (Figure 3) was measured at three different centrifuge facilities and values ranged between 10 and 23 cm (Wilson et al., 1994).

2.2 *NEES and current state-of the art in experimental modeling*

Over the past few decades, the (worldwide) geotechnical engineering community has seen significant advances in experimental simulations of the earthquake response and liquefaction of saturated soil systems. Specifically, experimental research using increasingly reliable element scale laboratory tests, insitu tests, and centrifuge experiments have provided the community with significantly improved understanding of the response and liquefaction of geosystems when subjected to dynamic loading. In the United States, the NEES (Network for Earthquake Engineering Simulation) initiative has been instrumental in upgrading the experimental facilities for earthquake engineering research. Today, the NEES centrifuge sites are equipped with excellent tools for preparation, characterization, instrumentation and testing of soil system models. Many recent NEES-Research projects have used these facilities to produce high quality experimental results for a variety of geotechnical engineering problems. Figure 3 illustrates the dramatic evolution in the state-of-the art of centrifuge modeling since the VELACS time. On one hand, more than 100 sensors were used in a NEES test along with three simultaneously tested model structures of shallow foundations and in-flight cone penetration testing to characterize the soil deposits (Dashti et al., 2008). On the other hand, merely 10 sensors were used in a VELACS model 12 of a single foundation.

2.3 *Computational modeling and validation needs*

The past decades were also marked by tremendous advances in computational power and computational methods. These advances enabled an unprecedented opportunity for the analysis of very large soil-structural systems using sophisticated constitutive and numerical modeling techniques (e.g., Zienkiewicz et al., 1998; Elgamal et al., 2003; Jeremic, et al., 2008). However, these advances in computational modeling were achieved quite often independently of the progress in experimentation and testing of soil systems. Thus, our computational tools are either not able or have not been properly validated to address a number of challenging, but common, liquefaction phenomena. These phenomena include, for instance, (1) large lateral displacements and the influence of stress (mostly shear) bias on ground deformation, and (2) the effects of soil fabric, void redistribution and preshaking on liquefaction susceptibility and evolution. The effects of multi-axial shaking and the presence of subsurface structural elements (e.g., foundation or utility lines) are also associated with other complex liquefaction and soil-structure interaction phenomena that still necessitate attention from the computational geotechnical community.

There is currently an urgent need for coordinated validation efforts to assess the capabilities and accuracy of computational tools used to predict the liquefaction phenomenon and its consequences on civil infrastructure systems. The overall objectives of the LEAP project fall within this context (Manzari et al., 2014). Achieving these objectives requires: (1) consistent standard for the validation of computational tools (Kutter et al., 2014), and (2) a high quality set of comprehensive and reliable experimental data. Such an undertaking will enhance our confidence in advanced computational tools and enable a wider acceptance within the community of practitioners.

Conceptually, the ultimate validation data correspond to case histories of thoroughly instrumented actual systems, such as the Wildlife Refuge site of NEES@UCSB (UCSB 2014). However, quite a few systems have been thoroughly instrumented. Furthermore, geotechnical systems are often immense and the responses of such systems depend on a large number of variables. Thus, it is almost impossible to record and collect enough experimental data to isolate the effects associated with a given phenomenon such as liquefaction. For this reason, a thorough validation of computational tools using case history analysis of a full-scale system often requires significant assumptions and may not be practical or feasible. The alternative is to use experimental data provided by tests of soil samples and small-scale centrifuge models under controlled conditions. These tests are now capable of producing superior experimental data in terms of both quality and quantity.

2.4 *Requirements for validation data*

The majority of experiments in geotechnical engineering are conducted primarily to: (1) advance the fundamental understanding of some physical phenomena (e.g., lateral spreading or void redistribution), (2) improve or possibly construct a mathematical model of these phenomena, or (3) assess the performance or safety of an engineering system (or subsystem). These experiments are often not adequate for specific validation tasks because of a number of reasons, including: (1) inconsistency between the validation objective and the experiment, (2) limited resolutions of measurements of response quantities (e.g., only global response parameters are measured), or (3) incomplete documentation of testing conditions (e.g., incomplete measurements of input quantities).

Thus, validation efforts to assess the accuracy of a computational tool in simulating a physical phenomenon generally require the design and conduct of specific experiments. Specifically, these experiments should be planned to capture clearly the essential physics of the phenomena of interest, and measure with adequate resolution and level of accuracy all response, initial and boundary condition parameters necessary to perform the validation with as little assumptions as possible. The purpose is to acquire data that enables a quantitative and conclusive assessment of the ability of the computational models with as little assumptions as possible. Furthermore, the process of validation has to be performed in a somewhat independent fashion of the experimental procedures and tests to ensure an "objectivity" of the assessments.

Within the context of a community projects such as LEAP, the requirement discussed above may be achieved by relying on a close collaboration and coordination among experimentalists and computational modelers to design adequate validation experiments and to use mostly blind (class A) predictions (Oberkampf et al., 2010).

3 EXPERIMENTAL DATA FOR VALIDATION

Development of reliable experimental centrifuge test data is an essential goal of LEAP. A quantitative calibration and validation of computational tools to predict specific aspects of soil response associated with liquefaction is contingent on the availability of adequate experimental data. The experimental data provide reference (response) measures against which the output of computational models of soil liquefaction are compared. Uncertainties are always present in experimental data (Drosg, 2007) and the validation process cannot assume that this data is fully correct. Thus, the model predictions can be credibly assessed and used in quantitative validations only if the accuracy and estimates of the uncertainty in the measured experimental data are explicitly taken into consideration (Oberkampf et al., 2010). In other words, the experimental data has to undergo an inspection process to assess the quality and possibly quantify the uncertainties of this data and ensure that it can be used with confidence as a reference for calibration and validation of computational model predictions.

There are different types of factors that lead to uncertainties in complex experiments such as centrifuge tests. These factors include experimental setup, instrumentation and procedures as well the testing facility characteristics. The uncertainties may be of systematic or random nature (Oberkampf et al., 2010). Systematic (also called epistemic) uncertainties are associated with a lack of knowledge (incomplete measurements or characterization of input motion). Random (or aleatory) uncertainties reflect an intrinsic random variability. Historically, these errors were often acknowledged, but rarely explicitly considered in validation efforts of computational tools used in geotechnical engineering.

Furthermore, liquefaction problems are complex and marked by the presence and coupling of different physics associated with the soil solid and fluid phases and interaction with any relevant foundation or structural element (having various levels of geometric complexity). A hierarchical strategy (Oberkampf et al., 2010) is used in LEAP to address this complexity in validating of soil liquefaction models. This strategy divides the complex validation problem into a series of progressively more complex sub-validations (Oberkampf et al., 2010) and includes both class C and A predictions:

(1) Validation against single element test data
(2) Class C calibration by comparing numerical model predictions to existing data from:
   a. Benchmark centrifuge model tests (relatively simple geometry such as 1D sloping ground tested using a laminar container).
   b. Physical model tests of systems (e.g. dams, soil-structure interaction, etc.).
   c. Benchmark simulations of liquefaction in the field (e.g. Christchurch).
(3) Class A validation by blindly comparing numerical model predictions to data from:
   a. New benchmark centrifuge model tests (relatively simple geometry such as 1D sloping ground tested in a laminar container or biaxial shaking of level sites using a 2D laminar container).
   b. New physical model tests of systems (e.g. dams, soil-structure interaction, etc.).

This approach recognizes that the relative quantity and resolution of information that is obtained from experiments vary substantially as a function of the complexity of the physical model and associated tests. Each step of the hierarchy is aimed at providing information that facilitates the following one.

3.1 *Class C calibration data*

The George E. Brown Network for Earthquake Engineering Simulation (NEES) has provided unprecedented opportunities for the earthquake engineering community in the USA and abroad to study various aspects of the response of civil engineering infrastructure to earthquake loading. Some of these projects involved centrifuge testing and had been curated and the associated data was made publicly available in NEEShub (NEES 2014). Many of the conducted experiments were intended to study mechanisms of behavior in relatively complex problems. Often, these experiments furnish good quality data, but do not provide self-contained high quality validation data set. The shortcomings are primarily because the experiments are not duplicated on multiple facilities (i.e., there is no assessment of uncertainty) and in most cases the experiments are too complex and cannot be used in validation of a liquefaction problem without additional experimental data. The experimental data from these projects are good candidates for class C predictions (or calibrations) of liquefaction computational tools. The following paragraphs provide an overview of the NEEShub data that may be used in such calibrations.

3.1.1 *NEES data for benchmark calibrations*

The NEEShub currently includes at least two projects with data appropriate for benchmark calibrations.

"*Experimental and micromechanical computational study of pile foundations subjected to liquefaction induced lateral spreading:*" This project (Gonzalez, 2008, Abdoun et al., 2013) involved a number of centrifuge experiments and corresponding full-scale tests of level and sloping ground sites. The project also included centrifuge tests for of soil pile systems. Sample results of a level site test are discussed below.

"*Advanced site monitoring and effective characterization of site nonlinear dynamic properties and model calibration:*" A number of centrifuge tests of level site deposits (of a saturated granular soil) were tested using a 2D shaker and a 2D laminar box (El Shafy et al., 2014). The tests provide unique opportunity of good quality benchmark data to assess the effects of multi-axial shaking on site dynamic response and liquefaction.

3.1.2 *NEES data for system calibrations*

The NEEShub also includes a number of projects that involved complex soil systems. The following are two selected projects that may be used in calibration of systems involving shallow foundations and site remediation.

"*Seismic risk mitigation for port systems:*" A number of centrifuge experiments of rather complicated soil systems were conducted. The experiments involved 3-dimensional problems associated

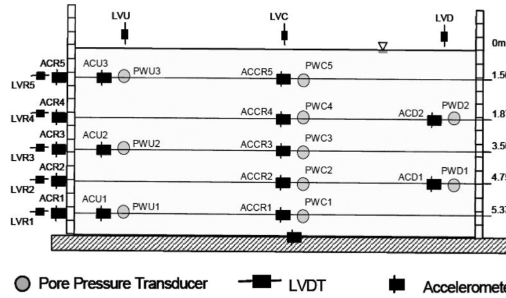

Figure 4. Variation of the shear modulus with confining pressure and void ratio for the stiff fabric synthetic soil (the discrete data points correspond to the triaxial test simulations and the solid lines to a least-squares fit).

with liquefaction drains, colloidal silica gel retrofit, along with others aspects. Nevertheless, this project also included an experiment of a gently sloping 2-layer (Kamai et al., 2008) which is a potential candidate as a benchmark model test.

"*Towards developing an engineering procedure for evaluating building performance on softened ground:*" This project involved experiments with good quality data for system calibration associated with foundation problems. These experiments included, for instance, multiple rectangular buildings placed on a layer of liquefiable soil of limited thickness, as sketched in Figure 3 (Dashti et al., 2008).

3.1.3 *Case study of a benchmark test*

A benchmark test of a level site (Gonzalez, 2008) was selected from NEEShub by the US LEAP team to illustrate some of the steps associated with the process of calibration and validation and assessment of the validation metrics (Kutter et al., 2014). This article presents some of the characteristics of the selected test and discusses the outcome of preliminary inspection analyses that are being conducted to assess the quality and appropriateness of the associated data.

Briefly, the test consisted of about 6 m (in prototype units) of a Nevada sand deposit tested in a laminar box (Figure 4). The soil was pluviated to achieve a relative density of 40% and then fully saturated with a viscous fluid to achieve a permeability of the order 10^{-4} m/s. The soil model was equipped with an extensive array of accelerometers, pore pressure transducers and LVDTs to measure both lateral displacements and surface settlements. The deposit was subjected to a base excitation that was aimed at exploring the response of a saturated soil over a wide range of conditions, as shown in Figure 5. Specifically the excitation consisted of 4 phases with relatively constant accelerations amplitudes which increased with phase (0.01 g, 0.05 g, 0.1 g, and 0.25 g for phase 1 to 4).

Figure 5 also displays the accelerations that were measure within the soil and on the laminates (at depths of 3.5 m and 4.75 m and the recorded excess pore pressures within the soil at these depths. The recorded pore pressures showed that the soil experienced high

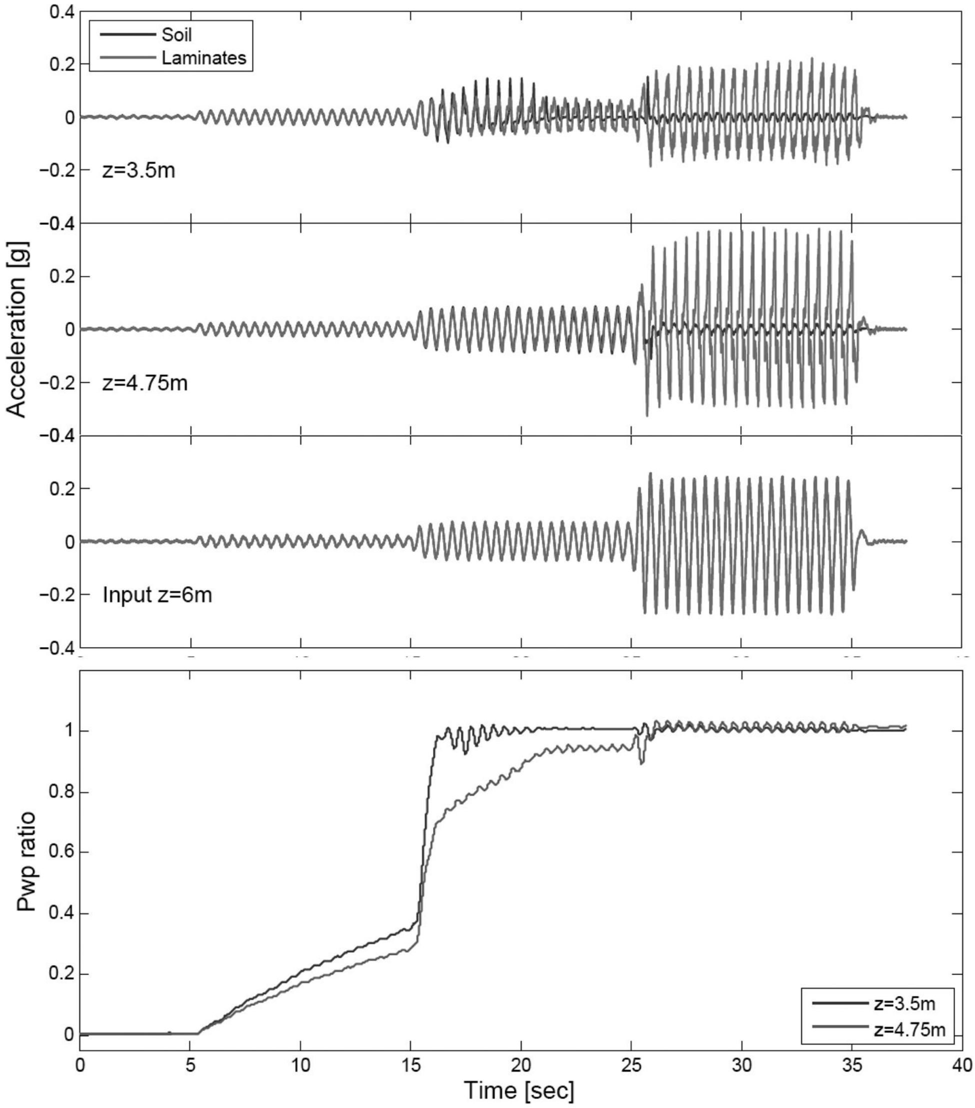

Figure 5. Input motion and selected accelerations and pore pressure time histories of the level site deposit of Figure 4.

pore pressure ratios during the third phase of excitations (starting at about 16 s). Nevertheless, during these phases the accelerations measured on the laminates showed a response more consistent with the input motion than the soil response (with remarkably large accelerations during the fourth shaking phase when the soil had fully liquefied). In other words, the laminated are not fully frictionless, and the interlaminate contacts are able to transmit significant accelerations.

The recorded accelerations within the soil and the permanent lateral displacements of the laminates were used to obtain the shear stress and strains with the soil deposit (Zeghal et al., 1995), as shown in Figure 6. The evaluated stresses and strains assume that the soil response within the central part of the deposit is dominated by shear-beam type deformations. The computed shear stress-strain response (Figure 6) appeared to be consistent with this assumption until about 26 s of shaking. For instance the obtained behavior shows a number of cycles with a significant dilative response (during the 10 s to 22 s window). During the last phase of shaking (22 s to 26 s), the computed shear stress-strain response had a significant amplitude even though the pore pressure ratios were close to 1.0. Also, the observed stress-strain response did not show a pattern consistent with that exhibited during the 10 s to 22 s window. Apparently, once the soil liquefied fully (i.e., pore pressure ratio of about 1.0), a significant portion of the measured soil accelerations were transmitted through the container laminates and normal waves through the soil. In other words, the fourth phase of shaking may not be used in a calibration analysis

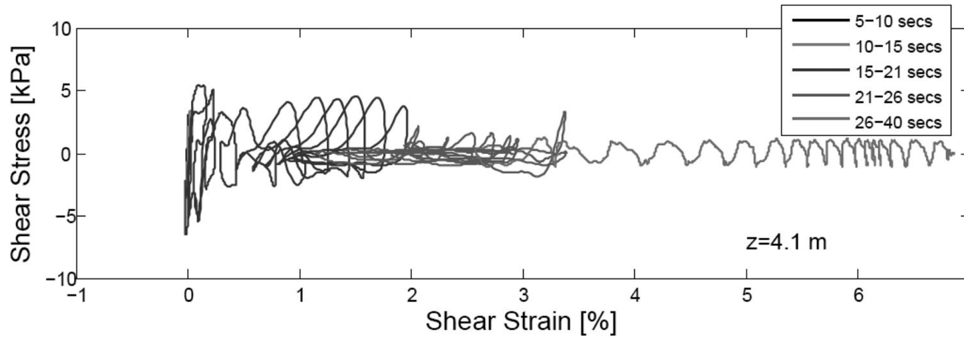

Figure 6. Shear stress-strain response (at about 4.1 m depth) of the level site deposit of Figure 4.

using a shear beam model of the deposit. This finding draws attention to the necessity of assessing the conditions under which a laminar container soil model may be used with a shear beam computational model. A thorough quantitative calibration or validation exercise of the centrifuge model shown in Figure 4 may require a realistic model of the laminated container that reflects the actual inter-laminate friction coefficient and the interaction between the soil and the laminates (both in the normal and tangential directions).

3.2 *Class A validation data*

The LEAP class A validation effort will follow the strategy described above. The details of the validation (using class A blind predictions) and data to be employed will be developed through a consensus of the geotechnical engineering community. The following is a description of the tests and requirements as envisioned by the US LEAP group.

3.2.1 *Benchmark centrifuge model tests*

The benchmark tests will consist of level and sloping ground deposits (Figure 5) tested using the same soils but with progressively more complex conditions. These tests will provide data to assess the ability of constitutive and numerical techniques to evaluate: (1) the effect of initial shear stress on the pore water pressure generation and dissipation, (2) large deformations and lateral displacements of the soil at different elevations (as well as related issues of possible transition of the soil behavior from contractive to dilative), and (3) the effects of fabric on the initiation and evolution of soil liquefaction (including soil stiffness properties and contraction and dilation). Two different fabrics will be used, and the models will be subjected a series of shaking events. In flight site characterization will employed between the shaking events will be used to provide the necessary data for assessing the ability of the constitutive models to account for evolution of density and fabric.

3.2.2 *System centrifuge model tests*

The system tests will be conducted to evaluate the response of the same cohesionless soil used in the

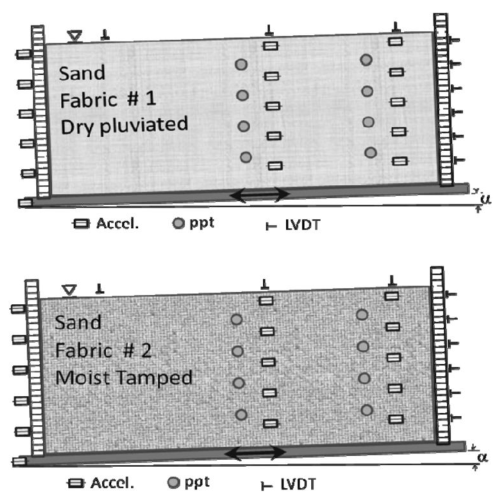

Figure 7. Schematic of benchmark centrifuge models of a gently sloping saturated soil deposit with two different fabrics.

benchmark tests in more complex configurations that involve a structure (e.g., a quay wall) with liquefiable backfill and foundation soils or a soil embankment. A schematic of potential configurations for centrifuge tests for system validations is shown in Figure 7.

3.2.3 *Data, quality assurance and experimental errors*

The planned tests for class A predictions will capitalize on the recent advances in testing enabling more effective and reliable methods in specimen preparation, saturation of the soil, and achieving target input motions. The associated models will be densely instrumented to achieve a high resolution in measuring the key state parameters (e.g., accelerations, pore pressure, lateral displacements, and settlements). In flight tools (e.g., miniature CPT) will be employed to characterize the soil and further define the initial conditions. Also, an extensive set of material and element tests will be conducted for the soils that will be used with the benchmark and system tests. These tests will provide all data necessary for constitutive modeling. It should be noted that VELACS included a parallel report summarizing

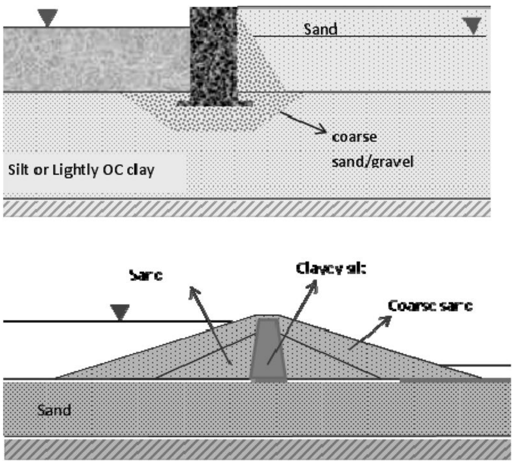

Figure 8. Potential configuration for centrifuge tests for system validations.

material properties of the soils used in the centrifuge tests (Arulmoli et al., 1992).

Quantification of experimental errors and biases has always been a challenge in testing of geotechnical soil elements and system. This is associated with the inherent random nature of geo-materials. Thus, it is not always possible to repeat test under identical conditions. Experimental errors associated with sensor limitations are presumed to be minor in view of the significant advance in the sensing technology. However, there is always variability in experimental results associated with the details of the different testing procedure used at separate facilities as well as the effects of centrifuge scaling laws. The LEAP project will rely on replication of tests and modeling-of-the-model to assess the associated level of biases and experimental errors.

4 CONCLUSIONS

This paper discussed a number of issues related to the characteristic of experimental data that may be used in the calibration and validation of computational models of soil liquefaction within the context of the LEAP project. Currently existing experimental data sets often have limitations and are potentially good only for model calibrations (or Class C predictions). In contrast, new experimental data are needed for a validation effort. Specifically, a hierarchical series of soil sample and centrifuge model tests, with full uncertainty quantification, are needed to generate experimental data that would enable efficient and conclusive Class A (blind) predictions.

ACKNOWLEDGEMENT

The planning phase of the LEAP project has been funded by the US National Science Foundation Geotechnical Engineering program directed by Dr. Richard Fragaszy (NSF proposal number 1344619). This support is gratefully acknowledged.

REFERENCES

Abdoun, T., Gonzalez, M. A., Thevanayagam, S., Dobry, R., Elgamal, A., Zeghal, M., Mercado, and El Shamy, U., (2013). "Centrifuge and large scale modeling of seismic pore pressures in sands: a cyclic strain interpretation," *Journal of Geotechnical and Geoenvironmental Engineering,* Vol. 139, No. 8, pp. 1215–1234.

Arulanandan, K., and R. F. Scott (1993–1994). "Verification of Numerical Procedures for the Analysis of Soil Liquefaction Problems," Proceedings of the International Conference on the Verification of Numerical Procedures for the Analysis of Soil Liquefaction Problems, Vols. 1 and 2, A. A. Balkema, Rotterdam, the Netherlands.

Arulmoli, K., Muraleetharan, K. K., Hossain, M. M., and Fruth, L. S. (1992). *VELACS: Verification of Liquefaction Analyses by Centrifuge Studies, Laboratory Testing Program, Soil Data Report*, Report, The Earth Technology Corporation, Project No. 90-0562, Irvine, California.

Dashti, S., Bray, J.D., Pestana, J. M., Riemer, M.F., and D. Wilson (2008). Centrifuge Test Plan for Test Series SHD03, NEESR-II Project: "Towards Developing an Engineering Procedure for Evaluating Building Performance on Softened Ground." http://nees.org/data/get/NEES-2006-0224/ Experiment-3/Analysis/SHD03_DataReport.pdf.

Dobry, R. and Taboada, V. (1994). "Possible Lessons from VELACS model No. 2 Results," *Verification of Numerical Procedures for the Analysis of Liquefaction Problems*, Arulanandan and Scott (eds.), Proceedings of Intl. Conf., Davis, CA, October 17–20, 1993, Vol. 2, A.A. Balkema, Rotterdam, The Netherlands, pp. 1341–1352.

Drosg, M. (2007). *Dealing with Uncertainties: a Guide to Error Analysis*, Berlin, Springer-Verlag.

Elgamal, A., Yang, Z., Parra, E., and Ragheb, A., (2003). "Modeling of Cyclic Mobility in Saturated Cohesionless Soils," *International Journal of Plasticity*, Pergamon, Elsevier Science Ltd., Vol. 19, Issue 6, pp. 883–905.

El-Shafee, O., Spari, M., Abdoun, T., and Zeghal, M. (2014). "Analysis of the response of centrifuge model of a level site subjected to bi-axial base excitation," *Geo-congress 2014: geo-characterization and modeling for sustainability*, ASCE, Atlanta, Georgia, February 23–26.

EPRI (1993). Electric Power Research Institute. Guidelines for determining design basis ground motions. Palo Alto, California: Electric Power Research Institute, vol. 1–5, EPRI TR-102293.

Gonzales, M. (2008). "Centrifuge modeling of pile foundation response to liquefaction and lateral spreading: study of sand permeability and compressibility effects using scaled sand technique, PhD Thesis, Rensselaer Polytechnic Institute, Troy, NY.

Jeremic, B., Cheng, Z., Taiebat, M., and Dafalias, Y. F. (2008). "Numerical Simulation Of Fully Saturated Porous Materials." International Journal for Numerical and Analytical Methods in Geomechanics, 32(13), 1635–1660.

Kamai, R., Howell, R. Conlee, C., Boulanger, R., Marinucci, A., Rathje, E., Rix, G. (2008). "Evaluation of the Effectiveness of Prefabricated Vertical Drains for Liquefaction Remediation." Centrifuge Data Report for UCD/CGMDR, June 25, 2008.

Kutter et al., (2014). "Proposed Outline for LEAP Verification and Validation Processes," the Fourth International

Conference on Geotechnical Engineering for Disaster mitigation and Rehabilitation (4th GEDMAR), 16–18 September, 2014, Kyoto, Japan.

Lambe, T.W. (1973) "Predictions in Soil Engineering" *Geotechnique,* Vol. 23, No. 2, pp. 149–202.

Manzari et al., (2014). "LEAP Projects: Concept and Challenges," the Fourth International Conference on Geotechnical Engineering for Disaster mitigation and Rehabilitation (4th GEDMAR), 16–18 September, 2014, Kyoto, Japan.

NEES (2014). https://nees.org/

Oberkampf, W. L., and Roy, C. J. (2010). *Verification and validation in scientific computing* (Vol. 5). Cambridge: Cambridge University Press.

Prevost, J. H. and Popescu, R. (1994). An assessment of VELACS. *Technical Report NCEER*, 94, 415–23.

UCSB (2014). http://www.nees.ucsb.edu/facilities/wla

Wilson, D.W., Farrell, T.M., and Kutter, B.L. (1994). "An Overview and Relevance of Experimental Data from VELACS Project Model Nos. 7, 11, and 12." Proceedings, Verification of Numerical Procedures for the Analysis of Soil Liquefaction Problems, Arulanandan and Scott,eds., Balkema, Rotterdam, Vol. II, pp. 1657–1680.

Zeghal, M., Elgamal, A.-W., Tang, H. T., and Stepp, J. C. (1995). "Lotung Downhole Seismic Array: Evaluation of Soil Nonlinear Properties." *Journal of Geotechnical Engineering*, ASCE, 121(4): 363–378.

Zienkiewicz, O. C., Chan, A. H. C., Pastor, M., Schrefler, B. A., and Shiomi, T. (1998). *Computational Geomechanics with Special Reference to Earthquake Engineering*. John Wiley and Sons, England.

Geotechnics for Catastrophic Flooding Events – Iai (Ed)
© 2015 Taylor & Francis Group, London, ISBN 978-1-138-02709-1

Benchmark centrifuge tests and analyses of liquefaction-induced lateral spreading during earthquake

T. Tobita
Disaster Prevention Research Institute, Kyoto University, Japan

M.T. Manzari
George Washington University, USA

O. Ozutsumi
Meisosha Co., Japan

K. Ueda
Railway Technical Research Institute (RTRI), Japan

R. Uzuoka
Tokushima University, Japan

S. Iai
Disaster Prevention Research Institute, Kyoto University, Japan

ABSTRACT: ABSTRACT: Over the past twenty years after the VELACS project, with major advancement of computer simulation technologies, research works on numerical constitutive modelling of liquefiable sand have been conducted intensively. Contribution of the VELACS project on the development of numerical modeling in this field has never been underrated. However, with the development of new and innovative models, we believe that now is the time to revisit the project and help define direction of research for possibly another twenty years'. As a pilot project for the future international collaborations to examine the capabilities of existing numerical techniques for liquefaction analysis through laboratory experiments and centrifuge tests, a Class A prediction is conducted by numerical modelers of four institutes for a series of centrifuge experiments of flat and inclined saturated sand deposits. A brief description of the experiments, results of the numerical predictions, and general remarks for the next step are presented in this paper.

1 INTRODUCTION

Over the past twenty years after the VELACS project (Arulanandan and Scott, 1993 and 1994), with major advancement of computer simulation technologies, extensive research work on constitutive modelling of highly non-linear material, such as liquefiable sand, under dynamic condition have been conducted and some have been successfully applied in practice. Contribution of the VELACS project on the development of numerical modeling on liquefiable ground has never been underrated. However, with the development of new and innovative models, we believe that now is the time to revisit it and help to define possibly direction of research on this field for another twenty years'.

As a pilot study aiming at future international collaborations to examine the capabilities of existing numerical models for liquefaction analysis through laboratory experiments and centrifuge tests, a series of dynamic centrifuge tests on liquefiable ground were conducted at the Disaster Prevention Research Institute, Kyoto University, Japan in 2012. These experiments were intended to provide the experimental base for a Class A validation exercise. This prediction/validation involved cooperative efforts of five participants: George Washington University, USA, Meisosha, Co., Railway Technical Research Institute, and Tokushima University, Japan. A small workshop was held on January 30, 2013 in Kyoto, Japan to compare and discuss not only numerical results, but also method of the centrifuge testing. Participants of this workshop were, in addition to the above mentioned institutes, from University of California, Davis (USA), Cambridge University (UK), National Central University (Taiwan), Tokyo Institute of Technology (Japan), and Ehime University (Japan). In what follows, a summary of this pilot project and some remarks for the next step is given.

Table 1. Test cases for centrifuge modelling.

Case	Ground Condition		Peak Hor. Input Acc. Amp. (m/s^2)	Relative density, Dr (%)	Degree of saturation od the ground, Sr (%)	Construction method of model ground
1	1	Horizontal	2.41	58.8	100% (assumed)	Water pluviation
	2		2.50	41.9		
	3		2.47	47.6		
2	1	Slope	1.52	48.6	100% (assumed)	
	2		2.04	48.2		
	3		4.22	46.6		
3	1		2.35	43.9	99.3	Saturated in the
	2		2.50	45.7	99.5	vacuum
	3		2.39	46.9	99.7	chamber

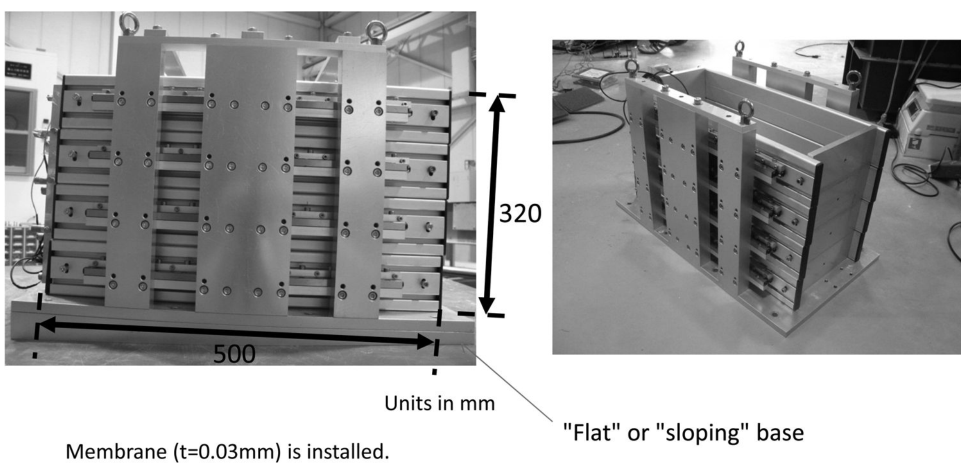

Figure 1. Hinged-wall shear box at DPRI, Kyoto University.

2 CENTRIFUGE TESTS ON LIQUEFIABLE GROUND

A series of centrifuge experiments were conducted under 50 g to observe dynamic behavior of a saturated sand deposit. As summarized in Table 1, in total nine cases were tested. In all cases the model ground was inclined at 2 degrees, except for Case 1-1 in which the ground was flat. A hinged-wall type shear box (L50 × W20 × H32 (cm)) (Fig. 1) was implemented for shaking table tests of both flat and sloping saturated sand deposit. In the case of sloping ground, the flat model ground was prepared first, then the box was attached on the base plate with inclined surface of 2 degrees (Fig. 1).

The model ground, made of Toyoura sand, was prepared either by water pluviation method (Case 1-1 to Case 2-3) or vacuum chamber method (Case 3-1 to Case 3-3) (Table 1) to have loose sand deposit of the relative density of 40–50%. The model ground was saturated with water, i.e., no viscous fluid was used, and shaken by the input acceleration with maximum amplitude of about 1.5 to 4.2 m/s^2 and frequency of approx. 2 Hz.

Sensor locations are specified in Figs. 2 to 4. In total 8 accelerometers, 7 potentiometers to measure lateral displacement of the hinged-wall, and 8 pore water pressure transduces were used to record the dynamic behavior of the model ground. Reason for not having used viscous fluid was just for its ease of handling because we had been at the phase of testing the effectiveness of the vacuum chamber method for fully saturating the model ground (Okamura & Inoue 2010). As shown in Table 1, the degree of saturation with vacuum chamber method is more than 99% which may be a satisfying value to take into account the repeatability of physical model testing.

Liquefaction strength curves and related information are shown in Fig. 5.

As pointed out by Scott (1994), in dynamic physical modelling the effect of vertical motion is inevitable. This will be shown later in comparison with numerical results.

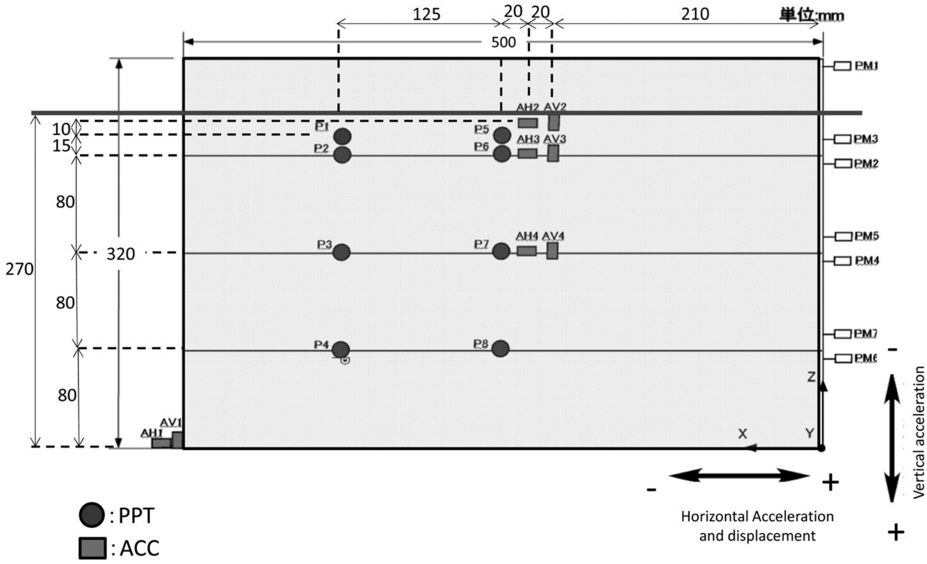

Figure 2. Sensor locations of Case 1-1.

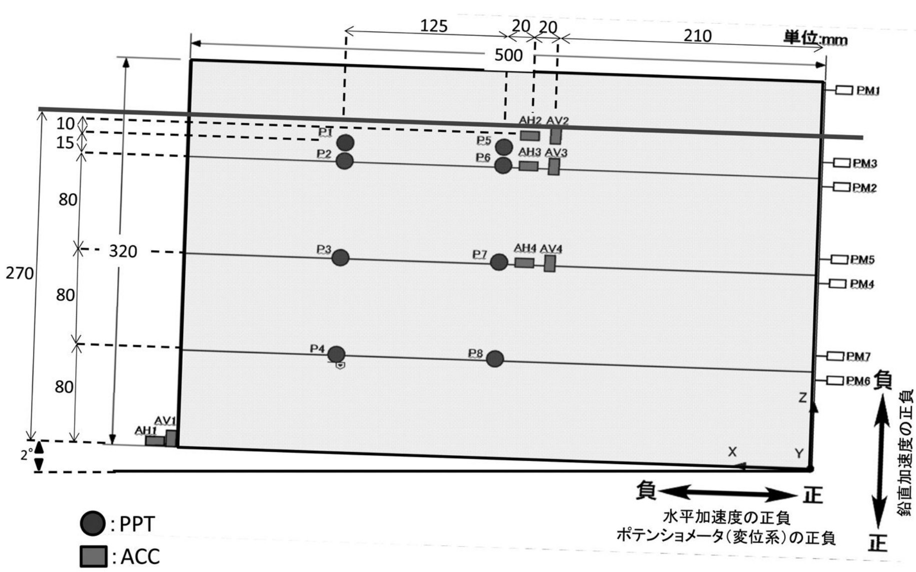

Figure 3. Sensor locations of Case 1-2.

3 DATA PROVIDED FOR CLASS A PREDICTION/VALIDATION

The following dataset was provided to the numerical modelers.

1. Hollow cylindrical torsional shear test results of Toyoura sand
2. Liquefaction strength curve of Toyoura sand
3. Grains size distribution curve of Toyoura sand
4. Time histories of input acceleration of all the test cases
5. Mechanical details of the hinged-wall shear box

Due to time limitation, some of the dataset was provided in Japanese only.

4 RESULTS OF NUMERICAL PREDICTION

As mentioned earlier, because the present study is a pilot program for future collaboration, in what follows, comparison with measured data will be made only anonymously. Results of 4 numerical models, Model A to D, are presented (Dafalias & Manzari (2004), Iai,

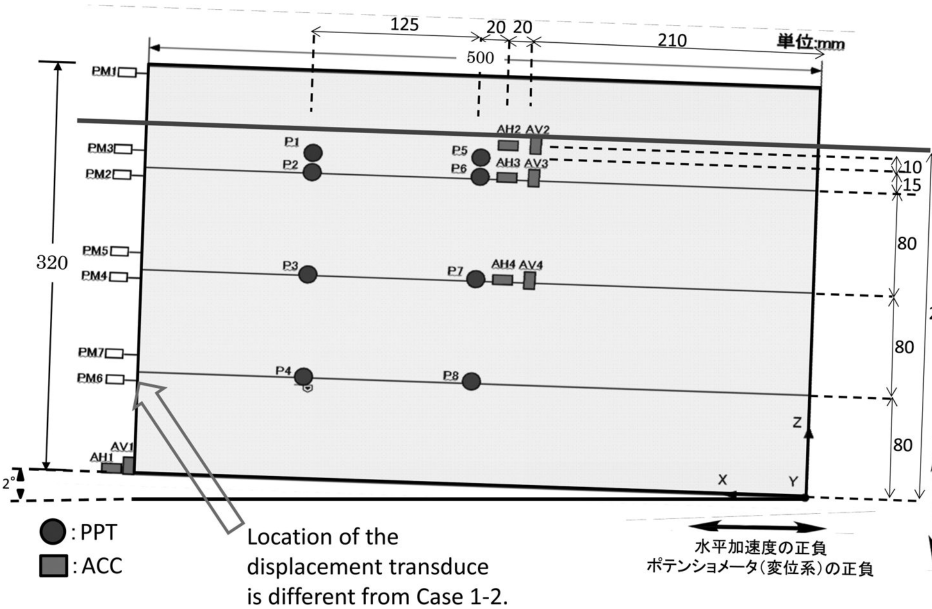

Figure 4. Sensor locations of Case 1-3 and later.

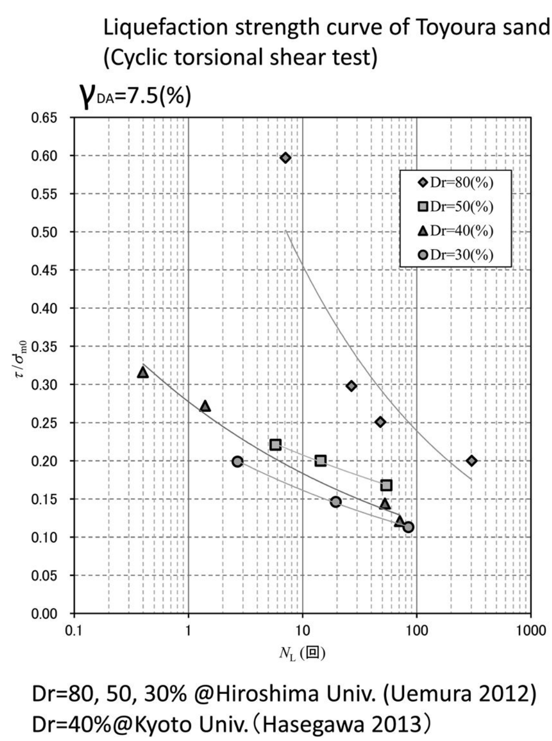

B values of the tests of Dr=40%

τ/σ'_{m0}	B Value
0.12	0.902
0.144	0.931
0.272	0.986
0.316	0.948

Properties of Toyoura sand

Specific gravity G_s	2.636
Min. density ρ_{dmin}	1.638
Max. density ρ_{dmax}	1.329
Max. void ratio: e_{max}	0.983
Min void ratio: e_{min}	0.609

Figure 5. Liquefaction strength curves and associated test data of Toyoura sand.

et al. (2011, 2013), Manzari (1996a, b), Manzari & Dafalias (1997), Oka, et al. (1999) (alphabetical order)). In all figures below, thicker red curves are predicted ones and thinner black curves are measured ones. Computational results were provided by time histories of acceleration, excess pore water pressure, and ground deformation. Submission of the results of model calibration with element test data was not requested. In Model A and D, the finite element mesh and deformation are provided.

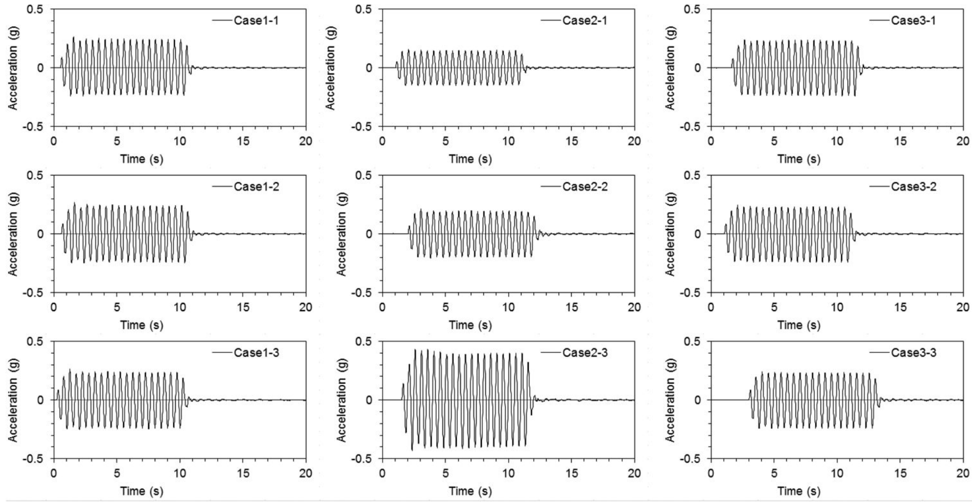

Figure 6. Time histories of the input acceleration measured in the centrifuge tests.

4.1 *Model A*

With this model, computation was made for all 9 cases (Table 1) (Figs. A-1 to A-36). Horizontal accelerations are slightly over estimated, while vertical acceleration are closely correlated. Large spikes on horizontal acceleration, characteristics of dilative behavior during lateral deformation of liquefied soil, are simulated well. Lateral displacements are under estimated. Excess pore water pressures are consistently over predicted. Deformed shapes computed for inclined cases are realistically simulated in a sense that a mass of the model ground is deformed and piled up in the downstream.

4.2 *Model B*

Results of Model B are presented for Cases 1-1, 1-3, 2-1, 2-3, and 3-1 (Figs. B-1 to B-15). Decay of horizontal acceleration at the onset of liquefaction is well simulated. Vertical accelerations are over estimated, especially in the inclined cases. Dilative response in horizontal acceleration due to lateral deformation under cyclic loading is not reproduced. Lateral displacement is over predicted. Excess pore water pressure builds up slightly faster in some cases but overall behavior seems to be well simulated.

4.3 *Model C*

Model C provides results for Cases 1-1, 1-2, 1-3, 2-1, 2-2, and 2-3 (Figs. C-1 to C-18). The modeler comments that the time histories of response acceleration originally provided was the relative acceleration. Thus, by adding the measured input acceleration to the measured response acceleration, time histories are plotted as absolute acceleration (Figs. C-1, C-4, C-7, C-13, and C-16). The acceleration time histories seem to agree well with the measured responses. Excess pore water pressure build up and its dissipation are well simulated. Lateral displacements are over estimated.

4.4 *Model D*

With Model D, numerical analysis for Cases 1-1, and 3-1 are demonstrated. In this model, results obtained from different formulations are compared, i.e., Infinitesimal, Total-Lagrangian and Updated-Lagrangian formulations. Decay of the horizontal acceleration at the onset of liquefaction is well simulated. Vertical acceleration is over estimated. Dilatancy response during lateral deformation is not properly reproduced. Lateral displacements by infinitesimal computation agree better than those of the total and updated Lagrangian formulation.

5 GENERAL REMARKS

Aiming at the future international collaborations, Class A prediction/validation exercise by 4 institutions was successfully conducted in a limited time schedule. Although lessons learned from this project seem to have been already summarized by Scott (1994), for the next step of the project, it suffices to say that

1. When studied in more details, the experimental results and the class A predictions reported in this paper would likely shed additional light onto the current state of physical and numerical modeling of soil liquefaction. They also serve as the first step toward a more comprehensive evaluation of the state-of-the of liquefaction analysis.
2. Repeatability of centrifuge experiments has to be validated by comparison with results of tests conducted by other institutes. As Scott commented that “One might say that the old happy pioneering days of centrifuge testing vanished as soon as

VELACS commenced." With this, he emphasized the issue of quality control on physical modelling. In the present study, particularly, we tried to fully saturate the model ground with the vacuum chamber method to achieve the degree of saturation more than 90%. This could be achieved by other institutes. However, other issues such as "(identical) Input motion" and "Multidirectional shaking (i.e., unwanted large vertical acceleration with high frequencies)" (Scott 1994) are more challenging issues.

3. In numerical analyses, as common practice, material constants might have been selected by fitting the element test data provided by the organizer. Scott commented that "The best way to determine numerical values of material properties is to know centrifuge test results, and to obtain the properties by a Class C prediction, which involves back-fitting the model to that test, but this was not the primary function of the VELACS exercise." This gives us insight into the next step, LEAP (Liquefaction Experiment and Analysis Project) to conduct a combination of Class A and C prediction. For example, material constants can be determined through a Class C prediction of a rather simple model test in combination with normal calibration procedure with element test data.
4. This pilot study identifies the strong need that all the participants in these collaborative projects should have to discuss in person continually in order to gradually improve and form a consistent understanding of the reasons and the sources of uncertainties in the experimental and numerical results. This fact implies that we need to have continual technical meetings through the course of the projects. The newly proposed framework of Liquefaction, Experiment and Analysis Projects (LEAP) aims at fulfilling this type of need.

ACKNOWLEDGEMENT

This research was partially supported by the Ministry of Education, Science, Sports and Culture, Grant-in-Aid for Scientific Research (B), 23310119, 2011–2013, and Grant-in-Aid for Scientific Research (C), 25420502, 2013–2015.

REFERENCES

Arulanandan, K. and Scott, R.F. 1993 and 1994. Verification of Numerical Procedures for the Analysis of Soil Liquefaction Problems. *Proceedings of the international conference on the Verification of Numerical Procedures for the Analysis of Soil Liquefaction Problems*, Vols. 1 and 2. A. A. Balkema.

Dafalias, Y. F. and Manzari, M. T. 2004. Simple plasticity sand model accounting for fabric change effects. *ASCE Journal of Engineering Mechanics*, 130(6): 622–634.

Manzari, M. T. and Dafalias, Y. F. 1997. A critical state two-surface plasticity model for sands. *Geotechnique* 49(2): 252–272.

Manzari, M. T. 1996a. On finite deformation dynamic analysis of saturated soils. *Archives of Mechanics* 48(2): 281–310.

Manzari, M. T. 1996b. Finite deformation analysis of liquefaction-induced flow failures in soil embankments. *Int. J. Geotech. Geolog. Engrg*. 14(2): 83–110.

Iai, S., Tobita, T., Ozutsumi O., Ueda, K. 2011. Dilatancy of granular materials in a strain space multiple mechanism model. *International Journal for Numerical and Analytical Methods in Geomechanics*: 35(3): 360–392.

Iai, S., Ueda, K., Tobita, T. and Ozutsumi, O. 2013. Finite strain formulation of a strain space multiple mechanism model for granular materials. *International Journal for Numerical and Analytical Methods in Geomechanics* 37(9): 1189–1212.

Oka, F., Yashima, A., Tateishi, A., Taguchi, Y. and Yamashita, S. 1999. A cyclic elasto-plastic constitutive model for sand considering a plastic-strain dependence of the shear modulus. *Geotechnique*, 49(5): 661–680.

Okamura, M., Inoue, T. 2010: Preparation of fully saturated model ground, '*Physical Modelling in Geotechnics – Sprimgman, Laue& Seward (eds)*, Vols. 1 & 2, Taylor & Francis Group, London, ISBN 978-0-415-59288-8: 147–152.

Scott, R. F. 1994. Lessons learned from VELACS project, *Proceedings of the international conference on the Verification of Numerical Procedures for the Analysis of Soil Liquefaction Problems*, Vols. 1 & 2. A. A. Balkema: 1773–1779.

MODEL A

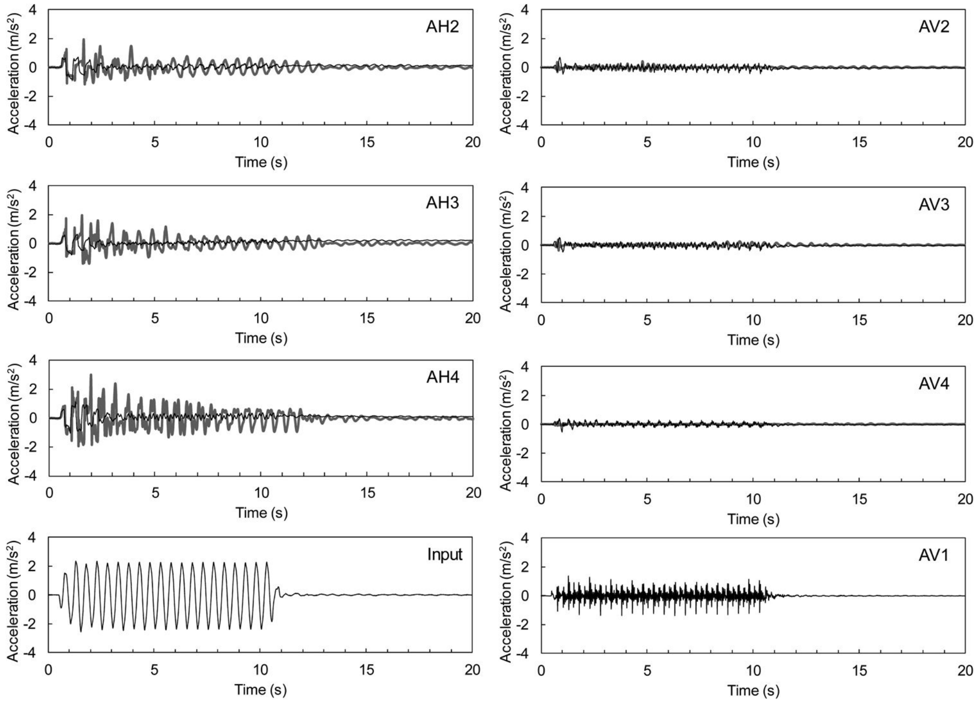

Figure A-1. Time histories of acceleration (Model A): Case 1-1.

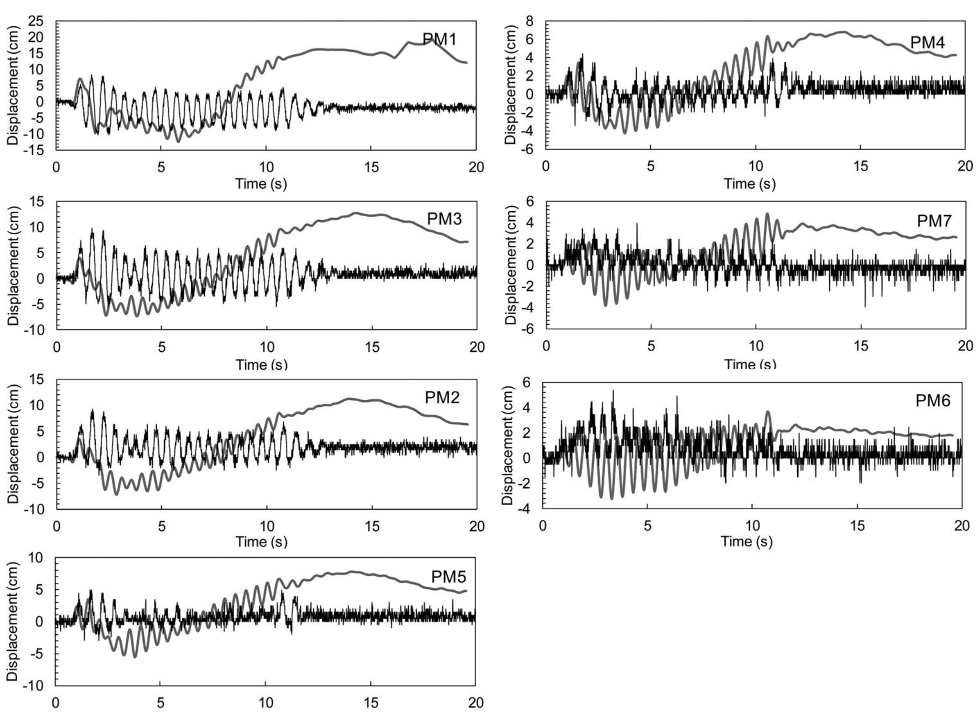

Figure A-2. Time histories of lateral displacement (Model A): Case 1-1.

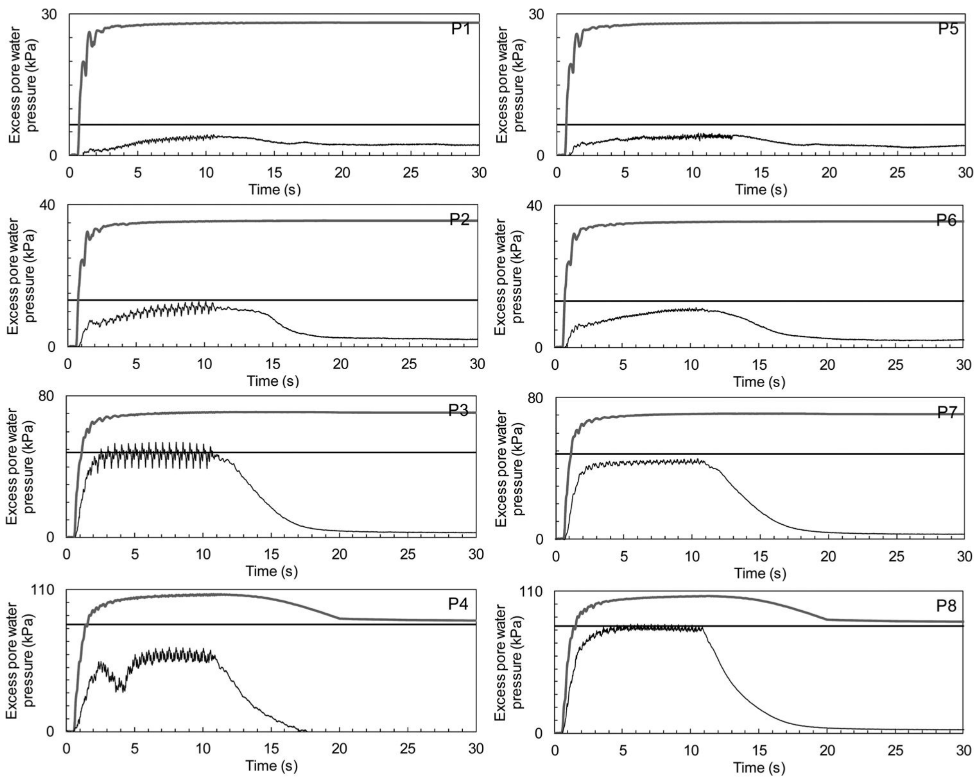

Figure A-3. Time histories of excess pore water pressure (Model A): Case 1-1.

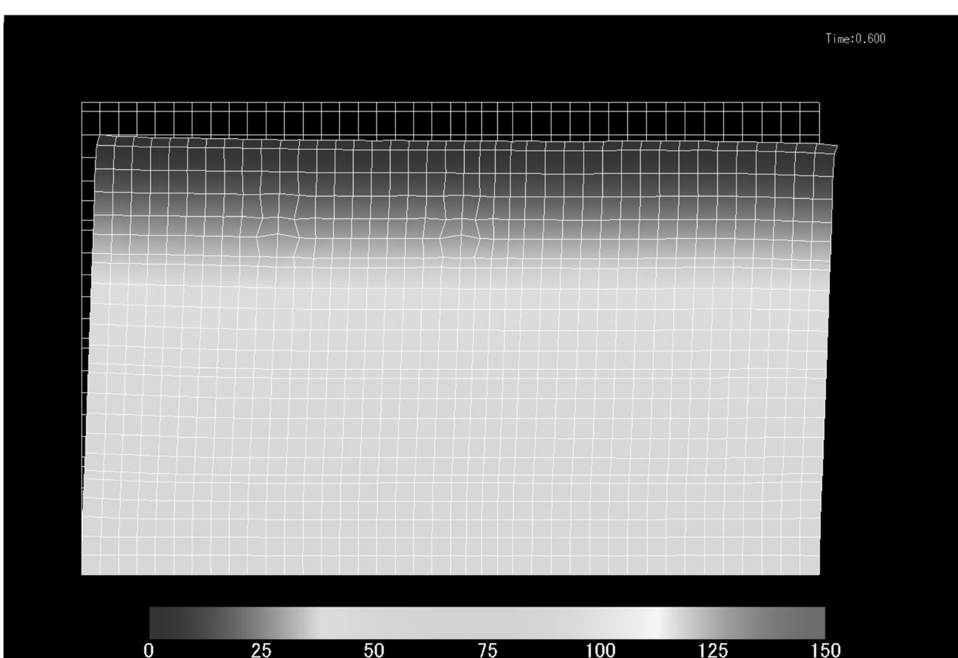

Figure A-4. Distribution of excess pore water pressure (kPa) at t = 30 sec. Deformation is exaggerated at 5 times (Model A): Case 1-1.

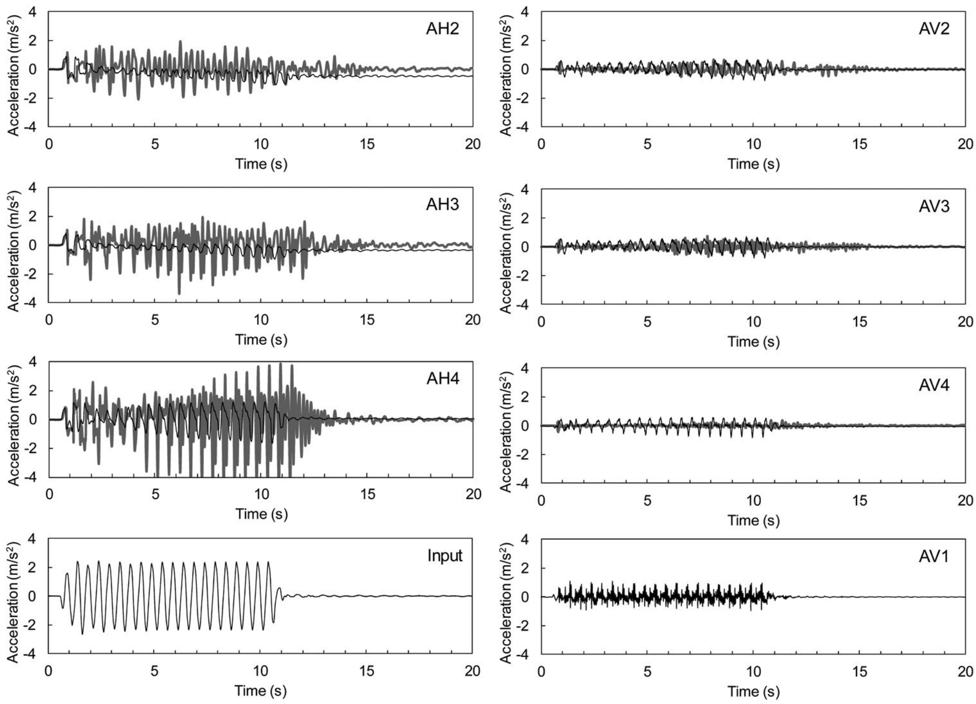

Figure A-5. Time histories of acceleration (Model A): Case 1-2.

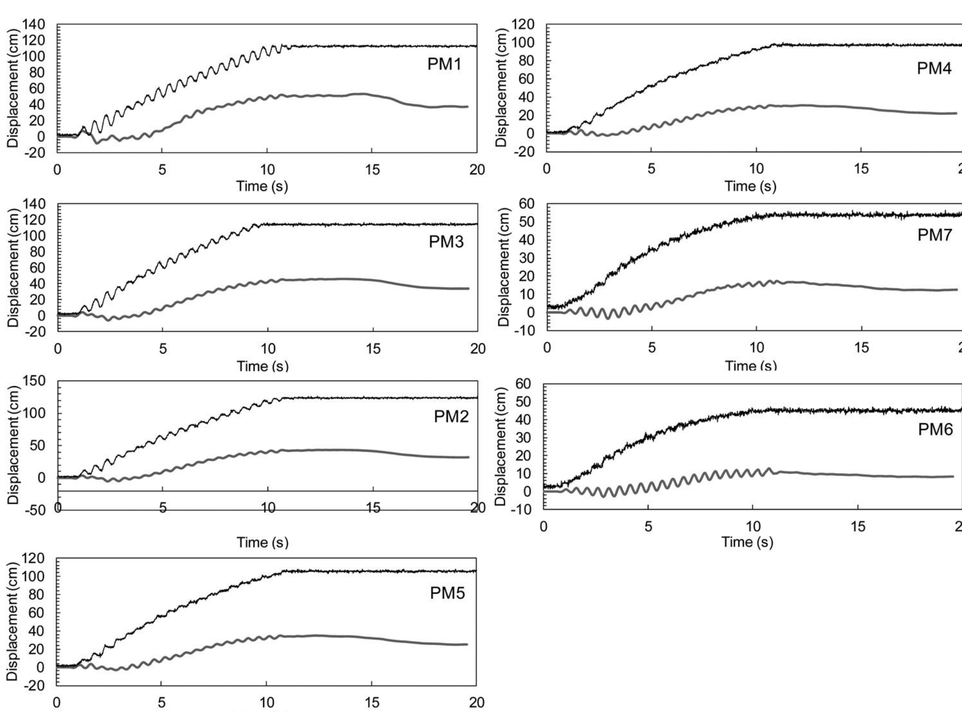

Figure A-6. Time histories of lateral displacement (Model A): Case 1-2.

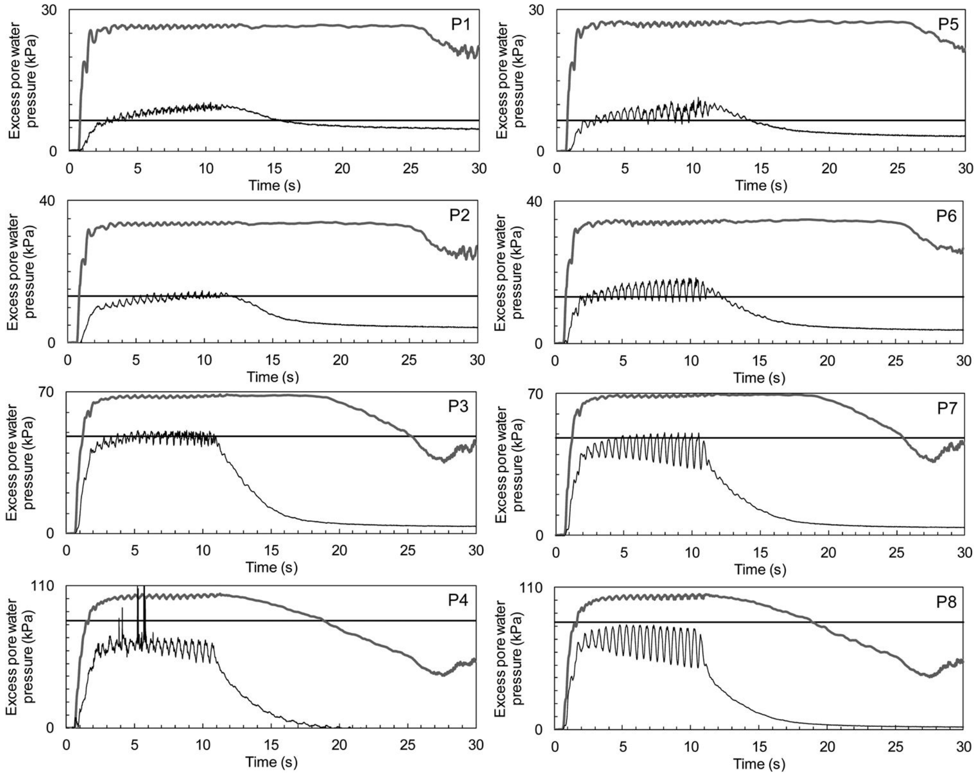

Figure A-7. Time histories of excess pore water pressure (Model A): Case 1-2.

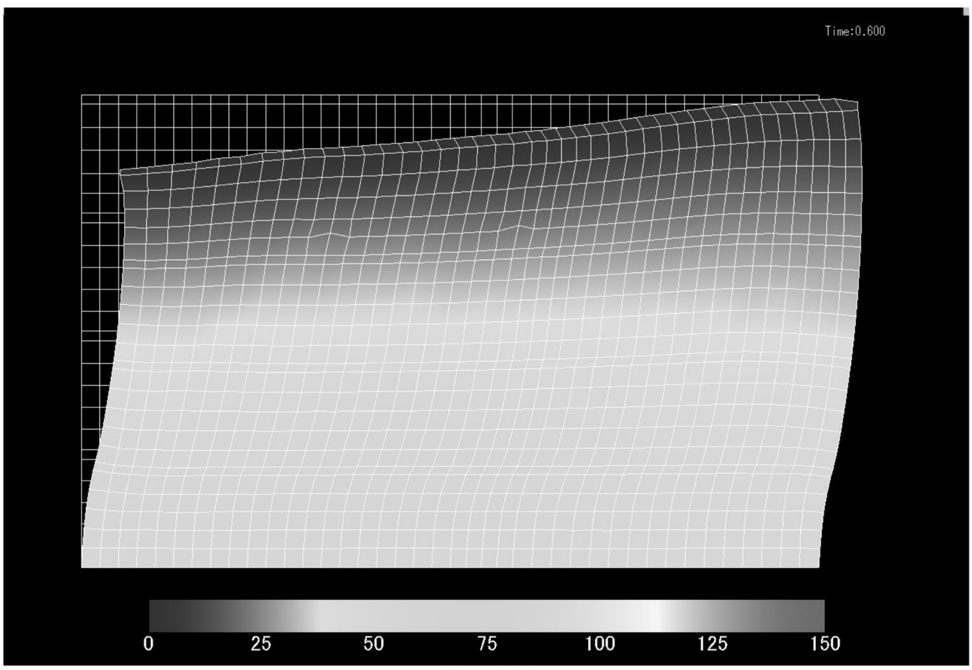

Figure A-8. Distribution of excess pore water pressure (kPa) at t = 30 sec. Deformation is exaggerated at 5 times (Model A): Case 1-2.

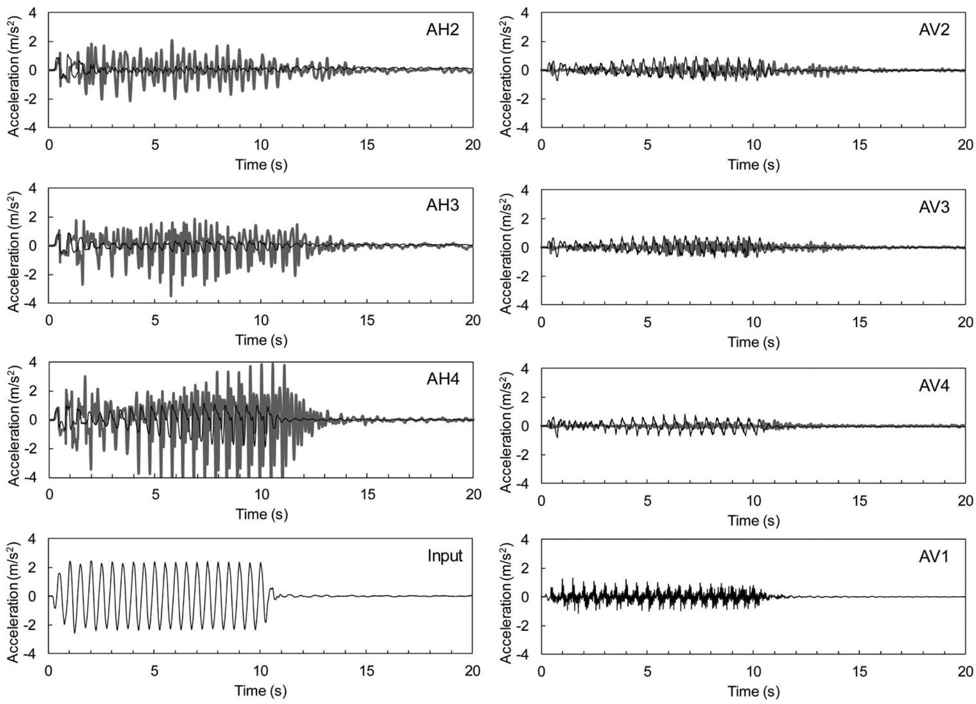

Figure A-9. Time histories of acceleration (Model A): Case 1-3.

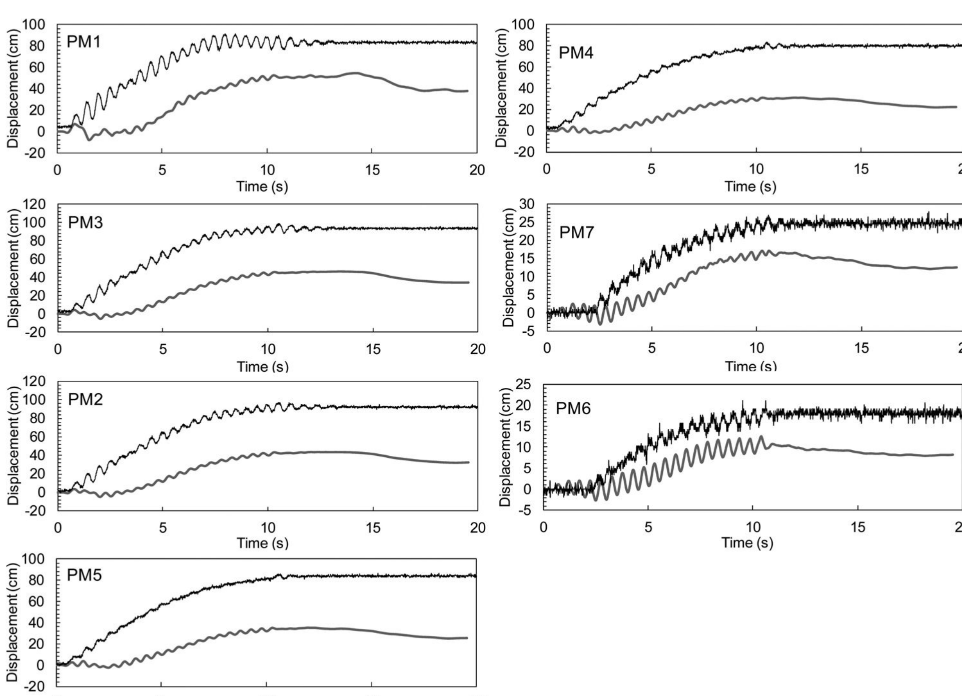

Figure A-10. Time histories of lateral displacement (Model A): Case 1-3.

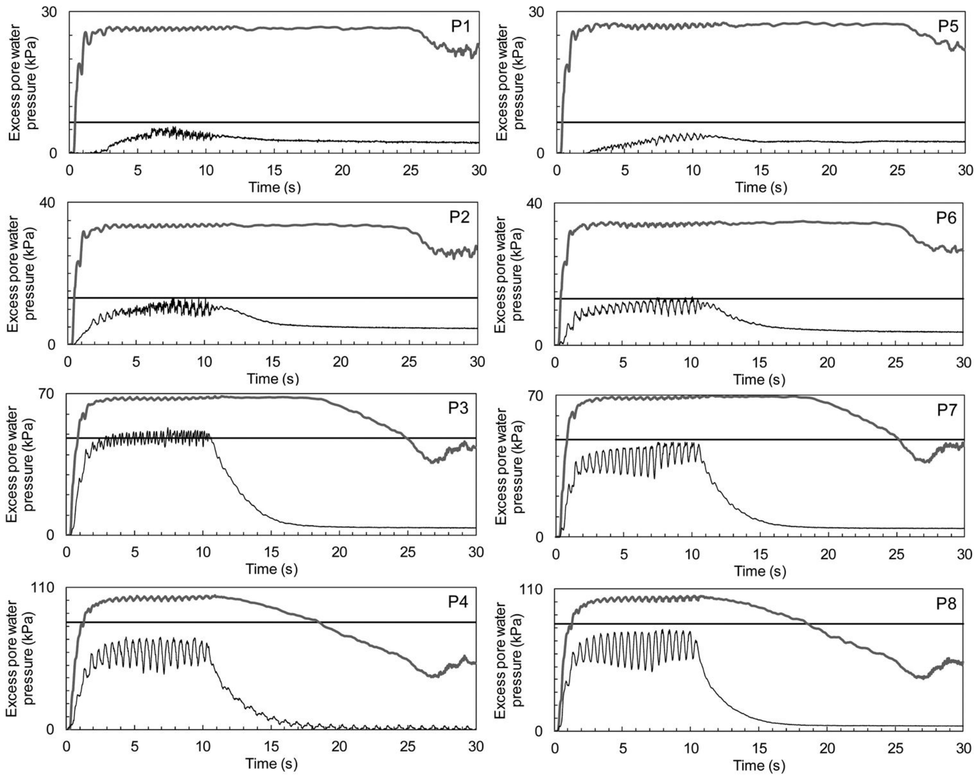

Figure A-11. Time histories of excess pore water pressure (Model A): Case 1-3.

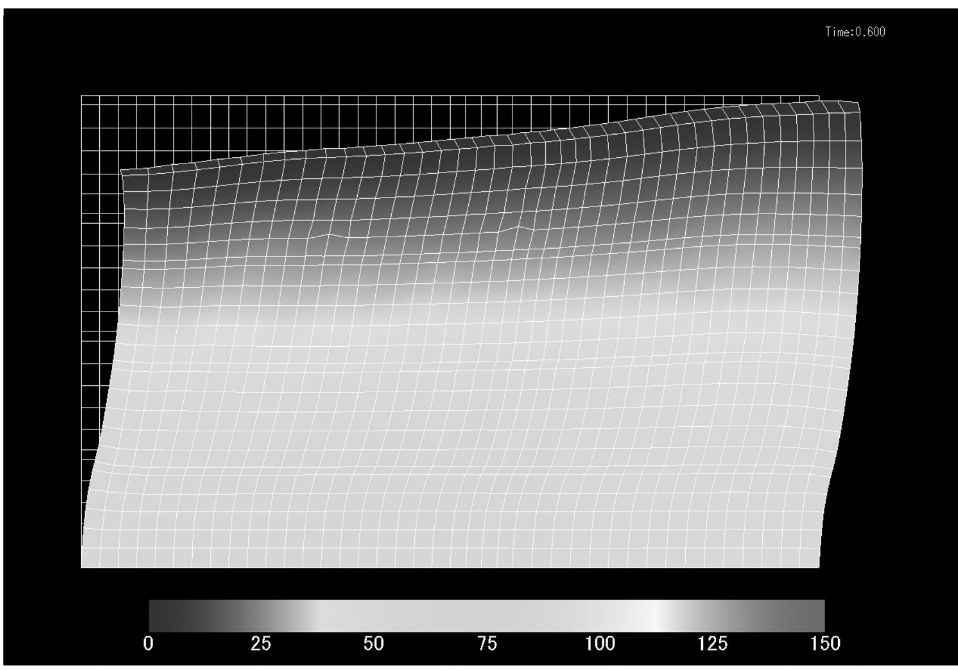

Case 1-3

Figure A-12. Distribution of excess pore water pressure (kPa) at t = 30 sec. Deformation is exaggerated at 5 times (Model A): Case 1-3.

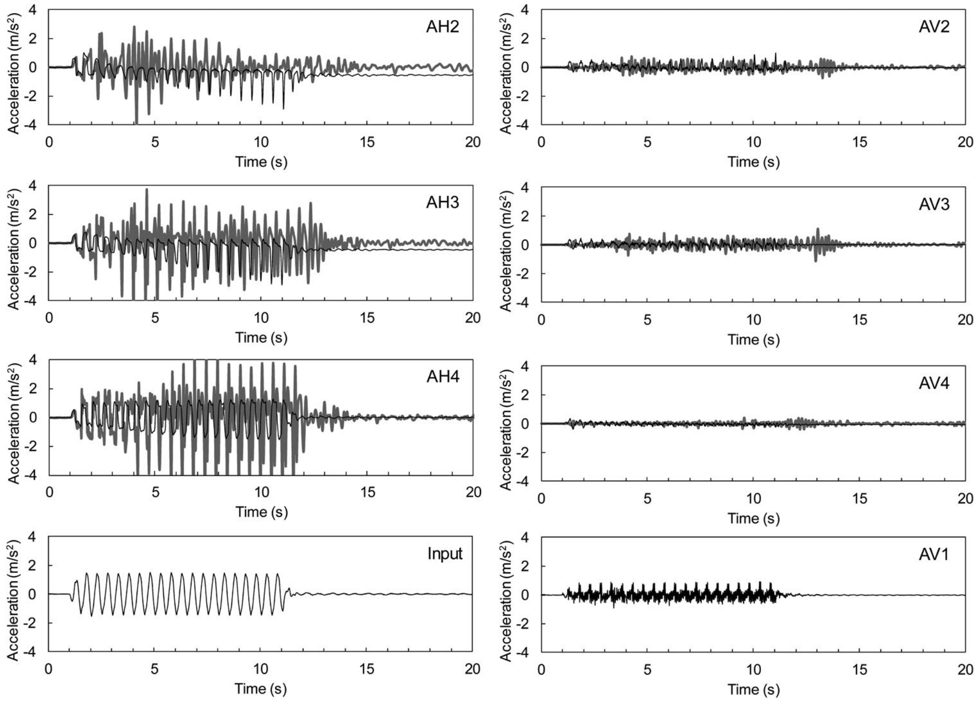

Figure A-13. Time histories of acceleration (Model A): Case 2-1.

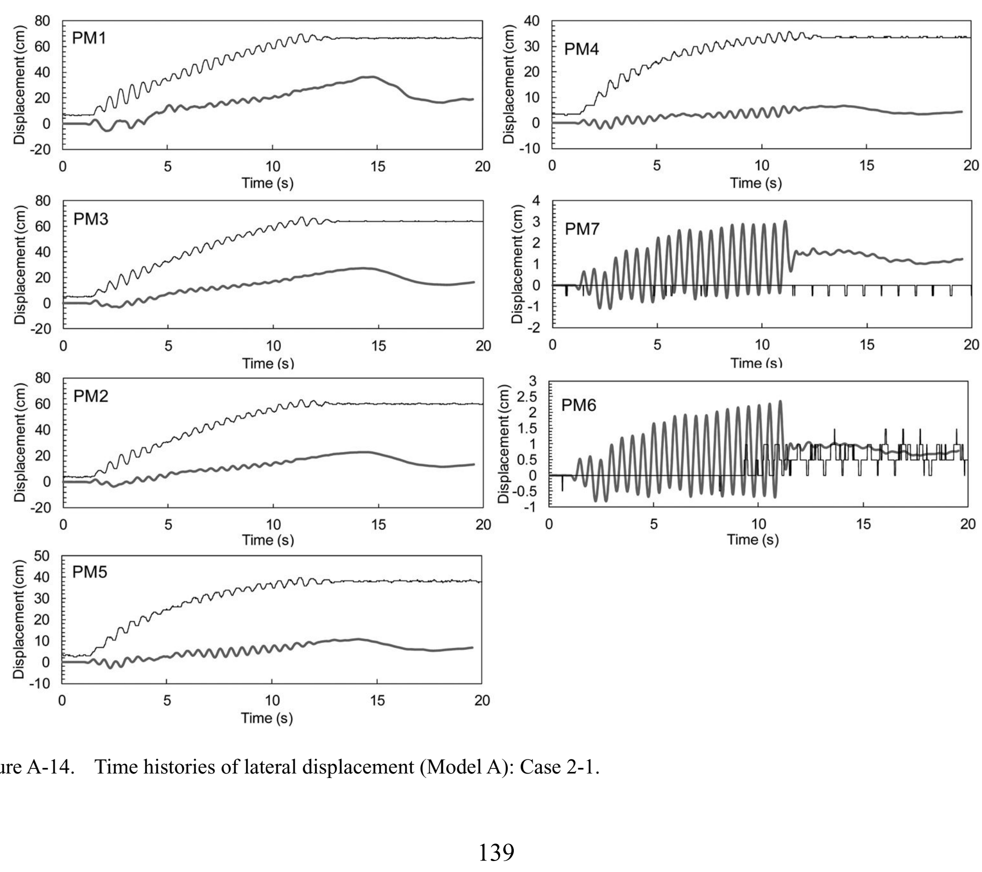

Figure A-14. Time histories of lateral displacement (Model A): Case 2-1.

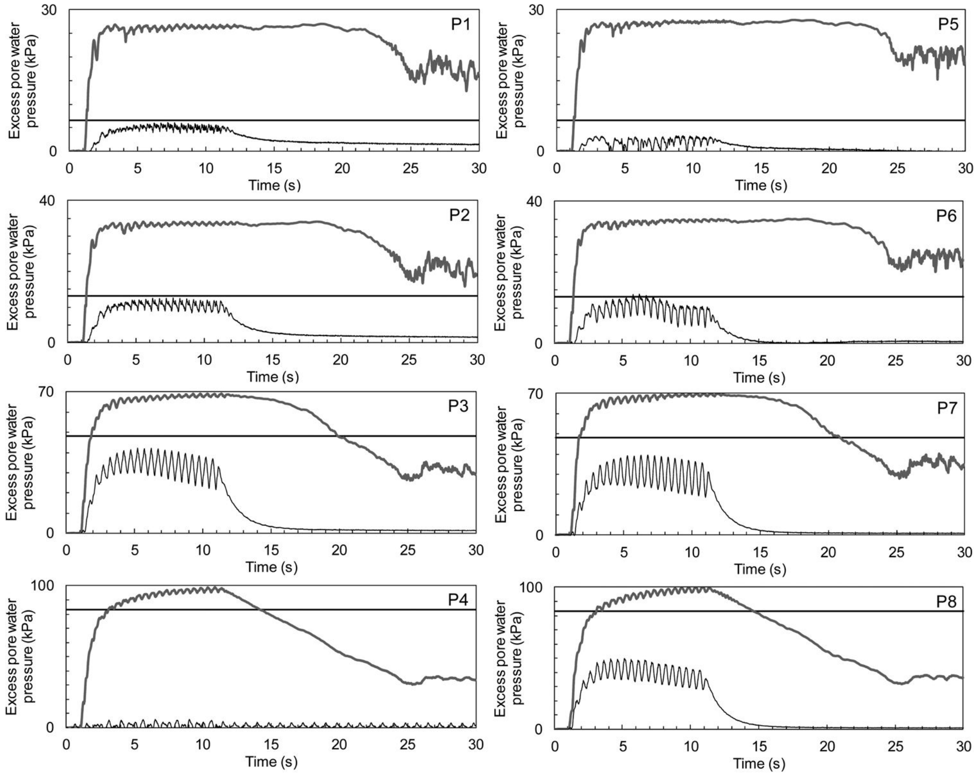

Figure A-15. Time histories of excess pore water pressure (Model A): Case 2-1.

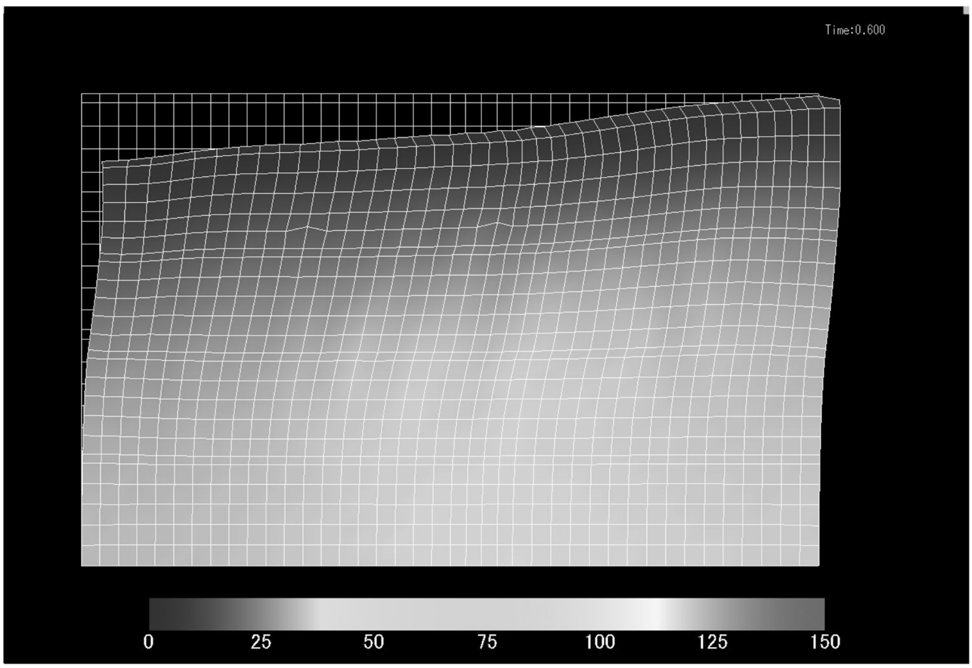

Figure A-16. Distribution of excess pore water pressure (kPa) at t = 30 sec. Deformation is exaggerated at 5 times (Model A): Case 2-1.

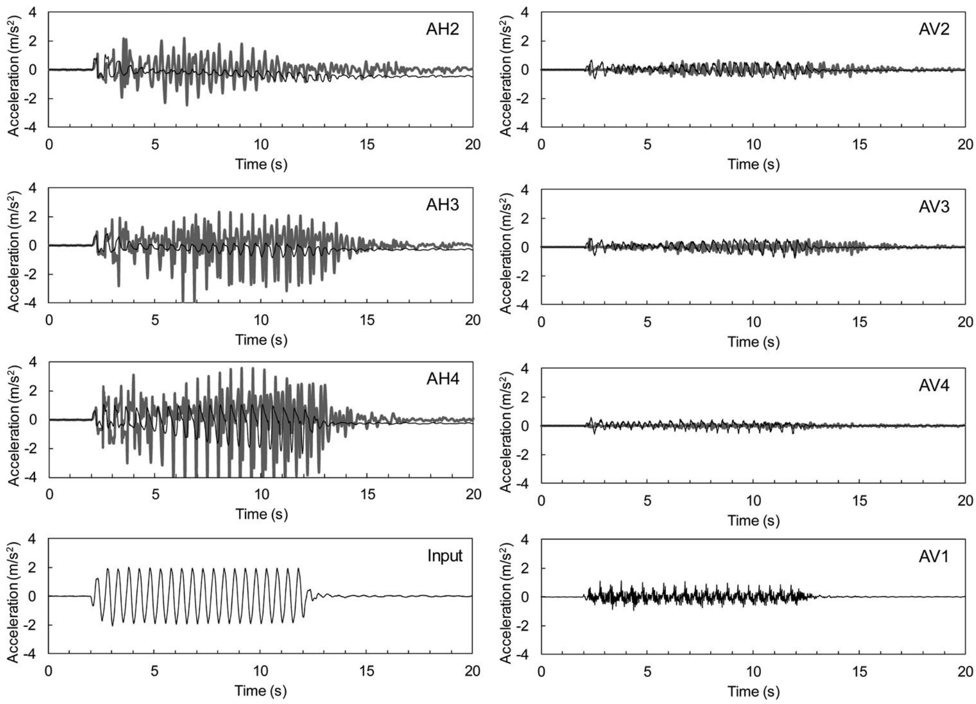

Figure A-17. Time histories of acceleration (Model A): Case 2-2.

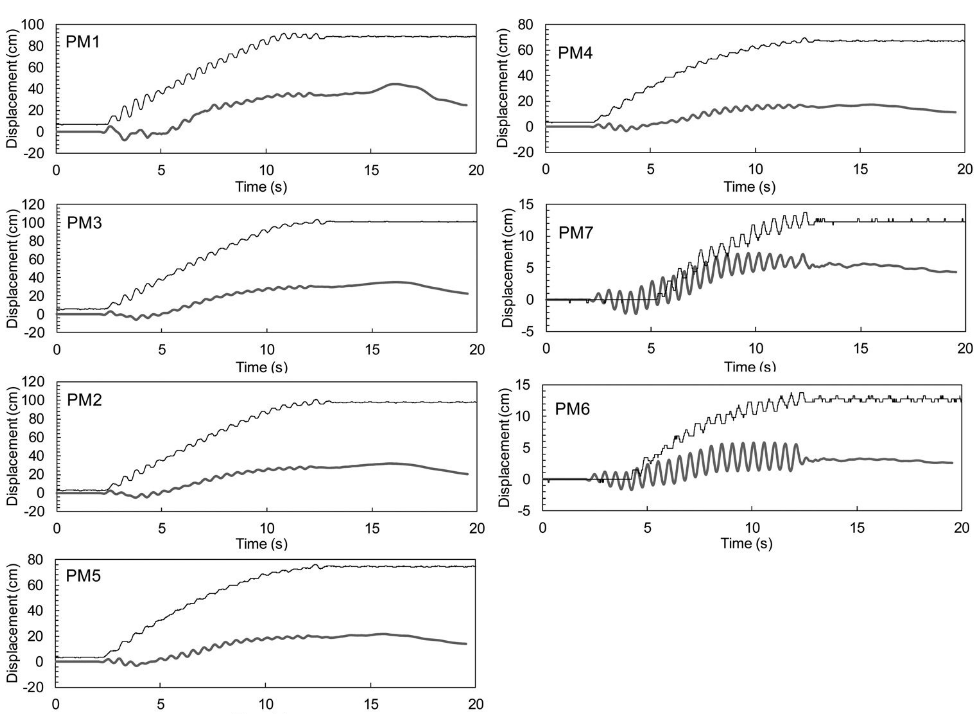

Figure A-18. Time histories of lateral displacement (Model A): Case 2-2.

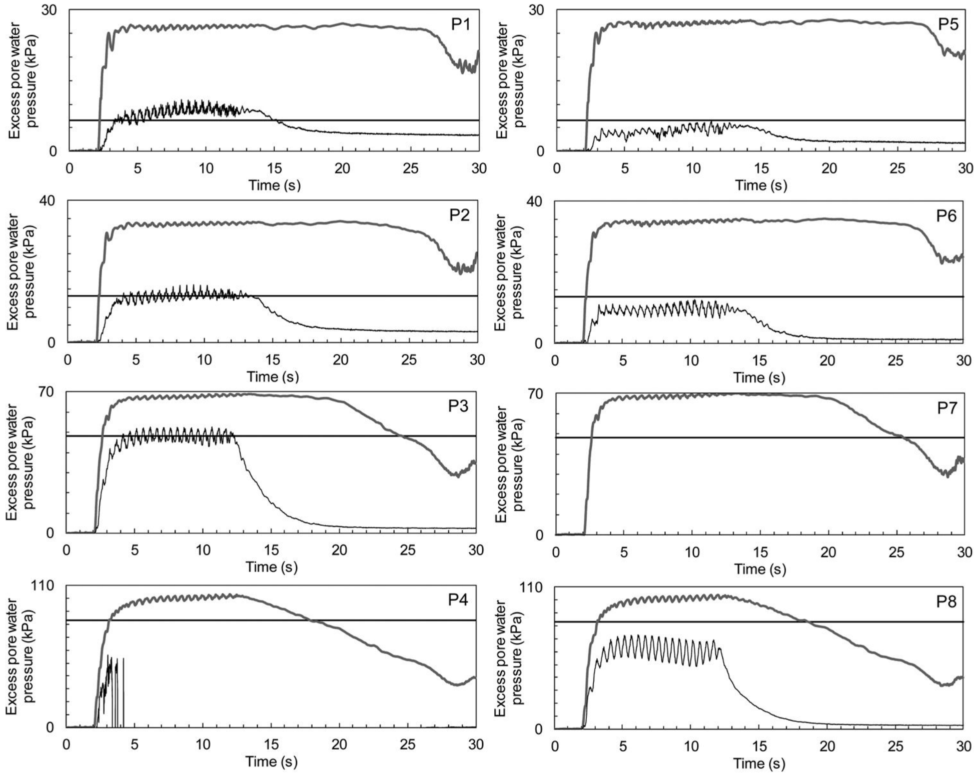

Figure A-19. Time histories of excess pore water pressure (Model A): Case 2-2.

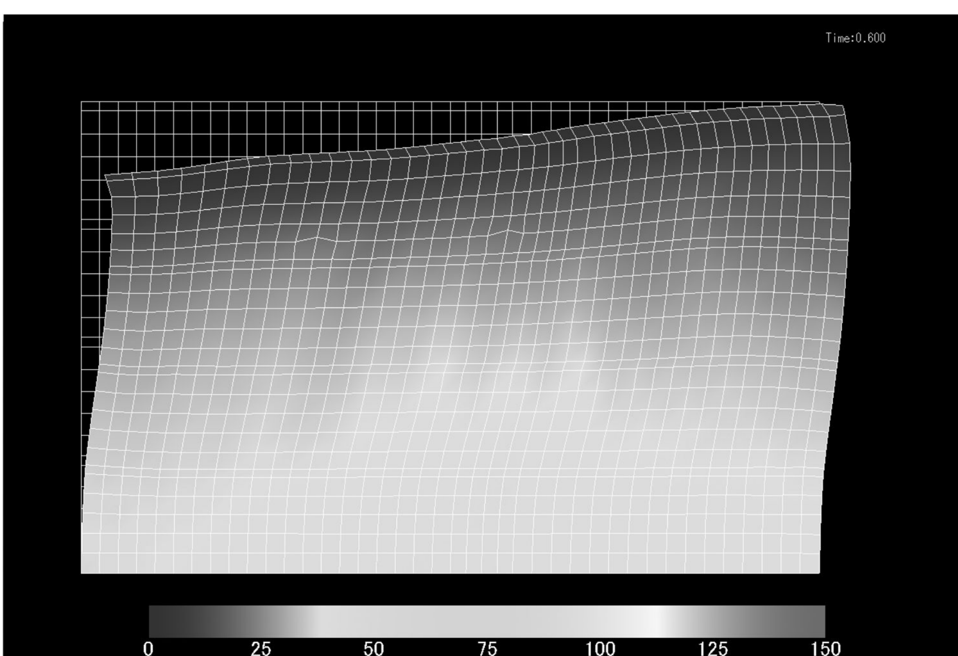

Figure A-20. Distribution of excess pore water pressure (kPa) at t = 30 sec. Deformation is exaggerated at 5 times (Model A): Case 2-2.

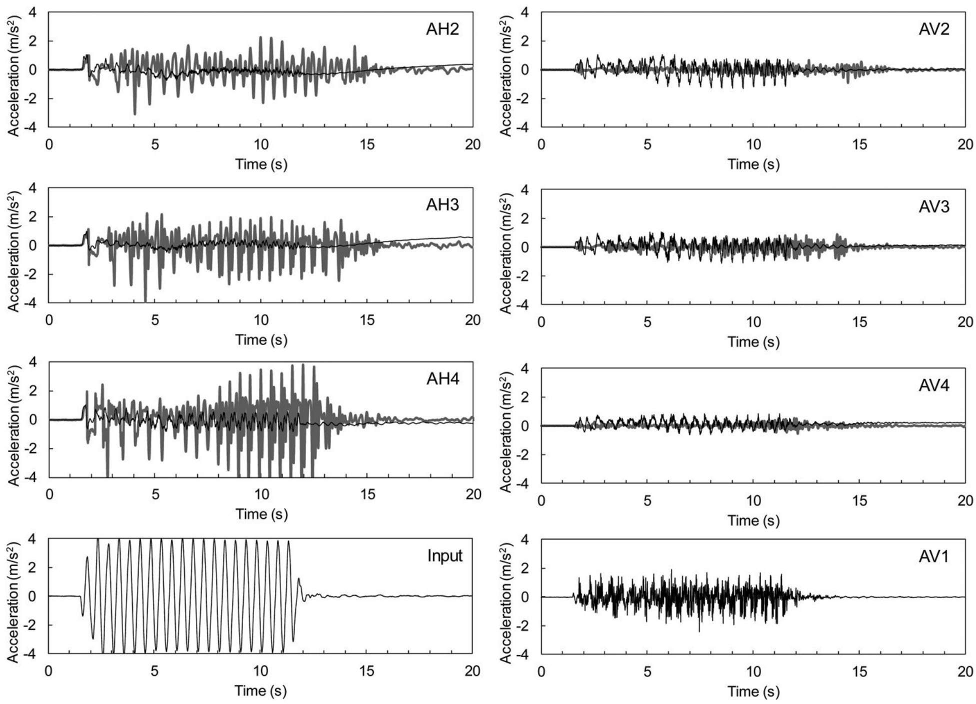

Figure A-21. Time histories of acceleration (Model A): Case 2-3.

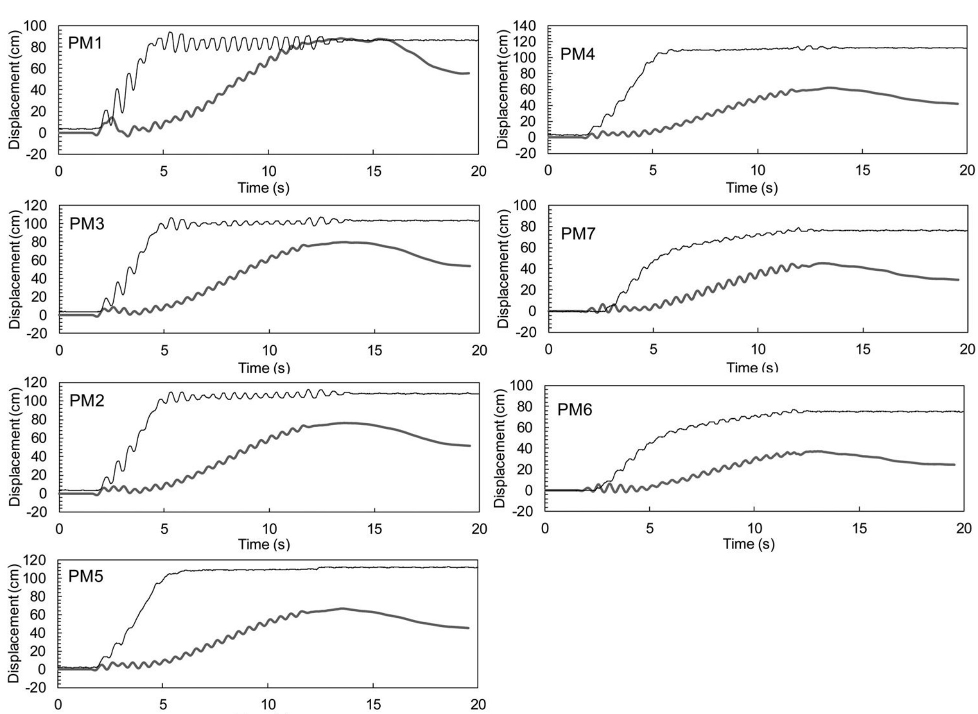

Figure A-22. Time histories of lateral displacement (Model A): Case 2-3.

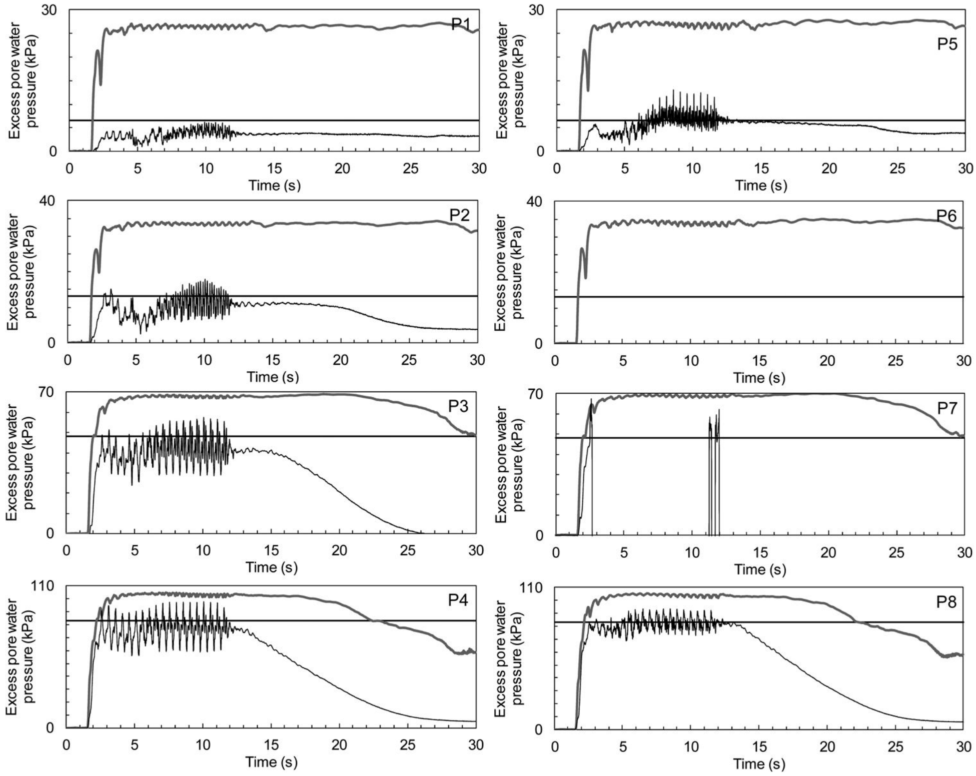

Figure A-23. Time histories of excess pore water pressure (Model A): Case 2-3.

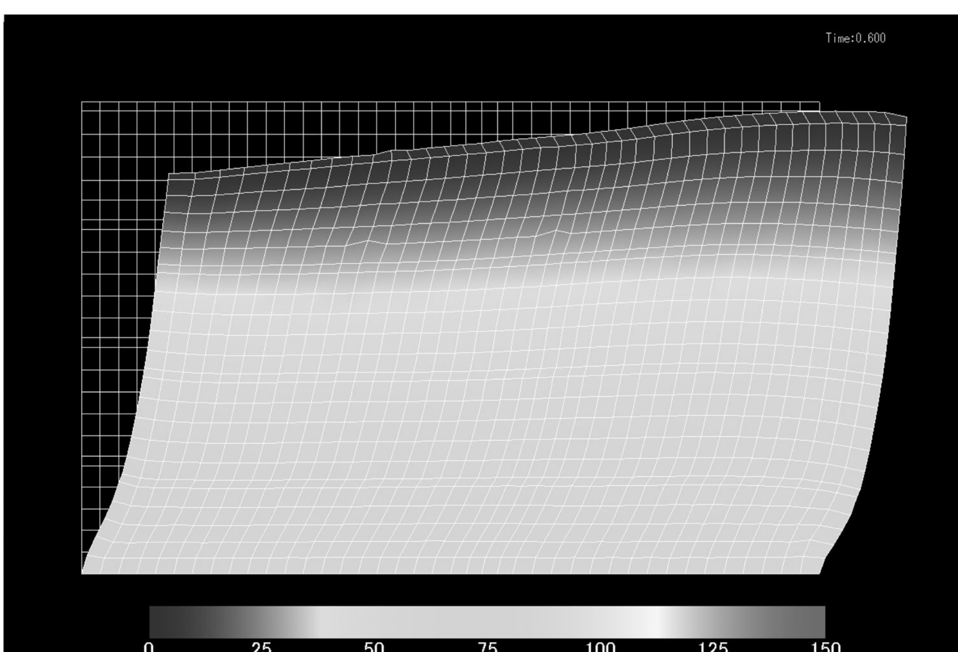

Figure A-24. Distribution of excess pore water pressure (kPa) at t = 30 sec. Deformation is exaggerated at 5 times (Model A): Case 2-3.

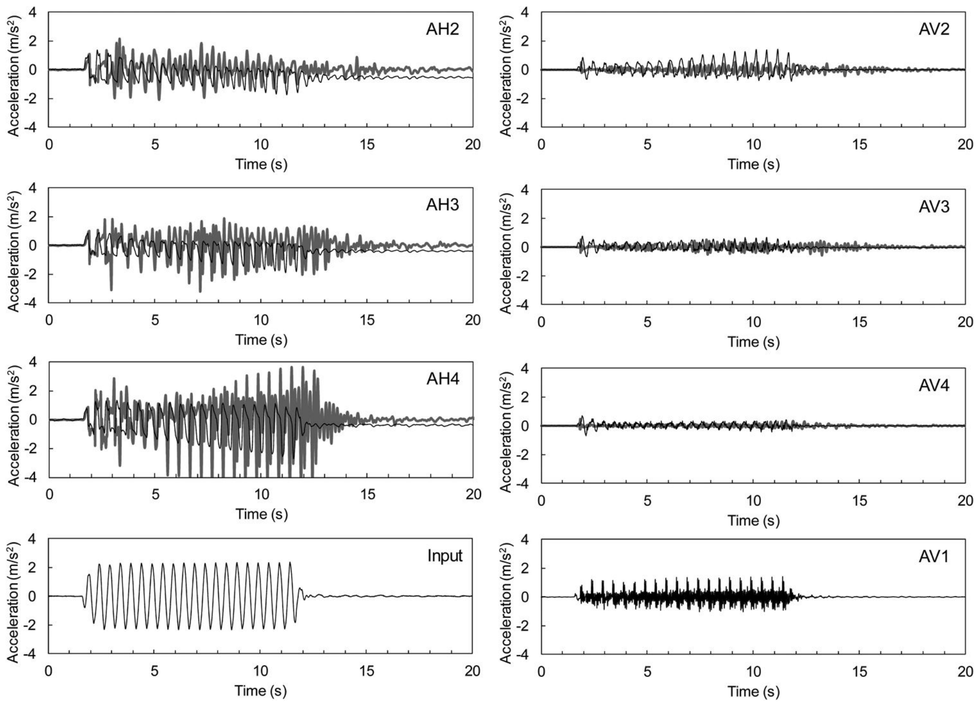

Figure A-25. Time histories of acceleration (Model A): Case 3-1.

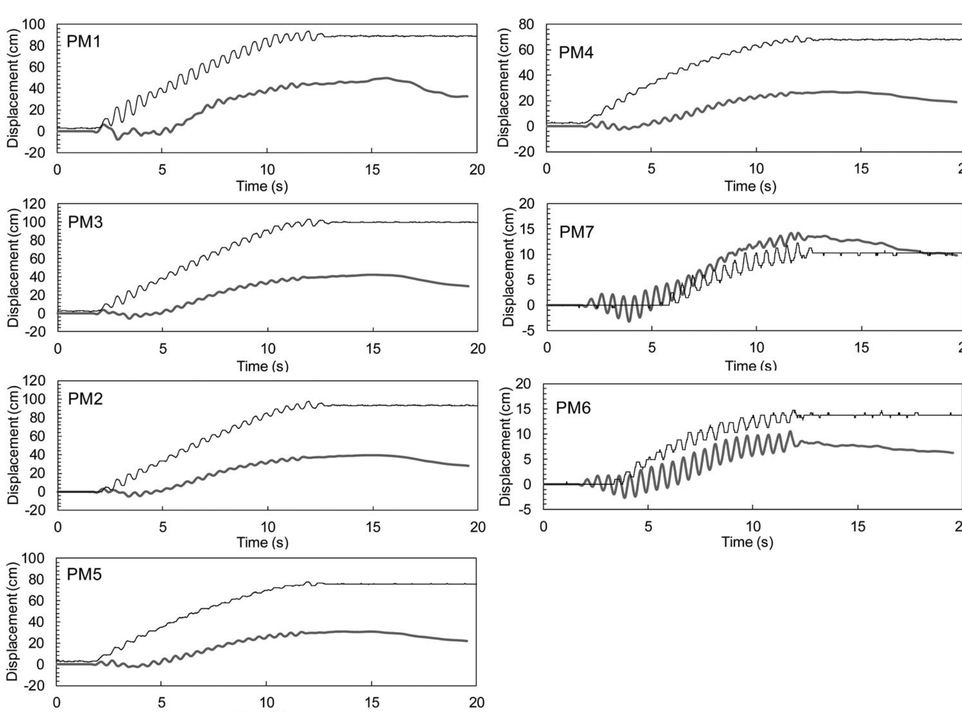

Figure A-26. Time histories of lateral displacement (Model A): Case 3-1.

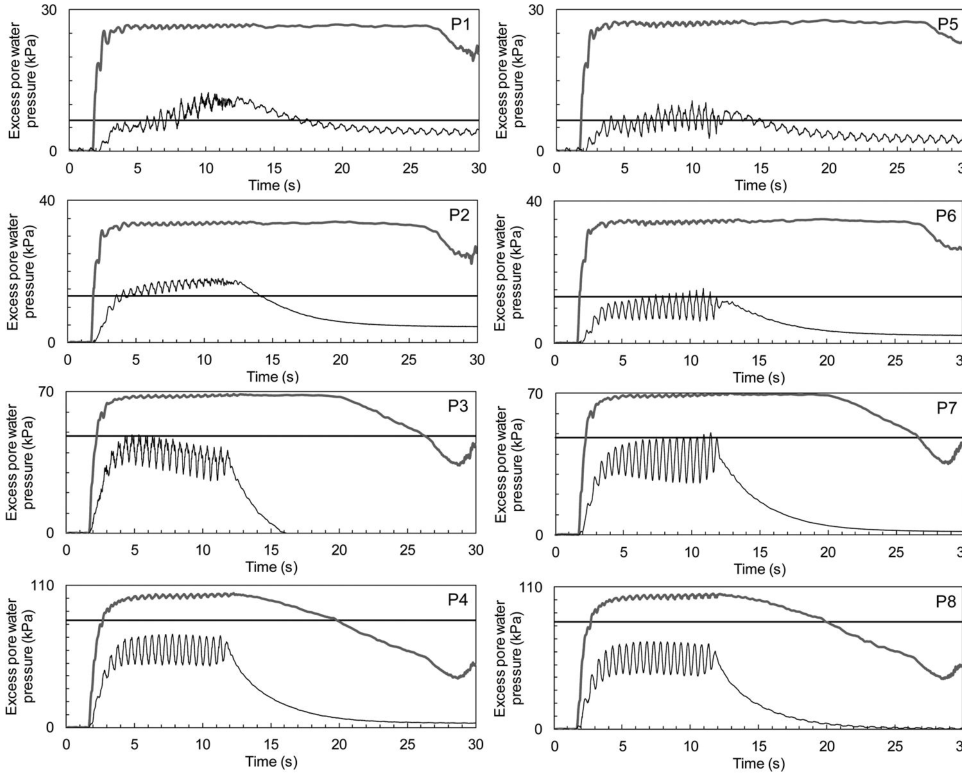

Figure A-27. Time histories of excess pore water pressure (Model A): Case 3-1.

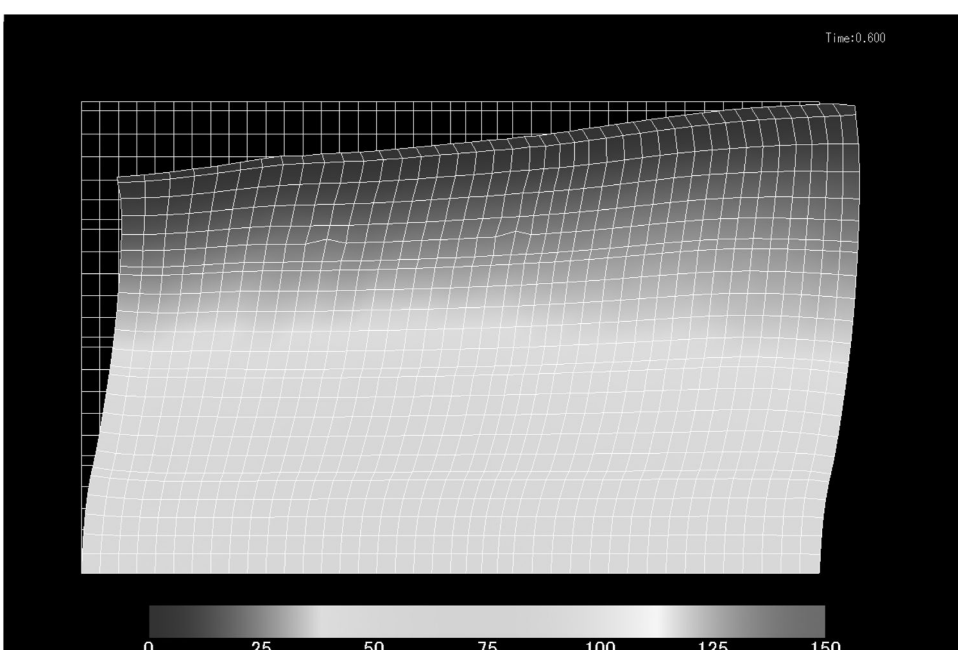

Figure A-28. Distribution of excess pore water pressure (kPa) at t = 30 sec. Deformation is exaggerated at 5 times (Model A): Case 3-1.

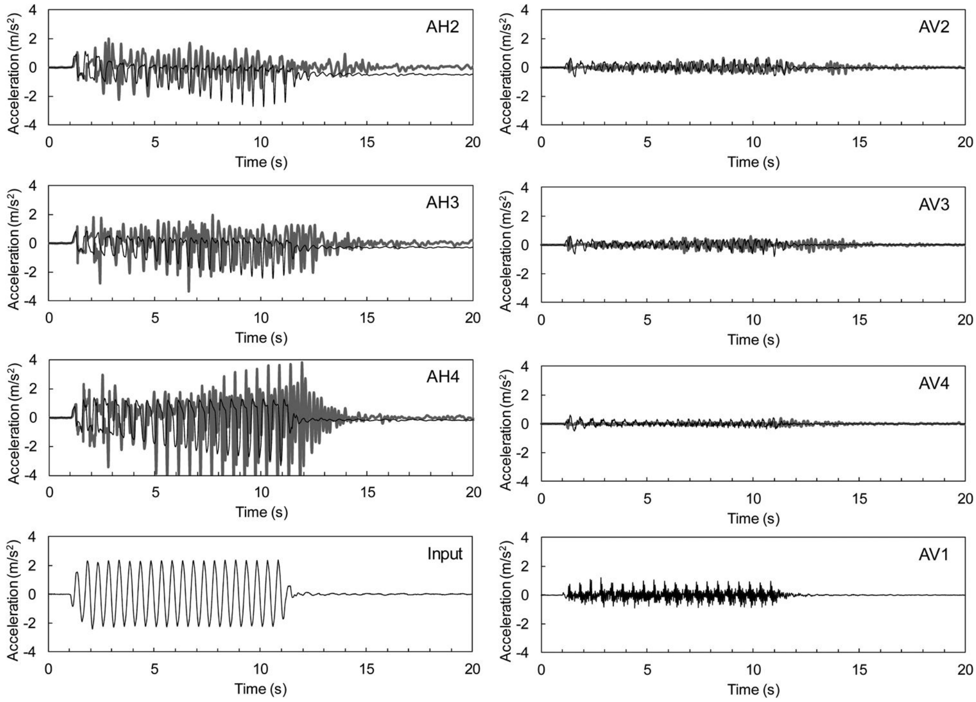

Figure A-29. Time histories of acceleration (Model A): Case 3-2.

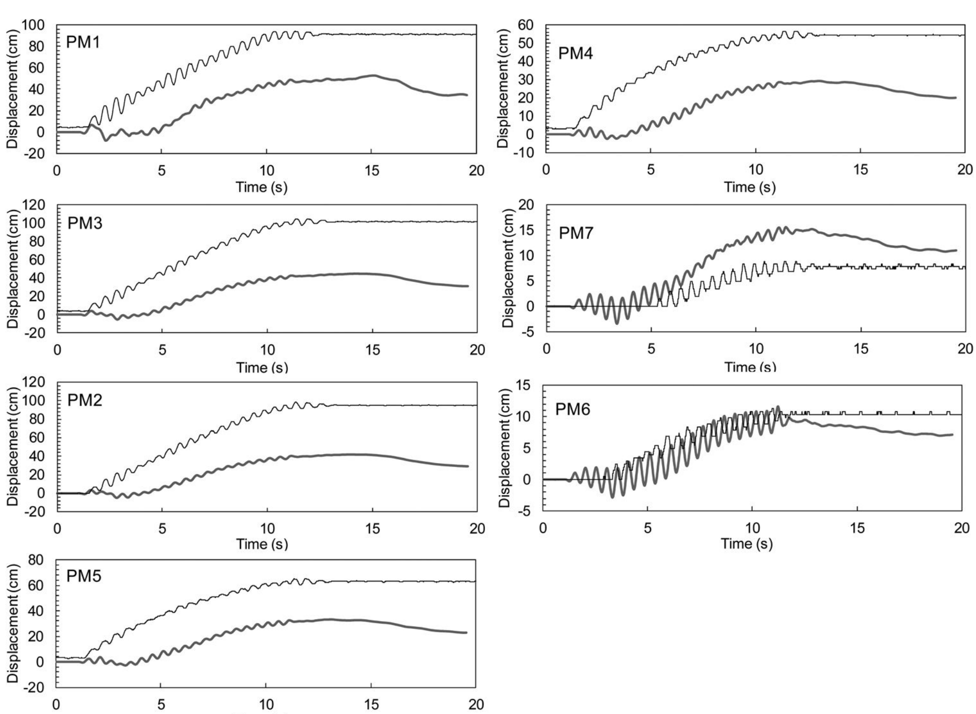

Figure A-30. Time histories of lateral displacement (Model A): Case 3-2.

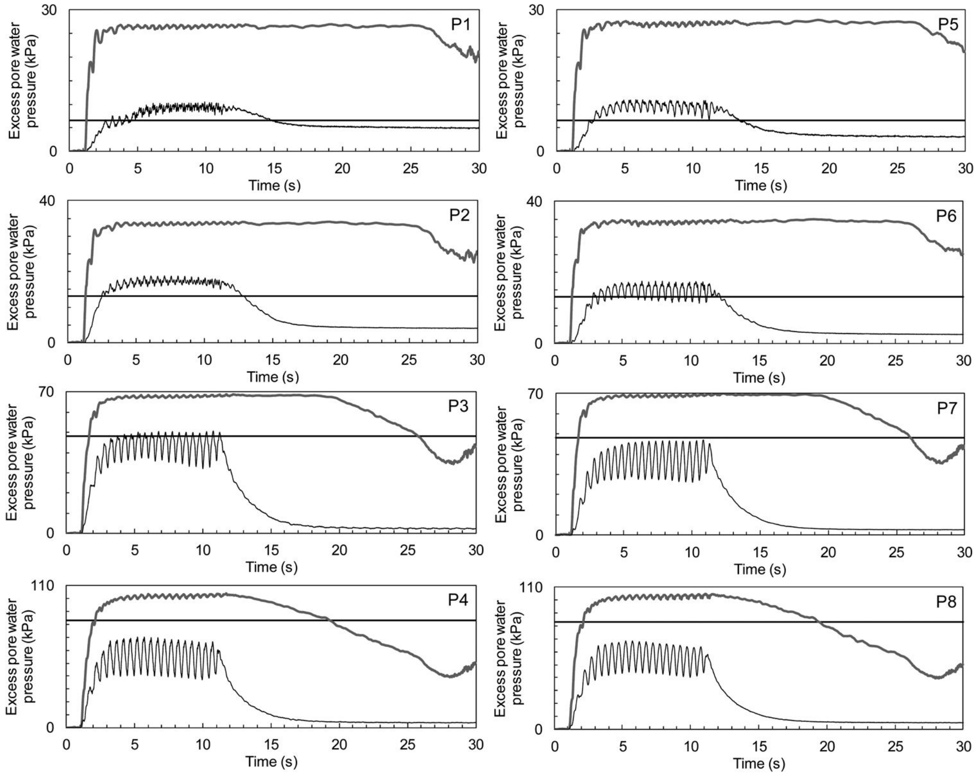

Figure A-31. Time histories of excess pore water pressure (Model A): Case 3-2.

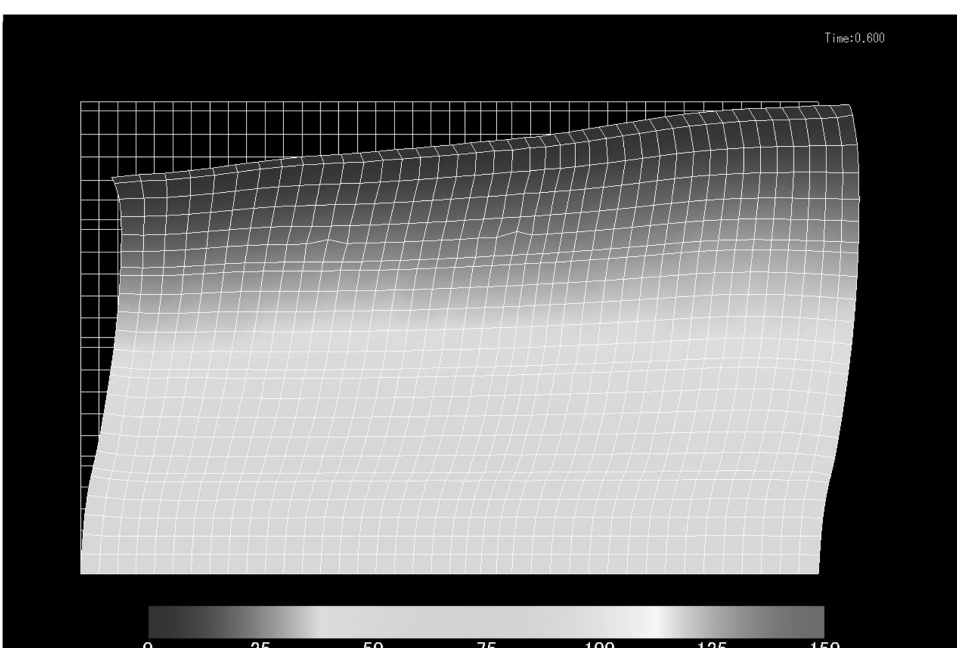

Figure A-32. Distribution of excess pore water pressure (kPa) at t = 30 sec. Deformation is exaggerated at 5 times (Model A): Case 3-2.

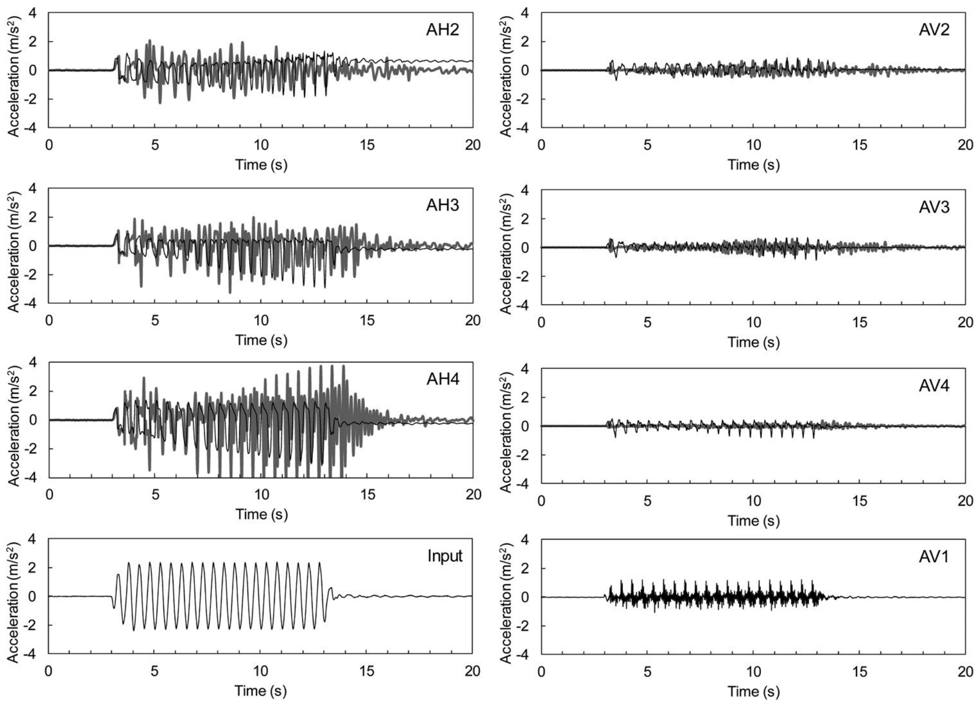

Figure A-33. Time histories of acceleration (Model A): Case 3-3.

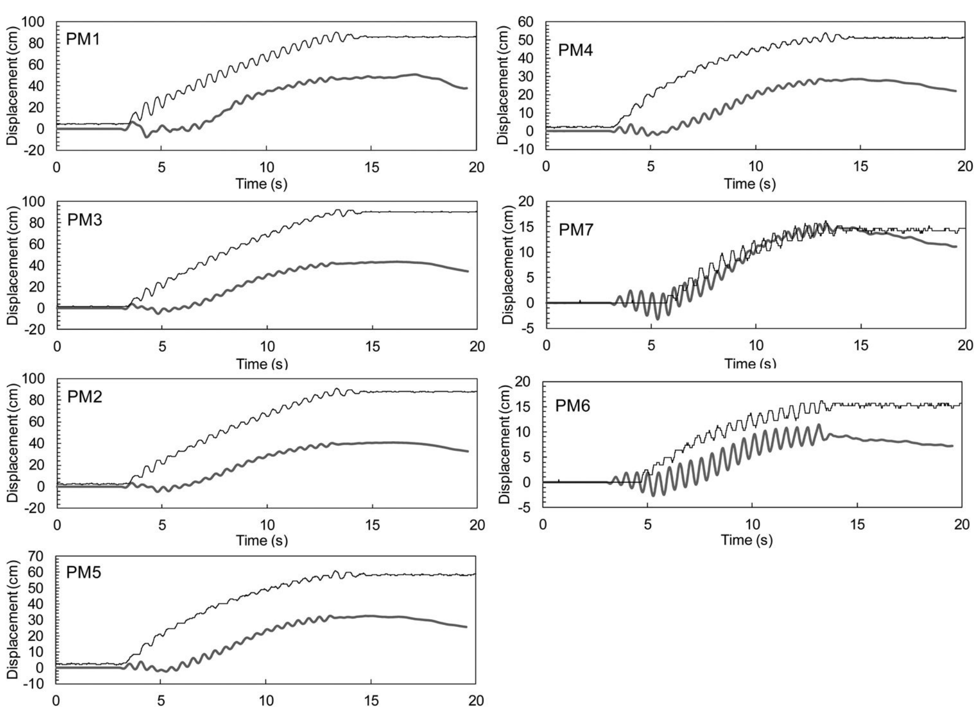

Figure A-34. Time histories of lateral displacement (Model A): Case 3-3.

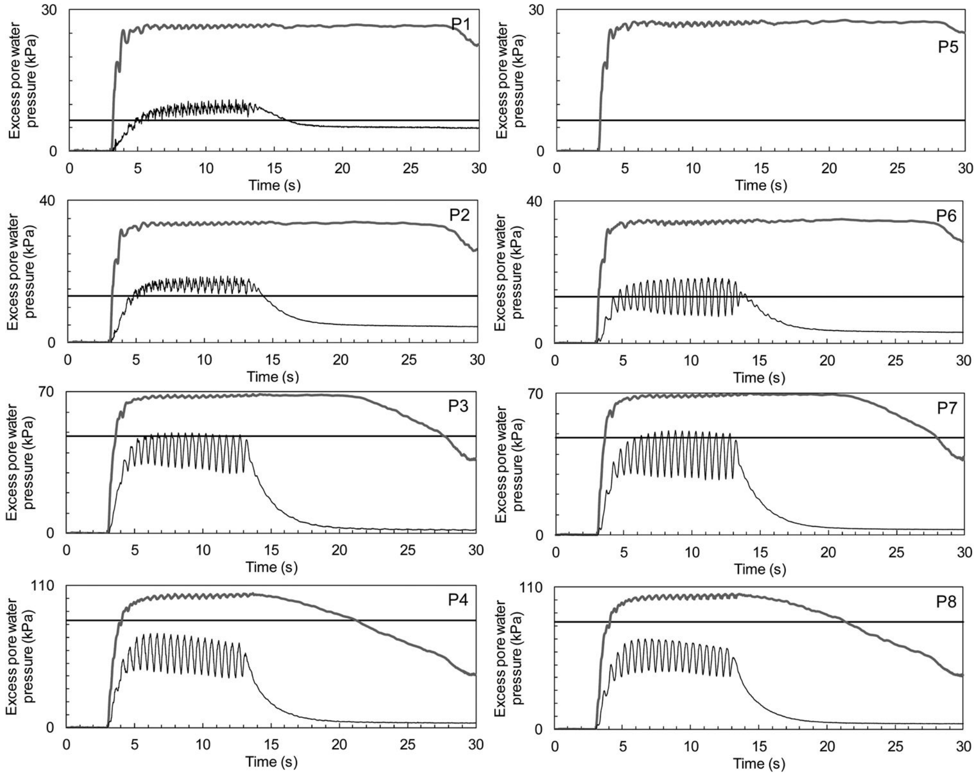

Figure A-35. Time histories of excess pore water pressure (Model A): Case 3-3.

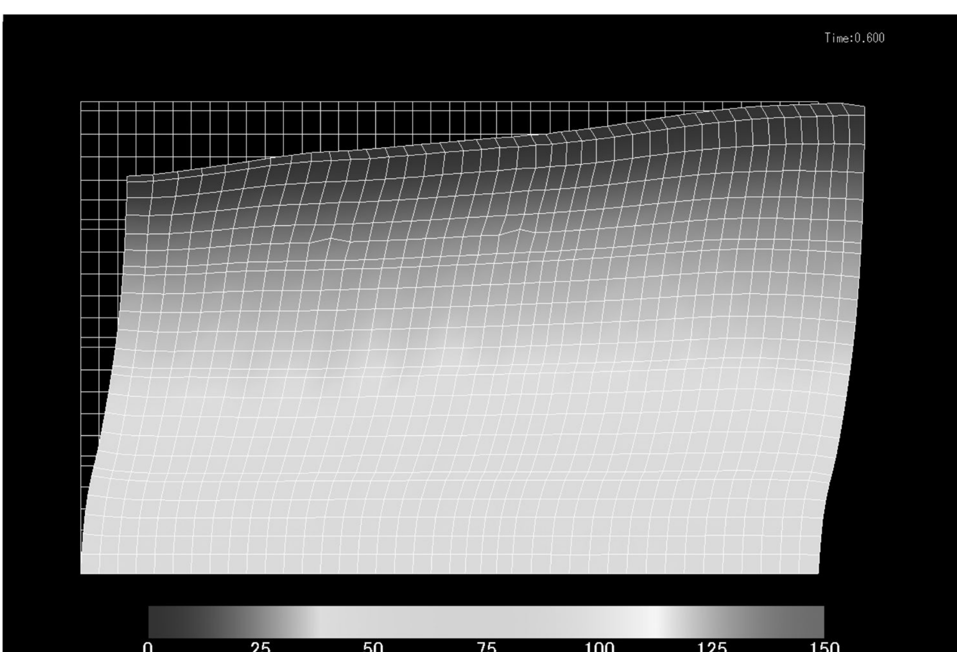

Figure A-36. Distribution of excess pore water pressure (kPa) at t = 30 sec. Deformation is exaggerated at 5 times (Model A): Case 3-3.

MODEL B

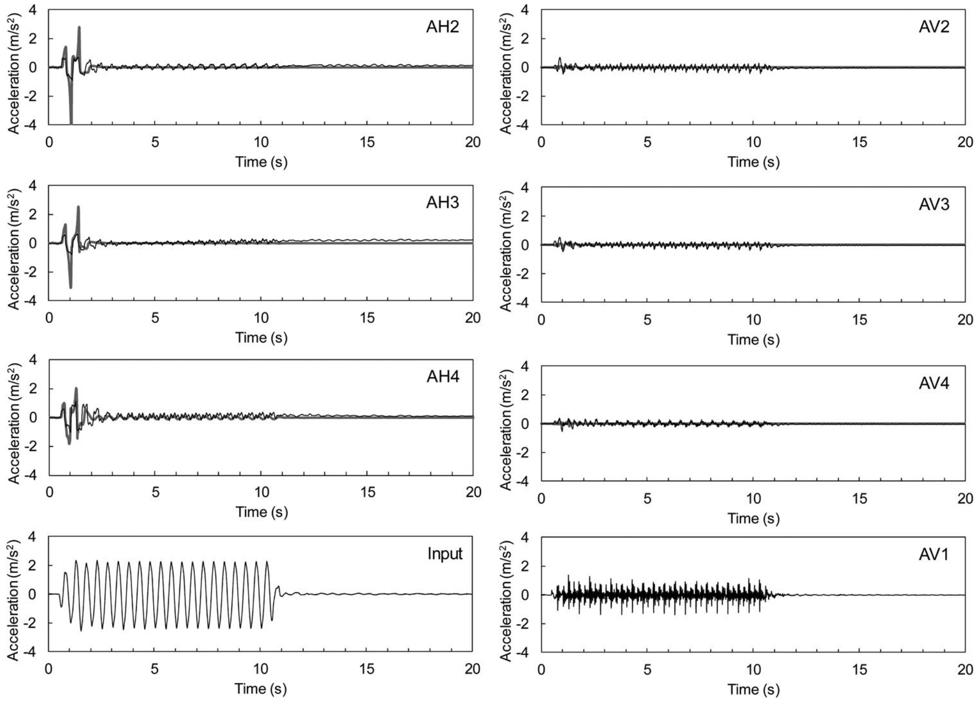

Figure B-1. Time histories of acceleration (Model B): Case 1-1.

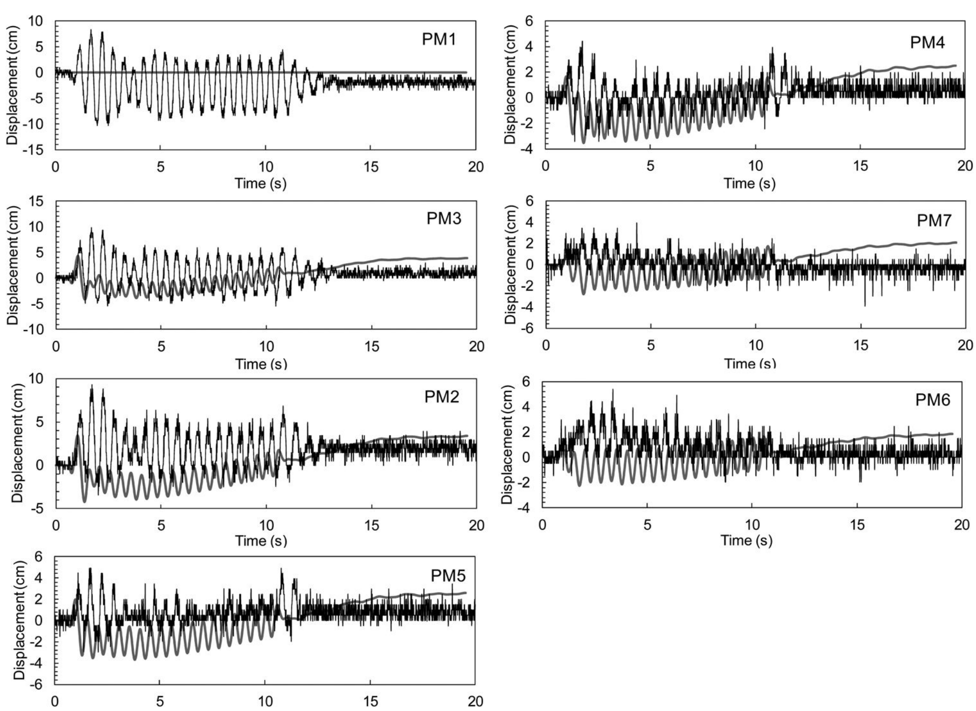

Figure B-2. Time histories of lateral displacement (Model B): Case 1-1.

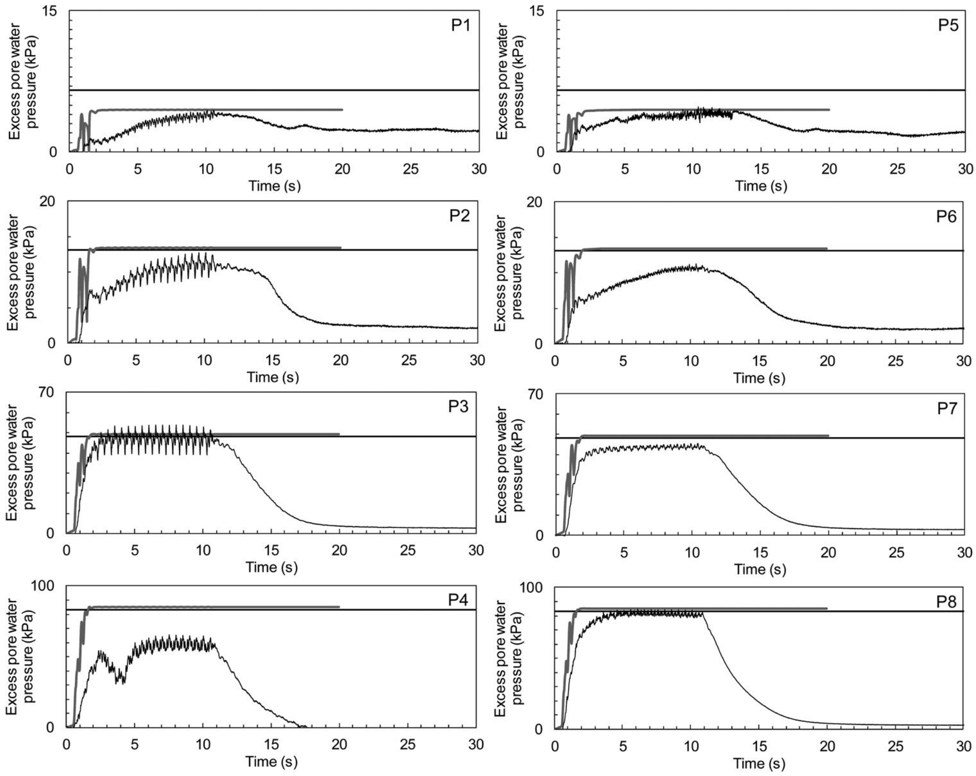

Figure B-3. Time histories of excess pore water pressure (Model B): Case 1-1.

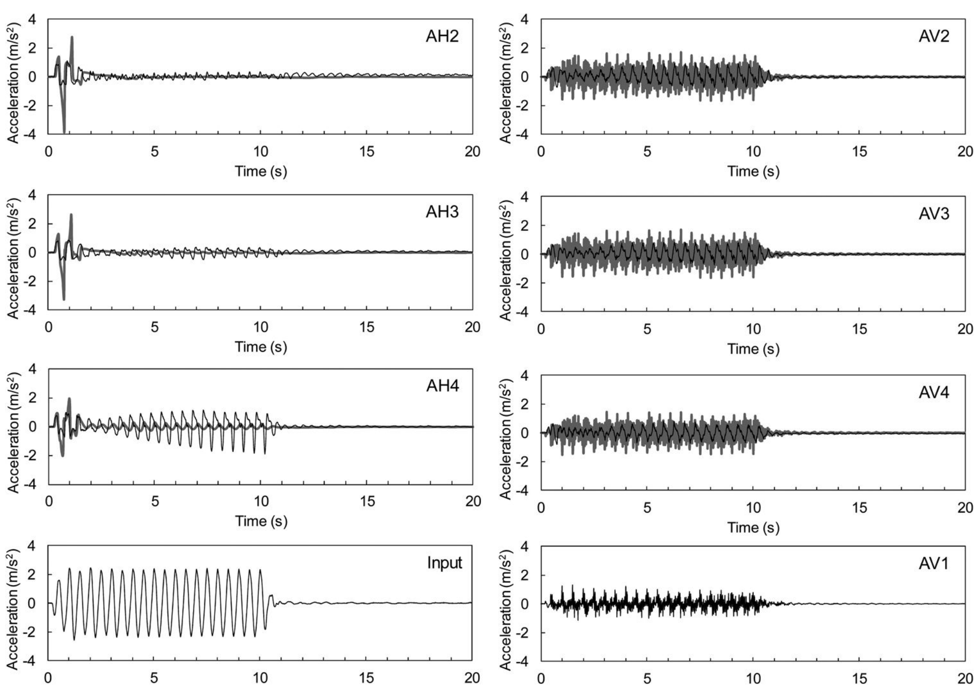

Figure B-4. Time histories of acceleration (Model B): Case 1-3.

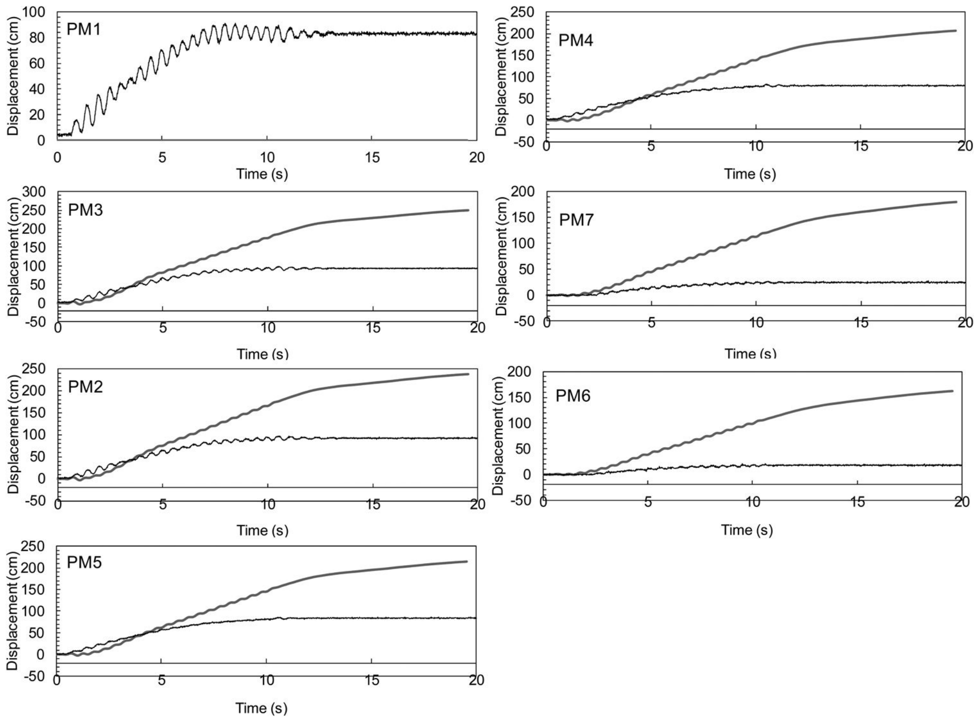

Figure B-5. Time histories of lateral displacement (Model B): Case 1-3.

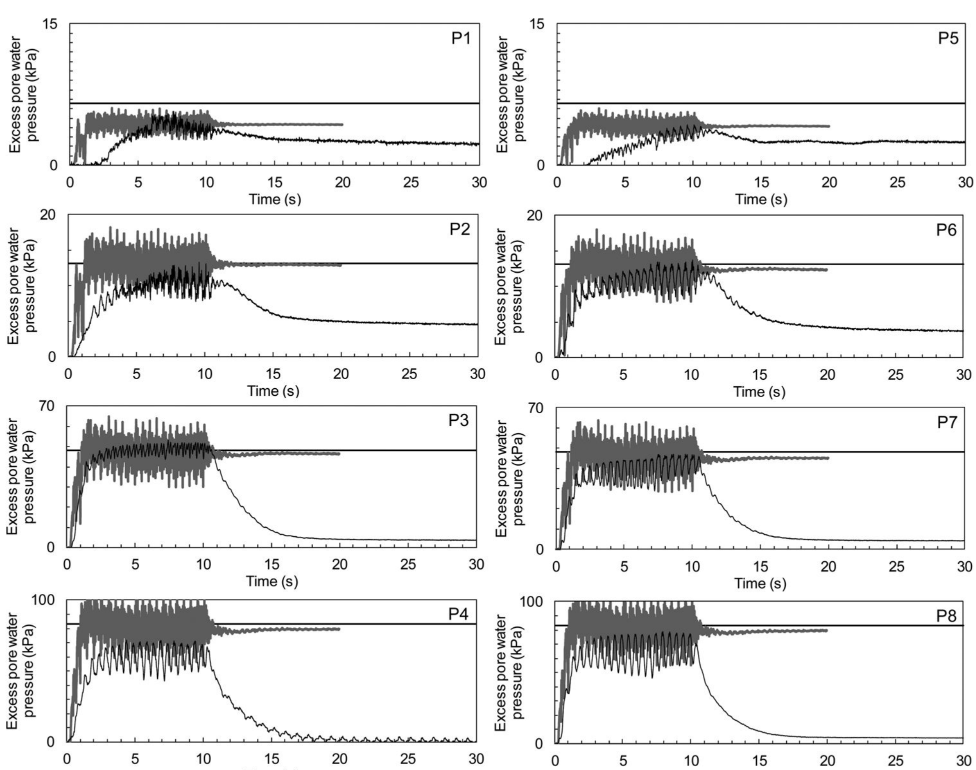

Figure B-6. Time histories of excess pore water pressure (Model D): Case 1-3.

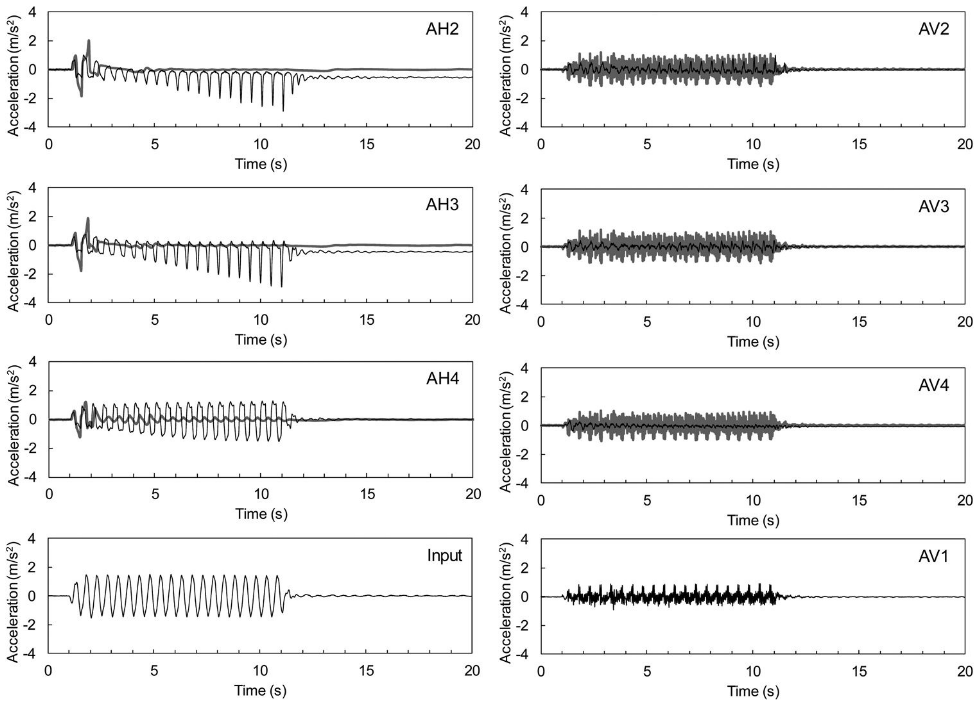

Figure B-7. Time histories of acceleration (Model B): Case 2-1.

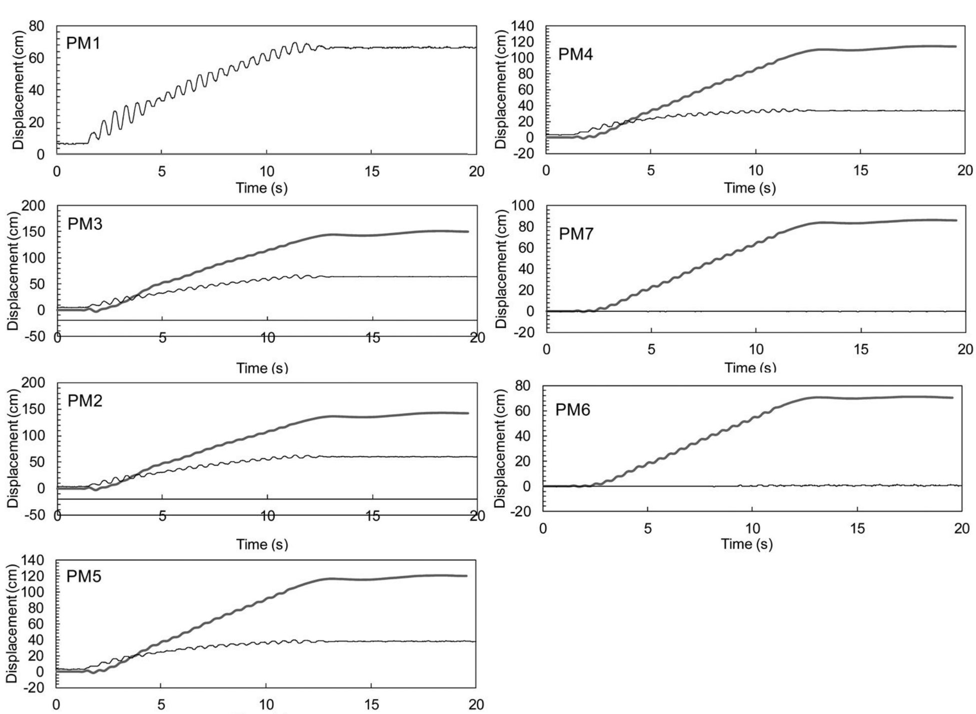

Figure B-8. Time histories of lateral displacement (Model B): Case 2-1.

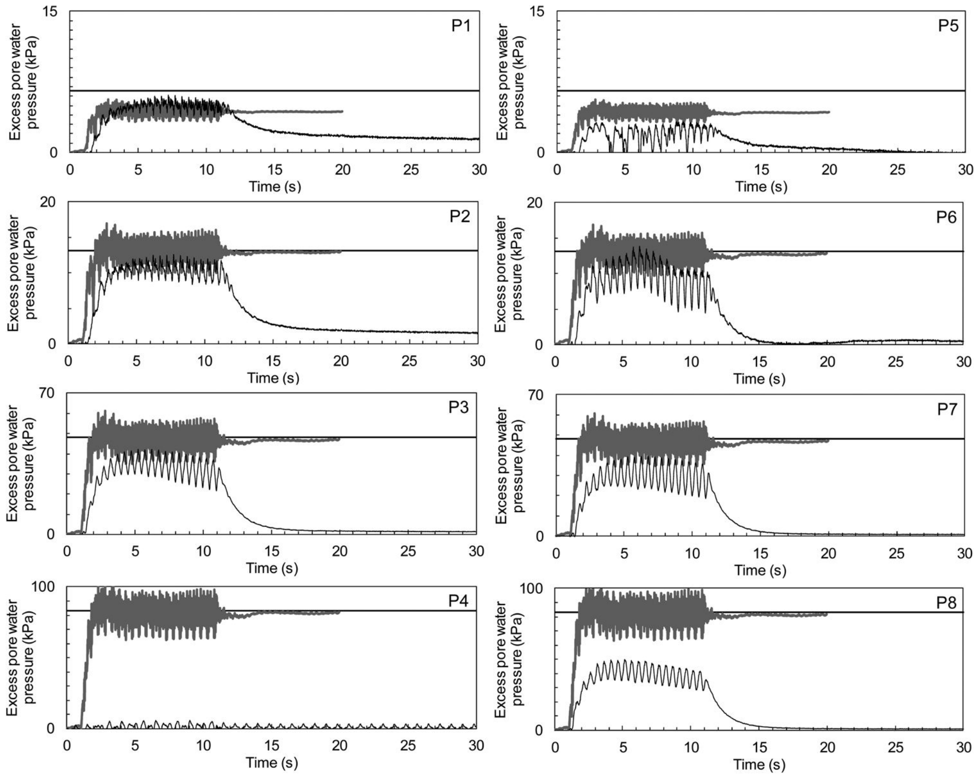

Figure B-9. Time histories of excess pore water pressure (Model B): Case 2-1.

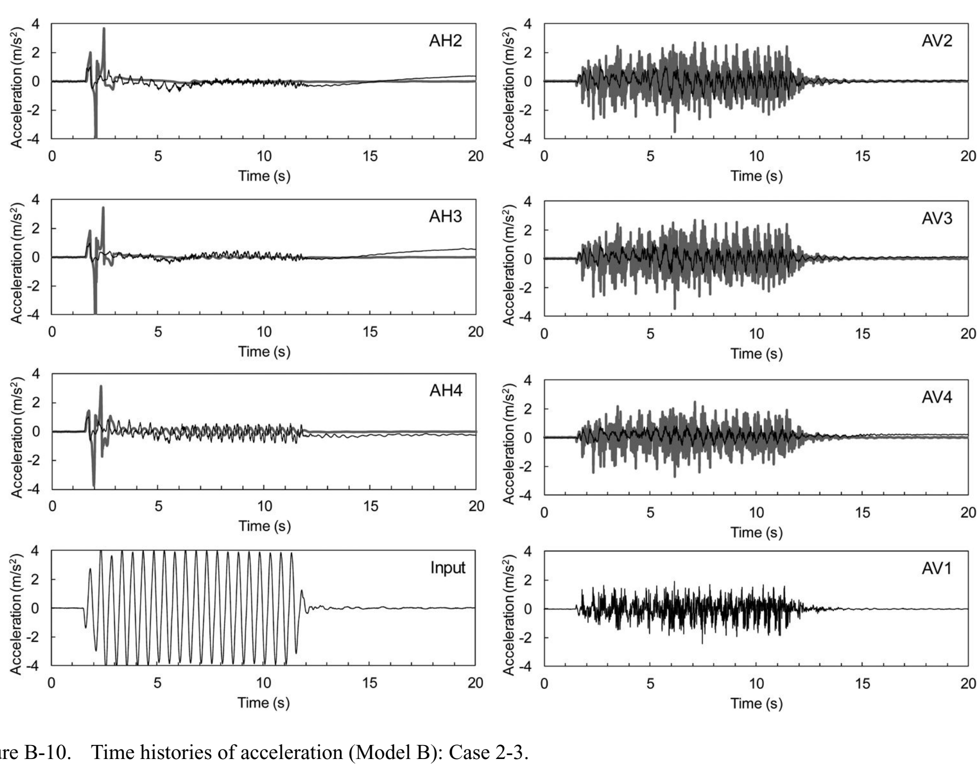

Figure B-10. Time histories of acceleration (Model B): Case 2-3.

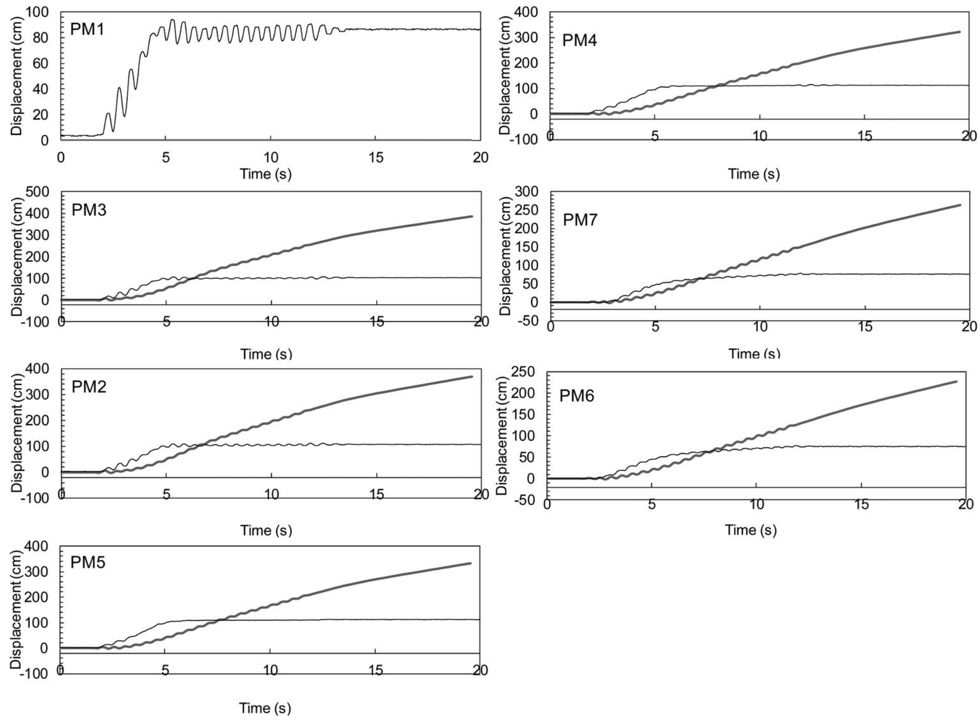

Figure B-11. Time histories of lateral displacement (Model B): Case 2-3.

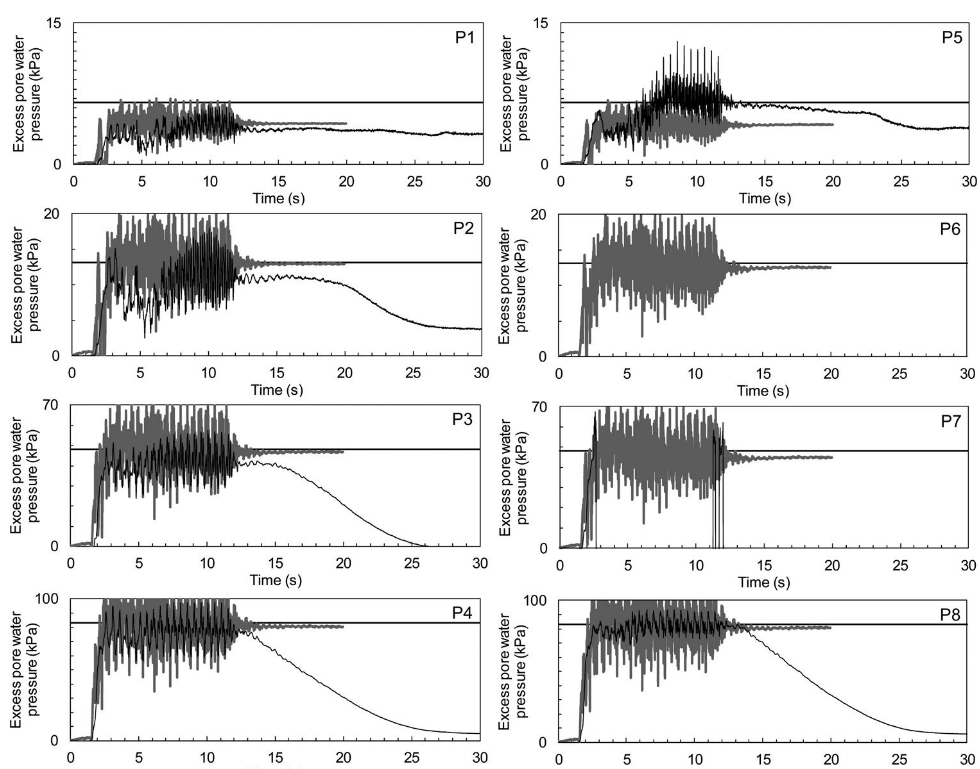

Figure B-12. Time histories of excess pore water pressure (Model B): Case 2-3.

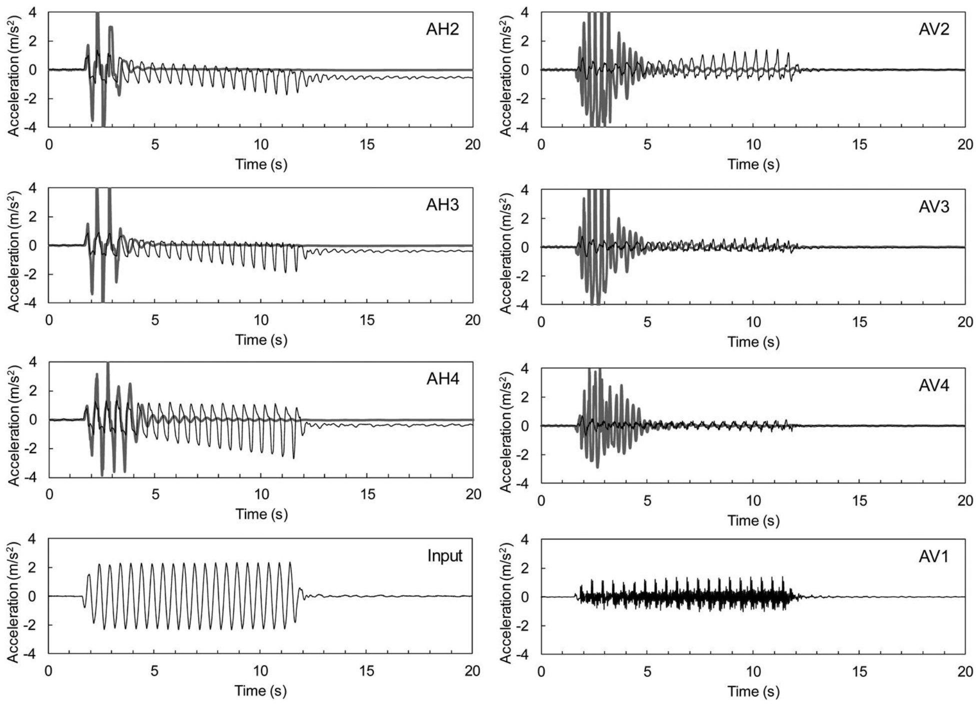

Figure B-13. Time histories of acceleration (Model B): Case 3-1.

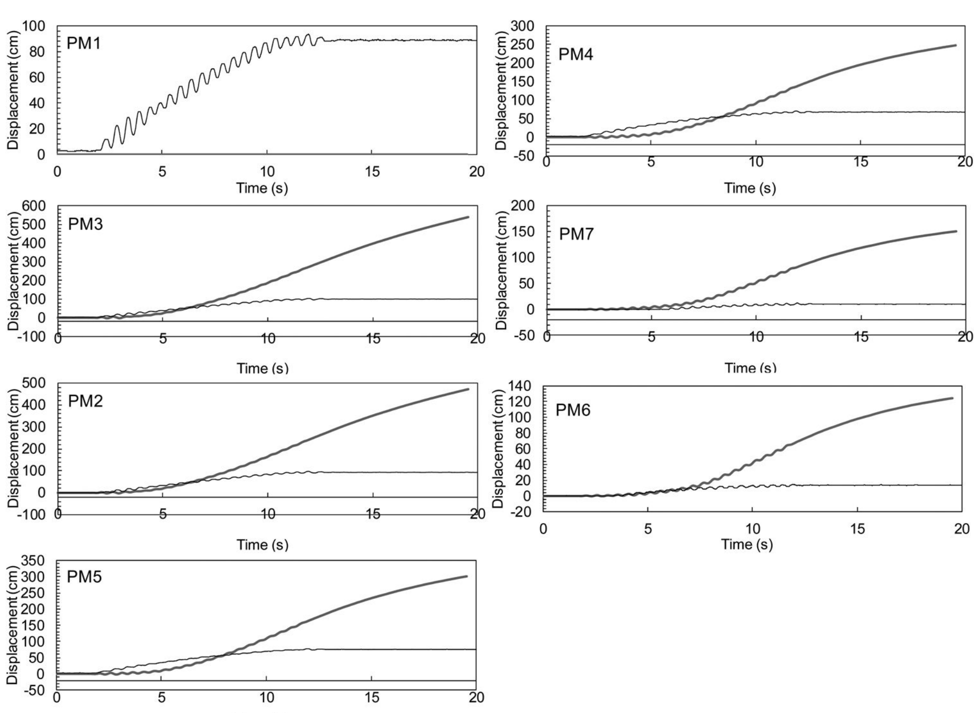

Figure B-14. Time histories of lateral displacement (Model B): Case 3-1.

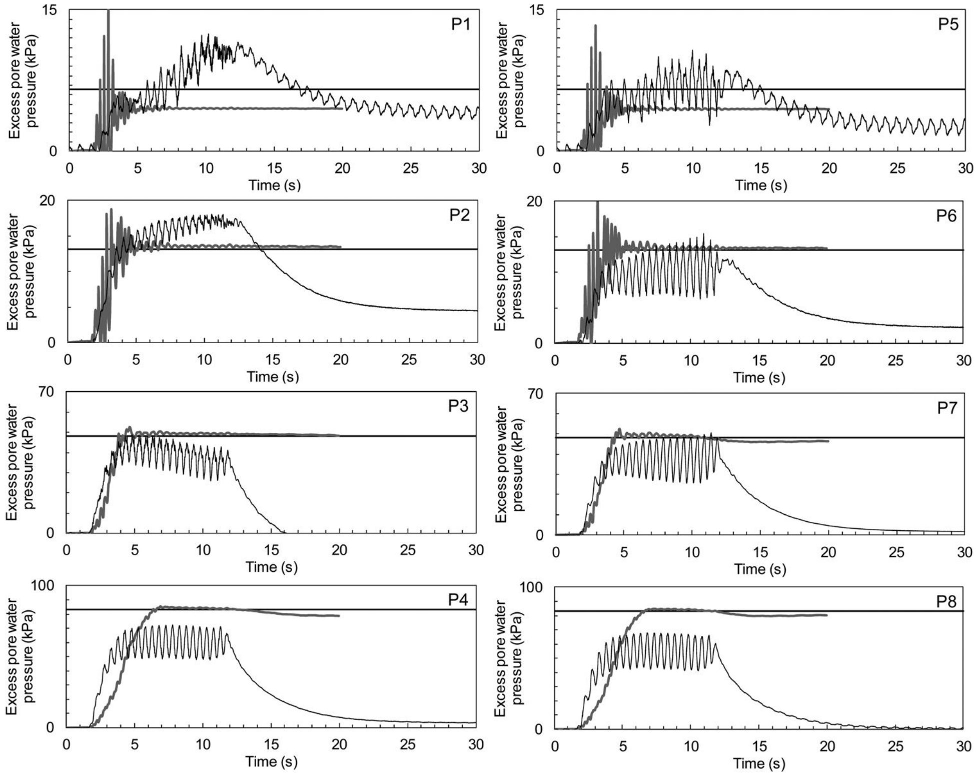

Figure B-15. Time histories of excess pore water pressure (Model B): Case 3-1.

MODEL C

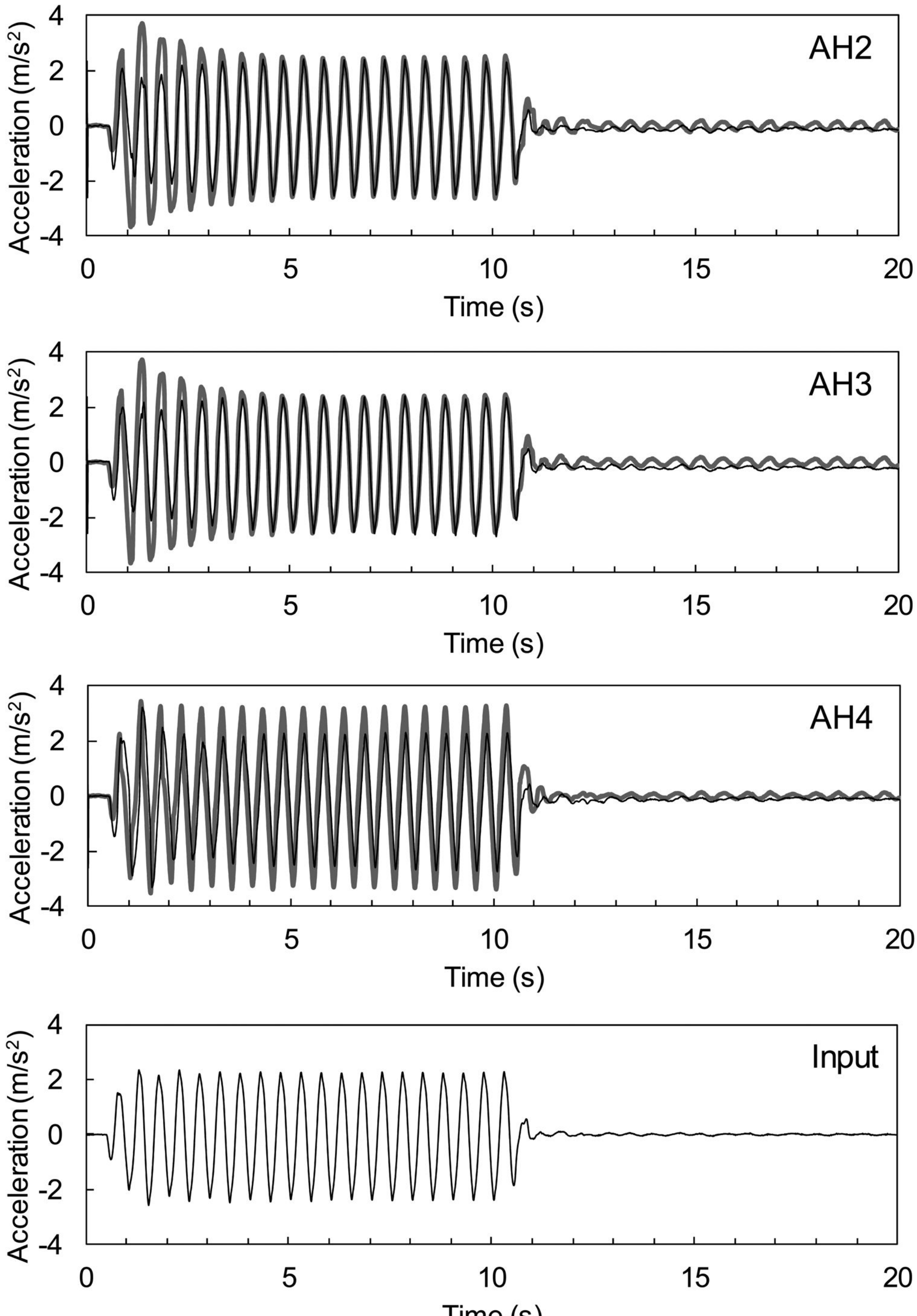

Figure C-1. Time histories of absolute acceleration (Model C): Case 1-1.

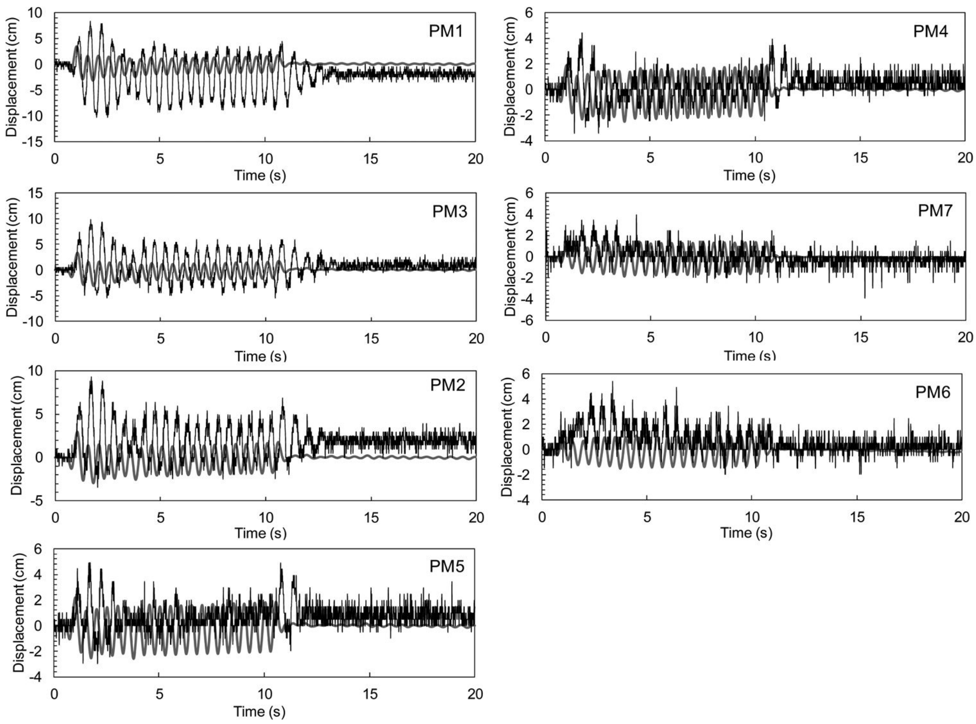

Figure C-2. Time histories of lateral displacement (Model C): Case 1-1.

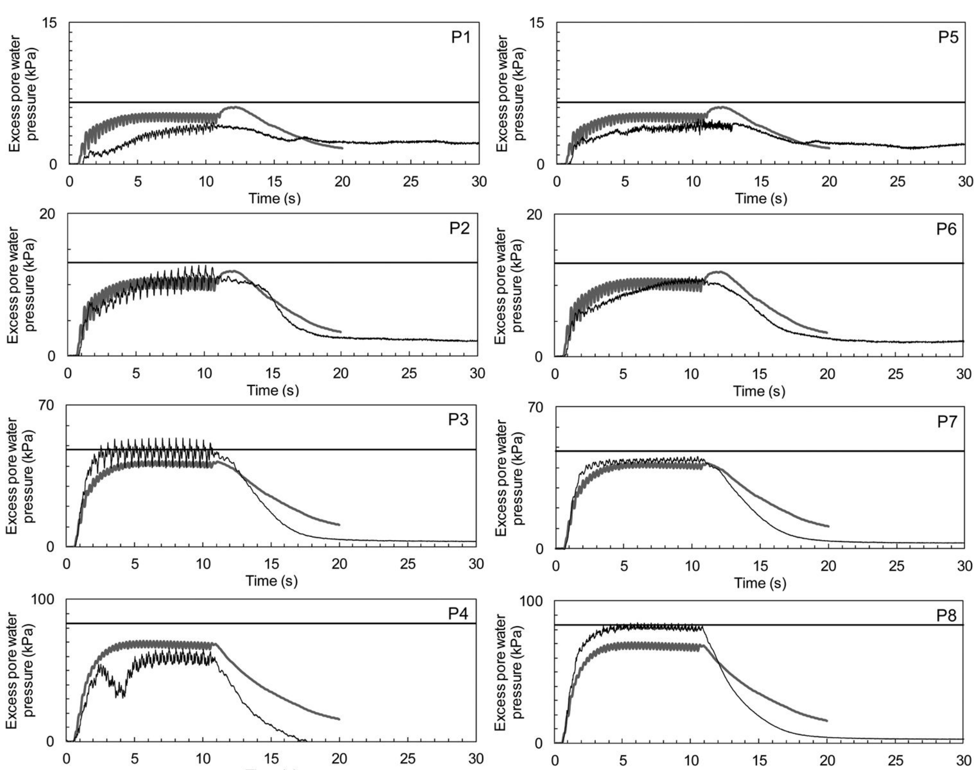

Figure C-3. Time histories of excess pore water pressure (Model C): Case 1-1.

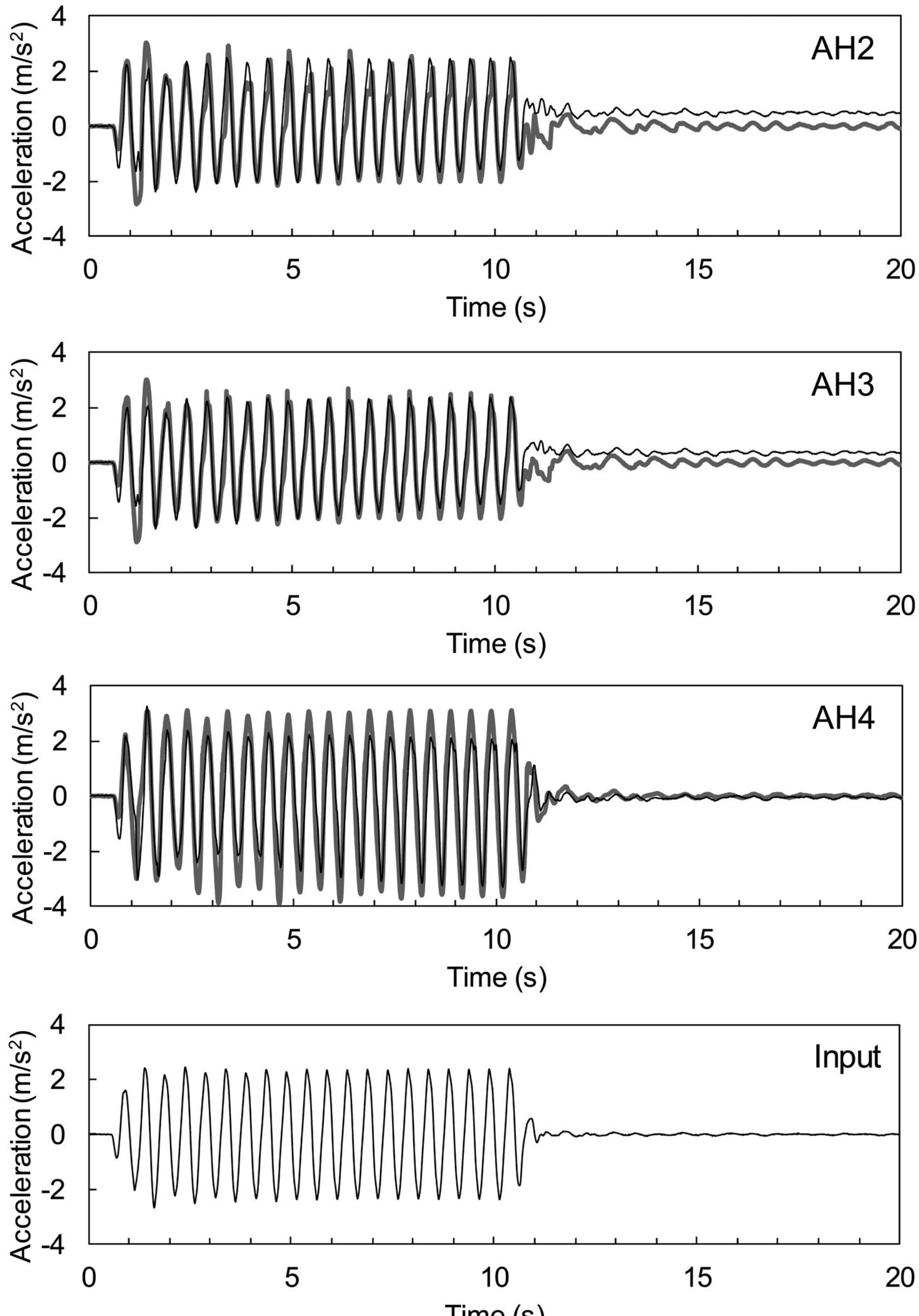

Figure C-4. Time histories of absolute acceleration (Model C): Case 1-2.

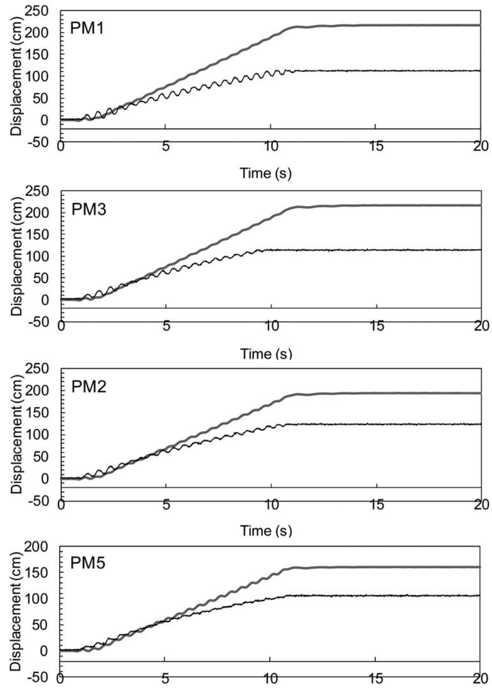

Figure C-5. Time histories of lateral displacement (Model C): Case 1-2.

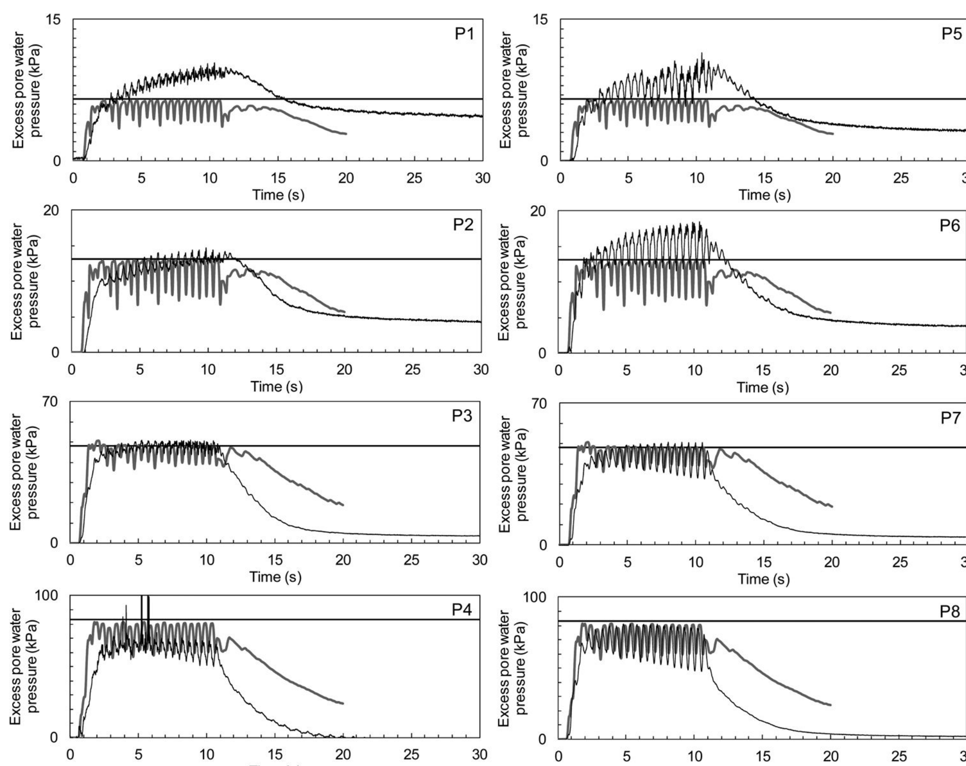

Figure C-6. Time histories of excess pore water pressure (Model C): Case 1-2.

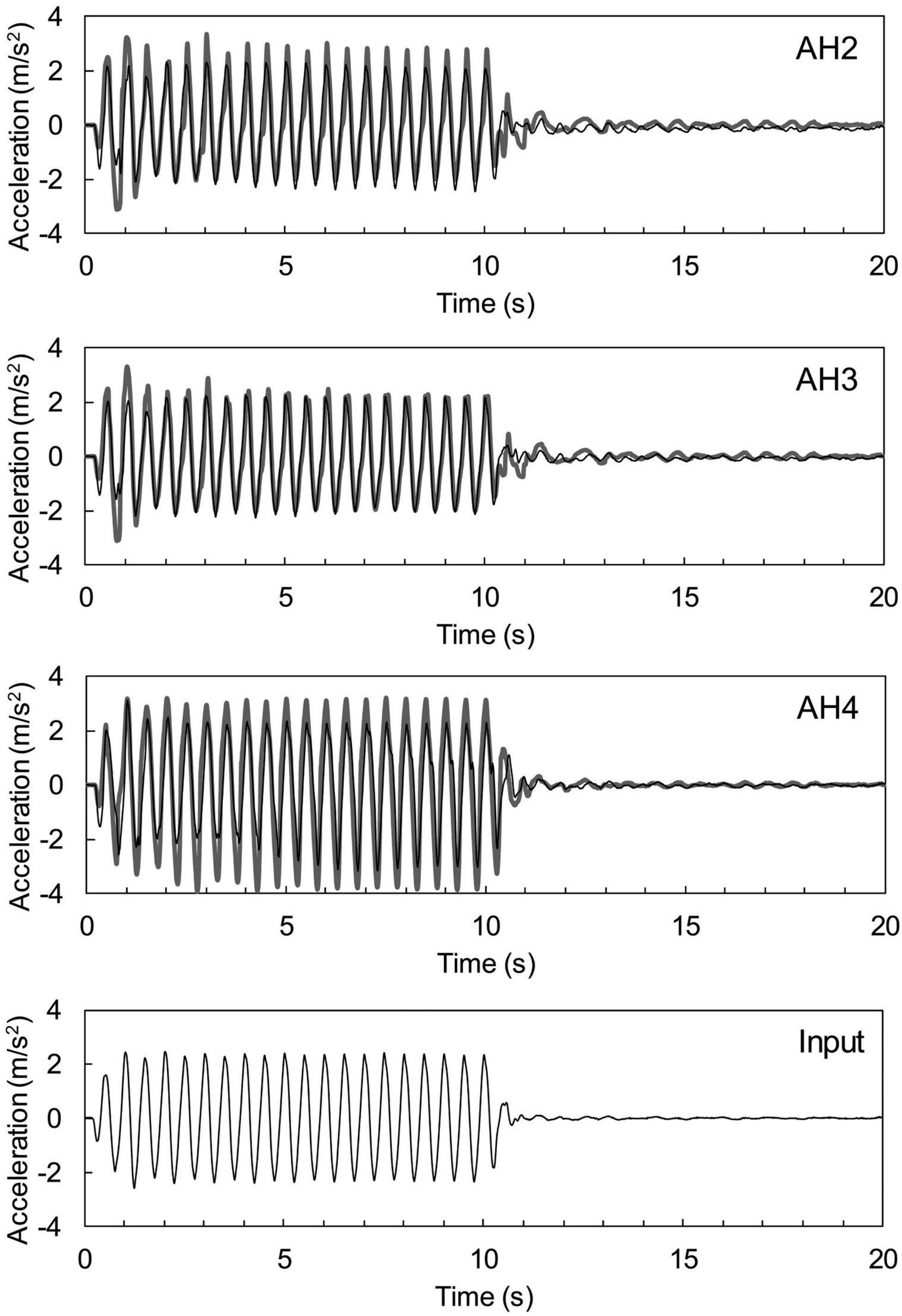

Figure C-7. Time histories of absolute acceleration (Model C): Case 1-3.

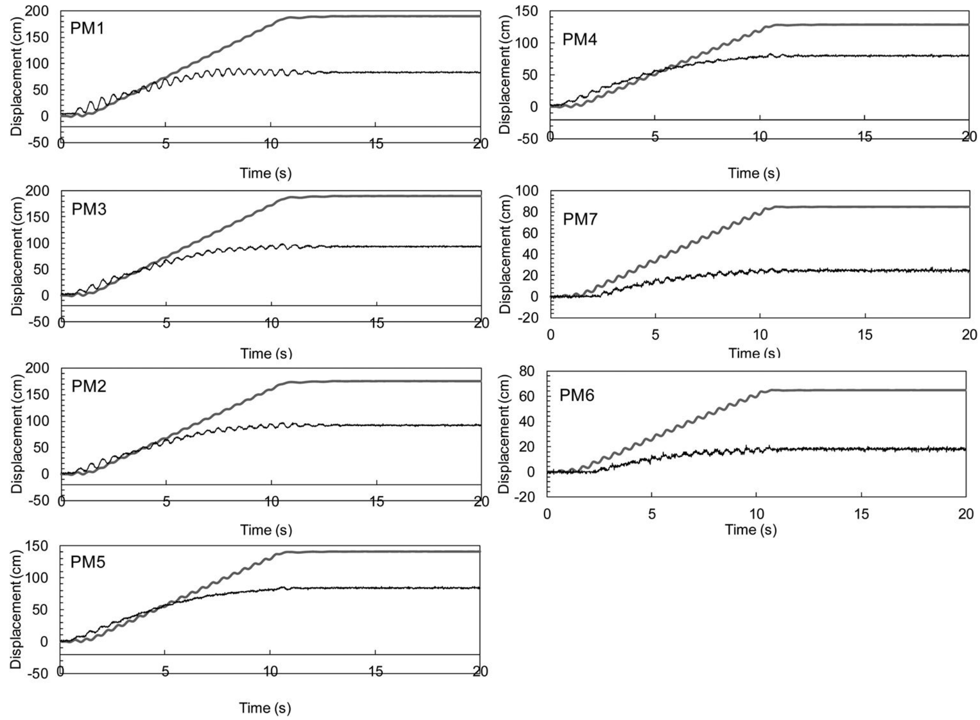

Figure C-8. Time histories of lateral displacement (Model C): Case 1-3.

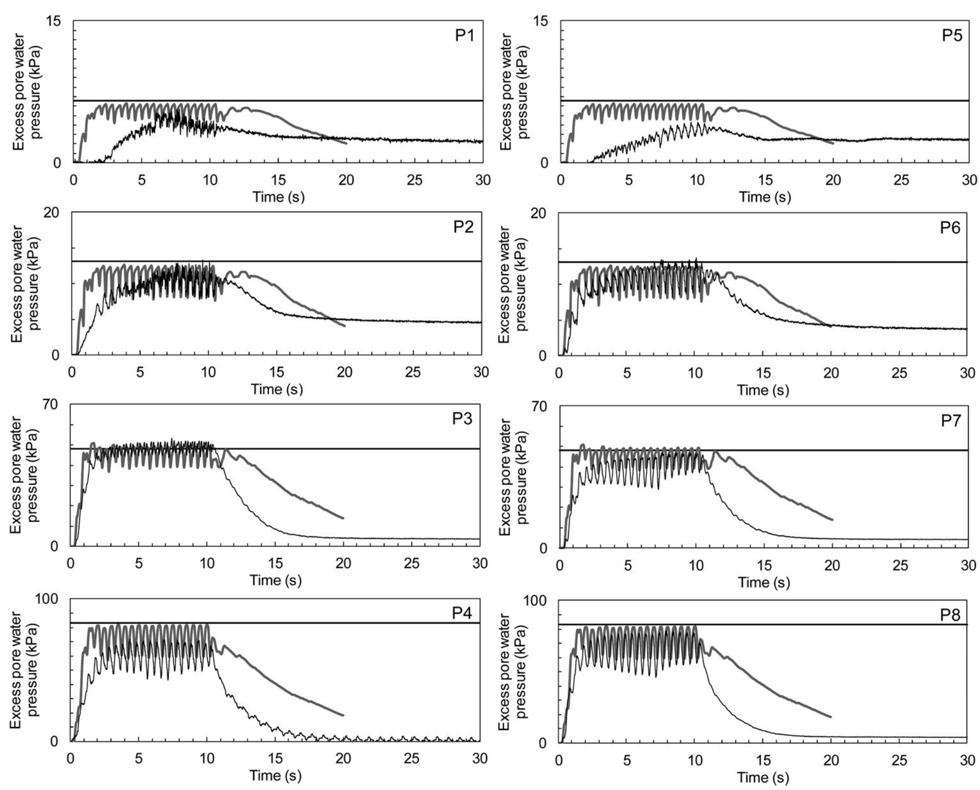

Figure C-9. Time histories of excess pore water pressure (Model C): Case 1-3.

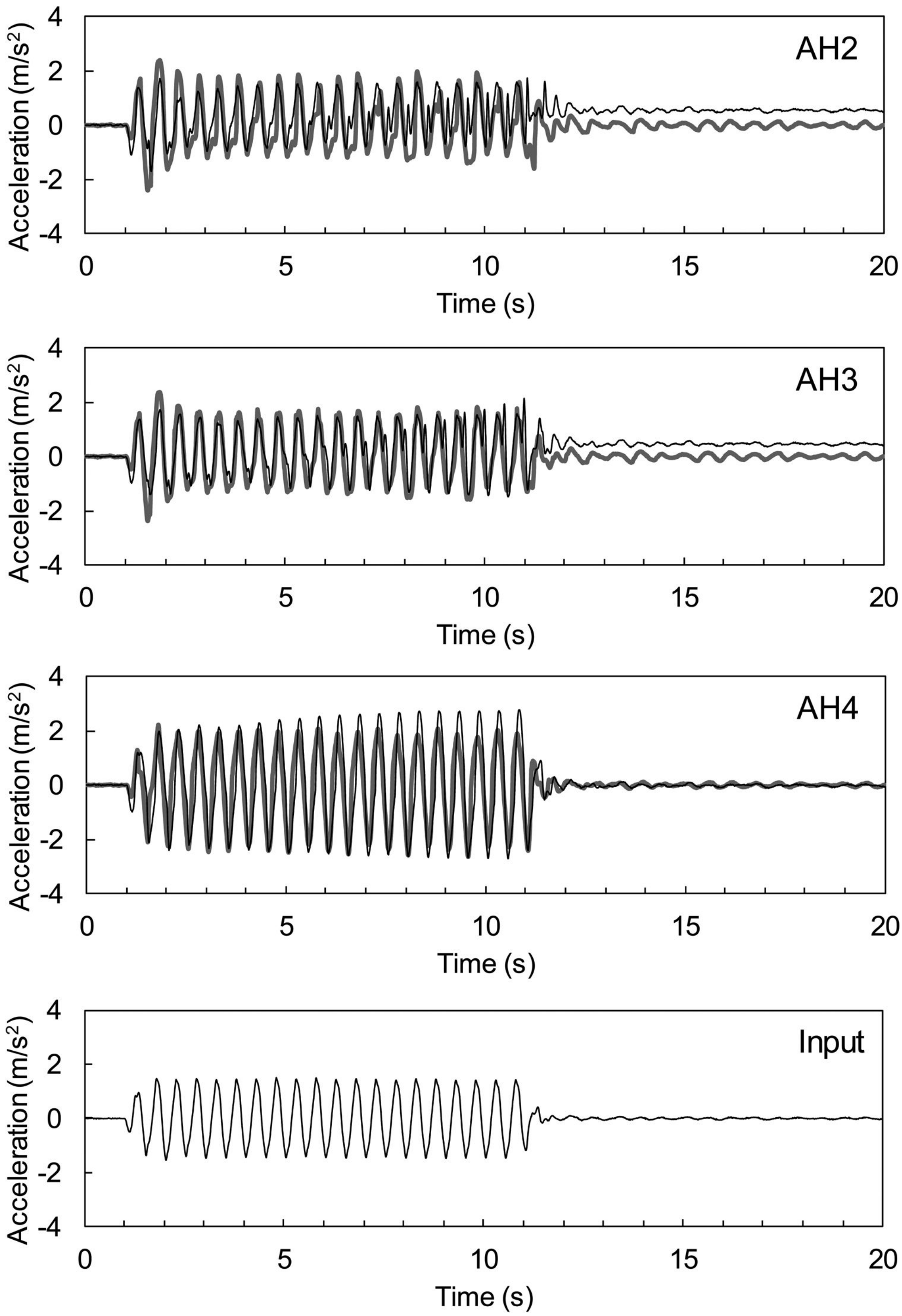

Figure C-10. Time histories of absolute acceleration (Model C): Case 2-1.

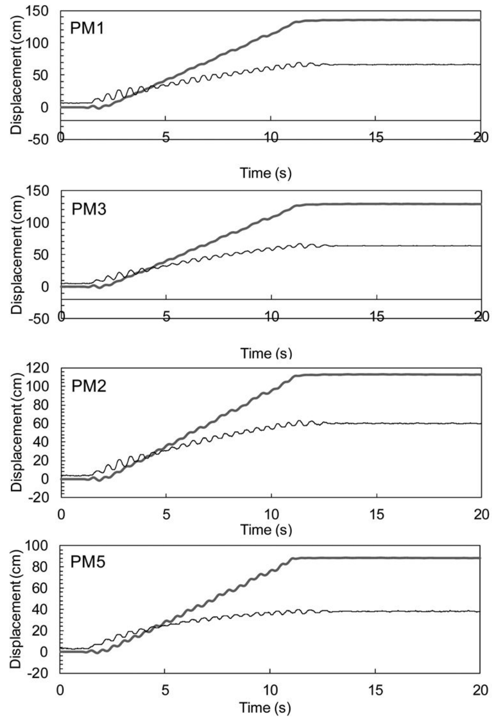

Figure C-11. Time histories of lateral displacement (Model C): Case 2-1.

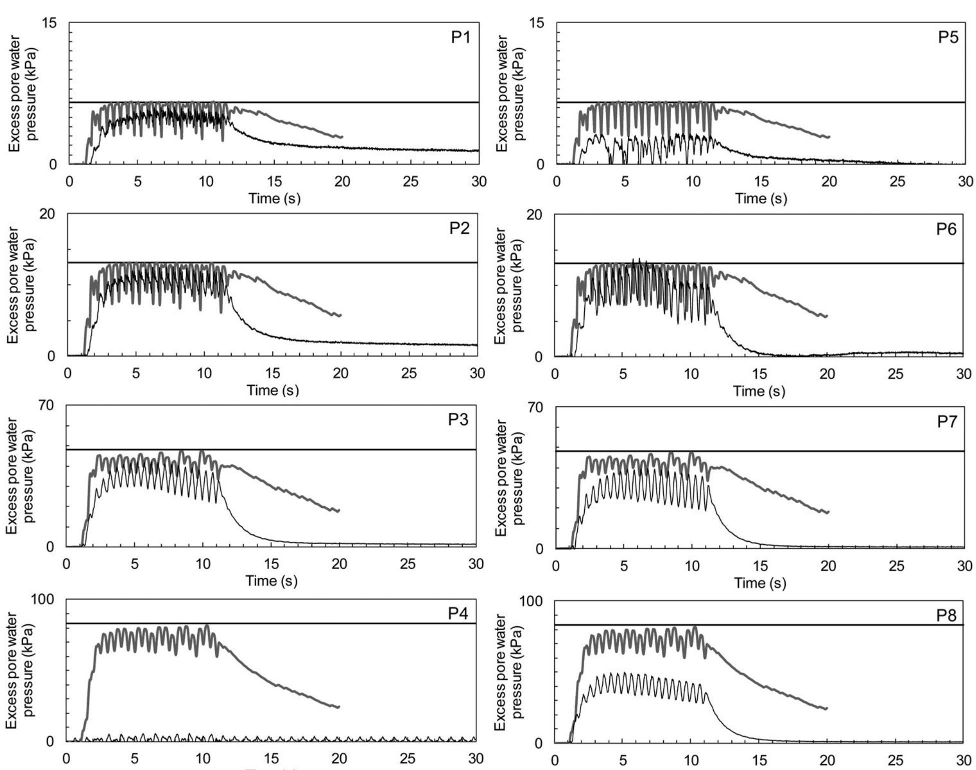

Figure C-12. Time histories of excess pore water pressure (Model C): Case 2-1.

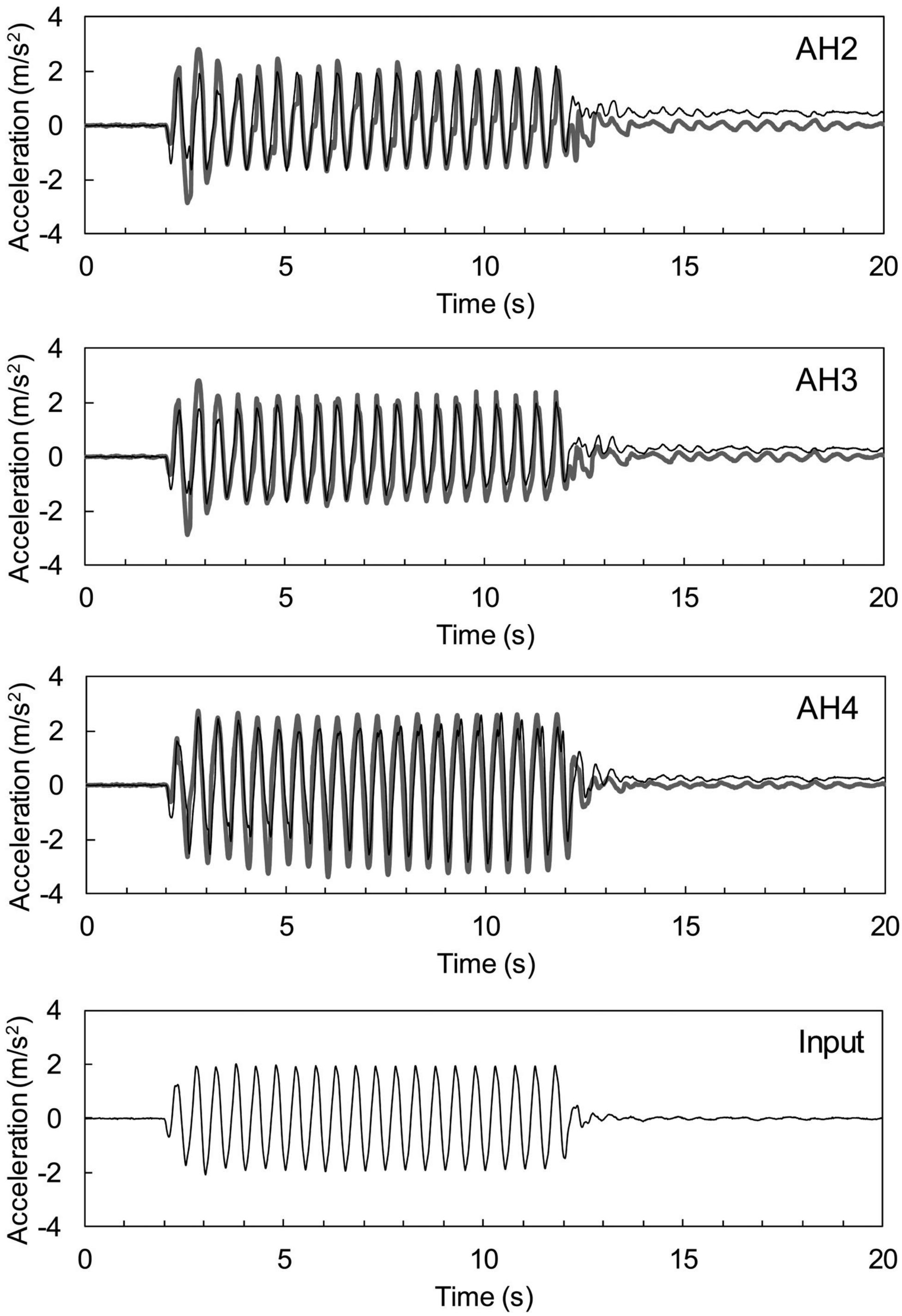

Figure C-13. Time histories of absolute acceleration (Model C): Case 2-2.

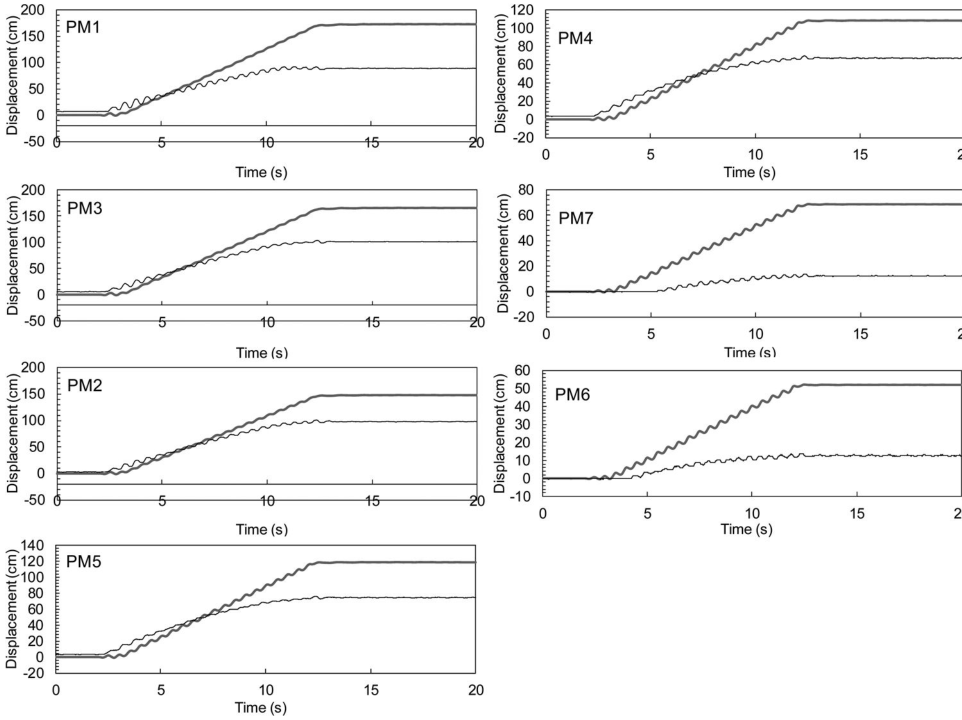

Figure C-14. Time histories of lateral displacement (Model C): Case 2-2.

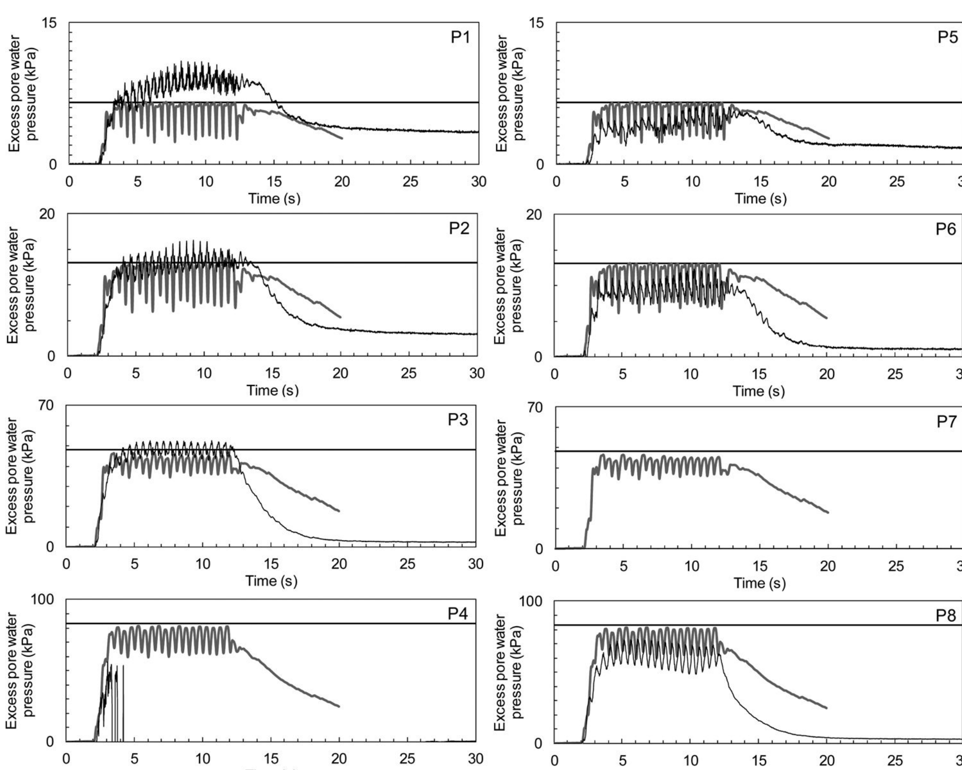

Figure C-15. Time histories of excess pore water pressure (Model C): Case 2-2.

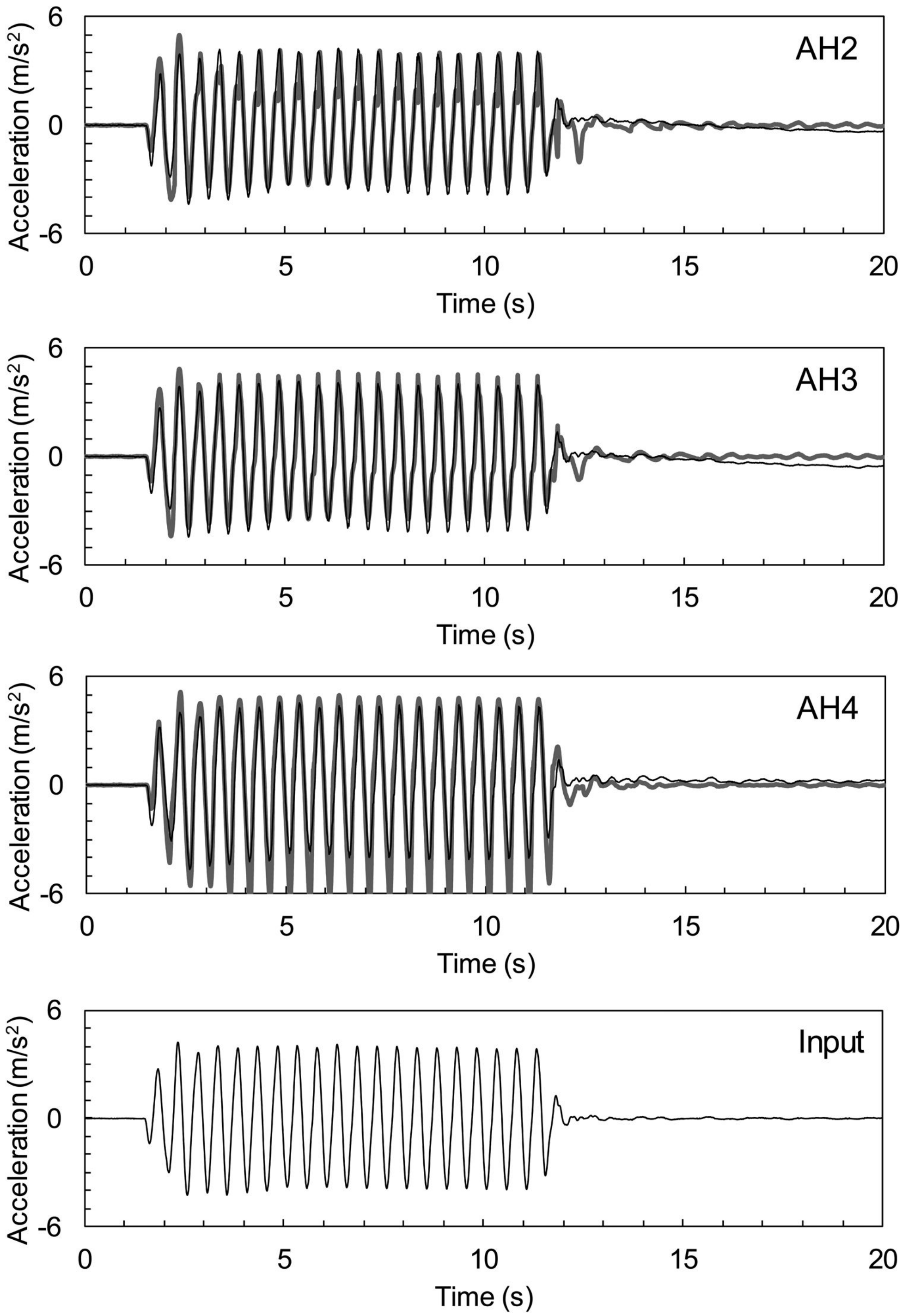

Figure C-16. Time histories of absolute acceleration (Model C): Case 2-3.

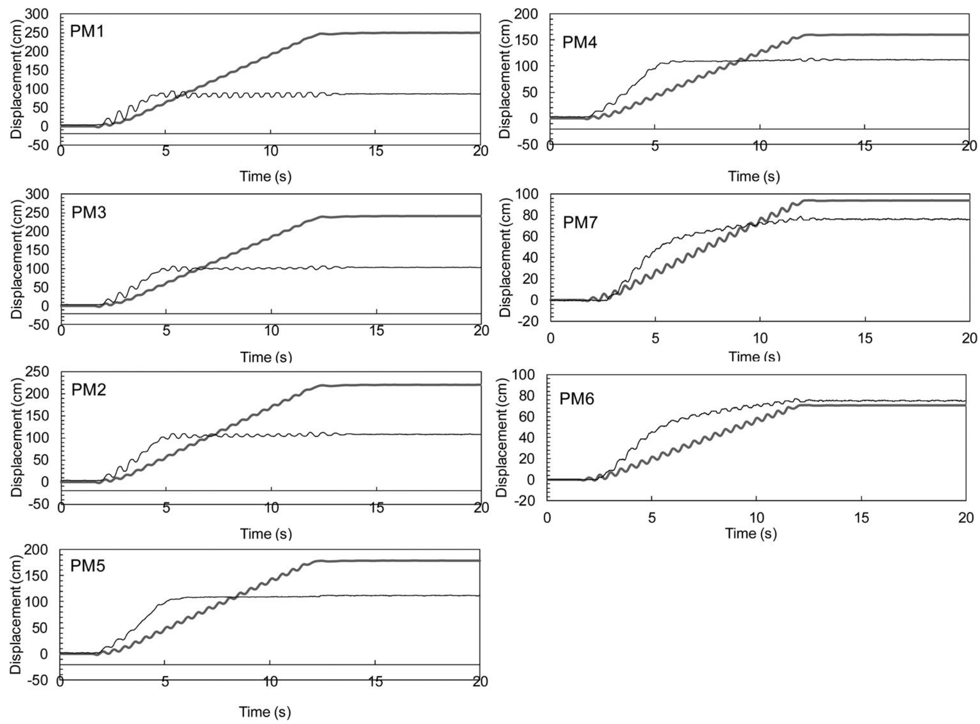

Figure C-17. Time histories of lateral displacement (Model C): Case 2-3.

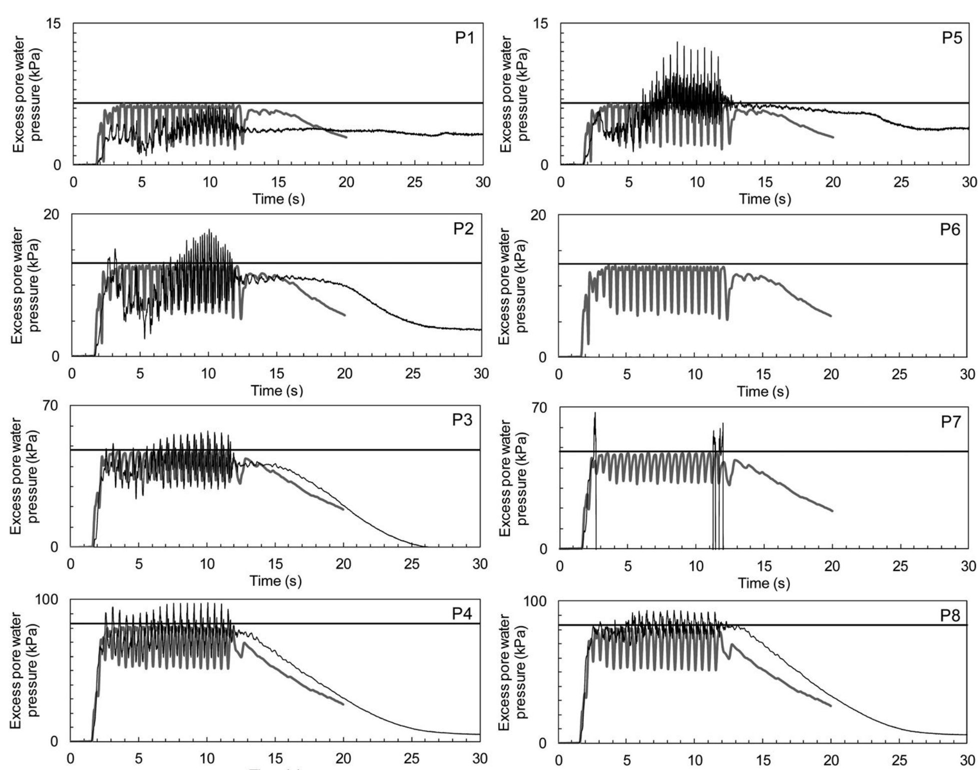

Figure C-18. Time histories of excess pore water pressure (Model C): Case 2-3.

MODEL D

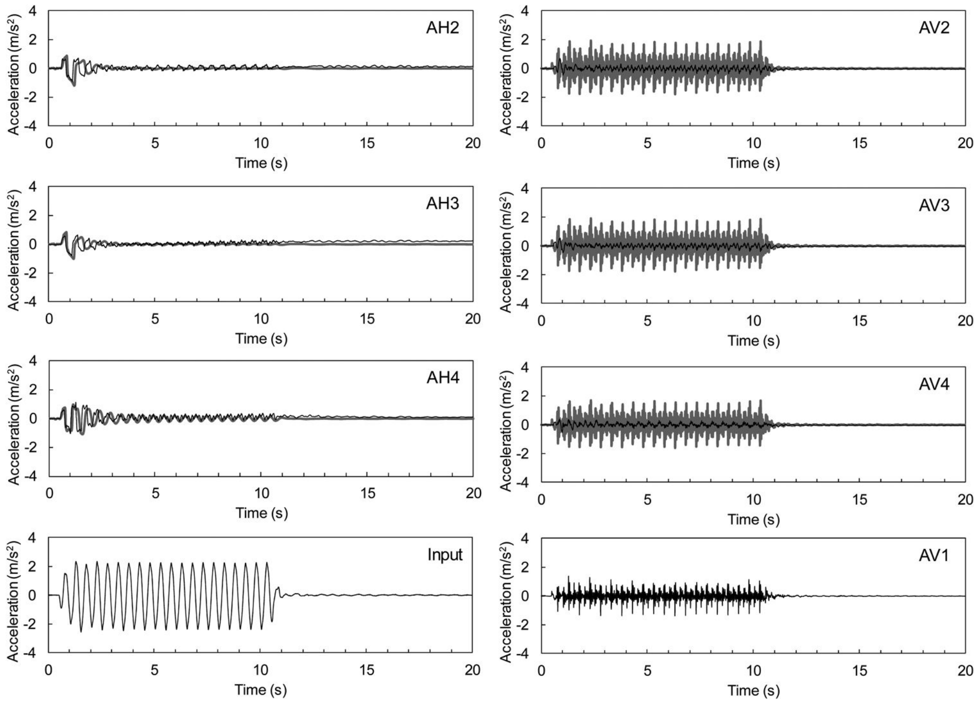

Figure D-1. Time histories of acceleration (Model D): Case 1-1 (undrained).

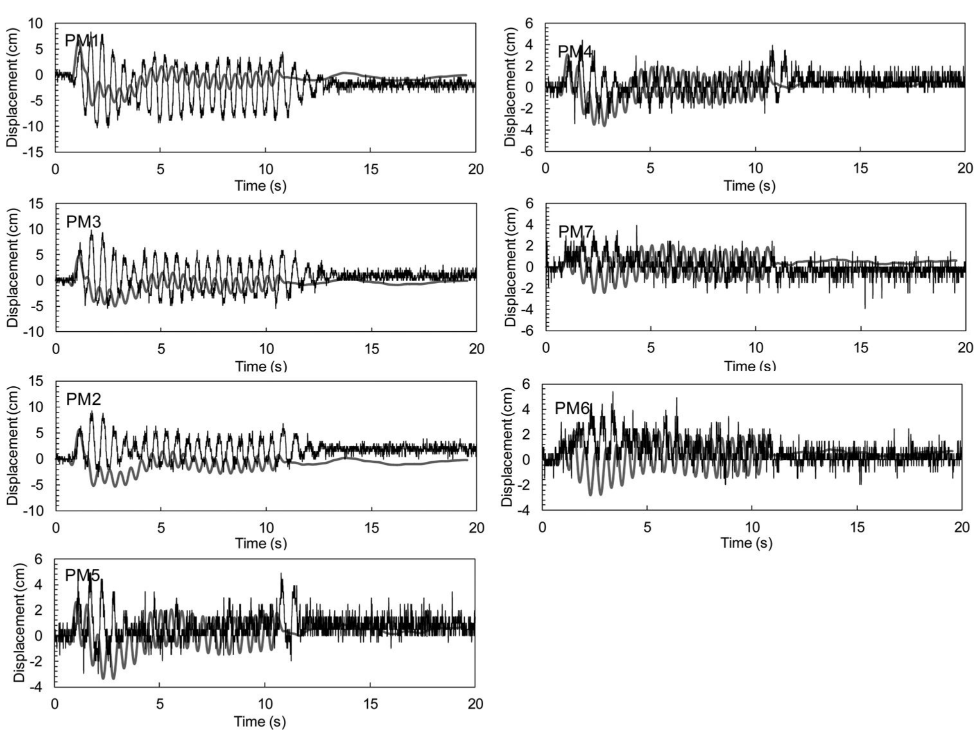

Figure D-2. Time histories of lateral displacement (Model D): Case 1-1 (undrained).

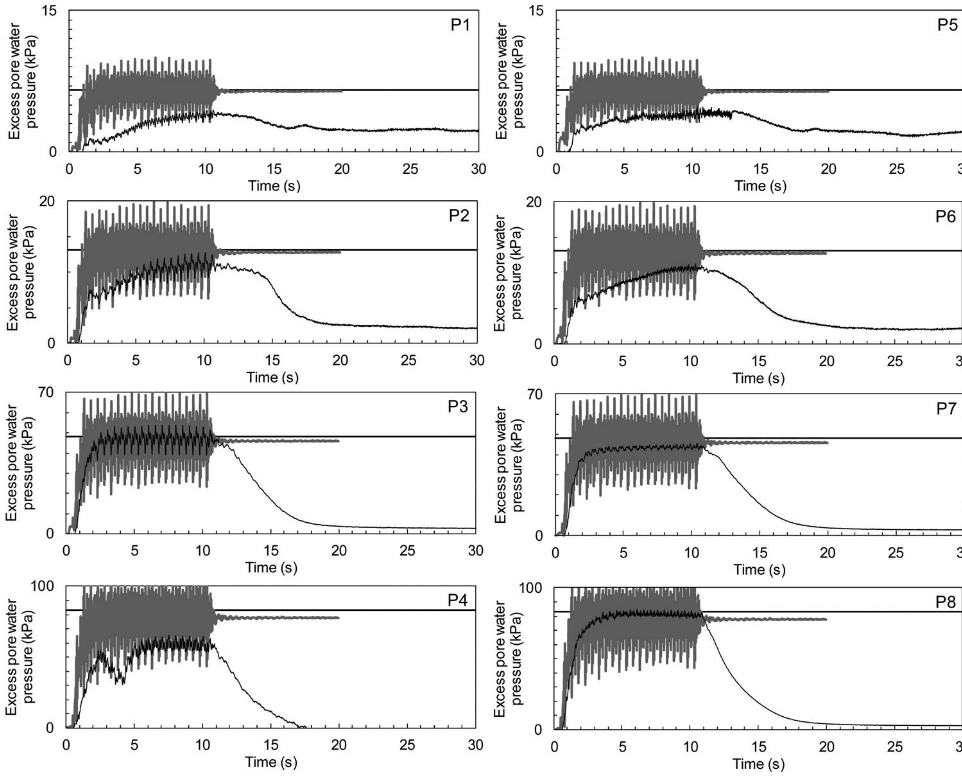

Figure D-3. Time histories of excess pore water pressure (Model D): Case 1-1 (undrained).

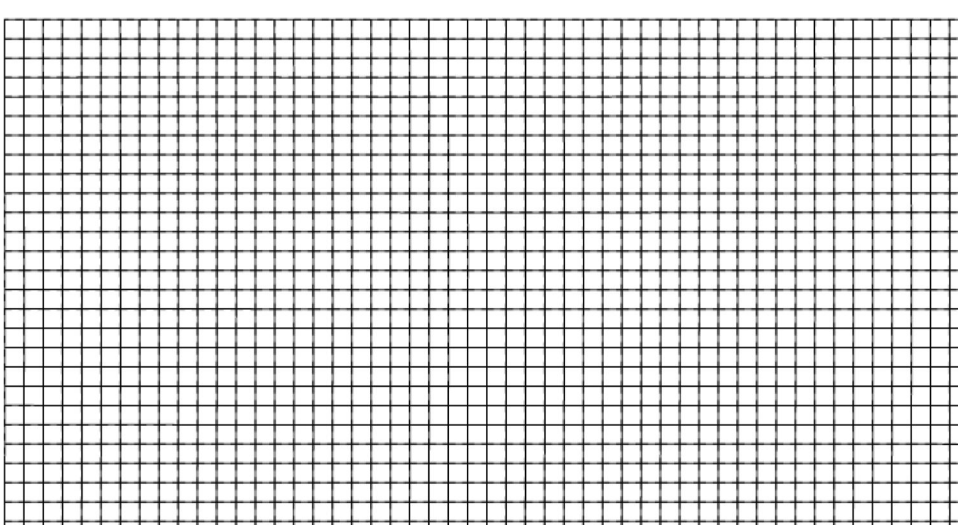

Figure D-4. Deformation after shaking (Model D): Case 1-1 (undrained).

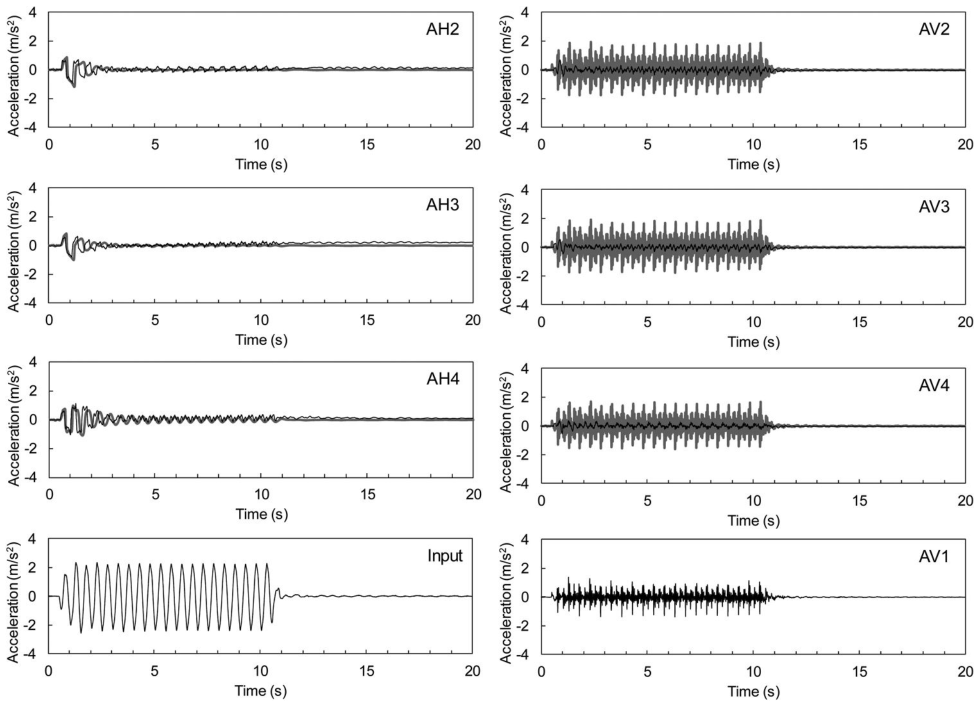

Figure D-5. Time histories of acceleration (Model D): Case 1-1 (TL-undrained).

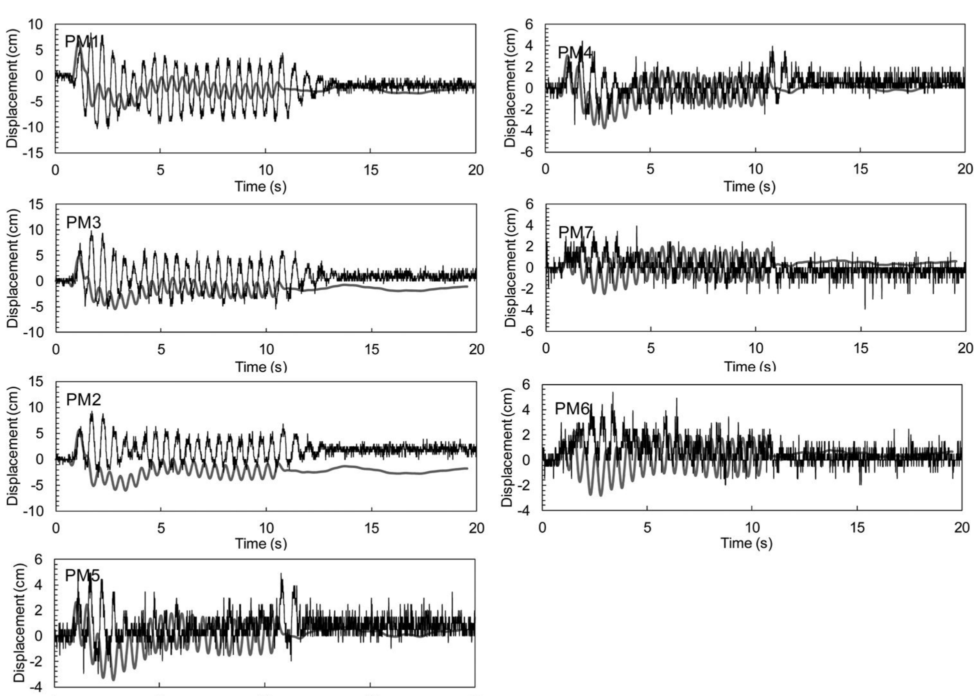

Figure D-6. Time histories of lateral displacement (Model D): Case 1-1 (TL-undrained).

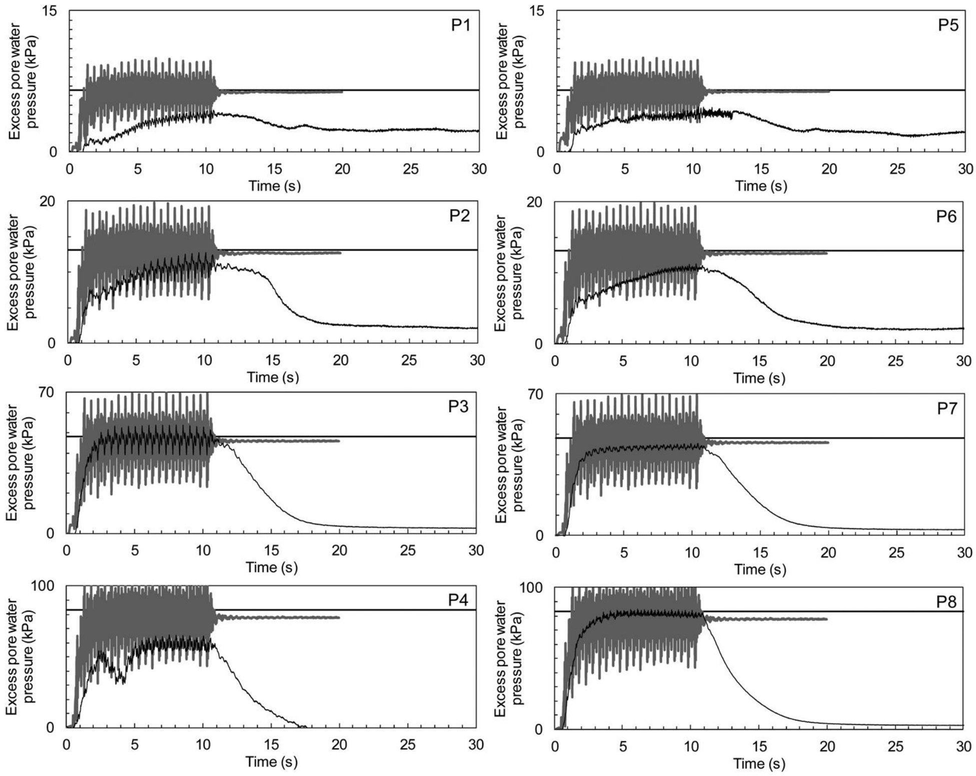

Figure D-7. Time histories of excess pore water pressure (Model D): Case 1-1 (TL-undrained).

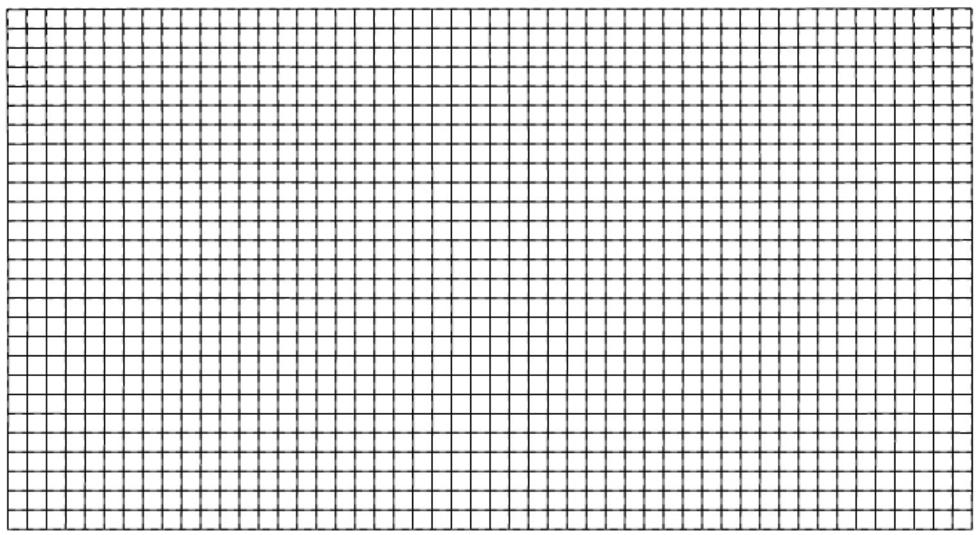

Figure D-8. Deformation after shaking (Model D): Case 1-1 (TL-undrained).

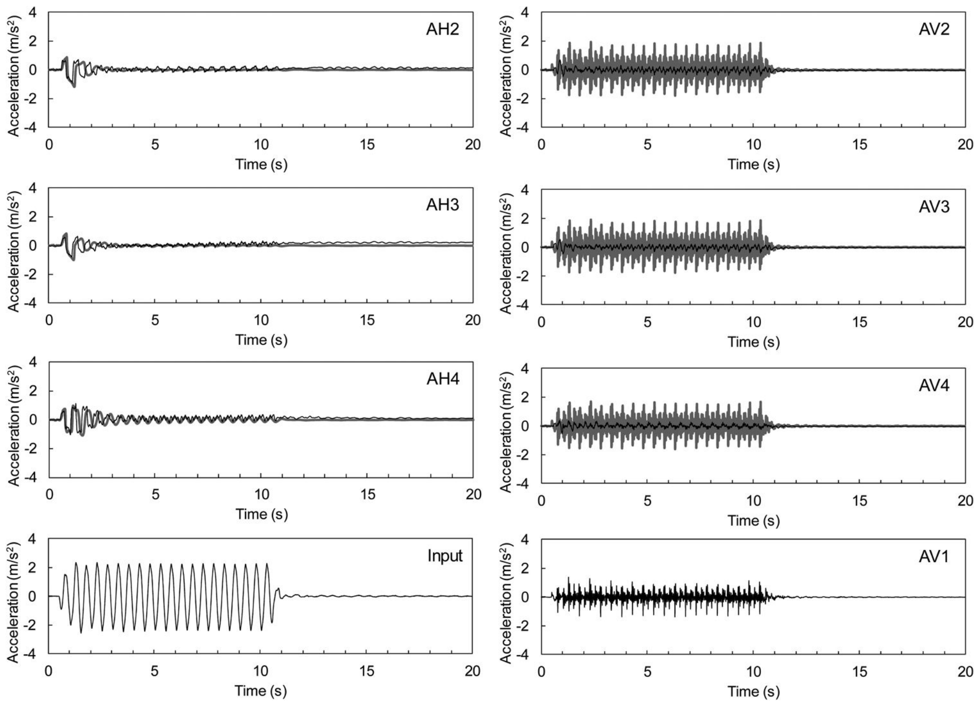

Figure D-9. Time histories of acceleration (Model D): Case 1-1 (UL-undrained).

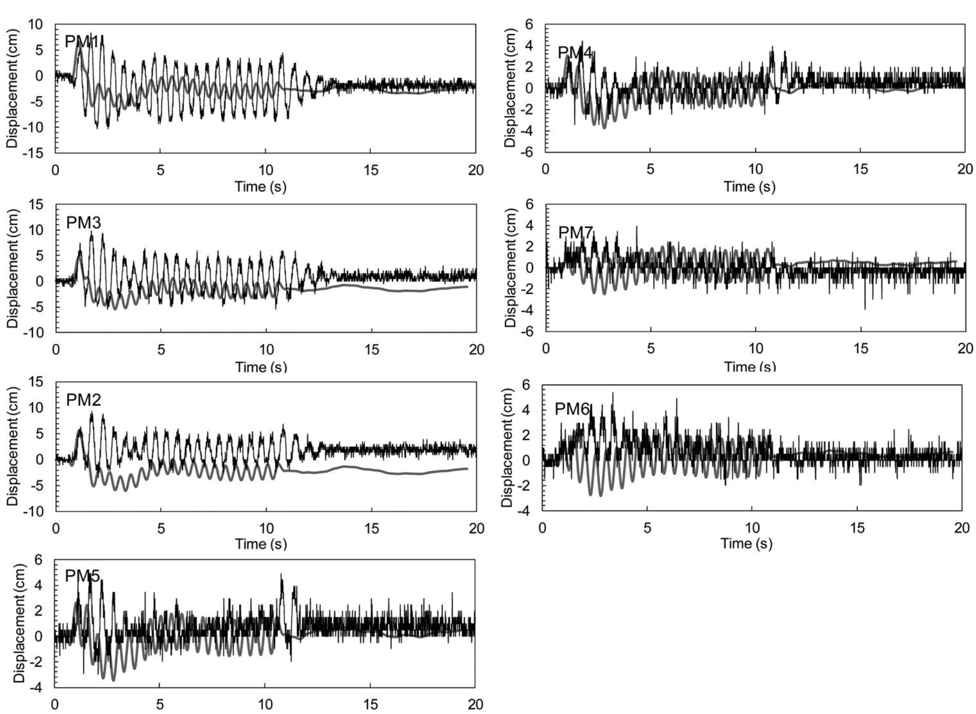

Figure D-10. Time histories of lateral displacement (Model D): Case 1-1 (UL-undrained).

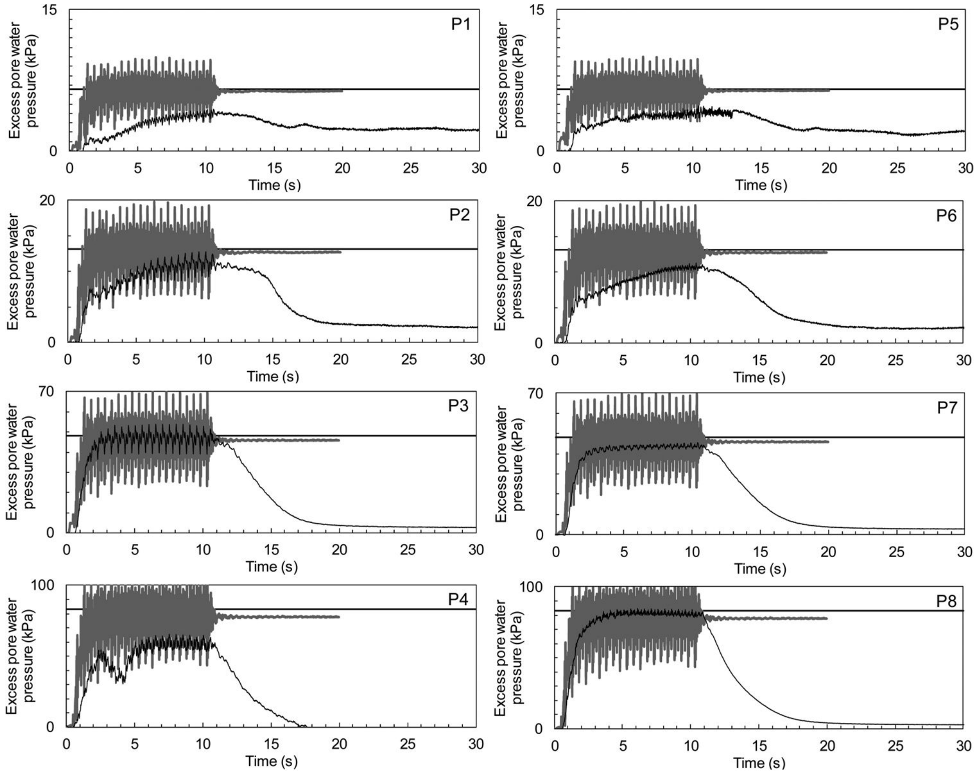

Figure D-11. Time histories of excess pore water pressure (Model D): Case 1-1 (UL-undrained).

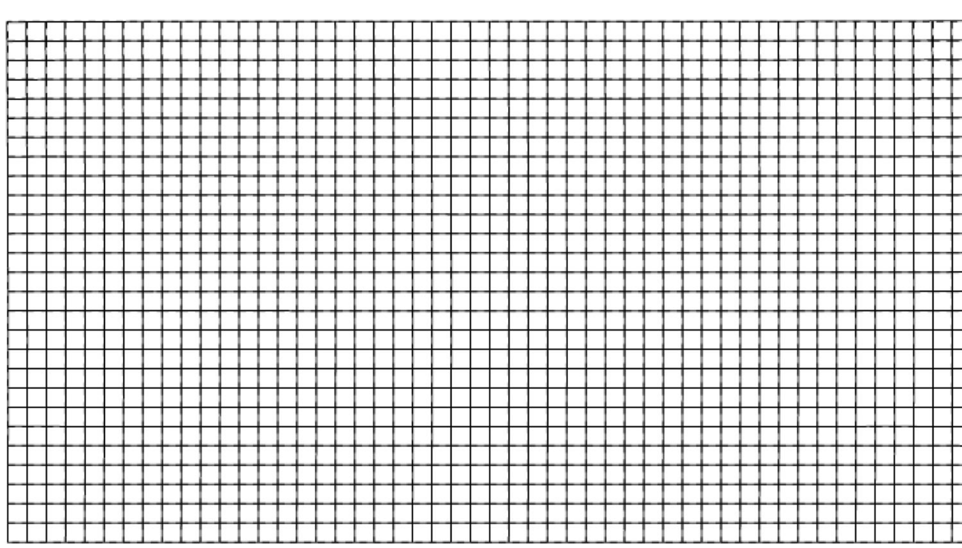

Figure D-12. Deformation after shaking (Model D): Case 1-1 (UL-undrained).

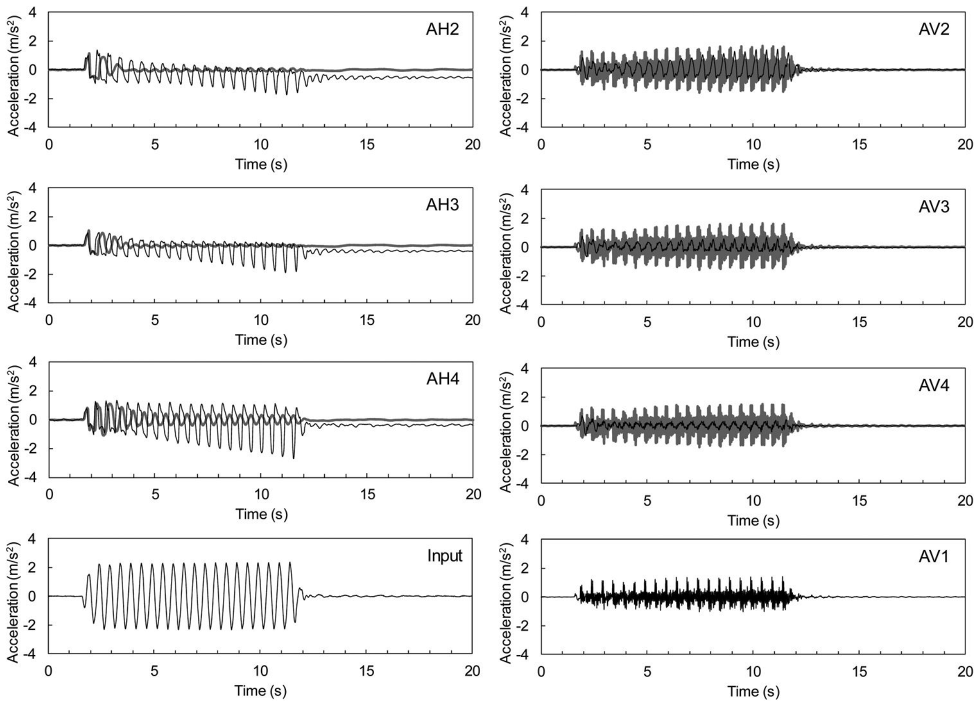

Figure D-13. Time histories of acceleration (Model D): Case 3-1 (undrained).

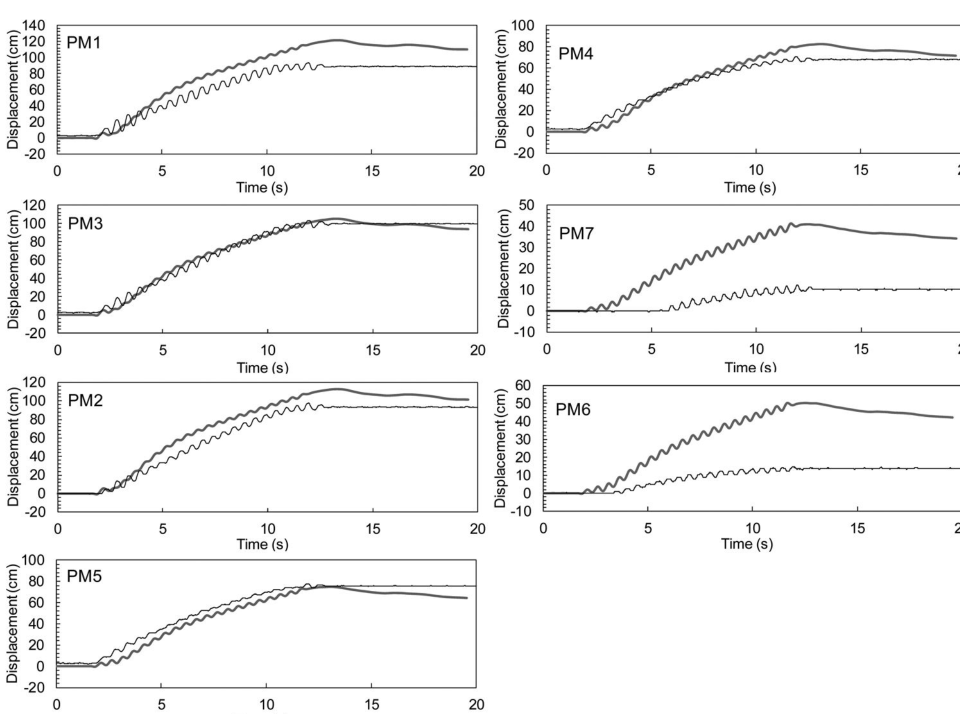

Figure D-14. Time histories of lateral displacement (Model D): Case 3-1 (undrained).

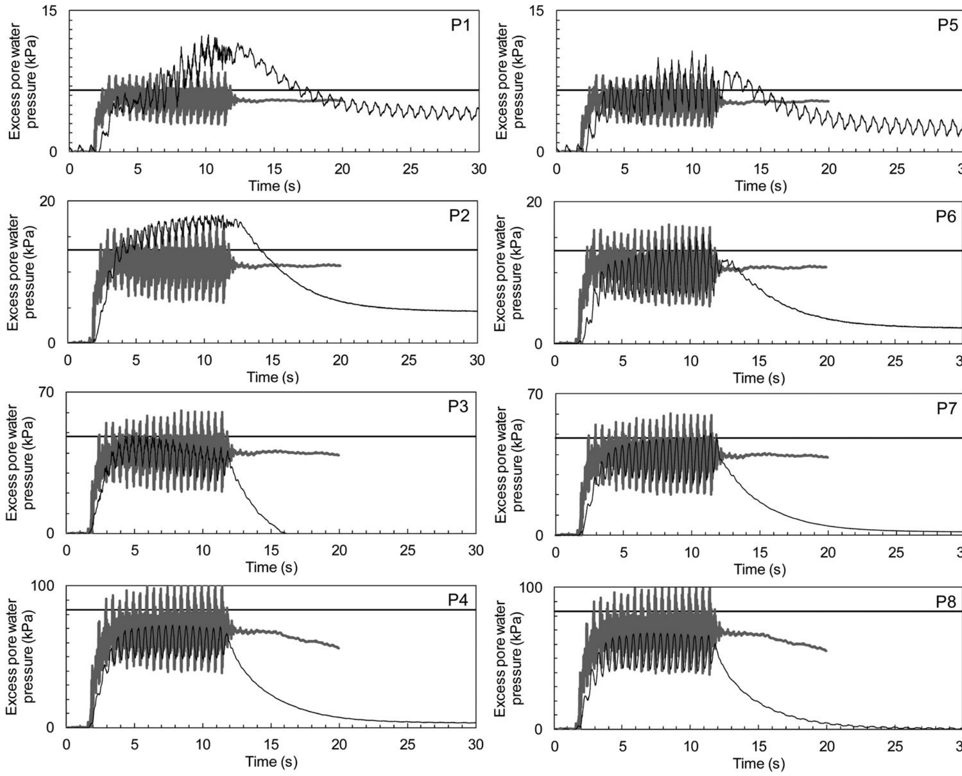

Figure D-15. Time histories of excess pore water pressure (Model D): Case 3-1 (undrained).

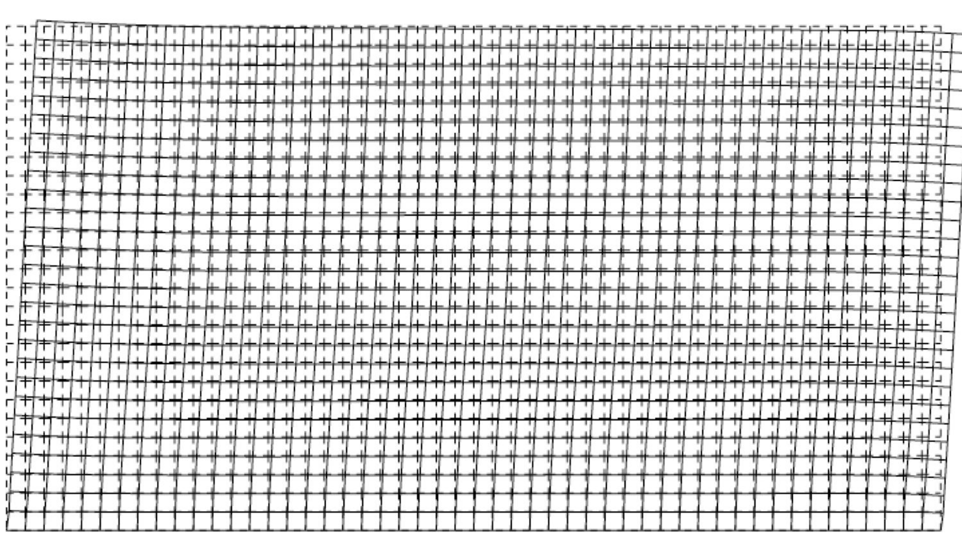

Figure D-16. Deformation after shaking (Model D): Case 3-1 (undrained).

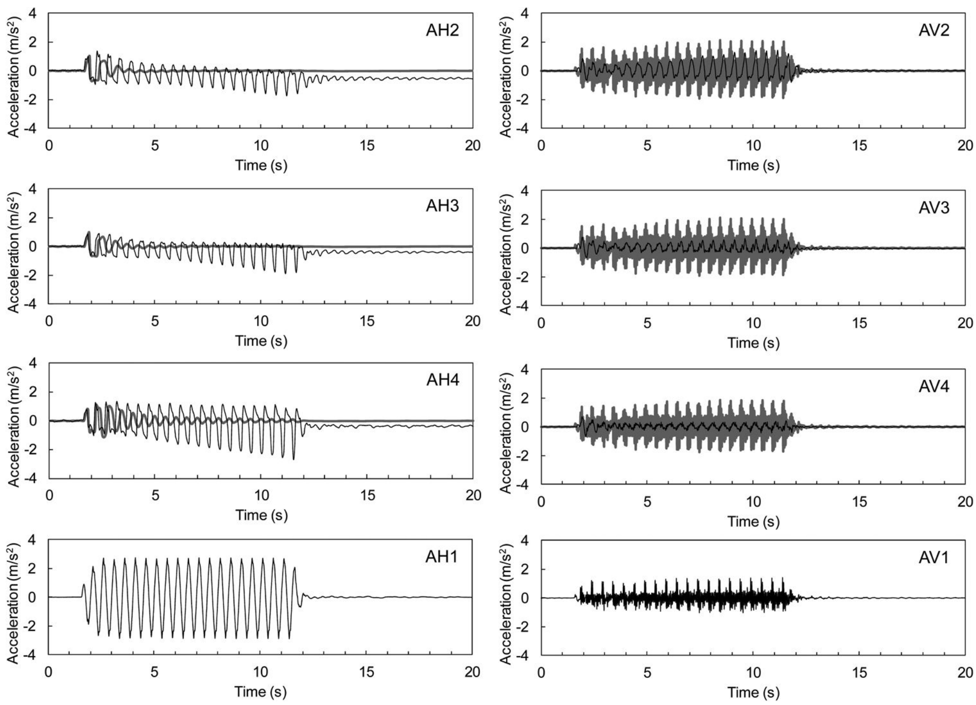

Figure D-17. Time histories of acceleration (Model D): Case 3-1 (TL-undrained).

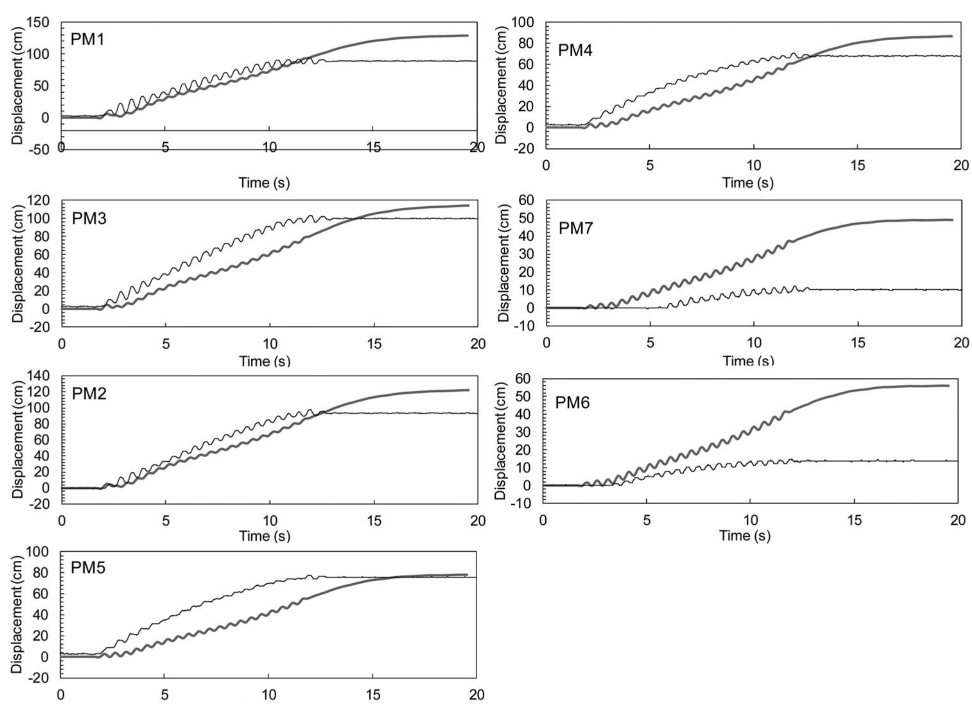

Figure D-18. Time histories of lateral displacement (Model D): Case 3-1 (TL-undrained).

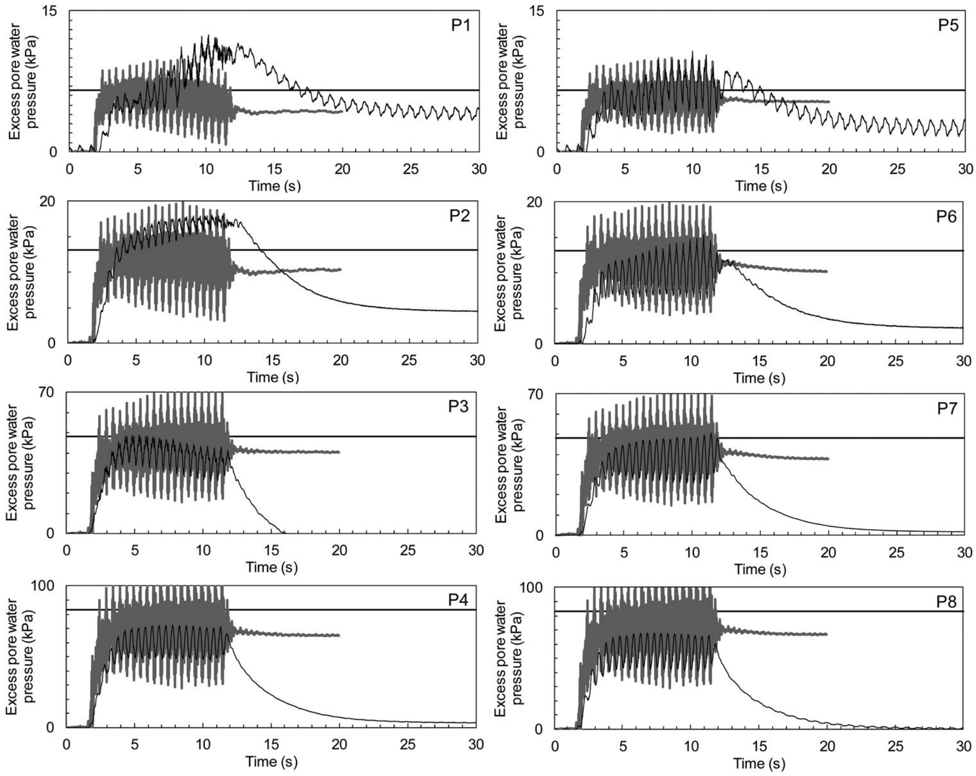

Figure D-19. Time histories of excess pore water pressure (Model D): Case 3-1 (TL-undrained).

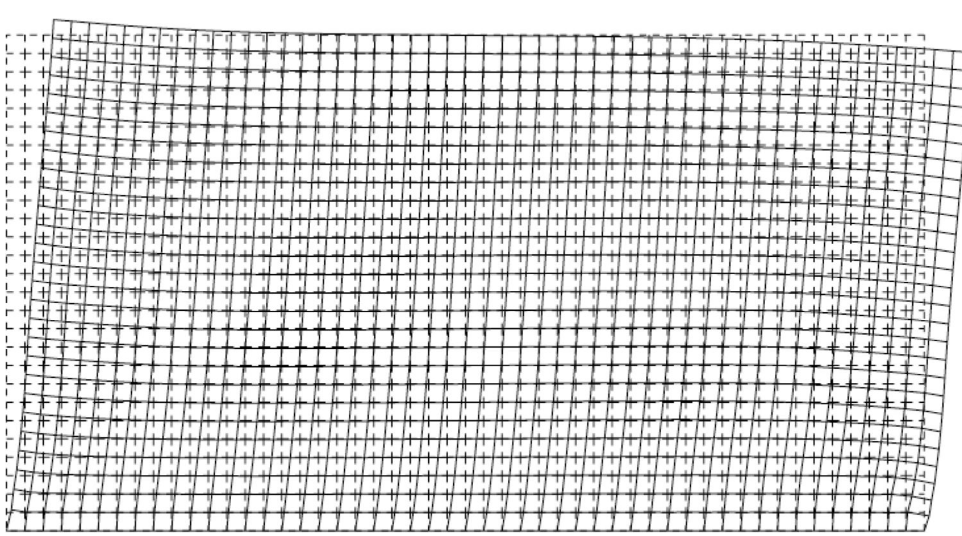

Figure D-20. Deformation after shaking (Model D): Case 3-1 (TL-undrained).

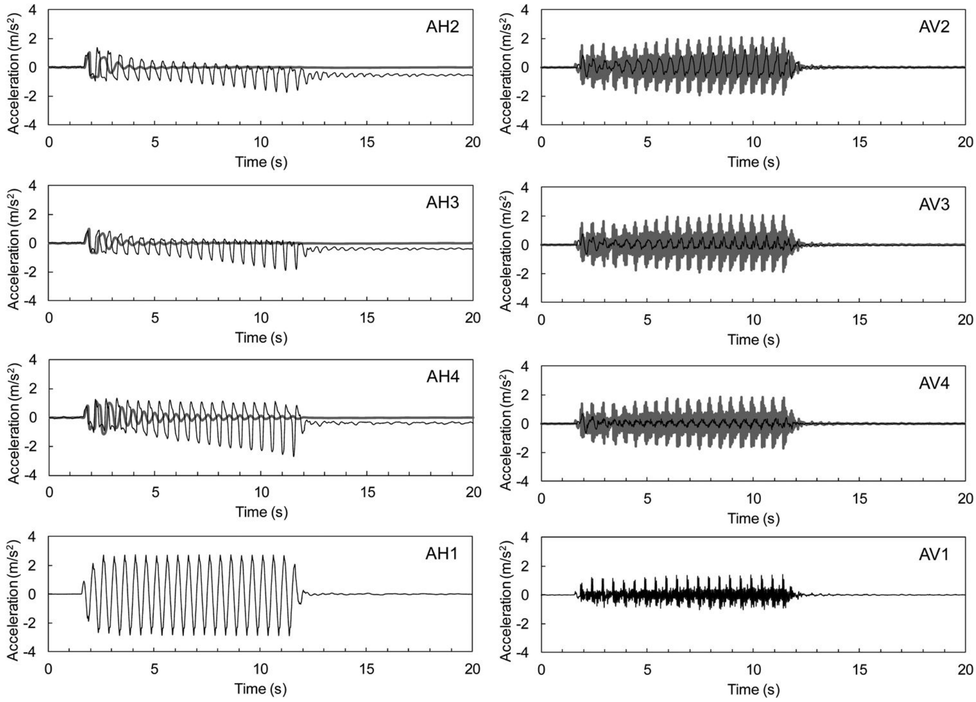

Figure D-21. Time histories of acceleration (Model D): Case 3-1 (UL-undrained).

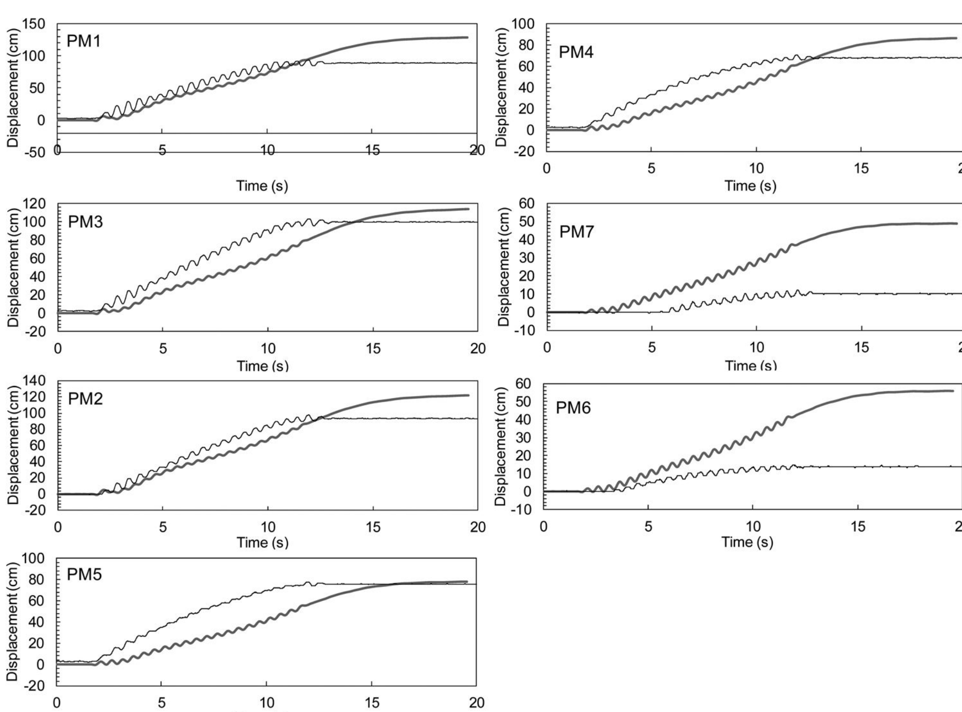

Figure D-22. Time histories of lateral displacement (Model D): Case 3-1 (UL-undrained).

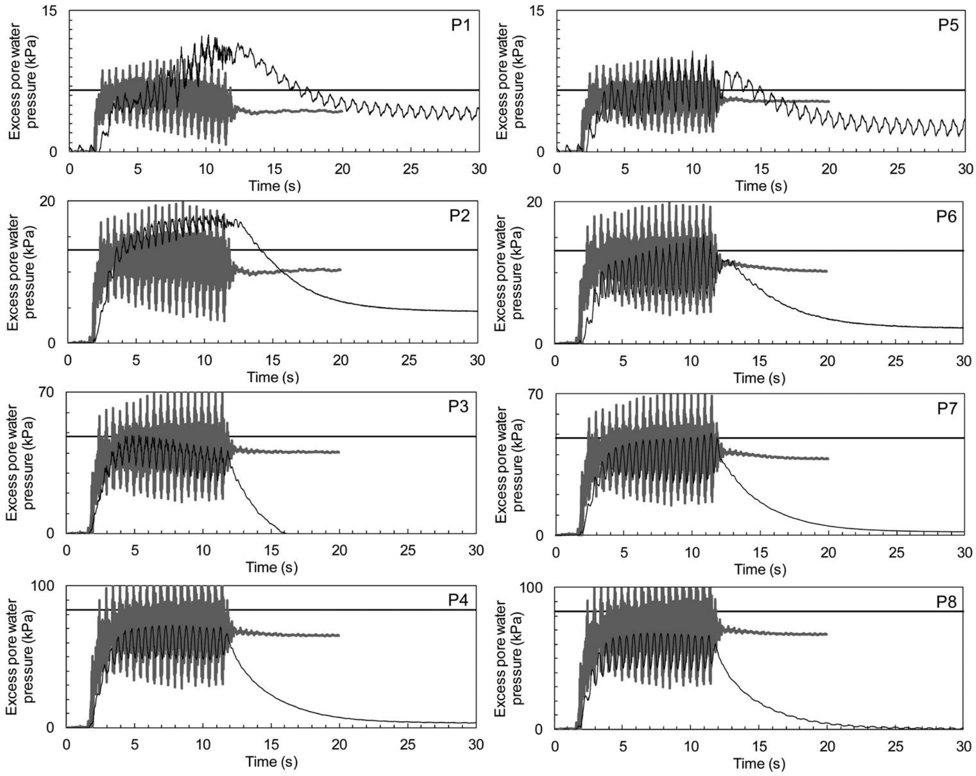

Figure D-23. Time histories of excess pore water pressure (Model D): Case 3-1 (UL-undrained).

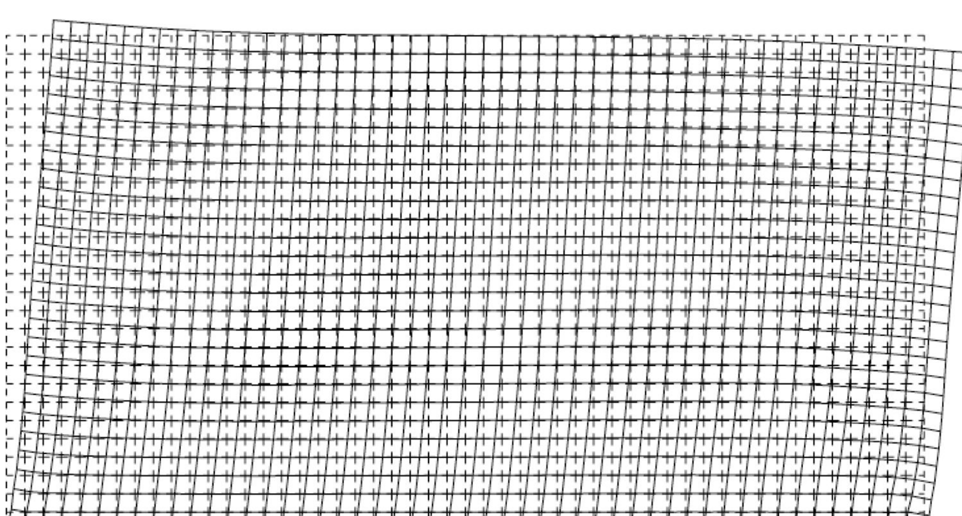

Figure D-24. Deformation after shaking (Model D): Case 3-1 (UL-undrained).

Workshop on guidelines and recommendations for local governments to mitigate flooding disasters

Geotechnics for Catastrophic Flooding Events – Iai (Ed)
© 2015 Taylor & Francis Group, London, ISBN 978-1-138-02709-1

Preparing 'Guidelines and Recommendations' for disaster mitigation – what is the lesson from recent flood and tsunami

K. Ichii
Hiroshima University, Hiroshima, Japan (TF 2 Leader of TC303)

ABSTRACT: TF2 in TC303 of ISSMGE have been working on the preparation of the 'Guidelines and Recommendations' for flood and tsunami disaster mitigation. For this purpose, a workshop is organized in GEDMAR 4th September 2014. This paper summarized the background and target of the activity. Then a brief summary of geotechnical engineers for tsunami hazard mitigation is summarized as a case study. The review of the case study clarifies the important viewpoints for the preparation of the 'Guidelines and Recommendations'. A sample image of the contents for the 'Guidelines and Recommendations' is also introduced.

1 INTRODUCTION

1.1 *Background: TC303 activity*

Technical Committee 303 (TC303) is organized in ISSMGE to discuss 'Coastal and River Disaster Mitigation and Rehabilitation' (short name 'Floods'). This activity started from 2009, and it belongs to the wider theme of 'Impact on Society'. Disasters such as tsunami in 2004 Sumatra earthquake in Indonesia, 2005 Hurricane Katrina in USA, and 2009 Typhoon Morakot in Taiwan are the background.

TC303 organized 3 task forces. Completion of a book, preparation of a guidelines and recommendations, organization of conferences are main target. This article is a review of the preparation process of the 'guidelines and recommendations', and a demonstration of a sample content.

1.2 *Target: Guidelines and Recommendations*

Tsunami disaster in 2004 Sumatra earthquake in Indonesia and flood disaster in 2005 Hurricane Katrina in USA, and 2009 Typhoon Morakot in Taiwan revealed the fragility of our society. These catastrophic disasters can happen at all over the world. The Great east-Japan Earthquake and Tsunami Disaster in 2011 is one of them.

One of the reasons why such miserable disasters never stop may be that we do not share our experiences enough. Researchers and scientist write technical papers to show their experiences to the world, and some well-trained engineers have chances to attend conferences or technical meeting to share the recent experiences, knowledge etc. However, the countermeasures against regional tsunami and flood hazard shall be discussed in the regional community, with the assistance of local engineers. The balance of the cost for countermeasures and the benefit by disaster mitigation efforts should be carefully discussed in the local community. In other word, the tsunami and flood hazard should be explained to the local people for effective implementation of countermeasures and development of adequate evacuation scheme in case of the disaster.

Thus, local government official, functionary of the local government, regional community managers should take the initiative for disaster mitigation. Sometimes, these leaders have a background of engineering (for example, in Japan, civil engineers in local government should play this role). However, these engineers are not specialized in geotechnical engineering but just having knowledge of civil engineering in general. Furthermore, in some other cases, these leaders may not have the background of engineering. Considering these situation, supplying a simplified guidelines and recommendations for the consideration of tsunami and flood disaster is quite important and effective to mitigate future disasters. This is the target of TF2 in TC303.

2 A CASE STUDY: EFFORTS TO MITIGATE TSUNAMI DISASTER

2.1 *Tsunami hazard map*

As an example of the important knowledge transfer, the author introduces some effort for tsunami disaster mitigation case in Japan.

The first step of the tsunami hazard mitigation is the preparation of a hazard map. Figure 1 is an example of tsunami hazard map (Kochi Prefecture). This is not the latest version of the maps, but it was opened for public from Kochi Prefecture several years ago. The maps were prepared for 2 cases: one was the case when embankments, floodgates or other coastal protection structures do not work and the other was the case when these structures work well. It can be said that these were the best case and the worst case. The reason why they prepare these 2 types of hazard maps

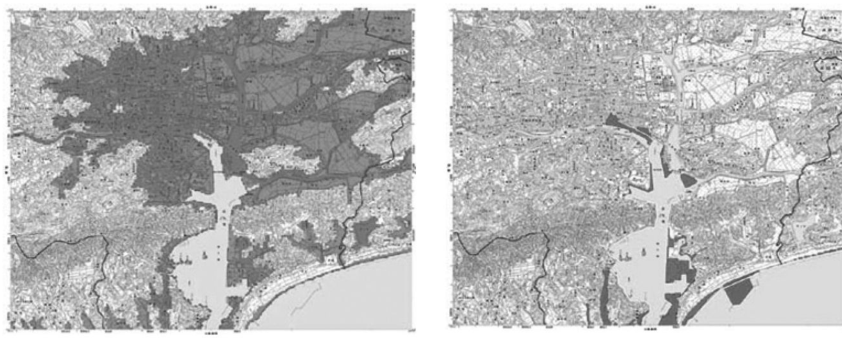

(a) The case when embankments, floodgates, etc. do not work

(b) …..work well…

Figure 1. An example of published tsunami hazard maps (Kochi Prefecture).

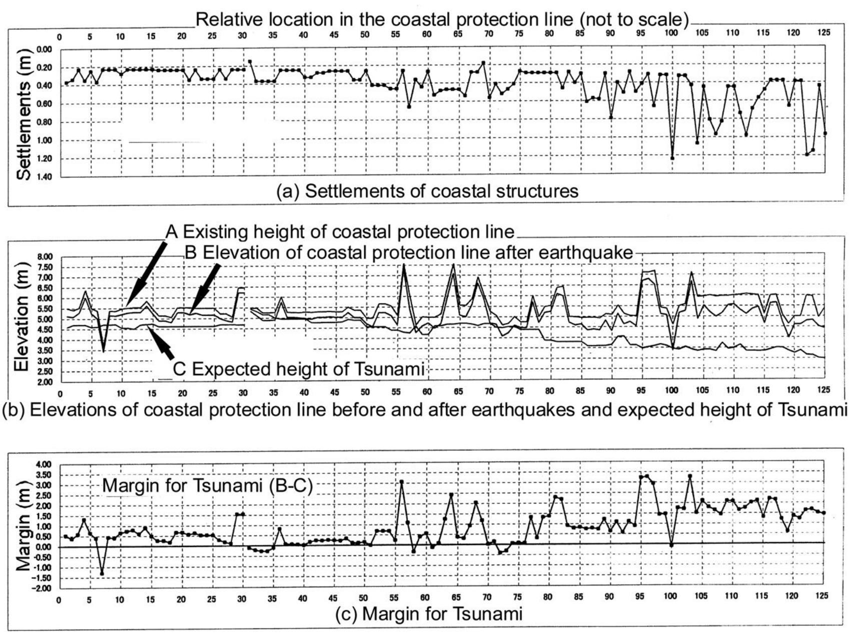

Figure 2. An example of seismic performance evaluation along a coast line (Osaka Prefecture).

was that they did not know the seismic performance of coastal structures. Another reason which I suppose is as follows. The real situation was close to the worst case shown in the left hand side in Figure 1. If we pay more efforts on seismic performance evaluation and improvements, the situation could turn into the better case (closer to the best case shown in the right hand side). In other word, the left side figure was the anticipated situation to realize the necessity of the countermeasures, and the right side figure was the target to be accomplished by engineers.

2.2 *Effort of geotechnical engineers to mitigate tsunami disaster*

As a duty for geotechnical engineers, clarification of the seismic performance of coastal structures should be done. Figure 2 is an example (Osaka Prefecture). This is the seismic performance evaluation results of sea side structures along a coastal line of Osaka Prefecture. In this area, total 125 types of structures locate in the coast line of 70km. For each structure, settlement induced by the anticipated ground motion was evaluated (Figure 2(a)). Then subtracting the evaluated settlement from the height of the structure (A in Figure 2(b)), the residual height of the coastal structure could be evaluated (B in Figure 2(b)). Comparing the residual height (B in Figure 2(b)) and the anticipated tsunami height announced by Japanese government (C in Figure 2(b)), the margin for tsunami (Figure 2(c)) could be evaluated. In the case shown in Figure 2, there were no margin at about 7 parts, and more detailed investigations or countermeasures were necessary for these parts.

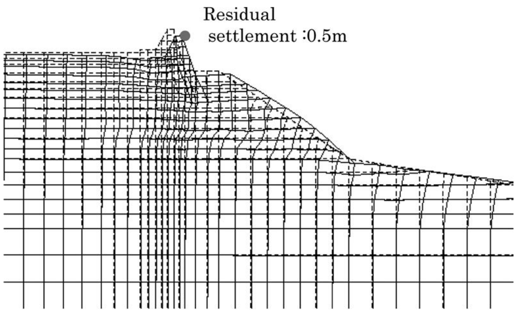

Figure 3. An example of FEM analysis results.

Figure 3. An example of FEM analysis results.

The evaluation of the settlement shown in Figure 2 was done by referring the summary of FEM parametric studies. An example of FEM analysis result is shown in Figure 3. The settlement at the crest can be evaluated. The applicability of the FEM program for coastal structures was confirmed by the comparison with case histories and model test results. An example of the model test results is shown in Figure 4. The concept of the analysis is published in many literatures (i.e. Iai et al., 1999).

But it was not cost effective to build FEM model for each site. Furthermore, such an advanced method is not appropriate for the regional leaders for disaster mitigation who sometimes have no background of engineering education.

In this sense, a simple but cost effective system to evaluate the settlement of coastal structures is expected. One of the effective approaches is referring the summary of FEM parametric studies (Ichii and Donahue, 2004). Recently, computer software is extremely improved, and even a complicated engineering calculation can be done in common software such as Microsoft Excel. For example, 1-D seismic response analysis with equivalent-linear method can be done in Microsoft Excel (Bardet, et al., 2000). Such effort to provide user friendly environment for advanced analysis may be very effective to improve our approach in disaster mitigation.

After the assessment of seismic performance of coastal structures, seismic retrofit at weak points shall be done. Sometimes, huge breakwaters are constructed to mitigate the expected tsunami height. Figure 5 is an example of breakwater against tsunami. The seismic retrofit including the improvement of the foundation layer and the construction of facilities for disaster mitigation are part of the duty of geotechnical engineers.

2.3 *The damage beyond our imagination*

The 2011 Great East Japan Earthquake (Mw = 9.0) was a huge scale earthquake, and it causes significant tsunami disaster. The observed tsunami height was larger than the prior expected one.

As the result of unexpected height of the tsunami, the observed tsunami inundation was far beyond the area given in the prior imagination. Figure 5 shows

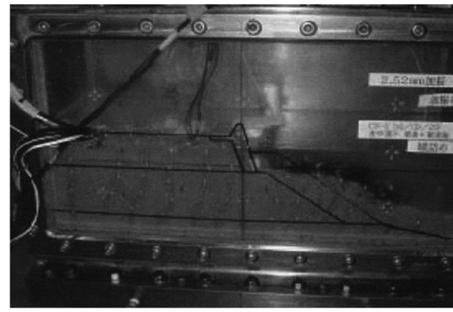

Figure 4. An example of centrifuge model.

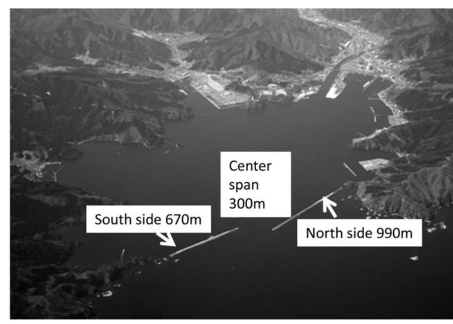

Figure 5. Kamaishi Port Gate Breakwaters. (Kamaishi Port Office).

the comparison between the tsunami inundation areas shown in the hazard maps and observed in the reality. The reality was quite severe than our prior imagination. As the result of this discrepancy between our preparation and the reality, many people died.

In addition to the people who could not evacuate, some people did not try the evacuation, I suppose. The reason why they did not evacuate may be as follows.

'I did not imagine the tsunami comes to my place where is far from the coast'

'I believed the breakwaters and sea walls made us safety enough'

These comments are fictions. I did not conduct interviews actually. But from the broadcasted interview reports on TV to the people who were really in danger, I have heard similar comments several times. And similar comments can be found in the discussions related to the failure of Fukushima Nuclear Power Plant. Note due to the limited information opened for public, the discussion related to the Nuclear Power Plant failure is skipped in this paper. However, as a philosophical issue, similar problems may be there.

3 OUTREACH: SAFETY AND RELIEF

3.1 *Cycles between safety and relief*

The expectation for the engineers from the society is to build a safety society and to give relief to the people. However, the facts observed in the 2011 Great East-Japan Earthquake and Tsunami Disaster remind us that

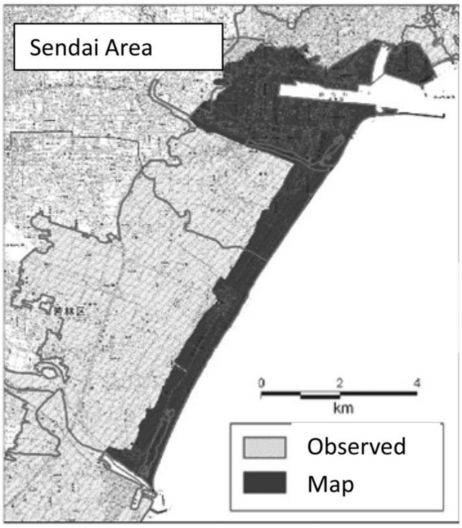

Figure 6. Tsunami inundation areas observed in reality and shown in the hazard maps. (Cabinet Office, 2011).

to build the safe and relief society is quite difficult. In short, the relieved people may not evacuate in case of the disaster, and the damage is easily increased. From the abovementioned discussion, what we learned are as follows.

a) The hazard in reality can be far beyond our expectation.
b) Publication of hazard maps or constructions of breakwaters as countermeasures were believed to be effective to mitigate tsunami disaster. However, these efforts not only give the society the feeling of relief, but also restrain the people from evacuating. Therefore, once the real hazard is severer than our expectation, the damage could be magnified.

The author thinks that these two points are related to the relationships between 'safety' and 'relief'. In these years, 'Safety and relief' has been a kind of buzz word in Japanese public administration and Japanese civil engineering industry. Many politicians appeal the activity to guarantee 'safety and relief' of the society. Many projects have been put into practice to build safety society and to give a relief to people.

The relationship between 'safety' and 'relief' can be schematically illustrated as shown in Figure 7. Safety can be established by preparation of countermeasures. And with the acknowledgement of the effect of countermeasures, relief to the people is realized. However, once the people get the relief, they lose the concern about the danger. The situation without consciousness of danger is a really unsafe condition. Therefore, we engineers should work hard for the edification of people. In a sense, this edification is a kind of agitation to make the people request countermeasures. Anyway, as the result of edification, they feel uneasiness and request the countermeasures. Thus, civil engineering project to provide safe society can be conducted based

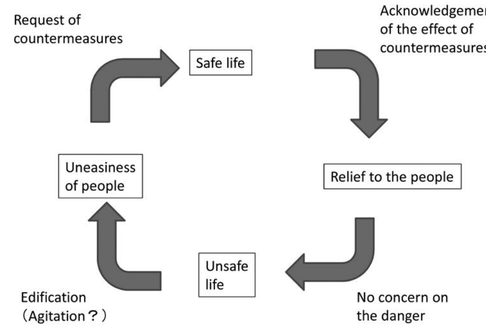

Figure 7. The possible relationship between 'safety' and 'relief'.

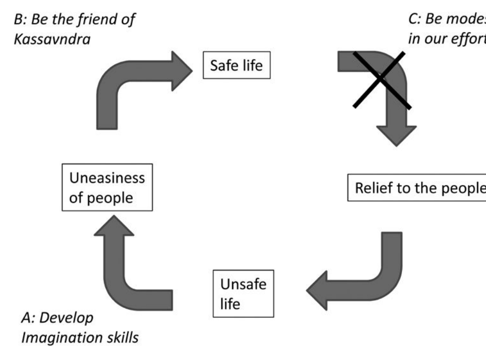

Figure 8. How can we stop the endless cycle?

on the request of people. This is a kind of endless cycle, and it will not ensure the safety for us.

3.2 *How to stop the endless cycle*

Considering the cycle shown in Figure 7, what we should learn from the experience to stop the cycle. It is summarized in Figure 8. There are 3 main lessons.

A) Develop imagination skills

We need to develop more imagination skills. In a sense, we did not recognize it before the earthquake that the people were too much relieved and were in unsafe condition. We engineers were also too much relieved considering our behavior which tends to choose safer side in practice. This was really because of the shortage of imagination.

B) Be the friend of Kassavndra

Kassavndra is a female prophet in Troy. Her prediction was right, but nobody believed. In general, people would not want to face the possibility of un-happy event, and they never believe these un-happy stories until it really happened. In short, we often neglect not-so-happy story and regard the person who told the story as a kind of Kassavndra. However, we need to be a friend of Kassavndra, and learn how to adapt to the story.

C) Be modest in our efforts

We often pride ourselves on our effort to the society. Especially for the effort to build safe society, the

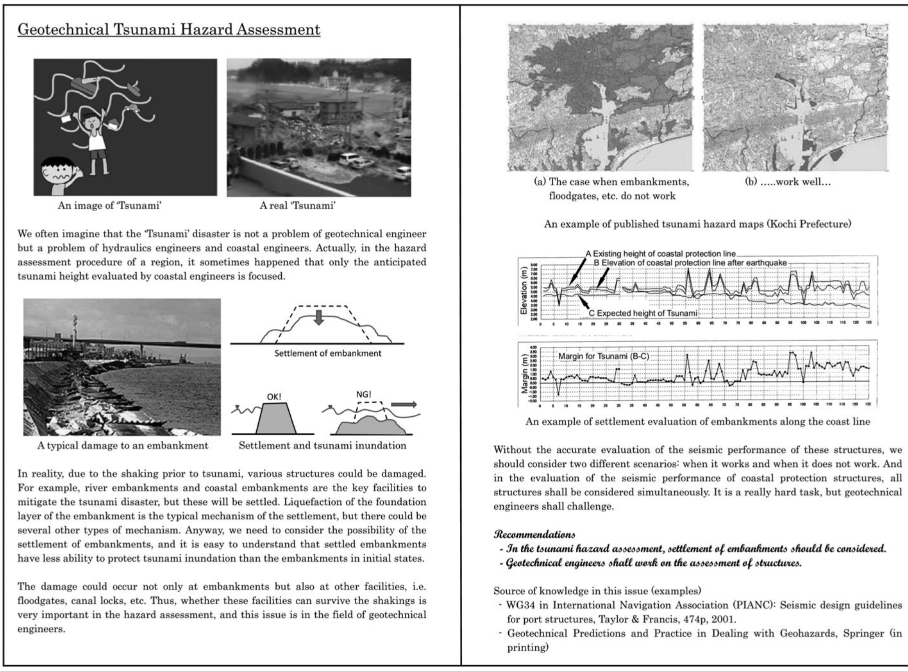

Geotechnical Tsunami Hazard Assessment

An image of 'Tsunami'   A real 'Tsunami'

We often imagine that the 'Tsunami' disaster is not a problem of geotechnical engineer but a problem of hydraulics engineers and coastal engineers. Actually, in the hazard assessment procedure of a region, it sometimes happened that only the anticipated tsunami height evaluated by coastal engineers is focused.

A typical damage to an embankment   Settlement and tsunami inundation

In reality, due to the shaking prior to tsunami, various structures could be damaged. For example, river embankments and coastal embankments are the key facilities to mitigate the tsunami disaster, but these will be settled. Liquefaction of the foundation layer of the embankment is the typical mechanism of the settlement, but there could be several other types of mechanism. Anyway, we need to consider the possibility of the settlement of embankments, and it is easy to understand that settled embankments have less ability to protect tsunami inundation than the embankments in initial states.

The damage could occur not only at embankments but also at other facilities, i.e. floodgates, canal locks, etc. Thus, whether these facilities can survive the shakings is very important in the hazard assessment, and this issue is in the field of geotechnical engineers.

(a) The case when embankments, floodgates, etc. do not work   (b) .....work well...

An example of published tsunami hazard maps (Kochi Prefecture)

An example of settlement evaluation of embankments along the coast line

Without the accurate evaluation of the seismic performance of these structures, we should consider two different scenarios: when it works and when it does not work. And in the evaluation of the seismic performance of coastal protection structures, all structures shall be considered simultaneously. It is a really hard task, but geotechnical engineers shall challenge.

Recommendations
- ***In the tsunami hazard assessment, settlement of embankments should be considered.***
- ***Geotechnical engineers shall work on the assessment of structures.***

Source of knowledge in this issue (examples)
- WG34 in International Navigation Association (PIANC): Seismic design guidelines for port structures, Taylor & Francis, 474p, 2001.
- Geotechnical Predictions and Practice in Dealing with Geohazards, Springer (in printing)

Figure 9. Image of the 2 pages formatted content in the 'Guidelines and Recommendation'.

appeals of our efforts contribute to the relief of people. However, in a sense, our efforts are overevaluated by the people, and their relief amplified the disaster. This is really an unexpected situation. We should be more modest. This is especially a severe issue in the discussion related to the failure of nuclear power plant.

3.3 *Outreach and communication*

Based on the three lessons mentioned above, the concept necessary for the 'Guidelines and Recommendation' can be as follows.

– Imagination skill for future disaster

  We need to have the ability to assess the possibility of future disaster. This may be done by sharing the tragic case histories occurred in the world. A brief summary of wide variety of disasters should be included.

– Scientific approach

  Imagination skill will give us possible not-so-happy stories. But some of them cannot occur (or rarely occur) in reality due to the difference in regional background. Understanding of the mechanism of disaster is important, and it shall be done in scientific way. Scientific background enables us to hear the not-so-happy story from Kassavndra.

– Probabilistic approach

  Imagination skill will give us possible not-so-happy stories. We need to face the possibility of these worst scenarios, however, adequate recognition of the possibility of these worst scenarios are also important. Otherwise, we cannot give the priority for our behaviors (i.e. implementation of countermeasures or not). These things should be done in probabilistic way. Probabilistic (reliability) evaluation of engineer's effort is quite reasonable.

– Outreach

  The 'Guidelines and Recommendation' should be used many places. Thus, it would be better to compile and publish as a brief but free guidebook (i.e. free downloadable PDFs). In this case, it can be used in the seminar or class for beginners.

3.4 *Image of 'Guidelines and Recommendation'*

Since our experiences of disaster and knowledge on disaster mitigation will increase continuously, the 'Guidelines and Recommendation' cannot be the perfect. It can be improved step by step. Therefore, preparation of the first trial version is anyway important.

In order to enable the step-by-step improvement of the document, 2 pages style format is considered. The contents should be divided into 4 categories: Case histories, Activities prior to the event (preparation), Activities during the event (emergency response), and Activities after the event (restoration work). All the content should be summarized in 2 figures, concrete recommendation and references.

Figure 9 is an example image for tsunami hazard mitigation explained in this paper. Similar types of contents are now coming to TF2, such as the emergency repair work by soil bags for the boiling damage to river embankment in flood case. TF2 is waiting for your contributions.

4 CONCLUSIONS

In this paper, a brief summary of geotechnical engineers for tsunami hazard mitigation is summarized as a case study. Then, important viewpoints for the preparation of the 'Guidelines and Recommendations' as the activity of TF" in TC303 of ISSMGE were clarified. A sample image of the contents is also introduced, and TF2 is waiting for contributions from various people.

ACKNOWLEDGEMENT

The authors would like to thank contributors for TF2 activities and support from TC303 members. The author also thanks to financial supported by FLIP Consortium, JSPS KAKENHI Grant Number 23310119 and 25420505.

REFERENCES

Bardet, J.P., Ichii, K. and Lin, C.H., 2000, EERA, A Computer Program for Equivalent Linear Earthquake Site Response Analysis, Dept. of Civil Eng, University of Southern California, USA.

Cabinet Office, 2011, White Paper on Disaster management 2011, Government of Japan. (in Japanese with English executive summary on the website) http://www.bousai.go.jp/hakusho/h23/index.htm, (downloaded on September, 2011)

Iai, S., Ichii, K., Liu, H. and Morita, T. (1998) 'Effective stress analysis of port structures', Special Issue of Soils and Foundations, Japanese Geotechnical Society, pp. 97–114.

Ichii, K. and Donahue, M. J. (2005) 'Evaluation of sea dike settlement due to sesmic shaking prior to tsunami attack', Solutions to Coastal Disasters 2005, ASCE, pp. 616–629.

Kamaishi Port Office: http://www.pa.thr.milt.go.jp/kamaishi/bousai/b01_03.html (in Japanese) (downloaded on September, 2011)

Kochi Prefecture: Website of Kochi prefecture in a past time. (The latest version can be found at http://www.pref.kochi.lg.jp/soshiki/010201/tunamisinsuiyosoku.html) (in Japanese)

Osaka Prefecture: Non-published information related to the committee of disaster prevention along the coastal line.

Geotechnics for Catastrophic Flooding Events – Iai (Ed)
© 2015 Taylor & Francis Group, London, ISBN 978-1-138-02709-1

Geotechnical lesson and application on earth bank for tsunami disaster prevention

Ken-ichi Tokida
Graduate School of Engineering, Osaka University, Suita, Japan

ABSTRACT: In the 2011 Off the Pacific Coast of Tohoku Earthquake in Japan, many sea walls along the seacoast were damaged by the tsunami overflow destructively. However, based on the field survey by the authors, it could be found that there were earth banks which were damaged slightly by the tsunami flood. In this paper, for verifying the reasons why the earth banks are tough against the tsunami overflow are discussed through the waterway overflow test and simplified permeability one. From the experimental results, the hardly-permeability of soils and banks can be clarified and the design concepts to apply the earth banks as the multiple defense for the tsunami disaster prevention are proposed from the geotechnical engineering views.

1 INTRODUCTION

Many infrastructures such as seawalls, river dikes etc. were damaged destructively by the tsunami overflow caused by the 2011 Off the Pacific Coast of Tohoku Earthquake (2011 Earthquake, and so on) in Japan. However, based on the field survey after the above earthquake, the authors could found several earth banks which were damaged and/or eroded slightly and deterred the tsunami flood along the coastal areas at Sendai Plain in Miyagi Prefecture. This finding will be very important to discuss the earth banks as the effective measures against the tsunami disaster.

On the other hand, in general, the earth bank can be indicated to have several advantages of economy, inspection, repair, preservation of environment and utilization of space comparing with the existing sea walls. Then the earth banks are expected to be the effective measures against the tsunami in the future.

However, the reasons why the earth banks are tough against the tsunami flood haven't been clarified enough, and then the practical and effective utilization of the earth banks as the sea walls against the tsunami is not going smoothly at present.

In this paper, the examples of the earth banks which give us hints on the toughness of earth banks in the above field survey and the several lessons obtained are introduced (Tokida and Tanimoto, 2012). Then, in order to know the fundamental characteristics and the improving method of earth banks against the tsunami overflow, the channel overflow simulation tests are conducted. Furthermore, assumed that the toughness of the earth banks against the tsunami overflow is due to the hardly-permeability of the overflow water into the earth banks, the permeable characteristics of soils under the water pressure are investigated with use of the simplified test device. Finally, the design concepts to apply the earth banks as the sea walls and one of functions of the multiple defenses for the tsunami disaster prevention in the future are discussed from the geotechnical engineering views.

2 DAMAGE OF EARTH BANK AND LESSONS

2.1 *Example damaged slightly by tsunami overflow*

Photo 1 is the satellite view around the river dyke newly constructed about 2 years ago before the 2011 Earthquake to heighten the existing low river dyke of Teizan Canal at Idoura in Sendai City. The new dyke was about 3.9 m high and 1.5 km long and located around the marsh whose width is about 200 m. The overflow depth at the crest of the dyke and the maximum overflow duration time are assumed to be about 3.85 m and 25 minutes based on the tsunami height measurement (Shibayama etc., 2011) and tidal wave meter record (Takahashi etc., 2011), respectively.

Photo 1. Aerial view around the river dyke damaged slightly at Idoura in Sendai City.

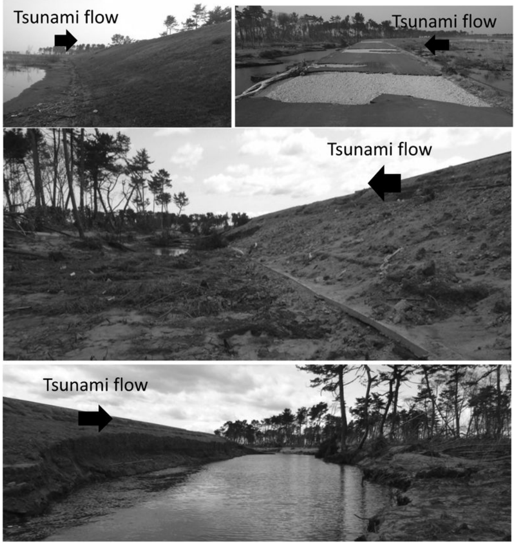

Photo 2. Earth river dyke at Idoura after the tsunami on 30 April, 2011. (Upper-left: front slope, upper-right: crest, middle: back slope without dug pool, lower: back slope with dug pool).

Photo 2 shows the state after the tsunami overflow focused on the front, crest and back of the dyke. The arrow in Photo 2 shows the direction of the leading wave. These photos hint very important lessons for the future measures against the tsunami flood.

The upper-left photo shows that the lawn planted at the front slope surface wasn't almost eroded. The upper-right one shows the crest of the levee which is paved with asphalt of 0.1 m thick. Though the asphalt is partially removed, the levee remained functioning. The middle and lower ones show the eroded condition at the back slope and toe of the river dyke without and with the water pool, respectively. It can be known clearly that the erosion at the back side of the levee is more severe than that at the front one and crest, however the erosion seems to be limited at the surface which will be related to the later discussion.

At this point, the water pool made by the flood stream named 'dug pool' in this paper and the slope failure in the Photo 2 can be considered to be slight damage keeping the dyke function from the geotechnical engineering views which will be discussed later.

Furthermore, it can be known that forest reserve located at the back side of the dyke with the dug pool was not flown away severely, which indicates that the dug pool may reduce the acting force on the structures. However the effective function of the dug pool against the tsunami flow is very interesting, it can be referred in the other discussion (Tanimoto and Tokida, 2012).

2.2 *Example deterring tsunami flood*

At the sand beach located in the east side of the Yuriage Fishing Port, the sand bank was found in the field survey on July 9, 2011. The upper in Photo 3 by the Japan Coast Guard (2011) shows the artificial bank covered with the geosynthetics sheet just attacked by the tsunami. The lower-left photo shows the macrograph of the bank, this bank is approxiately 5.6 m high and 150 m long, the crest is approximately 24 m wide, and the front slope at the sea side is approximately 1: 2.7. The overflow depth at the crest of the bank was estimated to be about 0.5 m.

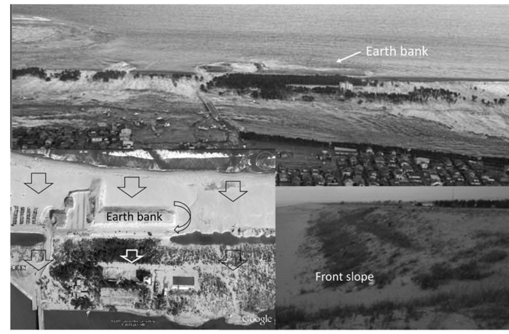

Photo 3. Artificial earth bank on the beach to deter the tsunami flood. (Upper: just attacking, lower left: macrograph around bank after tsunami, lower right: front slope after tsunami on July 9, 2011).

This example indicates remarkably that the tsunami wave at the front of the bank almost stopped and was forced to go around the bank, and the forest reserve at the back side of the bank was defensed. Furthermore, the lower-right one in Photo 3 shows the slightly eroded front slope similar to Photo 2.

As shown above, this example gives us the important lesson that the earth bank can deter the tsunami flood when the height is enough against the tsunami height which will be hinted for the later discussion on the design concept of the measures against tsunami.

2.3 *Example eroded slightly by tsunami flow*

The artificially made high bank was found at Wakabayashi Area in Sendai City shown in Photo 4. This high bank was constructed as a public ground for an adventure play named Boken Plaza and located at approximately 350 m from the coastal line. The bank is shaped like a ship and is approximately 400 m long and 80 m wide. The top of the bank is located in the sea side direction and the bank is sloped to the west. The height of the bank is 15.89 m and the estimated flooded depth by the authors is 10.55 m (Tokida and Tanimoto, 2012).

From the geotechnical engineering views, when the stability of the high bank is concerned, the erosion and/or failure of the bank should be considered. The lower-left and right photos show the eroded conditions at the side and front of the bank after the tsunami, respectively. The slopes of the earth bank surface are 1: 4–1: 5.

As shown above, it can emphasize that the earth bank which may be planted is difficult to be eroded by the tsunami flood flow with the depth of about 10 m

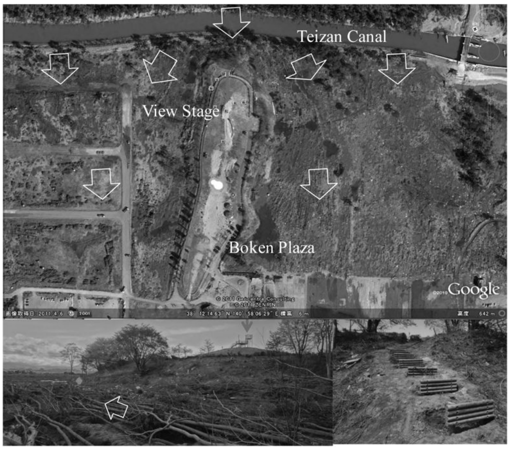

Photo 4. Artificial earth bank after tsunami slightly eroded at the front and sides by the tsunami flood flow. (Upper: aerial vies around bank, lower left: side view, lower right: step eroded at the front of bank on May 2, 2011).

and the duration time of about 30 minutes. In other words, there aren't fatal problems on the erosion and sliding failure of the earth bank against the tsunami flood from the geotechnical engineering views, whose reasons will be discussed later.

3 WAERWAY OVERFLOW TEST ON EROSION AND IMPROVEMENT OF EARTH BANK

The hardly erosive and permeable functions of the earth bank and their improving methods are investigated and discussed through the waterway overflow tests on the earth bank models by Tokida etc. (2014).

3.1 *Tests conditions*

As shown in Photo 5, the waterway is 55 m long and 1 m wide, and the heaved water flows over the earth bank model. The fundamental shape of the earth bank model prepared is 8 cm high, 14 cm wide at the crest, 46 cm wide at the base and the slope rate is 1:2. Fig. 1 shows 5 cases of the earth bank models which are fundamental models of Case 1 (Dry) and Case 2 (Wet) and the reinforced models of Case 3 (Wet, whole geosynthetics), Case 4 (Dry, partial geosynthetics) and Case 5 (Dry, crest plate).

The soil materials are silt sand and the over 2 mm grain-size particles are excluded. The mean particle size is 0.55 mm, optimum water content is 11.4% and maximum dry density is 1.98 g/cm^3. The wet condition of the water content of 12.0∼13.0% is the dry density, saturated coefficient of permeability and porosity are 1.90 g/cm^3, 1.86×10^{-5} cm/s and 0.340, respectively. The dry condition of the water content of 4.6∼6.7% is 1.71 g/cm^3, 2.35×10^{-4} cm/s and 0.266, respectively.

The inputted water depth at the front of the bank models is 11.1∼11.6 cm and the duration time of the first wave and second one overflowing the earth bank models is 17.20∼20.31 seconds.

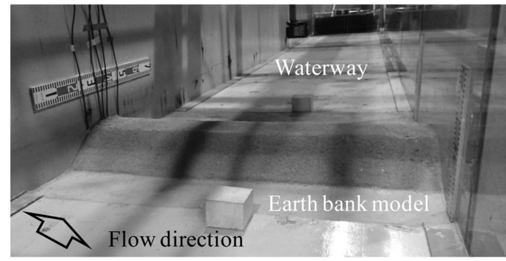

Photo 5. Overview of waterway and bank model.

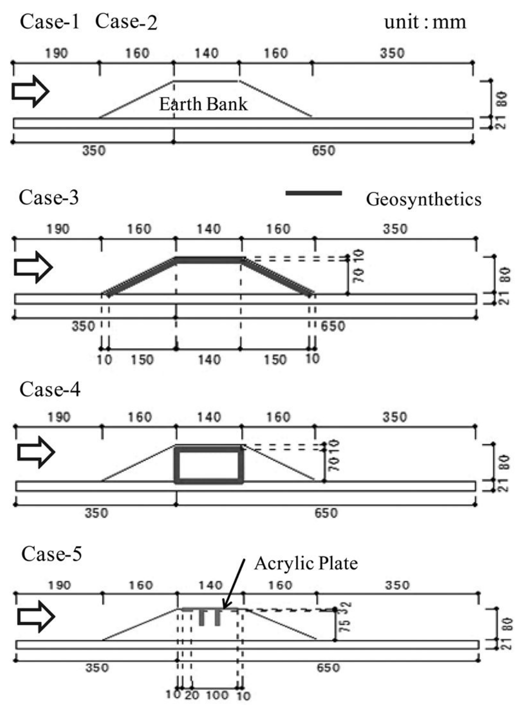

Figure 1. Fundamental and reinforced earth bank models of Case-1 and Case-2 not-reinforced and Case-3 to Case-5 reinforced.

3.2 *Typical tests results*

Photo 6 shows the state of earth bank model after the overflow and it can be found that the earth bank model begins to be eroded at the back toe and enlarged to back slope and crest. On the other hand, the front slope is eroded slightly. This result could be observed at the existing earth bank shown in Photo 2. Then it can be known that it's necessary to pay attention to the back slope and the base ground around the back toe for the effective measures.

The areas of the earth bank models before the overflow with that after one are measured with use of the laser sensor, and the measured results are summarized in Table 1.

Photos 7 and 8 show the eroded section reinforced by the geosynthetics sheet covered wholly in Case-3 and partially under the crest in Case-4, respectively.

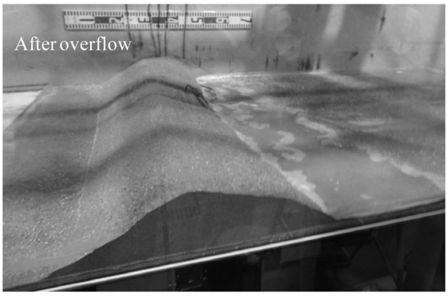

Photo 6. Earth bank model after overflow in Case-1.

Table 1. Rate of erosion of earth bank model by overflow.

Test Case	Front Slope Ratio/ Back Slope Ratio/ Soil Condition	Rate of Erosion (%)			
		Total	Front Slope	Crest	Back Slope
Case-1	1:2 / 1:2 / Dry	36.5	1.7	14.7	20.1
Case-2	1:2 / 1:2 / Wet	17.0	0.8	5.1	11.1
Case-3	1:2 / 1:2 / Wet	12.7	0.9	6.1	5.7
Case-4	1:2 / 1:2 / Dry	20.6	1.2	4.1	15.3
Case-5	1:2 / 1:2 / Dry	17.5	1.4	0.7	15.4

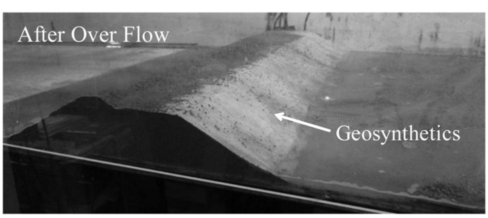

Photo 7. Reinforced earth bank after overflow in Case-3.

Photo 8. Reinforced earth bank after overflow in Case-4.

Based on Case-3, it can be learned that only the surface above the reinforced body with the geosynthetics is eroded in the low eroded ratio of 12.7%. On the other hand, based on Case-4 under the dry condition, it can be learned that the reinforced body is difficult to be eroded and enlarged with the eroded ratio of 20.6% smaller than that of 36.5% in Case-1 unreinforced under the dry condition.

From the above results, it can be learned that the reinforcement with the geosynthetics sheet is very effective to reduce the erosion and can control the eroded area.

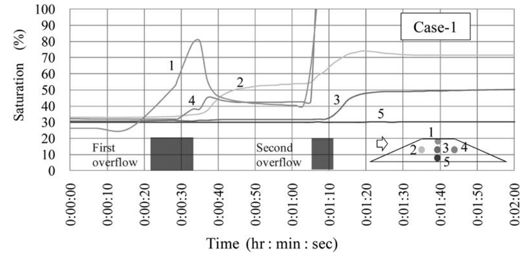

Figure 2. Time history of degree of saturation in bank: Case-1.

The permeable behavior of the first and second overflow water into the earth bank body is investigate with the water ratio meters set in the bank. The time history of the degree of saturation calculated from each water ratio meter is shown in Fig. 2, representatively. As for Case-1 under the dry condition in Fig. 2, the water saturation at the upper water ratio meter (No. 1) increases largely during the first overflow and the water saturation at the No. 4 meter and No. 2 one are followed to increase however the other two ones are not changed largely. Furthermore, during the second overflow, the seepage can be observed at 4 meters without No. 5 meter.

Summarized the above results including Case-2 to Case-5, it can be learned that the earth bank model, especially under the dry condition is difficult to be permeated and the water can be prevented not to permeate into the earth bank body with use of the geosynthetics sheet set wholly or partially in the earth bank body and the plate without permeability on the crest.

The followings can be obtained through the waterway overflow tests.

1) It can be confirmed that the earth bank begins to be eroded from the back slope, spreading to the crest and front slope gradually, which was lessoned from the actual earth bank in Chapter 2.
2) However the duration time of the water overflow is short in this waterway tests, the possibility of the hardly-permeability of the earth bank which is compacted adequately or reinforced with the geosynthetics can be obtained.
3) The reinforcement with use of the geosynthetics sheets set inside of the earth bank body (Case-3 and Case-4) and the cover plate at the crest (Case-5) can be shown to be very effective to reduce and/or control the erosion of the earth bank.

The above subjects on the waterway test conditions which are a little different from that at the field will be discussed in the following Chapter 4.

4 MODEL TESTS ON PEARMEABILITY OF SOILS UNDER WATER PRESSURE HEAD

The reasons why the earth bank is tough against the tsunami overflow observe in some examples shown in Chapter 2 is discussed through the simplified test device in this Chapter. The details on the experimental

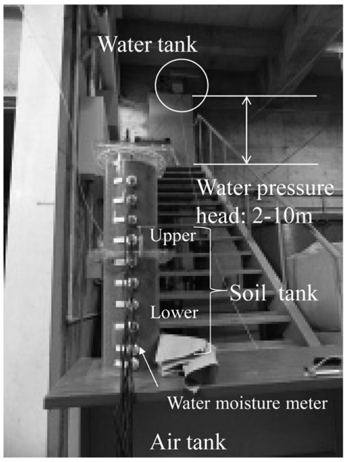

Photo 9. View of experimental device prepared.

methods and results is referred in the paper by Shimakawa etc. (2014).

4.1 *Lessons from experimental results*

Experimental conditions is referred to the site conditions of the river dyke at Idoura shown in Photo 1 introduced in Chapter 2. For this study, the simplified experimental device is prepared combining with the water tank to supply the water head, upper and lower soil tanks to model the earth bank surface of 0.75 cm thick and air tank to simulate the pore air in the soil body deeper than 0.75 m shown in Photo 9. The water pressure head loaded on the upper surface of soil layer is set modeling the actual water overflow depth of 2 m to 10 m and the overflow duration time of 30–60 minutes.

Typical relationship between the water permeable depth and the water traveling time of 0 to 60 minutes is summarized in Fig. 3. The fitted curves put down in Fig. 3 are drown assuming that the water permeable depth is in proportion to the square root of the water permeable time except for Cases 11 and 12 where the water permeates into the lower soil tank.

The interesting lessons obtained from the above tests can be summarized as follows.

1) The simplified test device combined with three tanks and the soil moisture meters can simulate the actual conditions such as the water pressure head level of 2 m to 10 m, the earth bank height of 4 m and the tsunami overflow duration time of 30–60 minutes.
2) The water permeation depth is in proportion to the square root of the water permeable time and trends to be increased according to the increase of the water permeation duration time and the water pressure head level, however which influence a little.
3) In case of the water pressure head level of 2 m and 10 m under the degree of saturation of 35%, the water permeable depth is only about 20 cm and 35 cm, respectively at the permeable duration time of 30 minutes.
4) The air tank condition of CLOSE or OPEN influence a little because of the hardly-permeability of soils.
5) The initial degree of saturation of soils influence a little largely on the water permeable depth. The water permeable depth measured under the initial saturation of around 35%, 45% and 65% is 25 cm, 45 cm and 58 cm, respectively at the permeable duration time of 30 minutes.
6) The enclosed pore air pressure occurred by the water permeability into the soil layer is very small.
7) The degree of saturation at the water permeated zone increases from the initial 35% to about 70 to 80%, which indicates that the water is permeable under the degree of saturation of 100%.

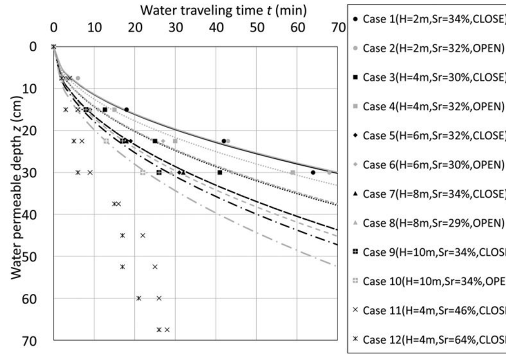

Figure 3. Relationship between water permeable depth and water traveling time in Case 1 to Case 12.

The above results indicate the hardly-permeability of the soils compacted adequately against the pressured water head.

4.1.1 *Modeling of water permeable depth*

For investigating the stability of the earth banks against the tsunami overflow, the water permeable depth is tried to be modeled considering the water pressure head level and the degree of saturation of the earth bank body.

Based on the experimental results on the water permeable depth for the initial degree of saturation of 35% at the permeable duration time of 30 minutes, the relationship modeled in Fig. 4 is proposed.

5 ESTIMATION OF STABILITY OF RIVER DYKE AT IDOURA

Applying the experimental results in Chapter 4, the reason why the river dyke damaged slightly shown in Chapter 2 is discussed as follows in the paper by Shimakawa etc. (2014).

As shown in Chapter 4, the degree of saturation of the earth bank before the tsunami is important. Because not only the river dyke body locates above

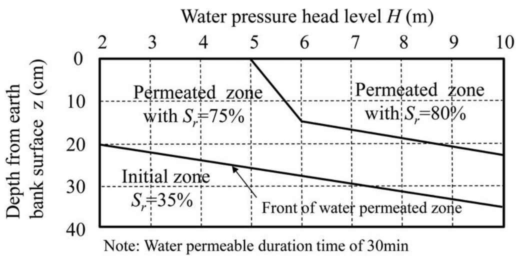

Figure 4. Modeling of water permeable depth considered water pressure head level and the degree of saturation of the earth bank body at permeable duration time of 30 minutes.

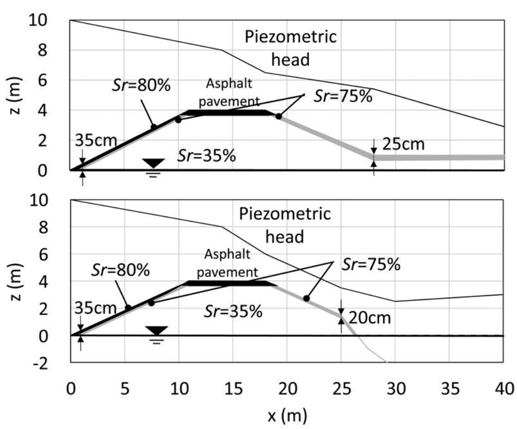

Figure 5. Estimated permeated state of river dyke just after tsunami overflow (Upper: Case 1, lower: Case 2).

the ground water but also it hadn't been rain for 2 months half before the tsunami, the degree of saturation of river dyke body is estimated to be very low, for example, 35% less than 45% in this case study. Furthermore, because the river dyke was constructed about 2 years before the tsunami, it may be compacted adequately and low permeable similar to the experimental conditions of soils in Chapter 4.

Applied the relation in Fig. 4 to the river dyke at Idoura in Photo 1, the water permeated state of the river dyke just after the tsunami overflow estimated can be shown in Fig. 5 where the upper and the lower show the states of Case 1 without the dug pool and Case 2 with the dug pool.

Shown in Fig. 5, the water permeated depth at the front slope and back one of the river dyke surface are assumed under the water pressure head of 10 m and 2 m or 4 m, respectively because the degree of saturation at the front slope and back one are assumed to be 75% and/or 80%, and 75%, respectively.

Considered the above results, it can be concluded that because the permeated zone whose shear strength is afraid to be decreased is very shallow compared with the river dyke height of 4 m, the sliding stability of the dyke overflown by the tsunami flood may be almost sustained. This is one of the reasons why the river dyke at Idoura shown in Photo 1 wasn't failed severely.

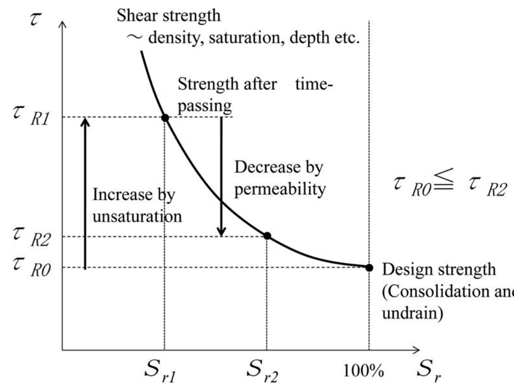

Figure 6. Concept on relationship between design shear strength and its change induced by the decrease of degree of saturation.

6 DISCUSSION ON MECHANIZM OF EROSION AND STABILITY OF EARTH BANK

Although typical two types of damages of the river dyke: sliding failure and erosion are hinted in Chapter 2 and the former is discussed in Chapter 5, the latter is also discussed as follows.

Firstly, because the shear strength of soils decreases by the change of degree of saturation, the concept on the relationship between the design shear strength before the tsunami overflow and its change induced by the water permeability, i.e. decrease of degree of saturation. The concept relationship between the hear strength of soils and the degree of saturation can be shown in Fig. 6.

When the shear strength τ_{R0} of the earth bank is designed as the consolidated and un-drained one, the earth bank body above the ground water level will be strengthen to τ_{R1} because the soils will be un-saturated (100% to S_{r1}) according to the time passing under the constant maximum dry density. At the state, when the tsunami overflow water permeates into the body, the shear strength of soils will be decreased to τ_{R2} because of the increase of degree of saturation (S_{r1} to S_{r2}). However, because the shear strength (τ_{R2}) is larger than the design one (τ_{R0}), the sliding stability of the earth bank can be ensured as far as the shape of the earth bank isn't changed by the erosion.

Secondly, the relationship between the water permeability into soils and the erosion acting on the soils can be explained as the erosion mechanism at the earth bank surface shown in Fig. 7. Just as the initial shear strength τ_R at the earth bank surface decreases by the water permeability induced by the tsunami overflow, in other words, induced increase of degree of saturation, the tractive stress τ_L which relates to the flow depth and flow velocity increases from zero to the level τ_{L0} same with the decreased shear strength τ_{R0}. Then the erosion at the earth bank surface begins to occurred. Then, the permeability and erosion continues as long as the flow stress is maintained to be more than the

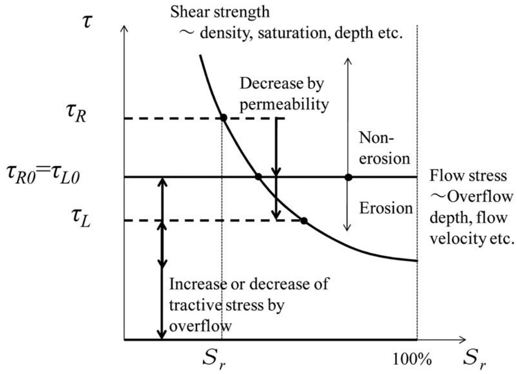

Figure 7. Concept for relationship between shear strength and flow stress to consider erosion of earth bank.

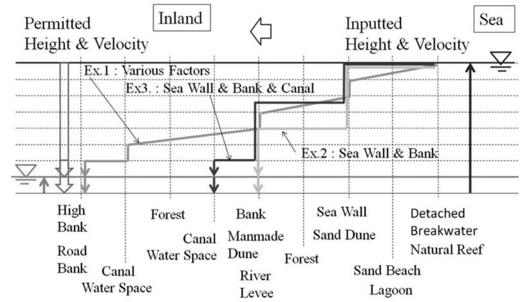

Figure 8. Performance-based design concept combining factors related to reduction of tsunami.

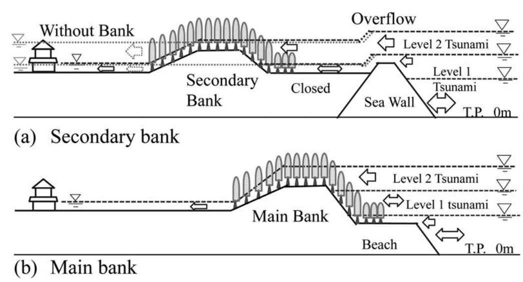

Figure 9. Design concepts of earth bank against tsunami.

Photo 10. Concrete example for design concept.

shear strength, i.e. $\tau_L > \tau_{R0}$. Afterwards, the erosion stops when the flow stress decreases to be lower than the shear strength, i.e. $\tau_L < \tau_{R0}$.

The above relation should be investigated in the future.

7 DESIGN CONCEPTS TO APPLY EARTH BANK TO MULTIPLE DEFENCE AGAINST TSUNAMI DISASTER

The typical structures which are related to reducing the water depth and/or flow velocity of the tsunami and clarified in the field survey conducted at Sendai Plane are detached breakwaters, natural reefs, sand beaches, lagoons, sea walls, forests, canals, river levees, manmade banks, and road embankments.

When the reducing function of each structure can be quantitatively estimated, the performance-based design concept shown in Fig. 8 may be generally proposed. As shown in Fig. 8, the input conditions of the tsunami at the coastal line such as the run up height and the flow velocity are gradually reduced through each reducing structure to output conditions such as the required flooded depth and flow velocity. The structures considered in the above design can be selected and 3 examples of Ex. 1, Ex. 2 and Ex. 3 are shown in Fig. 8.

After the 2011 Earthquake, the Central Disaster Management Council (2011) proposed the strategic concepts such as “multiple defenses” for the future tsunami disaster prevention. In order to perform the multiple defenses, the earth bank can be expected as the important and effective functions to prevent and/or reduce the tsunami flood in the future.

The design concepts to apply the earth bank as the main sea wall and the secondary sea wall can be propose in Fig. 9 considering the two tsunami level: Level 1 and Level 2. Especially, in case of the secondary sea wall, the earth bank at the back side of the sea wall designed against the tsunami flood of Level 1 can make up for a deficiency of the tsunami height expected in the tsunami flood of Level 2.

Photo 10 shows the examples of the earth banks to know the design concept in Fig. 9 concretely. This shows the combination of the sea wall and the earth bank at Asahi Coast in Chiba Prefecture which were flooded by the tsunami in the 2011 Earthquake. The earth bank at the back side of the sea wall is 2 m high and the overflow water depth at the crest of the bank is estimated to be about 0.5 m to 1.0 m (Tokida & Tanimoto, 2012). It can be indicated that if the earth bank was not existing, the flood depth of about 0.5 m to 1.0 m at the back ground may be increased to about 2.5 m to 3.0 m.

Furthermore, the design concept to apply the earth bank for the petrochemical complex at the bay area can be also proposed in Fig. 10 where many kinds of earth banks are related. The concrete image of the above concept can be shown in Photo 11 photographed at the Osaka Bay Area, in Japan. However this earth bank planted may be constructed only for the boundary green zone, this combination of the sea wall and the earth bank will be very effective for the future tsunami based on the above design concept.

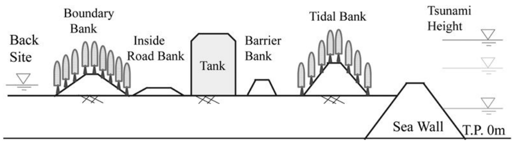

Figure 10. Design concept of several types of earth banks for petrochemical complex.

Photo 11. Concrete example of design concept combining sea wall with earth bank planted at Osaka Bay Area.

In order to apply the above design concepts, further works will be necessary to investigate and estimate the reducing function of the earth banks quantitatively.

8 CONCLUSION

In this paper, the hardly-permeability of earth banks is interested from the field lessons obtained in the 2011 Off the Pacific Coast of Tohoku Earthquake and investigated through the waterway overflow tests and the permeable tests using the simplified device. And based on the experimental results, the reason why the river dyke at Idoura were damaged slightly by the tsunami overflow is discussed. Furthermore, the design concept to apply the earth bank for the multiple defenses against the tsunami flood in the future.

The very interesting lessons from the geotechnical engineering views can be obtained as follows.

(1) In the 2011 Off the Pacific Coast of Tohoku Earth quake, the earth banks slightly damaged, deterring tsunami flood and eroded slightly are very important examples suggesting the toughness of the earth bank against the tsunami flood from the geotechnical engineering viewpoints.
(2) However the test conditions are limited, the possibility of the hardly-permeability of the earth bank and the improvement of the toughness of the earth bank can be obtained through the waterway overflow tests.
(3) The simplified test device combined with three tanks and the soil moisture meters made for this study is very effective to investigate the permeability of soils considering the actual conditions such as the water pressure head level of 2 m to 10 m, the earth bank height of 4 m and the tsunami overflow duration time of 30 to 60 minutes.
(4) Based on the permeability tests through the simplified test device, the hardly-permeability of soils which are compacted adequately and unsaturated is confirmed.
(5) The reason why the earth bank at Idoura was damaged slightly by the tsunami overflow can be estimated considering the hardly-permeability of soils because the permeable zone reducing the shear strength was very shallow.
(6) However the concepts on the hardly-permeability of earth banks relating not only the sliding failure indicated above but also the hardly-erosive are proposed, the details on the concepts is necessary to be discussed in the future.
(7) The design concepts to apply the earth bank as the measures to deter and/or reduce the tsunami flood are proposed, which are necessary to apply to the actual projects in the future.

ACNOWLEDGEMENT

The author would like to express sincere gratitude to Mr. Ryusuke Tanimoto of Ministry of Land, Infrastructure and Transport and Mr. Junpei Shimakawa of Graduate School of Engineering of Osaka University for their sincere works and Naruo Institute of Toyo Construction Co. Ltd. for the technical supports.

REFERENCES

Central Disaster Management Council. 2011: Report of the Committee for Technical Investigation on Countermeasures for Earthquakes and Tsunamis Based on the Lessons Learned from the "2011 off the Pacific coast of Tohoku Earthquake", 28 September.

Japan Coast Guard. 2011: Photograph by Aircraft MH906 of 2nd Regional Coast Guard Headquarters Sendai Air Station.

Shibayama, T., Matsumaru, R., Esteban, M. and Mikami, T. 2011: Damage Survey of Tsunami in Miyagi and Fukushima Prefecture, JSCE Prompt Report o Earthquake Disaster in the Great East Earthquake. (In Japanese)

Shimakawa, J., Tokida, K., Hata, Y. and Tanimoto, R. 2014: Study on Hardly-permeable Earth Bank against Tsunami Flood, 4th International Conference on Geotechnical Engineering for Disaster Mitigation and Rehabilitation, Theme 3: Disaster mitigation and rehabilitation. (Under contribution)

Tokida, K. & Tanimoto, R. 2012: Damages of Coastal Structures through Field Survey on the 2011 Off the Pacific Coast of Tohoku Earthquake. Journal of JSCE, A1, Vol. 68, No. 4, pp.1091–1112.

Tokida, K., Tanimoto, R., Tatta, N. and Suzuki, K. 2014: Earth Bank Reinforced with Geosynthetics against Tsunami Flood Learned in the 2011 Great East Japan Earthquake, 10th International Conference on Geosynthetics. (Under contribution)

Takahashi, S. and 33 researchers. 2011: Urgent Survey for 2011 Great East Japan Earthquake and Tsunami Disaster in Ports and Coasts, Technical Note of the Port and Airport Research Institute, No. 1231. (In Japanese)

Tanimoto, R. and Tokida, K. 2012: Study on Structure of Dug Pool Eroded by Tsunami Flood and Its Tsunami-reduction Function, International Symposium on Earthquake Engineering, Japan Association of Earthquake Engineering (JAEE), pp.143–150.

Geotechnics for Catastrophic Flooding Events – Iai (Ed)
© 2015 Taylor & Francis Group, London, ISBN 978-1-138-02709-1

On the failure mechanisms of different levee designs under extreme rainfall event – case studies in Southern Taiwan

Wen-Chao Huang & Ray-Kuo Chen
Department of Civil Engineering, National Central University, Jhongli, Taiwan

Meng-Chia Weng
Department of Civil and Environmental Engineering, National University of Kaohsiung, Kaohsiung, Taiwan

ABSTRACT: The exploration of possible failure mechanisms of levees located in southern Taiwan was focused. Two levees including Chiuliao 1st Levee and Gueishan Levee along Laonong River were chosen as the cases for analyzing possible failure mechanisms. For Chiuliao 1st Levee, the levee might fail under slope failure and sliding failure of retaining wall. For Gueishan Levee, overturning failure of the retaining wall could control the stability of the levee. With greater scouring depths the above levees could reach failure with moderate water level, although the failure mechanisms were different.

1 INTRODUCTION

Because Taiwan is located in a sub-tropic area, it is unavoidable to encounter severe disasters induced by typhoons during the summer season. An average precipitation of 2500 mm/year to 3000 mm/year could even be recoded in mountainous areas in southern Taiwan. The enormous rainfall could causes floods and if the levees were not designed and constructed properly, the outcome could be disastrous. On August 8, 2009, Typhoon Morakot invaded Southern Taiwan and caused significant loss of life and property (Lin et al. 2011; Wu et al. 2011; Weng et al. 2011). Many levees and revetments in southern Taiwan were damaged during this event, and the river basin suffered severe flood disasters. Out of the levees that were damaged in southern Taiwan, the levees along Laonong River have been investigated thoroughly due to the large population of residency along this river. A detailed description of levee failure conditions was shown in Table 1.

Among the levee breaches along Laonong River, the most serious disaster occurred at the Chiuliao 1st Levee, which is located in Kaoshu village in Pintung County. This levee was built on the left river bank near the confluence of the Laonong River and its branch, the Chokuo River. This levee is a gravity-type earthen levee with a height of approximately 10 m. During Typhoon Morakot, the levee broke away, providing an opening for water to scour the protected side of the structure. This event drew significant public attention to the issue of levee safety.

In addition, Gueishan Levee along Laonong River has also experienced levee breach. The total length of Gueishan Levee is 1328 m and the breach of this levee was about 200 m. The geologic location is different from that of the Chiuliao Levee. The Gueishan Levee is located in the middle part of Laonong River at the right bank, as shown in Figure 1. Kaomei Bridge, a local important infrastructure, is close to Gueishan Levee and therefore some of the analysis parameters were obtained from boring logs when the bridge was constructed.

Table 1. Flood induced levee failures along Laonong River during Typhoon Morakot in 2009 (Liu et al. 2009 and Huang et al. 2014).

No.	Levee/Length (m)	Failure Condition
1	Gueishan Levee/1328	Breached for about 200 m
2	Chiuliao 2nd Levee/815	Breached for about 270 m
3	Chiuliao 1st Levee/648	Total Collapse
4	Shinshin Levee/440	Total Collapse

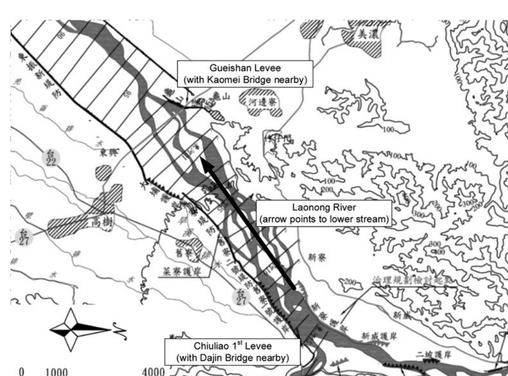

Figure 1. Locations of Chiuliao 1st Levee, Gueishan Levee and Laonong River.

The failure mechanisms of a levee system during a flood include several factors: (1) overtopping, (2) scouring of the foundation, (3) seepage/piping of levee body, and (4) sliding of the foundation (Ojha et al. 2001). These failure conditions are influenced by the levee's geometrical configuration, hydraulic conditions (e.g., river level, seepage, etc.), and material properties (e.g., grading, cohesion, compaction, and water salinity). Among these failure mechanisms, overtopping, which indicates the flood waters exceed the design capacity of the levee and flow over the structure, is a common failure mechanism. During Hurricane Katrina, the levee system surrounding New Orleans experienced catastrophic overtopping due to possible shoaling effect, bringing approximately 80% of the city under water. Many researchers have studied the stability of levees under overtopping flow (Seed et al. 2008a, b; Xu et al. 2012). However, in the case of Chiuliao 1st Levee, overtopping was not the main failure mechanism. According to the field investigation and the report of eyewitness after Typhoon Morakot (Li et al. 2009; Chang, 2012), no flood evidences on the protected side of the levee were found, such as flow traces or inundation in the lower area. Therefore, other mechanisms must have caused this levee breach. For Gueishan Levee, there is also no further evidence as to the reasons for the partial failure of the levee. However, the overall length of Gueishan Levee was 1328m, as shown in Table 1, with a breached section length of 200m. If overtopping occurred in Gueishan Levee, the whole length of Gueishan Levee could be under water, not just partial failure. With the above inference, we also expect that Gueishan Levee did not experience overtopping failure.

Overall, this study explores the main mechanisms for flooding disasters, which result in levee breaching and foundation failure. We first determined the geotechnical properties of the levee and the site, and then applied the limit equilibrium method to analyze the levee behavior and foundation stability when heavy rain occurred. This study attempts to identify the reasons for potential damage for different levee designs along Laonong River in Southern Taiwan.

2 SITE CONDITIONS AND LEVEE DESIGNS

2.1 *Levees Laonong river and its site conditions*

Laonong River Basin is located at southern part of Taiwan. The river is a tributary of the Gaoping River in Taiwan. The length of Laonong River is about 133 km. During Typhoon Morakot, the levees along Laonon River have experienced catastrophic breaches. Out of the eight levees (Gueishan Levee, Chiuliao 1st and 2nd Levees, Leegang Levee, Dongjengshin Levee, Tsailiao Levee, Toocool Levee, and Shinshin Levee, the total length of the above levees are about 23 km) along Lanong River, there were four levees that experienced catastrophic breaches. The total breached lengths were approximately 1.5 km. For the above failed levees, Chiuliao 1st Levee and Shinshin levee were washed away totally by the floods during Typhoon Morakot.

To perform analyses about the stability of the levees, site conditions along Laonong River has to be obtained. In this study, the site investigation information was collected from the borehole information of nearby bridges of the studied levees. Along Laonong River, the soil layers are mostly gravel layers to a depth of about 20 m. Specifically, the bridges near Chiuliao 1st Levee and Gueishan Levee are Dajin Bridge and Kaomei Bridge. We have analyzed the borehole information from these two bridges to represent the subsurface profiles of the above levees. For Chiuliao 1st Levee, it was shown that gravel layers is present to a depth of about 20 m and the bedrock lies at an elevation of about 125 m. The soil borings provided information about the standard penetration test (SPT-N) values, physical properties, and engineering properties of the soil. These reports summarized the physical properties of soils, including basic classification, natural water content, unit weight, void ratio, Atterberg Limits, specific gravity, and engineering properties such as friction angles and cohesions. The unit weight ranged from 19 to 22 kN/m^3, and the SPT-N values are close to a maximum of 50 blows. The friction angles listed in the report ranged from 30° to 35°. The bedrock is consisted of shale, slates and occasionally sandstones. For the stability analysis of the levees, the in-situ engineering properties of the gravel layers are required, however, based on the generalized soil profile, the soils are mostly gravel and the friction angles from laboratory testing seem to be too conservative. Therefore, we used the empirical equations of Schmertmann (1975) and Hatanaka (1996) as the followings to relate SPT-N values with friction angles, and the evaluated friction angles ranged from 37° to 45°.

$$\tan\phi \approx \left[\frac{N}{(12.2+20.3\frac{\sigma_{v0}'}{p_a})}\right]^{0.34} \quad \text{(Schmertmann, 1975)} \quad (1)$$

$$\phi = (20N_1)^{0.5} + 20 \quad \text{(Hatanaka, 1996)} \quad (2)$$

where ϕ is the friction angle, N is the in-situ SPT-N value, σ_{v0}' is the effective vertical stress, p_a is the reference stress (equal to atmospheric pressure), and N_1 is the SPT-N value modified based on effective stress. Therefore in this study, the friction angle of the in-situ gravel layer was assumed to be 40 degrees, with cohesion is equal to zero. The friction angle for the backfills of the levees was also assumed to be 40 degrees.

As for Gueishan Levee, because it is located close to Kaomei Bridge, the borehole information during the construction of the bridge was employed to estimate the in-site soil engineering properties. In this area, the soil layers are also mostly gravel layers with SPT-N values are greater than 50 blows, therefore we have also assumed a friction angle of 40 degrees for the following stability analyses. The reasons that we did not use the empirical equations as suggested for the Chiuliao 1st Levee are that the recorded SPT-N values close to this site seemed to be overestimated and

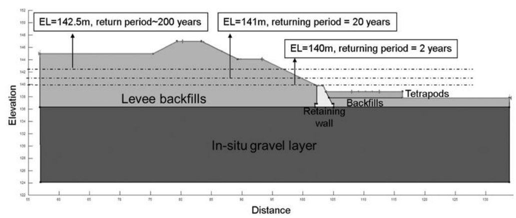

Figure 2. Design Cross Section of Chiuliao 1st Levee Before Typhoon Morakot.

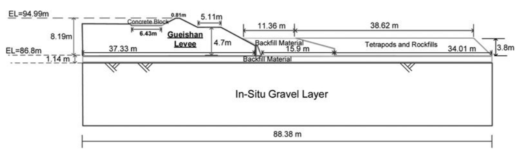

Figure 3. Design Cross Section of Gueishan Levee Before Typhoon Morakot.

some may not be correct, therefore we have assumed a reasonable friction angle based on common values for gravel layers.

2.2 *Levee designs in case studies*

In addition to the site conditions of the levees for the stability analyses of the levees, the design cross sections were also needed for the analyses. In this study, Chiuliao 1st Levee and Gueishan Levee were selected to perform the analyses due to its availability of the design cross sections. For these two levees, we have collected the design cross sections before Typhoon Morakot. Due to the fact that after the typhoon the above levees experienced failures, most of the current and available design cross sections were all conducted after Typhoon Morakot. The design cross sections before Typhoon Morakot became very limited to certain levees.

The design cross section for Chiuliao 1st Levee before Typhoon Morakot was shown in Figure 2. It was shown that the foundation of the levee laid on the surface of the in-situ gravel layer, with backfill of 1.5 m thick at the flood side of the levee. In addition, another layer of rockfill (tetrapods) was also placed on top of the backfill layer to protect the backfill from souring. In the figure, the design water level for different flood return period was also shown in the figure. It can be seen that the water level with a flood return period of 200 year is about ½ of the levee design height before Typhoon Morakot.

About Gueishan Levee, it is located at the right bank of Laonong River close to Kaomei Bridge, and the length of Gueishan is about 1300 m. The design cross section is shown in Figure 3. The levee itself is placed directly on top of a layer of backfill material with a retaining wall close to the toe of the levee. The backfill material (with a thickness of 1.1 m) laid on top of the in-situ gravel layer. In addition, another layer of backfill was placed in front of the levee at the flood side of the levee. The thickness of this backfill layer is 3.8 m. The backfill layer extended to the river side to a length of about 50 m, and rockfill layers were placed further outward to the river direction.

3 FAILURE MECHANISMS AND ENGINEERING FACTORS

3.1 *Analyzed failure mechanisms*

Based on the research results by Huang et al. (2014), the major failure mechanisms for Chiuliao 1st Levee are the slope failure of the levee and sliding failure of the retaining wall under steady state seepage. The corresponding water levels and scouring depth are high water level close to top of levee and a scouring depth of 0.5 m. Based on the above analysis results and available levee information along Laonong River, we considered the following failure mechanisms for Chiuliao 1st Levee and Gueishan Levee. For Chiuliao 1st Levee, a more in-depth discussion about the variations of scouring depth to the failure mechanisms were conducted in this study. The failure mechanisms of Chiuliao 1st Levee were also compared with Gueishan Levee in order to summarize the influences of different design cross sections on the potential failure mechanisms of different levees.

In this study, the stability of slopes (the two levees) and retaining walls close to the toe of the levees was analyzed. Due to possible drainage and clog conditions at the protected and flood sides of the levee, the water levels at two sides of the levee might be different. This results in seepage conditions in the levee. The distribution of pore water pressure inside the levee, as well as along the impervious boundary along the bottom of the retaining wall has to be obtained for further stability analysis. Therefore, for slope stability analysis, seepage analysis was performed in advance and coupled with slope stability analysis to understand the influence of the seepage condition inside the levee. Additionally, the pore water pressure distribution along the bottom of the retaining was also obtained, in order to calculate the corresponding uplift force to the retaining wall. The uplift force was employed to evaluate the stability of the retaining wall from a sliding and overturning failure point of view.

For a more detailed discussion about the analysis of retaining wall stability, an illustration of the retaining wall was shown in Figure 4. The forces acting on the retaining wall included the active force from the levee backfill, the passive force from the backfill material at the flood side of the levee. It was assumed that the passive force from the backfill still exists at the flood side for less conservative analysis. This passive force may be reduced to some extent when water level started to rise. At both sides of the retaining wall, there are also water pressures acting from left and right side of the retaining wall. As mentioned in the previous paragraph, the uplift force along the bottom of the retaining wall could also hamper the stability of the retaining

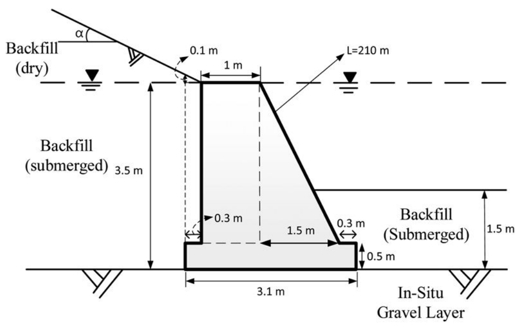

Figure 4. Retaining Wall Design Cross Section of Chiuliao 1st Levee (Huang et al. 2014).

wall (thus result in the failure of the levee), therefore in the sliding and overturning failure analysis, the uplift forces resulted from the pore water pressure distribution were also included.

For slope stability analyses coupled with seepage analysis, the software Slope/W and Seep/W in Geostudio was employed. For slope stability analysis in Slope/W, the factor safety by Spencer's theory was reported in this study. Spencer's slope stability theory assumed that there is force and moment equilibrium between the slices and the vertical and horizontal forces between the slices were also considered. In addition, because of the water level difference in protected and flood side of the levee, seepage analysis was performed before slope stability analysis, in order to consider the effect of the seepage inside the dam and in-situ soil layers. The pore water pressure at the bottom of the retaining wall was also recorded from seepage analysis for retaining wall stability analyses. In summary, the failure mechanisms considered in this study include the following:

(1) Slope stability of the levee considering steady state seepage.
(2) Retaining wall stability (includes sliding and overturning failure) considering steady state seepage. Bearing capacity failure of the retaining wall is less possible in this study given that the in-situ friction angle is very high, therefore in this study, bearing capacity failure was not analyzed.

3.2 *Influencing engineering factors*

There are two types of variable employed in the stability analysis of the levees. The first type is the water level (protected side and flood side of levee). The water level (WL) is defined as the water height on the flood side from the in-situ ground surface. Because there is difference between protected-flood sides of the water level, the difference is termed as water level difference (WLD). The second type is the scouring depth (SD) of the river bed on the flood side. Scouring depth is defined as the depth from the surface of the original backfill at the flood side. Figure 5 shows the definitions of parameters to enable better comprehension of the analyzed cases. Based on our preliminary analysis,

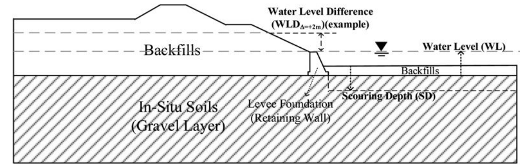

Figure 5. Definitions of variables (WLD, WL and SD) in the stability analyses of levees (Huang et al. 2014).

although it was also shown that the strength parameter of the in-situ gravel layer plays an important role in the performance of the levees, the sensitivity of this strength parameter was not as significant as the above two types of variables. Therefore in this study, the engineering properties of the in-situ gravel layer were assumed to be a constant friction angle.

As mentioned previously, possible levee failure mechanisms include: (1) overtopping, (2) scouring of the foundation, (3) seepage/piping of levee body, and (4) sliding of the foundation. For overtopping levee failure, the most recent case was in New Orleans, LA, USA during Hurricane Katrina. Due to the unprecedented water level height of the shoaling effect, the levees outside of the city center experienced overtopping failure. However, for the case studies in Southern Taiwan after Typhoon Morakot, interviewing results with the local residents have shown that there was no clear evidence of overtopping for the Chiuliao 1st Levee, and some have even indicated that the levee failure occurred right after the water at the flood side started to recede. This result was consistent with the analyzed results by Huang et al. (2014). Furthermore, the preliminary analyses of the seepage inside the levee also showed that the exit gradient is far less than the critical hydraulic gradient. Therefore in this study, the failure mechanisms were focused on two major mechanisms triggered by two variables. The in-situ engineering properties of the gravel layer were assumed to be a constant value according to empirical equations and literatures related to gravel material.

4 ANALYSIS RESULTS

4.1 *Stability of chiuliao 1st levee*

The stability analysis of levees in this study includes the slope stability and retaining wall stability under steady seepage condition. The variables employed in this study include the water level height and scouring depth. As shown in Figure 6, the water level height at the protected side is defined as h_1, while the water level height at the flood side is defined as h_2. For Chiuliao 1st Levee, the backfill thickness at the flood side is 1.5 m, therefore we have analyzed three distinct scouring depths of 0.5, 1.0 and 1.5 m. The case without the consideration of scouring was also analyzed by Huang et al. (2014). It was found that the safety factor became most critical when water level at the protected side is close to the top of the levee and some amount of water

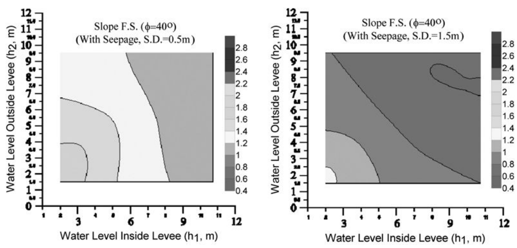

Figure 6. Slope stability of Chiuliao 1st Levee with SD of 0.5 and 1.5 m.

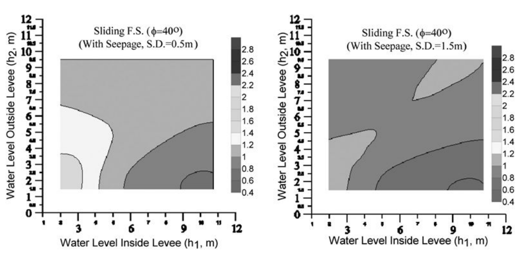

Figure 7. Retaining Wall Sliding FS of Chiuliao 1st Levee with SD of 0.5 and 1.5 m.

level difference can cause levee reached slope failure. As shown in Figure 6 with scouring depths of 0.5 and 1.5 m, it was found that with only about 1/3 scouring of the backfill material at the flood side (i.e. SD = 0.5 m), the water level has to be close to the top of the levee (which is about 10.7 m) for the safety factor reduces (but still greater than 1.0). However, as the scouring depth became 1.5 m (which indicated that the backfill material was eroded completely), the safety factor could become less than 1.0 as the water levels at both sides of the levee were about 6.0 m. This water level height is about 3/5 of the design levee height, slightly higher than the water level height of a flood returning period of 200 year.

As shown in Figure 7, a retaining wall was also present in the design cross section before Typhoon Morakot. The retaining wall stability was also analyzed based on sliding and overturning failure modes under different scouring depths as mentioned previously. According to the analyzed results of the retaining wall stability when there was no scouring, it was found that the corresponding water level height has to be close to the top of the levee at the protected side and a significant amount of water level difference was required for the sliding and overturning safety factor to be less than 1.0. This may not be a possible scenario since the design water level height of the 200 year returning period is somewhere in the middle of the levee.

However, as shown in Figure 7 for the retaining wall sliding stability with scouring depths of 0.5 and 1.5 m, the safety factor reduces as the water level inside the levee increases, furthermore, as the water is close to the top of the levee in the protected side (i.e. h_1 is large), sliding failure became critical and as the water

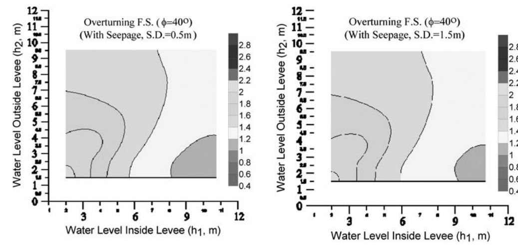

Figure 8. Retaining Wall Overturning FS of Chiuliao 1st Levee with SD of 0.5 and 1.5 m.

in the flood side receded to about 6.5 m, sliding failure occurred as the scouring depth was 0.5 m. As the backfill material in the protected side was eroded completely (i.e. SD = 1.5 m), the required water level in the protected side for the levee foundation reached sliding failure is even as small as 6m, with flood side water level slightly less than the water level at the other side.

As shown in Figure 8 for the retaining wall overturning stability with scouring depths of 0.5 and 1.5 m, the safety factor also reduced as the water level increases, however, most of the safety factors were greater than 1.0, only when the water level at the protected side was at the top of levee with a significant amount of water level difference could the retaining wall stability became critical (safety factor between 1.0 to 1.2). In short, the retaining wall of the Chiuliao 1st Levee has less possibility to reach overturning failure, even when the scouring depth was 1.5 m (i.e. backfill material was eroded completely).

Based on the above analysis results, the possible failure mechanisms for the Chiuliao 1st Levee could be a combination of slope failure and retaining wall sliding failure. The above failure modes could occur under the following scenarios: (1) when there is no local scouring of the flood side backfill material, the water level at the protected side has to be close to the top of the levee, once the water started to recede from the flood side, the sliding failure of the retaining wall could occur. This is a consistent result with the findings of Huang et al. (2014), (2) when there is small amount of local scouring (such as 1/3 of the thickness of the backfill material), sliding failure of the retaining wall could occur when there is water level difference of about 4m and (3) when the backfill layer was eroded completely (a total thickness of 1.5m of the backfill layer was eroded), slope failure and retaining wall sliding failure could occur only with water level height of about half of the design levee height. Overturning of the retaining wall is less likely because before critical condition occurred for this type of failure, other two failure conditions could have occurred already.

4.2 *Stability of gueishan levee*

The second analyzed case is Gueishan Levee. Geuishan Levee is located at the right bank of Laonong River with a total length of about 1300 m. During Typhoon Morakot in 2009, about 200 m length of the levee experienced failure. Although the failed section was not as

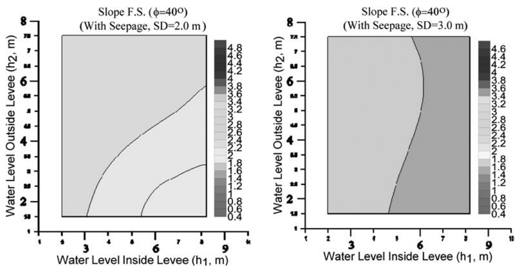

Figure 9. Slope stability of Gueishan Levee with SD of 2.0 and 3.0 m.

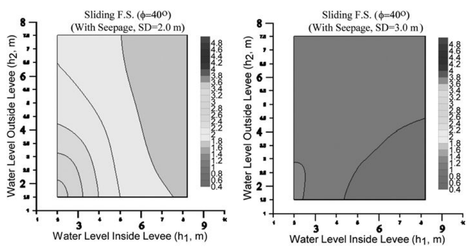

Figure 10. Retaining Wall Sliding FS of Gueishan Levee with SD of 2.0 and 3.0 m.

complete as Chiuliao 1st Levee, we have been able to collect the design cross section, as well as the borehole information close to this levee, therefore Gueishan Levee was selected as the second studied case. As mentioned previously, a retaining wall was also present at the toe of the levee, with a backfill thickness of about 3.8 m present at the flood side of the levee. The whole levee was constructed on top of a backfill layer of about 1.1 m. In the following analysis, similar failure mechanisms were also analyzed under different water levels and scouring depths. The scouring depths analyzed for Gueishan Levee were 0, 2.0, 3.0 and 3.8 m, in which a scouring depth of 3.8 m indicated that the backfill material at the flood side was eroded completely.

As shown in Figure 9, the results for slope stability analysis of the levee under scouring depths of 2.0 and 3.0 were presented. Cases without any scouring showed that the safety factor for slope failure is much greater than 3.0 under any given water levels. Figure 9 showed that with a scouring depth of 3.0 m, the slope failure safety factor was greater than 1.4 under any water level situation. As the scouring depth reached 3.8 m, the levee could fail with this mechanism even when the water level at the flood side was only about half of the design levee height with about 3.6 m water level height in the flood side of the levee. For the slope stability of Gueishan Levee, it was concluded that the levee could not fail under this mode when there is a scouring depth of 3.0 m or less.

For the retaining wall stability of Gueishan Levee, as shown in Figures 10 and 11. It was found that safety factor varies with the change of water level and scouring depths. When the scouring depth was less than 2.0 m, the sliding and overturning safety factors were all acceptable. However, as the scouring depth was

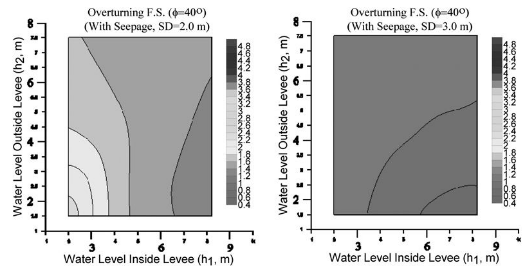

Figure 11. Retaining Wall Overturning FS of Gueishan Levee with SD of 2.0 and 3.0 m.

greater than 3.0 m, the safety factor against sliding and overturning failure could be less than 1.0 under the situation when the water level was close to the top of the levee. Under the above water level height, overturning failure of the retaining wall could happen when the water level at the flood side was about 3 m lower than that of the protected side. Under this situation, the sliding of the retaining wall may not occur (but it may become critical with FS slightly greater than 1.0). As the backfill material at the flood side of the levee was eroded completely (i.e. scouring depth was 3.8 m), sliding and overturning failure of the retaining wall became imminent for most of the water level heights. This is due to the loss of the passive resistance of the backfill material at the flood side of levee.

As the scouring depth may increase gradually, when the scouring depths are less than 2.0 m, the failure of the levee may be less likely for the three failure mechanisms under any water level conditions. However, as the scouring depth reached 3.0 m, based on the analysis results, the retaining wall might reach overturning failure first when the water level at the protected side is close to the top of levee and with the receding of the water level at the flood side by about 3 m. Under the above condition, safety factor against slope failure and retaining wall sliding failure is slightly greater than 1.0. As the backfill material was eroded, the safety factor against slope failure, sliding and overturning failure of the retaining became critical for most of the water level heights. A summary of the possible failure mechanisms and the corresponding triggering conditions of the analyzed levees was shown in Table 2.

5 FAILURE MECHANISMS OF CASE LEVEES IN SOUTHERN TAIWAN

Based on the analysis results of Chiuliao 1st Levee and Gueishan Levee, it was found that the two levees could still be stable with partial erosion of the backfill material at the flood side of the levee. Under partial scouring, failure could still occur only when the water level was close to the top of levee at the protected side of the levee with a significant amount water level difference at the flood side. When the backfill material was washed away completely due to flood, the levee could fail only with moderate water level height. Under

Table 2. Summary of Possible Failure Mechanisms for Chiuliao 1st and Gueishan Levees.

Levee	Water level and scouring depth	Possible failure mechanisms
Chiuliao 1st Levee	No scouring	Failure unlikely
	Scouring depth greater than 0.5 m	Slope failure and sliding failure of the retaining wall controlled the stability of levee. The above could occur at medium water level or above
Gueishan Levee	Scouring depth less or equal to 2 m	Overturning FS is between 1.2～1.4 for high water level
	Scouring depth greater than 3.0 m	Overturning failure of the retaining wall controlled the stability of the levee. The above occurs at medium water level or above

this case, Chiuliao 1st Levee could be controlled by the slope failure and sliding failure of the retaining wall, while for Gueishan Levee, overturning failure of the retaining wall might control the stability of the levee.

For the triggering factors that were considered in this study, safety factors of any failure mechanism could be the most critical when the water level is close to the top of the levee with water receding from the flood side of the levee. As the scouring depth increases, the safety factor decreases accordingly, however, the two cases showed partial ability to resist small amount of scouring, as the scouring depth becomes large, levee failure could occur even with relatively low water level.

6 CONCLUSIONS

In recent years the occurring frequencies and intensities of the extreme rainfall conditions have caused numerous loss of human lives and properties around the world. To avoid the damages that may be caused by the extreme rainfalls, levees were constructed in low-rise or prone-to-inundation areas. If the design of levees did not consider the effect of extreme rainfall, such as seepage condition in the levee or various failure mechanisms, possible failure might occur with unexpected mechanisms. For example, levee failures during Hurricane Katrina in the U.S. and Typhoon Morakot in southern Taiwan experienced unexpected performances during extreme rainfall events. The rainfall record in southern Taiwan during Typhoon Morakot was even close to the world record. In this study, it was focused on the exploration of failure mechanisms of levees located in southern Taiwan. Two levees including Chiuliao 1st Levee and Gueishan Levee along Laonong River that have experienced failure were chosen as the cases for analyzing possible failure mechanisms. The failure triggering factors that were employed in this study are the water level height and the scouring depth. Three major failure mechanisms were considered, including the slope failure of the levee, sliding and overturning failure of the retaining wall. Due to possible different water levels at both sides of the levee, the above failure mechanisms were also analyzed with a steady state seepage condition coupled.

For Chiuliao 1st Levee, the levee might fail under several scenarios. First of all, when there is no scouring, all failure mechanisms are unlikely. As the scouring depth is about 0.5 m (about 1/3 of the backfill layer thickness) and the water level was close to the top of levee at the protected side, slope failure and sliding failure of the retaining wall could occur once the water at the flood side started to recede. When the scouring depth was 1.5 m (i.e. the backfill material was eroded completely), the levee could fail under slope failure and sliding failure of retaining wall when the water level height was only in the middle of the design levee height.

For Gueishan Levee, as the scouring depth is less than 2.0 m, analysis results have shown that none of the failure modes could occur under all possible water level heights. However, as the scouring depth is greater than 3.0 m (the backfill layer thickness is 3.8 m), overturning and sliding of the retaining wall could occur under medium height of water level. To be more specific for Gueishan Levee, overturning failure of the retaining wall could control the stability of the levee because the water level condition could be reached first for this failure mechanism.

It was found by comparing with the analyzed results for the above two levees that Chiuliao 1st Levee and Gueishan Levee can sustain a small amount of scouring, a scouring depth about 1/3 to 1/2 of the backfill layer thickness. However, with greater scouring depths the above levees could reach failure with only moderate water level, although the failure mechanisms were different.

In the past the design of levees (especially for local levees in a suburban area), it is more common to adopt a general design cross section for the whole length of a levee. However, the induced water level height during extreme rainfall might be different at different cross sections of the river, if the design or analysis did not consider the effect of the extreme rainfall under various failure mechanisms, unexpected failures of the levee could occur, just like the cases shown in this study. Although three major failure mechanisms were chosen to be analyzed based on site investigation and interviews with local residents, for other levees, it is crucial to consider the stability from all possible failure mechanisms, especially under the extreme rainfall conditions and local scouring effect. In this way possible failures of the levees under the influence of extreme weather condition could be avoided by designing with the most possible failure mechanism in mind and the loss of human lives and properties could be minimized.

ACKNOWLEDGEMENT

The research was sponsored by the National Science Council of Taiwan, Grant No. NSC101-2218-E-002-001. The authors also thank Directorate General of Highways and Water Resources Agency of Taiwan for providing associated information about the analyzed cases.

REFERENCES

CHANG, L. P. 2012. The disaster investigation and improvement measures of hydraulic facilities after Typhoon Morakot. Risk assessment for geotechnical facilities under extreme events. Taipei, Taiwan.

HATANAKA, M. & UCHIDA, A. 1996. Empirical correlation between penetration resistance and effective friction of sandy soil. Soils and Foundations 36, 1–9.

HUANG, W.-C., WENG, M.-C. & CHEN, R.-K. 2014. Levee failure mechanisms during the extreme rainfall event: a case study in Southern Taiwan. Natural Hazards, 70, 1287–1307.

LI, W. S., YEH, K. C., LIN, C. C., SHIEH, C. L., WEN, J. C., YEH, Y. L., HSIEH, L. S., CHEN, L. Q., LI, H. C. & WANG, Y. W. 2009. Disaster survey and analysis of Morakot Typhoon. Taipei, Taiwan: National Science Council, Taiwan.

LIU, C. B., TSAI, W. H., HEISH, K. J., LIN, C. H. & CHANG, D. C. 2009. Survey and improvement measures on Southern Taiwan hydraulic facilities after 88 Flood. Sino-Geotechnics 122, 95–104.

LIN, C. W., CHANG, W. S., LIU, S. H., TSAI, T. T., LEE, S. P., TSANG, Y. C., SHIEH, C. L. & TSENG, C. M. 2011. Landslides triggered by the 7 August 2009 Typhoon Morakot in southern Taiwan. Engineering Geology, 123, 3–12.

OJHA, C., SINGH, V. & ADRIAN, D. 2001. Influence of porosity on piping models of levee failure. Journal of Geotechnical and Geoenvironmental Engineering, 127, 1071–1074.

SCHMERTMANN, J. H. Measurement of in-situ shear strength. Proceedings of a Conference on in-situ measurement of soil properties, 1975. 57–138.

SEED, R. B., BEA, R. G., ABDELMALAK, R. I., ATHANASOPOULOS-ZEKKOS, A., BOUTWELL, G. P., BRIAUD, J. L., CHEUNG, C., COBOS-ROA, D., EHRENSING, L., GOVINDASAMY, A. V., HARDER, J. L. F., INKABI, K. S., NICKS, J., PESTANA, J. M., PORTER, J., RHEE, K., RIEMER, M. F., ROGERS, J. D., STORESUND, R., VERA-GRUNAUER, X. & WARTMAN, J. 2008. New Orleans and Hurricane Katrina. I: Introduction, Overview, and the East Flank. Journal of Geotechnical and Geoenvironmental Engineering, 134, 701–717.

SEED, R. B., BEA, R. G., ATHANASOPOULOS-ZEKKOS, A., BOUTWELL, G. P., BRAY, J. D., CHEUNG, C., COBOS-ROA, D., COHEN-WAEBER, J., COLLINS, B. D., HARDER, J. L. F., KAYEN, R. E., PESTANA, J. M., RIEMER, M. F., ROGERS, J. D., STORESUND, R., VERA-GRUNAUER, X. & WARTMAN, J. 2008. New Orleans and Hurricane Katrina. IV: Orleans East Bank (Metro) Protected Basin. Journal of Geotechnical and Geoenvironmental Engineering, 134, 762–779.

WENG, M. C., WU, M. H., NING, S. K. & JOU, Y. W. 2011. Evaluating triggering and causative factors of landslides in Lawnon River Basin. Engineering Geology, 123, 72–82.

WU, C. H., CHEN, S. C. & CHOU, H. T. 2011. Geomorphologic characteristics of catastrophic landslides during typhoon Morakot in the Kaoping Watershed, Taiwan. Engineering Geology, 123, 13–21.

XU, Y., LI, L. & AMINI, F. 2012. Slope stability analysis of earthen levee strengthened by high performance turf reinforcement mat under hurricane overtopping flow conditions. Geotechnical and Geology Engineering, 30, 893–905.

Geotechnics for Catastrophic Flooding Events – Iai (Ed)
© 2015 Taylor & Francis Group, London, ISBN 978-1-138-02709-1

Impact of the recent earthquake and tsunami on Chilean port

F. Caselli, M. Beale & M. Reyes
Escuela de Ingeniería Civil Oceánica, Universidad de Valparaíso, Valparaíso, Chile

ABSTRACT: The recent earthquake with Mw of 8.3 attacked the northern Chile on the April 1, 2014 resulted in considerable damages to quay structures of the port of Iquique. In contrast, the recently renovated/reinforced quays of the port stayed at minor damage. This document summarizes the information available for the impact over the port of Iquique, due to the recent seismic sequence in northern Chile, with the aim of assess causal relation between the quay structure damages, quay renovation/reinforcement methods and city system behavior and its influence on the port operation, all in the context of risk analysis for BCP studies.

1 INTRODUCTION

The earthquake and tsunami that occurred on February 27th 2010 in central Chile caused a profound change in terms of how tsunami disasters in Chile are perceived, and revealed multiple vulnerabilities in crucial aspects of their management. Soon after that event the government of Japan, through the Japanese International Cooperation Agency (JICA) and the Japan Science and Technology Agency (JST), proposed to the Chilean government the development of a joint research project on tsunami disasters (SATREPS Project). One year later, the Great East Japan Earthquake and Tsunami prompted more urgent efforts in researching the mitigation of tsunami disasters around the world. The aim of the joint Chilean-Japanese project is "To Develop Technologies to Improve Communities and People in Chile, Japan and other countries to be Well-prepared and Resilient against Tsunami", and is organized into four groups working on different aspects of tsunami disaster mitigation. This research is part of Working Group 4, which aims to generate programs to create a well-prepared/resilient populace/communities. Within this overall objective is an "Investigation of a planning method for local government system[s] to be functional after the disasters/Business Continuity Plan (BCP)". For several reasons, Iquique city was chosen as the pilot zone on which to focus the research. Among those reasons, the seismic gap in front of the northern part of Chile was highlighted as a probable zone for earthquake and tsunami generation in short term.

With the scientific attention focused on northern Chile, because of the seismic gap since 1868 and 1877 events, a seismic sequence stroke during March and April 2014, with a main shock of Mw 8.2 on April 1st (González et al. 2014).

This document summarizes the information available for the impact over the port of Iquique, due to the recent seismic sequence in northern Chile, with the aim of assess causal relation between the quay structure damages, quay renovation/reinforcement methods and city system behavior and its influence on the port operation, all in the context of risk analysis for BCP studies.

2 GENERAL VIEW OF EARTHQUAKE AND TSUNAMI DISASTER RISK

2.1 *Iquique city*

Iquique is the capital of the administrative region of Tarapacá, located at 20.2°S and 70.1°W. With a total population of around 186,000 people, it is the largest city in its region. The workforce is composed of nearly 87,000 people, representing 46% of the total population (INE, 2013).

The economy of the city is mostly commercial, followed by mining, construction and fishing, among other forms of economic activity. The port plays an important role in the local economy, as a connection to the world for the import and export of goods, to or from Chile as well as to or from the Bolivian market.

The Free Tax Zone of Iquique (hereinafter ZOFRI) is the largest employer of the city, with almost 36,000 workers directly and indirectly related to its activity (ZOFRI, 2012).

As capital of the region, the offices of the regional government, which is part of national government, are located in downtown Iquique. The city is also the capital of Iquique's province, surrounded from the north by the Province of Arica (Region of Parinacota), east by Tamarugal Province (which limits with Bolivia), south by Tocopilla Province (Region of Antofagasta) and west by Pacific Ocean (Fig. 1).

The city is connected to the rest of the country through domestic flights, highways and by merchant ships. There are no commercial ships for people transportation along Chilean coast. As Iquique is located in a desert area, the access by road can be very fragile in

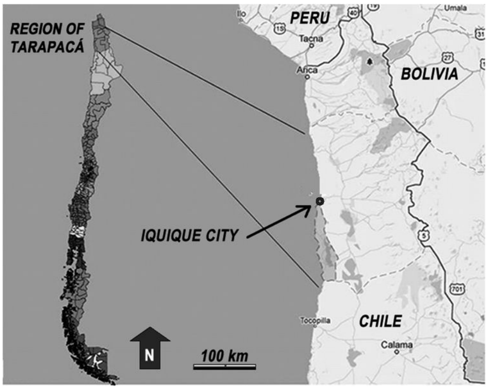

Figure 1. Location of Iquique City in Chile (Region of Tarapacá). Modified from Google maps (2014)

case of earthquakes. The main access route to Iquique is route 16, that connects with the neighboring commune of Alto Hospicio and later with route 5-North, which goes through almost the entire country. In the southern part of the city there is a coastal route (Route 1) connecting with Antofagasta city.

2.2 *Conceptualization of tsunami disaster risk*

The application of risk theory in different disciplines and with different kinds of hazard has led to the development of various definitions of risk and methods for its calculation within the scientific community. There is a diverse range of applications of risk research, and among these is disaster management. However, there is no agreement on terminology, and there are several definitions of risk, depending on the type of disaster, technical approach or scientific theory. All these factors often result in confusion for risk management processes (Pliefke et al., 2007).

An attempt to standardize the concept has been proposed by Reyes & Miura (2013), with the core idea of the study of risk as a highly multidisciplinary activity. Based on that work, and for the purposes of this research, the definition of disaster risk is to be considered as follows:

"The probability of harmful consequences, or expected loss of lives, people injured, property, livelihoods, economic activity disrupted (or environment damaged) resulting from interactions between natural and human induced hazards and vulnerable conditions."[UNDP, cited in (Pliefke et al., 2007)]

Hereinafter, this paper is intended to analyze the behavior of Iquique port and city, in terms of the major or more relevant vulnerabilities and its associated impact due to the last seismic sequence, in an attempt to prepare the conditions for risk assessment and analysis.

2.3 *Characterization of hazard*

2.3.1 *Earthquake*

The continental territory of Chile is located just over the subduction zone where the Nazca and South American plates converge. For this reason, Chile is prone to earthquakes and tsunamis, as can be observed in historical data and geologic evidence, from several studies. In fact, since 1562 more than 31 near-field tsunamis have ravaged the coasts of Chile, producing even the devastation of entire cities like Arica in 1604 and Concepción in 1751 (Winckler et al., 2010).

The historical record shows that more than 110 earthquakes with a magnitude greater than 7.0 have occurred since the year 1570 CE (Winckler et al., 2010).

From these documented earthquakes 79% did not generate destructive tsunami, and only 11% generated destructive tsunami. Some locations show recurrence of tsunami impact, and several towns have even been moved from their original sites to safer locations (Reyes & Miura 2013).

Generally speaking the majority of earthquakes in Chile meet the conditions of being tsunamigenic, so tsunami generation scenarios must be always considered in the coastal regions of Chile.

The statistical behavior of earthquakes and tsunamis shows some tendency in very specific parts of the long coast of the country. However, it is not possible to generate forecast information from that. For seismic design, the building code includes an acceleration spectrum that has been prepared on the base of historical earthquakes, and after the earthquake of February 27th, 2010, some aspects of local seismicity and soil related risks has been introduced for improvement of the code. In the case of tsunami, just some supposition of tsunamigenic zones based on historical data, are the usual input for estimation of inundation maps. All the biggest coastal cities has inundation maps, developed by the Hydrographic and Oceanographic Service of the Navy (hereinafter SHOA), but its precision is not enough for detailed risk estimation, and had been used just to define evacuation zones and procedures (Reyes & Miura 2013). Additionally, there are not full introduction of tsunami resistant design of structures, but there is an official standard recommended for that purpose, since year 2013.

The specific case of northern Chile concentrates several conditions that introduce uncertainties for earthquake and tsunami hazard probabilistic analysis, even in comparison to other regions of the country. Reyes & Miura (2013) highlights among those conditions the following:

- Environmental conditions, due to the lack of water as an obstacle for human settlement and paleotsunami research;
- Industrial Development since the first half of 19th century;
- Administrative aspects, related to the conquest of this territory by Chile after the Pacific war against Perú and Bolivia (1879–1883);
- Infrastructural challenges for railways and roads construction in desertic conditions, as another obstacle for human settlement and historical recording of seismic and/or tsunami events

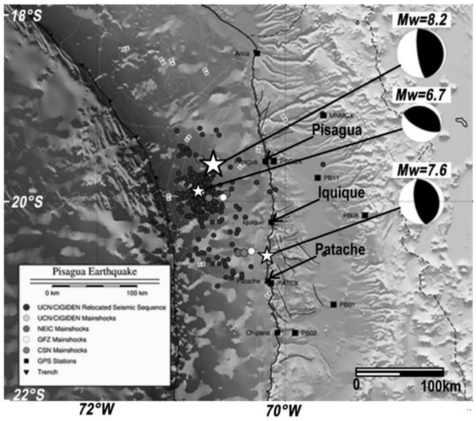

Figure 2. Location of Pisagua – Patache Seismic Sequence, including mainshocks Mw 6.7, Mw 8.2 and Mw 7.6. Modified from González et al. (2014).

In spite of the scarcity of historical information, there were scientific arguments to consider the southern Perú and northern Chile as a seismic gap, since the occurrence of the great events of 1868 and 1877, with estimated magnitudes around Mw 8.6–8.8 (Comte & Pardo, 1991).

On April 1st 2014, at 23:46:50 UTC (20:46:50 local time) a portion of the aforementioned seismic gap release part of the cumulated energy through a Mw 8.2 subduction earthquake, with epicentre off the coast of Pisagua, a coastal town localized 68 km north of Iquique (Fig. 2). The hypocenter was located at 19.572°S,70.908°W and 38.9 km depth (Barrientos, 2014).

The seismic sequence started with several foreshocks, the main one on March 16th with a Mw 6.7 earthquake. The foreshock activity lasted for thirteen days, followed by a quiet period of 2.5 days. At the end of that, a new rupture occurred south of Iquique on April 3rd at 2:43:14 UTC (21:43:14 local time), with a Mw 7.6 foreshock, marking the end of significant activity for this seismic sequence. The main shock of the sequence triggered a minor tsunami that affected the coastal infrastructure in several towns, including Iquique (González et al. 2014).

Notwithstanding the occurrence of this latest event, is clearly understandable that the most complete and confident data available for tsunami hazard description is mainly concentrated during the last 150 years, an almost negligible time lapse for geological analysis. And, because of the late introduction of seismic recording technology, for the major part of Chilean earthquakes it is only known epicentre, focal depth, magnitude, approximate seismic moment and estimated size of the rupture surface (Kausel & Campos, 1992)

Several studies has been conducted to determine the seismic potential of the northern part of Chile, and the southern part of Perú, all concluding the existence of seismic gaps along the Perú-Chile trench, in the subduction interface between Nazca and South American plates (Chlieh et al., 2011; Béjar-Pizarro, 2010; Comte and Pardo, 1991; Kausel and Campos, 1992). Among the interseismic coupled areas detected from Lima to Antofagasta (12°S to 24°S), the largest blocked segment was the northern Chilean gap with estimated potential to generate an earthquake of Mw~8.6 to 8.8 (Chlieh et al., 2011). However, many uncertainties or unsolved questions must be considered for that estimations and its tsunamigenic potential:

– The elastic behaviour hypothesis for the upper crust has been not fully demonstrated (Chlieh et al., 2011).
– There are factors as structural complexities, thermal gradient or other discontinuities, that exert influence over the subduction interfaces or its frictional properties. Those factors are not fully understood (Béjar-Pizarro, 2010; Chlieh et al., 2011; Kausel and Campos, 1992).
– Regarding to the lessons from the Great East Japan Earthquake of March 2011, the assumption of system's reset assigned for the events of 1868 and 1877 cannot be totally demonstrated (McCaffrey, 2007, MacCaffrey 2008, Satake & Atwater 2007, Kagan & Jackson 2011). That is also reinforced by the uncertainties related to the rupture length estimation of 1877's earthquake (Motagh, 2010).
– The lack of sea-bottom geodesy near the trench (Chlieh et al., 2011).

As stated in Reyes & Miura (2013), there are several theories aiming to explain the tectonic behaviour in subduction zones, and there is not total agreement on the occurrence of megathrust earthquakes, especially under consideration of the exposed uncertainties. The April 1st's event and its associated seismic sequence introduce a new factor to take into consideration in forecasting for future events.

2.3.2 *Tsunami*

The three main ruptures (Mw 6.7, Mw 8.2 and Mw 7.6) generated tsunamis, which affected the nearby areas of the epicentre. However. the Mw 6.7 and Mw 7.6 were just instrumentally detected, while the Mw 8.2 generated affectation of Arica, Pisagua, Iquique and some small fishing coves and villages located southward of Iquique. González et al. (2014) carried out a post tsunami survey, six days after the event. At Caleta Riquelme, besides Iquique port, the run']up reached a maximum elevation of 3.15 m.a.s.l. and maximum inland horizontal penetration of 90.08 m. Over the area of influence of the tsunami, the maximum run']up measured in that survey was 4.4 m.a.s.l. at the fishing cove of Patache, while the maximum measured horizontal penetration was 315 m at Ike-Ike Beach (González et al. 2014). Figure 3 summarizes the measurement performed.

2.4 *Characterization of Vulnerabilities*

Reyes & Miura (2013) systematized the city of Iquique, through the generation of a problem's tree that was transformed into a tree of vulnerabilities, as shown in figure 4. Thus, the impact of earthquake and tsunami hazard over port infrastructure and its operations is included as impact over Transportation Facilities. Else, Reyes & Miura (2013) proposes that the global vulnerability of the port can be assessed as a multi variable vulnerability, considering the following aspects:

- Structural vulnerability to liquefaction
- Structural vulnerability to shaking
- Structural vulnerability to tsunami impact
- Structural vulnerability to debris/vessels impact
- Floating objects trajectories/final location/recovery
- Headquarters location/communication network
- Ship evacuation protocol
- Combustible spots/fire control systems/protocols

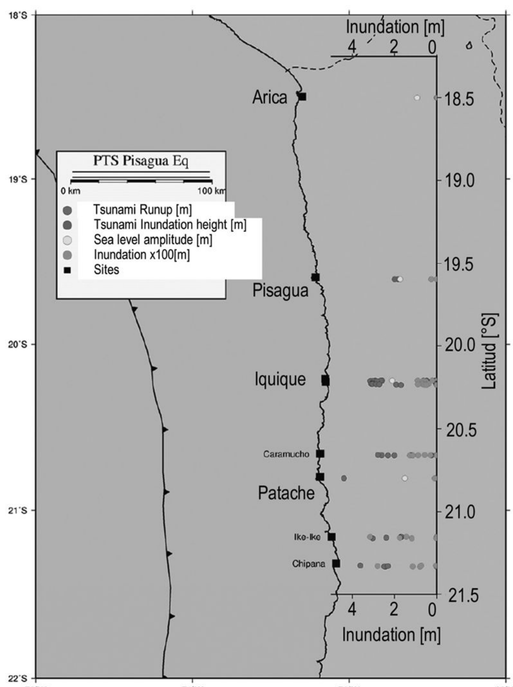

Figure 3. Post tsunami survey results, for the April 1st's tsunami. (González et al. 2014).

- Drill experience – Personnel training/evacuation
- Damage survey protocol
- Dredging operations/debris removal
- Safe quay for emergency operations
- Alternative operational routes
- Alternative land access routes
- Critical information backup/protection
- Business Continuity Planning
- Considering a major hypothetical earthquake and tsunami, the authors calculated a critical level of risk for port operation, in case of hazard occurrence within the next ten years (Reyes & Miura 2013).
- In the following sections of this article, the impact of the recent Mw 8.2 earthquake and its associated seismic sequence will be analyzed, based on this vulnerabilities systematization, with special focus on geotechnical and structural aspects, and introducing the consideration of the Port as part of a greater system: Iquique city.

2.5 *Impact associated to the April 1st 2014 Earthquake and Tsunami at Iquique city*

As pointed in section 2.1, and considering the systematization of the city proposed by Reyes & Miura (2013), the impacts produced by the recent Mw 8.2 earthquake revealed the relative importance of specific vulnerabilities of the city, some of those being key conditions for the operation and recovery of productive issues, as well as for people's normal life. Among observed impacts due to earthquake and tsunami should be considered the following:

- Severe damage to buildings and houses, mainly concentrated in the neighbour town of Alto Hospicio (Building Damage)
- Blocking and damage due to landslides in the access route to Alto Hospicio (Transportation Facilities)
- Shortage of water and electricity, for several days (Lifelines Facilities)
- Structural damage to commercial facilities (Other Facilities)
- Structural damage in port infrastructure and loss of one of the three tug boats (Transportation Facilities)
- Psychological impacts due to the large amount of aftershocks, among other related factors (Life Difficulties)

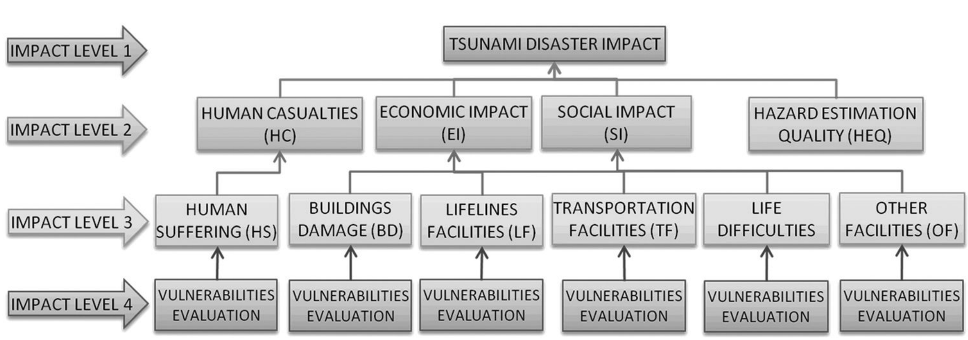

Figure 4. Simplified vulnerabilities tree (Reyes & Miura 2013).

Figure 5. Location of Iquique Port in the city of Iquique. (Google Maps 2014).

Figure 6. Main ports of the west coast of the center region of South America. Modified from Google maps (2014).

- Human suffering due death or injured people (Human Suffering)
- Damage to boats and other issues of the fishing cove “Caleta Riquelme” (Other Facilities)

The operation of Iquique port was seriously affected by some of the impacts mentioned above, even through indirect damages.

3 IMPACT ON IQUIQUE PORT

3.1 *General information of Iquique Port facilities and operators*

Iquique Port is located at 20°11′59″S and 70°09′25″W, built on a small island connected to the city through a breakwater (Fig. 5).

The city is located in the center region of South America, along with Perú, Bolivia, Paraguay, northern region of Argentina and southern region of Brazil. The west coast of this region has several public ports, among them the peruvian ports of Callao, Matarani and Ilo, and the chilean ports of Arica, Iquique, Mejillones and Antofagasta. Close to Iquique there are also the private ports of Patillos and Patache. The Figure 6 displays the mentioned region and ports.

During the year 1997, the Chilean government enacted the law N° 19,542 that modernized the state-owned port sector, hereinafter “Port Act”, thus creating 10 independent port companies and assigning to them the main role of manage, operate, develop, and maintain state-owned ports. Empresa Portuaria Iquique (Iquique Port, hereinafter “EPI”) is one of these companies and began operations in April 1998, becoming the owner and manager of two port terminals: Terminal N°1, which includes berths 1 and 2, both for commercial ships, and one area for fishing boats service, and Terminal N°2, including berths 3 and 4, both for commercial ships. On year 2000 the operation of the Terminal N°2 was given in concession to Iquique Terminal Internacional S.A. (hereinafter “ITI”) which operates under a mono-operator mode, unlike EPI that operates under a multi-operator mode. In 2013 starts the process to tender port concession of Terminal N°1, but this must be delayed because of the damage caused by the earthquake on the quay structure.

Nowadays Iquique Port has been specialized in containerized cargo, representing 76,6% of the total in 2013, according to operational statistics provided by EPI. Much of this freight transfer corresponds to Terminal N°2 and it is explained by the fact that EPI have not invested in container transfer equipment for Terminal N°1. This evolution of freight transfer by each terminal from 2008 through 2011 is shown in Table N°1 and Table N°2 (Tribunal de la Libre Competencia, 2013)

Leaving aside the containerized cargo, the main products transshipped in Iquique Port correspond to: copper, fishmeal, fish oil, sulfur and vehicles (EPI, 2012), the latter being the only one corresponding to imported cargo.

According to EPI’s information, the average of the imported cargo transfered the last 5 years correspond to 58% of the port operations; is interesting that most of that cargo correspond to containerized cargo that goes to several clients, each representing 1% or less of the total. This is explained by ZOFRI, which gathers several businesses that sell the 26% of the total of the imported products to customers primarily in Bolivia (ZOFRI 2013), as well as to other destinies in the central region of South America (Fig. 6). As consequence of this fact, most of the containers that leave the port are directed toward storage areas in ZOFRI.

Furthermore, and consistent with Table N°2, the main clients for exports are mining companies operating in the region as well as fisheries. Note that this means that most of the containers arriving to Iquique with cargo must leave empty; according to EPI’s personnel these empty containers are transported to the center of the country where they will be used.

Table 1. Freight transfer [ton], Terminal N°1, from 2008 through 2011. Modified from Tribunal de la Libre Competencia (2013).

Type of freight	2008	2009	2010	2011
Break bulk	213,408	162,522	209,749	279,728
Containerized	665,097	381,476	288,689	99,792
Bulk	28,865	28,417	70,051	197,878
Total	90,737	572,415	568,489	577,398

Table 2. Freight transfer [x1000 ton], Terminal N°2, from 2008 through 2011. Modified from Tribunal de la Libre Competencia (2013).

Type of freight	2008	2009	2010	2011
Break bulk	324.4	24.6	26.9	248.0
Containerized	1,585.0	1,340.4	1,802.0	1,801.1
Bulk	201.6	75.0	90.2	80.0
Total	2,111.0	1,661.0	2,160.8	2,129.1

Table 3. Main operating features of Terminal N°1 and Terminal N°2, Iquique Port. (EPI 2012).

	Berths 1-2	Berth 3	Berth 4
Commercial length [m]	400	335	294
Maximum allowable draught [m]	9.3	9.3	11.25
Apron's width [m]	20	20	30
Structure type	Gravity wall blocks	Gravity wall blocks	Gravity wall blocks with extension and driven piles
Construction year	1928–1932	1928–1932	2005–2012
Operated by	EPI	ITI	ITI

3.2 *Port facilities and operators*

As part of the concession contract ITI performed works to: widening of berth 4 (2005), extension of the same berth (2009) and works of seismic retrofitting in the structure of berth 3 (2011). Table 3 shows main operating features of both terminals (including construction year), and in Figure 7 is displayed the port facilities layout.

3.3 *Impact over port infrastructure*

The evaluation of the damage to port infrastructure was done in two stages: first a preliminary assessment performed by port engineers, and second an underwater inspection and measuring of bathymetry and topography by external consultant.

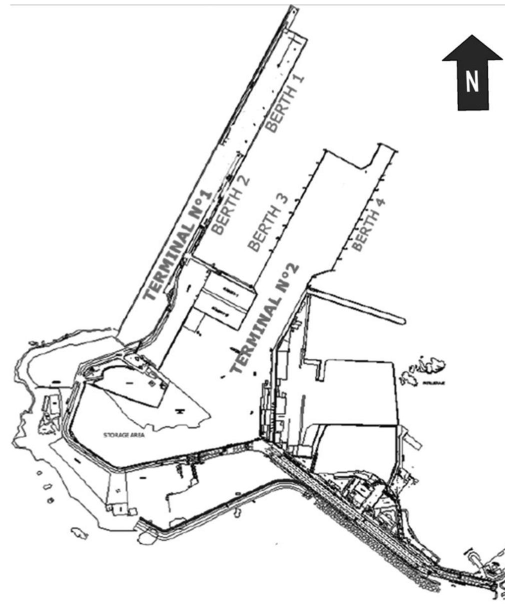

Figure 7. Layout of the Iquique Port (Tribunal de la libre competencia, 2013).

In the preliminary assessment, port engineers (from EPI and ITI) checked the displacement of blocks of the quay wall using a plumb line, this procedure was done around the perimeter of the 4 berths, breakwater and fishing site; also, they sought debris on the seabed near the pier. The figure 10 shows the Terminal No.1 segmented according to defined sections in the report prepared in the preliminary assessment.

As a result of this inspection it was determined that the breakwater wall had slight damage, finding cracks in Sector C and some degree of misalignment in the central zone B. In the structure of the head, there is a crack exposed to the sea that drains the fill, at high risk of collapse. The structure of the north wall has a collapsed section, together with a major unevenness of the yard behind it, with cracks and fissures on the surface, even exposed to wave action. The wall structure of the quay was damaged in several ways depending on the section: between bitts N°18 to 10 there's no apparent damage; however, closer to the head of pier there is an increasing damage, ranging up to the bitt N°1 at the end of the pier, with serious damage to the verge of collapse. The structure of the access bridge has minor damage and uneven cracks, so it has limited access only to light vehicles. The esplanades have variable damage, from mild to collapsed points, finding slopes and cracks, apparently due to liquefaction effects (EPI 2014).

On the other hand, according to information provided by EPI, at berth N°3 minor settlements were found in an approximate width of 5 m measured from the apron; moreover, at berth N°4 no visible damage were found. Therefore, the maritime authority authorized the use of the sites N°3 and N°4 on the basis of the

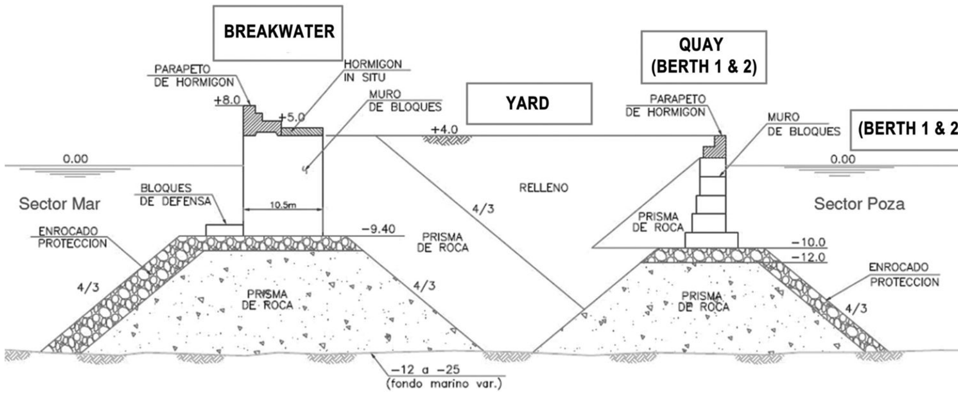

Figure 8. Cross section of the wharf, Terminal N°1 (EPI 2014).

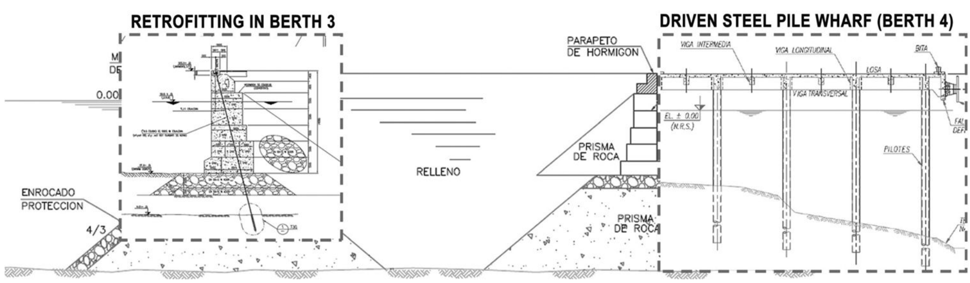

Figure 9. Cross section of the wharf , Terminal N°2 (EPI 2014).

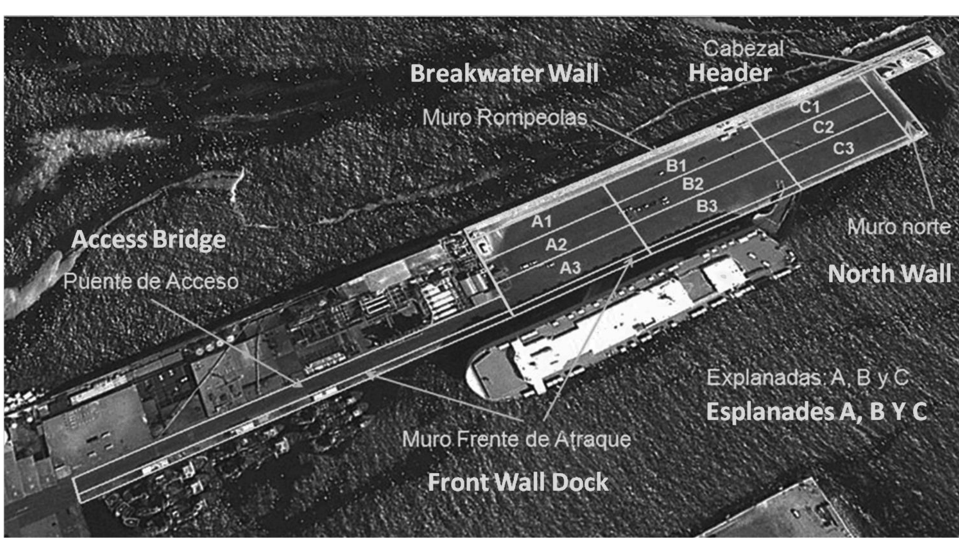

Figure 10. Terminal N°1 segmented according to preliminary evaluation results (EPI 2014).

report from the Port and the Maritime Works Bureau (hereafter DOP) of the Ministry of Public Works, indicating the constraint of limiting the heavy traffic in the damaged area of the site N°3. It's interesting to add that both organizations, EPI and DOP, have been part of the SATREPS project, specifically in group 4b, in the process of developing a BCP for Iquique Port; therefore both have been discussing the actions after this kind of event. So, even considering the early stages of this project, they have realized the effectiveness of BCP and related analysis and activities.

Notwithstanding that the operation on the berth N°3 was authorized, ITI's dockworkers expressed their concern about their safety when working on the damaged pavement. Because of this the DOP instructed actions for rehabilitation works on the quay in order to avoid accidents by operation of cranes along uneven ground.

3.4 *Effect of preventive measures against the quake*

The assessment results indicates that berths N°1 and N°2 were the most damaged, being one of the most important effects the change in the verticality of the quay wall blocks, which leant forward to the sea side about 50 cm. This deviation is concentrated between bitts N°1 (at the head of the pier) through N°8, between bitts N°8 to N°18 no variation were found (EPI 2014).

Analyzing the effects of the earthquake in both terminals, it is clear that the minor effects on Terminal N°2 are explained by the seismic retrofitting work applied to the gravitational blocks at berth N°3, as well as the satisfactory seismic response of wharf founded on driven steel piles used for the berth N°4. Figures N°8 and 9 shows the cross section of the wharf of each Terminal.

3.5 *Impact on port due damage on external zones*

Among the impacts mentioned in 2.5 there are three particularly relevant to be considered for analyzing the impacts on the port: damages on ZOFRI, damage on the road to Alto Hospicio and the loss of one of the tug boats that give service to the port.

Due to the earthquake several warehouses in ZOFRI were affected, in a local newspaper it is stated that 66 of them had to be closed due to fails in meeting the minimum safety requirements, and 27 of them remained closed after April 29th (El Longuino de Iquique, 2014). Because of that situation the access to the site was limited, which led to an increase in the number of containers stored in port areas, instead of leaving the port to be stored at ZOFRI facilities, as mentioned in 3.1. On April 24th, another local newspaper stated that the number of containers unloaded in ZOFRI dropped to one-fifth of the normal transfer (La Estrella de Iquique, 2014).

Furthermore, as a consequence of the road blocking between Iquique and Alto Hospicio, arose several transportation difficulties for workers to get to their job positions at Iquique. That situation was also important for dock workers of the port, and according to Port personnel this caused some difficulties in resuming activities during the first stage after the Mw = 8.2 event.

Additionally, due to the tsunami one of the three tug boats operating in the port was shipwrecked, with slight damage to the boat but unable to be released by its own means. In spite of that Iquique port could continue operating, since most of the ships arriving at the port uses at most two tugs, this presents an additional risk in the event of failure of any of the remaining tug boats, and adds challenges for evacuation procedures in case of major tsunami.

4 PORT CAPACITY MITIGATION AND FURTHER DEVELOPMENT

Given the good performance of the terminal N°2, the operation on berths N°3 and N°4 were allowed two days after the event occurred, although the berth N°3 with restrictions. This meant that approximately 80% of the port operations were restored.

On the other hand, the damages in Terminal N°1 compel to make reconstruction works, specifically for sections B, C, north wall and head of the pier. Furthermore, the process to tender port concession of Terminal N°1 (along with develop and operate a future new berth), had to be stopped since the terms include that the concessionaire could operate berths N°1 and N°2 while the works of the terminal improvement and expansion are performed. Therefore, it must be decided how will be altered the tender for the port concession, already including the requirement of seismic retrofitting for berths N°1 and N°2. Should be noted that one of the objectives of this new concession is to expand the port for arrival of new Panamax ships, enabling the port of Iquique get competitive advantages in its hinterland.

5 CONCLUSIONS

The seismic sequence that stroke northern Chile and in particular Iquique city during March and April 2014, with a main shock of Mw = 8.2 on April 1st, has been a challenging situation for people, government and scientific community in Chile, notwithstanding the awareness from the seismic gap associated. The consequences of this event can be analyzed from a positive perspective, because the damage level was not so large and preventive measures were effective. However, as it is proposed in the reference (Reyes & Miura 2013), the vulnerabilities of the system should be considered in its multivariable context, thus giving more choices to understand and control the risk, and realizing that the consequences of a major earthquake and tsunami can reach critical levels.

In fact, the economic core of the city is very susceptible to be affected by earthquake and tsunami hazard, as can be observed through the effects on the Port infrastructure and its operations, as well as the effects on ZOFRI facilities. Together with the road network fragility, in the context of desertic conditions, the resilience capacity of Iquique can be seriously diminished in its productive base.

As has been observed, the Chilean codes for earthquake resistant design of buildings and other structures has incorporated the experience and new knowledge through the years, reaching to a safe infrastructural condition. However, the elements built long time ago and without modern standards for structural design, as the case of Iquique port quays, are very vulnerable to earthquake and tsunami impact. Else, the tsunami resistant design code is recent and there are not structures designed under its recommendations in

Iquique city. Then, can be stated that in case of a major earthquake and tsunami the core infrastructure of the port will be seriously affected if there are not retrofitting improvements. Must be taken into account in this context that generally speaking the majority of earthquakes in Chile meet the conditions of being tsunamigenic, so tsunami generation scenarios must be always considered in the coastal regions of Chile.

In terms of the port operations, the global impact of hazard in the city is a relevant aspect to be considered in BCP. This doesn't mean that the infrastructural damage is not important, on the contrary, is a highlight for the consideration of multivariable aspects of vulnerabilities, where those related to infrastructure are very important and urgent. Aspects like the accessibility of dock workers after earthquake strike, or the availability of tug boats after tsunami impact, are key factor for a soon recovery of local economy, with the port as main engine. In that context, the consequences on the port due to the damages on ZOFRI facilities reveal the importance of wide and detailed consideration of the supply chain, especially in defining the scope of a BCP for ports. This time the port was able to restore its main operations, but the damages on ZOFRI forced the port to increase the amount of stored containers in the yards. This fact creates difficulties in the operation of the port, but also generates an increase in dangers due to stacked containers (especially empty ones) in the case of the occurrence of a large-scale tsunami.

The early stages of BCP studies already performed with EPI and DOP staff has been a positive improvement of their capacity to cope the emergency and basic stages of recovery. The authors are convinced that an integral BCP strategy will be a key factor for improvement of resilience capacity in Iquique city.

REFERENCES

Barrientos, S. 2014. Technical report Iquique Earthquake, Mw = 8.2, April 1st 2014. National Seismological Centre, Universidad de Chile. (in Spanish).

Béjar-Pizarro, M., 2010. Asperities and barriers on the seismogenic zone in North Chile: state-of-the-art after the 2007 Mw 7.7 Tocopilla earthquake inferred by GPS and InSAR data. Geophysical Journal International, pp. Vol. 183, 390–406.

Chlieh, M. et al., 2011. Interseismic coupling and seismic potential along the Central Andes subduction zone. Journal of Geophysical Research, p. Vol. 116.

Comte, D. & Pardo, M. 1991. Reappraisal of Great Historical Earthquakes in the Northern Chile and Southern Peru Seismic Gaps. Natural Hazards, pp. Vol 4: 23–44.

El Longuino de Iquique, 2014. Salud suspende el funcionamiento de 66 galpones tras el terremoto, 29 de abril, página 8.

EPI 2012. Master Plan Port of Iquique. Iquique Port, 2012. (in Spanish).

EPI 2014. Experience from Iquique earthquake and tsunami. Presentation for Workshop "Earthquake and Tsunami: Experiences of the Chilean port system". Santiago of Chile, 2014. (in Spanish).

González G., Salazar, P., González J. & Shrivasta M., 2014. The 16th March – 3 April 2014, Pisagua-Patache Seismic Sequence Rapid Response Internal Report. EERI, Iquique Chile Earthquake and Tsunami Clearinghouse. 2014.

Google Maps. (2014). North of Chile. Retrieved from https://www.google.cl/maps/@-21.8578914,-71.2848408,5z

Google Maps. (2014). Center region of south america. Retrieved from https://mapsengine.google.com/map/edit?mid=zPo7AOXKknN0.klhDq12T8cxs

INE. 2013. Regional economic report, Santiago of Chile: National Institute of Statistics (INE). (in Spanish)

Kagan, Y. and Jackson, D., 2011. Tohoku earthquake: A surprise? SAO/NASA Ads.

Kausel, E. and Campos, J., 1992. The Ms = 8 tensional earthquake of 9 December 1950 of northern Chile and its relation to the seismic potential of the region. Physics of the Earth and Planetary Interiors, pp. Vol. 72, 220–235.

La Estrella de Iquique, 2014. Réplicas acentúan daños en EPI e ITI colapsa con cargas, 24 de abril, página 2.

McCaffrey, R., 2007. GEOPHYSICS> The Next Great Earthquake. Sciencew, p. Vol. 315.

McCaffrey, R., 2008. Global frequency of magnitude 9 earthquakes. Geology, pp. Vol. 36, 263–266.

Motagh, M., 2010. Subduction earthquake deformation associated with 14 November 2007, Mw 7.8 Tocopilla earthquake in Chile: Results from InSAR and aftershocks. Tectonophysics, pp. 60–68.

Pliefke, T. et al. 2007. A Standardized Methodology for Managing Disaster Risk – An attempt to Remove Ambiguity. Ghent, Belgium, Taerwe and Proske, pp. 283–294.

Reyes M. & Miura F., 2013. A Proposal of Tsunami Risk Assessment Method for Iquique, Chile. Bulletin of the International Institute of Seismology and Earthquake Engineering ISSN 0074-655X CODEN IISBB2. 2014, vol. 48, pp. 103–108.

Satake, K. and Atwater, B., 2007. Long-Term Perspectives on Giant Earthquakes and Tsunamis at Subduction Zones. Annual Review of Earth and Planetary Sciences, pp. Vol. 35, 349–374.

Tribunal de la libre competencia (Court for Defense of Free Competition, TLC). 2013. Request report on competition terms to tender port concession of Terminal N° 1 of Iquique Port. (in Spanish).

Winckler, P., Reyes, M. and Sepúlveda, I., 2010. The tsunami of February 27, 2014 in Robinson Crusoe Island, Archipelago of Juan Fernandez, Valparaiso: Universidad de Valparaiso. (in Spanish).

ZOFRI, 2012. Yearbook, Iquique: Free Tax Zone. (in Spanish).

ZOFRI, 2013. Statistical bulletin. Free Tax Zone of Iquique. (in Spanish).

This page intentionally left blank

Geotechnics for Catastrophic Flooding Events – Iai (Ed)
© 2015 Taylor & Francis Group, London, ISBN 978-1-138-02709-1

Numerical analysis of Darcy/Navier-Stokes coupled flows and seepage-induced erosion of soils

K. Fujisawa
Graduate School of Agriculture, Kyoto University, Japan

ABSTRACT: The numerical analysis of the soil erosion induced by seepage flows is presented in this article. To the end, the following three aspects need to be computed: Water flow fields, onset and speed of erosion and boundary tracking between the soil and the water phases. The authors employ the Darcy-Brinkman equations in order to compute the water flow fields around the soils, which easily enable the simultaneous analysis of the Darcy flows in the porous media and the Navier-Stokes flows in the fluid domain. The onset and the speed of the seepage-induced erosion is predicted by an empirical formula from the flow velocity and the pressure gradient of the seepage water. The boundary tracking scheme based on the phase-field equation is applied for tracking the soil boundary changing with the erosion. The numerical results reveal that the combination of the above three aspects achieves the stable computation of the seepage erosion.

1 INTRODUCTION

Recently, the damages and failures of soil structures, such as levees and small embankment dams for irrigation reservoirs, has occurred more frequently because of a greater chance of severe typhoons and localized heavy rains. Piping, which is induced by the soil erosion due to the seepage flows is known as a primary cause of embankment breaks. Actually, Foster et al. (2000) statistically investigated the failures and the incidents involving embankment dams around the world, and reported that the seepage-induced erosion accounted for approximately 45% of these incidents. The seepage-induced erosion is considered to be a major threat to the structures made of earth materials and the objective of this article is to develop a numerical method to compute and predict the phenomenon.

To this end, this article begin with the simultaneous computation of seepage flows in porous media and regular flows in fluid domains, because the erosion of soils is affected by water flows inside and outside the soils, and these two flow fields need to be grasped in order to predict how the erosion develops. Hereafter, the domain of porous media is called the 'Darcy phase' and the flow in the domain is called the 'Darcy flow', because the Darcy's law is applied for simplicity. On the other hand, the domain occupied by only water is called the 'fluid phase' and the flow in the fluid domain is called the 'Navier-Stokes flow', because its behavior is governed by Navier-Stokes equations.

Thus far, there have been several numerical studies dealing with the coupled analysis of the Navier-Stokes and the Darcy flows (e.g., Girault & Rivière, 2009; Cai et al., 2009; Mu & Xu, 2007). They adopted different governing equations between the fluid and the Darcy phases, as shown in Equation 1 and 2;

$$\frac{\partial u_i}{\partial x_i} = 0 \tag{1a}$$

$$\frac{\partial u_i}{\partial t} + \frac{\partial u_i u_j}{\partial x_j} = -\frac{1}{\rho}\frac{\partial p}{\partial x_i} + \nu \frac{\partial^2 u_i}{\partial x_j \partial x_j} \tag{1b}$$

$$\frac{\partial}{\partial x_i}\left(\frac{k}{\rho g}\frac{\partial p}{\partial x_i}\right) = 0 \tag{2}$$

where u_i, p, ρ, ν, k and g denote the flow velocity, the piezometric pressure, the density of water, the kinematic viscosity of water, the hydraulic conductivity and the gravitational acceleration, and t and x_i are time and Cartesian coordinates.

However, their interest is mainly in the mathematical treatment used to connect the numerical solutions in the two different phases and the numerical procedure for satisfying the conservation of mass and momentum at the interface is not as easy as is applicable to practical problems. As described in the next chapter, the authors employ the Darcy-Brinkman equations as the governing equations for this problem and propose a numerical method to simultaneously solve the Navier-Stokes and the Darcy flows which is uncomplicated and applicable to the practical problems.

Combining the boundary tracking with the simultaneous analysis of the Darcy and the Navier-Stokes flows, the computation of the seepage induced erosion is carried out. In order to determine the moving speed of the soil boundary due to the erosion, an empirical formula predicting the discharge rate of the soils is utilized. The numerical method of Sun & Beckermann (2007) is applied to tracking the soil boundary changing with the erosion. The method proposed by them enables the sharp interface tracking based on the phase-field equation.

The numerical simulation of the seepage-induced erosion is presented in the end of this article, which shows that the combination of the above numerical methods and the empirical formula achieves the stable computation of the seepage-induced erosion.

2 GOVERNING EQUATIONS

2.1 *Water flow fields*

The authors focus on the following partial differential equations, called Darcy-Brinkman equations, as the governing equations for the coupled analysis of the Navier-Stokes and the Darcy flows;

$$\frac{\partial u_i}{\partial x_i} = 0 \tag{3a}$$

$$\frac{\partial u_i}{\partial t} + \frac{\partial}{\partial x_j}\left(\frac{u_i u_j}{\lambda}\right) = -\frac{\lambda}{\rho}\frac{\partial p}{\partial x_i} + \nu\frac{\partial^2 u_i}{\partial x_j \partial x_j} - \frac{\lambda g}{k}u_i \tag{3b}$$

where λ denotes the porosity and the flow velocity u_i appearing in Equation 3 corresponds to the Darcy velocity in the Darcy phase. The Darcy-Brinkman equations can be derived by taking the volume-average of the Navier-Stokes equations over the domain of porous media. The concise derivation is written in Bars & Worster (2006). It should be noted that Equation 3 is the same as the Navier-Stokes equations, given $\lambda = 1.0$ and $1/k = 0$.

The non-dimensionalization of Equation 3b makes it easier to understand what it implies. Defining the non-dimensional quantities of u_i^*, x_i^*, t^* and p^* as follows;

$$u_i = ku_i^* \ , \ x_i = hx_i^* \ , \ t = \frac{h}{k}t^* \ , \ p = \rho ghp^* \tag{4}$$

and substituting Equation 4 into Equation 3b, it is reduced into the following form;

$$\frac{k^2}{gh}\left[\frac{\partial u_i^*}{\partial t} + \frac{\partial}{\partial x_j}\left(\frac{u_i^* u_j^*}{\lambda}\right)\right] = -\lambda\left(\frac{\partial p^*}{\partial x_i^*} + u_i^*\right) + \frac{k\nu}{gh^2}\frac{\partial^2 u_i^*}{\partial x_j^* \partial x_j^*} \tag{5}$$

When the value of the hydraulic conductivity k approaches to zero, the left hand side and the second term of Equation 5 vanish at the rate of the second and first order of k, respectively, and the following relation is obtained;

$$\frac{\partial p^*}{\partial x_i^*} + u_i^* = 0 \tag{6}$$

Equation 6 is identical to the Darcy's law.

Equation 3 can describe the Navier-Stokes equations in the fluid phase by giving $\lambda = 1.0$ and $1/k = 0$, and can approximate the Darcy's law in the Darcy phase. Therefore, the Darcy-Brinkman equations allow us to simulate the Darcy and the Navier-Stokes flows without employing the different governing equations between the fluid and the Darcy phases.

2.2 *Boundary tracking*

The governing equation based on the phase-field equation is herein used for boundary tracking. This method regards the zero contour of the phase-field variable ϕ as the interface between two different phases, and the phase-field variable ϕ has a hyperbolic tangent profile across the interface. The usual phase-field method allows us to track the interface by solving the following equation derived from the general interface advection equation.

$$\frac{\partial \phi}{\partial t} + a|\nabla\phi| = b\left[\nabla^2\phi + \frac{\phi(1-\phi^2)}{W}\right] \tag{7}$$

where ϕ, a, b and W denote the phase-field variable, the moving velocity normal to the interface, the curvature coefficient and a measure of the width of the hyperbolic tangent profile, respectively. However, this equation treats not only the normal interface motion but also the curvature driven motion which is not necessary for the motion of the interface due to the seepage-induced erosion. Hence, the equation developed by Sun & Beckermann (2007) below is employed, which can avoid the curvature-driven interface motion.

$$\frac{\partial \phi}{\partial t} + a|\nabla\phi| = b\left[\nabla^2\phi + \frac{\phi(1-\phi^2)}{W} - |\nabla\phi|\nabla\cdot\left(\frac{\nabla\phi}{|\nabla\phi|}\right)\right] \tag{8}$$

As seen in the right hand side of Equation 8, the curvature term included in the right hand side of Equation 7, i.e., $\nabla^2\phi + \phi(1-\phi^2)/W$, is cancelled out by the counter term, i.e., $|\nabla\phi|\nabla\cdot\nabla\phi/|\nabla\phi|$, whereby the interface motion driven only by the velocity normal to the interface (i.e., a) can be computed by Equation 8.

3 NUMERICAL METHOD

In this chapter, the numerical method developed by the authors, which achieves the stable computation of the Darcy-Brinkman equations, is explained. The numerical computation for the boundary tracking is well described in Sun & Beckermann (2007). The detailed procedures for solving equation (8) are omitted due to space limitations, but can be found in their paper.

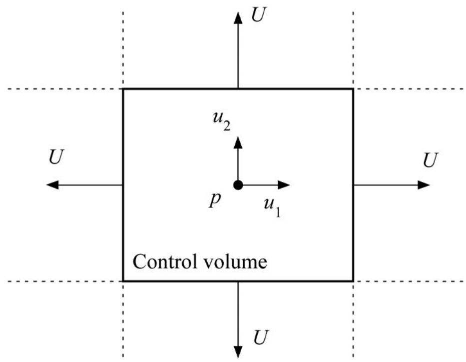

Figure 1. Finite volume cells and variables.

3.1 *Numerical procedures for solving the Darcy-Brinkman equations*

The method presented herein is based on the one proposed by Kim & Choi (2000), which can solve the Navier-Stokes equations for incompressible fluids by the finite volume method with unstructured grids. Their method is characterized by the grid system shown in Figure 1. The velocity and the pressure are stored at the center of the finite volume cells and the flux U is additionally computed at the mid-point of each cell face, which has the following definition;

$$U = (u_i)_{face} n_i \tag{9}$$

where $(u_i)_{face}$ and n_i denote the flow velocity and outward-normal unit vector on the cell face, respectively.

Applying a fractional step method and the Crank–Nicolson method to the time integration of Equation 3, and spatially integrating it over the finite volume cells, Equations 10 to 15 are obtained;

$$\frac{u_i' - u_i^m}{\Delta t} = -\frac{\lambda g}{2k}\left(u_i' + u_i^m\right) \tag{10}$$

$$\begin{aligned}\frac{\hat{u}_i - u_i'}{\Delta t} = &-\frac{1}{A}\oint_l \frac{1}{2\lambda}\left(\hat{u}_i U^m + u_i^m \hat{u}_j n_j\right) dl \\ &-\frac{1}{A}\cdot\frac{\lambda}{\rho}\oint_l p^m n_i dl + \frac{1}{A}\cdot\frac{\nu}{2}\oint_l \frac{\partial}{\partial n}\left(\hat{u}_i + u_i^m\right) dl\end{aligned} \tag{11}$$

$$\frac{u_i^* - \hat{u}_i}{\Delta t} = \frac{1}{A}\cdot\frac{\lambda}{\rho}\int_l p^m n_i dl \tag{12}$$

$$\oint_l \frac{\lambda}{\rho}\frac{\partial p^{m+1}}{\partial n} dl = \frac{1}{\Delta t}\oint_l U^* dl \tag{13}$$

$$\frac{u_i^{m+1} - u_i^*}{\Delta t} = -\frac{1}{A}\cdot\frac{\lambda}{\rho}\oint_l p^{m+1} n_i dl \tag{14}$$

$$\frac{U^{m+1} - U^*}{\Delta t} = -\frac{\lambda}{\rho}\frac{\partial p^{m+1}}{\partial n} \tag{15}$$

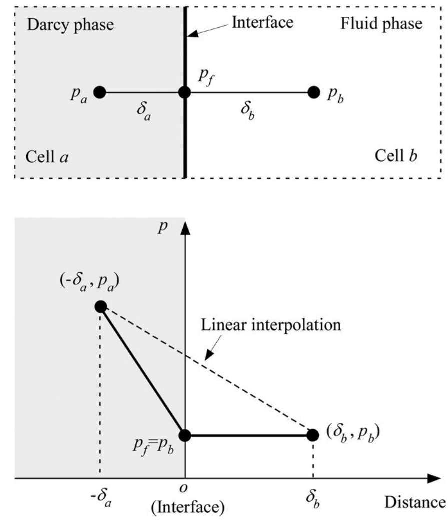

Figure 2. Interpolation of pressure at the interface between the Darcy and the fluid phases.

where A, l, n_i and Δt denote the area of the cell, the length of the cell faces, the outward normal unit vector at the cell faces and the time interval, respectively, and the superscript m implies the number of time steps. u_i', $\hat{u}_i$ and u_i^* are the intermediate velocities between u_i^m and u_i^{m+1}. U denotes the flux defined at each cell face and U^* $(=u_i^* n_i)$ is the intermediate one. The numerical procedure involves computing Equations 10 to 15 in the above order with the aid of the interpolation techniques explained in the next section. Equations 11 and 13 result in the linear systems for $\hat{u}_i$ and p^{m+1}, which require the inversion of the matrices.

3.2 *Interpolation*

In order to compute the integrals appearing in Equations 11 to 14, the velocities, the pressure and their directional derivatives need to be evaluated at the mid-point of each cell face. The values of the velocities and the pressure are interpolated from those at the centers of neighboring cells. Then, the manner of interpolating these variables plays an important role in the stable computation at the interface between the Darcy and the fluid phases. This section introduce an interpolation scheme, as shown in Figures 2 and 3, to achieve the stable and physically-natural computation of the Darcy-Brinkman equations.

For simplicity, rectangular finite volume cells are considered herein. It should be noted that the simple linear interpolation of the variables may induce the physically unrealistic oscillations at the interface of the two different phases, although the reason is omitted due to space limitations. In order to avoid the oscillations, the interpolation method described by the following equations is successful;

$$p_f = \left(\frac{k_a}{\delta_a} p_a + \frac{k_b}{\delta_b} p_b\right) \Big/ \left(\frac{k_a}{\delta_a} + \frac{k_b}{\delta_b}\right) \tag{16}$$

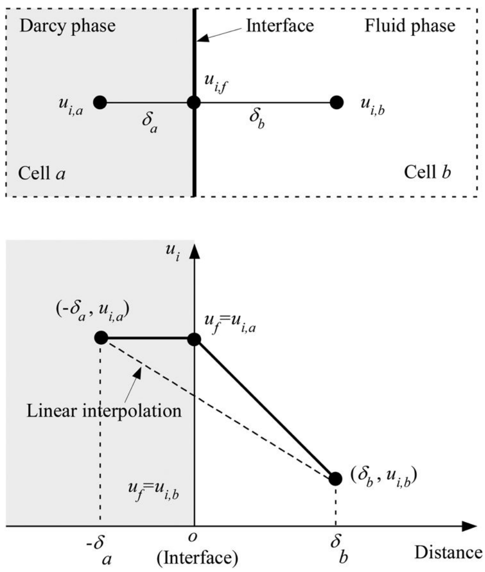

Figure 3. Interpolation of velocity at the interface between the Darcy and the fluid phases.

$$\left.\frac{\partial p}{\partial n}\right|_a = \frac{p_b - p_a}{\delta_a + \delta_b} \quad , \quad \left.\frac{\partial p}{\partial n}\right|_b = \frac{p_a - p_b}{\delta_a + \delta_b} \tag{17}$$

$$u_{i,f} = \left(\frac{k_b}{\delta_a} u_{i,a} + \frac{k_a}{\delta_b} u_{i,b}\right) \Big/ \left(\frac{k_b}{\delta_a} + \frac{k_a}{\delta_b}\right) \tag{18}$$

$$\left.\frac{\partial u_i}{\partial n}\right|_a = \frac{u_{i,f} - u_{i,a}}{\delta_a} \quad , \quad \left.\frac{\partial u_i}{\partial n}\right|_b = \frac{u_{i,f} - u_{i,b}}{\delta_b} \tag{19}$$

where p_f and $u_{i,f}$ denote the values of the pressure and the velocity at the interface, respectively, and δ is the distance from the cell center to the interface. The subscripts a and b indicate that the values are related to the cells a and b (the left and the right cells in Figures 2 and 3).

Equation 16 means that when a cell face is located on the interface between the Darcy and the fluid phases, the value of the pressure stored in the cell of the fluid phase is given to the interface (See Figure 2 and note $k_b = \infty$). On the other hand, the velocity is interpolated in an opposite manner, i.e., the velocity of the Darcy phase is given to the interface (See Figure 3). While the cell face is within the Darcy or fluid phase, the pressure and the velocity are linearly interpolated onto the cell face.

4 NUMERICAL SIMULATION

The numerical simulation of the seepage-induced erosion is accomplished by the combination of solving the Darcy-Brinkman equations and tracking the boundary between the Darcy and the fluid phases. Herein, the numerical simulation of the seepage-induced erosion is presented after the simultaneous analysis of the seepage and the Navier-Stokes flows is illustrated.

4.1 *Preferential flows in porous media*

The preferential flow in a soil block is simulated by the above mentioned numerical scheme. Figure 4 shows the geometry and the boundary conditions of this problem. The computation was carried out on the rectangular domain with the dimensions of 400 mm in length and 50 mm in width. The soil block was installed at the right of the domain and had the dimensions of 300 mm in length and 50 mm in width. The porosity and the hydraulic conductivity were assumed to be 0.40 and 5.0E-4 m/s, respectively. A flow pipe with the dimensions of 200 mm in length and 20 mm in width was artificially created in the soil block to induce the preferential flow. The fluid phases were located at the flow pipe and the left 100 mm long region of the computational domain. The inflow rate of 0.002 m/s was given to the left extreme of the computational domain, while the free outflow boundary condition was imposed and the water pressure was assumed to be 0 kPa at the right side. Both the upper and lower sides had the free-slip boundary condition. Assuming the flow velocity and the pressure to be zero as the initial conditions, the numerical computation was conducted until the flow field reached the steady state with the time interval of $\Delta t = 2.0\text{E-}4$ s.

Figure 5 shows the vector plot of the flow velocity under the steady state. The field of the flow velocity in the left fluid phase is approximately uniform. After the water flow enters the Darcy phase, it accelerates to the other fluid phase, i.e., the flow pipe. The velocity at the right side of the Darcy phase almost vanishes and the profile of the water flow within the flow pipe at the exit looks parabolic as is known as the Hagen-Poiseuille flow.

Figure 6 shows the detailed profiles of the horizontal flow velocity u_1 within the flow pipe at the cross sections of $x = 0.206$, 0.218 and 0.394 m. The positions of $x = 0.206$ and 0.218 are located at the left side of the flow pipe where the seepage water concentrates into the fluid phase. On the other hand, x=0.394 is located at the right extreme of the computational domain where the water flow discharges. As seen in the figure, there exists the horizontal flow velocity around the Darcy phase near the left side of the flow pipe, while it is nearly vanishes near the exit (See the velocity in $0 < y < 0.015$ and $0.035 < y < 0.05$ in Figure 6). However, it should be noted that the horizontal component of the flow velocity vanishes at the interface between the Darcy and the fluid phases, i.e., $y = 0.015$ and 0.035, and it gradually increases as the vertical coordinate departs from the flow pipe. The profile of the horizontal velocity is not parabolic at the inlet of the flow pipe, but it quickly approach to the parabolic shape with the increase of the horizontal coordinate.

The red solid line in Figure 6 indicates the theoretical profile of the Hagen-Poiseuille flow assuming that the whole influent water thoroughly concentrate into the flow pipe. The velocity profile of $x = 0.394$

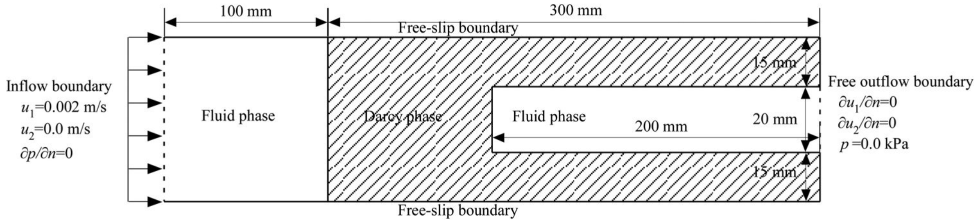

Figure 4. Geometry and boundary conditions for preference flow.

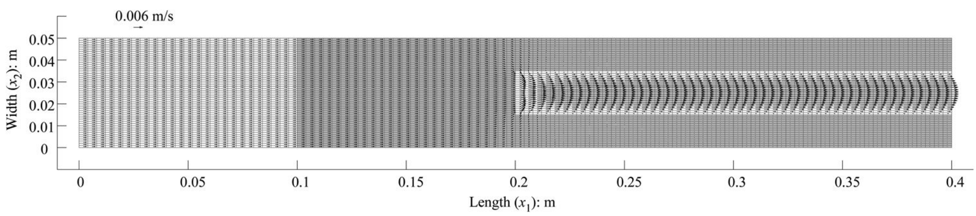

Figure 5. Computed velocity profile of preferential flow.

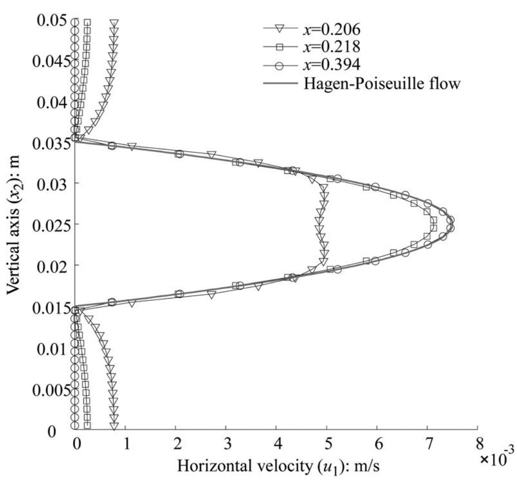

Figure 6. Horizontal velocity profiles at the cross sections of $x = 0.206$, 0.218 and 0.394 m.

is adequately similar to the theoretical one. This result shows that the proposed method can accurately simulate the Darcy and the Navier-Stokes flows in detail, and the detailed prediction of the preferential flows is realized.

4.2 *Backward seepage erosion*

The moving speed of the interface denoted by a in Equation 7, corresponds to the discharge rate of soils. The interface speed a can be estimated by the following equation;

$$a = \frac{u_n}{\lambda} - \left\{ f + (1-\lambda)\frac{\partial p}{\partial X} \right\} \frac{k}{\lambda^2 \rho g} \tag{20}$$

where u_n, X and f denote the outward normal seepage flow velocity at the interface, the coordinate normal to the interface and the maximum resisting force exerted onto the sand particles. Equation 20 is derived from the experiments by Fujisawa et al. (2012) and is based on the equilibrium of the forces exerted onto the sand particles in a direction perpendicular to the interface. The profile of the boundary between the Darcy and the fluid phases is updated by solving Equation 7 at each time step after the values of a is obtained from the numerical solutions of the pressure and flow velocity of the Darcy-Brinkman equation.

An example shown in this section is the numerical simulation of the backward erosion. Figure 7 shows the geometry and the boundary conditions. The Darcy phase of a 125 mm long soil block was installed at the middle of the computational domain and the rightward water flow was induced by the imposed boundary conditions. The right side of the Darcy phase was made concave, which intended to accelerate the seepage flow to the exit and to concentrate the seepage-induced erosion to the center of the Darcy phase. The other region was occupied by water, i.e., the fluid phase.

As for the boundary conditions, the horizontal velocity of 0.0016 m/s was given to the left side of the computational domain and the free outflow boundary condition was set on the right side. The free-slip condition was imposed on both the upside and the downside. The hydraulic conductivity and the porosity of the Darcy phase were assumed to be 1.0×10^{-3} m/s and 0.4, respectively. After the initial flow velocity and the initial water pressure were set to zero, the numerical computation was carried out until the penetration of the soil block occurred.

Figure 8 shows the profile of the computed interface between the Darcy and the fluid phases changing due to the erosion. As seen in the figure, the boundary moves in a direction opposite to the seepage flow (The backward seepage erosion is seen).

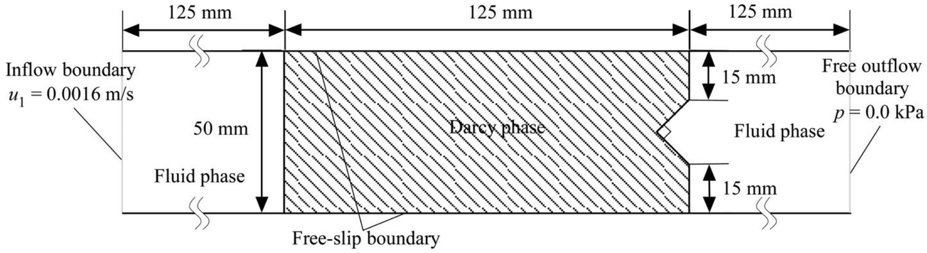

Figure 7. Geometry and boundary conditions for the numerical analysis of backward seepage erosion.

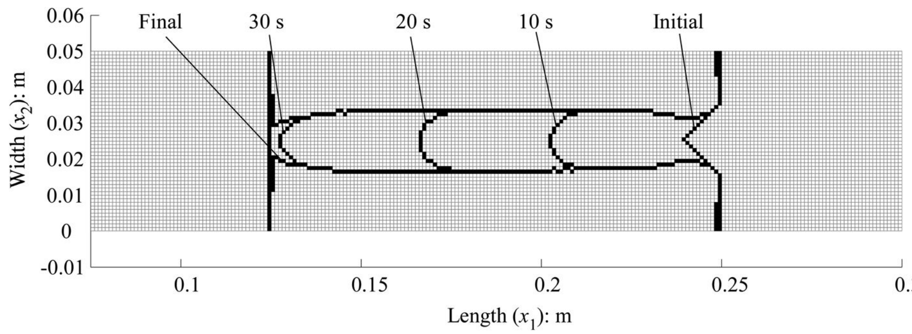

Figure 8. The profile of the interface altering with elapsed time due to the seepage-induced erosion.

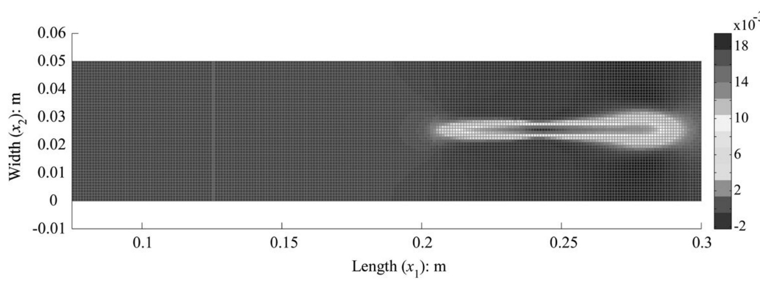

Figure 9. Horizontal velocity 10 seconds after the start of erosion (Unit: m/s).

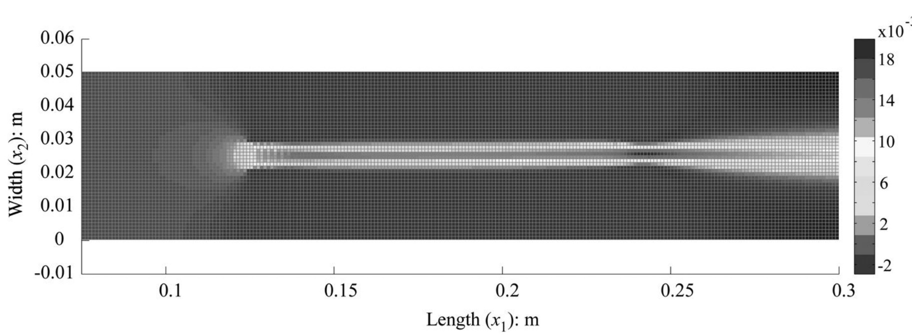

Figure 10. Final horizontal velocity after penetration (Unit: m/s).

Figures 9 and 10 show the contour plots of the horizontal flow velocity 10 seconds after the erosion started and after the penetration, respectively. These results show that the flow velocity in the region where the soil is eroded became even greater than the other region, which concentrated the water flow into the eroded region and developed the seepage-induced erosion straightly upstream. After the soil block was penetrated, the erosion no longer proceeded because the water flow almost fully concentrated to the connected fluid phase.

5 CONCLUSIONS

This article has presented a numerical method for the computation of the soil erosion induced by seepage flows. This method is built from the three parts, i.e., the simultaneous analysis of the Darcy and the Navier-Stokes flows, the estimation of the erosion rate and the computation of the boundary tracking. The authors employed the Darcy-Brinkman equations as the governing equations to achieve the simultaneous analysis of the Darcy and the Navier-Stokes flows. The erosion rate was estimated by the experimental formula of Fujisawa et al. (2012) and the tracking of the interface between the Darcy and the fluid phases was conducted by solving the phase-field equation modified by Sun & Beckermann (2007).

The preference flow was simulated by solving the Darcy-Brinkman equation, which has shown that it can produce the stable and physically realistic numerical solutions and that the detailed flow field of the fluid phase can be computed. The numerical results of the backward seepage erosion has revealed that the numerical method explained in this article can predict the typical behavior of the seepage-induced erosion, which straightly develops upstream.

REFERENCES

Bars, M.L. and Worster, M.G. 2006. Interfacial conditions between a pure fluid and a porous medium: implications for binary alloy solidification, *Journal of Fluid Mechanics* 550: 149–173.

Cai, M., Mu, M. and Xu, J. 2009. Numerical solution to a mixed Navier–Stokes/Darcy model by the two-grid approach, *SIAM Journal on Numerical Analysis* 47(5): 3325–3338.

Chan, T.F., Gallopoulos, E., Simoncini, V., Szeto, T. and Tong, C.H. 1994. A quasi-minimal residual variant of the Bi-CGStab algorithm for nonsymmetric systems, *SIAM Journal on Scientific Computing* 15(2): 338–347.

Foster M., Fell R. and Spannagle M. 2000. The statistics of embankment dam failures and accidents. *Can. Geotech. J.* 37: 1000–1024.

Fujisawa K., Nishimura S., Nakatani A. and Murakami A. 2012. Velocity of sand particles transported by upward seepage flow during sand boil, *IDRE Journal* 80(5): 409–416

Girault, V. and Rivière, B. 2009. DG approximation of coupled Navier-Stokes and Darcy equations by Beaver-Joseph-Saffman interface condition, *SIAM Journal on Numerical Analysis*, 47(3): 2052–2089.

Kim, D. and Choi, H. 2000. A second-order time-accurate finite volume method for unsteady incompressible flow on hybrid unstructured grids, *Journal of Computational Physics* 162: 411–428.

Mu, M. and Xu, J. 2007. A two-grid method of a mixed Stokes-Darcy model for coupling fluid flow with porous media flow, *SIAM Journal on Numerical Analysis* 45(5): 1801–1813.

Sun Y. and Beckermann C. 2007. Sharp interface tracking using the phase-field equation. *Journal of Computational Physics* 220: 626–653.

This page intentionally left blank

Geotechnics for Catastrophic Flooding Events – Iai (Ed)
© 2015 Taylor & Francis Group, London, ISBN 978-1-138-02709-1

Effect of incidence angle of current and consolidation pressure on the hydraulic resistance capacity of clayey soil

Y.S. Kim, S.H. Jeong, T.M. Do & C. Lee
Department of Marine and Civil Engineering, Chonnam National University, Yeosu, Jeollanamdo, Republic of Korea

K.O. Kang
Department of Civil and Environmental Engineering, Hiroshima University, Kagamiyama, Higashi Hiroshima, Japan

ABSTRACT: Until now, study on the hydraulic resistance characteristics of the ground at the river and the ocean current has been focused on the behavior under uni-directional flow without considering directional change of flow. However, recent research results show that scour rates which were measured under the bi-directional flow was much higher than those measured under uni-directional flow for both fine grained and coarse soil. Since the direction of inflow and return flow at the shore, where the structure will be constructed, is not always 180°, effect of the incidence angle on the hydraulic resistance capacity of the ground should be examined. Using the improved EFA which can consider the directional change of flow, hydraulic resistance capacities of the artificially composed clayey fine-grained soil and clayey sandy soil under 0°, 90°, 135°, and 180° incidence angles of flow were assessed. Test result shows that hydraulic resistance capacity decreases, while scour rate increases, with the increase of the incidence angle between inflow and return flow. Eventually, since the larger the incidence angles between inflow and return flow, the larger the scour rate, hydraulic resistance capacity under bi-directional flow (0°↔180°) should be examined for the design purpose.

1 INTRODUCTION

Constructions of long-span bridges and tunnels, which connect land to island or island to island, over narrow water courses, that at sometimes have concentrated water flow, are active lately in Korea, along with the island and coastal development, which is vigorously underway for balanced regional development. Plans and constructions of various offshore and undersea structures are also afoot, calling for priority consideration on the soundness of the foundations for the stability of such superstructures. In particular, risks associated with the erosion of soil and bedrock around the foundations are at the center of attention because the foundations for the structures on the sea are penetrated through the upper soft soil and built on weathered rock or the bed rock. Scour in the marine environment exhibits much more complicated mechanism than that in the river, as it undergoes the combined influence of different factors such as bi-directional tidal flow, interaction of wave flow, and cohesive soil (Jeong, 2007). The biggest general difference is that the river has steady uni-directional flow and continuous supply of soil, whereas the sea has directional change of current twice a day due to a tidal movement. Moreover, clear-water contraction, which does not result in deposition, takes place in the narrow waterways between lands or between islands (Kim & Kim, 1998).

According to the recent research trends in the scour in maritime condition, a number of experimental formulae or empirical formulae have been published through different types of hydraulic model experiments and numerical analysis. Typical examples include the empirical formula considering the bi-directional tidal current (Nakagawa & Suzuki, 1976), the formula considering the uni-directional flow of tidal current (Breusers *et al.*, 1977), and the formula considering both wave and current. In addition, Rudolph *et al.* (2004) made a field measurement of scour depth around the foundations of offshore structures in the neritic area, which is subject to wave and bi-directional tidal current in the North Sea, and compared the measured result with those predicted by existing formulas. As a result of the comparison of the measured scour depths with predicted values under bi-directional tidal current, uni-directional flow, and both wave and uni-directional flow, the measured scour depth was closest to the predicted value by the formula considering only bi-directional flow, and the formula considering both waves and uni-directional flow turned out to be underestimated. Zevenbergen *et al.* (2005) conducted an assessment on the tidal effect only qualitatively at the spot where a structure

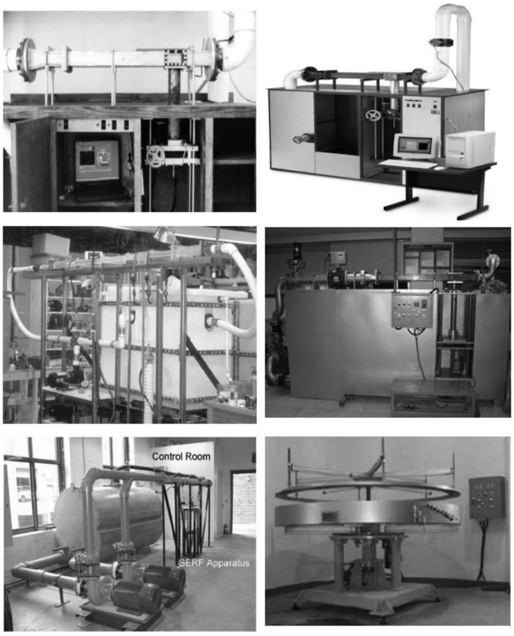

Figure 1. Hydraulic resistance measurement apparatus for uni-directional flow.

is built and computed scouring amount without considering a tidal effect. Empirical scour formula for river is also used depending on whether or not soil is transported like in clear-water contraction or live-bed contraction (Richardson & Davis, 2001).

In this research, a quantitative comparison of hydraulic resistance characteristics under uni-directional flow that occurs in the river and multi-directional flow was conducted for artificially composed soil samples with different compositions and consolidation stress history. Based on the comparison, the effect of directional change of the tidal current on the hydraulic resistance capacity of clayey soil ground was assessed and the methods to make a reasonable assessment on the hydraulic resistance capacity of ground under various tidal currents were reviewed to ensure their validity.

2 HYDRAULIC RESISTANCE APPARTUS

EFA test measures the flow velocity of erosion of 1mm soil caused by the water flowing in a rectangular pipe by placing one end of the standard-size thin wall tube with 76mm outside diameter on the bottom of the rectangular pipe and using a piston to push the soil in the sampling tube until it protrudes 1mm into the pipe. Scour rates are measured under the same velocity after the soil sample is rotated to the aimed angle by using the sample rotating part controller to simulate the change of incidence angle of current. Since the purpose of this study was to check the effect of directional change of the current on the scour characteristics

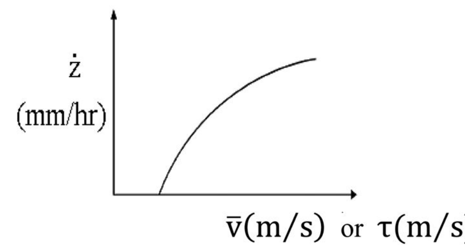

Figure 2. Representative test results of the EFA.

of the ground, the frequency of the actual sea current was used for that of directional current change of the seabed soil, but same total sustainment time of flow velocity which was applied to uni-directional current test was used to this test. The test procedure follows the approach described in NCHRP. See Kim & Kang (2011) for details.

EFA test result generates the scour rate change $\dot{z}$ curve to flow velocity ($\bar{v}$) and the mean shear stress τ, arising from the surface of the soil sample due to the water flowing in the pipe, can be obtained from Equation 1. Here, critical velocity is defined as the velocity of flow right before the scour rate becomes to be 1mm/hr, and the shear stress imposed on the ground by the water at the critical flow velocity is defined as the critical shear stress τ_c (Briaud *et al.*, 1999).

$$\tau = \frac{1}{8} f \rho V^2 \tag{1}$$

where f = friction factor obtained from the Moody chart; ρ = mass density of water (1000 kg/m^3), V = mean flow velocity in the pipe (m/s). Friction factor f is the function of the Reynolds number of the pipe $R_e(=VD/\nu)$ and relative roughness ϵ/D; D = diameter of the pipe (m); ν = dynamic viscosity coefficient of the water (10^{-6}m^2, 20°C); ϵ = Roughness.

3 EXPERIMENT AND EVALUATION

3.1 *Artificial soil specimens*

In this research, artificial soil samples were made by mixing Kaolinite and Jumunjin sand by weight ratio. The mixed soil sample had 100% initial water content, and it was thoroughly stirred and was set aside for 1day at 100% water content to ensure de-aeration and stabilization of the slurry. To assess the geotechnical characteristics of the artificial soil sample, unconfined compression test was performed to determine un-drained shear strength, and basic material test was carried out to identify water content, liquid limit, plastic limit, unit weight, void ratio, specific gravity, particle size distribution, etc. Physical and mechanical properties of the artificial soil are summarized in Table 1.

Table 1. Physical and mechanical properties of artificial soils.

consolidation pressure, σ_c (kPa)	composition ratio	ω(%)	Gs	e	LL(%)	PI(%)	γ_d(kN/m^3)	γ_t(kN/m^3)	s_u(kPa)	USCS
75	K80S20	59.59	2.65	1.73	66.70	30.69	9.51	15.20	9.24	MH
	K50S50	38.80	2.67	1.05	56.44	25.94	12.75	17.65	8.42	SM-SC
200	K80S20	44.14	2.65	0.98	66.70	30.69	13.14	16.48	28.05	MH
	K50S50	32.60	2.67	0.82	56.44	25.94	14.42	18.14	21.96	SM-SC

ω: Water content, Gs: Specific gravity, e: Void ratio, LL: Liquid limit, PI: Plasticity index, γd: Dry unit weight, γ_t: Total unit weight, s_u: Undrained shear strength, USCS: Unified soil classification system.

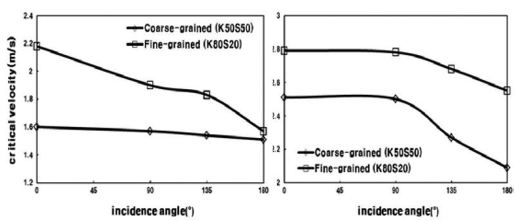

(a) 75kPa (b) 200kPa

Figure 3. Incidence angle-critical velocity relationship.

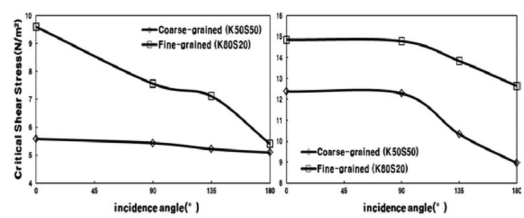

(a) 75kPa (b) 200kPa

Figure 4. Incidence angle-critical shear stress relationship.

3.2 *Effect of incidence angle of current and consolidation pressure on the hydraulic resistance capacity of clayey soil*

In order to assess the effect of incidence angle of current on the hydraulic resistance capacity of ground, EFA tests to determine critical flow velocity and critical shear stress were carried out under uni-directional flow (rivers) and under the flow that has various incidence angles (the sea) for 4 clayey soil sample cases: fine-grained soil K80S20 and coarse-grained soil K50S50 composed under 75 kPa and 200 kPa consolidation pressures, respectively. For the test carried out under uni-directional flow, scour amount of 1 mm was observed for one full hour, whereas for the test considering change of the incidence angle of tidal flow, the soil sample was rotated in the order of 0° → 90° → 0° → 90° every 15 minutes during the same one hour, while shutting off the water flow upon each rotation, taking into account the twice-a-day tidal cycle in Korea. Hydraulic resistance capacity was measured repeatedly, while gradually raising flow velocity from low to high, and was drawn to a graph of scour rate versus flow velocity, which was converted again to the relationship between critical shear stress and scour rate using Equation 1.

The test result confirmed that critical flow velocity and critical shear stress, at which scouring begins, tend to decrease with the increase of the incidence angle, regardless of the consolidation pressure, as shown in Fig. 3∼4.

As a result, bi-directional flow condition (0° ↔ 90°, 0° ↔ 135°, 0° ↔ 180°) seemed to make soil more susceptible to scour than uni-directional flow condition (0°) as published in the research by Kim & Kang (2011). Under 75 kPa consolidation pressure, in coarse-grained soils (SM-SC), scour occurred easily due to generally lesser critical flow velocity and critical shear stress regardless of the incidence angle, while in fine-grained soils, scour took place easily when incidence angle increased as the critical flow velocity and critical shear stress drastically decreased with the increase of the incidence angle. Meanwhile, in case of the soils formed under relatively deeper depth, which were consolidated to 200 kPa, both coarse-grained soil and fine-grained soil showed an insignificant difference in critical flow velocity and critical shear stress until the incidence angle reached 90°, demonstrating that the higher the consolidation pressure, the stronger the scour-resistance capacity, but showed a sharp fall when the incidence angle was increased to 135°. For the soils under confining pressure of 200 kPa, fine-grained soil (MH) showed smaller decrease in critical flow velocity and critical shear stress with the increase of the incidence angle, as compared to coarse-grained soil (SM-SC), unlike the result under 75 kPa consolidation pressure.

In summary, fine-grained (MH) soil turned out to be more erodible when hydraulic resistance capacity plunged as a result of the incidence angle change in the layer under lower consolidation pressure, while coarse-grained soil (SM-SC) became more erodible when hydraulic resistance capacity fell sharply with the increase of the incidence angle to some degree even under deep depth with high consolidation pressure. Fig. 5 shows the relationships of average scour rate ratio that was measured at various incidence angles against the value measured under uni-directional flow.

In fine-grained soil (MH), scour rates increased slower than in coarse-grained soil (SM-SC),as a result

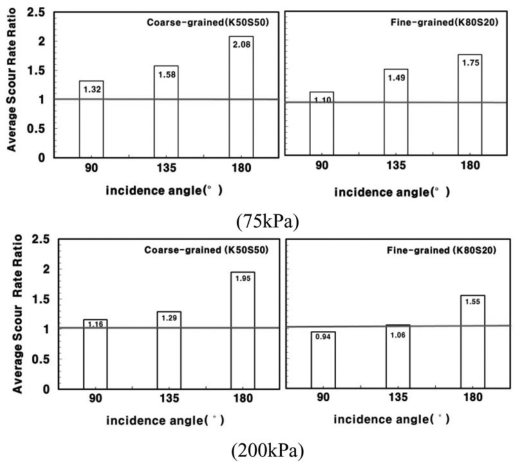

Figure 5. Incidence angle-average scour rate ratio relationship.

of increase in the incidence angle of flow, but the rates were maximum 75% higher at 180^o incidence angle than those measured under uni-directional flow. In coarse-grained soil (SM-SC), average scour rate ratio was 1.16~2.08, and the scour rate increased more seriously than in fine-grained soil (MH) when the incidence angle increased, showing the scour rate increase with the increase of the incidence angle, in most cases.EFA test on bi-directional flow (0° ↔ 180°) only will be sufficient enough for understanding the hydraulic resistance capacity under various flow incidence angles for the purpose of conservative design, given the fact that the hydraulic resistance capacity fell most substantially when the incidence angle between inflow and return flow was 180° than at other incidence angles for both clayey coarse-grained soil (SM-SC) and fine-grained soil (MH). Also, hydraulic resistance capacity decreased more substantially due to directional change of current in clayey fine-grained soils (MH) of the shallow ground under low consolidation pressure, while the same phenomenon occurred in clayey coarse-grained soils (SM-SC) of the deep ground under high consolidation pressure.

4 CONCLUSION

Hydraulic resistance capacity of fine-grained soil (MH) is relatively larger – low scour rate, high critical flow velocity, and high critical shear stress – than that of coarse-grained soil (SM-SC), regardless of consolidation pressure and incidence angle of bi-directional current. Hydraulic resistance capacity decreased more substantially due to directional change of current in clayey fine-grained soils (MH), which has large hydraulic resistance capacity, of the shallow ground under low consolidation pressure, while the same phenomenon occurred in clayey coarse-grained soils (SM-SC) of the deep ground with high consolidation pressure. In the study on the effect of the incidence angle of flow on the hydraulic resistance capacity of clayey coarse-grained soil (SM-SC) and fine-grained soil (MH), hydraulic resistance capacity decreased gradually with the increase of the incidence angle from 90°, 135°, to 180° and fell most substantially under bi-directional flow at incidence angle of 180° than others. EFA test on bi-directional flow (0° ↔ 180°) only will be sufficient enough for the conservative design purpose of a structure requiring the consideration of various incidence angles of flow.

ACKNOWLEDGEMENT

This research was supported by Basic Science Research Program through the National Research Foundation of Korea(NRF) funded by the Ministry of Education(grant number 2013011403).

REFERENCES

Breusers, H.N.C., Niccollet, G. & Shen, H.W. (1977) Local scour around offshore cylindrical pier. Journal of Hydraulic Research, 15(3), 211–215.

Briaud, J.L., Ting, F., Chen, H.C., Gudavalli, S.R., Perugu, S. & Wei, G. (1999) SRICOS: Prediction of scour rate in cohesive soils at bridge piers, Journal of Geotechnical and Geoenvironmental Engineering, Vol. 125, No. 4, ASCE, Reston, Virginia, USA, 237–246.

Jeong, H.C (2007)Geotechnical Characteristics of the Scour of Soft Seafloor Ground, Master Thesis, Graduate School, Chonnam National University.

Kang, K.O (2012). Experimental Study on Hydraulic Resistance Capacity of Cohesive Soils Considering Direction Change of the Tidal Current, Master Thesis, Graduate School, Chonnam National University.

Kim, N.H & Kim, Y.S. (1998)Offshore structure and foundation, One Technology.

Kim, Y.S. & Kang, K.O (2011) Experimental Study on Hydraulic Resistance of Sea GroundConsidering Tidal Current Flow, Journal of Korean Society of Costal and Ocean Engineers. 23(1), 118–125.

Nakagawa, H. & Suzuki, K. (1976) Local scour around bridge pier in tidal current. Coastal Engineering in Japan, 1(19), 89–100.

Richardson, E.V. & Davis, S.R. (2001) Evaluating Scour at Bridge, Hydraulics Engineering Circular No. 18, Fourth Edition, FHWA NHI 01-001, Federal Highways Administration, Washington, D.C.

Rudolph, D., Bos, K.J. &Luijendijk, A.P. (2004) Scour around offshore structures analysis of field measurement, Proceedings of Second International Conference of SCOUR and EROSION. Vol 1.

Zevenbergen, L.W., Lahasse. P.F., & Edge, B.L. (2005) Tidal Hydrology, Hydraulics and Scour at Bridges 1st edition, FHWA BHI, Federal Highway Administration, Hydraulic Engineering Circular No. 25, Washington, D.C.

Geotechnics for Catastrophic Flooding Events – Iai (Ed)

Evaluation of liquefaction susceptibility of soils using Dynamic Weight Sounding test

S. Sawada
Engineering Headquarters, OYO Corporation, Japan

ABSTRACT: A new index ΔN_{sw} is proposed for estimating liquefaction susceptibility of soils. The index is calculated using the results of two types of Swedish weight sounding test. One test is the originally quasi-static weight sounding test, from which, $N_{SW\text{-}S}$, the numbers of half turns per 1 m of penetration is obtained. The other is a newly developed dynamic weight sounding, in which an electrical hammer drill is installed at the top of sounding rod and $N_{SW\text{-}D}$, the number of half turns per 1 m of penetration is obtained. Liquefaction potential can be evaluated by ΔN_{SW} which is the difference between $N_{SW\text{-}S}$ and $N_{SW\text{-}D}(\Delta N_{SW} = N_{SW\text{-}S} - N_{SW\text{-}S})$. An example of in-situ quasi-static and dynamic weight sounding tests was conducted in order to show the effectiveness of the new index. This dynamic weight sounding test is an economically sounding and simple in-situ test method for estimating the liquefaction susceptibility of soils.

1 INTRODUCTION

The Swedish Weight Sounding (SWS) test, based on the Technical Specification of the reference number is ISO/TS 22476-10 (2005)), is one of the most convenient tools for shallow subsoil investigation and many operations have been made in recent decades for evaluation of bearing capacity of housing lots. This paper addresses a new development of weight sounding with dynamic hammer drill equipment. The validation test results indicated that this newly developed equipment is highly useful for mitigation of liquefaction-induced problems due to earthquakes.

This article addresses the new development of dynamic weight sounding device that is equipped with a rock hammer drill. It is shown herein that the new device, which is called the Dynamic Weight Sounding (DWS) test, is a time-efficient tool that can evaluate the liquefaction risks such as the high or low possibility. The time efficiency makes it possible to study a large area in a relatively short period.

2 TEST EQUIPMENT AND DATA PROCESSING

A schematic figure of Dynamic Weight Sounding test (DWS) test proposed in this paper is shown in Figure 1. The DWS test system is mounted on SWS test equipment with a dynamic hammer drill at the top of sounding rod. SWS test consists of a screw-shaped point, 19mm diameter rod, weights or other loading system and a handle or a rotating device. The weight sounding test is made as a static sounding in soft soils

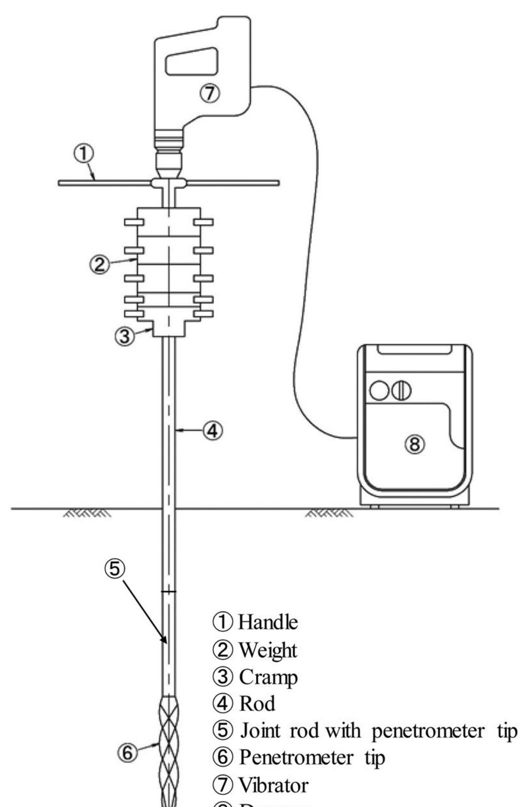

Figure 1. Schematic figure of "Dynamic Weight Sounding (DWS)" test.

Figure 2. View of “Dynamic Weight Sounding (DWS)” test.

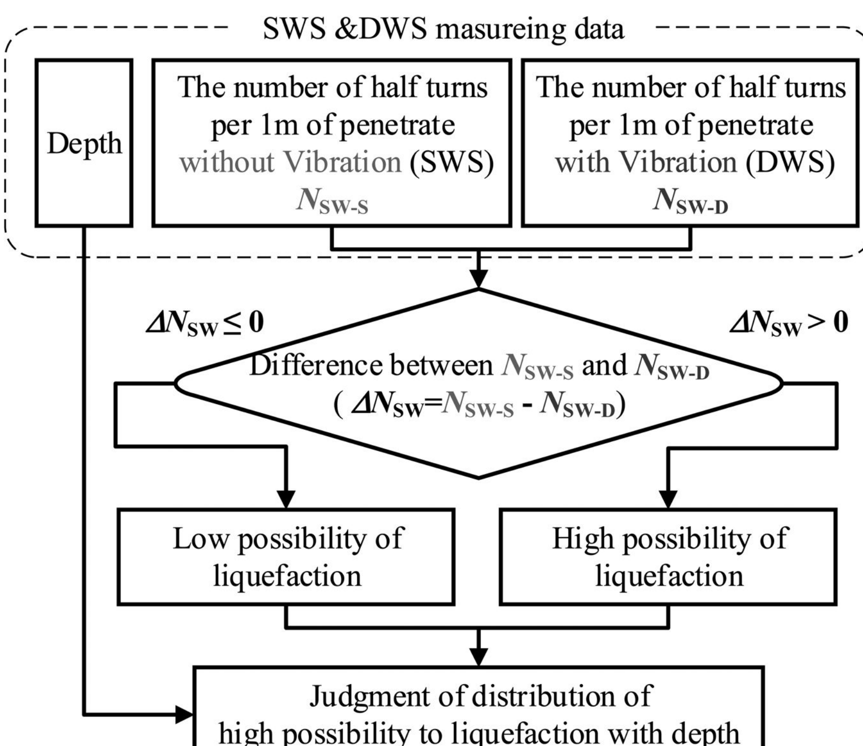

Figure 3. Flow chart for judgment of liquefaction susceptibility.

where the penetration resistance is less than 1 kN. When the resistance exceeds 1 kN the penetrometer is rotated, manually or mechanically, and the number of half turns for a given depth of penetration is recorded. The SWS test is primarily used to give a continuous soil profile and an indication of the layer sequence. The penetrability in even stiff clays and dense sand is good. The weight sounding test is also

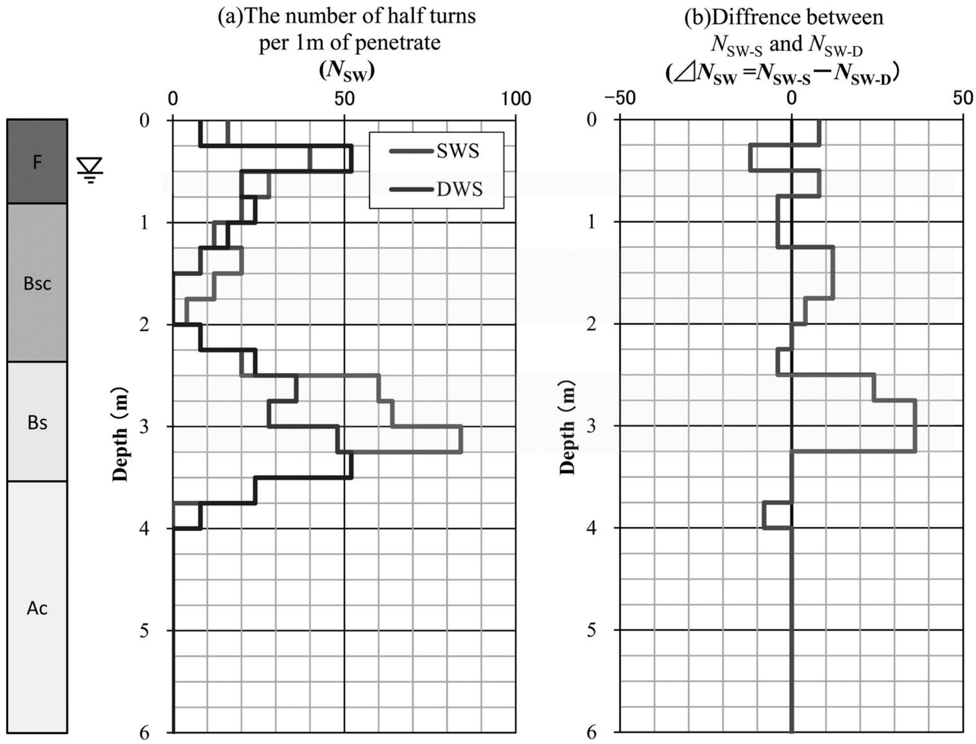

Figure 4. An example data of Dynamic Weight Sounding (DWS).

used to estimate the density of cohesionless soils and to estimate the depth to very dense ground layer indicating the length of end-bearing piles. The system has a very simple structure and is very cheap. Figure 2 shows a view of DWS test system with a dynamic hammer drill in the field test conducted in order to make sure of the effectiveness in the field. This view shows a half-automatically SWS test system and a dynamic hammer drill.

The penetration resistance is defined as the number of half turns per 1 m of penetrate (N_{SW}) required to rotate the penetrometer tip 20 cm downwards under the quasi-static drainage condition. These numbers of half turns per 1 m indicate the static resistance of SWS test N_{SW}-values ($N_{SW\text{-}S}$). On the other hand, numbers of half turns indicate the dynamic resistance of DWS test N_{SW}-values ($N_{SW\text{-}D}$). The difference at the same depth between $N_{SW\text{-}S}$ and $N_{SW\text{-}D}$ indicates the liquefaction susceptibility of soils as follows,

$$\Delta N_{sw} = N_{SW\text{-}S} - N_{SW\text{-}D} \quad (1)$$

The DWS test system can be easily brought into the fields without truck vehicles and can be set up within 5 minutes. The DWS test system consists of the above mentioned SWS test equipment with a dynamic hammer drill.

The flow chart for data processing to estimate depths with high possibility of liquefaction by SWS & DWS-method is shown in Figure 3. All datacan be obtained by SWS & DWS measurement.

3 TEST SITE CONDITIONS & EXAMPLE DATA

The test site is located in the Kanto plains area along The Tone River, Japan. The soil profile and the number of half turns per 1 m penetration are shown in Figure 4. The soil profile is investigated usind Piezo Drive Cone (PDC) has been proposed by Sawada (2009). The surface soil layer is an unsaturated fill (F), which mainly consists of dredged sandy soil, inter-bedded with several clays of 5–10 cm in thickness. The bank (B) layer exists down to 3.4 m in depth above a natural sedimentary alluvial clay layer (A_C). The groundwater level is 0.5 m below the ground surface. The sandy soil like an intermediate soil layer (B_{SC}) is deposited from 0.9 m to 2.3 m in depth. The uniformed sand layer (B_S) is medium sand with some fine contents. These numbers of half turns per 1 m penetrate N_{SW} observed within the sandy soil is 100; indicating SWS test results are almost greater than DWS test result.

Figure 4(b) illustrates the distribution ΔN_{sw} for depth. The result of the differential between the number of half turns DWS and SWS test can take into account locally higher value in the loose sandy soil layer rather than in the clay layer. In order to evaluate the liquefaction potentials at each step of DWS test, a new index ΔN_{sw} is now defined as equation (1). The discontinuity of ΔN_{sw} is seen in the layers between 2.4 m and 3.2 m below the ground surface. Therefore, the liquefaction potential index ΔN_{sw} directly indicates the degree of liquefaction susceptibility. The threshold value of this index, indicating whether the soil layers are liquefiable or not, is 0.0 in this study.

4 CONCLUSION REMARKS

The following conclusions were obtained from a series of SWS & DWS test results.

(a) The new index ΔN_{sw} has the possibility for estimating liquefaction susceptibility of soils.
(b) The liquefaction potential index ΔN_{sw} directly indicates the degree of liquefaction susceptibility.
(c) The threshold value of this index, indicating whether the soil layers are liquefiable or not, is 0.0 in this study.

REFERENCES

ISO/TS 22476-10 (2005). *TECHNICAL SPECIFICATION*, Geotechnical investigation and testing – Field testing – Part 10: Weight sounding test.

Sawada, S., (2009), Evaluation of differential settlement following liquefaction using. *Piezo Drive Cone, 17th International Conference on Geotechnical Engineering, Alexandria, Egypt*, 1064–1067.

Geotechnics for Catastrophic Flooding Events – Iai (Ed)
© 2015 Taylor & Francis Group, London, ISBN 978-1-138-02709-1

Earthquake and tsunami damage estimation for port-BCP

Yasuhiro Akakura & Kenji Ono
Disaster Prevention Research Institute, Kyoto University, Japan

Koji Ichii
Hiroshima University, Japan

ABSTRACT: As a preparation for the possible future large-scale earthquakes and tsunami, Business Continuity Plan (BCP) has been in progress in Japanese ports. In BCP of ports (port-BCP), based on the seismic damage evaluation results, fragility of ports and possibility to restore the function of ports in designated level and period shall be evaluated. In this paper, the damage situation of port facilities in the Great East Japan Earthquake and Tsunami Disaster is reviewed. Then, from a practical point of view, the development of a simple earthquake-tsunami damage evaluation method necessary for port-BCP is discussed.

1 INTRODUCTION

In Japan, possibility of future large-scale disasters induced by earthquakes in southern sea side area (Nankai Trough Earthquakes) or just beneath the capital (Tokyo Inland Earthquakes) has been worried. In the estimate by the cabinet office, damages by Nankai Trough Earthquakes and by Tokyo Inland Earthquakes are about 22 billion US dollars and about 11 billion US dollars, respectively. Compared to the GDP in Japan is about 47 billion US dollars in 2012, these estimated damages will give a quite large impact to Japanese economy.

In order to mitigate these possible future large-scale earthquakes and tsunami damage, various countermeasures are under preparation both in governmental sectors and private sectors. As one of the countermeasures, preparation of Business Continuity Plan (BCP) has been in progress in Japanese ports (port-BCP).

In port-BCP, fragility of ports and possibility to restore the function of ports in designated level and period shall be evaluated. The evaluation of the fragility of ports shall be based on the seismic damage evaluation results for port facilities. However, there is no practical scheme to evaluate the damage of port facilities induced by both earthquake and tsunami simultaneously. FEM (Finite Element Method) is often used for seismic design, but this is time and cost consuming. Furthermore, the impact of tsunami of port facilities cannot be evaluated in conventional FEM.

Considering the current situation summarized above, in this paper, from the practical point of view, the development of a simple earthquake-tsunami damage evaluation method necessary for port-BCP is discussed. Although there are various types of port facilities, quay walls (facilities for the mooring of ships) are focused in this paper.

2 PORT-BCP

2.1 *Ports in Japan*

Since Japan is surrounded by sea, ports are very important for Japanese economy and people's life. For example, in 2008, 88% of energy and 61% of foods are imported in Japan, 99.7% (in weight) of the imported material come from ports.

In Japan, there are 125 commercial ports (more than major port class) including 5 International Hub Ports (Figure 1).

2.2 *Impact of the great East Japan earthquake and tsunami disaster*

In the Great East Japan Earthquake and Tsunami Disaster, March 11, 2011, various types of damage including failures of breakwaters and quay walls, liquefaction at the apron, burial of debris, vehicles and containers to the channel, were observed in pacific side ports of eastern Japan. Right after the termination of the Tsunami Warnings/Advisories, activities to clear the channel at a rapid rate was done by governments (MLIT: Ministry of Land Infrastructure, Transport and Tourism, and prefectural governments). As the results of these efforts, temporary use of some quay walls was possible in all major ports by the end of March, 2011.

It took more time to start the full scale restoration. For example, 3 months was necessary to re-open the berth No.1, and a half year was necessary to be the container crane was operational, in Takasago-container terminal in Sendai-Shiogama Port. This fact indicates that the Takasago-container terminal could not response to the needs of cargo transport from/to the region. Although ports in the Sea of Japan side (west side of Tohoku area) were used as the

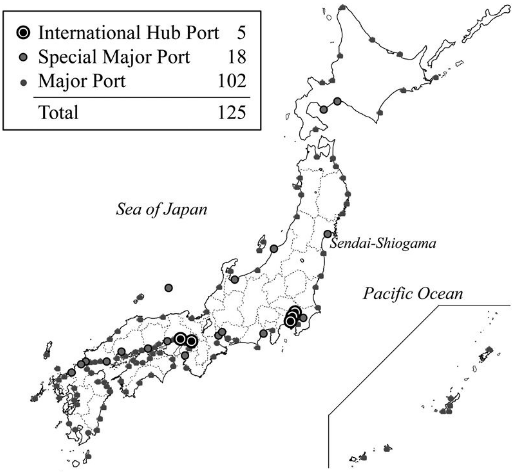

Figure 1. Location of Ports in Japan.

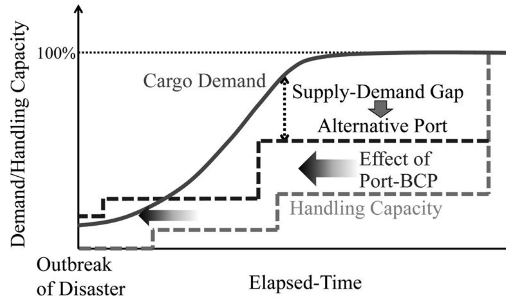

Figure 2. Conceptual Diagram of Port-BCP.

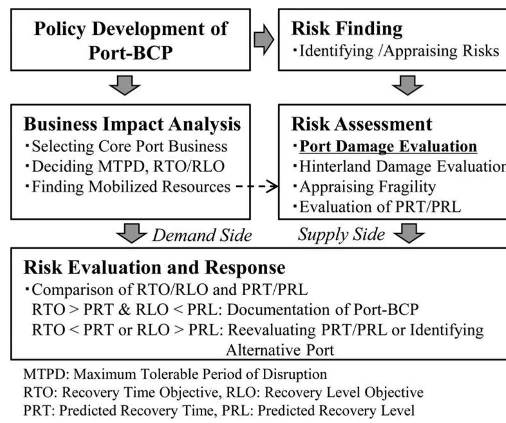

Figure 3. Procedures for Preparing Port-BCP.

alternative, this suspension of the Takasago-container terminal induced stagnation of international cargo transport. It also cut the supply chain for various companies, and enlarged the damage to Japanese economy.

Based on this situation, the council of MLIT reported the fundamental policy for earthquakes and tsunami countermeasures for ports (June, 2012). In this report, following 2 important policies are shown.

(1) Preparation of port-BCP and sharing the BCP among the stakeholders are necessary to enable the effective and rapid restoration of cargo transport function of port under the limited human/material resources.
(2) In port-BCP, the back-up ports should be identified in advance.

2.3 *Outline of Port-BCP*

BCP is a plan of action, to be prepared in advance for the purpose of the continuous existence of the subject of making the plan, not only to prepare the initial response such as secure of the employee or prevention of secondary disaster, but also to enable the continuity or restoration in shortest period of important activity of the subject. (Niki 2012, Ono et al. 2014).

In 1995, the function of Kobe Port was completely suspended by the earthquake occurred at just beneath the port. The restoration of the Kobe Port took a long time. During the restoration period, although other ports such as Osaka Ports worked as the alternative, most of the transship container cargo of Kobe Port moved to Busan Port. These moved cargos do not come back to Kobe Port even after the complete restoration of Kobe Port.

From the lesson in the past disaster mentioned above, the purpose of the port-BCP can be summarized as anchoring of users to the port by restoration of the function of the port to the target service level in target restoration period. For this purpose, (1) Toughening (such as seismic retrofit) of port facilities, (2) Acceleration of rehabilitation by the preparation of rehabilitation process and system, and (3) Ensuring substitute function by alternative ports, are important.

Figure 2 shows the relationship between Cargo Demand and Cargo Handling Capacity in port-BCP. Right after the outbreak of the disaster, handling capacity may be not enough. However, toughening enables to maintain the minimum function to satisfy the cargo demand. Prior preparation may accelerate the rehabilitation. If cargo handling capacity is still insufficient (gap in demand and supply), alternative ports enables to maintain the continuity of the port function.

The process to prepare port-BCP is shown in Figure 3. As the demand side approach, BIA (Business Impact Analysis) is utilized to determine MTPD (Maximum Tolerable Period of Disruption) and RTO/RLO (Recovery Time Objective/Recovery Level Objective). As the supply side approach, RA (Risk Analysis) is used to evaluate PRT/PRL (Predicted Recovery Time/Predicted Recovery Level). RTO/RLO and PRT/PRL were compared, and when RTO is longer than the PRT and RLO is less than PRL, the preparation of the BCP is completed.

In the risk analysis (RA) in this BCP preparation, the damage of port facilities is estimated and the negative impact (fragility) of the suspension of

Location	Displacement	Horizontal	Vertical
Crown of Berth	Residual	-0.87 m	-0.25 m
	Maximum	-1.13 m	-0.28 m

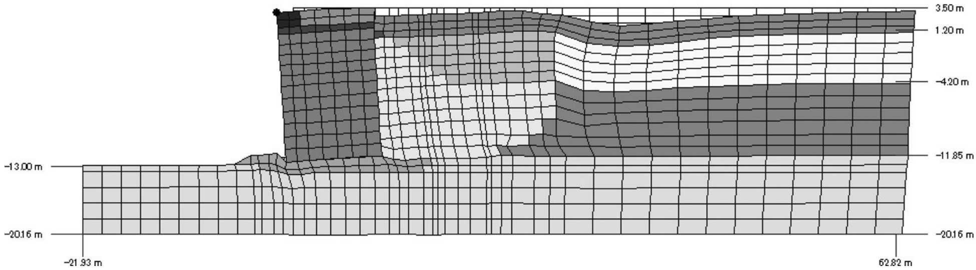

Figure 4. Estimation Result of Residual Displacement of Berth at Port of Hachinohe by Using FLIP (Aomori Prefecture 2013).

the damaged facilities shall be evaluated. Thus, the restoration period is the important result from the analysis.

As the port facilities to be considered in the port-BCP, there are various types of facilities, such as quay walls and piers (facility to mooring ships), channels, breakwaters, cranes (cargo handling facilities), port road, etc. In this paper, as one of the most important facility in cargo handling, quay walls are focused.

3 EXISTING DAMAGE EVALUATION PROCEDURE OF PORT FACILITY

3.1 *Finite element analysis*

Design of Japanese port facilities shall follow the design standard (OCDI 2009). In this design standard, finite element analysis is implemented to evaluate the seismic performance of the facilities, especially against the level-2 earthquake motions. As the benefit of the application of the finite element analysis, the non-linear behavior of soil and soil-structure interaction can be considered appropriately. Furthermore, although liquefaction phenomenon have been observed in ports in case of earthquakes, advanced finite element analysis such as FLIP (Iai et al. 1990) can evaluate the liquefaction induced damage to port facilities.

In port-BCP, finite element analysis is sometimes utilized to evaluate the damage to port facilities. Figure 4 shows an example of seismic damage evaluation of a quay wall in Hachinohe port (Aomori Prefecture 2013). In this example, displacement of a caisson is evaluated for the BCP preparation. After the anticipated earthquake, occurrence of 87 cm horizontal displacement is estimated. From the viewpoint of the operation, 100 cm is a threshold for the performance in the design standard. Thus, in port-BCP, this quay wall can be regarded to have acceptable seismic performance.

Furthermore, based on this analysis results, necessity of the temporarily restoration of pavement is clarified. To do the removal of the asphalt pavement and re-installation of rubble pavement, 24 days of restoration period, 20 workers at the peak time, equipment such as concrete cutter, shovel, trucks, breakers and road rollers are necessary.

However, in general, finite element analysis is quite time and cost consuming approach. Especially, detailed data including geotechnical profiles is necessary to obtain adequate results. Since the purpose of port-BCP is different from the seismic design but is only to provide fundamental data to consider the action plan to maintain the function of the port. Therefore, the detailed damage estimation as shown in Figure 4 is not necessary in many cases, and great use of finite element analysis is not appropriate. For example, in the case of Hachinohe port, 3 quay walls out of 37 public quay walls in the port were analyzed by the FEM.

In addition, for the risk analysis, the probabilistic information is preferable. However, the FEM result is not expressed in the probabilistic way in usual.

3.2 *Fragility curve*

Japanese Government (Cabinet Office) and prefectural governments sometimes evaluate the damage to port facilities as a part of the earthquake or tsunami damage evaluation of the region (i.e. Cabinet Office 2013, Hiroshima Prefecture 2013, Osaka prefecture 2014). In many cases of these regional damage evaluations, fragility curves for gravity type quay walls (Ichii 2004) were utilized. This fragility curve is obtained by the parametric study by FEM. The accuracy of the FEM is evaluated by case histories, and the evaluated accuracy is probabilistically reflected to the fragility curves. Thus, as shown in Figure 5, the probability of the damage occurrence to input motion level (peak acceleration at the basement) is given. The possible damage is categorized into 4 levels: level I (Serviceable), level II (Repairable), level III (Near collapse) and IV (Collapse). This category is based on the seismic design guidelines by International Navigation Congress, WG34 (PIANC 2001).

Although this fragility curve was proposed for gravity-type quay walls, it is applied for various types of quay walls except for seismic-reinforced type quay

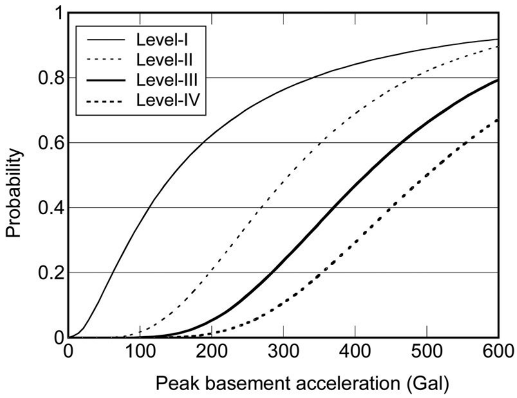

Figure 5. Fragility Curve for Gravity-Type Quay Walls (Ichii 2004).

Photograph 1. Combined Damage by Earthquake and Tsunami at Port of Soma (Taken by Tohoku Regional Bureau of MLIT).

walls. Furthermore, the fragility curves are prepared for various conditions in terms of geotechnical profiles (SPT N values and depth of foundation layers) and shape of caisson (usually corresponds to the seismic coefficient used in the design), however, adequate curves corresponds to the conditions rarely used for the damage estimation due to insufficient background data preparations in the risk analysis.

The fragility curve approach is very powerful and applicable to the port-BCP. Preparation of the curves for various types of structures and adequate preparation of the background data for all quay walls in the risk analysis is the problem to be solved.

3.3 *Tsunami damage estimation*

In current design standard for port structures in Japan, tsunami is not considered. For breakwaters, from the experience in the Great East Japan Earthquake and Tsunami Disaster, the mechanism of failure by tsunami was clarified (Arikawa et al. 2013) and consideration to build resilient breakwater is in progress. However, the consideration of the design of quay wall against tsunami is not in progress yet.

In the damage evaluation by Cabinet Office and prefectural governments, various types of consideration is implemented. In the evaluation by the Cabinet Office (2013), damage to the quay wall by tsunami is neglected and performance of breakwaters was judged by the height difference of tsunami wave and structural design wave. In the evaluation by Osaka Prefecture (2014), damage to quay walls was neglected. The settlement of breakwater by shaking and liquefaction is considered, and the breakwater is failed when tsunami height exceed the height of the breakwater. In the evaluation by Hiroshima Prefecture (2013), the function of the quay wall is suspended when the tsunami height exceeds 4 m.

These considerations are very simple and easy to apply. However, considering the damage situation in the Great East Japan Earthquake and Tsunami Disaster, these methods are not fit to the reality.

Table 1. Damage Level of Each Port in The Great East-Japan Earthquake and Tsunami Disaster.

Port	Seismic Intensity	Tsunami Inundation	Damage Level (0% 25% 50% 75% 100%)
Hachinohe	5+	2.7m	
Kuji	5-	4.4m	
Miyako	5+	3.8m	
Kamaishi	6-	7.9m	
Ofunato	6-	10.3m	
Ishinomaki	6-	3.9m	I II III
Shiogama	6+	1.7m	
Sendai	6+	4.9m	
Soma	6-	7.6m	
Onahama	6-	1.5m	

Damage Level I: No damage or can be used in a few days.
Damage Level II: Can be used in a few months by emergency rehabilitation.
Damage Level III: A few years' restoration work is needed.
Data: Tohoku Regional Bureau of MLIT

4 NEEDED DAMAGE ESTIMATION FOR PORT-BCP

The seismic evaluation methods for port-BCP shall need to satisfy the following three requirements.

(1) The complex damage due to both earthquake motion and tsunami can be considered.
(2) Easy to apply for the damage evaluation scheme in prefectural government.
(3) The damage level shall be evaluated by the required restoration period.

As for the requirement (1), at present, there is no method to consider the both effect of earthquake motion and tsunami on the damage of quay walls. In reality, there is a report showing that quay walls may be damaged by liquefaction at first, and then the damage may be increased by the tsunami (Shimosako 2013) (i.e. Photograph 1). From the seismic damage reported by Tohoku Regional Bureau of MLIT, the damage level in Soma Port and Onahama Port, where intensive

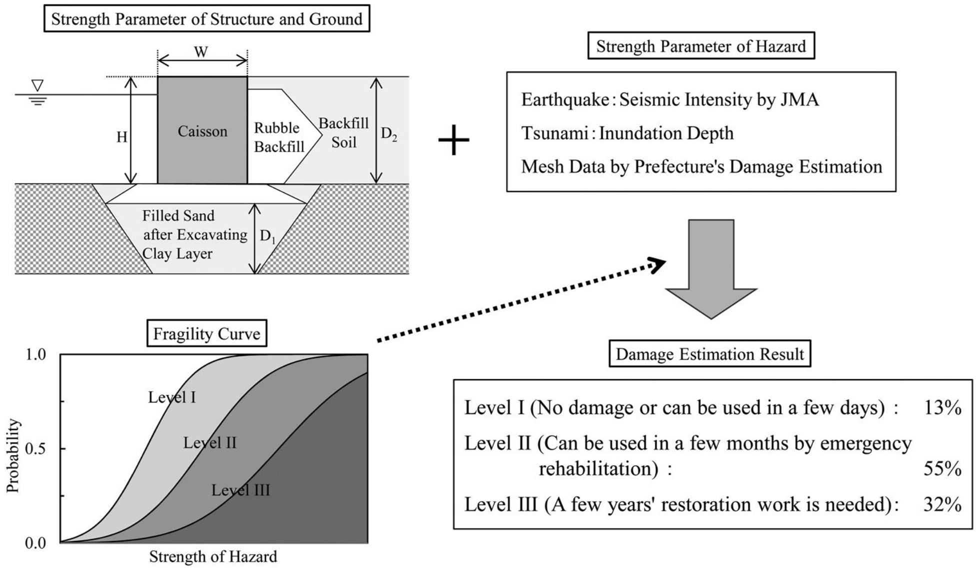

Figure 6. Conceptual Diagram of Damage Estimation of Berthing Facility for Port-BCP.

liquefaction was observed, is higher than the damage level in Sendai-Shiogama Port (Ishinomaki Port, Shiogama Port and Sendai Port), where strong shaking may be observed due to the small distance to the epicenter (Table 1 from the data by Tohoku Regional Bureau of MLIT). A method to evaluate the damage to quay wall, based on the estimation of strong motion, liquefaction and tsunami at the site is requested.

As for the requirement (2), most of ports in Japan are managed by prefectures (and large city government in some case), and the result of port-BCP shall be consistent with the damage evaluation by these prefectures or large city government. Therefore seismic hazard for port-BCP (shaking intensity and tsunami inundation height) may be given as mesh map, from the damage evaluation by these prefectures or large city government. Although these damage evaluations usually use simplified input data (without no data such as detailed geotechnical profile, site characteristics of strong motions, etc.), if the data for port-BCP can be transferred, the implementation of port-BCP is quite effective. As an example, JMA seismic intensity and tsunami inundation height shall be the parameter in the damage evaluation, since these parameter are often indicated in the damage evaluation by these prefectures or large city government.

As for the requirement (3), the purpose of damage evaluation in port-BCP is only for the estimation of restoration period. In most of the damage evaluation for port facilities, engineering parameters such as residual displacement, stress state of steel components are focused. These parameters are important for the stability and operation of the facility, however, this not the final goal in port-BCP. How long does it take to be recovered to the initial state is the most important concern. The damage level should be discussed from this viewpoint.

In addition, the results of the damage evaluation should be expressed in probabilistic way. Since the seismic induced damage is the consequence of quite complicated phenomenon, some quay walls with less seismic resistance accidentally can survive the earthquake but other quay walls with high level of seismic design accidentally collapsed. This complicated reality shall be considered in probabilistic way.

Figure 6 shows the summary of damage evaluation scheme for port-BCP. Based on both the strength parameters for structure and ground, and the strength parameter of hazard, probabilities of failure (corresponds to various level of damage in terms of restoration period) of the quay wall shall be calculated by fragility curves.

5 CONCLUSIONS

In this paper, from the practical point of view, the development of a simple earthquake-tsunami damage evaluation method necessary for port-BCP is discussed. At present, seismic design of quay wall cares only strong motions (including liquefaction), but it does not care the effect of tsunami. From the experience in the Great East Japan Earthquake and Tsunami Disaster, it is necessary to develop a method to evaluate the complex damage to quay wall induced by strong motion, liquefaction and tsunami. In this method, the parameters for hazard shall be consistent with the index used in the damage level evaluation by prefectures or large city government (i.e. JMA seismic intensity and tsunami inundation height are typical parameters to be used).

The damage level of facilities shall be classified based on the required restoration period, and the probability of failure of facilities for these damage level should be evaluated in port-BCP.

Although the damage evaluation for quay wall is focused in this paper, similar damage evaluation for various facilities such as channel, breakwaters, etc. are necessary. For example, the closure of channel by burial material (debris, vehicles and containers) shall be evaluated by the tsunami height and amount of floating objects.

Port-BCP and seismic induced damage evaluation for port-BCP are no necessary to be perfect in the beginning. It can be improved step by step. Therefore, preparation of the first trial version is anyway important and the authors wish this paper could be a good step for the first development of port-BCP.

ACKNOWLEDGEMENT

The authors would like to thank Tohoku Regional Bureau of MLIT for assistance during this study. This study was supported by JSPS KAKENHI Grant Number 25289165.

REFERENCES

Aomori Prefecture 2013. *Hachinohe Port BCP*. (In Japanese)

Arikawa T., Satou M., Shimosako K., Tomita T., Yeon G. & Niwa T. 2013. Failure Mechanism and Resiliency of Breakwaters under Tsunami, *Technical Note of The Port and Airport Research Institute, No.1269*. (In Japanese)

Cabinet Office 2013. *Damage Estimation of Nankai-Trough Mega Earthquake 2nd Report*, Conference Material No.4, Damage Estimation Item and Outline of Procedure. (In Japanese)

Hiroshima Prefecture 2013. *Survey Report of Earthquake Damage Estimation of Hiroshima Prefecture*. (In Japanese)

Iai, S., Matsunaga, Y. & Kameoka, T., (1990). Strain space plasticity model for cyclic mobility, *Report of the port and harbour research Institute*, Japan, Vol.29, No.4, pp.27–56.

Ichii, K. 2004. Fragility Curves for Gravity-Type Quay Walls Based on Effective Stress Analyses, *13th World Conference on Earthquake Engineering*, *Paper No. 3040, August 1–6 2004*, Vancouver B.C., Canada.

Niki, K. 2012. *Risk Management 2nd Edition*: Toyo Keizai Inc. (In Japanese)

Ono K., Takino, Y. & Akakura Y. 2014. Development of Making Procedure of Business Continuity Plan for Port Logistics by Using Business Impact Analysis, *Proceedings of Infrastructure Planning of Japan Society of Civil Engineers, Vol.49, 6–7 June 2014.* Sendai: Japan. (In Japanese)

Osaka Prefecture 2014. Damage Estimation Procedure, *Review Meeting for Response to Nankai-Trough Mega Earthquake, 5th Meeting*, Reference Material No.1. (In Japanese)

Overseas Coastal Area Development Institute of Japan 2009. *Technical Standards and Commentaries for Port and Harbour Facilities in Japan.* (Japanese Ver.: Port and Harbours Association of Japan).

PIANC, 2001, *Seismic design guidelines for port structures*, Balkema.

Shimosako K., Breakwater Failure due to Tohoku Earthquake Tsunami, *Nagare, Vol.32, No.2, pp.27–32, The Japan Society of Fluid Mechanics.* (In Japanese)

Geotechnics for Catastrophic Flooding Events – Iai (Ed)
© 2015 Taylor & Francis Group, London, ISBN 978-1-138-02709-1

Reliability on the stability of long continuous earth-structures

T. Hara, M. Nonoyama, Y. Otake & Y. Honjo
Gifu University, Gifu, Japan

ABSTRACT: This paper shows a reliability estimation example of the present seismic verification and retrofit design on a continuous earth-structure from the viewpoint of uncertainties, such as reproducibility of geotechnical analysis and quantity of subsurface exploration, and discuss the future direction of the seismic measure scheme of long continuous earth-structures.

1 INTRODUCTION

The seismic verification and the retrofit design of continuous earth-structures, such as river dike, road embankment and water canal, are carried out with using geotechnical analysis at the points of subsurface exploration executed at intervals of several hundred meters. In this scheme, the seismic response of the target structure, which is obtained from geotechnical analysis, such as FEM, is treated as a deterministic value and the structural soundness is evaluated from the comparison between the response and allowable value with considering safety factor to the limit value. The approach of the scheme, unfortunately, cannot evaluate the structural soundness in various areas with the same safety level, because the reproducibility of the seismic response is different depending on what geotechnical analysis the designer used and the reliability distribution of the geo-model is different depending on the quantity of subsurface exploration.

Therefore, this paper describes a reliability estimation example of the present scheme, seismic verification and retrofits design on a continuous earth-structure, and discusses the future direction of the seismic measure scheme of long continuous earth-structures.

2 PROCEDURE FOR THIS STUDY

Figure 1 shows the procedure for this study. The seismic verification and the retrofit design on the target structure, which are based on the present scheme, with respect to the assumed conditions in this example are carried out at first. And then next, the reliability of the results based on the present scheme is estimated with considering uncertainties of geotechnical analysis reproducibility and geo-model. Here, in order to consider the uncertainty effect of the geo-model to the estimated response by geotechnical analysis,

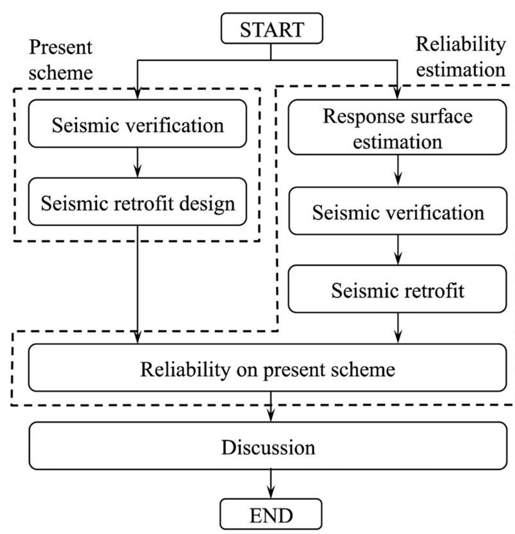

Figure 1. Procedure for this study.

response surface method (Honjo 2011) is adopted in this study. At last, the future direction of seismic measure scheme is discussed from the estimated reliability of the present scheme.

3 EXAMPLE CONDITIONS

3.1 *Target structure*

The embankment canal of 5 km, which is built on liquefiable ground during earthquake, as shown in Figure 2 to 5 is to be the target structure as a continuous earth-structure in this example. The allowable subsidence of the canal is 0.6 m with considering safety factor of 2.0 to the limit one of 1.2 m.

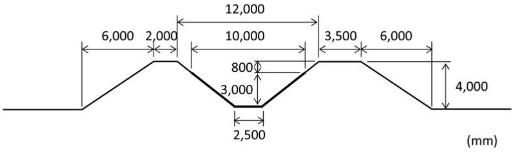

Figure 2. Target structure.

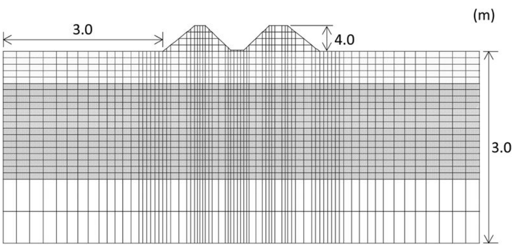

Figure 3. FEM mesh of the target structure.

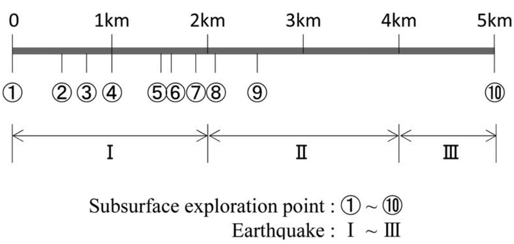

Figure 4. Subsurface exploration points.

3.2 *Geotechnical analysis*

The seismic response of the target structure is estimated by dynamic effective stress FEM (LIQCA, Oka 1994) in this example. Figure 3 shows the FEM mesh. The soil layer composition of the mesh (geo-model) is varied depending on one of the respective subsurface exploration point. The geotechnical parameters to input to FEM were determined by the element simulation with respect to the dynamic laboratory tests of the specimens obtained from one of subsurface exploration points.

3.3 *Subsurface exploration*

10 standard penetration tests (SPT) had been carried out in this range. Figure 4 and 5 show the subsurface exploration points and each SPT result, respectively. Here, 2.5 km interval is included in the subsurface exploration though, extreme condition is assumed to know the effect of subsurface exploration interval to the reliability in this example.

3.4 *Target earthquake*

3 deterministic earthquakes, as shown in Figure 4, are considered as the target ones in this example. Figure 6 shows the target earthquakes.

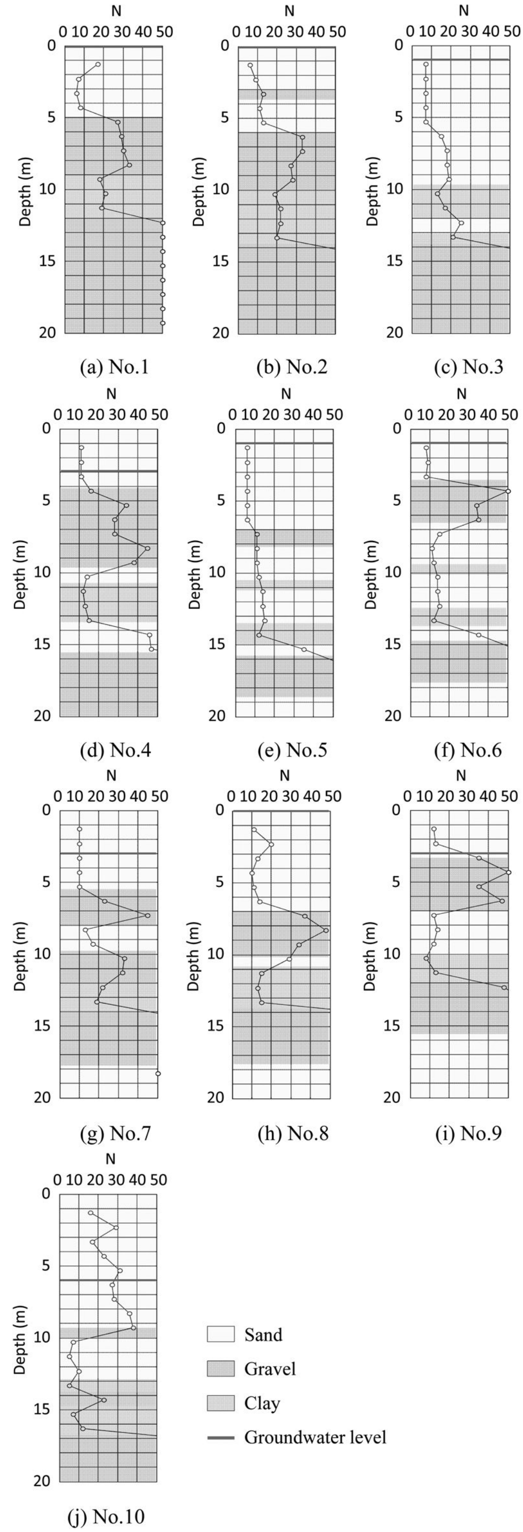

Figure 5. SPT result of each subsurface exploration points.

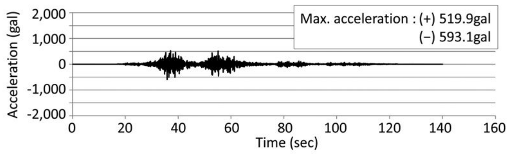

(a) Earthquake 1

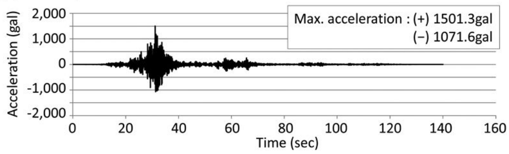

(b) Earthquake 2

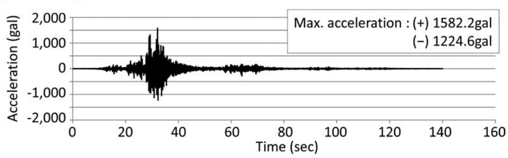

(c) Earthquake 3

Figure 6. Earthquakes adopted in this example.

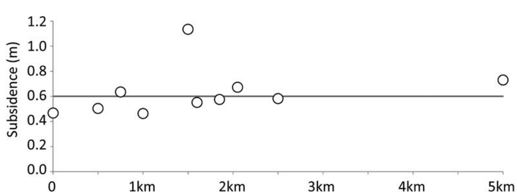

Figure 7. Seismic verification result.

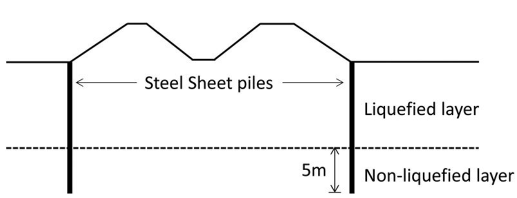

Figure 8. Countermeasure using steel sheet piles.

4 PRESENT SCHEME

4.1 *Seismic verification*

Figure 7 shows the seismic verification results of the target structure. According to the results, it is considered that the canal without countermeasure exceeds the allowable subsidence at 4 points of subsurface exploration.

4.2 *Seismic retrofit design*

Two countermeasures, one using steel sheet piles with drainage, as shown in Figure 8, another one is chemical grouting, are targeted in this example. The range of the countermeasure execution is usually determined by engineering judgment though; it was assumed as the range between the middle points of two subsurface exploration points, which are ones exceeding and un-exceeding allowable subsidence, in this example. Figure 9 shows the countermeasure range and the effect of the countermeasure to seismic response.

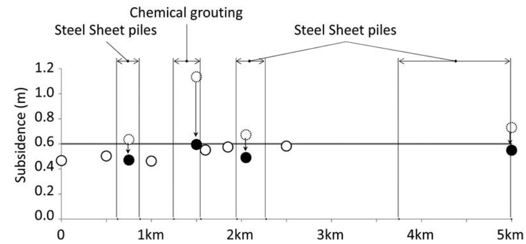

Figure 9. Countermeasure range and the effects.

5 RELIABILITY ESTIMATION

5.1 *Response surface estimation*

Response surface (Honjo 2011), approximate relationship between the seismic response obtained by FEM analysis and contribution factors to the response, is studied at first, in order to estimate the seismic response depending on the uncertainty of geo-model, such as soil layer composition, stiffness of each layer and liquefaction extent of the liquefiable layers.

Equations 1 to 4 present the response surfaces of each condition, which were obtained from parametric studies.

Case without countermeasure;

($H_a > 0.62$)

$$S = \left[5.15 - 6.44\left\{1 - EXP\left(-\frac{H_a - 0.6}{0.3}\right)^{0.14}\right\}\right] \cdot \left[1 - EXP\left(-\frac{FS_{03} - 1.8}{1.8}\right)^{0.7}\right] \tag{1}$$

($0.1 < H_a <$ or $= 0.62$)

$$S = 3.67\left[1 - EXP\left(-\frac{0.7 - H_a}{0.3}\right)^{0.13}\right] \cdot \left[1 - EXP\left(-\frac{FS_{03} - 1.8}{1.8}\right)^{0.7}\right] \tag{2}$$

Case with steel sheet pile countermeasure;

$(H_a > 0.62)$

$$S = \left[5.75 - 7.62\left\{1 - EXP\left(-\frac{H_a - 0.6}{0.29}\right)^{0.12}\right\}\right] \cdot \left[1 - EXP\left(-\frac{FS_{03} - 1.8}{2.5}\right)^{0.7}\right] \tag{3}$$

$(0.1 < H_a <$ or $= 0.62)$

$$S = 3.09\left[1 - EXP\left(-\frac{0.7 - H_a}{0.3}\right)^{0.09}\right] \cdot \left[1 - EXP\left(-\frac{FS_{03} - 1.8}{2.5}\right)^{0.7}\right] \tag{4}$$

where, S = subsidence (m), H_a = average shear stiffness of the ground range of 20 m depth from the surface (10^5 kPa), which is calculated by Equation 5,

$$H_a = \sum_0^{20} a \cdot G_{N1} \cdot F_L^2 \cdot dx \Big/ 20 \tag{5}$$

a = correction coefficient concerning depth of liquefiable layer from the surface, which is presented Equation 6,

$$\begin{aligned} a &= 1.0 \quad (F_L \geq 1.0) \\ a &= 0.1x \quad (F_L < 1.0) \end{aligned} \tag{6}$$

x = depth from the ground surface (m), F_L = resistance ratio against liquefaction, which is calculated by Equation 7,

$$F_L = R \big/ L \tag{7}$$

R = liquefaction strength ratio, L = cyclic shear stress ratio during earthquake, G_{N1} = shear modulus (kPa), which is calculated by Equation 8,

$$G_{N1} = \frac{\gamma_t}{g} \cdot V_{sN1} \tag{8}$$

γ_t = wet unit weight of soil (kN/m^3), g = gravitational acceleration (m/s^2), V_{sN1} = shear wave velocity (m/s), which is calculated by Equation 9,

$$V_{sN1} = 80 \cdot N_1^{1/3} \tag{9}$$

N_1 = revised SPT-N value by confining pressure, which is calculated by Equation 10,

$$N_1 = \frac{170N}{\sigma_v' + 70} \tag{10}$$

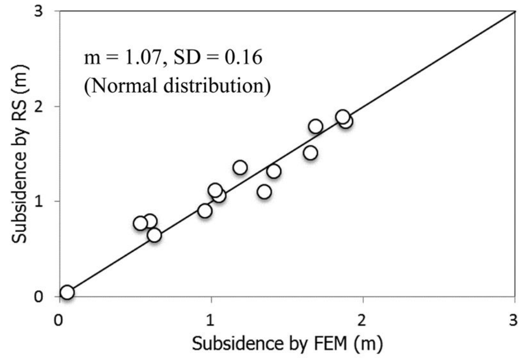

(a) Case without countermeasure

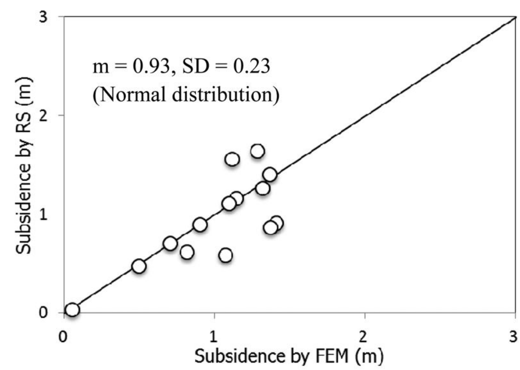

(b) Case with steel sheet pile countermeasure

Figure 10. Reproducibility of the response surfaces.

N = SPT-N value, σ_v' = effective confining pressure (kPa), FS_{03} = integral acceleration Fourier spectra of 0–3 Hz (gal), FS_{03} of earthquake 1, 2 and 3 are 2.94, 5.00, 10.1, respectively, for instance.

The reproducibility of the response surfaces (RS) with respect to the responses estimated by FEM analyses, which is obtained from parametric studies, is shown in Figure 10.

5.2 *Uncertainty of FEM reproducibility*

Figure 11 shows the uncertainty of FEM reproducibility with respect to the dynamic experimental responses of the embankment built on liquefied ground during earthquake, which is obtained from blind tests (JICE 2002). Because of blind test, the setting error of the geotechnical parameters to input into the FEM is included in the uncertainty.

5.3 *Uncertainty of subsurface exploration*

Figure 12 shows the variation of H_a value as the uncertainty of subsurface exploration. Here, H_a value at the investigated point is to be deterministic value, and mean value and variation are calculated by Kriging method (Dagan 1982, Otake 2012) with using the

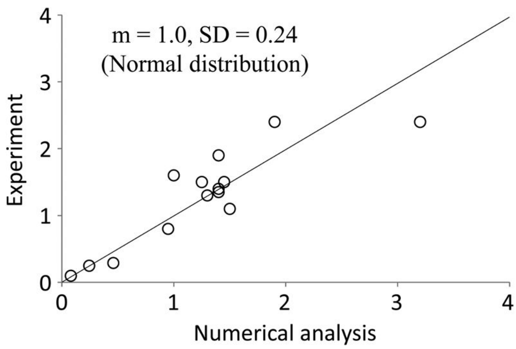

Figure 11. FEM reproducibility (LIQCA).

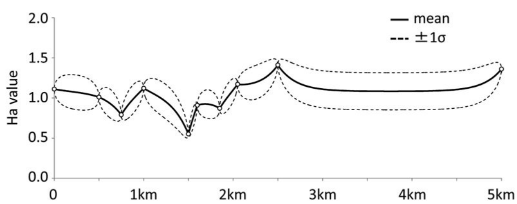

Figure 12. Uncertainty of subsurface exploration.

uncertainty of H_a value and autocorrelation distance of all data.

In the present scheme, the application range of the investigated point data is determined by engineering judgment. The judgment based on enough experiences is, of course, important though; there must be anxiety the designers feel, because everyone knows that uncertainty exists in the application of investigated data to other area of invisible ground content. This paper tried to express the anxiety by the uncertainty of the application with using Kriging method. The uncertainty increase so as to be long the interval to the next point or as to be large the difference from the next point data.

5.4 *Reliability on seismic verification*

The failure probability of seismic verification with respect to the limit subsidence, 1.2 m, at a given point is estimated from the performance function presented by Equation 11 and 12.

The distribution of subsidence and the failure probability are shown in Figure 13 and 14, respectively.

($H_a > 0.62$)

$$g = R - S \geq 1.0$$
$$= 1.2 - \left(\begin{array}{l} \left[5.15 - 6.44 \left\{ 1 - EXP\left(-\dfrac{H_a \cdot \delta_{Ha} - 0.6}{0.3} \right)^{0.14} \right\} \right] \\ \cdot \left[1 - EXP\left(-\dfrac{FS_{03} - 1.8}{1.8} \right)^{0.7} \right] \end{array} \right) \tag{11}$$
$$\cdot \delta_{RS} \cdot \delta_{FEM} \geq 1.0$$

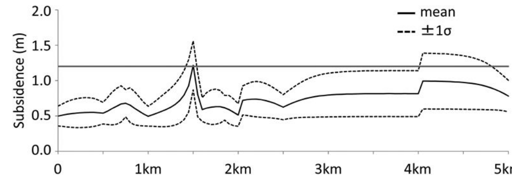

Figure 13. Subsidence with considering H_a variation.

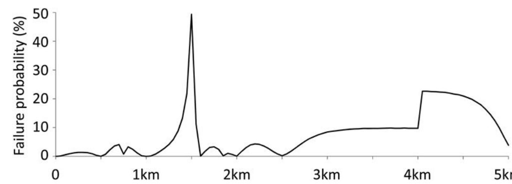

Figure 14. Failure probability without countermeasure.

($0.1 < H_a <$ or $= 0.62$)

$$g = R - S \geq 1.0$$
$$= 1.2 - \left(\begin{array}{l} 3.67 \left[1 - EXP\left(-\dfrac{0.7 - H_a \cdot \delta_{Ha}}{0.3} \right)^{0.13} \right] \\ \cdot \left[1 - EXP\left(-\dfrac{FS_{03} - 1.8}{1.8} \right)^{0.7} \right] \end{array} \right) \tag{12}$$
$$\cdot \delta_{RS} \cdot \delta_{FEM} \geq 1.0$$

where, δ_{Ha} = random variables of H_a value estimated by Kriging method at a given point, δ_{RS} = random variables of the response surface reproducibility with respect to the response obtained by FEM in case without countermesure, m = 1.07 and SD = 0.16 with normal distribution, δ_{FEM} = random variables of FEM reproducibility with respect to experimental data, m = 1.0 and SD = 0.24 with normal distribution.

5.5 *Reliability on seismic retrofit design*

The failure probability of seismic retrofit design in the case using steel sheet pile walls with respect to the limit subsidence, 1.2 m, at a given point is estimated from the performance function presented by Equation 13 and 14. In the case of chemical grouting, the probability is estimated by Equation 11 and 12 with the F_L value of the liquefiable layers is set to be 1.0.

The distributions of subsidence in both measured cases of using steel sheet pile with drainage and chemical grouting are shown in Figure 15 and 16, respectively.

($H_a > 0.62$)

$$g = R - S \geq 1.0$$
$$= 1.2 - \left(\begin{array}{l} \left[5.75 - 7.62 \left\{ 1 - EXP\left(-\dfrac{H_a \cdot \delta_{Ha} - 0.6}{0.29} \right)^{0.12} \right\} \right] \\ \cdot \left[1 - EXP\left(-\dfrac{FS_{03} - 1.8}{2.5} \right)^{0.7} \right] \end{array} \right) \tag{13}$$
$$\cdot \delta_{RS} \cdot \delta_{FEM} \geq 1.0$$

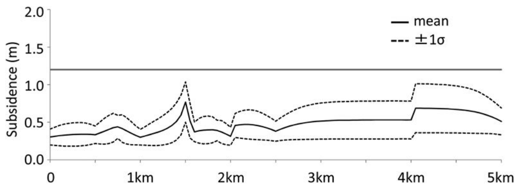

Figure 15. Subsidence (with using steel sheet pile).

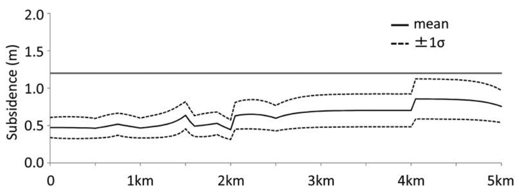

Figure 16. Subsidence (with using chemical grouting).

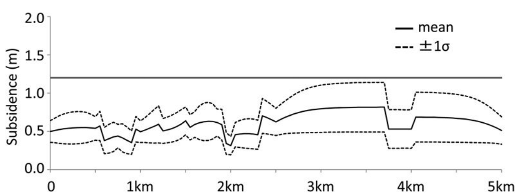

Figure 17. Subsidence of the retrofitted water canal.

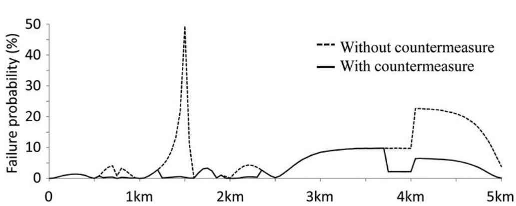

Figure 18. Failure probability of the present scheme.

$(0.1 < \mathrm{H_a} < \text{or} = 0.62)$

$$g = R - S \geq 1.0$$
$$= 1.2 - \left(\begin{array}{l} 3.09\left[1 - EXP\left(-\dfrac{0.7 - H_a \cdot \delta_{Ha}}{0.3}\right)^{0.09}\right] \\ \cdot\left[1 - EXP\left(-\dfrac{FS_{03} - 1.8}{2.5}\right)^{0.7}\right] \end{array} \right) \qquad (14)$$
$$\cdot \delta_{RS} \cdot \delta_{FEM} \geq 1.0$$

where, δ_{RS} = random variables of the response surface reproducibility with respect to the response obtained by FEM in case with steel sheet pile counter measure, m = 0.93 and SD = 0.23 with normal distribution.

5.6 *Reliability on the present scheme*

The subsidence distribution and the failure probability with respect to the limit subsidence, 1.2 m, of the seismic retrofit design based on the present scheme, which

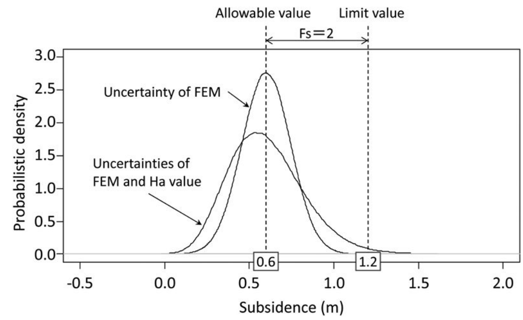

Figure 19. Implicit failure probability in the present design.

is described at the section 4.2, are shown in Figure 17 and 18, respectively.

According to the results, it can be confirmed that the failure probabilities exist in the case of the seismic retrofit design based on the present scheme and they are not small.

6 DISCUSSION

This paper presented an example of reliability estimation on the present seismic verification and retrofit design on a long continuous earth-structure from the viewpoints of geotechnical analysis reproducibility and subsurface exploration intervals. And the existence of failure probability that cannot be ignored was confirmed as the result.

This study describes the importance of reliability estimation from following the viewpoints:

(1) Designers can recognize the potential hazard of their design based on the uncertainties of the geotechnical analysis they adopted and subsurface exploration used in the design.

For example, although designers implicitly consider the target failure probability of nearly 0% from the viewpoint of both safety factor and FEM reproducibility, there must be uncertainty depends on subsurface exploration, and the uncertainty affect to failure probability as shown in Figure 19. As the result, the residual failure probability, which is one of somewhere exceed the limit value within the entire canal, on the seismic retrofit design based on the present scheme is 96.6% in this example.

(2) If designers know the reliability on the design, application of appropriate and effective measure can be studied, additional subsurface exploration for instance. For example, if the uncertainty of the geo-model is reduced, the failure probability of the latter canal of 2.5 km may be able to be decreased in this example. There are many cases that additional subsurface exploration is the most reasonable measure to reduce failure probabilities.
(3) Reliability estimation can be applied to risk assessment and management. Furthermore, designers can study the most reasonable measure from

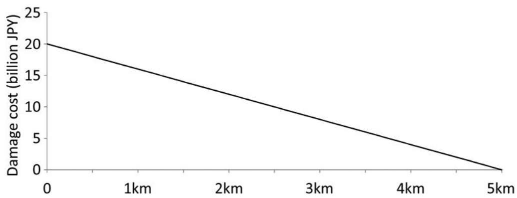

Figure 20. An assumption of damage cost distribution.

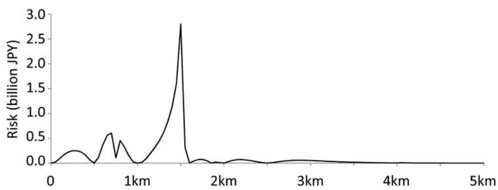

(a) Risk distribution before retrofit execution

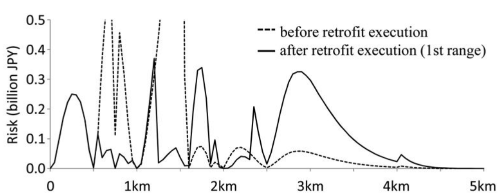

(b) Risk distribution after the retrofit execution to the 1st range

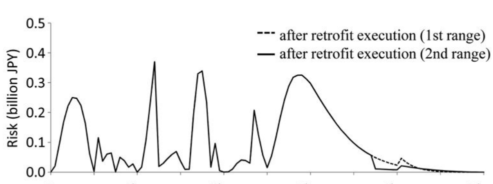

	0 ~ 2.5km	2.5km ~ 5km	Total
Risk0	13.22	0.88	14.10
Cost1	2.98	-	2.98
Risk1	4.64	4.90	9.54
Cost2	-	2.22	2.22
Risk2	4.64	4.72	9.36
Benefit	8.58	0.18	4.74
B/C	2.88	0.08	0.91

(c) Risk distribution after the retrofit execution to latter range

Figure 21. Risk analysis of the present scheme.

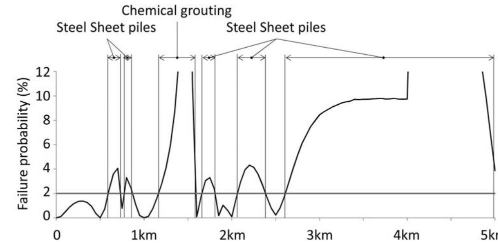

(a) Target reliability approach

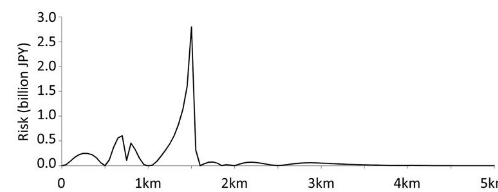

(b) Risk distribution before retrofit execution

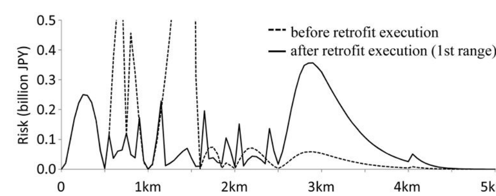

(c) Risk distribution after the retrofit execution to the 1st range

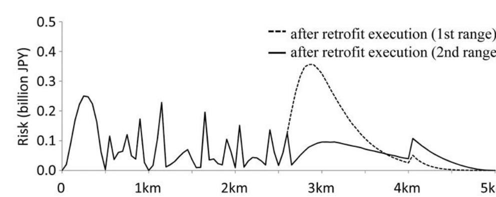

	0 ~ 2.5km	2.5km ~ 5km	Total
Risk0	13.22	0.88	14.10
Cost1	3.14	-	3.14
Risk1	3.82	5.36	9.18
Cost2	-	4.10	4.10
Risk2	3.82	2.81	6.63
Benefit	9.40	2.55	7.47
B/C	2.99	0.62	1.03

(d) Risk distribution after the retrofit execution to latter range

Figure 22. An example of risk management.

the viewpoint of the cost-effectiveness of B/C, the ratio of the risk reduction and the measure cost.

For example, if the damage cost of the 5km water canal was assumed as Figure 20, the risk reduction and the B/C of the seismic retrofit based on the present scheme is estimated as shown in Figure 21. Here, the risk of given points with considering the effect of upstream failure probability to the given points are estimated by Equation (15).

$$R_n = (1-p_1)\cdot(1-p_2)\cdots(1-p_{n-1})\cdot p_n \cdot D_n \tag{15}$$

where, R_n: risk of the n-th block, the length of 1 block is 50 m in this example, p_n: failure probability of the n-th block, D_n: damage cost of n-th block.

In Figure 21(c), Risk0 means the respective risks of the first and latter ranges before retrofit execution. Cost1 and 2 mean respective countermeasure costs of the first and latter ranges. Risk1 means the respective risks of the first and latter ranges after retrofit execution to only the first range. Risk2 means the respective risks of the first and latter ranges after retrofit execution to latter range. Benefit of the first range is evaluated by the difference of Risk0 and 1, one of the latter range is evaluated by the difference of Risk1 and 2.

According to the result, it can be confirmed that the seismic retrofit design based on the present scheme is not appropriate, because the risk reduction by the execution of seismic retrofit is 4.7 billion JPY against the retrofit cost of 5.2 billion JPY, $B/C = 0.91 < 1.0$, as shown in Figure 21(c). This is the reason, why the allocation of the seismic retrofit is not appropriate. For example, in case of considering from 2 ranges of the first 2.5 km and latter 2.5 km, the risk of latter range is increased by the seismic retrofit execution to the first range, as shown in Figure 21(b) though, the allocation of seismic retrofit based on the present scheme cannot decrease effectively the risk of the latter range as shown in Figure 21(c).

On the other hand, if the risk management based on the reliability estimation with an assumption of target reliability, 2% for instance, is conducted as shown in Figure 22 (a), effective seismic retrofit, B/C = (risk reduction: 7.5 billion JPY)/(retrofit cost: 7.2 billion JPY) = 1.03, can be achieved, because of the appropriate seismic retrofit allocation to the latter range.

As shown in the example above, reliability estimation can be applied to reasonable seismic retrofit design of continuous earth structures.

7 CONCLUSION

The importance and the effectiveness of reliability estimation to the future seismic retrofit design on long continuous earth structures were discussed from a reliability estimation example of an embankment water canal in this paper. This paper is concluded as follows;

(1) Residual failure probability exists after the execution of seismic retrofit based on the present scheme.
(2) Uncertainty of subsurface exploration as well as one of geotechnical analysis reproducibility affect to the residual failure probability.
(3) The residual failure probability can be quantitatively estimated by reliability estimation.
(4) If the residual failure probability is cleared, designers can study on the most reasonable seismic retrofit design.
(5) Additional subsurface exploration is one of the effectiveness countermeasures to reduce the residual failure probability.
(6) Reliability estimation can be applied to risk management.
(7) There are cases that the seismic retrofit design based on the present scheme is not effective treatment from the viewpoint of risk reduction and cost-effectiveness, B/C.
(8) There are cases that designers can find the most effective treatment of seismic retrofits from risk management based on reliability estimation.

Although risk estimation is not only desirable approach, the authors expect that the reliability consideration can be applied to development of more reasonable seismic retrofit design approach than the present one.

REFERENCES

Dagan, G. 1982. Stochastic modeling of groundwater flow by unconditional and conditional probabilities, 1, Conditional simulation and the direct problem, *Water Resourced Research*: Vol.18, No.4, 813–833.

Honjo, Y. 2011. Challenges in geotechnical reliability based design; *Proc. of the 3rd intern. symp. On Geotechnical Safety and Risk, 11–27*, Munich, 2–3 June 2011.

Japan Institute of Construction Engineering (JICE). 2002. Analysis method of seismic river dike deformation, *JICE Document*: Col.102001.

Oka, F., Yashima, A., Shibata, T., Kato, M. & Uzuoka, R. 1994. FEM-FDM coupled liquefaction analysis of a porous soil using an elasto-plastic model, *Applied Scientific Research*: Vol.52, 209–245.

Otake, Y. & Honjo, Y. 2012. A practical geotechnical reliability based design employing response surface – Seismic design of irrigation channel on liquefiable ground –, Journal of Japanese Society of Civil Engineering (JSCE): Vol. 68 No.1, 68–83.

Panel Discussions "How to meet catastrophic flooding events?"

This page intentionally left blank

Geotechnics for Catastrophic Flooding Events – Iai (Ed)
© 2015 Taylor & Francis Group, London, ISBN 978-1-138-02709-1

Prelude to Panel Discussion: How to meet catastrophic events

W.D. Liam Finn
University of British Columbia, Vancouver, BC, Canada

ABSTRACT: Initial thoughts on three questions posed by Chairman Professor S. Iai for the Panel Discussion at the Kyoto Conference.

1 QUESTION 1. WHEN YOU WERE YOUNG HOW DID YOU COME UP WITH NEW IDEAS AND EXPLOIT THEM?

My profession is geotechnical earthquake engineering and I entered the field in 1964 in the aftermath of the Niigata and Alaska earthquakes. Almost nothing quantitative was known about the mechanisms by which earthquakes affected sites, caused liquefaction and damaged port structures. The devastation caused by these two earthquakes sharply focused the attention of geotechnical engineers on these problems. New ideas were easy to come by because they were driven by the need to solve the fundamental questions about seismic response posed by the events in Niigata and Alaska. The way things should develop was also constrained: it was obvious that soil testing methods that simulated the cyclic loading by earthquakes was fundamental to all other studies; to quantify earthquake induced motions required methods for site response analysis and methods of seismic slope stability had to be developed. As a result of the difficulty of getting undisturbed samples of soil, in situ methods based on SPT and CPT were developed for assessing liquefaction potential. All research was driven by obvious needs and it was usually fairly obvious how to go about providing answers. From 1964 to about 1984 was the golden age of geotechnical earthquake engineering. Today the field is mature and sophisticated. It is much more difficult to develop truly creative new ideas. This may partly explain the big effort devoted to developing new constitutive models even though already at least 100 are available.

2 QUESTION 2. GEOTECHNICAL MEASURES TO MEET CATASTROPHIC FLOODING EVENTS

Two major geotechnical concerns are the stability of saturated slopes with or without surface runoff and the stability of flood protection dikes. Earlier in this year 130 people lost their lives in Washington State when their small community was hit by a major slope failure in saturated soils. The important elements in levee safety are to ensure no erosion of the river side slopes and avoidance of seepage induced failures on the landslide slopes. Overtopping of the levee is also a major concern which can lead to breaching of the levee by erosion. The risk of overtopping depends on the flood height to the government is willing to raise the levees. This decision should be based on a detailed study of past floods and the use of a flood projection model that preferably should contain a component related to climate change. With respect to climate change, it should be noted that insurance companies in Canada are now considering not to insure against floods unless there is a modern flood map available for the location that takes in account climate change.

A devastating flash flood inundated Calgary, Alberta in 2013 causing billions in damage and leading to about 125,000 people being evacuated. It was one of Canada's great disasters. The city of Calgary, in planning for the future is considering boring a 5km tunnel under the city to carry off flood water.

Engineering measures to deal with future flooding are very important but with fiscal restraints on what can be the residual risk is always substantial. Therefore the most important weapon for mitigating the dangers from flooding is informed risk management. A risk management plan drafted by a qualified professional should be the foundation for planning effective emergency response measures and drafting public policy regarding floods. Such policy is needed if zonation in the flood plain is to be one tool in the mitigation of flood threats and damage.

3 QUESTION 3. ADVICE TO YOUNG RESEARCHERS IN GEOTECHNICAL ENGINEERING

I asked this question many years ago of the late Professor Harry Seed. His answer was simple and direct. "Do something important and you will have the satisfaction of contributing to society and getting recognition". I have followed his advice in my own career and have had no cause to regret it.

Today it is much more difficult to develop truly innovative research problems because geotechnical engineering is a mature field – nearly all the easy problems have been dealt with satisfactorily. The main areas for research innovation are particle physics in which sand is treated as sand particles, not as a continuum and constitutive modelling. However, the latter, in an effort to explain everything, have become very complicated with anywhere from 12 to 24 constants which render them not suitable for general practice. It is too difficult and uncertain to calibrate them to field conditions. There is scope for program validation by field case histories, particularly for programs used in practice. Centrifuge testing offers similar opportunities.

Geotechnics for Catastrophic Flooding Events – Iai (Ed)
© 2015 Taylor & Francis Group, London, ISBN 978-1-138-02709-1

Prelude to Panel Discussion: How to meet catastrophic events

Michel J. Pender
Department of Civil and Environmental Engineering, University of Auckland, New Zealand

ABSTRACT: Personal reflections in response to the three questions raised by Chairman Professor S. Iai for the Panel Discussion at the Kyoto Conference.

1 QUESTION 1. WHEN YOU WERE YOUNG HOW DID YOU COME UP WITH NEW IDEAS AND EXPLOIT THEM?

My first comment is that I was passionate about understanding soil behaviour. The sense of relief at completing my undergraduate studies with all the associated compulsory learning was enlivening. Now I was studying a discipline that I found to be fascinating, was ripe for new development, and was likely to produce understanding that was useful in engineering practice. I started my graduate studies in the middle 60's. I spent much of the first six months of my PhD time in the library. I was able to review all the issues of Geotechnique, Soils and Foundations, the Journal of the ASCE Soil Mechanics and Foundations Division, the Canadian Geotechnical Journal, as well as the proceedings of all the conferences of the International Society of Soil Mechanics and Foundation Engineering. So at the end of six months I had a good overview of what was happening in soil mechanics. (This is an opportunity not available to starting researchers today as the literature is now vast.)

The most important realization that came from this was that soil was not an elastic material, despite the often used assumption in geotechnical engineering. That in turn led to a fascination with Critical State Soil Mechanics and the Cam clay and Modified Cam clay models for soil stress-strain-strength behaviour.

From there I was fortunate enough to suggest an incremental development of the Critical State models that catered for the nonlinear behavior of overconsolidated soil; the subsequent paper published in Geotechnique still receives an occasional citation. From there I wanted to extend the model to cyclic behavior of soil and the phenomenon of cyclic mobility. In this I was not successful, although others have since achieved this. The lesson from this is two-fold. First really good ideas do not come often. They are preceded by many unsuccessful concepts. The best chance of success comes, I think, from a willingness to explore many and different approaches and not allowing one's thinking to be bounded by the fashions presented in the current literature. So persistence is important, not becoming discouraged, being ready to take a clean sheet of paper and start again! This process requires a certain amount of confidence in oneself. Second there is often an element of luck involved.

The actual process by which ideas arise is rather mysterious. However, total immersion in a topic area is essential. Surprisingly, I find that new ideas don't come while one is actually thinking about the subject at hand, but, once total immersion has been established, they pop into one's mind at times when one is otherwise engaged – perhaps there is a subconscious processing mechanism at work.

2 QUESTION 2. GEOTECHNICAL MEASURES TO MEET CATASTROPHIC FLOOD EVENTS.

Recently we have witnessed a number of huge natural catastrophes. A defining aspect of these is that they extend further than one type of hazard; no doubt the reason the term multi-hazard has come into use recently. Geotechnical matters, then, are just one facet of a bigger picture.

The discussion question asks about flooding and geotechnical issues. Recent experience in New Zealand confirms, yet again, that liquefaction is associated with nearly all major earthquakes and how the consequences of this may be associated with flooding (see below). Clearly land stability is affected by flooding, in this case erosion of material at the base of slopes being an important mechanism. Again earthquake induced slope instability in steep terrain is known to form landslide dams in rivers, the overtopping of which leads to further problems downstream. Flooding is usually a consequence of intense rainfall. Recently there have been examples of catastrophic landslides from hill slopes that have become saturated. Another consequence of intense rainfall is the loss of agricultural pasture from hill county slopes so the flood debris may be more than runoff water. Geotechnical insight is important in the design of stop-banks to contain flood waters. These systems, like all infrastructure, require regular inspection and maintenance and even re-building when new understanding comes to hand.

Recent experience in NZ reveals links between flooding and liquefaction. First, the town of Kaiapoi, a little north of Christchurch, was established in the second half of the 19th century. A sequence of serious floods of the Waimakariri river affected the town. The residents embarked on several ambitious projects to alter the course of the river. This was achieved. Sand filling was then placed in and around the town. However, when the earthquakes occurred in 2010 and 2011 there was major liquefaction in those parts of Kaiapoi which had the sand filling (Wotherspoon et al 2011). Here we have an example of human activity to alleviate problems from one type of natural hazard, flooding, which inadvertently led to problems from another, liquefaction. Unfortunately that is not the end of the flooding problems in Christchurch. The major liquefaction in the eastern parts of Christchurch in 2010 and 2011 caused a regional subsidence of about 1 m. This has led to potential flooding problems. The spring tides were handled by placing stopbanks along the Avon and Heathcote rivers. But there is still a part of Christchurch that is now affected by flooding when there is heavy rainfall as a basin structure has formed without a natural escape route for the water – there have been several instances of this flooding after heavy, though not unusually so, rainfall in 2014. So in this case the flooding problem is a longer term consequence of the earthquake and the liquefaction.

3 QUESTION 3. ADVICE TO YOUNG RESEARCHERS IN GEOTECHNICAL ENGINEERING

Become acquainted with current developments in some aspect(s) of the subject that is intellectually demanding. This is the type of thing young minds can grasp with comparative ease and stays with one for a long time.

Get involved in some real engineering – in other words learn to calibrate your research interests to projects of interest to the local community and so ensure that your research is relevant.

Develop and maintain an awareness of where the discipline is, where it is going, and how where your contribution fits-in.

Find good mentors. Generally they are only too willing and respond well to youthful enthusiasm and the need for guidance.

REFERENCE

WOTHERSPOON, L. M., PENDER, M. J., and ORENSE, R. P. (2011) Relationship between observed liquefaction at Kaiapoi following the 2010 Darfield earthquake and former channels of the Waimakariri River. Engineering Geology 125, 45–55.

Geotechnics for Catastrophic Flooding Events – Iai (Ed)
© 2015 Taylor & Francis Group, London, ISBN 978-1-138-02709-1

Contribution to Panel Discussion: How to meet catastrophic events

H. Ohta
Chuo University, Tokyo, Japan

ABSTRACT: 'Preliminary thoughts on three questions posed by Chairman Professor S. Iai for the Panel Discussion at the Kyoto Conference.

1 QUESTION 1: WHEN YOU WERE YOUNG HOW DID YOU COME UP WITH NEW IDEAS AND EXPLOIT THEM?

Two ideas were produced by me in my younger days in the last part of 1960's:

(i) an elasto-plastic constitutive model developed as an extension of the experimental works on negative dilatancy (contractancy) of normally consolidated clays published by Professor Toru Shibata in 1963,
(ii) estimation of constant-volume shear strengths of compacted fill materials by introducing a concept of (equivalent) preconsolidation pressure related to the compaction efforts.

It took several years for me to fully develop these ideas before finalizing both of them which happened to be published in the same year of 1977 when I was in my early 30's.

In 1960's when I was a student, I was told by my supervisor, Professor Shojiro Hata, that I should try to create some new ideas in the field related both to soil mechanics and construction activities. He suggested me not to come into the typical soil mechanics subjects which were consolidation and shear strength at that time. He encouraged me to visit many of the tunneling and dam construction sites and stay there for a couple of weeks or more to observe what are happening in the sites. Based on the observation during my stay at more than 10 sites, I started to realize that the earth reacts to the human construction activities in a path-dependent way.

A process of "dig and fill" results in a reaction of the earth different from that induced by a "fill and dig" process. This implies that elasticity can never simulate what happens to the earth during the construction works because elastic materials do not behave in a path-dependent way. To me, at that time, the simplest path-dependent constitutive model was incremental elasto-plastic stress-strain relations such as the one I learned by reading a paper of Cam Clay model authored by Professors Roscoe, Schofield and Thurairajah in 1963. From their paper I learned about the plastic flow rules etc. and reached a constitutive model which Professor Andrew Schofield called Kamo Clay model. Kamo is the name of a river flowing through the middle of Kyoto city where Kyoto University is located.

2 QUESTION 2: GEOTECHNICAL MEASURES TO MEET CATASTROPHIC FLOODING EVENTS

I made several series of trip visiting coastal areas in the North-East Japan where people had suffered from the huge tsunamis on 11th March, 2011. One of those trips was made together with Prof. and Mrs. Michael Pender and my wife Saeko. Each trip gave me new information which made me feel even sadder. There were many points I found from the geotechnical point of view. Among those, I would like to attract engineers' attention to the effect of buoyancy.

Typical configuration of large breakwaters completely washed away by the tsunamis in 2011 was a huge concrete caisson (30m high) sitting on rubble mound (40m high) placed on the seabed. The concrete caisson was filled with gravels and was thought to be heavy enough to resist the tsunami force. The high water comes around the breakwater giving the effect of buoyancy, since the water does not come into the caisson as quickly as the water outside the caisson. This produces instantaneous buoyancy which, I guess, has not been considered in the current design works. In case that the height of the tsunami water is much more than a few meters, thus induced instantaneous buoyancy can be big enough to produce instantaneous instability of huge breakwaters.

Oil storage tanks placed near the sea water are typically surrounded by circular low fence to let the possible leaking oil stay around the tank and prevent it from flowing away. When these tanks suffer from large tsunami waves much higher than their circular fence, the buoyancy can be big enough to pull the tanks off their foundations. Oil storage tanks will float away like vessels with full of burning oil fired by sparks produced when the steel tank walls are hit by the steel top cover plates. I guess the effect of buoyancy has not been considered in the current design methods.

3 QUESTION 3: ADVICE TO YOUNG RESEARCHERS IN GEOTECHNICAL ENGINEERING

Suppose I have a cup of glass that we usually use when we drink the water. The shape of such a glass cup is perfectly described by a pair of concentric circle (plan) and an inverted trapezoid (elevation). Let me have a glass cup in my hand and show it to you who are sitting around me. I say to you "Please draw a picture of this glass cup" and you will produce pictures consisting of two ellipses being connected to each other by two straight lines. Overall pictures drawn by you are different from each other depending on the location where you are looking at the glass cup held by me.

We are geotechnical engineers handling phenomena related to the earth. Any of the geotechnical problems are seen by us from the engineering point of view. However, nature does not care about our concern and behaves in its own way in reacting to the external agencies such as force, temperature, pressure etc. resulted from our activities such as construction works and/or natural hazards. We usually try to understand how the nature, soils and rocks, behaves by carefully observing nature from OUR engineering viewpoint. This is similar way that you did in drawing a picture of a glass cup in my hand. Your pictures are different from each other depending on your viewpoints.

I advice young geotechnical researchers "Do not try to accurately draw two ellipses being connected to each other by two straight lines, because it is not an easy task. It is a difficult task far more than you expect if you want to get an accurate picture like a photo. Instead, draw a pair of concentric circle (plan) and an inverted trapezoid (elevation). It will be much easier and more accurate. Do not look at a phenomenon from your own viewpoint. Look at it from a viewpoint that nature itself looks at it. Try to find out such nature's viewpoint. Then your work will be much easier and finer. Good luck!

This page intentionally left blank

Geotechnics for Catastrophic Flooding Events presents the keynote lectures (book, 264 pages) and keynote lectures and general papers (CD-ROM, 608 pages) presented at the Fourth International ISSMGE-Conference on Geotechnical Engineering for Disaster Mitigation and Rehabilitation (4th GEDMAR, Kyoto, Japan, 16-18 September 2014). The contributions discuss hurricane, rainstorm and storm surge induced riverine and coastal flooding events, such as the 2004 Sumatra earthquake in Indonesia, the 2005 Hurricane Katrina disaster in New Orleans, USA, Typhoon Morakot, which devastated parts of Taiwan in 2009 and the 2011 earthquake and tsunami disaster in Eastern Japan, when combined failure mechanisms, multiple hazards, and rare events with huge consequences occurred.

The book is divided into the following sections:
– Keynote lectures
– Liquefaction experiment and analysis project (LEAP)
– Guidelines and recommendations for local governments to mitigate flooding disasters
– Materials and modeling
– Natural hazards
– Disaster mitigation and rehabilitation

Geotechnics for Catastrophic Flooding Events will be of interest to researchers, academics, industry practitioners and other professional involved in earthquake geotechnical engineering, foundation engineering, and earthquake engineering and structural dynamics.

ISBN 978-1-138-02709-1

CRC Press
Taylor & Francis Group
an informa business
www.crcpress.com

6000 Broken Sound Parkway, NW
Suite 300, Boca Raton, FL 33487
Schipholweg 107C
2316 XC Leiden, NL
2 Park Square, Milton Park
Abingdon, Oxon OX14 4RN, UK

an **informa** business